Frequency-magnitude distribution and spatial fractal dimension of seismicity at the geysers geothermal area and long valley caldera, California

Barton, David J.

Frequency-Magnitude Distribution and Spatial Fractal Dimension of Seismicity at The Geysers Geothermal Area and Long Valley Caldera, California

David J. Barton

A thesis submitted in partial fulfilment of the requirements for the degree of Doctor of Philosophy

Department of Geological Sciences,

University of Durham

September 1998

Frequency-Magnitude Distribution and Spatial Fractal Dimension of Seismicity at The Geysers Geothermal Area and Long Valley Caldera, California

David J. Barton

Abstract

Although there is no obvious reason why seismic *b*-value and the spatial fractal dimension of earthquakes, *D*, should be related, there are several reports of observed empirical correlations between these two quantities. In order to investigate this phenomenon, and attempt to relate it to different types of earthquakes, industrially induced seismicity in The Geysers geothermal area, California and earthquake swarms in Long Valley caldera, California were analysed. Raw seismograms from the Unocal-NEC-Thermal network in The Geysers were processed automatically, calculating magnitudes from coda lengths and locating them using a three-dimensional velocity model. Seismicity correlated with the locations of commercial wells and surface fault locations. The entire Geysers dataset was too complex for clear correlations between *b*, *D*, seismicity and injection to be observed. In several cases, short pulses of injection induced bursts of seismicity of either small-magnitude, clustered events or large-magnitude diffuse seismicity, resulting always in a transient anomaly of negative *b/D*. However, sometimes pulses of injection were not accompanied by *b/D* transients and sometimes *b/D* transients were not accompanied by known injection. The latter cases may or may not indicate undisclosed injection activity. A seismic crisis in Long Valley caldera was associated with major *b/D* anomalies that accompanied migration of the activity from a hydrothermal zone on the south edge of the resurgent dome to the right-lateral, blind, near-vertical South Moat fault to the immediate south. The results indicated that the hydrothermal zone is an inhomogeneous structure whereas the South Moat has a mature, coherent fault plane, capable of generating magnitude $M = 6$ earthquakes and posing a threat to the town of Mammoth Lakes.

Declaration

I declare that this thesis, which I submit for the degree of Doctor of Philosophy at the University of Durham, UK is my own work and is not substantially the same as any which has previously been submitted for a degree at this or any other university.

David John Barton
University of Durham
September 1998

Dedica

Alla mia fidanzata Cristina,
il mio vero amore.
Grazie per tutto.

Acknowledgements

As I leave the loving arms of academia for micro-serfdom in a multinational computer company, I would like to thank:

My supervisor Gill Foulger, for helping me complete this thesis within a tight deadline. Thank you also to Jeremy Henderson, my 'other' supervisor. Also Angus, Alwyn, Rashmin, Du and Kostas. Heartfelt thanks to my personal tutors, Gilbert Larwood and Neil Goulty for their support. Gilbert unfortunately died in the spring of 1997; this thesis is dedicated to his memory.

My father, my brother Stephen and the rest of my family for the support they have given me over the past nine years at university.

Cristina's friends and family for making me feel so welcome this summer in Sicily, especially Faby for making my stay fun. Most of all, thank you to Cristina's mother, Carmen Vitanza, and father, Gary Licata, for making me feel welcome and loved.

Friends and members of the Geology Department for making my time in Durham slightly more bearable, especially Rob, Thani, Alex, Anthony, Andy, Julia, Sarah, Richard, Glenn, José, Ashwina and Edy. Five years is a long time to be in a place as small as Durham. Thank you also to the Graduate Society, the House Committee past and present, and Durham University.

M. Ali Khan at the DOGGR, for answering my many questions about the well data and helping me make sense of the public record. Thank you to Doug Neuhauser for supplying the raw seismogram data, and to David Oppenheimer, John Langbein and Bruce Julian at the USGS for advice and help.

John Gatehouse and George Ruth for the loan of the Macintosh Powerbook during summer 1998. Without them I would never have finished on time.

The IT centre for the help they have given me over the years.

The Natural Environment Research Council for my Ph.D. studentship.

Finally, I would like to thank my fiancée Maria Cristina for her love, friendship, support and capable typing while preparing this thesis. Her help has been invaluable and I am very grateful.

List of Contents

List of Figures

List of Tables

Chapter 1

Introduction

1.1 Introduction

A tool to predict individual earthquakes is one of the 'Holy Grails' of geophysics. Unfortunately, identifying earthquake precursors at a useful level of significance has proved problematic. This lack of clear cut precursors may be due to either the inability of current instrumentation to measure reliable earthquake precursors, or the extreme sensitivity of the underlying non-linear physics to initial conditions, so making it impossible for a reliable precursor to exist *(Brune, 1979; Kagan, 1994)*. Some possible precursors have been identified, such as seismic quiescence before strong aftershocks, foreshocks, and the decrease in radon concentration before a large event *(Wyss, 1991)*, though these are not universally observed.

Another approach considers the fractal nature of earthquake populations. Both earthquake magnitude and earthquake locations have been shown to be fractal (Chapter 2). Of great interest is the claim that the seismic *b*-value (the 'fractal dimension' of the distribution of earthquake sizes) and the fractal dimension of earthquake hypocentres, D, vary in a systematic way related to the earthquake process *(e.g. Henderson et al., 1994)*. Previous authors have attempted to harness this to produce a tool to understand the seismic process, and several models have been produced (Sections 2.1.4, 2.2.1 and 2.3). Since it is not clear what processes are operating during the seismic cycle, the causes of changes in *b* and *D* are not clear, so casting doubt on the validity of these models.

In this thesis, the seismic processes in two areas in California were investigated by calculating the temporal variation of *b* and D. The first, The Geysers geothermal

area, is a highly developed area of commercial geothermal steam production (Chapter 3). The majority of the seismic activity is due to either steam production or the re-injection of condensate, which is done in an attempt to recharge the field with fluid following over-exploitation during the 1980s. The second study area is Long Valley caldera, California (Chapter 6). During late November 1997, there was a severe seismic crisis in the South Moat area of the resurgent dome (Figure 6.1). This intense seismic activity occurred in the same area as previous activity associated with the reactivation of the vertical, west-north-west striking, blind South Moat fault.

In these studies I have attempted to relate the fractal characteristics of earthquake processes to other observations, including industrial well activity and ground deformation. This work contributes to understanding the reasons why b and D vary, and the limitations of these parameters in predicting seismic activity. Whether changes in b and D may some day comprise a useful prediction tool is still unclear. Before such a tool can become a reality, further work aimed at understanding the micro-scale processes that accompany elastic and inelastic deformation and how they affect macro-scale processes is needed.

1.2 Structure of this thesis

The structure of this thesis is as follows:

Chapter 1 contains a short introduction and an outline of the structure of this thesis.

Chapter 2 is a brief overview of fractal theory, the seismic *b*-value and the relationships between *b*-value and the fractal dimensions of earthquake epicentres and hypocentres. Concepts and methods to estimate these parameters are introduced.

Chapter 3 is a description of the geology, geophysics and seismicity of The Geysers Geothermal Area, California. This chapter examines the seismological impact of steam production, and investigates the methods used to prolong the life of this resource.

Chapter 4 describes the processing of seismic data from The Geysers, recorded by the UNOCAL-NEC-Thermal (UNT) network between 1989 and 1994. An assessment of the quality of the "Barton catalogue" generated is presented, along with a comparison with data recorded by the state-wide North California Seismic Network (NCSN). This chapter also contains a study of the steam production and condensate injection wells in The Geysers.

Chapter 5 contains an analysis of the Barton catalogue using the fractal dimension and b-value estimation techniques described in Chapter 2. These quantities are estimated both for the whole catalogue and for discrete subsets (clusters) within it. The temporal development of these quantities is then compared with the well histories introduced in Chapter 4, and cases of systematic behaviour highlighted.

Chapter 6 presents seismic data from Long Valley caldera, California. In November 1997 there was a seismic crisis in the South Moat of the caldera. Using the same fractal dimension and b-value estimation techniques used for the data from The Geysers (Chapter 5), the systematics of the South Moat earthquake activity are examined. Ground deformation data from the same period are also presented.

In the final chapter, Chapter 7, I summarise and draw conclusions from the results described in the previous chapters. The behaviour observed at The Geysers and Long Valley is used as the basis for suggesting theoretical models. Finally, I make suggestions for future work.

The appendices contain listings of the computer programs I wrote to process the raw seismogram data (Appendices 1 to 4), a summary of the well data that I assembled from diverse federal and private sources (Appendix 5), the listing for the program I wrote to perform the *b/D* analysis (Appendix 6) and a summary table of parameters I used in the analyses (Appendix 7).

Chapter 2

Fractals and b-values

2.1 Estimation of the fractal dimension

2.1.1 What is a fractal?

A fractal is a rough or fragmented geometric shape that can be subdivided into parts, each of which is similar to the whole in some way *(Feder, 1989)*. Fractals generally exhibit scale-invariance, whereby an object can appear identical (or "self similar") over a variety of scales. Fractal structures are common in mathematics, e.g. the Sierpinski triangle (Section 2.1.2), the Koch snowflake and the Mandelbrot set. Fractals can either be self-similar (i.e. they exhibit isotropic scale-invariance) or self-affine (i.e. they have orientation-dependent scale-invariance).

When studying scaling aspects, the natural world is more usefully described using fractal geometry than by using Euclidean objects. However, fractal objects in natural systems are only self-similar over a limited range of scales. For example, the coastline of an island appears to be self-similar over a range of scales, but is limited by grain size on a microscopic scale, and by the size of the island on a macroscopic scale. Geometrical fractal objects (Section 2.1.2) are self-similar over an infinite range. Self-similarity has been observed in many geological and geophysical phenomena, such as rock fragments, faults, earthquakes, volcanic eruptions, mineral deposits and oil fields. The frequency-size distributions of these systems exhibit a power-law dependence, and it can be shown that such distributions are fractal. Most fractal systems in nature are self-affine.

2.1.2 Simple geometrical fractal sets

The fractal set can be defined by:

$$N_n = \frac{C}{r_n^D} \tag{2.1}$$

where N_n is the number of objects with a characteristic linear dimension r_n, D is the fractal dimension, n is the order of the fractal and C is a constant of proportionality. When the fractal dimension is an integer, it is equivalent to a Euclidean dimension. For example, for a point $D = 0$, for a line $D = 1$, for a square $D = 2$ and for a cube $D = 3$. In general, however, the fractal dimension is not an integer, but a *fractional dimension.*

Two well-known examples of mathematical fractal structures are the Cantor Set and the Sierpinski Carpet. Mathematical fractal structures are deterministic, i.e. their initial conditions and equations are fully specified and not random or stochastic *(Turcotte, 1992)*. The Cantor Set (Figure 2.1a) is constructed from a line of unit length (the initiator) divided into three parts (the generator) so that $r_1 = {}^1/_3$. The two end segments are retained so that $N_1 = 2$, and the central segment is discarded. The process is repeated so that $r_2 = {}^1/_9$ and $N_2 = 4$ etc.

By rewriting Equation 2.1 as:

$$D = \frac{\ln\left(\frac{N_{n+1}}{N_n}\right)}{\ln\left(\frac{r_n}{r_{n+1}}\right)} \tag{2.2}$$

it can be shown that $D = 0.6309$ for the Cantor Set. If the subdivision process described above is carried out n times, the line length following the n^{th} subdivision, r_n, is related to the original line length, r_0, by:

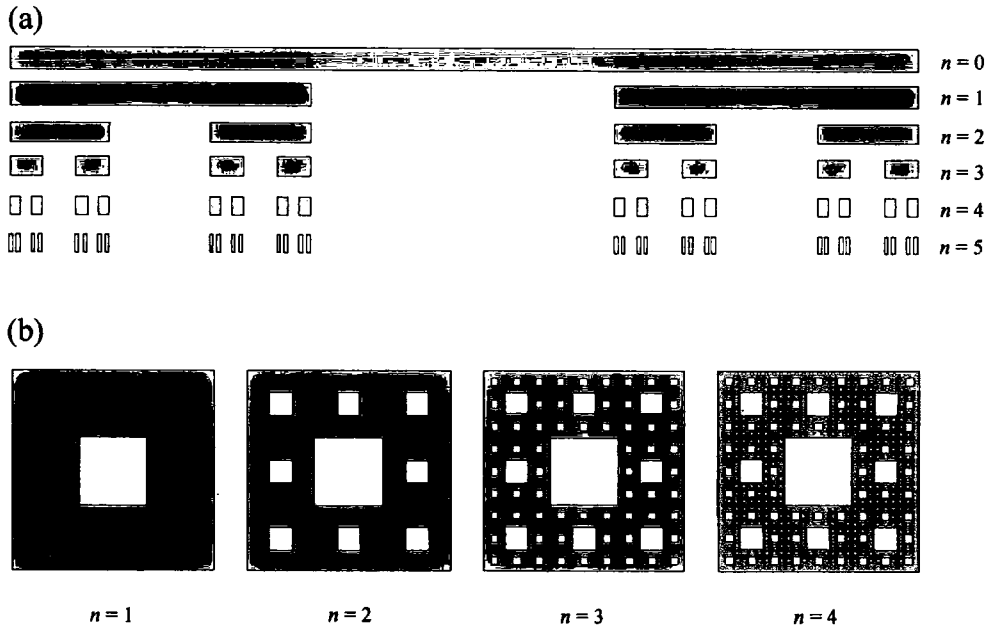

Figure 2.1 Simple deterministic fractals. (a) The Cantor set, $D = 0.6309$. The initiator is a line of unit length. The generator removes the middle third. n = order. (b) The Sierpinksi carpet, $D = 1.8928$. The initiator is a square. The generator is made up of $N = 8$ squares. *(from Feder, 1989)*

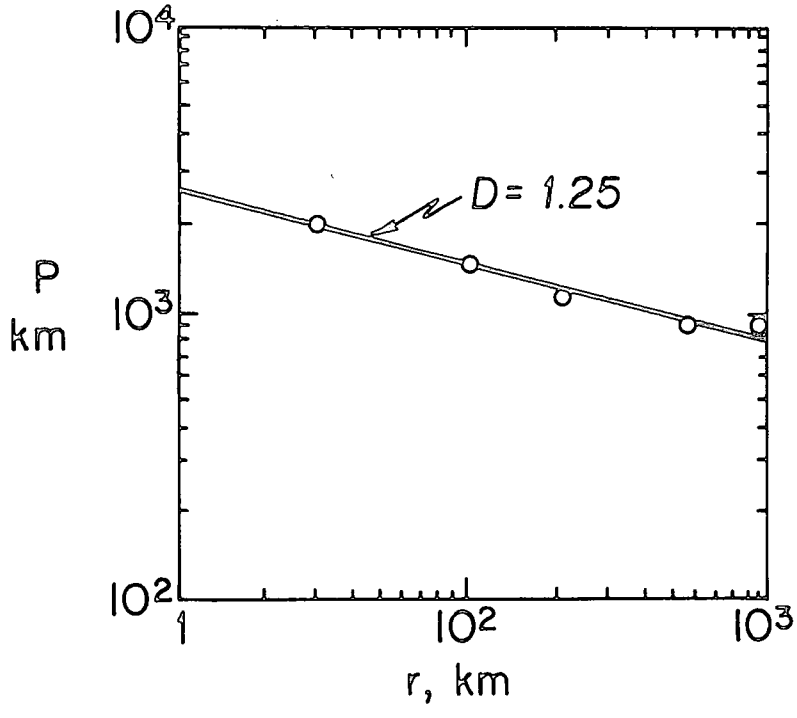

Figure 2.2 Length P of the west coast of Great Britain as a function of the length, r, of a measuring rod. Using equation 1.5, $D = 1.25$ *(from Turcotte, 1992).*

$$\frac{r_n}{r_0} = \left(\frac{r_1}{r_0}\right)^n \tag{2.3}$$

Thus, as $n \rightarrow \infty$, $r_n \rightarrow 0$. At this limit the Cantor Set is known as 'Cantor Dust' and is an infinite set of clustered points.

The Sierpinski Carpet (Figure 2.1b) is constructed by applying the method used above to a square. At each order (i.e. each step) the central square is removed. This process is then repeated many times. At first order, $r_1 = {}^1/_3$, $N_1 = 8$, at second order, $r_2 = {}^1/_9$, $N_2 = 64$, and so on. Application of Equation 2.2 yields $D = 1.8928$. These simple fractal sets were useful for testing the fractal dimension calculating programs written for this thesis.

2.1.3 Estimation of the fractal dimension for non-deterministic fractal sets

2.1.3.1 The ruler method and box counting

The ruler method and box counting are simple geometrical methods of estimating the fractal dimension of an object. In the ruler method, a ruler of a fixed length, r_n, is used to measure the length of an object's perimeter. The process is then repeated for other different fixed lengths. The measured perimeter length, P_n, for a ruler length r_n is given by:

$$P_n = r_n N_n \tag{2.4}$$

where N_n is the number of lengths r_n required to measure the length of the perimeter. By substituting for N_n in Equation 2.1,

$$P_n = \frac{C}{r_n^{D-1}}. \tag{2.5}$$

The gradient of a straight line fitted to a plot of log (perimeter length) against log (ruler length) is equal to 1-*D*, where *D* is the fractal dimension. The ruler method can be used to measure the fractal dimension of coastlines and contours *(e.g. Mandelbrot, 1967)* (Figure 2.2).

The box counting method uses boxes to cover an object to find the fractal dimension. Consider the coastline of an island (Figure 2.3a). To find its fractal dimension, the coast is overlain by a grid of a fixed line spacing, *r*, and the number of squares, *N*, required to cover the coastline is determined. This procedure is repeated for other line spacings. Finally, log (*N*) is plotted against log (*r*). If a linear relationship between log *r* and log *N* exists, then Equation 2.2 is used to calculate *D*. The fractal dimension found using the box counting method is known as the capacity dimension, D_0 *(Legrand et al., 1996)*. The types of fractal dimension discussed in this thesis are presented in Table 2.1.

The box counting method can also be applied to a distribution of points. To produce a reasonable estimate of *D* for a distribution of points using the box counting method, $N \sim 10^d$ points are needed, where *d* is the 'embedding dimension', the Euclidean dimension of the space around the fractal *(Takens, 1984)*. Hence the box counting method is impractical for calculating the fractal dimension of non-isotropic (i.e. self-affine) objects where $d > 3$ *(Farmer, 1982; Bai-Lin, 1984; Greenside et al., 1982; Theiler, 1990)*. The box counting method has been used to find the fractal dimension of the volcanic tuff fracture network at Yucca Mountain, Nevada *(Barton & Larsen, 1985)*.

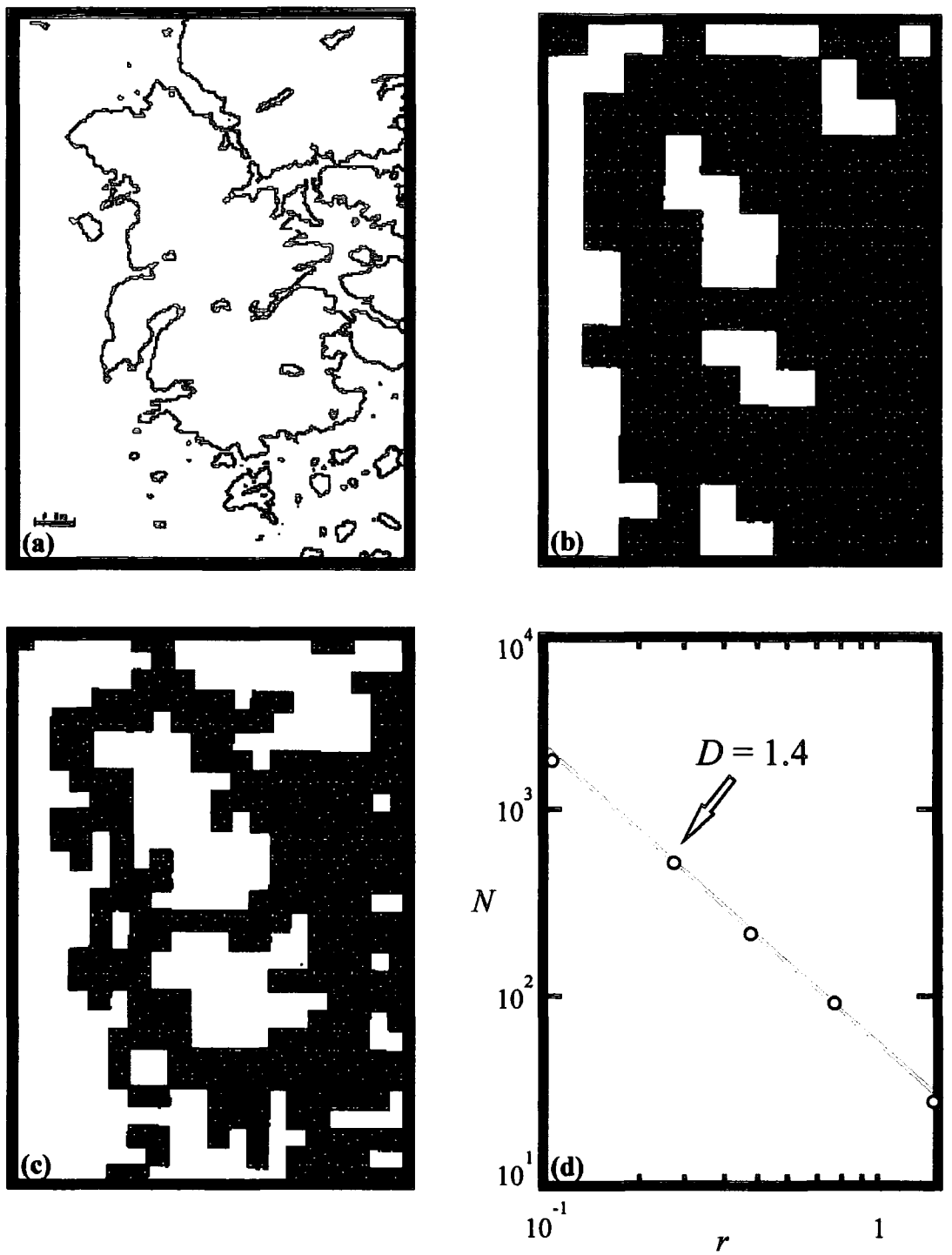

Figure 2.3 Using the box counting method for estimating the fractal dimension of a rocky coastline. (a) is a map of the coastline of Dear Island, Maine. (b) The shaded area contains the square boxes with $r = 1$ km required to cover the coastline; $N = 98$. (c) As (b), but with 0.5 km boxes; $N = 270$. (d) Plot of N against r, yielding $D = 1.4$. *(Turcotte, 1992)*

Table 2.1 Types of fractal dimension

Type	Name	Description
D_0	Capacity dimension	Complete space containing the fractal set is covered with boxes of a set size. The capacity dimension is a measure of the number of non-empty boxes (Section 2.1.3.1). Also known as the Hausdorff dimension.
D_1	Information dimension	Like box counting, but the number of elements in each box are also counted.
D_2	Correlation dimension	Takes into account the way one element of the fractal object is correlated to all the others (Section 2.1.3.2).
D_q	Generalised fractal dimension	Extension of the correlation dimension to the order q (see 'future work' in Chapter 7).

2.1.3.2 The correlation dimension method

In using the correlation dimension method, the spatial correlation between each point in the fractal set is considered *(Forrest & Witten, 1979; Grassberger & Procaccia, 1983a; Legrand et al., 1996)*. Consider a *d*-dimensional "box" of size R (either a cube or sphere), where d is the embedding dimension. Within the "box" is a fractal object comprised of a series of points. The number of points, N, which are within a distance, r, of a randomly chosen point, x, is given by (Figure 2.4):

$$N(r,R) \propto \left(\frac{r}{R}\right)^{d_{box}} \tag{2.6}$$

If the mean value of N is taken over all the possible points of the fractal, the Correlation Integral, $C(r)$ is,

$$C(r) = \lim_{N\to\infty} \frac{1}{N^2} \{\text{number of pairs } (x_i, x_j)_1^N \text{ whose distance } \overline{x_i x_j} > r\} \tag{2.7}$$

where x_i and x_j are the i^{th} and j^{th} points respectively within the fractal structure.

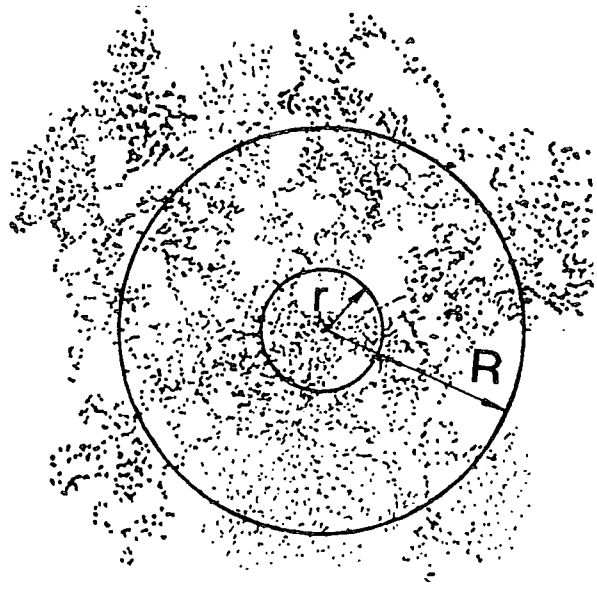

Figure 2.4 Schematic diagram showing the fractal measurement method for the correlation dimension *(from Xie & Pariseau, 1993)*.

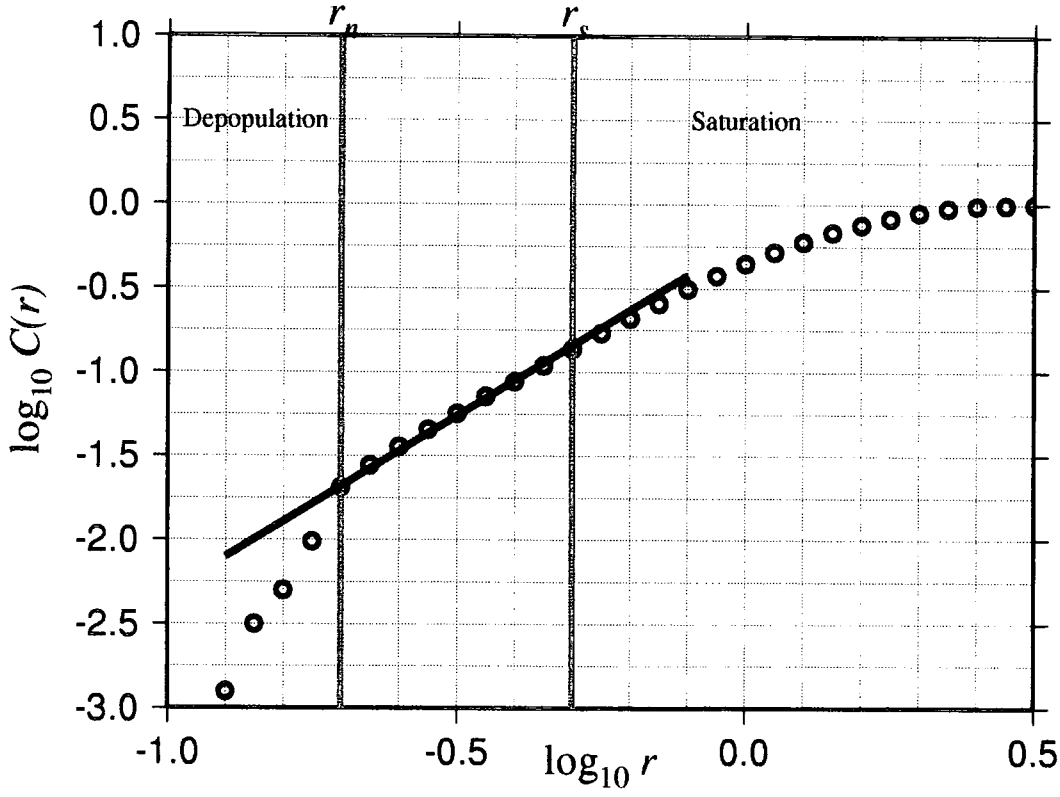

Figure 2.5 Estimation of the correlation dimension, D_2, the gradient of a plot of $\log_{10} C(r)$ against $\log_{10} r$. Black line represents least squares fit to points in the range $r_n < r < r_s$.

Or alternatively:

$$C(r) = \lim_{N\to\infty} \frac{1}{N^2} \sum_{i=1}^{N} \sum_{j=1}^{N} H\left(r - |x_i - x_j|\right) \tag{2.8}$$

where $H(x) = 0$ for $x < 0$ and $H(x) = 1$ for $x > 0$. In simpler terms, $C(r)$ is the probability that two points will be separated by a distance less than r.

For fractals, $C(r)$ scales as:

$$C(r) \propto r^{D_2} \tag{2.9}$$

where D_2 is the correlation fractal dimension.

Equation 2.9 can be rewritten as:

$$D_2 = \frac{\log C(r)}{\log r}. \tag{2.10}$$

If the dataset is self-similar over an infinite range, the correlation dimension, D_2, is the gradient of a plot of log $(C(r))$ against log (r). In practice fractal systems in nature are self-similar over a finite range (Figure 2.5), so D_2 must be estimated from a range insensitive to the finiteness of the set.

The extremes of the finite range of scales generate undesirable edge effects. Consider a dense cluster of points in an otherwise unpopulated region of space. When r is less than the smallest inter-point distance in the fractal dimension, both $C(r)$ and D_2 would tend to zero. This extreme is known as 'depopulation'. At the other extreme, when the value of r exceeds the diameter of the dense cluster of points, $C(r)$ would reach a maximum limit when all the available pairs of points would have been counted. This is known as 'saturation'. Both depopulation and saturation will appear in a data set that consists of a limited number of data points

within a volume of finite size, even if there are no measurement errors. Now consider what happens to the value of D_2 close to the extremes of depopulation and saturation. When r is small, $C(r)$ is unaffected by the lack of points outside the cluster. Hence, $C(r)$ increases rapidly with r and D_2 is large. Therefore, if a scaling range using small values of r is used to calculate D_2, strong clustering would correspond to an *increase* in D_2. When r approaches the diameter of the cluster, the rate at which $C(r)$ increases with r decreases and D_2 will be small. Hence, if a scaling range using large values of r are used to calculate D_2, strong clustering would correspond to a *decrease* in r. This implies that, depending on the range of r chosen, a dense cluster of points can yield both high and low values of D_2.

When calculating the range in r over which to calculate D_2, most authors arbitrarily choose the straightest segment of the plot. However, simply selecting the straightest part of the plot visibly is not enough *(Eneva, 1996)*. Depopulation and saturation do not just affect the parts of the curve which are visibly non-linear, but also the straighter portions too. Consequently there is a need for a proper scaling method that takes account of these effects. By considering a uniform distribution of N points within a hypercube of edge $2R$, it is possible to define the distances of depopulation, r_n, and saturation, r_S, as:

$$r_n = 2R(1/N)^{1/d} \tag{2.11}$$

$$r_S = \frac{R}{(d+1)} \tag{2.12}$$

where d is the embedding dimension *(Nerenberg & Essex, 1990)*.

Applying these equations, a proper scaling range is $r_n \leq r \leq r_S$ (Figure 2.5). If $r_S \leq r_n$, then a proper scaling region does not exist. It has been shown empirically that it is safe to use a lower limit of $r_n/3$ *(Eneva, 1996)*, and this was adopted for the

data analysed in this thesis. Note that r_n is dependent on N and that r_S is not, meaning that using more points to calculate D_2 only extends the scaling range at the depopulation end.

It has been suggested that at least 42^d points are needed to obtain a good estimate of D_2 *(Smith, 1988)*. This implies that correlation dimension calculations are limited to data sets with at most 5 or 6 dimensions, even on supercomputers. Other authors have found that smaller data sets are adequate if it is the *relative* values of D_2 which are of interest rather than the absolute values *(Nerenberg & Essex, 1990)*. This is particularly true for non-stationary dynamic systems *(Havstad & Ehlers, 1989; Eneva, 1996)*. The error in D_2 has been estimated by comparing the value of D_2 generated using a dataset of 12,800 points with that calculated using 100 points *(Havstad & Ehlers, 1989)*. The value of D_2 estimated using the smaller sample was within 10% of that generated using the larger dataset. The error in D_2 for the data analysed in this thesis was therefore assumed to be of this order; i.e. 10% of the value of D_2. The correlation dimension technique was used in preference to other methods of estimating fractal dimension because of its computational simplicity.

2.1.4 The fractal nature of seismicity

Several aspects of seismicity have been shown to be fractal. The geometry of the fracture surface of rocks (i.e. joints and faults) are fractal, and have been observed in rocks over scales of 10^{-6} m to 10^5 m *(Hirata, 1989)*. Surface traces of faults in the San Andreas fault zone have been shown to be fractal *(Aviles et al., 1987; Okubo & Aki, 1987)*. For the fault trace of the main San Andreas fault, $D \sim 1.001$ over a length scale range of 1 - 100 km *(Aviles et al., 1987)*, and is slightly higher ($D \sim 1.01$) for smaller scales. Another study that included branches of the San Andreas fault found that D was between 1.12 and 1.42 *(Okubo & Aki, 1987)*. A similar study in Japan found a fractal geometry over a scale range of 2 - 20 km, with D varying from ~ 1.5 at the centre of the Japan Arc to ~ 1.05 further from the

centre *(Hirata, 1989)*. Surface traces of fractures in the Mojave desert have been shown to have a fractal dimension of ~ 1.7 *(Sournette et al., 1991)*. Fractal fracture analysis has also been conducted in Japanese mines *(Merceron & Velde, 1991)*.

Earthquakes with magnitudes < 6 have been shown to be fractally clustered in time *(Kagan & Knopoff, 1981)*. The inter-event times of earthquakes near Efate Island in the New Hebrides also show fractal clustering *(Smalley et al., 1987)*. The temporal clustering of seismicity there between 1978 and 1984 exhibits self-similar behaviour over time ranges from a few minutes to about a month.

The epicentral and hypocentral distributions of earthquakes are also fractal. A study by *Sadowiskiy et al. (1984)* demonstrated that the spatial distribution of earthquakes on a global scale and earthquakes local to the Nurek region in the former USSR are fractal. Subsequent studies have discovered fractal earthquake locations in Japan, Italy, Brazil and California (Table 2.2). Fractal behaviour has also been observed in rock bursts and in laboratory microseismicity studies (Table 2.2).

Temporal variation of D_2 has been observed in earthquake sequences. Depending on whether a high value of D_2 corresponds to stronger or weaker clustering, D_2 will either increase *(e.g. Henderson et al., 1994)* or decrease *(e.g. De Rubeis et al., 1993)* respectively after a large earthquake. Similar results have been observed in laboratory microseismic studies *(e.g. Hirata et al., 1987)* and for rock bursts in mines *(Trifu et al., 1993)*. These observations indicate the importance of understanding the response of D_2 to clustering when comparing previous studies.

Table 2.2 Some examples of previous work on the fractal nature of earthquake locations.

Reference	Seismicity	Method of fractal Estimation	High D corresponds to:	Phenomena observed
Hirata et al. (1987)	Laboratory microseismicity on Oshima granite.	Correlation dimension.	Weaker clustering	D_2 decreased and greater clustering of microfractures observed during creep phase of rock deformation.
Henderson & Main (1992)	Earthquake epicentres in Parkfield, California	Correlation dimension	Stronger clustering	Following large earthquakes, D_2 increased.
De Rubeis et al. (1993)	Earthquake epicentres from Italy.	Correlation dimension	Weaker clustering	Prior to a large earthquake, D_2 increases. Following the event, D_2 falls due to an increase in seismicity and clustering. D_2 then rises again.
Trifu et al. (1993)	Rock burst hypocentres from mines in Ontario, Canada.	Correlation dimension	Stronger clustering	Increase in D_2 after large event.
Xie & Pariseau (1993)	Rock burst hypocentres in mines.	Correlation dimension	Weaker clustering	Prior to a rock burst, D_2 decreases as greater fracture clusters are formed.
Henderson et al. (1994)	Earthquake hypocentres in Brazil.	Correlation dimension	Stronger clustering	Increase in D_2 after large events.

A model to explain the behaviour of D_2 throughout seismic cycles was suggested by *De Rubeis et al. (1993)*. In this model, a high value of D_2 corresponds to weaker clustering. A major earthquake or swarm marks the end of a seismic cycle. The first phase of the next cycle is characterised by seismic activity migrating away from the main fault, which remains locked and aseismic. During the first phase, D_2 increases from the minimum value reached at the end of the previous cycle. In the second phase, stress begins to build up within the fault system. As the stress increases, accumulated strain energy is dissipated by failure on minor faults spread throughout the seismogenic volume. When the peak stress is reached, two scenarios are possible. Either the accumulated strain energy is released by aseismic creep or by a major earthquake. This can either occur without a significant precursory change in the fractal nature of the background activity (no change in

D_2) or may be preceded by a spatial clustering of activity (a precursory drop in D_2). This model also agrees with the observed changes in D_2 in acoustic emission microseismicity studies in the laboratory, and for rock burst seismicity in mines.

2.2 Estimation of the seismic b-value

2.2.1 What is a b-value?

The power-law relationship between the magnitude of earthquakes and their frequency of occurrence has been recognised for nearly a hundred years. *Omori (1902)* showed a table of the frequency distribution of maximum amplitudes recorded by a seismometer in Tokyo, which, when plotted on log-log paper, showed a power-law distribution. This relationship was expressed formally by the equation of *Ishimoto & Iida (1939)*:

$$n(A) = kA^{-m} \tag{2.13}$$

where $n(A)$ is the number of earthquakes with amplitude A and magnitude m, and k is a constant. The relationship between earthquake magnitude and frequency of occurrence is more commonly expressed by the Gutenberg-Richter equation. This equation states that the rate of occurrence of earthquakes of a magnitude greater than m is proportional to 10^{-bm}.

$$\log \dot{N} = -bm + \log \dot{a} \tag{2.14}$$

where $\dot{N}$ is the number of earthquakes per unit time with magnitude greater than m and $\dot{a}$ and b are constants *(Gutenburg & Richter, 1942)*. The constant $\dot{a}$ is a measure of the seismic rate. The constant b is known as the b-value. Although the value of b varies from region to region, it typically lies in the range $0.8 < b < 1.2$

(Evenden, 1970). A high value of *b* indicates a greater proportion of smaller events and a low value of *b* indicates a greater proportion of larger events.

Several authors have reported temporal changes in *b*-value in seismic sequences, both in natural earthquakes and in laboratory experiments (Table 2.3). Four types of behaviour have been observed. First, *b*-value decreases before a large event *(e.g. Scholz, 1968; Weeks et al., 1978; Hirata et al., 1987; Lockner et al., 1991)*. This phenomenon has been reported in earthquake data and in laboratory data using granites and sandstones, and is the most commonly observed. Second, *b*-value increases prior to and then decreases sharply before a large event *(e.g. Ma, 1978; Smith, 1981 & 1986; Henderson & Main, 1992)*. This has been observed in both natural earthquake and microseismic laboratory data obtained using hardstones.

Table 2.3 Some examples of observations of seismic *b*-value behaviour

Reference	Seismicity	Method of *b*-value calculation	Phenomena observed
Scholz (1968)	Laboratory rock microfractures in San Marcos gabbro.	Relationship between *b*-value and earthquake amplitude *(Asada et al., 1951)*.	High *b* observed in ductile rock; low *b* in brittle rock. Fall in *b* before rock failure.
Gibowicz (1973)	Aftershock sequences and an earthquake swarm in New Zealand.	Aki equation *(Aki, 1965)* (Equation 2.23)	Aftershock sequences: *b* increases rapidly after the main shock, decreases until the largest aftershock, and increases thereafter. Earthquake swarms: *b* decreased with time.
Wyss & Lee (1973)	Earthquakes in California	Aki equation *(Aki, 1965)*	*b*-value decreased before and after large earthquakes.
Gibowicz (1974)	Earthquakes in New Zealand 1955 - 1969.	Aki equation *(Aki, 1965)*	*b* varies with time with an oscillatory character with a period of 7 - 8 years.
Fieldler (1974)	Seismicity during the 1967 Caracas earthquake.	*b*-value calculated from frequency-magnitude plots	*b*-value decreased before the main shock.
Ma (1978)	Earthquakes in China.	Aki equation *(Aki, 1965))*	Before a large earthquake there is an increase in *b* followed by a decrease.
Weeks et al. (1978)	Microseismic events in the laboratory on Westerly granite.	Relationship between *b*-value and earthquake amplitude *(Asada et al., 1951)*.	Fall in *b*-value before failure.

Table 2.3 Previous observations of seismic *b*-value behaviour (continued)

Reference	Seismicity	Method of *b*-value calculation	Phenomena observed
Smith (1981)	Earthquakes in New Zealand, California and Venezuela.	Aki equation *(Aki, 1965)*	Before a large earthquake there is an increase in *b* followed by a decrease.
Imoto & Ishiguro (1986)	Earthquakes in central Japan.	Temporal changes in magnitude ratios *(Akaike, 1973).*	Before a large earthquake there is an increase in *b* followed by a decrease.
Smith (1986)	Earthquakes in New Zealand and California.	Zhang & Song equation *(Zhang & Song, 1981)* (Equation 2.24).	Before a large earthquake there is an increase in *b* followed by a decrease.
Hirata et al. (1987)	Laboratory microseismicity on Oshima granite.	Gutenberg-Richter equation, using amplitude magnitudes.	Decrease in *b* prior to failure.
Foulger (1988)	Earthquake swarms near the Hengill triple junction, Iceland	Frequency - magnitude plots	Decrease in *b* at the start of the swarm, increase during, and then returned to initial level afterwards.
Meredith et al. (1990)	Microseismic events in the laboratory on Westerly granite and Darley Dale sandstone.	Empirical relationship between stress intensity and *b*-value *(Meredith & Atkinson, 1983).*	Decrease in *b* prior to failure.
Lockner et al. (1991)	Microseismic events in the laboratory on Westerly granite.	Relationship between *b*-value and earthquake amplitude.	Decrease in *b* prior to failure.
Henderson & Main (1992)	Earthquakes in Parkfield, California / laboratory microseismicity on Darley Dale sandstone.	Aki equation *(Aki, 1965)* (Parkfield). Relationship between crack length and *b*-value (laboratory).	Before a large earthquake there is an increase in *b* followed by a decrease (Parkfield). Increase and then decrease in *b* prior to failure (laboratory).
Sammonds et al. (1992)	Microseismic events in the laboratory on Darley Dale sandstone.	Relationship between stress intensity and *b*-value *(Meredith & Atkinson, 1983).*	Decrease in *b* prior to failure.
Trifu et al. (1993)	Rock bursts in Canadian mines.	*b*-value calculated from frequency-magnitude plots	Changes in *b* not related to rock bursts.
Henderson et al. (1994)	Seismicity in Brazil.	Aki equation *(Aki, 1965).*	Decrease in *b* before a large event.

Third, *b*-value has been observed to change throughout an aftershock sequence *(e.g. Gibowicz, 1973).* Fourth, *b*-value varies over large areas and long time intervals, not apparently related to large events *(e.g. Gibowicz, 1974; Trifu et al., 1993).*

The first two types of behaviour in *b* can be explained using a one-dimensional fracture model *(Henderson & Main, 1992)* (Figure 2.6). A fault within a block of material is modelled as an isolated series of elements with differing fracture toughnesses (i.e. rock strengths). A crack is modelled as an element or series of elements whose fracture toughness have been exceeded by the local stress. The entire model is subject to a uniform remote stress. As the remote stress is increased, parts of the fault fail, forming isolated cracks. Since the presence of cracks amplifies the local stress field, these cracks will propagate as long as the local stress exceeds the fracture toughness. In this model, a high fractal dimension, estimated using the box counting method, corresponds to stronger fault clustering.

In the early stages of rock damage crack growth is not continuous. At low remote stresses, the growth of isolated cracks is inhibited by a stress relieving 'domain' around them *(Costin, 1983 & 1987)*. Consequently, well ordered crack distributions develop, suggesting a predictability, or 'persistence' of the system. These crack distributions have lower values of D_0. As small cracks predominate, *b*-value will be high, as observed in the type two behaviour. As the remote stress increases, the likelihood that two cracks might develop in the same volume increases, despite the inhibiting effect of stress-relieving domains, and volumes of the rock fail due to crack interaction. This fault clustering suggests an unpredictability, or 'antipersistence' of the system. Eventually, the whole fault is consumed by this process and undergoes catastrophic failure. In this phase, cracks are clustered (high D_0) and contain a larger proportion of bigger cracks (low *b*). This agrees with both type one and type two *b*-value behaviour.

Other factors can also cause *b*-value variations. Rock heterogeneity has been shown to increase *b*-value *(Mogi, 1962)*. Changes in the stress level can be caused by pore fluid pressures and thermal stresses *(Warren & Latham, 1970; Wyss, 1973)*. These three factors can cause *b*-value variations in volcanic areas *(e.g. Wiemer & McNutt, 1998)*.

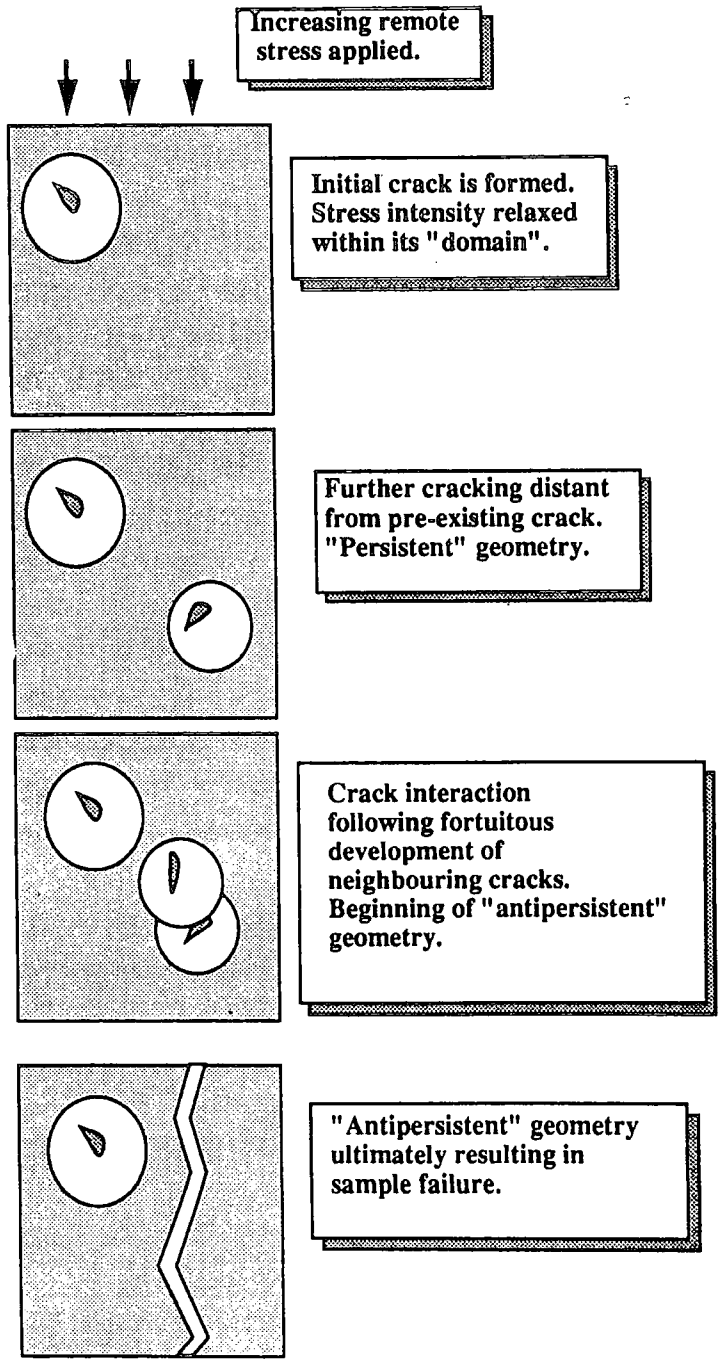

Figure 2.6 Cartoon illustrating the processes hypothesised to occur during the fracture of rocks *(from Henderson & Main, 1992)*.

2.2.2 The fractal nature of the seismic b-value

Since the Gutenberg-Richter equation (Equation 2.14) states that there is a power law relationship between the frequency of earthquakes and their magnitudes, it has been suggested that the *b*-value is related to the fractal dimension of earthquake magnitude, D_{mag} *(e.g. Aki, 1981; Turcotte, 1992).* The relationship between *b* and D_{mag} can be derived by expressing the *Gutenberg-Richter* equation (Equation 2.14) in terms of seismic moment, *M*, and fault-break area, *A*, for a set of earthquakes occurring along a single fault *(Aki, 1981).* The relationship between earthquake moment and the area of the rupture is *(Kanamori & Anderson, 1975)*:

$$M = \alpha A^{3/2} \qquad \text{where } \alpha \text{ is a constant.} \tag{2.15}$$

Earthquake magnitude, *m*, is related to moment by:

$$\log M = cm + d \tag{2.16}$$

where *c* and *d* are constants. It has been shown that *c* = 1.5 *(Kanamori & Anderson, 1975)* and that *d* = 9.1 for the case of surface wave magnitudes *(Kanamori, 1978; Hanks & Kanamori, 1979).*

Combining Equations 2.14, 2.15 and 2.16 gives:

$$\log \dot{N} = -\frac{3b}{2c} \log A + \log \dot{\beta} \tag{2.17}$$

where $$\log \dot{\beta} = \frac{db}{c} - \frac{b}{c} \log \alpha + \log \dot{a}$$

Equation 2.17 can be rewritten as:

$$\dot{N} = \dot{\beta} A^{-3b/2c} \tag{2.18}$$

If $N = \frac{C}{r^D}$ (Equation 2.1 - the definition of a fractal) and $A \sim r^2$, substituting these into Equation 2.18 gives:

$$\frac{C}{r^{D_{mag}}} = \dot{\beta}(r^2)^{-3b/2c} \tag{2.19}$$

$$\frac{C}{r^{D_{mag}}} = \frac{\dot{\beta}}{r^{3b/c}} \tag{2.20}$$

$$\therefore \quad D_{mag} = \frac{3b}{c} \tag{2.21}$$

If $c = 1.5$, then $D_{mag} = 2b$.

The fractal dimension of magnitude is thus twice the b-value. This relationship applies for tensile fractures in small samples, based on empirical laboratory evidence *(Hatton et al., 1993)*. Whether this hypothesis holds for earthquakes in nature is still not known, though it has been assumed implicitly in many recent studies *(Turcotte, 1992)*. A study of Japanese seismicity has shown that the fractal dimension of magnitudes is not related to spatial fractal dimension *(Hirata, 1989)*.

2.2.3 Calculation of the b-value

Since seismic recording stations have finite detection thresholds, it is not possible to detect all the low magnitude earthquakes in an area. Thus, to find the best estimate of the b-value for a set of earthquakes, the range of magnitudes above a minimum magnitude corresponding to the detection threshold, m_{min}, should be used. Maximum likelihood methods of estimating b were used in this work.

The simplest approach utilises the Aki equation *(Aki, 1965)*:

$$b = \frac{\log_{10} e}{\overline{m} - m_{\min}} \pm \frac{1.96b}{\sqrt{n}} \text{ (95\% confidence limits)} \qquad (2.23)$$

where $\overline{m}$ is the mean magnitude, $m_{\min}$ is the threshold magnitude and n is the number of events above the threshold magnitude. A better estimate of b is given by Zhang & Song, *(1981)*:

$$b = \frac{(n-1)\log_{10} e}{n(\overline{m} - m_{\min})} \qquad (2.24)$$

For the sample sizes used in most studies, including that of this thesis (50 to 400 events) the Aki and Zhang & Song equations are approximately equivalent.

The Aki equation only gives a good estimate of b when the range of magnitudes is greater than two or three orders. The range of magnitudes for the data used in this thesis was relatively small. To take account of these small magnitude ranges, it was necessary to use a more rigorous version of the Aki equation to calculate b, called the Page equation *(Page, 1968)*.

$$b = \log_{10} e \left[\overline{m} - \frac{m_{\min} - m_{\max} e^{-b'(m_{\max} - m_{\min})}}{1 - e^{-b'(m_{\max} - m_{\min})}} \right]^{-1} \qquad (2.25)$$

where $b' = \dfrac{b}{\log_{10} e}$ and $m_{\max}$ is the maximum magnitude.

The solution for b in this equation was found using the method of bisection *(Press et al., 1988)*, as were the solutions to the equations for the 95% confidence limits for b given by:

$$\sqrt{n}\left[\frac{1}{b'^2}+\frac{(m_{b\max}-m_{b\min})^2}{2-e^{b'(m_{b\max}-m_{b\min})}-e^{b'(m_{b\min}-m_{b\max})}}\right]^{-\frac{1}{2}}$$

$$\times\left[\frac{1}{b'}+\frac{m_{b\min}-m_{b\max}e^{-b'(m_{b\max}-m_{b\min})}}{1-e^{-b'(m_{b\max}-m_{b\min})}}-\overline{m}\right]=\pm 1.96 \qquad (2.26)$$

A comparison of the three maximum likelihood methods for 200 event samples of data from The Geysers (Chapter 3) showed that the Aki equation (Equation 2.23) and the Zhang & Song equation (Equation 2.24) consistently produced values of *b* about 12% larger than those generated by the Page equation (Equation 2.25) (Figure 2.7). Visual inspection of frequency-magnitude plots showed that the Page equation produced the best fit to the data.

2.3 The relationship between b-value and fractal dimension

There is no obvious reason why *b*-value and the spatial fractal dimension of epicentres or hypocentres, *D*, should be related, since they are controlled by different characteristics of the seismicity. However, there are a number of reports of correlation between the two quantities (Table 2.4).

When analysing the changes in *b* and *D* within a earthquake catalogue, non-uniformity of the catalogue must be taken into account. For example, a study of earthquakes in the Tohoku region of Japan between 1926 and 1986 revealed a negative correlation between *b* and D_2 *(Hirata, 1989)*. However, changes in the earthquake location accuracy over the study period probably affected the apparent clustering characteristics of the seismicity. Similarly, a study of seismicity in the North Anatolian fault zone, Turkey, revealed a long- term negative correlation between *b* and D_2 *(Öncel et al, 1995)*. This was attributed to changes in instrument deployment rather than any real change in seismicity.

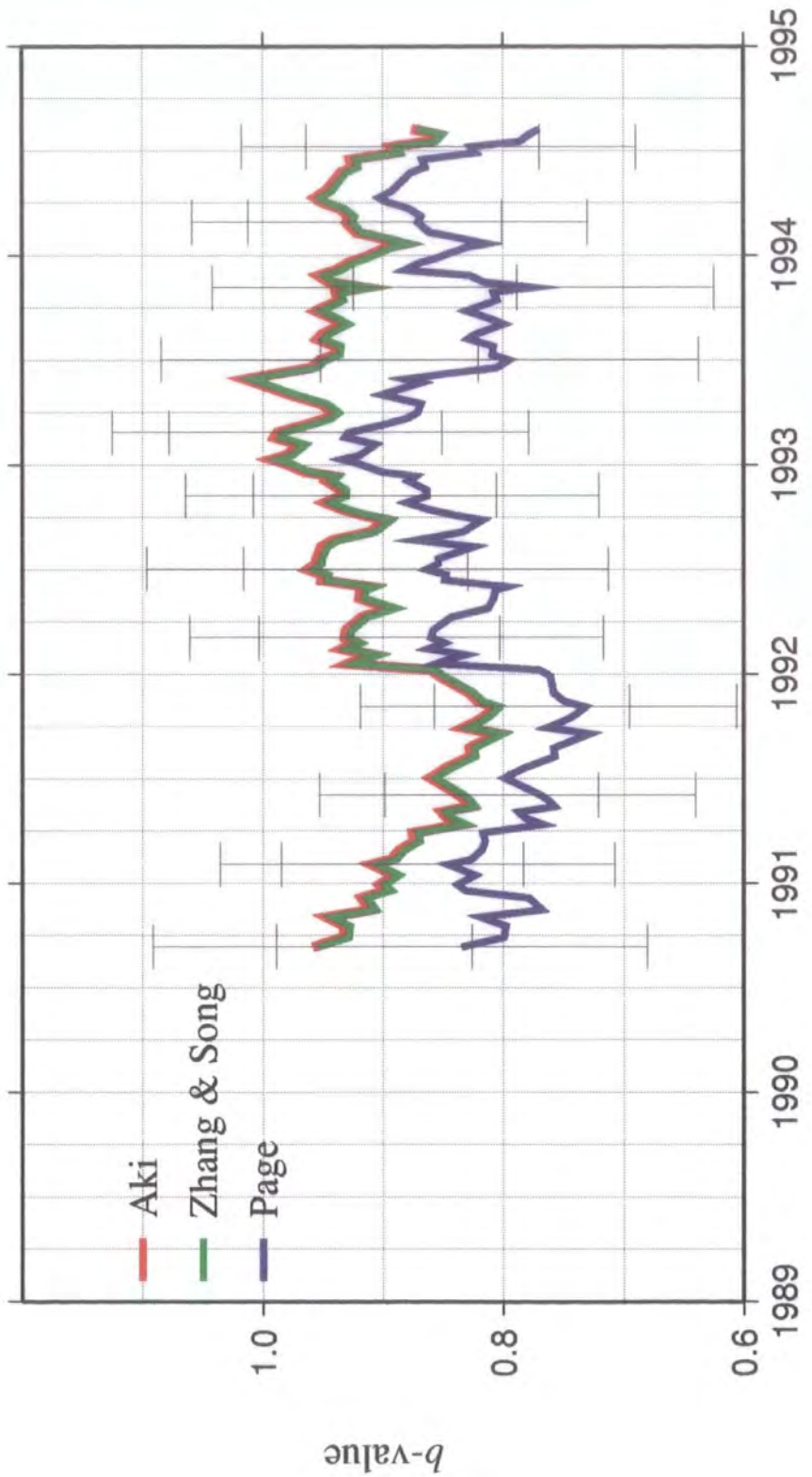

Figure 2.7 Comparison of *b*-values calculated using the Aki, Zhang & Song and Page equations. Data is from seismicity adjacent to well 09790231 in The Geysers geothermal area (Chapter 5). The Aki and Zhang & Song values are roughly equivalent and ~ 12% greater than those calculated using the Page equation. *b*-values are plotted at the middle of each window. Errors are the 95% confidence limits for the Aki and Page equations.

Henderson & Main (1992) studied data recorded between 1970 and 1990 from the Parkfield area, California, a 60 km segment of the San Andreas fault. The study included the major 1983 Coalinga event. The catalogue used was corrected for spurious changes in the detection rate *(Wyss et al., 1990)*, though recent work suggests that problems may still remain with the catalogue *(Wiemer, pers. comm., 1998)*. A high value of D_2 corresponded to strong clustering. Prior to the Coalinga event there were increases in b and D_2. During this event, b fell and D_2 increased (Figure 2.8), in agreement with the fracture model described in Section 2.2.1. There was an overall negative correlation between b and D_2 for the whole dataset (Figure 2.9).

Temporal changes in b-value and fractal dimension have also been examined close to the small town of João Câmara, in Rio Grande do Norte state, north-east Brazil. The area has been seismically monitored after the occurrence of a magnitude 3.0 earthquake on 5 August 1986 and several subsequent M = 5.0 events *(Takeya et al., 1989)*. A sequence of earthquakes between 1987 and 1988 showed that seismicity was occurring along a single major fault *(Henderson et al., 1994)*. This seismicity was divided into clusters, and the two largest were analysed (Figure 2.10). In this study, high values of D_2 correlated with strong clustering. One cluster exhibited high values of D_2 and decreases in b during large events, and an overall negative correlation between the two variables (Figure 2.11). This behaviour was similar to that observed at Parkfield.

The other cluster was characterised by a period of high activity at the start of the study period, with high values of D_2 and low b (Figure 2.12). For the rest of the study period there was little variation in b and D_2 and a weak positive correlation between the two variables. The explanation for this latter period in the second cluster was that a large earthquake had created a fracture zone, allowing the migration of fluids into the zone. This would increase the pore pressure and generate groups of small (high b) clustered (high D_2) events.

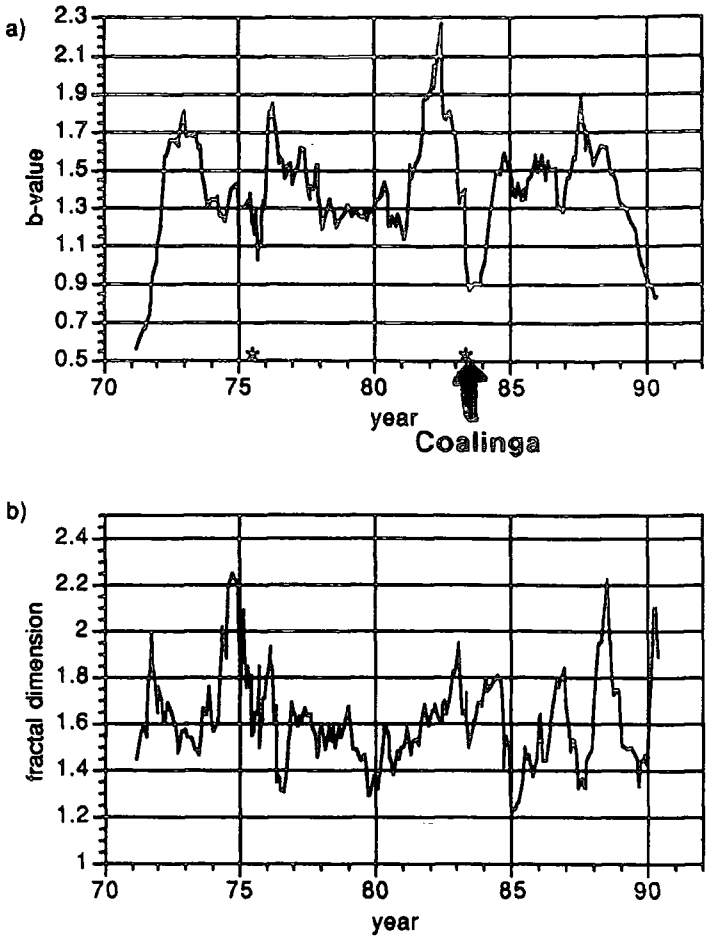

Figure 2.8 Graph showing (a) *b*-values and (b) fractal dimensions estimated for the Parkfield area, California. The time co-ordinate is the last earthquake in the 100-event analysis window. Large earthquakes are shown by stars *(from Henderson et al., 1992).*

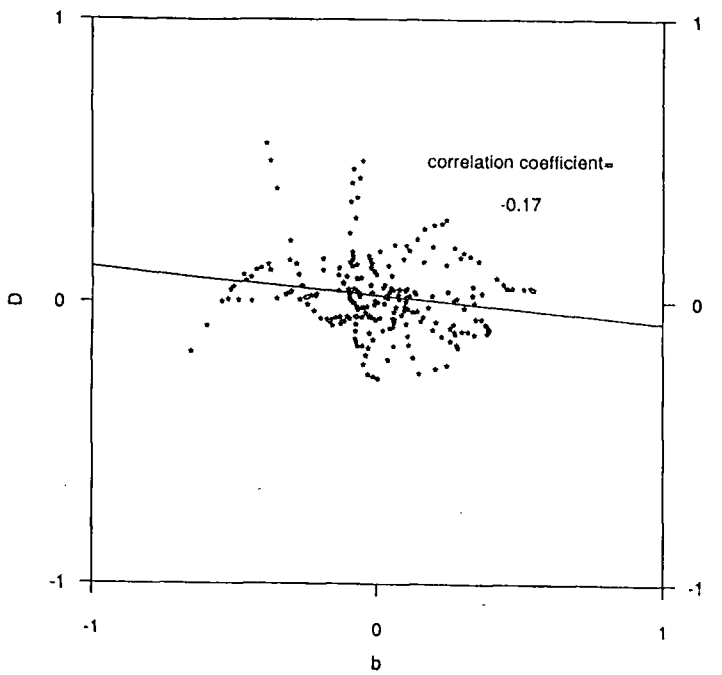

Figure 2.9 Graph showing the correlation of *b*-value and fractal dimension for the Parkfield area, California. Line is fitted using the least-squares method *(from Henderson et al., 1992).*

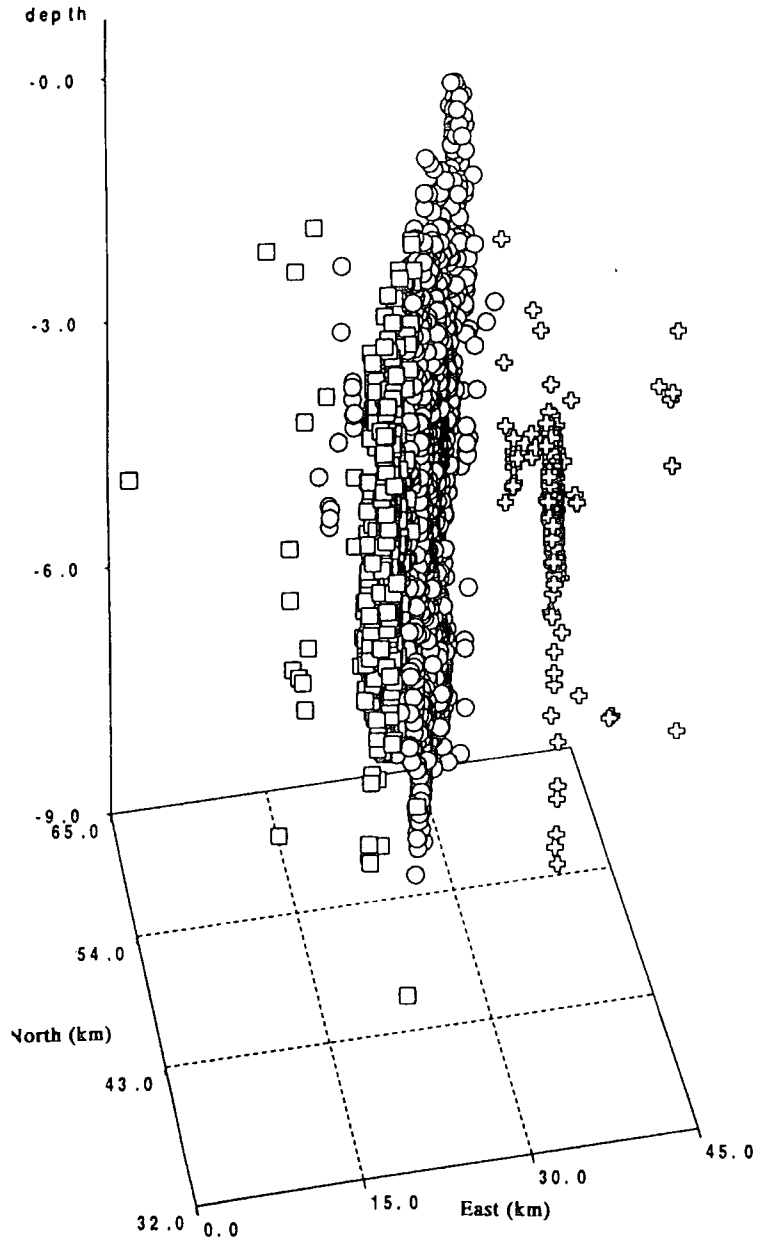

Figure 2.10 Perspective view of the seismicity, after cluster analysis, from João Câmara, north-eastern Brazil. Symbols represent data points belonging to cluster 1 (circles),cluster 2 (squares), and cluster 3 (crosses). Distances on axes are in kilometers measured from an arbitrary origin *(from Henderson et al., 1994)*.

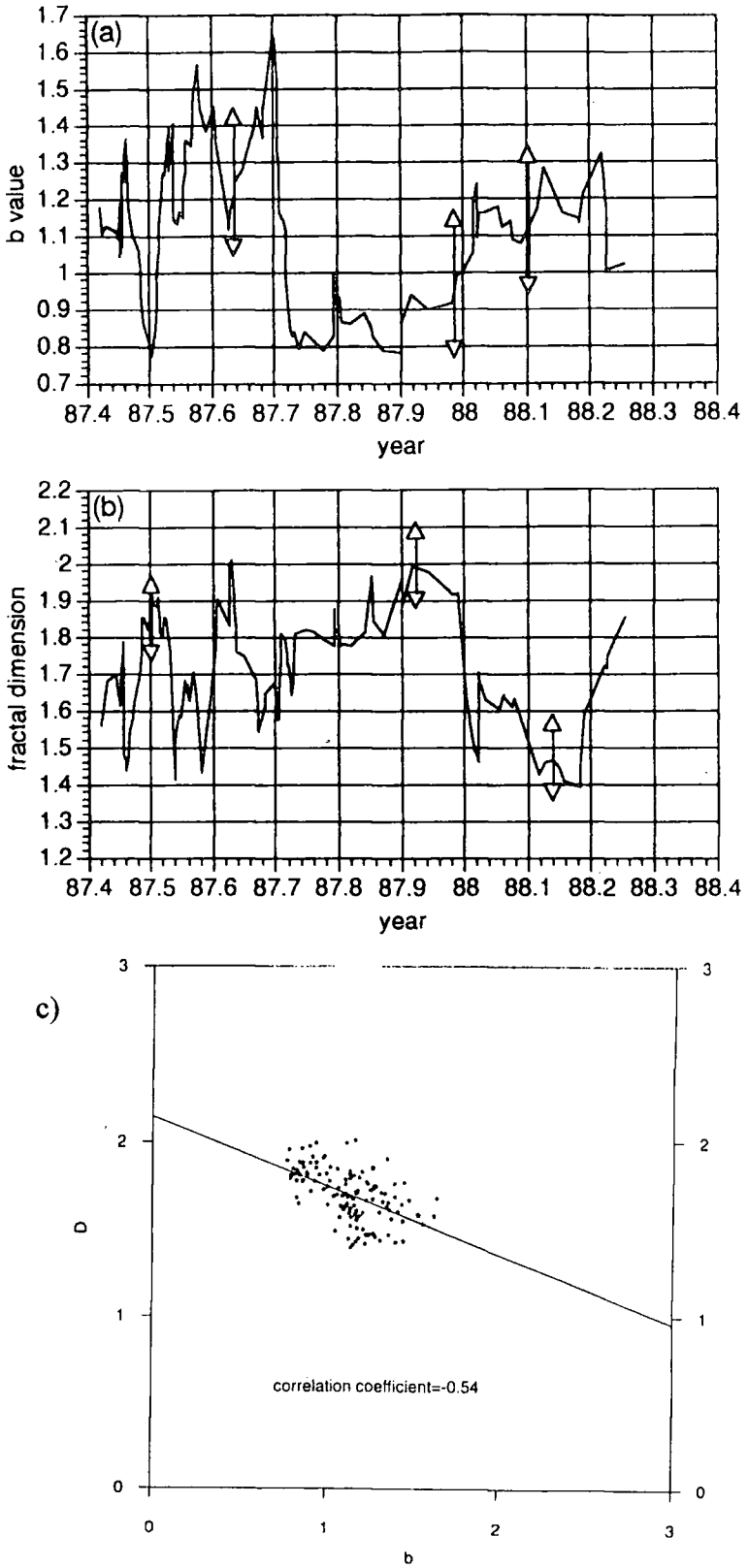

Figure 2.11 Diagrams showing, for cluster 1, the evolution of (a) the *b*-value and (b) the fractal dimension. Error estimates are 95% confidence limits for *b*, and ± 10% for *D*. These are indicated by the vertical double-ended arrows. (c) shows the negative correlation between *b* and *D* for cluster 1 *(from Henderson et al., 1994).*

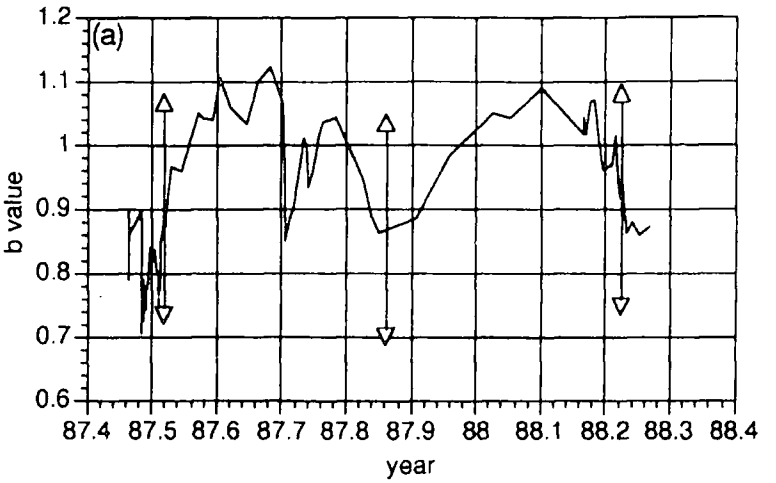

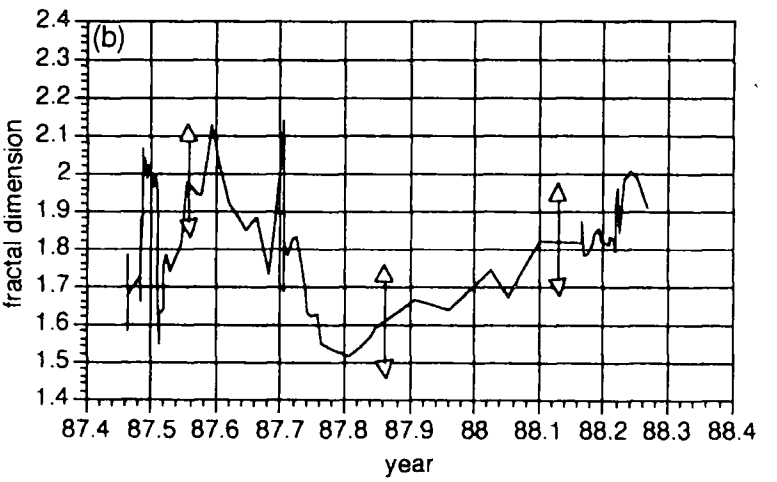

c)

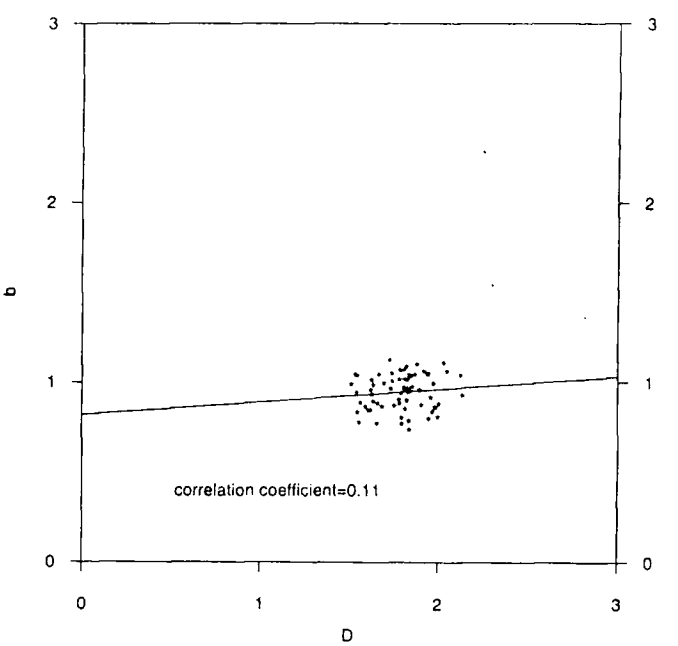

Figure 2.12 As figure 2.11, but for cluster 2 *(from Henderson et al., 1994).*

Comparisons have been made of *b* and *D* in laboratory microseismicity studies *(Hirata et al., 1987)*, rock bursts in mines *(Trifu et al., 1993)* and for gas induced seismicity *(Volant & Grasso, 1994)*. No correlation was found between *b* and *D* in these studies.

Table 2.4 Some examples of previous work on the correlation between *b*-value and spatial fractal dimension, *D*.

Reference	Seismicity	Methods of calculating *b* and D.	High *D* =	Phenonema observed
Hirata et al. (1987)	Laboratory microseismicity on Oshima granite.	*b*: Gutenberg-Richter equation, using amplitude magnitudes. *D*: correlation dimension	Weaker clustering	No correlation between *b* and *D*.
Hirata (1989)	Tectonic earthquakes from Japan 1926 – 1986 (epicentres).	*b*: Aki equation Magnitude *D* : box counting Spatial *D*: Correlation dimension	Weaker clustering	Long-term negative correlation between *b* and spatial *D*. Magnitude *D* spatial *D*. Possible errors due to location accuracy.
Henderson & Main (1992)	Tectonic earthquakes from Parkfield, California 1970 – 1990 (epicentres) .	*b*: Aki equation Spatial *D*: correlation dimension	Stronger clustering	Long term weak negative correlation between *b* and D_2. Following a large earthquake, *b* decreases and *D* increases.
Trifu et al. (1993)	Rock burst hypocentres in a mine in Ontario, Canada.	*b*: calculated from magnitude-frequency plots. Spatial *D*: correlation dimension	Stronger clustering	No correlation between *b* and *D*.
Henderson et al. (1994)	Seismicity in João Câmara, Brazil (hypocentres).	*b*: Aki equation Spatial *D*: correlation dimension	Stronger clustering	Tectonic cluster: long term strong negative correlation between *b* and *D*. Fluid induced cluster: initial period of high activity with a negative correlation (high *D*, low *b*), followed by a longer period with a positive correlation.
Volant & Grasso (1994)	Gas extraction induced seismicity in Lacq gas field, France (hypocentres).	*b*: Maximum Likelihood method (Aki?). Spatial *D*: correlation dimension.	Stronger clustering	No correlation.
Öncel et al. (1995)	Tectonic seismicity in the western part of the North Anatolian Fault Zone, Turkey (epicentres).	*b*: Aki equation Spatial *D* : correlation dimension	Weaker clustering	Long term negative correlation between *b* and *D*. Changes in *D* possibly due to changes in instrument deployment.

2.4 Summary

A fractal is a object that exhibits scale invariance (i.e. appears identical over a range of scales) and has a fractional (non-integer) topological dimension. Several aspects of seismicity have been shown to be fractal, such as fault geometry, inter-event times of clustered events and earthquake epicentres and hypocentres.

The correlation fractal dimension, D_2, is a measure of the spatial correlation between each point and all the others within a fractal structure. Since fractal systems in nature exhibit self-similarity over a finite range of scales, the correlation dimension must be calculated over a finite range, taking care to avoid edge effects known as 'saturation' (for large r) and 'depopulation' (for small r). Depending on the range of scales chosen, increased event clustering can correspond to a larger or smaller value of the correlation dimension.

The seismic b-value, defined by the Gutenberg-Richter power-law relationship between magnitude and event occurrence, is a measure of the proportion of larger to smaller events within a set of earthquakes. b typically takes a value in the range $0.8 < b < 1.2$. Types of temporal change in b that have been reported: (1) b-value decreases before a large earthquake, (2) b-value increases prior to, and then decreases sharply, immediately before a large earthquake, (3) b-value changes throughout an aftershock sequence and (4) b-value exhibits variation over large areas and long time intervals, not apparently related to large events. The first two types of behaviour can be explained using a one-dimensional fracture model.

Seismic b-value is related to the fractal dimension of magnitude, D_{mag}, by the relationship $D_{mag} = 2b$. This relationship applies for tensile fractures in the laboratory, though it is not known whether it holds for earthquakes. The fractal dimension of magnitudes is not related to the spatial fractal dimension. There is no obvious reason why b and spatial fractal dimension should be related though

several previous authors have noted some empirical correlation between these two quantities.

Chapter 3

The geology, seismicity and exploitation of The Geysers geothermal area

3.1 The tectonics and seismicity of northern California

3.1.1 Regional tectonics

Northern California is dominated by the San Andreas fault system and the Mendocino triple junction (MTJ), the junction between the Gorda, North American and Pacific plates (Figure 3.1). At about 30 Ma, the subduction of the Gorda plate under the North American plate commenced, forming the MTJ, a trench-transform-transform triple junction *(Furlong, 1993)*. The MTJ has since migrated north along the North American plate boundary from southern California, reaching the Geysers-Clear Lake area at ~ 3.3 Ma. The MTJ is presently at Cape Mendocino and is currently migrating north at a rate of 5 cm/year. Migration of the MTJ along the plate boundary terminated subduction and at about 30 Ma it initiated the broad right-lateral transform San Andreas fault system.

South of the MTJ are two main groups of faults (Figure 3.2). The first, dominated by the aseismic Garlock Fault, runs from the south-west to the north-east in the south of the State. This group of left-lateral faults were responsible for building the mountain range along the northern edge of the Mojave desert. The second group contains the San Andreas fault and its associated, distributed, right-lateral fault system. The San Andreas fault zone extends for approximately 1000 km parallel to the Californian coast.

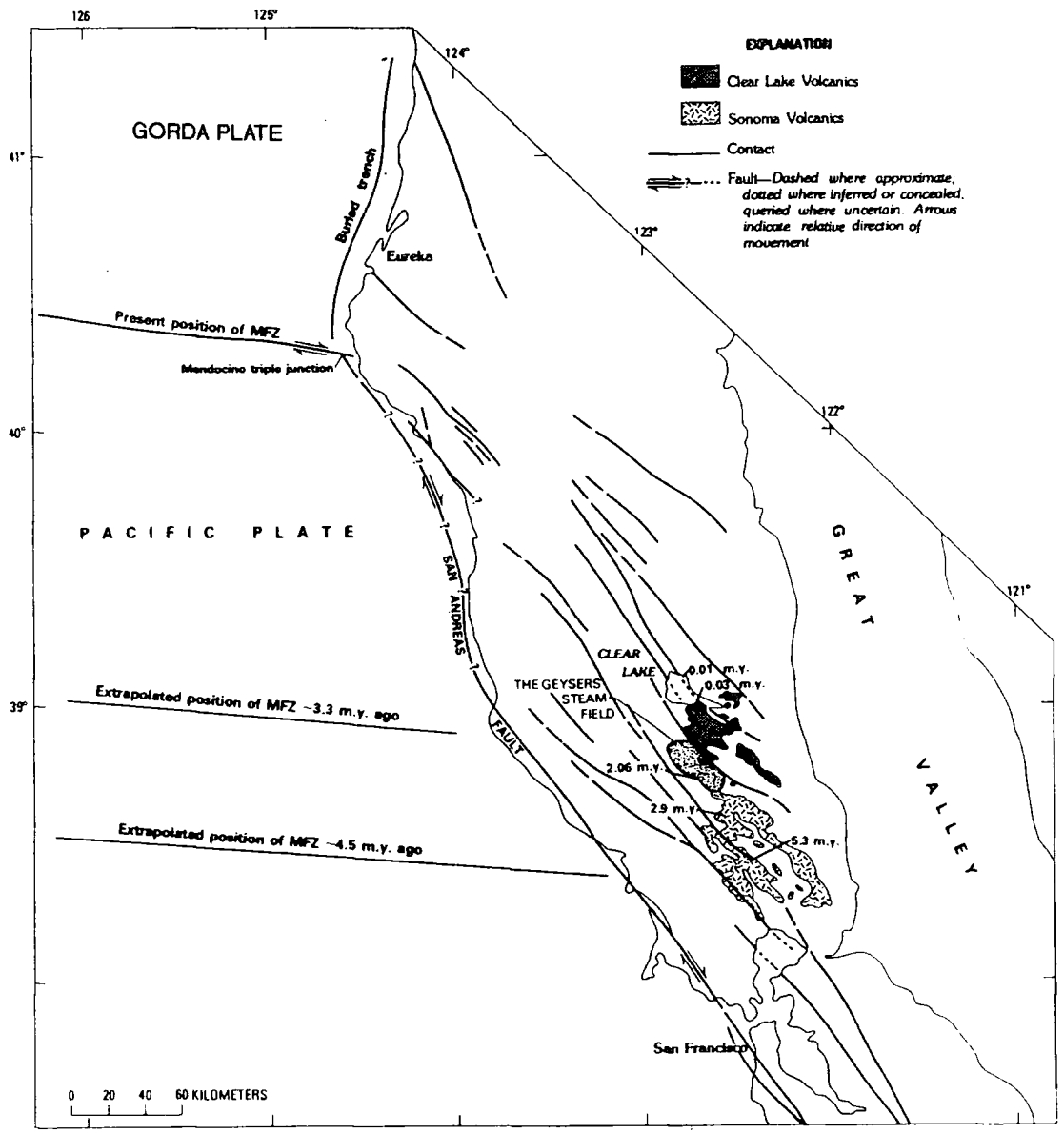

Figure 3.1 Diagram showing the northward progression of Tertiary and Quaternary volcanism with time, the San Andreas fault and the extrapolated positions of the Mendocino Triple Junction between 3 and 5 Ma *(from McLaughlin, 1981)*.

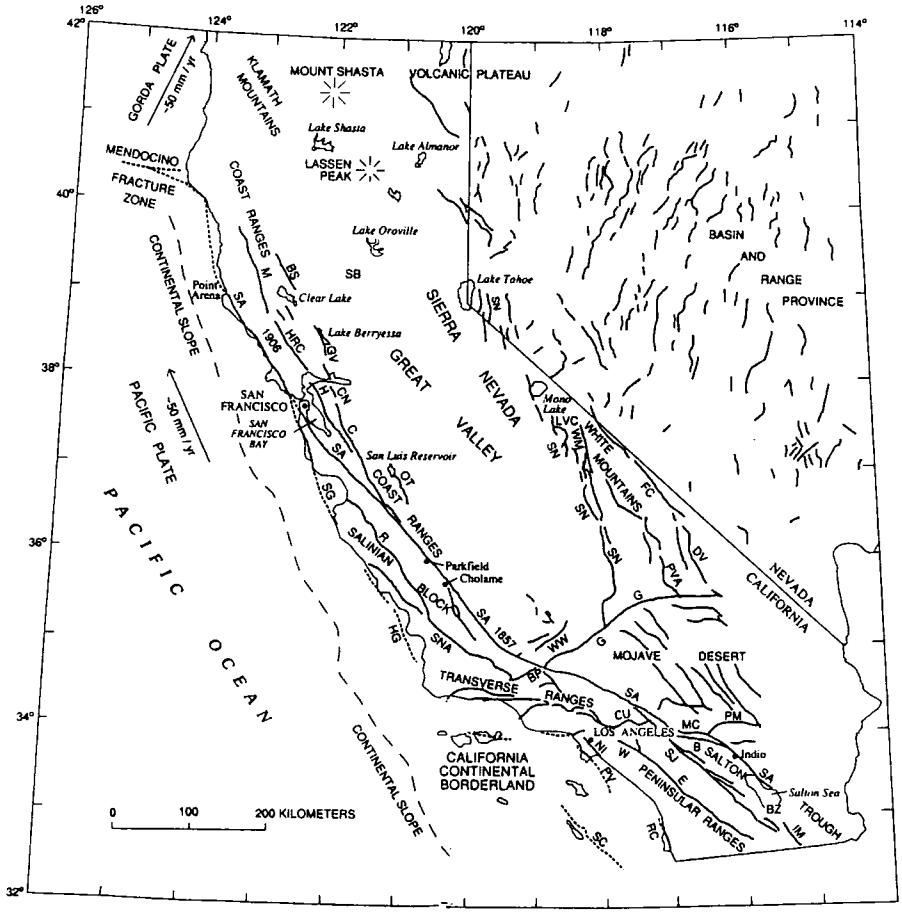

Figure 3.2 Map of California showing major fault zones. Faults are shown as black lines (dotted where concealed). Arrows and numbers indicate direction and amount of motion of the Pacific and Gorda plates with respect to the North American plate *(from Hill et al., 1990).*

Key: B = Banning; BP = Big Pine; BS = Bartlett Springs; BZ = Brawley seismic zone; C = Calaveras; CN = Concord; CU = Cucamonga; DV = Death Valley; E = Elsinore; FC = Furnace Creek; G = Garlock; GV = Green Valley; H = Hayward; HG = Hosgri; HRC = Healdsburg-Rodgers Creek; IM = Imperial; LVC = Long Valley Caldera; M = Maacama; M = Mission Creek; NI = Newport-Ingelwood; OT = Ortigalita; PM = Pinto Mountain; PV = Palos Verdes; PVA Panamint Valley; R = Rinconada; RC = Rose Canyon; SA = San Andreas; SC = San Clemente Island; SG = San Gregorio; SJ = San Janinto; SN = Sierra Nevada; SNA = Sur-Nacimiento; W = Whittier; WM = White Mountains; WW = White Wolf.

3.1.2 Regional seismicity

California is highly seismically active and has experienced earthquakes exceeding magnitude 8. In an attempt to monitor and understand earthquakes and fault systems in California, the United States Geological Survey (USGS) initiated a program of seismic station installation in 1969. By 1979, the North California Seismic Network (NCSN) had reached its current configuration of about 550 stations covering all of California. With this network all earthquakes with magnitudes greater than about 1.0 are located. Currently, NCSN includes more than a hundred, mostly 1 Hz, vertical component sensors, between San Francisco and the MTJ.

The distribution of seismic activity in northern California is controlled by the tectonic stress regime imposed by the plate boundary that follows the Californian coastline. North of the MTJ, there is oblique subduction of the Gorda plate below the North American plate *(Cockenham, 1984; Walter, 1986; Castillo & Ellsworth, 1993, Hill et al., 1990)*. The extent of the subducted plate is shown by earthquake hypocentres, which gradually deepen from the coast towards the east-south-east to a maximum depth of 87 km defining a 20°- 30° dipping Wadati-Benioff zone (Figure 3.3). These earthquakes are distinct from the shallow ones in the North American plate which are related to compression in the subduction environment. Epicentres cluster in the vicinity of the MTJ, and are more diffuse to the north, east and south-east *(Hill et al., 1990)*.

Most of the relative plate motion in the San Andreas fault system to the south of MTJ is accommodated in great ($M > 8$) earthquakes which occur roughly once per century. Between these large events, smaller-magnitude seismicity occurs, mostly along lesser faults within the San Andreas system. Work on the North Coast Ranges *(Hill et al., 1990; Castillo & Ellsworth, 1993)* show that earthquake epicentres define lineations east of the San Andreas fault running sub-parallel to it (Figure 3.4). These lineations indicate sub- parallel fault zones, 2-3 km wide, e.g. the Maacama and Bartlett Springs fault zones.

A north-west - south-east cross-section of the seismicity close to The Geysers (Figure 3.5a) shows a continuous level of activity with an undulating seismic base, varying from ~10 km in the north-west to ~ 12 km in the south-east. The seismic

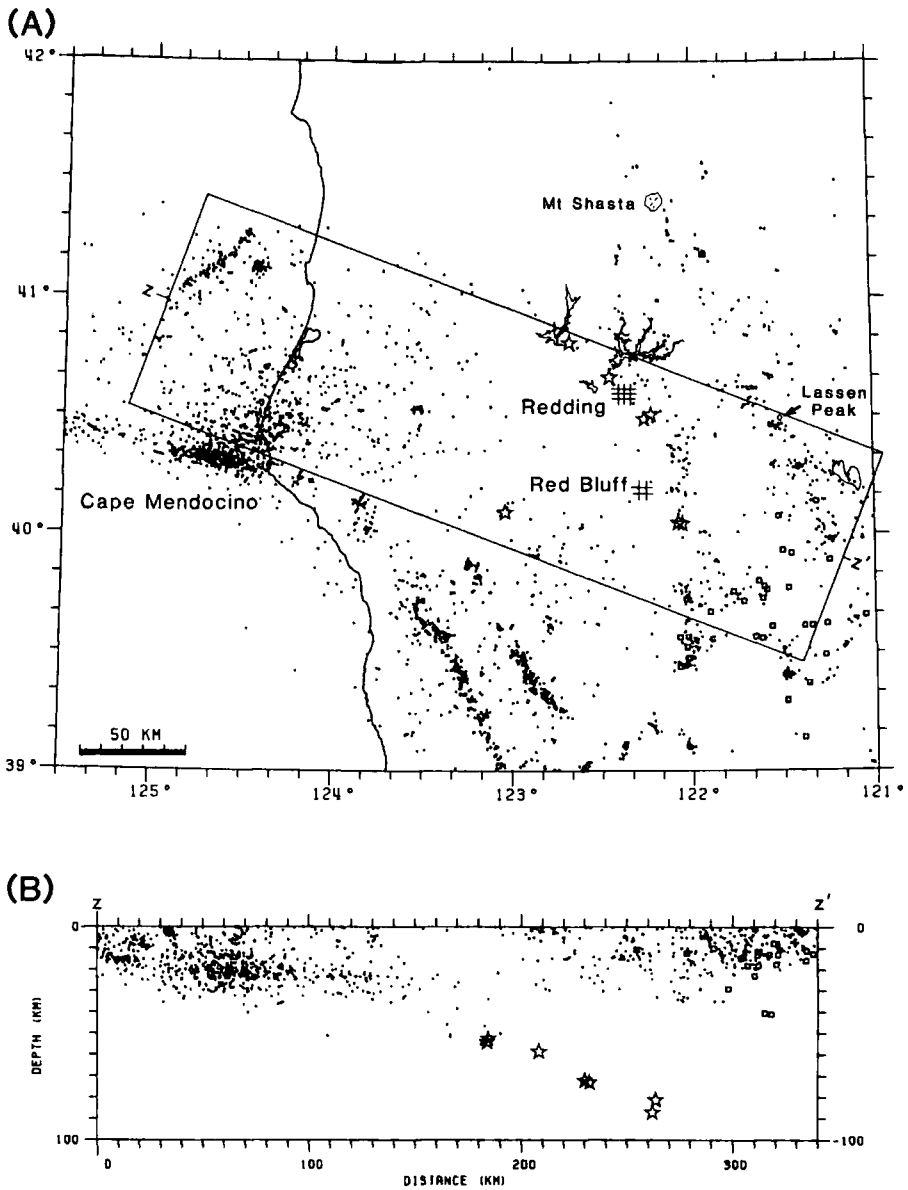

Figure 3.3 (A) Seismicity adjacent to the Mendocino Triple Junction. (B) Cross-section of seismicity from (A). The hypocentral pattern shows the subduction of the Gorda plate beneath the North American plate *(from Walter, 1986)*.

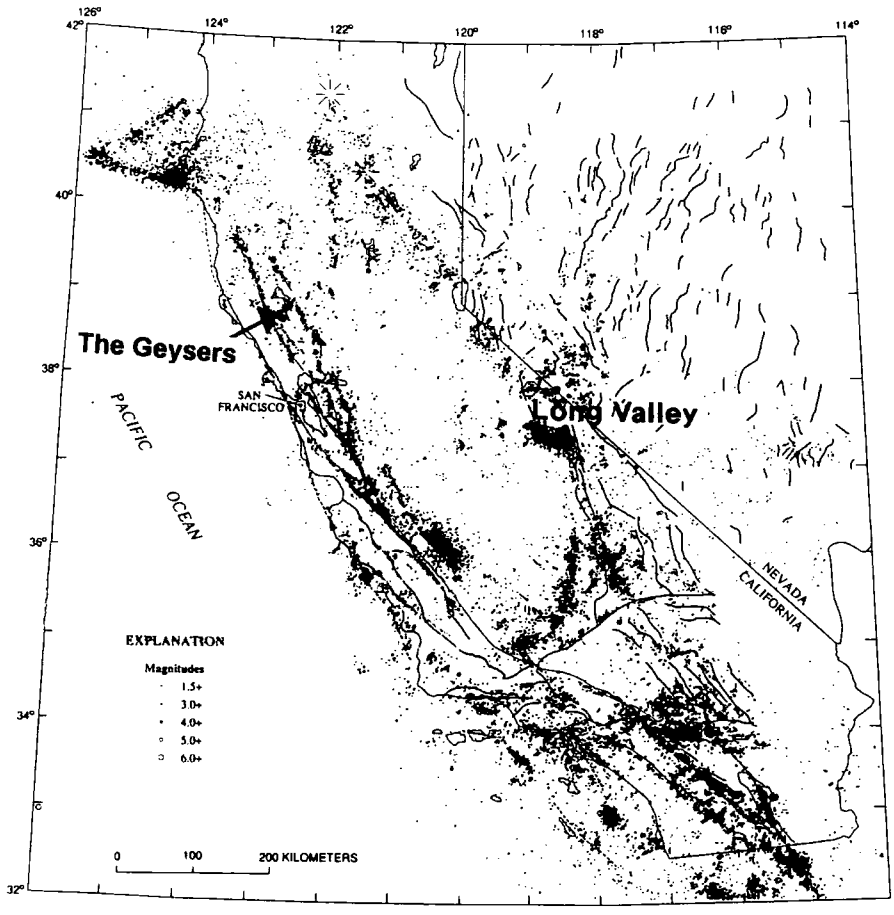

Figure 3.4 Locations of earthquakes with $M \geq 1.5$ in California and western Nevada 1980 - 86, and mapped Holocene faults *(from Hill et al., 1990)*.

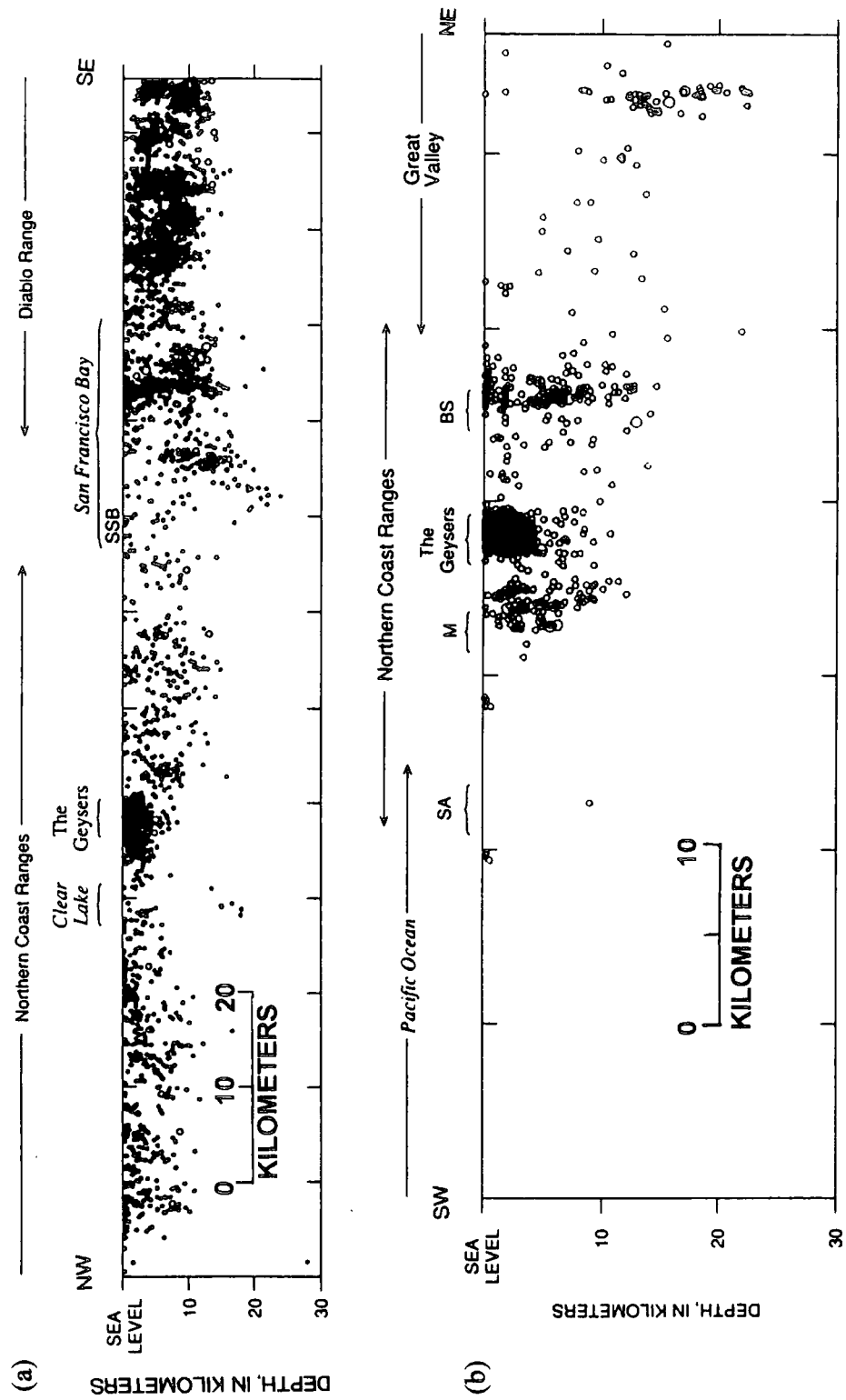

Figure 3.5 (a) North-west to south-east cross-section showing earthquakes with $M \geq 1.5$ adjacent to The Geysers 1980 - 86. (b) As (a) but for a south-west to north-east cross-section *(from Hill et al., 1990)*.

Key: M = Maacama, BS = Bartlett Springs, SA = San Andreas

base is shallowest at ~ 5 km beneath The Geysers. Complementary north-east - south-west cross-sections (Figure 3.5b) delineate the Maacama and Bartlett Springs fault zones, but fail to show the San Andreas fault. The regional hypocentral trend deepens to the east from ~ 10 km at the Maacama fault to ~ 25 km at Great Valley.

3.2 The Geysers geothermal area

3.2.1 Introduction

The Geysers geothermal area is the world's largest development of geothermal steam for electricity production. It is located about 120 km north of San Francisco in northern California, and is presently supplying ~ 6% of northern California's power (Figure 3.6). The developed area is elongated parallel to the trend of the regional fault zone and is roughly 600 km^2 in size.

The rocks of The Geysers are thought to form three geological units (Figure 3.7). Shallowest is an impermeable serpentinite caprock. This is underlain by fractured greywacke reservoir rock containing steam and hot water. Below is thought to be a magma source. These units are bounded to the south-west and north-east by major fault zones. The Geysers is one of the most seismically active areas in California. This seismicity is almost exclusively limited to the commercially developed area and is thus thought to be industrially induced.

3.2.2 Geology of The Geysers area

The Geysers area consists of two Jurassic-Cretaceous units assigned to the Franciscan and Great Valley sequences (Figure 3.8), partially capped by Quaternary volcanics. The Franciscan assemblage was intruded during the Pleistocene by a composite batholith known as the "felsite".

The Franciscan assemblage is a heterogeneous body of intensely-deformed and mildly- metamorphosed sandstone, chert and mafic igneous rocks ranging in age from late Jurassic in the east to Miocene in the west (Figure 3.8). The Franciscan assemblage is thought to have been deposited in a trench environment over an

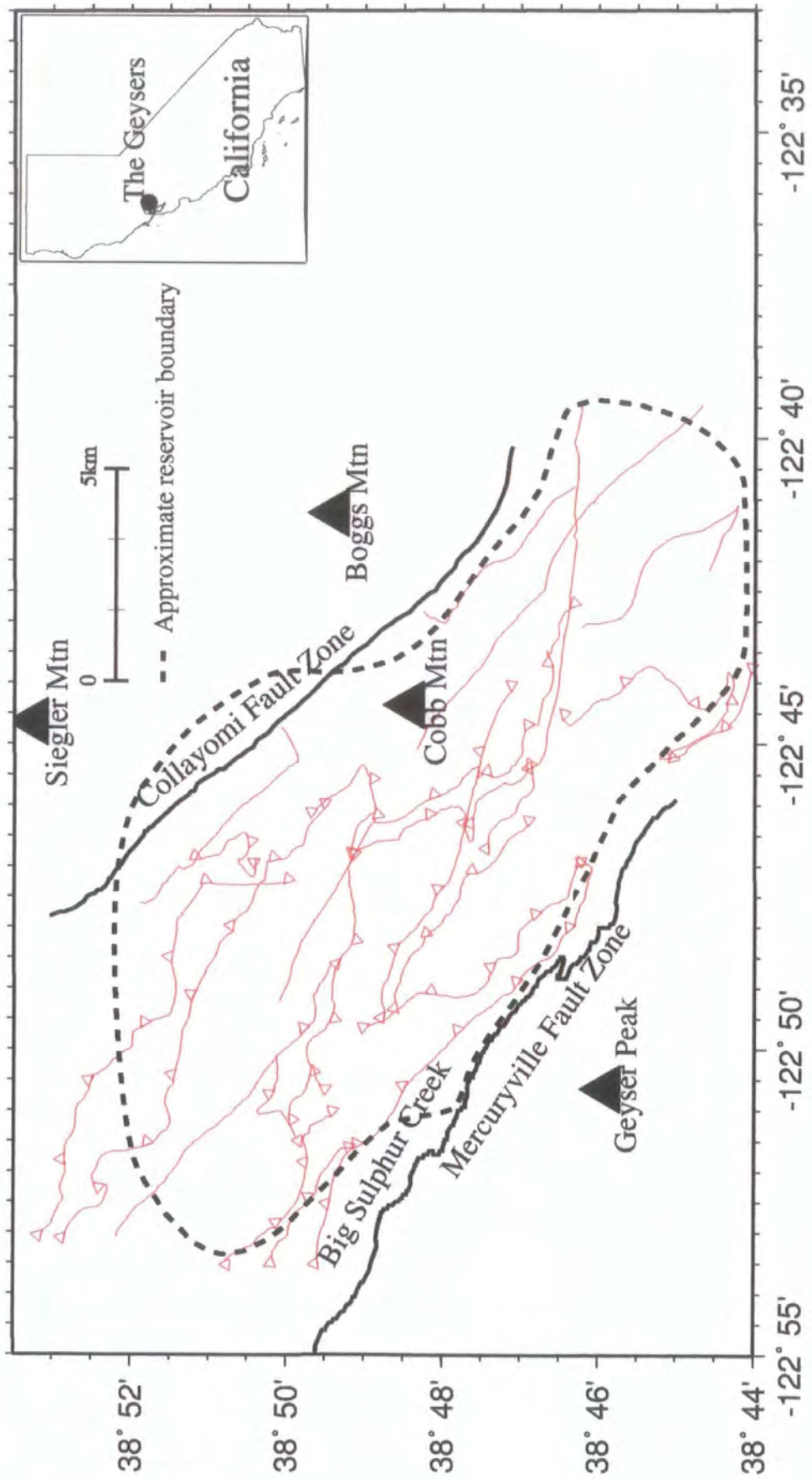

Figure 3.6 Map of The Geysers showing the approximate reservoir boundary (dashed line) and major fault zones (solid lines). Inset - Location of The Geysers in California.

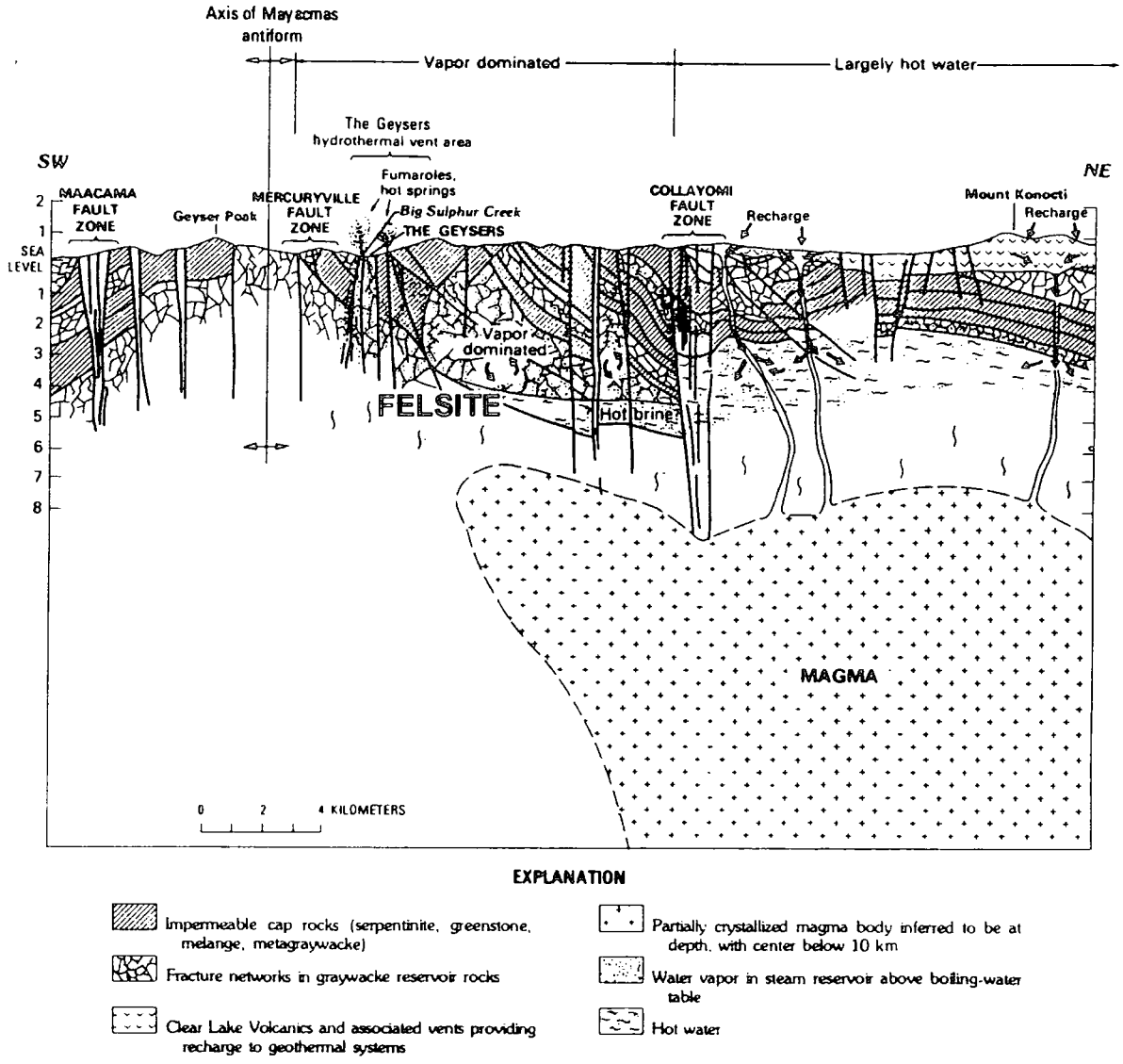

Figure 3.7 Structural model of The Geysers geothermal system *(from McLaughlin, 1981)*.

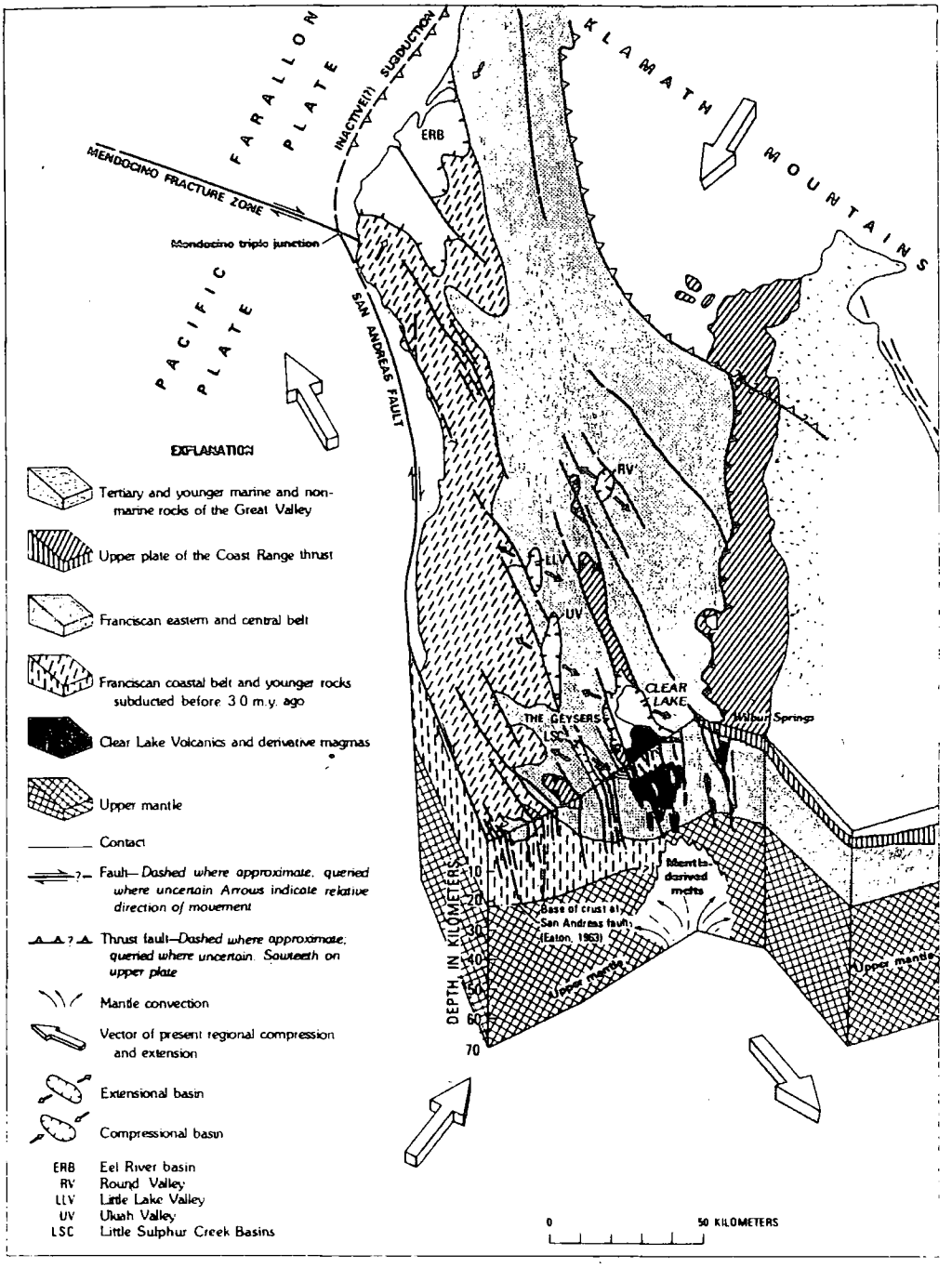

Figure 3.8 Major crustal features of northern California and their relation to the emplacement of magma beneath The Geysers *(from McLaughlin, 1981).*

easterly-dipping subduction zone. The mafic igneous rocks and chert are thought to have had an oceanic origin but the sandstone units may be derived from a terrestrial (i.e. island arc or continental) source.

The Great Valley sequence (Figure 3.8) is composed of moderately-deformed Late Jurassic to Late Cretaceous marine sedimentary rocks deposited in a series of submarine fans within an arc-trench gap or fore-arc basin environment. It overlies the fragmented late Jurassic Coast Range Ophiolite, thought to represent ancient oceanic crust. The Franciscan assemblage and Coast Range Ophiolite are separated by a great north-east dipping regional thrust called the Coast Range thrust *(Bailey et al., 1970)*.

The Clear Lake volcanic field was extruded onto Franciscan assemblage and Great Valley sequence rocks east and north-east of The Geysers during the Quaternary, and covers an area of approximately 400 km^2 (Figure 3.8). These rocks are the eruptive products of mantle heating, crystal fractionation and assimilation of rocks from the Franciscan assemblage, Great Valley sequence and the lower crust. Volcanic activity commenced at about 2 Ma and ceased approximately 10,000 years ago. The K/Ar age dates indicate that the volcanic rocks get progressive younger in a northerly direction within the volcanic field. The formation of this field may relate to the passage of the Mendocino triple junction through these areas or to the movement of the North American plate over a stationary hotspot *(McLaughlin, 1981; Hearn et al., 1981; Furlong et al., 1989)*.

The felsite batholith, intruded into the Franciscan Assemblage during the Pleistocene, is a composite body consisting of rhyolite porphyry, granite and granodiorite. Close temporal and geochemical similarities between the felsite and outcrops on Cobb Mountain suggest that they are equivalents *(Hulen & Nielson, 1993)*. Despite geochemical similarities, the felsite is too old to be an equivalent of the Clear Lake volcanics (1.3 vs. 1.07 Ma respectively). Although the felsite has a close spatial relationship with the steam reservoir, it is too old to be the heat source of the geothermal system *(Dalrymple, 1992)*. It has been suggested that The Geysers reservoir is 'mining' heat from a body at 7-10 km, consisting of either hot intrusions, magma or a mixture of the two, which is younger than 0.1 Ma *(Truesdale et al., 1993)*.

3.2.3 Tectonic history

The Geysers-Clear Lake region has a complex history of deformation representing a transition from a subduction to a shear regime during the Cretaceous to the Early Tertiary. During this period, the Franciscan and Great Valley Sequence units were deformed and probably underwent significant strike slip. These were then uplifted to their current position later during the Tertiary.

The major fault zones in The Geysers, such as the Maacama, Mercuryville and Collayomi fault zones, trend north-west to south-east parallel to the regional trend (Figure 3.8). These zones have complicated displacement histories on high-angle and north-east dipping surfaces reflecting periods of reverse, normal and right lateral strike-slip motion *(Hearn et al., 1981; McLaughlin, 1981)*. Numerous high-angle faults occur between these major fault zones. Their structural trend varies from north-east, north-north-west and north-west oriented normal faults and north-west trending strike-slip faults *(Hearn et al., 1976b)*.

3.2.4 The steam reservoir

3.2.4.1 Geology and tectonics

The steam reservoir is confined to the north-eastern limb of the Maacama antiform (Figure 3.7). It is bounded on the south-west by the Mercuryville fault zone and on the north-east by the Collayomi fault zone. These major fault zones trend north-west to south-east, parallel to the regional trend. The reservoir boundaries to the north-west and south-east are less well defined. It is thought that the reservoir extends no further 38^0 52' to the north-west and 38^0 44' to the south-east (Figure 3.6).

Much of the reservoir is within fractured Franciscan assemblage greywacke sandstone. The fracture network was enhanced and intensified by repeated episodes of felsite intrusion *(Truesdale et al., 1993)*. Consequently, most of the porosity in the reservoir is fracture related and its distribution related to the depth of greywacke and its distance above the felsite. The porosity of the reservoir greywacke is typically 2.3%, compared to 1.6% exhibited by non-reservoir

greywackes *(Gunderson, 1992)*. Upper portions of the felsite also form part of the reservoir, with a mean porosity of 2%. Fractures within the reservoir are mostly vapour-filled *(Truesdale & White, 1973)*. In the north-west Geysers, the thickness of the reservoir is only 600 - 1000 m, with the first steam entries at 760 - 1370 m below sea level. The thickness of the normal reservoir increases to ~1500 m and possibly to 5000 m in the central and south-east areas. Here the first steam entries are much shallower, at 610 - 760 m below sea level.

The reservoir can be divided into two distinct parts - a field-wide 'normal' reservoir with temperatures up to 235°C, and a vapour-dominated, high-temperature reservoir (HTR) at about 342°C which underlies the normal reservoir in the north-west of the steam field (Figure 3.9). The normal reservoir and the HTR are separated by a large temperature gradient over a 100 - 200 m depth interval *(Truesdale et al., 1993)*. The steam pressure is the same in both reservoirs, implying that they are connected. The difference in temperature in the two reservoirs is thought to be a result of different heat transfer methods *(Truesdale et al, 1993)*. According to this model, heat transfer in the HTR occurred by conductive heating from an igneous intrusion, whereas heat transfer in the normal reservoir occurred by a more efficient "heat pipe" process. By this process, heat is rapidly transmitted by a fluid that vaporises at one end of the pipe and condenses at the other, so resulting in counter-flows of vapour and liquid along the 'pipe'. Three boiling centres are thought to exist in the central and south-east Geysers *(Truesdale et al., 1993)*. Water flashes to steam there, then rises upwards and condenses at the top of the reservoir before returning to the boiling centre. This convection system is absent in north-west Geysers.

3.2.4.2 Formation and evolution

The Geysers has hosted at least three distinct hydrothermal systems. The first was an ancient regional metamorphic system at 170-200°C that formed in response to rapid burial in the presence of a normal geothermal gradient. The second was a hot water system at 170-350°C which was fuelled by a magmatic source. The third was a vapour-dominated reservoir evolved from the earlier hot water system operating at a temperature of 235 to 342°C *(Walters et al., 1992)*.

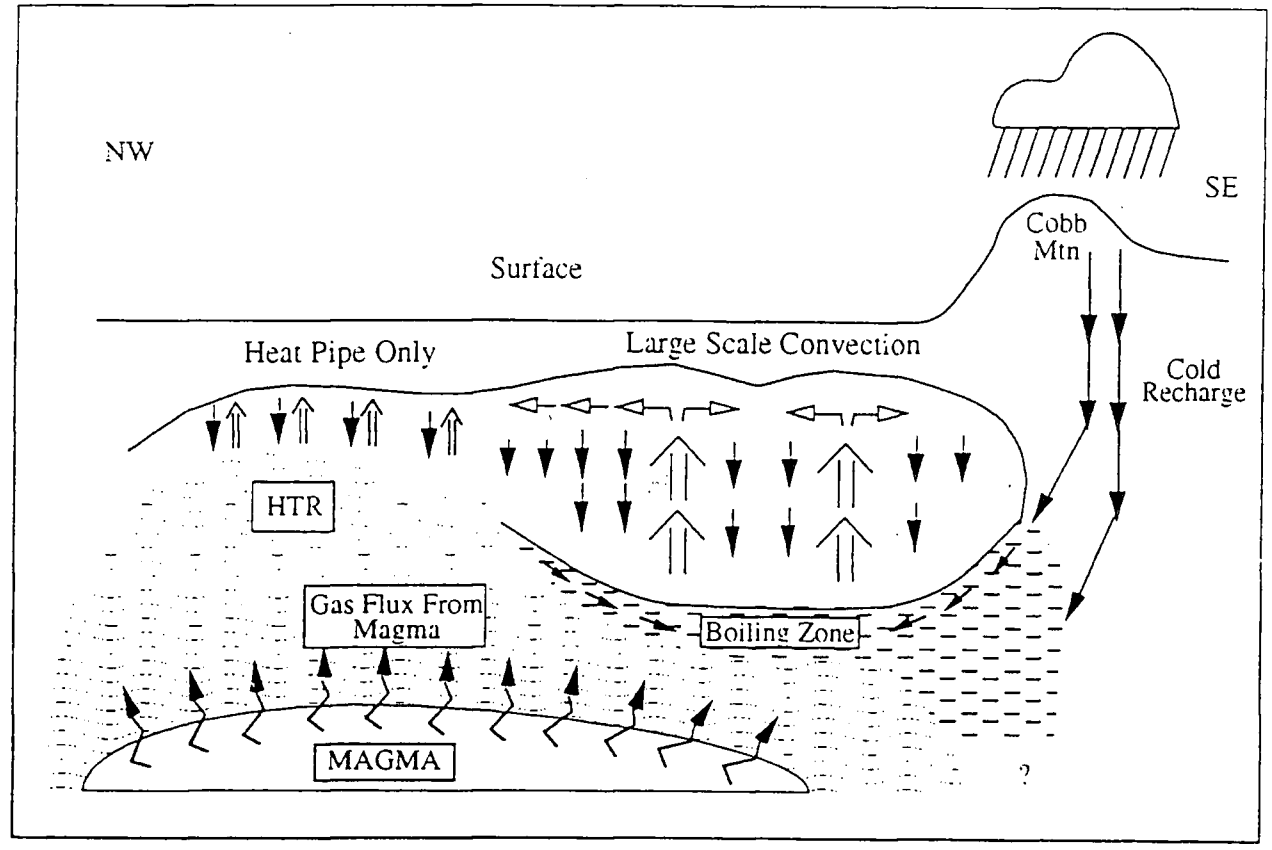

Figure 3.9 Schematic conceptual model of The Geysers geothermal system. HTR = high temperature reservoir. Open arrows represent the flow of steam. Closed arrows represent the flow of water (condensate and water) *(from Trusdale et al., 1993)*.

Several models have been suggested for the formation of the normal and HTR reservoirs. The shallow emplacement of the felsite body in the central and south-east Geysers produced a fracture system that reached the surface in those areas *(Walters et al., 1992)*. This caused venting and decompression of the liquid-dominated geothermal system and initiated boiling, so forming the normal reservoir. Then the reservoir lost most of its original gaseous content and was flushed by meteoric water. In the north-west Geysers the fracture system was deeper and did not reach the surface, leading to a slower evolution of the reservoir. Venting was first achieved along faults and fractures in the normal reservoir and then was artificially enhanced by commercial exploitation in central areas of the field. The poorer connection with the surface in north-west Geysers ensured that less condensable gas was vented and dilution by meteoric water was less important.

The HTR may also be a fossil of an earlier liquid-dominated system that is still cooling *(Walters et al., 1992)*. Alternatively, a possible absence of a liquid saturation zone in the HTR has meant that liquid from the normal reservoir has been evaporated on hot, dry rocks, heated by conduction from a deeper magmatic source *(Truesdale et al., 1993)*. Another model suggests that the HTR was formed by magma injection, which rapidly heated and boiled the existing reservoir liquid *(Kennedy & Truesdale, 1994)*.

3.2.4.3 Reservoir recharge

Compared to the amount of commercially injected fluid (Section 3.6), the amount of natural recharge is essentially nil. One source of recharge for the normal reservoir is thought to be meteoric water from Cobb Mountain (Figure 3.6). Although there is no known subsurface connection between the normal reservoir and Cobb Mountain, recharge might be possible through the reservoir greywacke or the felsite. Recharge may also be possible through volcanic vents *(Goff et al., 1977)*, or through reservoir outcrops in the south-east Geysers. The great thickness of low-permeability Franciscan rocks in the north-west of the geothermal field makes surface recharge of the HTR unlikely. HTR recharge is more probably from magmatic and metamorphic sources.

3.2.4.4 The reservoir caprock

In the south-east Geysers, Franciscan greenstone, chert and serpentinised periodite form the caprock to much of the reservoir (Figure 3.7). This caprock is typically 1100 m thick. In the north-west Geysers, the caprock is formed by outcropping greywacke. The greywacke caprock is identical to reservoir greywacke apart from a paucity of fractures. In the north-west Geysers the caprock is typically 3300 m thick (Figure 3.7).

3.3 Geophysical exploration in The Geysers

3.3.1 Gravity, magnetic and electrical surveys

Gravity surveys by the Californian Division of Mines and Geology (DMG) and the USGS revealed a ~ 30 mGal negative gravity anomaly centred near Mount Hannah, with a smaller negative anomaly near The Geysers *(Chapman, 1966; Isherwood, 1975)* (Figure 3.10a). Most studies have agreed that these enclosed gravity anomalies are probably produced (in part or totally) by a partially-molten magma chamber at depth. Early models of the gravity data featured a low-density, spherical magma chamber with a 6.5 km radius, centred at ~ 13.5 km below sea level *(Isherwood, 1981)*. More recent models feature a body of partial melt centred at depths of 15-20 km with a complex shallow crustal structure *(Blakely & Stanley, 1993)* (Figure 3.11). The negative anomaly in The Geysers is thought to be a combination of high-temperature, excess-porosity, low-density sources (e.g. magma) at depth, steam-filled rocks and hydrothermal alteration *(Denlinger & Kovach, 1981)*. Aeromagnetic data collected by the DMG and the USGS show two negative magnetic anomalies of -120 nT (10 km south of The Geysers) and -60 nT (10 km north-east of Mount Hannah), separated by a 60-nT positive anomaly centred on the Collayomi Fault zone (Figure 3.10b) *(Isherwood, 1976)*. The data were interpreted as Coast Range ultramafic rocks (e.g. serpentinite) and Clear Lake volcanics *(Isherwood, 1976)*. The magnetic and gravity anomalies do not coincide.

A geoelectrical cross-section compiled from direct-current, bipole-dipole, time-domain electromagnetic and magnetotelluric measurements shows that resistivities

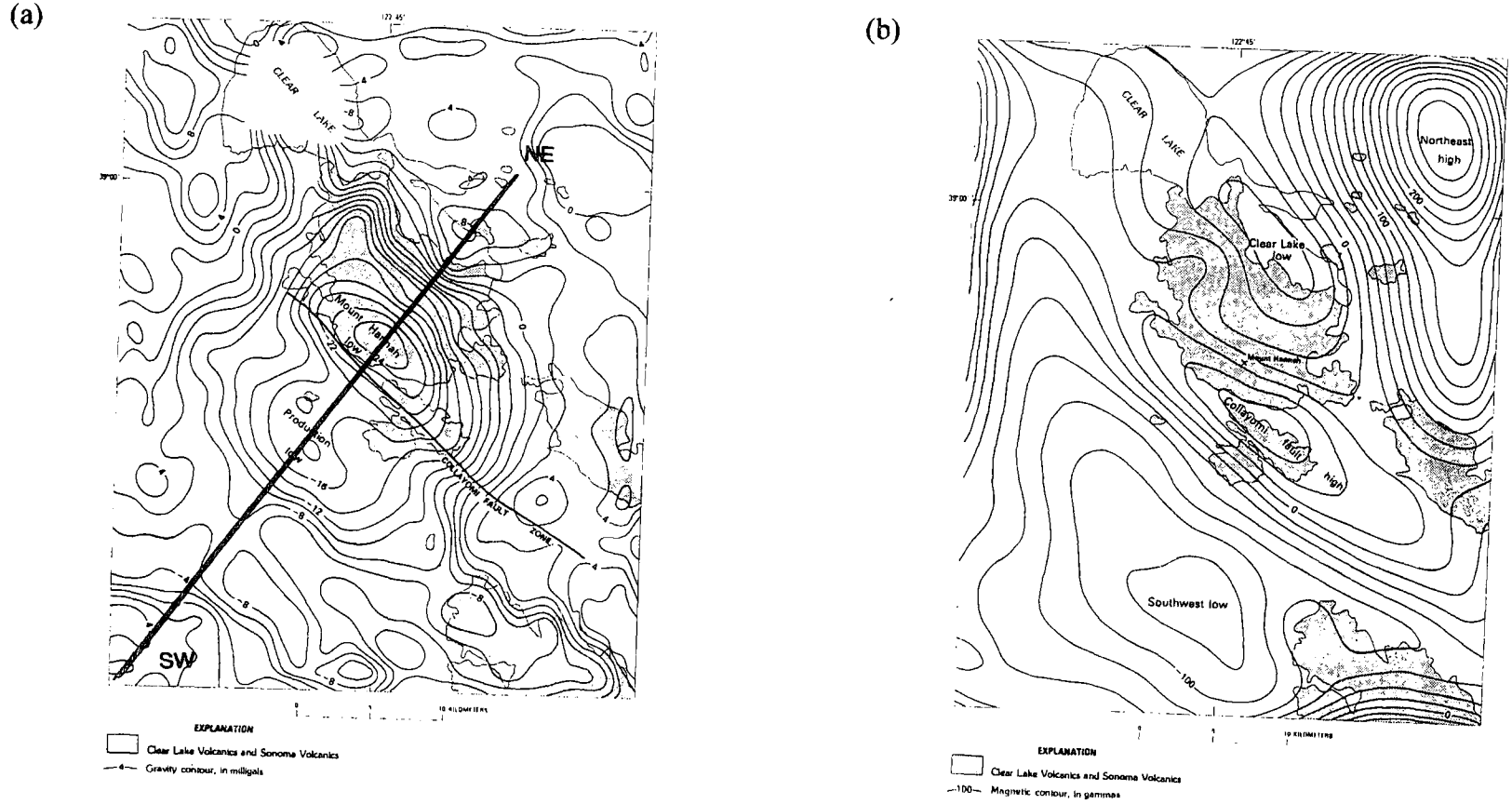

Figure 3.10 (a) Map of The Geysers, showing residual gravity based on reduction densities of 2.67 g/cm^3. Contour interval = 2 mGal, *(from Isherwood, 1975)*. (b) Map of The Geysers showing magnetic field continued upward to 3 km. Contour interval, 20 gamma *(from Isherwood, 1975)*. The south-west to north-east line refers to the cross-section used for gravity and magnetic field modelling (Figure 3.11).

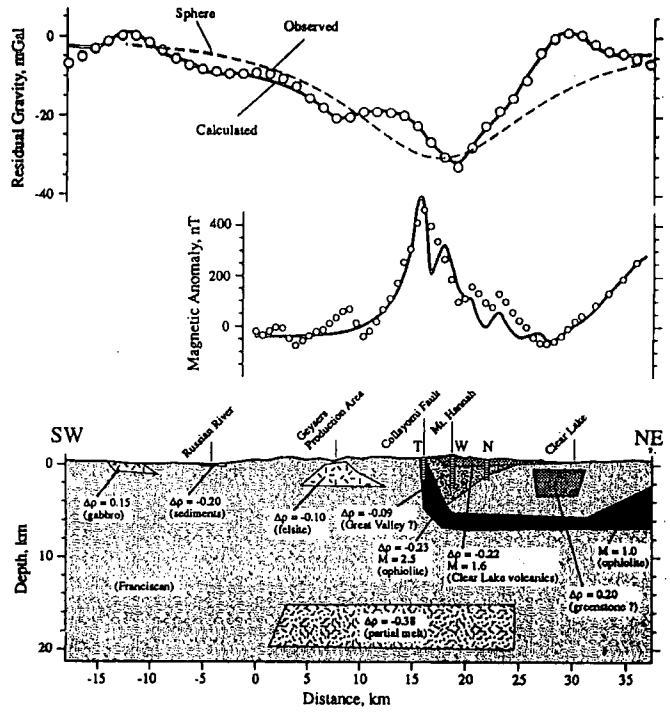

Figure 3.11 Gravity and magnetic field modelling for the cross-section shown on Figure 3.10. (a) Calculated and observed gravity fields, along with the gravity field calculated for a spherical body centred at 13.5 km depth. (b) Calculated and observed magnetic fields along the same profile. (c) Crustal model from gravity and magnetic modelling *(from Blakely & Stanley, 1993; Isherwood, 1975).*

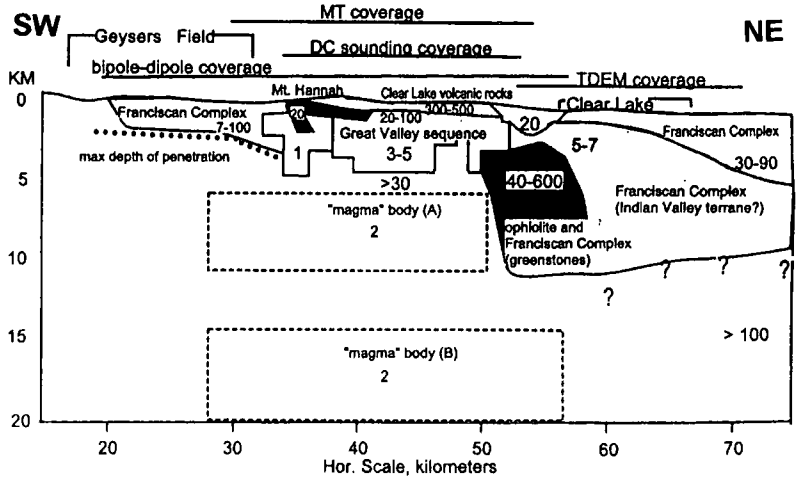

Figure 3.12 Geoelectrical modelling for the cross-section shown on Figure 3.10. The model was compiled from direct current soundings, bipole-dipole mapping data, time domain electromagnetic soundings and a two-dimensional magnetotelluric (MT) model. Numbers indicate resistivities (in ohm-m) of the units in the model. (A) and (B) represent alternative 2 ohm-m magma bodies added to test the sensitivity of the data *(from Blakely & Stanley, 1993).*

in The Geysers range widely from 7 to 100 Ωm *(Stanley & Blakely, 1995)* (Figure 3.12). The lower resistivity units have been interpreted as altered greywackes in the reservoir and the higher resistivity ones as unfractured graywackes, greenstones and mafic rocks. The magma body beneath The Geysers is modelled as having a resistivity between 0.3 - 3 Ωm, depending on the amount of melt and the water content *(Wannamaker, 1986)*.

3.3.2 Seismic surveys

Active seismic techniques have had limited success in The Geysers due to the rugged terrain and hetereogeneous surface geology. Two VSP surveys have been conducted to detect the extent of fracturing within the reservoir using P- and S-wave vibrators. *Majer et al. (1988)* detected anomalous shear wave behaviour above the reservoir and an 11% anisotropy in S-wave velocity which was attributed to fracture content. The second survey was undertaken in the felsite body in the south-west Geysers *(Majer et al., 1988)*, and similar V_p/V_s ratios to the first survey were observed. The only documented reflection survey *(Denlinger & Kovach, 1981)* met with limited success due to energy scatter. Reflectors at 2.5 to 3 km were detected and a lower boundary at < 4 km was interpreted as a tectonic boundary within the Franciscan Assemblage. Refraction profiles have revealed anomalously high P- and S-wave velocities and low attenuation at shallow depths (< 3 km) in the production area when compared to regional values *(Majer & McEvilly, 1979)*.

Teleseismic P-waves have been used to image the lithosphere beneath The Geysers *(Iyer et al., 1981; Oppenheimer & Herkenhoff, 1981; Benz et al., 1992)*. These studies have suggested that there are low-velocity bodies > 4 km beneath The Geysers consistent with silicic partial melt. P-wave arrival-time studies showed delays of one second under the steam field, and 0.9 seconds under Seigler Mountain and Mount Hannah (Figure 3.6; Figure 3.10). This represents a regional velocity decrease of 15% and up to 25% under Mount Hannah and in the production area. From these studies it was estimated that the crust under The Geysers is about 24 km thick.

3.3.3 Local earthquake tomography

Several models of the velocity structure in The Geysers have been presented by previous workers (Table 3.1).

Table 3.1 Statistics for local earthquake tomography of The Geysers geothermal area *(After Ross, 1996)*. NA = information not available.

Reference	Modelled parameter		Number of seismic stations		Number of earth-quakes	Number of seismic phase arrivals		Dimensions of modelled volume
	V_p	V_p/v_s	3 comp	Vertical	3 comp	P-wave	S-wave	(km)
Eberhart-Phillips (1986)	Yes	No	14	64	170	NA	NA	18x15x5
O'Connell (1986)	Yes	Yes	9	8	38	469	294	NA
Zucca et al. (1994)	Yes	No	NA	NA	NA	NA	NA	8.5x5.5x5
Romero et al. (1994)	Yes	Yes	16	0	480	9700	2700	5x5x4
Julian et al. (1996)	Yes	Yes	20	16	185	4032	944	20x20x7
Foulger et al. (1997)	Yes	Yes	7	15	146	2522	656	20x20x7

A study by *Julian et al. (1996)* used data from the UNT (Section 4.1.1) and IRIS (Section 3.4.3) networks from April 1991. A strong -9% V_p/V_s (P-wave velocity/S-wave velocity) anomaly was observed to coincide with the most exploited part of the geothermal field in the depth range 0-3 km . This anomaly was not observed in the V_p model. This three-dimensional V_p and V_s model was used to locate the earthquakes analysed in this thesis (Section 4.3.4.2). A similar study using data from a later time period, 1994 *(Foulger et al., 1997)* showed that the V_p/V_s anomaly had increased by ~4% since 1991, consistent with the expected effects of continued pressure reduction and the conversion of pore water to steam by steam extraction.

3.3.4 Geodetic studies

Surface deformation monitoring since the 1970s shows that The Geysers area has been subsiding *(Lofgren, 1981)*. The mean subsidence rate, relative to a point 20 km from the reservoir, was ~ 4.8 cm/year between 1973 and 1977, and was

centred on the most exploited areas of the reservoir. A causal relationship between reservoir pressure decline and surface subsidence has been suggested *(Lofgren, 1981)*. Another model *(Denlinger & Kovach, 1981)* suggested that the subsidence was due to cooling caused by phase changes and subsequent steam extraction within the reservoir. Three GPS studies conducted between 1994 and 1996 showed a mean subsidence rate of 4.7 cm/year *(Mossop & Segall, 1997)*. Subsequent modelling using these data showed that the reservoir pressure decline was a more likely cause for the motion than cooling.

3.4 History of seismic monitoring in The Geysers

3.4.1 Early seismic monitoring

Before 1975, seismic monitoring in The Geysers was restricted to temporary networks deployed in short term experiments. The details of these networks and dates are given in Table 3.2. These studies established the need for continuous monitoring.

Table 3.2 Summary of seismometer networks operated at The Geysers

Network / Reference	Dates	# of stations	Array diameter (Km)	# of events
Lange & Westphal (1969)	10-19 October 1968 (120 hours)	6 vertical component	Not available	19
Hamilton & Muffler (1972)	16 March - 7 April 1971	7 remote, 1 base station	Not available	53
NCSN	From 1975 in The Geysers	8 stations within The Geysers; 40 within detection threshold	15 (in The Geysers)	120 $M_d \geq 1.2$ events / month
O'Connell (1986)	26 days in 1982	Not available	6	Not available
UNT Partnership	From 1985	22 (in 1995)	15	40-50 events / day
GEO (NW Geysers)	1988 - 1994	16	4	5000
IRIS	April - May 1991	15	15	3096
LBL (SE Geysers)	1992 - 1995	13	7	~ 75 events / month

3.4.2 The NCSN network

In 1975, the USGS set up permanent seismometer stations in The Geysers, to monitor continuously the local earthquake activity *(Marks et al., 1978)*. Eight seismic stations are located within a 25 km radius of The Geysers and more than 40 regularly detect earthquakes within the production area *(Eberhart-Phillips & Oppenheimer, 1984)* (Figure 3.13) (Table 3.2). Analogue signals from stations in The Geysers are transmitted to the USGS Western Region Headquarters at Menlo Park, California. There the signals are digitised at 100 samples per second, the P-wave arrivals picked automatically and the hypocentres and coda-length magnitudes calculated. NCSN earthquakes are catalogued at the Northern California Earthquake Data Centre (NCEDC) at the University of California, Berkeley. The NCEDC database is updated daily with the NCSN earthquake data recorded in the previous 24 hours. The NCSN network had a magnitude detection threshold of M_d = 1.2 in 1975. Subsequent improvements in the network since 1981 have reduced the threshold to M_d = 0.5. Typically ten events in The Geysers are recorded every day, but there are many more small-magnitude events in the geothermal area than can be located by NCSN. The installation, beginning in 1985, of a dense, local network operated by the UNOCAL - NEC - Thermal industrial partnership, addressed this need (Section 4.1.1).

3.4.3 Other networks

Several small, dense, permanent networks have been operated intermittently in the north-west and south-east Geysers (Table 3.2). In 1988, Geo East Mesa Limited Partnership (GEO) installed a network in the north-west Geysers *(Romero et al., 1995)*. This 4 km diameter array contained 16 high-frequency borehole sensors. The Lawrence Berkeley Laboratory (LBL) installed a network in the south-east Geysers in 1992. It contained 13 high-frequency (4.5 Hz) digital surface seismometers in a 7 km array.

The IRIS network was operated by the USGS / University of Durham for one month in 1991 (Figure 3.13). It recorded local earthquakes within The Geysers, which were used for local earthquake tomography (Section 3.3.3) and to study earthquake moment tensors *(Julian et al., 1996)*. The network consisted of fifteen

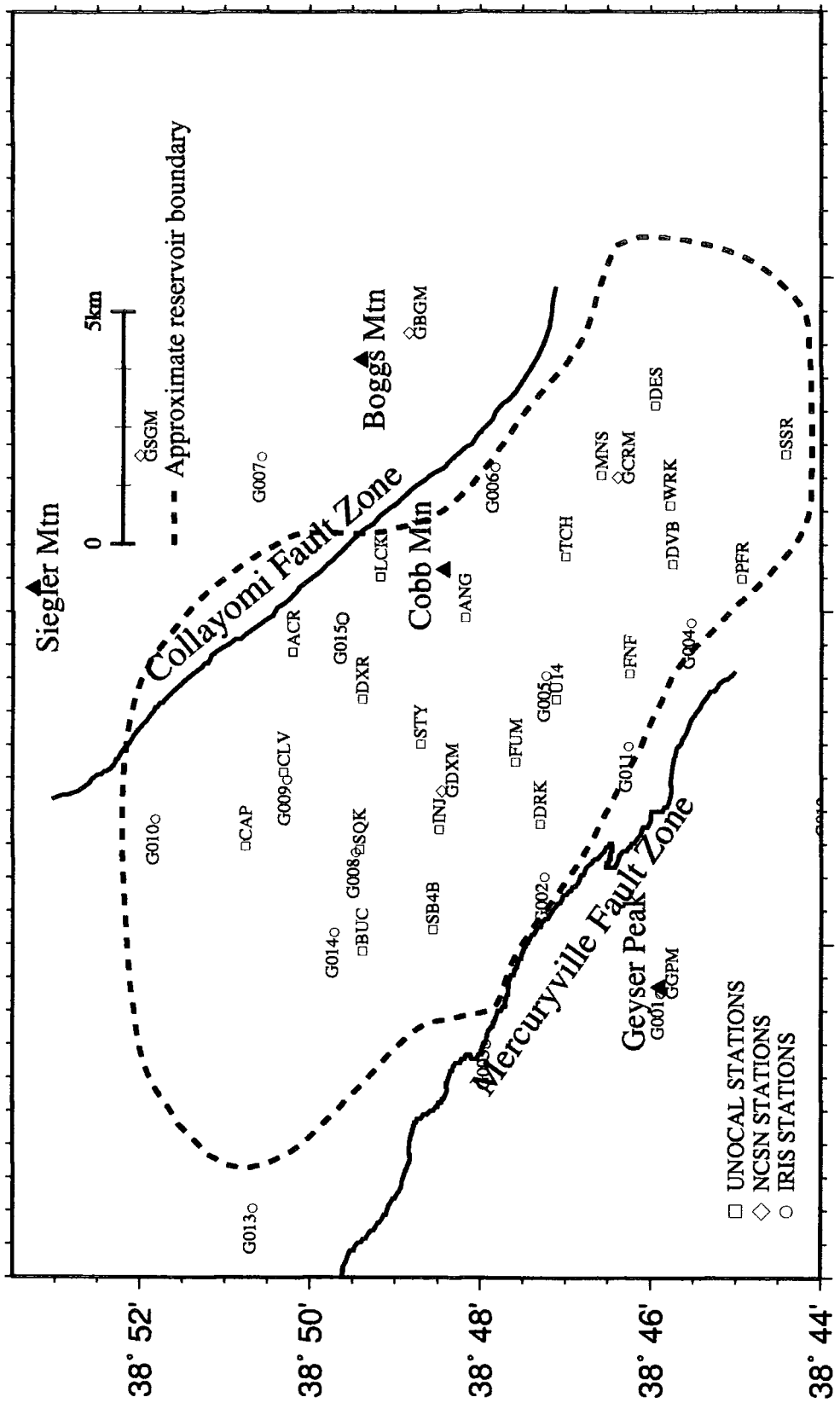

Figure 3.13 Map of The Geysers showing locations of NCSN, IRIS and UNOCAL recording stations. Correlation plots between coda length and NCSN magnitude for the stations marked in red are shown in Figure 4.7.

three-component sensors in a 15 km array. All stations used 2 Hz sensors apart from one which used an existing 4.5 Hz borehole sensor of the GEO network. The seismic data were recorded at 100 samples per second. During the 1-month monitoring period, 3906 earthquakes were recorded. Of these, 500 were located and 296 were used to derive the tomographic model.

3.5 Seismicity within The Geysers

According to the NCSN catalogue, The Geysers is about 45 times as active as the rest of northern California (Section 3.1.2) *(Ludwin et al., 1982)*. Figure 3.14 is a plot of NCSN epicentres and cross-sections for periods of one year between 1972 and 1995. The data presented is complete from 1975, when the NCSN threshold magnitude was M_d = 1.2. Prior to the installation of NCSN seismometers in The Geysers in 1975, insufficient sensor coverage prevented the detection of the majority of the earthquakes.

Between 1975 and 1995 there was a dramatic increase in the number and spatial distribution of earthquakes within the geothermal area. In 1975, seismic activity was limited to the central part of The Geysers. Since then, the seismicity has occupied two distinct volumes; one from 0 - 2.5 km below sea level and the other from 4 - 5 km. The rocks in the aseismic zone between 2.5 and 4 km below sea level are thought to be less fractured than the rest of the reservoir, and are consequently not as seismogenic *(Ross, 1996)*. The dearth of deeper earthquake activity is thought to be due to elevated temperatures at shallow depths within The Geysers-Clear Lake region, perhaps due to a molten or partially molten magmatic body *(Bufe et al., 1981)*.

During the late 1970s and early 1980s, the seismogenic volumes spread to the north-west and south-east. Distinct epicentral clustering first becomes obvious in about 1979. Between 1981 and 1989, the period corresponding to rapid development of the production area (Section 3.6), the number of events contained in these clusters increased (Figure 3.14). An aseismic 'deadzone' in the central Geysers is a constant feature from about 1984 onwards. Seismicity in previously aseismic areas (e.g. the north-west and south-east Geysers) was scattered and shallow. From 1989 and during the early 1990s a more diffuse seismicity pattern developed (Figure 3.14b(f) → (h)). The shallower seismogenic volume became

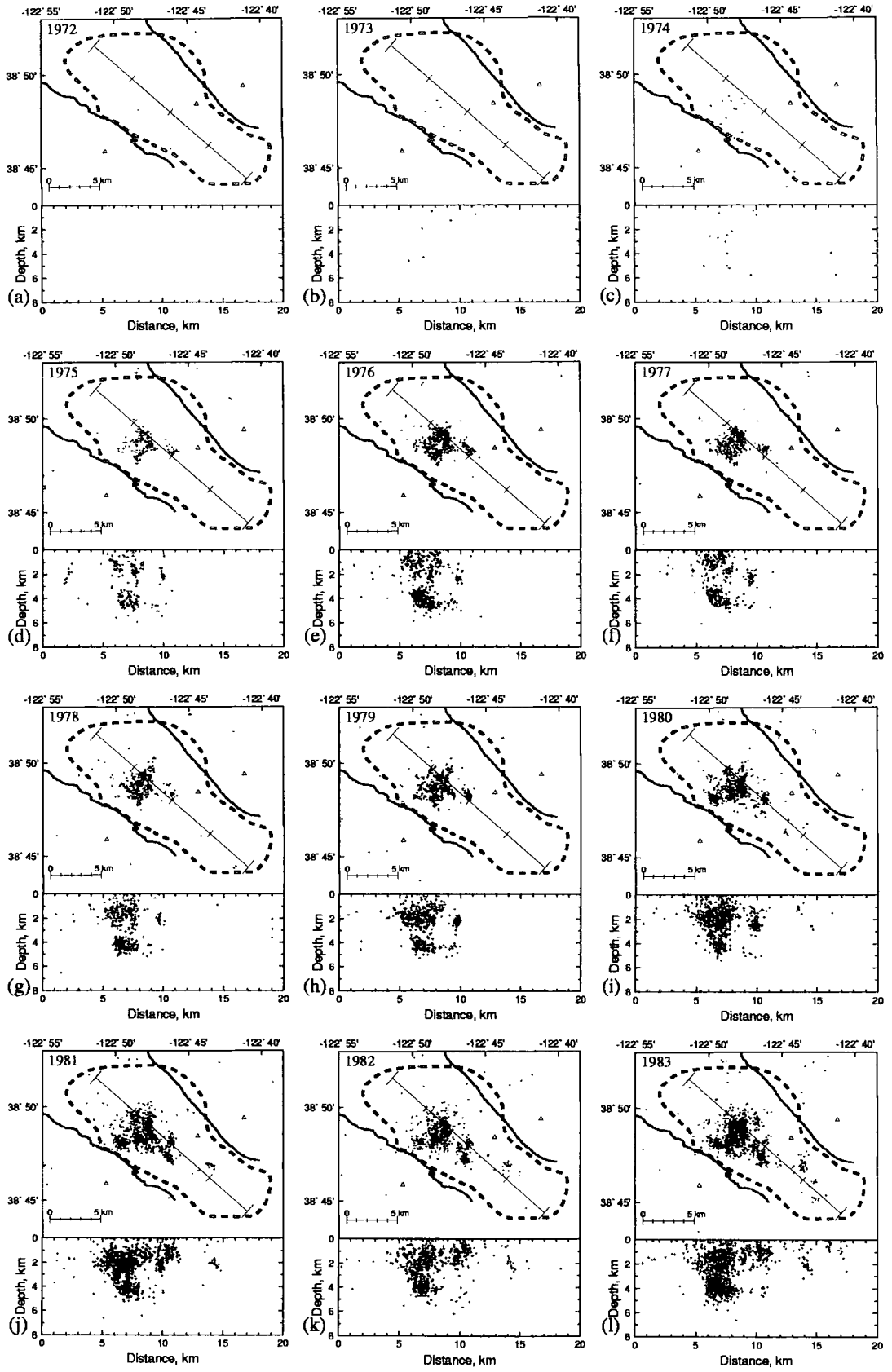

Figure 3.14a Epicentre maps and cross-sections for NCSN data from 1972 to 1983, M_d >= 1.2.

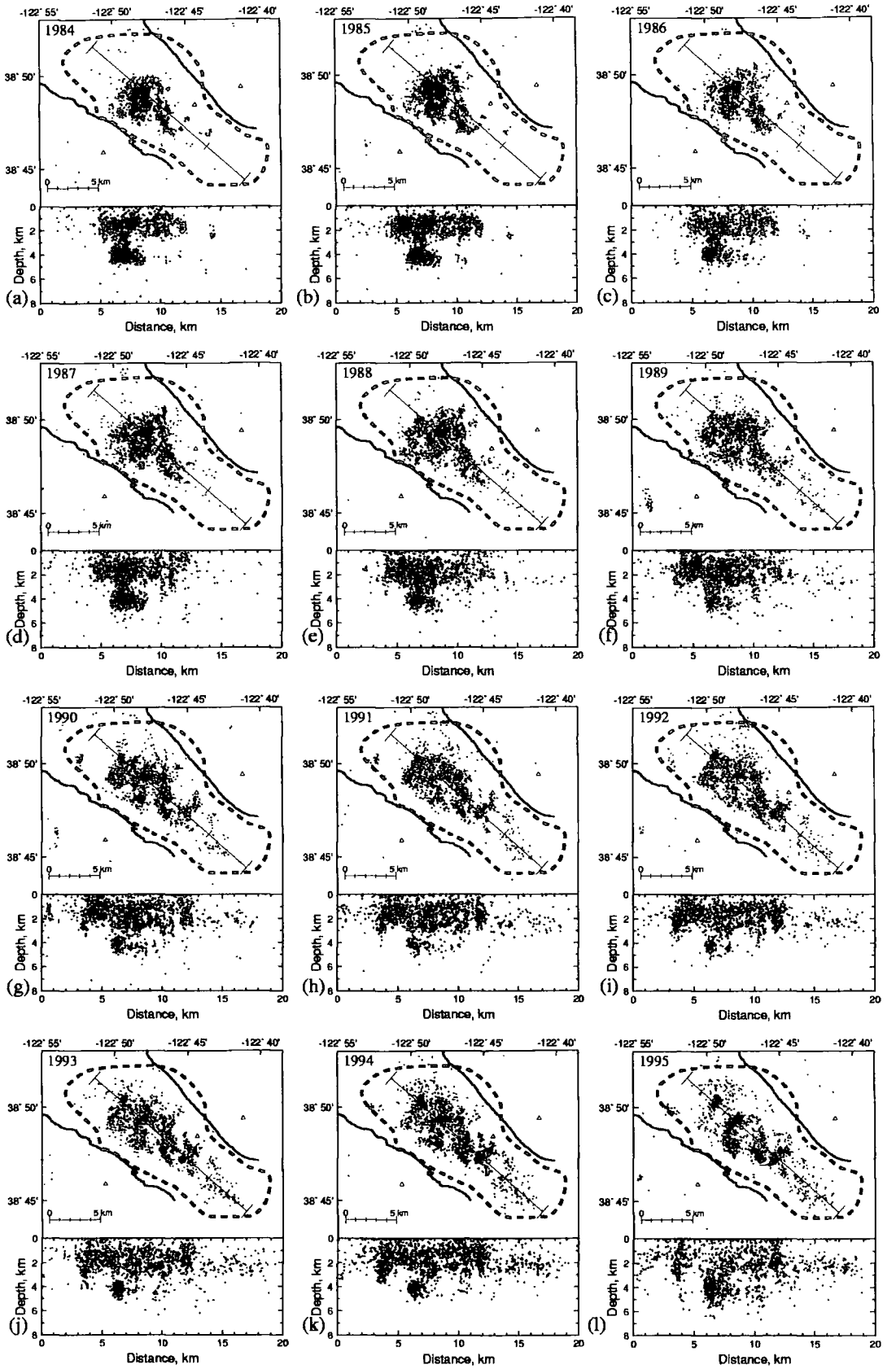

Figure 3.14b Epicentre maps and cross-sections for NCSN data from 1984 to 1995, $M_d >= 1.2$.

less well defined, spread to the north-west and south-east and then merged more with the deeper seismic volume. The epicentral clusters merged to form a single zone in the central Geysers, though the 'deadzone' was still visible. By the mid-1990s, distinct clusters had reappeared in the central Geysers (Figure 3.14b(l)). Outside the geothermal area, tectonic seismicity occurred along the Maacama and Bartlett Spring fault zones (Figure 3.5).

3.6 Commercial exploitation of The Geysers

The Geysers area has been commercially exploited for approximately 140 years. The first development was in the 1860s when a resort hotel south of Big Sulphur Creek (Figure 3.6) used the nearby fumaroles and hot water springs. In 1922 steam from wells drilled north of Big Sulphur Creek was used for electrical power production using a 1 KW generator. This project was abandoned in 1940 after the steam corroded the pipes and the generator.

Large-scale commercial development started in the mid 1950s after the development of new stainless-steel alloys designed to withstand the corrosive effects of hot steam. In 1955 a well-drilling program was initiated that had, by 1958, sufficient wells to supply a small electrical power generating unit. In September 1960 the first Pacific Gas and Electricity (PG&E) Utility (Unit 1, a 12-MW power unit) was brought into production (Figure 3.15). Steam was provided by a consortium of developers. Production at this time was modest, being about 0.1×10^6 kg/hour in 1960 rising to 0.73×10^6 kg/hour in 1968 (Table 3.3). This capacity stayed constant until the mid-1970s. The resource was estimated to have a maximum capacity of 3000 MW and a lifetime of 30 years *(Kerr, 1991)*. These projections were based upon estimates of the amount of available heat to generate steam. It was largely assumed that there would be enough water to carry the heat to the surface. Research into the reservoir and its mechanisms were neglected *(Kerr, 1991)*.

In 1971, with the arrival of the Union Oil Company of California (UNOCAL) in The Geysers, a period of sustained growth commenced. The partnership between PG&E and UNOCAL was very successful with UNOCAL drilling wells and providing steam for PG&E's power plants. Between 1971 and 1981 twelve power plants were installed. The average generating capacity increased by 67 MW per

year to an installed generating capacity of 943 MW in 1981. The mass of steam withdrawn from the reservoir mirrored the increase in power production with an average increase per year of 0.56×10^6 kg/hour, resulting in a total production of 6.58×10^6 kg/hour by 1981.

Table 3.3 History of development at The Geysers

Development Phase	Period	Installed generating capacity (MW)	Yearly increase in power generation (MW)	Steam withdrawal kg / hour
1	1960-1968	82	10	0.1×10^6 (1960) 0.73×10^6 (1968)
2	1969-1981	943	67	6.58×10^6 (1981)
3	1981-1989	2043	150	13.61×10^6 (1987)

A third phase of development began in 1981 with the installation of a further fourteen power plants between 1982 and 1989. This rapid development was encouraged by the success of the UNOCAL/PG&E partnership, the rising price of oil and the introduction in 1980 of US Federal incentives to encourage research and development into alternative energy resources. Steam production doubled at a rate of 1.16×10^6 kg/hour to a maximum of 13.61×10^6 kg/hour in mid-1987. By the end of the 1980s, five utilities, three developers and three developer/utility companies were exploiting The Geysers (Figure 3.16; Table 3.4).

In 1987 there was a sharp decrease in steam pressure within the reservoir. By 1988, steam pressure had decreased from > 3.5 MPa to < 1.38 MPa in some areas *(Barker et al., 1992)*. This showed that liquid reserves were being converted into steam at a much greater rate than they were being replenished by recharge, and that the field was over-developed.

Since then, steam production decline rates for UNOCAL-NEC-Thermal (UNT) areas have been 15%/year in the south-east Geysers, 7%/year in the north-west and 11%/year over the entire field. Unfortunately, due to a lack of communication between the operating companies and the belief that the drops in pressure were localised, new generating units were still being built as late as 1989. This hastened the decline in steam pressure further. During the 1990s pressure within the reservoir continued to decline, with the reservoir currently operating at $^2/_3$ its 1989 capacity. No new wells on UNT leases have been built since 1989.

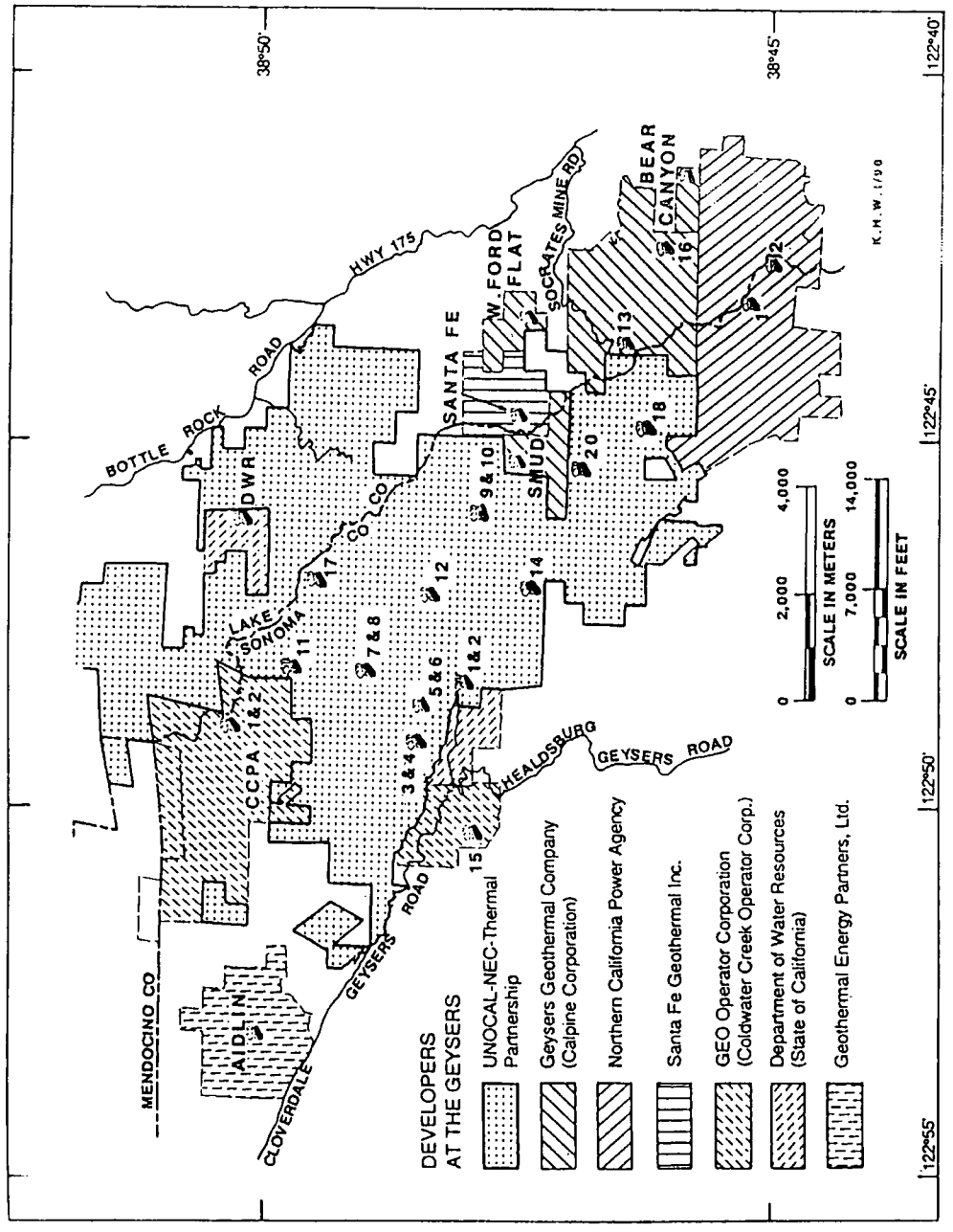

Figure 3.15 Map of The Geysers production area showing the area operated by each developer in 1992 *(from Barker 1992)*. The location of power generating units is indicated by the symbol with associated number. Information on the generating units is given in Table 3.3.

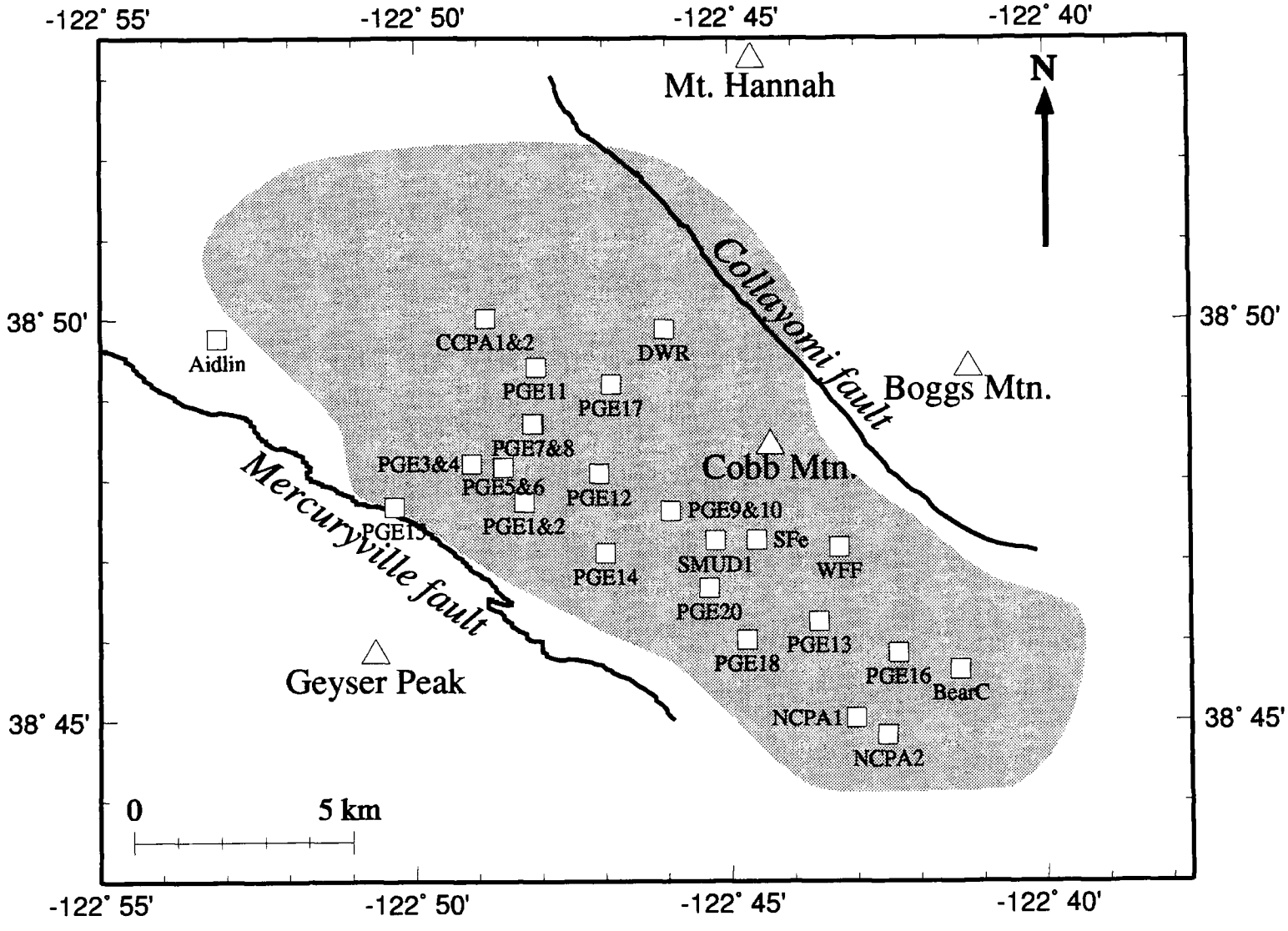

Figure 3.16. Map showing the location of power generating units at The Geysers geothermal area. At sites where two units are indicated, they are housed in the same building. Key: BearC: Bear Canyon; SFe: Santa Fe; WWF: West Ford Flat; see also Table 3.4. *(from Ross, 1996)*

Table 3.4 Power generating units at The Geysers *(from Barker, 1992)*

Power generating unit	Date on-line for commercial operation	Steam Supplier	Gross capacity (MW)	Cumulative capacity (MW)
PGE-1	09-1960	Retired 1991	12	12
PGE-2	03-1963	Retired 1992	14	26
PGE-3	04-1967	Retired 1992	28	54
PGE-4	11-1968	Retired 1992	28	82
PGE-5	12-1971	UNT	55	137
PGE-6	12-1971	UNT	55	192
PGE-7	11-1972	UNT	55	247
PGE-8	11-1972	UNT	55	302
PGE-9	11-1973	UNT	55	357
PGE-10	11-1973	UNT	55	412
PGE-11	05-1975	UNT	110	522
PGE-12	03-1979	UNT	110	632
PGE-15	06-1979	Retired 1989	62	692
PGE-13	05-1980	Calpine-SRGC	138	829
PGE-14	09-1980	UNT	114	943
PGE-17	12-1982	UNT	117	1062
NCPA-1	01-1983	NCPA	110	1172
PGE-18	02-1983	UNT	119	1291
SMUDGEO-1	10-1983	GGC	72	1363
Santa Fe	04-1984	SFI	80	1443
DWR-Bottle Rock	03-1985	DWR	55	1298
PGE-16	10-1985	Calpine-SRGC	119	1617
PGE-20	10-1985	UNT	119	1736
NCPA-2	11-1985	NCPA	110	1846
CCPA-1	05-1988	GEO	65	1911
Bear Canyon	09-1988	GGC	20	1931
CCPA-2	10-1988	GEO	65	1996
West Ford Flat	12-1988	GGC	27	2023
Aidlin	06-1989	GEP	20	2043

Overproduction of The Geysers may have been averted if better resource management had been adopted, with a research program examining the effects of commercial activity on the output of the field. If this had been done, predictions of the decline of the field might be taken more seriously. If production had been maintained at 1980 levels, power production might still be at full strength *(Kerr, 1991)*. Now that the field is in decline, developers and operators are seeking methods to prolong its useful life. Proprietary data have been released to the scientific community to help research.

Water injection has been used to slow the decline of the field. Heat within the reservoir is largely stored in the rock rather than in the water, so replacing the water lost by production would lengthen the life of the resource. Before starting injection in a well, the fracture distribution, rock permeability, temperature, steam

pressure, rock type and liquid saturation need to be examined. Injection is simply a matter of pouring fluid into the well as the reservoir pressure is lower than the hydrostatic pressure, though care must be taken to avoid extensive chilling of adjacent rock surfaces. During the 1980s, a field-wide total of 700 kg/s was injected at 25-30^{0}C. A condensate re-injection program returned 25% of the extracted steam and fresh water from Big Sulphur Creek back into the reservoir. In some other cases, injection resulted in a modest steam production recovery of 7%, though water has been found in the bottom of some production wells rather than it flashing to steam. In general, water injection has been of moderate long-term benefit to the recovery of the field.

In September 1997, two pipelines carrying partially treated sewage from neighbouring towns to the south-east Geysers were completed *(S.E. Geysers Wastewater Recycling System Website, 1998)*. These inject an additional 200 kg/s of 'grey water' at the low temperature of < 10^{0}C. An estimated 1.2 x 10^{10} kg of effluent water are delivered to the Geysers annually by this system. It is expected that 40 - 100% of the injected fluid will be converted to steam, and, assuming a steam recovery rate of 50%, electrical output at The Geysers should increase by 70 MW. However, any improvement in power production is difficult to assess. Since March 1998, UNOCAL wells have been operated in a cyclical pattern within the geothermal field, making it difficult to identify increases in steam production. In addition, fluid has only been injected at operational levels since December 1997, so at the time of writing (September 1998) too short a time period has elapsed for the full effect of the reinjection to manifest itself *(Atkinson, 1998)*. The environmental impact of pumping huge quantities of 'grey' water into the south-east Geysers has yet to be assessed, though the Northern California Power Agency (NCPA) operating company has reported a large drop in the amounts of non-condensensable gases (e.g. H_2S) found in the extracted steam.

A similar effluent injection pipeline from the City of Santa Rosa to The Geysers is currently at the planning stage *(Frye, 1997)*. That pipeline is designed to carry 1.5 x 10^{10} kg annually, and is scheduled for completion by 2001.

3.7 Relationship between seismicity and geothermal exploitation in The Geysers

Although there is very little information about the level of seismicity in The Geysers prior to the installation of the NCSN network in 1975, there is evidence that the area was significantly less active prior to exploitation. A survey of all the seismic activity in northern California within a 60 km radius of the University of California Calistoga seismic station 1962-63 and 1975-77 showed that level of seismicity ($M_d \geq 2.0$) was twice as much during the latter period *(Marks et al., 1978)*. The majority of this increase was attributed to The Geysers geothermal area. These findings are supported by the dramatic increase in activity recorded by the NCSN network since 1975, and by the greater number of reports of local felt activity and the amount of earthquake damage to local property (Figure 3.14).

The increase in earthquake activity is thought to be directly related to both the extraction of steam and the injection of fluid. A causal relationship between seismicity and commercial activity was first hypothesised in 1972 *(Hamilton & Muffler, 1972)*. Further work has supported this *(e.g. Majer & McEvilly, 1979; Ludwin & Bufe, 1980; Allis, 1982; Ludwin et al., 1982; Eberhart-Phillips & Oppenheimer, 1984; Stark, 1992; Romero et al., 1994; Kirkpatrick et al., 1995)*, and several mechanisms have been suggested to explain these relationships (Section 3.8). There is strong evidence that 50% of earthquake activity in The Geysers is caused by fluid injection, with the remainder of the activity caused by steam extraction and tectonic processes *(Stark, 1992)*.

Although seismicity due to tectonic processes does contribute to the overall level of seismicity in The Geysers, it is difficult to ascertain its contribution without seismic data prior to exploitation. An indication of the background level of seismicity in The Geysers is given by early studies of earthquake activity when there was little geothermal development. In the late 1960s / early 1970s, production was ~ 80 MW and the seismicity rate was ~ 4 events/day *(Lange & Westphal, 1969; Hamilton & Muffler, 1972)*.

There are some impressive correlations between seismicity and production-related activities on both local and field-wide scales. During the period 1975-82, earthquake activity in previously aseismic areas started soon after production

commenced (Figure 3.17) *(Eberhart-Phillips & Oppenheimer, 1984)*. A study of seismicity and the location of the electrical power plants after 1982 yielded similar results *(Ross, 1996)* (Figure 3.17). Although power plants are not directly responsible for injection or steam extraction, for engineering purposes they are positioned close to wells where these activities are taking place. Seismic activity in the central Geysers correlated exclusively with the operational generating units, and the deepest earthquakes occurred in the most exploited areas. Furthermore, areas with rapid increases in seismic rate had been recently heavily exploited, suggesting a causal relationship (Figures 3.17e-h). Seismicity in the south-east Geysers has remained comparatively low.

Following the pressure decline in 1987 and subsequent slowing of development (Section 3.6), the seismicity rate decreased. By the mid 1990s, seismicity had become largely limited to isolated clusters adjacent to ongoing injection and production activities. Areas where injection and production activities ceased have become relatively seismically quiet (Figures 3.17h - l). There is also a correlation between the average rate of steam extraction and the number of earthquakes per year (Figure 3.18) *(Ross, 1996)*. Between 1975 and 1988 the rate of steam extraction and the seismicity rate at The Geysers are closely correlated. The poor correlation after 1992 may be due to injection strategies not incorporated into the decline-curve calculations and unexpected changes in steam flow.

Fluid injection is another likely cause of seismic activity caused by commercial geothermal activities. Although other authors have suggested that production, rather than injection is the principal cause of the seismicity in The Geysers *(e.g. Eberhart-Phillips & Oppenheimer, 1984)*, studies of proprietary operational and geochemical data have revealed a spatial and temporal correlation between injection and seismicity *(Stark, 1992)*. Several mechanisms have been suggested to explain this phenomenon (Section 3.8). Possible applications of injection-induced seismicity include path-tracking of fluid through reservoirs and estimates of reservoir bathymetry *(Stark, 1992)*. Injection induced seismicity has also been observed in vapour-dominated geothermal fields in Larderello and Travale, Italy *(Batini et al., 1985)*, and in liquid dominated fields in Italy *(Batini et al., 1985)*, New Zealand *(Sherburn, 1984; Sarmiento, 1986)* and in the Philippines *(Bromley et al., 1986)*.

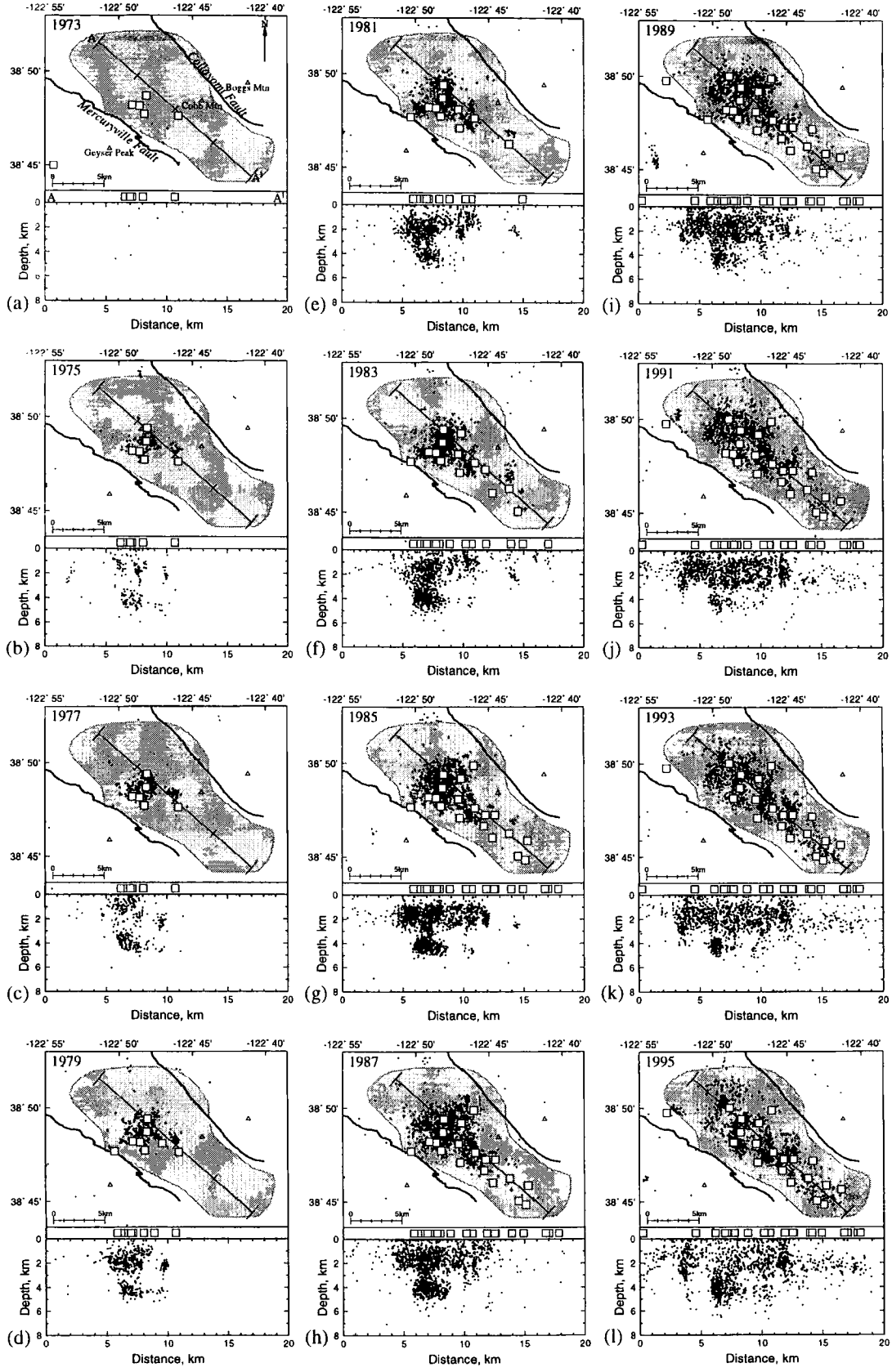

Figure 3.17 As 3.14, but with the locations of power generating units operating during the year represented superimposed on the seismicity *(from Ross, 1996).*

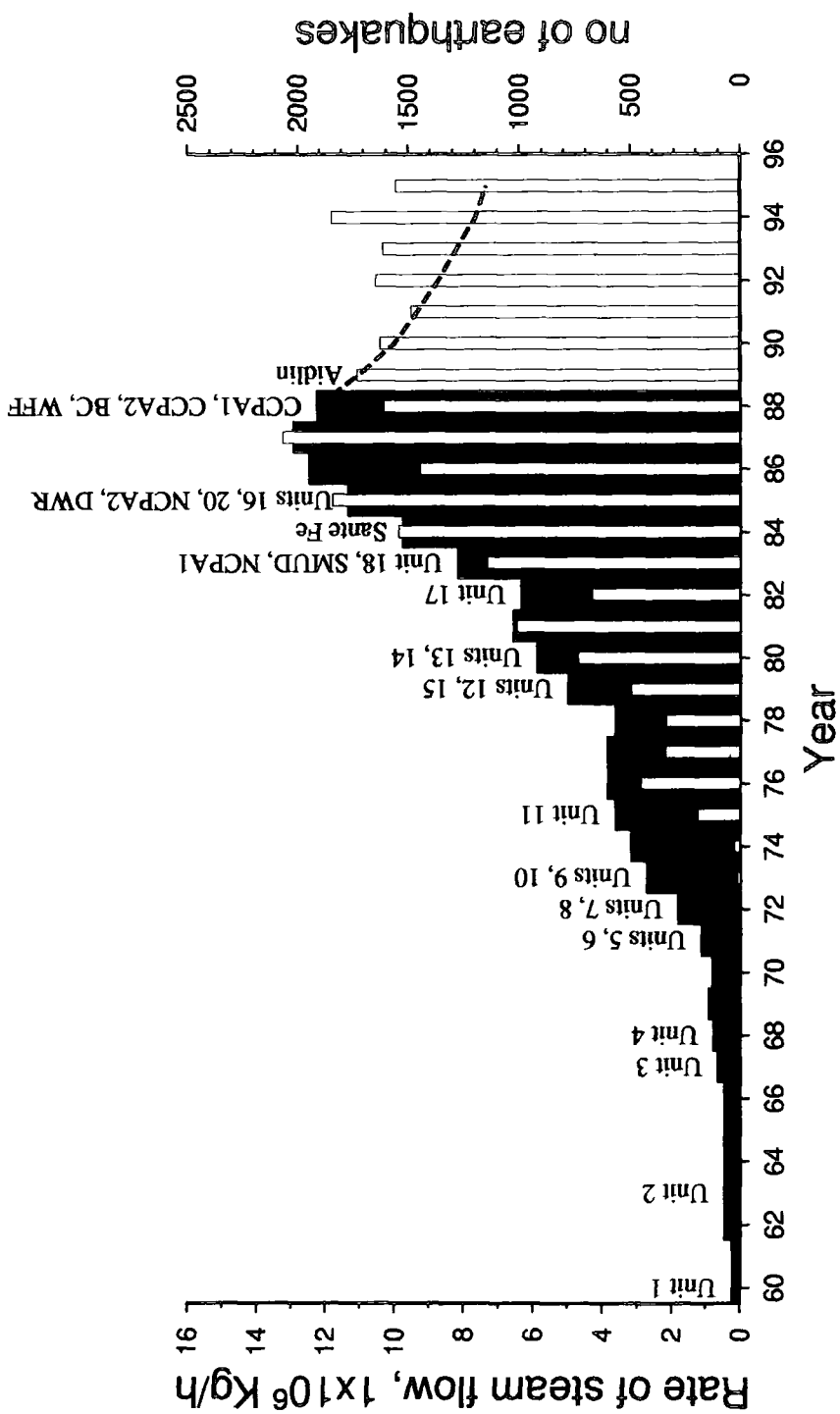

Figure 3.18 Histogram showing the average steam flow rate per hour between 1960-88 (filled columns) (modified from (*Barker et al., 1992*). The dashed line indicates the projected steam flow rate from 1989-95 (modified from *Williamson, 1992*). The white columns indicate the number of $M_D \geq 1.2$ earthquakes recorded in The Geysers by NCSN between 1973-95 (from the NCEDC). Installation histories of electrical power generating units at The Geysers are indicated (*from Ross, 1996*).

Figure 3.19 shows an example of how injection episodes can induce earthquakes in The Geysers. Adjacent to well DX-61, the seismicity rate was 18 events per month prior to injection episode in 1988 (Figure 3.19b). After the episode the seismicity rate rose to 61 events per month and a plume of earthquakes occurred in a zone dipping to the south-west of the injection well (Figure 3.19b). Similar results were reported for the north-west and south-east Geysers *(Romero et al., 1994)*.

The completion of the 'grey water' injection pipelines provides an opportunity to study the effects of fluid injection in the south-east Geysers. Figure 3.20 is a plot of average monthly delivery rates between September 1997 and June 1998. Delivery rates have been constant at ~ 360 kg/s since January 1998, bringing the total amount of injected fluid into The Geysers to 1060 kg/s.

Before the completion of the pipeline, 120 $M_d \geq 1.2$ earthquakes were occurring per month. Assuming that injection is the cause of 50% of earthquake activity in The Geysers *(Stark, 1992)*, the seismicity rate should increase by 30 - 40 $M_d \geq 1.2$ earthquakes per month. Figure 3.21 shows the number of NCSN-recorded earthquakes per month August 1997 - August 1998. Prior to the completion of the pipeline in September 1997, there were 125 $M_d \geq 1.2$ earthquakes per month. Afterwards, the seismicity rate increased by 50 - 80 earthquakes per month. Epicentral plots and cross-sections (Figure 3.22) show that prior to the operation of the new pipelines in September 1997, seismicity was concentrated in clusters in the central Geysers. The south-east Geysers was relatively aseismic at this time. When the pipeline commenced operations, seismicity increased noticeably in the central Geysers, while the south-east Geysers remained at the same level of seismicity.

Operating companies were at first reluctant to admit that their activities were inducing seismicity. In the light of evidence indicating that commercial steam extraction and injection *were* causing earthquakes, claims that the seismicity was low-level, small- magnitude and did not pose a seismic hazard were made. Despite these assurances, there is growing public opposition to further development, both of the steam field (unlikely though that is), and of the use of injection to prolong the life of the reservoir.

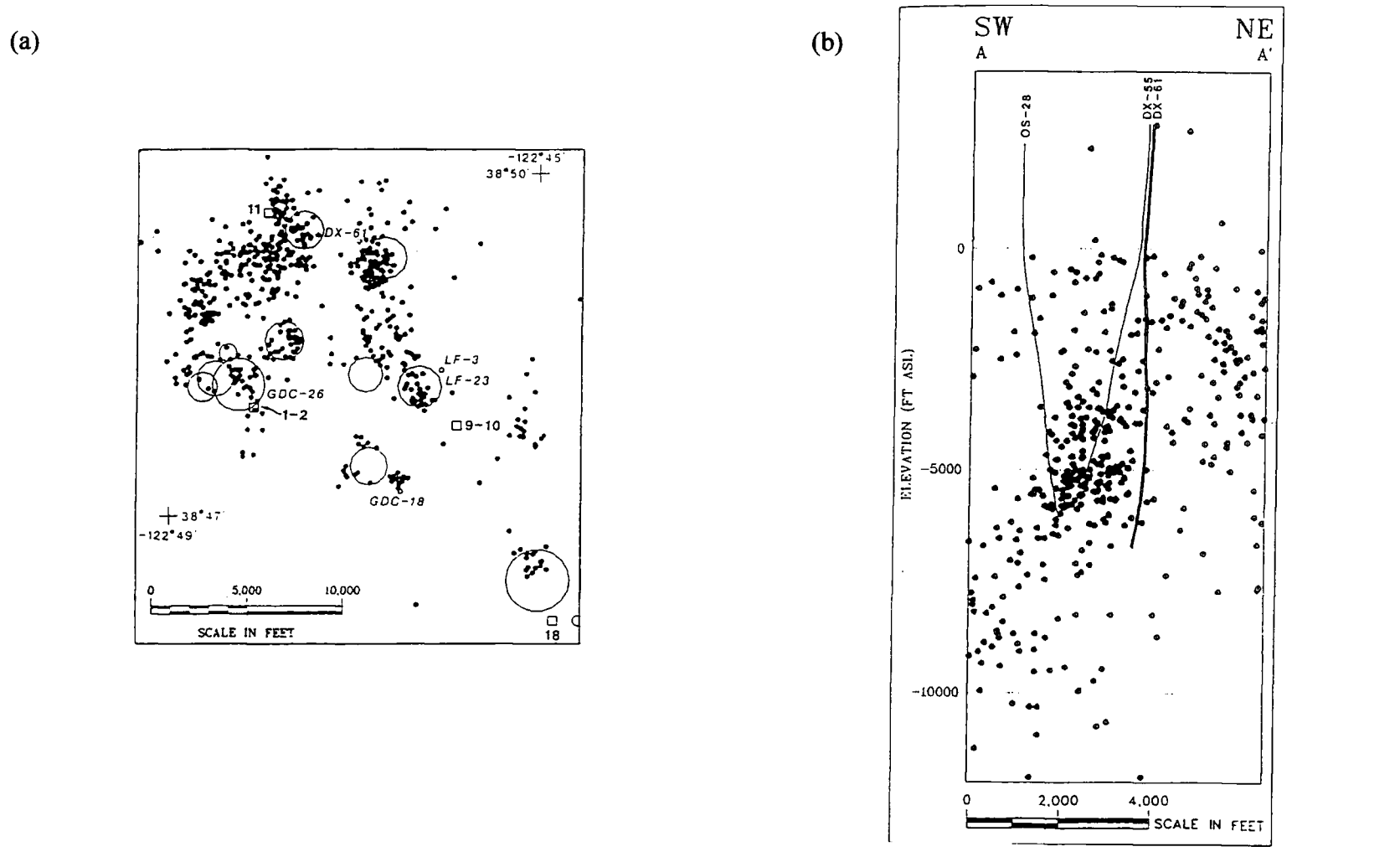

Figure 3.19 (a) Epicentres (dots) located by the UNT network (Section 4.1.1) between 11/1988 and 8/1989 with $M_d > 0.7$. Open circles represent UNOCAL injection wells, with circle area proportional to the volume injected over the aforementioned period. Numbered squares are selected PG&E power plants. (b) Cross-section showing earthquakes located in the vicinity of injection well DX-61 September to December 1986 *(from Stark, 1992)*.

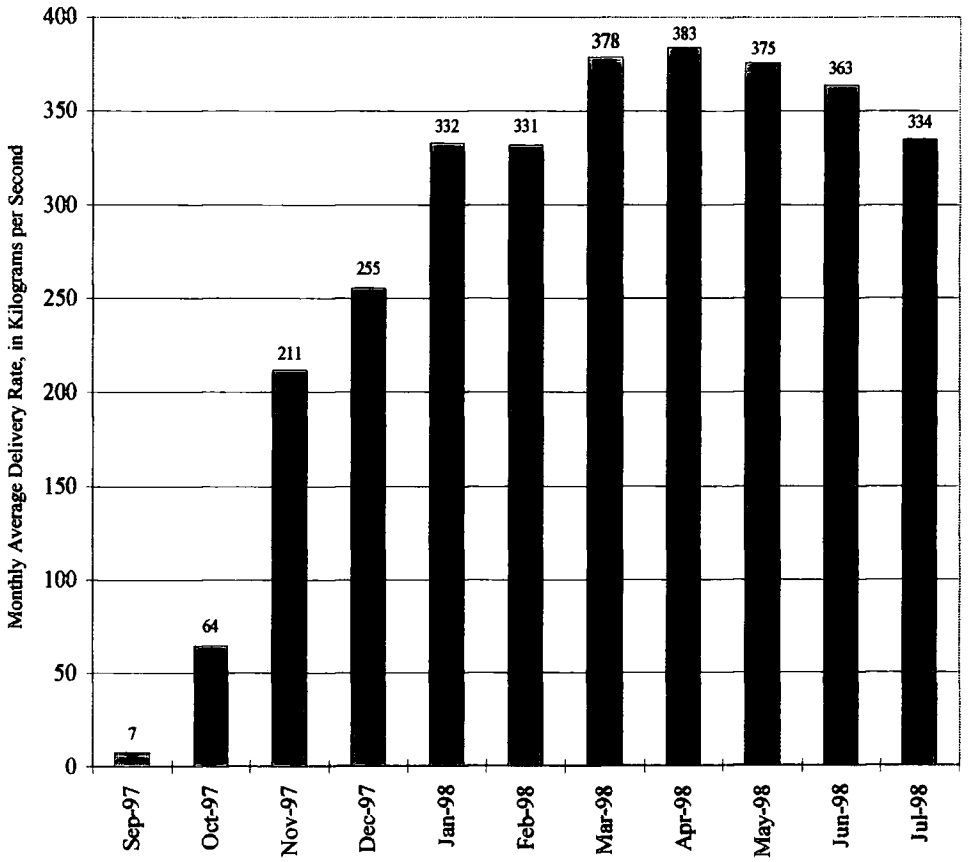

Figure 3.20 Plot of monthly average delivery rates for the south-east Geysers effluent pipe project *(http://www.geysers-pipeline.org/)*.

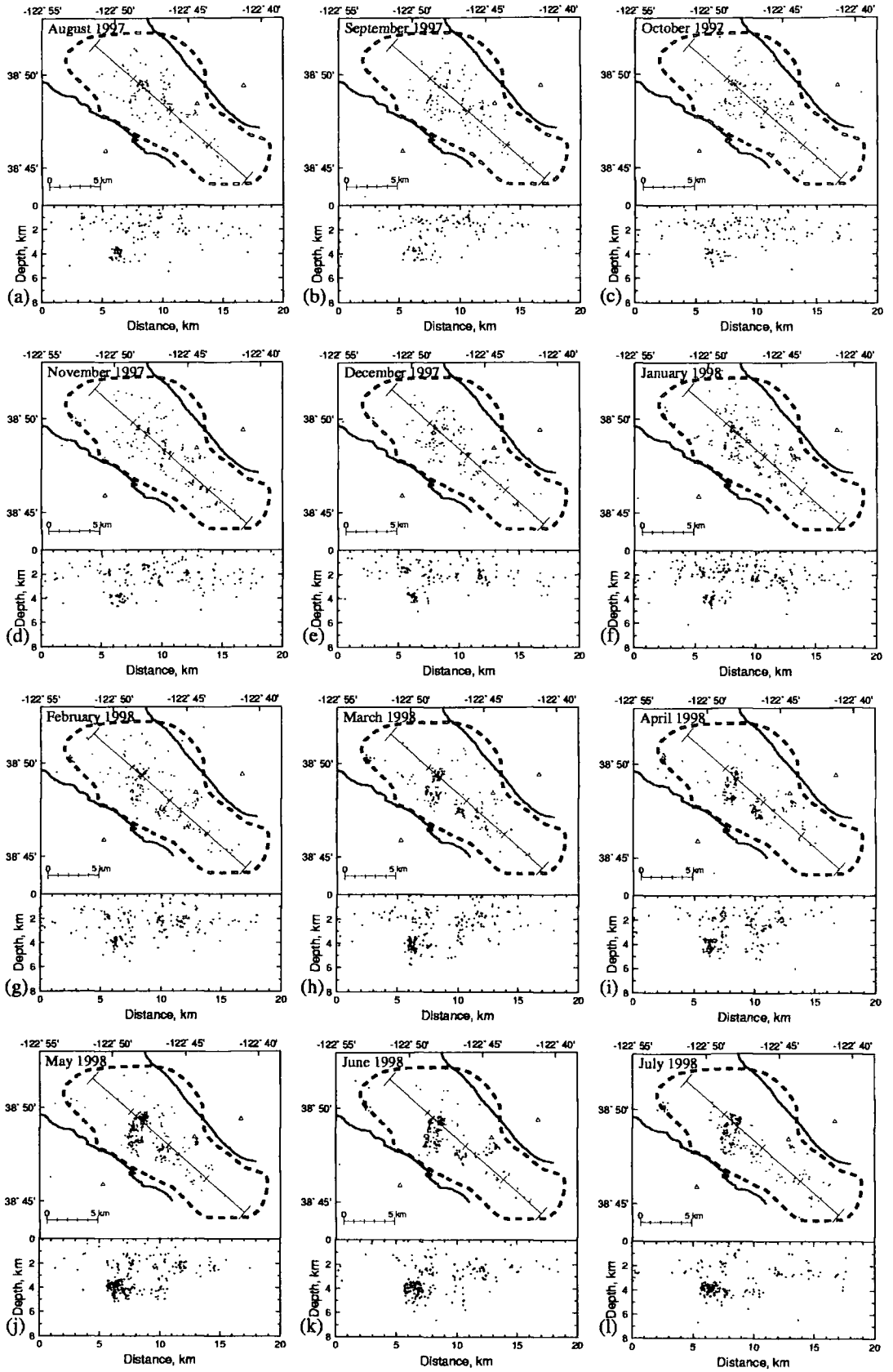

Figure 3.21 Epicentre maps and cross-sections for NCSN Geysers data from August 1997 to July 1998, M_d >= 1.2.

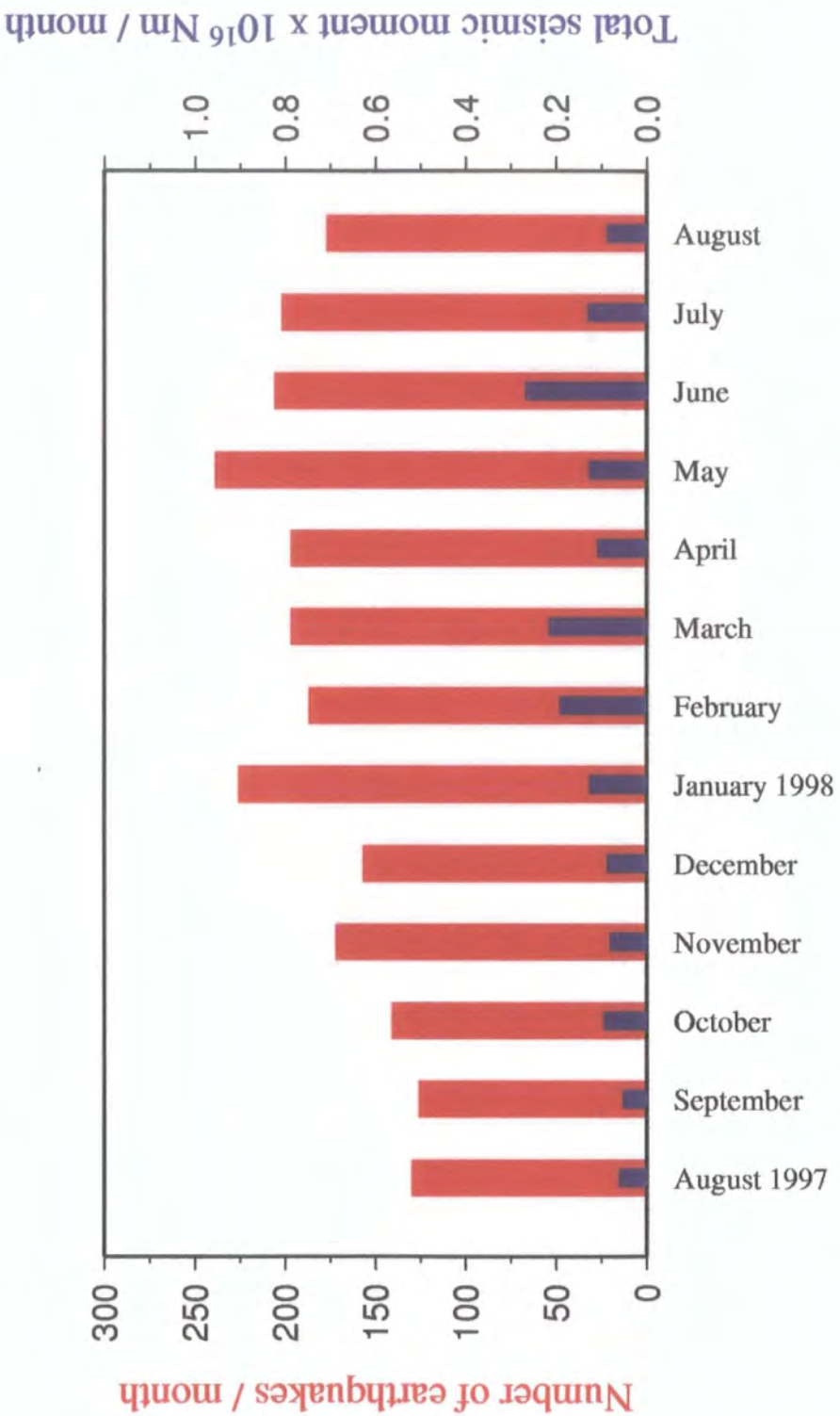

Figure 3.22 Number of events and total seismic moment per month for NCSN earthquakes with $M >= 1.2$ in The Geysers August 1997 - 1998.

3.8 Mechanisms of earthquake genesis at The Geysers

Although it is clear that commercial activities and seismicity are related, the exact mechanism of this process is poorly understood. Mechanisms involving temperature, pressure, volume and reservoir changes have been suggested. These are summarised in Table 3.5.

Table 3.5 Summary of seismic induction mechanisms

Method	Reference	Production induced seismicity?	Injection induced seismicity?
Pore pressure increase, lowering of effective normal stress	*Hubbert & Rubey (1959)*	No	Yes
Shear stress response to volume changes	*Majer & McEvilly (1979)*	Yes	No
Increase in reservoir strength	*Majer & McEvilly (1979), Allis (1982)*	Yes	No
Cooling due to extraction & injection	*Denlinger (1980)*	Yes	Yes
Fracture deflation	*Denlinger & Bufe (1982)*	Yes	No
Declines in temperature & pressure causing deformation change from creep to stick-slip	*Denlinger & Bufe (1982)*	Yes (unlikely in The Geysers)	No

The *Hubbert & Rubey (1959)* mechanism shows how changes in pore fluid pressure can trigger rock failure. Failure occurs when the shear stress exceeds the effective normal stress (the difference between normal stress and pore pressure) by a critical value. When a rock volume is already near failure, a small increase in pore pressure could thus induce failure. Considering the sub-hydrostatic pressures within the reservoir and the fact that condensate can be injected at zero well-head pressure, previous authors were doubtful that failure could occur by this method *(Majer & McEvilly, 1979; Allis, 1982; Denlinger & Bufe, 1982; Eberhart-Phillips & Oppenheimer, 1984)*. However, water levels within operating injection wells stabilise hundreds of metres above the well base. Since the hydraulic pressure of a 100 m column of water is about ~ 1 MPa, and reservoir pressures vary from 1.4 to 3.5 MPa, a column of water several hundreds of metres high would generate sufficient pressure to cause failure by the mechanism suggested by *Hubbert & Rubey (1959) (Stark, 1990)*.

Cooling in response to field-wide steam extraction and localised condensate injection *(Denlinger, 1980)* could cause a reduction in the normal stress across fracture surfaces so resulting in localised failure. As it is thought that rocks in The Geysers are close to failure, this failure mechanism seems likely. Long term-injection of fluid may change the rock deformation regime from near ductile (typical for rocks at depths of 3 km and greater) to brittle. This process may occur in conjunction with the mechanism suggested by *Hubbert & Rubey (1959)*.

Some of the seismicity in The Geysers may result from changes in the shear stress field in response to volume changes *(Majer & McEvilly, 1979)*. Geodetic studies in the production area have shown that there has been horizontal and vertical contraction in areas of greatest commercial exploitation, supporting this hypothesis *(Lofgren, 1981; Mossop & Segall, 1997)*. Fracture deflation could cause increases in shear stress, thus inducing failure *(Denlinger & Bufe, 1982)*. Fracture deflation would increase the shear stress within one crack length of the tip by 33 - 66% of the crack pressure decline. This mechanism requires a continuous pressure decline to generate a constant level of seismicity. Before the onset of production, tectonic motion is thought to be due to aseismic creep; afterwards due to stick-slip deformation so causing seismic activity *(Majer & McEvilly, 1979; Allis, 1982; Denlinger & Bufe, 1982)*. Three mechanisms have been suggested for this change. First, the transition could be caused by a large fluid-pressure decrease, possibly accompanied by a water-dominated to steam-dominated reservoir change *(Allis, 1982)*. The Geysers reservoir is vapour dominated, so this mechanism is unlikely. Second, the transition from aseismic creep to seismic stick-slip could be caused by deposition of silica on existing fracture surfaces precipitated from boiling reservoir fluids, so increasing the coefficient of friction *(Allis, 1982)*. Third, temperature and pressure declines in laboratory experiments have caused the transition from creep to stick-slip *(Byerlee & Brace, 1972; Stetsky et al., 1974)*, though a lack of cool rock in the reservoir makes this process unlikely in The Geysers.

3.9 Summary

The Geysers geothermal area is the world's largest development of geothermal steam for electrical production, currently supplying 6% of northern California's power. The rocks of The Geysers form three geological units: (1) a serpentinite

caprock, underlain by (2) a fractured greywacke vapour-dominated reservoir rock, which is heated from below by a (3) heat source thought to be magma. The Geysers area consists of two Jurassic-Cretaceous units assigned to the Franciscan and Great Valley sequences, partially capped by Quaternary volcanics. The Franciscan assemblage was intruded during the Pleistocene by a composite batholith known as the felsite. The reservoir, bounded by major fault zones to the north-east and south-west, can be divided into two distinct parts - a field-wide 'normal' reservoir and a high temperature reservoir lying under the normal field to the north-west. Porosity within the reservoir is fracture related, enhanced by repeated episodes of intrusion by the felsite. Compared to the amount of commercially injected fluid, the amount of natural reservoir recharge is essentially nil.

The Geysers is one of the most seismically active areas in California. This seismicity is almost exclusively confined to the commercially developed area and has been monitored by a succession of temporary and permanent networks. The NCSN network, expanded into The Geysers in 1975, shows that the seismicity in the most heavily exploited areas increased dramatically during the rapid development of the resource during the 1980s. Seismicity is thought to be a result of commercial activity.

In the late 1980s, pressure decline occurred in the reservoir, indicating that The Geysers had become over-developed. Condensate injection is currently used to delay the decline of the geothermal field, using former production wells and pipelines carrying treated sewage from neighbouring towns. This method has limited success, but has induced more seismicity. 50% of Geysers seismicity is thought to be caused by fluid injection, with the remainder caused by steam extraction and tectonic processes. Since September 1997, sewage has been injected into south-east Geysers by two pipelines. Although there has been an increase in seismicity since then, most of this is Central Geysers and may not be linked to the pipeline activity. Several mechanisms have been suggested for induced seismicity. Currently The Geysers is generating only 66% of its total installed capacity of 2043 MW.

Chapter 4
Seismic Data Processing & Well Data

4.1 The UNOCAL - NEC - Thermal network

4.1.1 Network Specifications

Since 1975, micro-earthquake activity in The Geysers has been monitored using the NCSN network, operated by the US Geological Survey *(Eberhart-Phillips & Oppenheimer, 1984)* (Section 3.4.2). After installation of this network, it soon became apparent that there were far more earthquakes in The Geysers than could be located. In 1985, a Union Oil of California (UNOCAL) - NEC - Thermal partnership, the "UNT Partnership", began proprietary seismic recording in order to monitor the environmental impact of industrial activity in The Geysers. By 1989, a dense network of continuously recording seismic stations covered most of the producing steam field *(Stark & Davis, 1996)*. The network was designed to provide an even distribution of stations over the study area (Figure 4.1). Currently, the network of twenty-two recording stations form a dense 15-km diameter array with an average station spacing of 1500 m. Half of the seismometers are in 39-m deep boreholes, one is in a 85-m deep borehole and the remainder are at the surface. All the seismometers are 4.5 Hz instruments.

Since 1989, the network has undergone three stages of development, the *W*, *G* and *F* networks (Figure 4.1). The *W* network, in operation during 1989, consisted of two three-component and ten vertical-component stations (Table 4.1a). During the interim period between the *W* network and when the subsequent *G* network came online in late 1989, there were several gaps in the monitoring due to equipment failure (Figure 4.2). Consequently, few earthquakes were detected during this period. The *G* network, which had twice the gain of the *W* network,

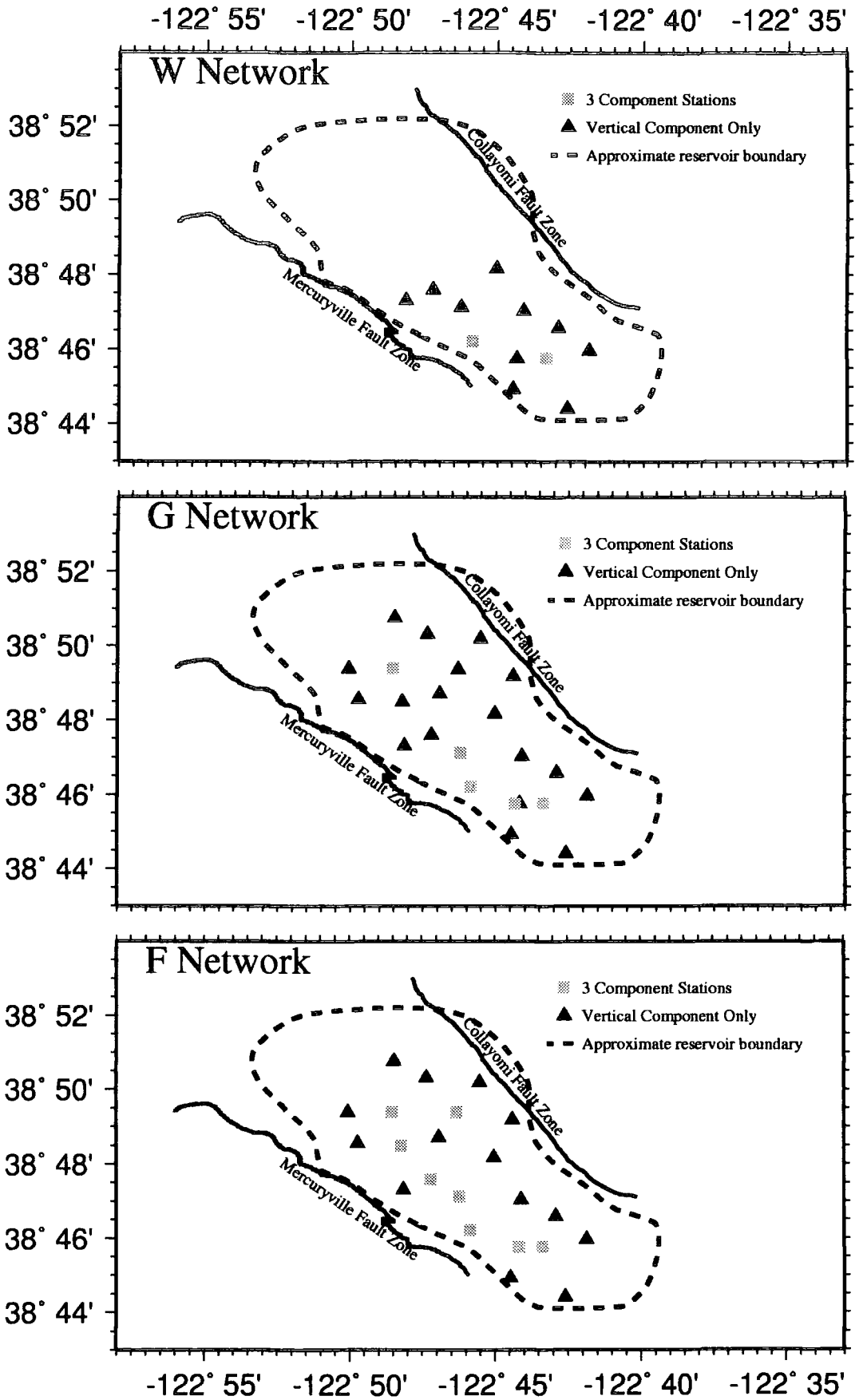

Figure 4.1 Map of The Geysers showing the UNT seismic station locations.

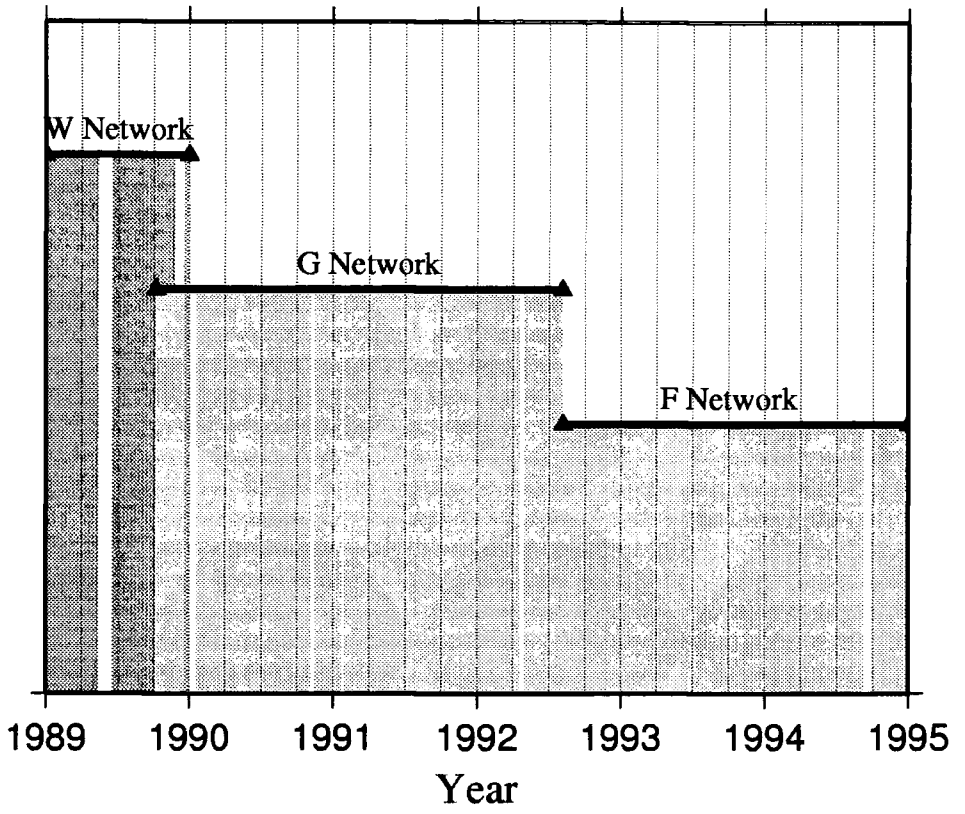

Figure 4.2 Operation histories of the UNT networks. Shaded areas indicate times when the networks were in operation.

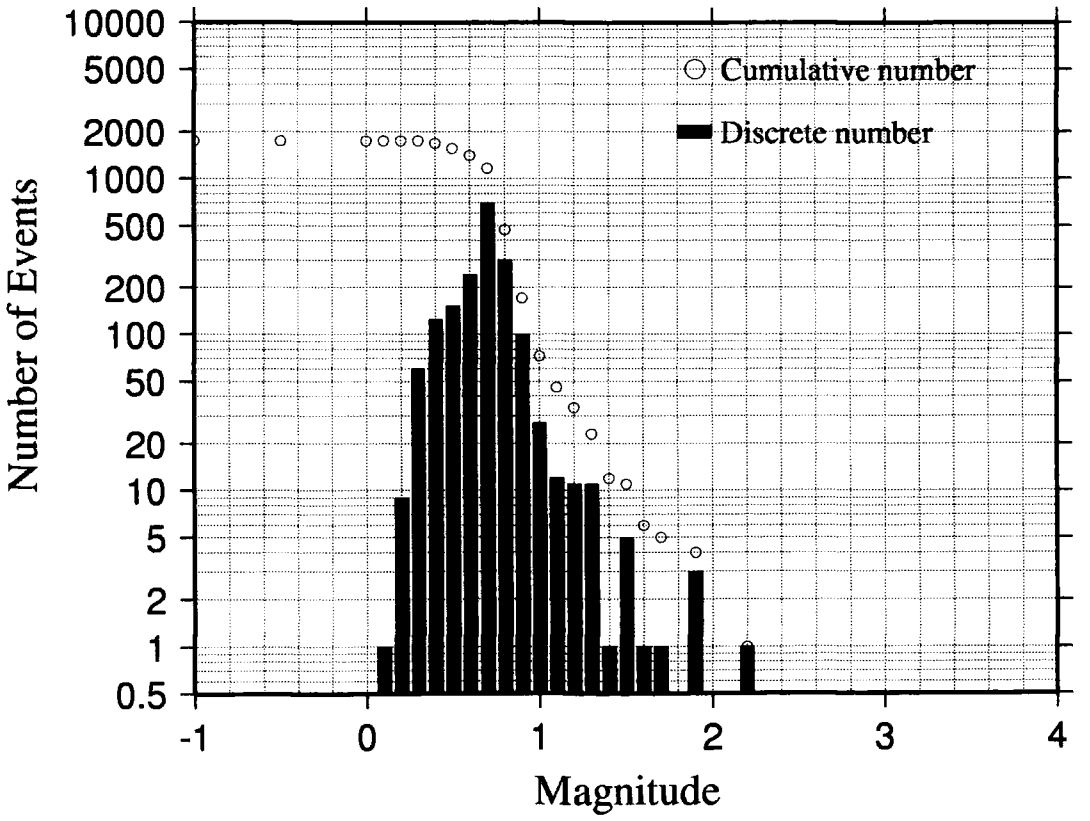

Figure 4.3 Log-frequency - magnitude plot of UNT seismic data for April 1991.

Table 4.1 Details of UNT seismic networks

Table 4.1a W Network (1989 - 1990)

Station Name	Latitude (degrees)	Longitude (degrees)	Number of Components
ANG	38.80278	-122.75067	1
DES	38.76617	-122.69783	1
DNV	38.76244	-122.73895	1
DRK	38.78858	-122.80242	1
FNF	38.77037	-122.76431	3
FUM	38.79323	-122.78673	1
MNS	38.77633	-122.71533	1
PFR	38.74883	-122.74117	1
SSR	38.74017	-122.71000	1
TCH	38.78389	-122.73502	1
U14	38.78542	-122.77084	1
WRK	38.76283	-122.72267	3

Table 4.1b G Network (late 1989 to day 218, 1992)

Station Name	Latitude (degrees)	Longitude (degrees)	Number of Components
ACR	38.83661	-122.75848	1
ANG	38.80278	-122.75067	1
BUC	38.82315	-122.83423	1
CAP	38.84608	-122.80771	1
CLV	38.83867	-122.78917	1
DES	38.76611	-122.69775	1
DNV	38.76244	-122.73895	3
DRK	38.78858	-122.80242	1
DVB *	38.76267	-122.73633	3
DXR +	38.82283	-122.77167	1
FNF	38.77037	-122.76431	3
FUM	38.79323	-122.78673	1
INJ +	38.80820	-122.80357	1
LCK *	38.81967	-122.74002	1
MNS	38.77640	-122.71530	1
PFR	38.74892	-122.74115	1
SB4B	38.80945	-122.82871	1
SSR	38.74019	-122.70995	1
SQK	38.82344	-122.80892	3
STY	38.81181	-122.78204	1
TCH	38.78389	-122.73502	1
U14	38.78542	-122.77084	3
WRK	38.76276	-122.72272	3

* = Station commenced operation after 1989

+ = vertical-component only station converted to three-component

Table 4.1c F Network (Day 218, 1992 to present)

Station Name	Latitude (degrees)	Longitude (degrees)	Number of Components
ACR	38.83661	-122.75848	1
ANG	38.80278	-122.75067	1
BUC	38.82315	-122.83423	1
DES	38.76611	-122.69775	1
CAP	38.84608	-122.80771	1
CLV	38.83867	-122.78917	1
DRK	38.78858	-122.80242	1
DVB	38.76267	-122.73633	3
DXR	38.82283	-122.77167	3
FNF	38.77037	-122.76431	3
FUM	38.79323	-122.78673	3
INJ	38.80820	-122.80357	3
LCK	38.81967	-122.74002	1
MNS	38.77640	-122.71530	1
PFR	38.74892	-122.74115	1
SB4B	38.80945	-122.82871	1
SQK	38.82344	-122.80892	3
SSR	38.74019	-122.70995	1
STY	38.81181	-122.78204	1
TCH	38.78389	-122.73502	1
U14	38.78542	-122.77084	3
WRK	38.76276	-122.72272	3

was in operation between day 279 in 1989 and day 218 in 1992, and consisted of five three-component and sixteen vertical-component stations (Table 4.1b). The *F* network came into operation on day 218 in 1992 and is still in use. This network has eight three-component and fourteen vertical-component stations (Table 4.1c). The gain of the *F* network is the same as that of the *G* network.

The UNT network currently locates typically up to 40 or 50 events per day and has a location threshold of coda magnitude, $M_d \sim 0.2$ *(Stark & Davis, 1996)*. Data recorded are automatically digitised at 100 samples per second. Satellite timing is used. Up until mid-1992 the events were identified and located by a NEWT Inc. processor, but this subsequently has been done by a PC-based system called ***iaspei*** *(Lee, 1992)*. UNT propriety software, incorporating the location program ***hypoinv*** *(Lee & Lahr, 1975)*, is used to calculate hypocentral locations. The one-dimensional velocity model used is similar to that of *Eberhart-Phillips &*

Oppenheimer (1984) (Figure 4.8), with station corrections based on calibration shots. The UNT locations have vertical hypocentral errors of ~ 0.4 km and horizontal errors of ~ 0.2 km *(Stark & Davis, 1996)*.

4.1.2 The quality of UNT magnitude data

Figure 4.3 is a log-frequency magnitude plot UNT catalogue magnitude data for the month of April 1991. The data above the threshold magnitude do not approximate to a straight line as might be expected. This suggests that the automatic coda-magnitude picking routines used to calculate the UNT catalogue magnitudes may not be reliable. Closer examination of the seismograms for this month show that, in a significant number of cases, more than one event was recorded on each trace. Figure 4.4 shows some examples. In several cases, the coda magnitude had been calculated using the P-wave pick from the first event on a trace and a coda pick from the last. This has led to an over-estimate of many earthquake magnitudes. In order to avoid these errors, for this project all the events were repicked from the raw seismograms and the locations and magnitudes were recalculated for the entire dataset. This also gave the opportunity to use a three-dimensional velocity model for The Geysers from prior tomographic inversions *(Foulger et al., 1996)*, to locate the earthquakes (Section 4.3.4.2).

4.2 Earthquake Magnitudes

4.2.1 What is an earthquake magnitude?

The first earthquake size scale was developed in 1931 *(Wadati, 1933)*. Earthquake magnitude was introduced by Richter in 1935 *(Richter, 1958)* in an attempt to quantify Californian earthquakes using a scale based on instrumental data called the Richter Local Magnitude scale.

$$M_L=\log_{10}(a) - \log_{10}(a_0(\Delta)) \qquad (4.1)$$

where M_L = local magnitude, a = maximum amplitude measured (after attenuation corrections) and a_0 = maximum amplitude at a epicentral distance Δ for a "zero" earthquake.

Richter selected for a "zero" earthquake one which he thought was the smallest earthquake of interest. Subsequently, still smaller earthquakes became of interest and thus these have negative magnitudes. The Richter Local Magnitude scale has two limitations. First, the earthquake amplitude should be measured on a seismogram recorded by a Wood-Anderson torsion seismometer *(Eaton et al., 1970)*. Second, the amplitude attenuation correction used to calculate M_L may only be valid for earthquakes in southern California. To overcome these difficulties, other magnitude scales were developed, such as the surface wave magnitude *(Gutenberg, 1945)* and the body wave magnitude scales *(Gutenberg & Richter, 1956)*.

Magnitude does not correspond to any physical parameter. However, it is quick and easy to measure and can give a rough idea of the size of an earthquake. Also it may be empirically related to other physical parameters which can be difficult to measure otherwise, such as the seismic moment *(Brune, 1968)* and the energy released by an earthquake *(Gutenberg & Richter, 1956)*.

4.2.2 Coda Magnitudes

Many of the earthquakes recorded by the UNT network saturated the system (Figure 4.4) so making amplitude measurements impossible. Fortunately, the magnitude of an earthquake can also be estimated from the duration of the earthquake *(Real & Teng, 1973)*.

1) A single event (time=07:37:39.860 on 14/4/1991)

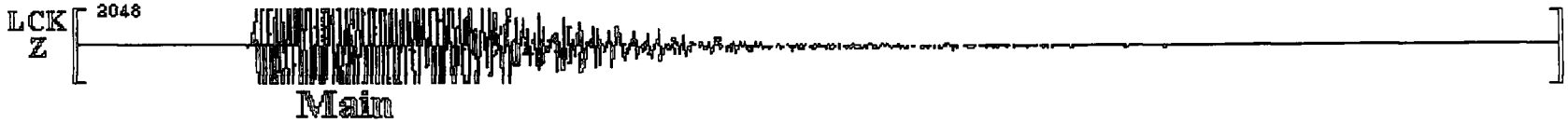

2) A small foreshock before a larger event (time=14:26:07.32 on 25/4/1991)

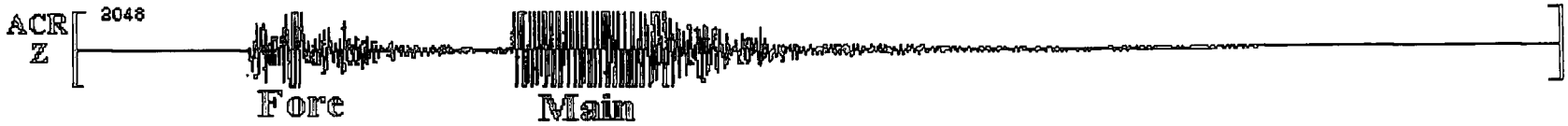

3) Several aftershocks after the main event (time=22:43:51.46 on 5/4/1991)

4) Several aftershocks merging into the main event so giving the appearance of a single large event (time=07:59:03.12 on 4/4/1991)

Figure 4.4 Sample raw seismogram traces from the UNT data set

This is called the coda or duration magnitude, M_d.

$$M_d = a_1 + a_2\log_{10}(\tau) + a_3(\Delta) + a_4h \qquad (4.2)$$

where M_d = duration magnitude, τ = duration of an earthquake or coda length, Δ = epicentral distance from recording station (km), h = focal depth (km) and a_1, a_2, a_3 and a_4 are constants.

Since the duration magnitude scale is empirically calibrated by comparison to other magnitudes, the coda length, τ, may be defined differently for each dataset. In this thesis, the amplitude cut-off threshold was defined as an arbitrary peak to peak amplitude of 100.0 amplitude units for the *W* network and 200.0 for the other two networks (Section 4.1.1). In California, the focal depths, h, of earthquakes are mostly between 1 and 10 km, i.e. within a relatively narrow range. This means that the a_4h term is almost constant, so this term can be combined with a_1. Also, a_3 is very small, typically 0.003 *(Lee et al., 1972)*. Consequently, the magnitude dependence on epicentral distance is also small and the $a_3(\Delta)$ term can be ignored. The simplified equation (Equation 4.3) implies a simple linear relationship between coda magnitude and the logarithm of the coda length of an earthquake:

$$M_d = a_1 + a_2\log_{10}(\tau) \qquad (4.3)$$

4.3 Calculating locations and magnitudes

4.3.1 Conversion of the raw data and file name conventions

The raw UNT seismograms for the period 1989 to 1994 were provided on nine exabyte tapes by Doug Neuhauser at the NCEDC. The data were in UNOCAL Corporation PCQL trace file (standard input default) format and consisted of ~ 25-35,000 seismograms per year - a total of approximately 20 Gbytes of data. Since a

limited amount of disk space was available, raw seismograms were read off the exabyte tapes in batches of ~ 200 days at a time, processed and then deleted. The catalogue files for each batch of 200 days were then concatenated into a single catalogue file when all the seismograms had been processed. The data were converted into the XDR (External Data Representation) version of Lamont's AH (AdHoc) format, using the program ***pcql2ah***, *(B. Julian, pers. comm.)*, incorporated into a shell script called ***pcql2ah_script*** (Appendix 1). ***pcql2ah*** inputs a list of stations for each of the recording networks to conduct the conversion.

Each event file was identified by a unique file name. The PCQL files were named using the format:

19yy/19yy.ddd/dddtime.netyear

where *yy* = year, *ddd* = day of year, *time* = the time in hours, minutes and seconds, expressed in hexadecimal, and *net* is the network that recorded the data (either *W*, *G* or *F*).

A similar scheme for the AdHoc (AH) data files was adopted:

net/netyyddd/ddd.hhmmss.n.ah

where *n* = the earthquake number on the trace, *hh* = time expressed in hours, *mm* = minutes and *ss* = seconds. A list of the traces contained within each file, i.e. the traces associated with a single earthquake, was created using a script called ***mkahlist*** (*B. Julian, pers. comm.*). These files were given the suffix '.list'. Output files containing picks from the raw seismograms were given the suffix '.ep' if they were hand-picked, or '.ap' if they had been picked automatically.

4.3.2 P and coda picks

4.3.2.1 autopick

Since the UNT raw seismogram dataset was so large, an automated picking method was adopted. The programs developed were based on the program ***autopick*** (*R. Crosson, Mary O'Neill and Angus Miller, pers. comm.*), which can measure P-wave arrival times, polarities and qualities from digital AH seismograms.

The ***autopick*** algorithm is based on the ratio of two sliding, triangularly weighted sums of the seismogram amplitudes, called an 'fbcurve'. Such a curve is expected to have a maximum value at the arrival time of a seismic phase. To make a P-wave pick, ***autopick*** makes two passes along each trace and calculates an 'fbcurve' for each pass. The first pass uses the entire seismogram to detect whether there are any phase arrivals that could be P-waves and to calculate an approximate arrival time. The second pass uses a more detailed 'fbcurve' to refine the pick in the portion of the seismogram identified in the first pass. To achieve this, the area of interest is processed using a low pass filter, and an 'fbcurve' with narrower triangles is calculated using the absolute seismogram amplitudes. In both cases, a pick is only made if the 'fbcurve' meets certain user-defined threshold criteria. If a pick cannot be refined, it is discarded.

The output from ***autopick*** was in the binary form used by the seismogram analysis program ***epick*** which was used to verify the ***autopick*** results. P-wave picks were marked with a 'P' when verified using ***epick***.

*4.3.2.2 **noisepick***

noisepick** (Miller, 1996)* is a simplified version of ***autopick. Using the output from ***autopick*** as input, ***noisepick*** measured the root mean square of the ambient noise for the second before the P-wave pick. The noise-level pick made by this program is written to the .ap file. Noise picks were marked with a 'N' when verified using ***epick***. ***noisepick*** was used for two purposes. The first was to gauge the noise level over a subset of the data to find an acceptable noise threshold for the rest of the UNT dataset. The subset used was April 1991, from which 13,245 samples were picked. The noise threshold, above which data were discarded, was defined as the value less than or equal to the noise in 80% of seismograms, and was 10.75 uncalibrated amplitude units (Figure 4.5). The output format of the original version of ***noisepick*** was modified by the author so that the P-wave picks and output from ***noisepick*** could be read by ***codapick*** (Section 4.3.2.3).

4.3.2.3 codapick

This program is an adaptation of ***autopick*** by the author, based on an algorithm by *Lee et al. (1972)*. A coda pick is made where the seismogram peak-to-peak amplitude falls below an arbitrary amplitude threshold. In practice, a modified algorithm had to be adopted because of the types of seismograms encountered. The arbitrary amplitude threshold had to be set at a higher level than the ambient noise level. Some sample seismograms were analysed manually and a suitable value chosen. Due to different network gains, the amplitude threshold was 100 uncalibrated amplitude units for the *W* network and 200 uncalibrated amplitude units for the other two networks.

Measuring the first time where the peak-to-peak amplitude falls beneath the arbitrary amplitude threshold may produce anomalously small coda lengths since real earthquakes do not decay uniformly. Thus the coda picks were made where

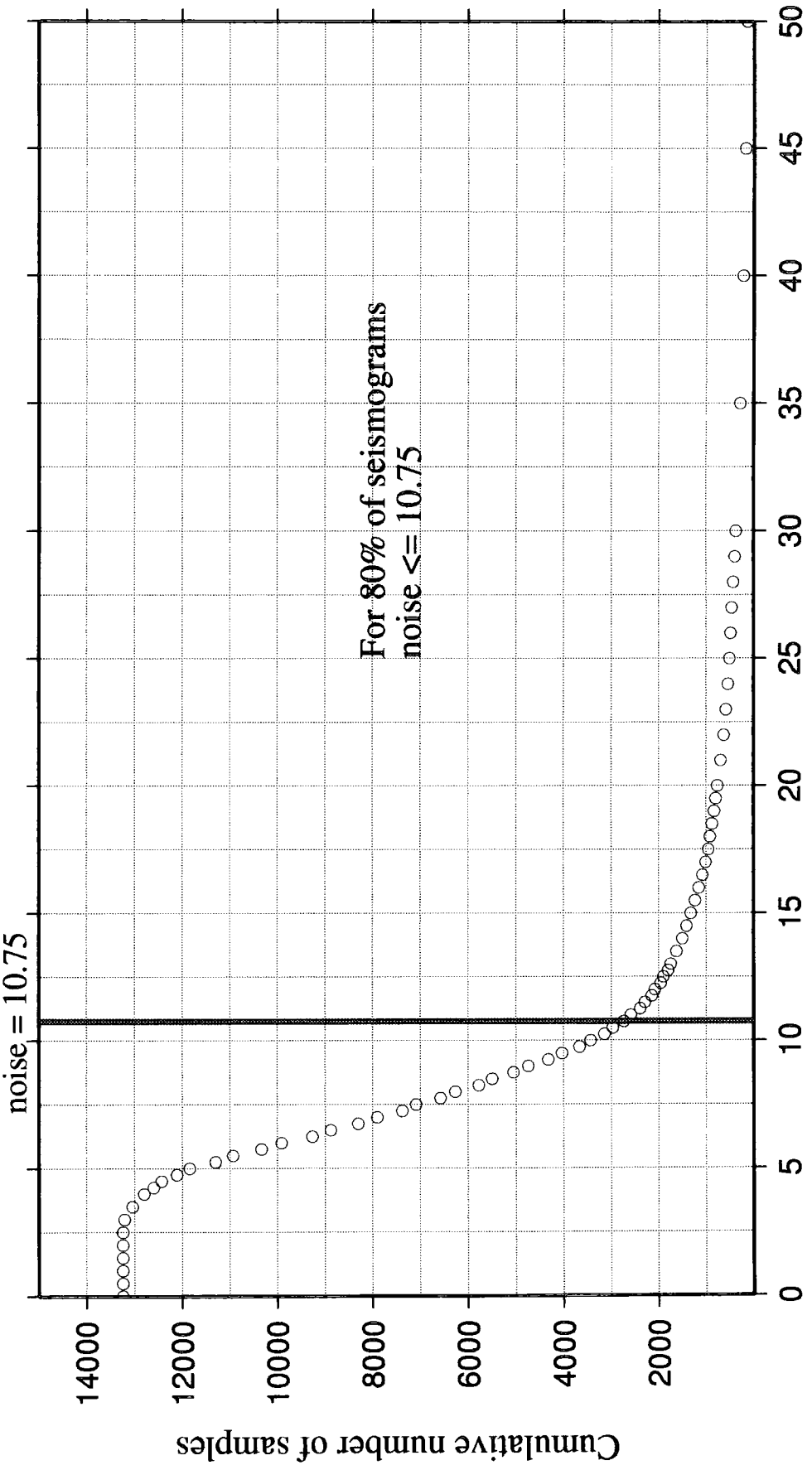

Figure 4.5 Plot of cumulative number of samples against RMS noise for UNT seismicity from April 1991.

the peak-to-peak amplitude fell below the arbitrary threshold magnitude and remained so for one second.

Some earthquakes were observed where a small-amplitude P-wave decayed into noise before the arrival of the S-wave. Consequently, the coda pick would be made before the arrival of the S-wave in these cases. This problem was solved by identifying the largest peak-to-peak amplitude between the P-wave pick and end of the seismogram and making the coda pick where the event signal had decayed after the maximum amplitude point. ***codapick*** is listed in Appendix 2. The output from ***codapick*** was also written to the .ap file. Coda picks were labelled 'Coda' where checked using ***epick***.

4.3.2.4 Other pick information

Only the vertical components from the three-component stations were processed. Station SQK was incorrectly labelled. Instead of the vertical and the two horizontal components being labelled SQK(Z), SQK(X) and SQK(Y), as was the case for the other three component stations, they were labelled SQK(Z), SQKX(Z) and SQKY(Z). This was also seen occasionally for stations FUM, FNF and DVB. When this occurred, the X and Y components were filtered out. During the sample month used for the magnitude calibrations (April 1991), seven different traces were given the label SQK(Z). Since it was not possible to differentiate between traces that had been correctly labelled and those that had not, traces from this station were discarded.

The picking programs described above were incorporated into a Bourne shell script called ***ah2codapick*** (Appendix 3). Figure 4.6 is a flow diagram for ***ah2codapick***.

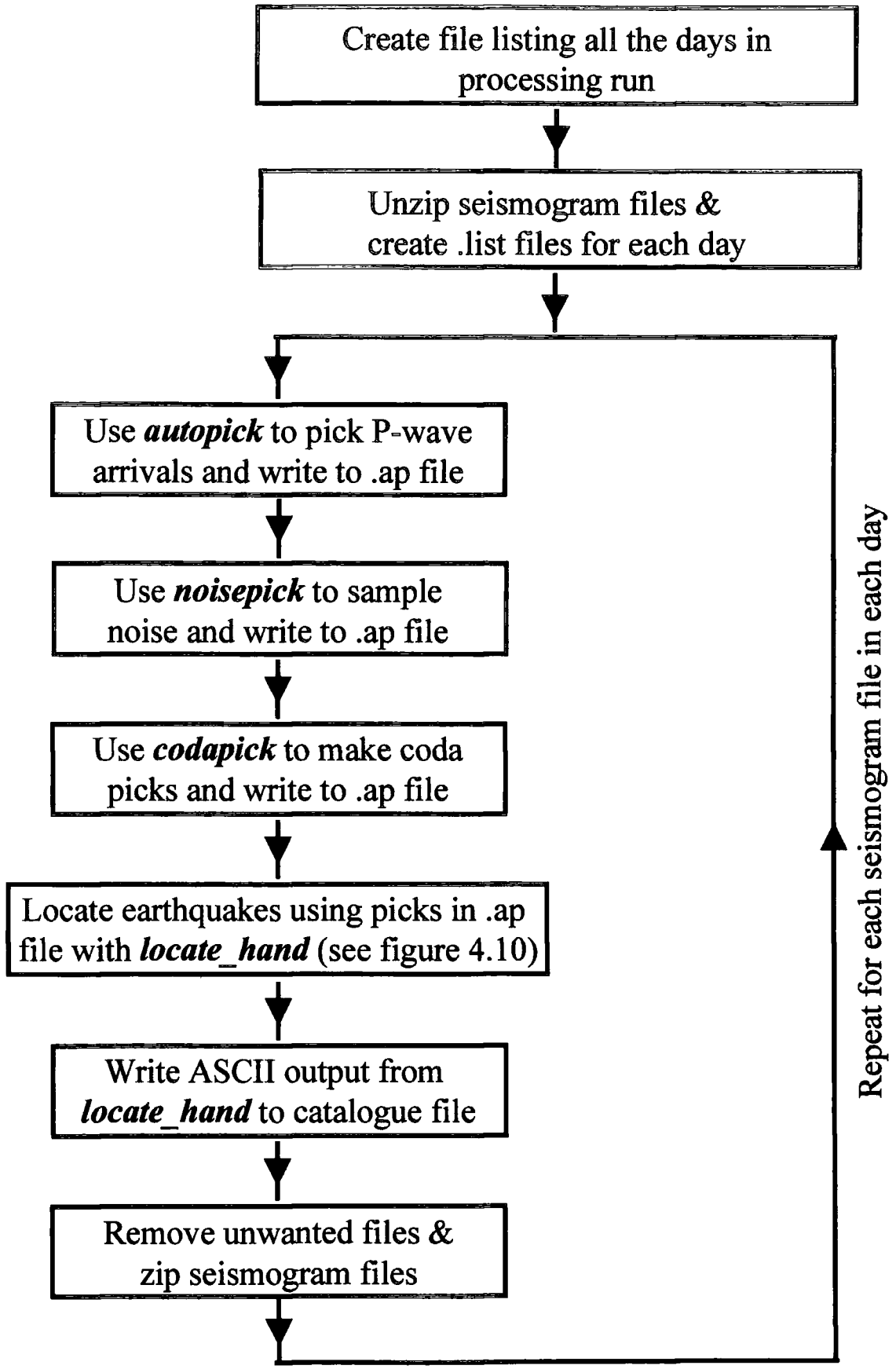

Figure 4.6 Flow diagram for program ***ah2codapick***

4.3.3 Calibrating the coda lengths to obtain magnitudes

Equation 4.3 gives the relationship between magnitude and coda length. To find the values of the calibration constants a_1 and a_2, the measured coda lengths were compared with a known dataset of magnitudes. The NCSN dataset was chosen, and events from April 1991 present in both the UNT and NCSN datasets were identified. The UNT coda length durations for the calibration were initially measured using the automated picking routines described above, but the large number of multi-event traces caused an overestimate of the number of larger earthquakes. Hand picking each of the calibration events, though laborious, guaranteed that each had been correctly picked.

Calibration plots of NCSN magnitude against the logarithm of the coda length were plotted for each UNT station. Plots of this type exhibit a slight curvature, increasing with severity at higher magnitudes *(Lee et al, 1972; Real & Teng, 1973; Lee & Wetmiller, 1976; Bakun and Lindh, 1977)*. However, for the range of magnitudes of events from The Geysers ($0 < M_d < 4$) this phenomenon was not observed, so it was assumed that a straight line would be the best fit to the data. The straight line was fitted using minimum deviation and least squares fitting methods *(Press et al., 1988)*. Since no two recording stations would have identical instrumentation calibration nor nearby geological conditions, each station had its own values for a_1 (the intercept on the calibration graph) and a_2 (the gradient). Using the minimum deviation method it was found that $0.09 < a_1 < 0.71$ and $1.41 < a_2 < 2.09$. For the least squares method, $-0.04 < a_1 < 0.48$ and $1.70 < a_2 < 2.09$. The least squares fit method results for a_1 and a_2 were a better fit to the data, so these were used to calculate UNT magnitudes.

During April 1991, the stations DNV, INJ, MNS, TCH, U14 and WRK all exhibited poor signal-to-noise ratios, so making it difficult to pick a reasonable number of P-wave and coda picks for these stations. These stations were thus not calibrated. Table 4.2 shows the number of events picked for each of the remaining

sixteen UNT stations, plus their values for a_1 and a_2. Figure 4.7 shows the correlation plots for ACR and LCK.

Table 4.2 Magnitude - Coda duration data for the NCSN calibrated UNT stations

Station Name	*Number of Hand Picks*	*least squares fit*		*minimum deviation fit*	
		a2	*a1*	*a2*	*a1*
ACR	150	1.711	0.207	1.415	0.371
ANG	91	1.906	0.236	1.722	0.380
BUC	94	1.893	0.362	1.954	0.329
CAP	128	2.010	-0.049	1.871	0.035
CLV	120	1.873	0.225	1.592	0.350
DES	76	1.921	0.145	1.508	0.433
DRK	113	1.706	0.189	1.575	0.246
DVB	59	1.942	0.223	1.797	0.313
DXR	93	1.808	0.230	1.839	0.224
FNF	81	1.873	0.336	1.587	0.504
FUM	131	1.725	0.210	1.629	0.251
LCK	106	2.006	-0.083	1.745	0.091
PFR	38	2.006	0.480	1.574	0.709
SB4B	86	1.791	0.306	1.792	0.289
SSR	33	2.091	0.258	2.093	0.256
STY	71	1.928	0.376	1.600	0.593

4.3.4 Locating the events

4.3.4.1 qloc

The earthquakes were located using program ***qloc*** *(B. R. Julian, unpublished program)*, controlled by the UNIX Bourne script ***eloc***. ***qloc*** performs an iterative, damped inversion of P-wave arrival time data from each recording station to minimise the sum of the travel time residuals. The initial hypocentral estimate for each earthquake was a point 3 km below sea level directly beneath the station. The UNT earthquakes were located using both one-dimensional and three-dimensional velocity models.

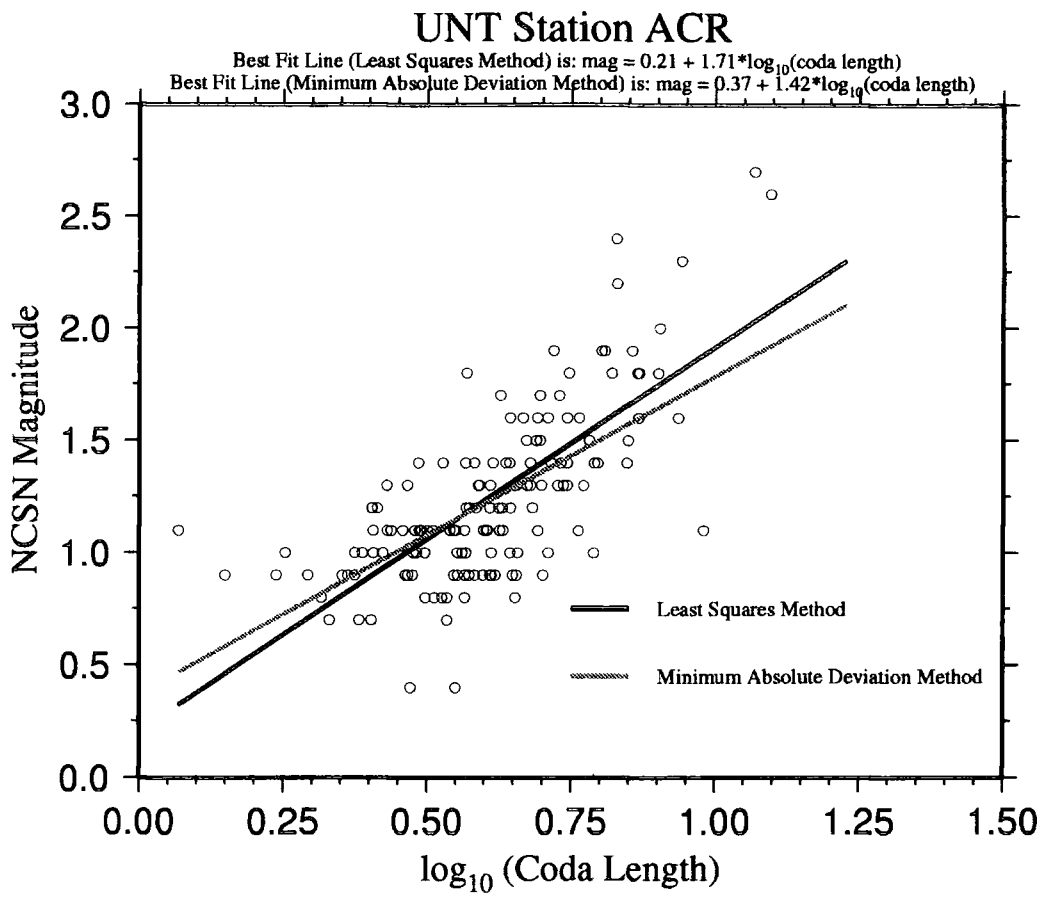

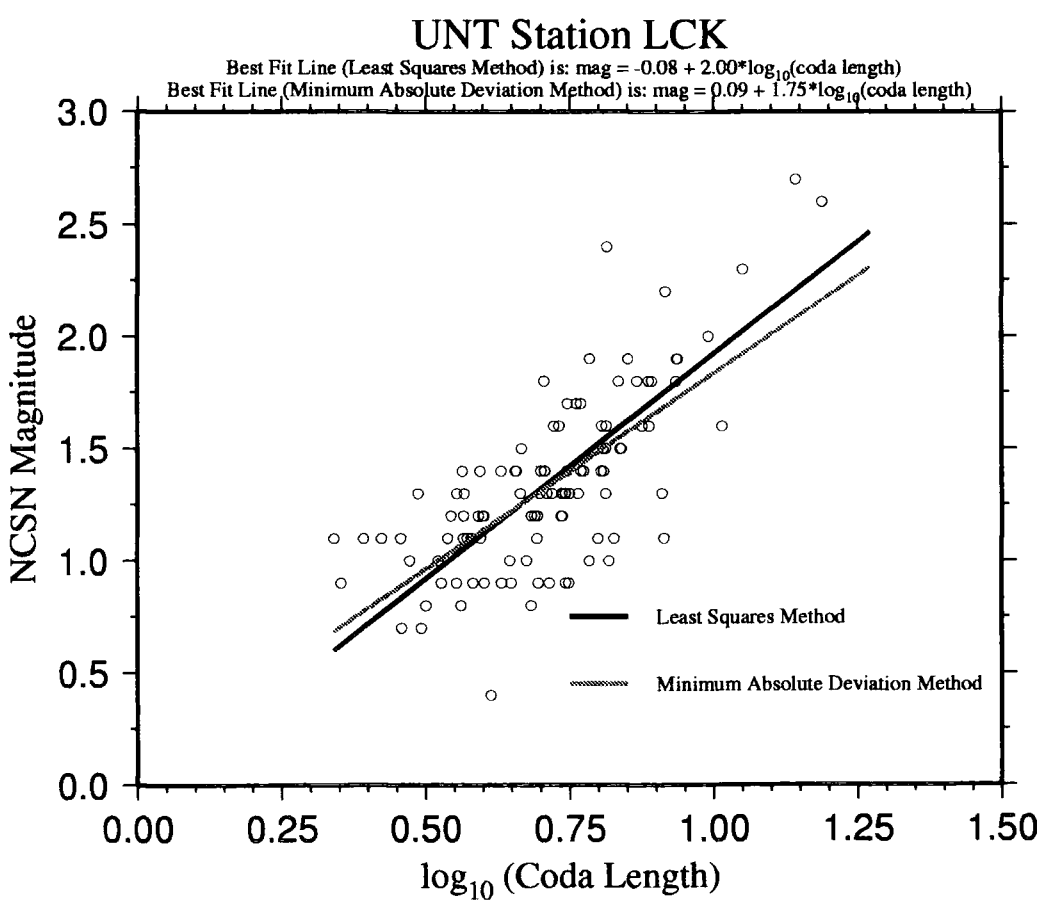

Figure 4.7 Sample correlation plots between UNT coda lengths and NCSN magnitudes.

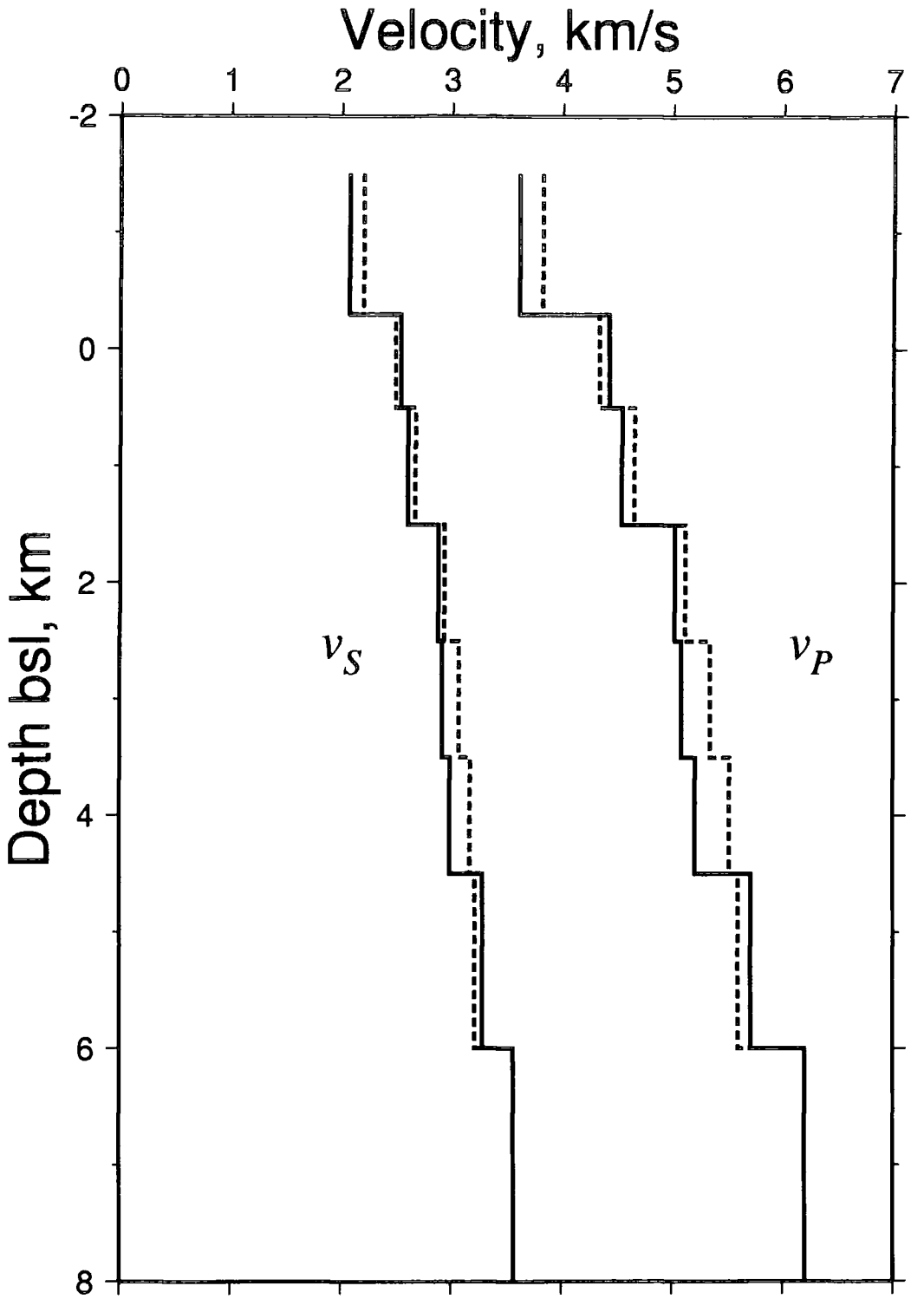

Figure 4.8 One-dimensional v_p model derived from VELEST (black line). The regional one-dimensional v_p model is represented by a dashed line. The one-dimensional v_s model was calculated from v_p model assuming a constant v_p / v_s ratio of 1.74. The regional v_s model was calculated from the v_p model assuming a v_p / v_s ratio of 1.80 *(from Ross, 1996).*

4.3.4.2 The one- and three-dimensional velocity models used

The one-dimensional velocity model used for this work had been generated from local earthquakes using the inversion program *velest (Kissling et al., 1994; Ross, 1996)*. By simultaneously updating hypocentral locations and travel times, the inversion program iteratively improved estimates of the one-dimensional velocity model until the best fit for the set of earthquake travel-time measurements was generated (Figure 4.8).

The three-dimensional Geysers velocity model used *(Julian et al., 1996)* was created by a tomographic inversion of local earthquakes arrival times. It was generated using 4032 P-wave and 944 S-wave arrival times from 185 earthquakes recorded by UNT and the IRIS network (Section 3.3.3) in 1991. The study area was 20 x 20 km with a depth range of -1 to 6 km. Arrival times were measured to an accuracy of 0.01 seconds for P- waves and 0.02 seconds for S- waves.

The tomographic inversion was done using the ***SIMULPS12*** program *(Eberhart-Phillips, 1993)*, which solved for V_p and V_p/V_s simultaneously with earthquake locations and crustal structure using a iterative least squares method. Compared with the initial one-dimensional model, the final three dimensional model gave a 70% reduction in variance, with RMS residuals of 0.022 seconds for P-waves and 0.048 s seconds for S- waves.

The maximum resolution of the V_p model was ~ 1 km (Figure 4.9). V_p was 10% lower in north-west Geysers compared to the Central Geysers area. This anomaly, coincident with the HTR (Section 3.2.4.1), probably reflects variations in lithology, temperature or increased compressibility of the pore fluid. There is a shallow low velocity anomaly centred on Cobb Mountain coinciding with mapped units of the Clear Lake volcanics (Section 3.2.2). The low velocity anomaly to the north-east of the Collayomi fault correlates with the Clear Lake volcanics at shallow depths and the Coast Range Ophiolite at depth.

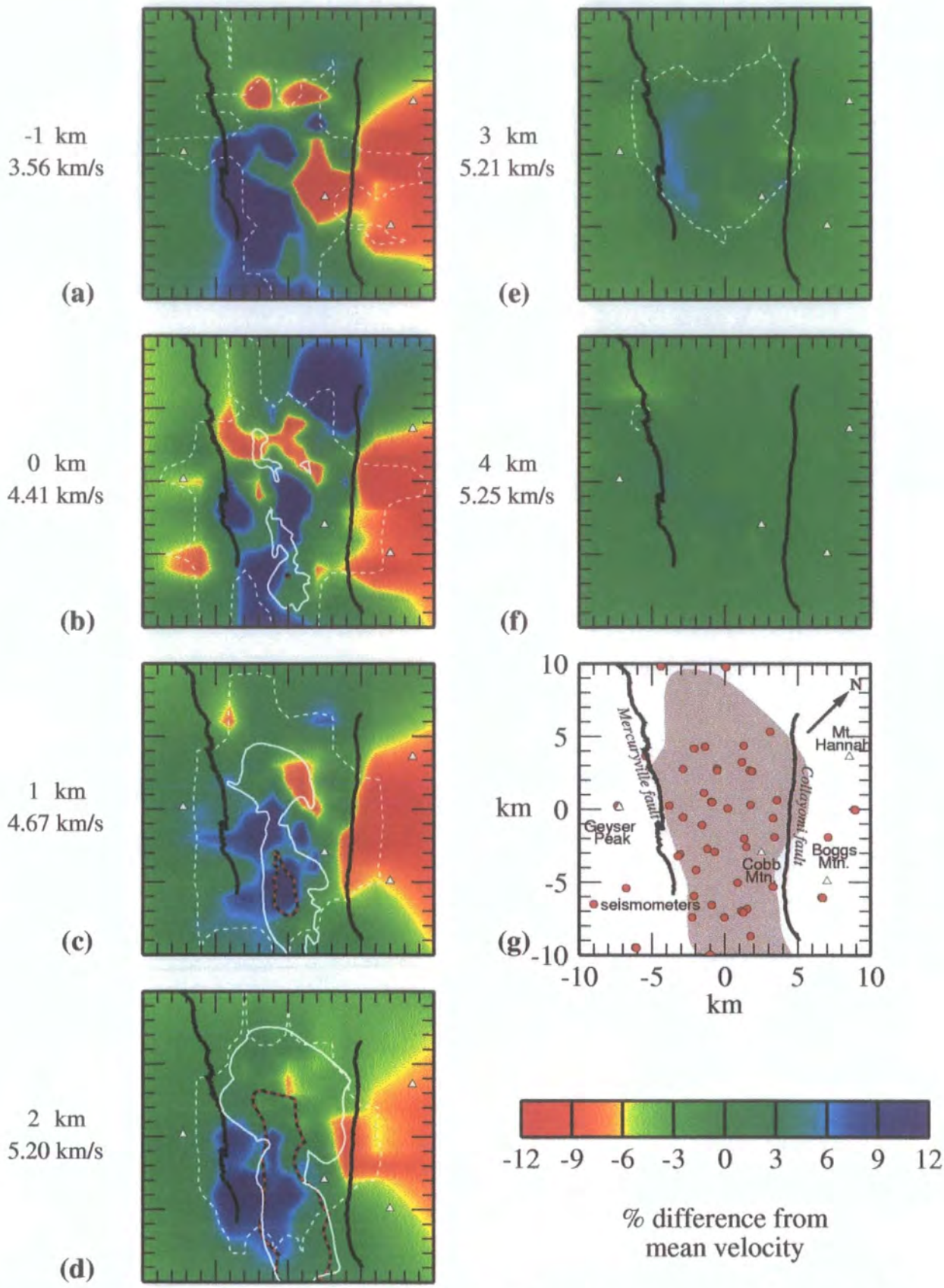

Figure 4.9a. Maps showing percentage variation in v_p from mean values for horizontal depth slices through the model (values to the left of map). The location map (g) details surface features within the modelled volume including the 1992 production area (shaded) and seismometers (red circles). Areas enclosed by white dashed lines (a-f) are well resolved (spread < 4 km). Solid white lines: boundary of steam reservoir; black and red lines: boundary of the felsite batholith; white triangles: mountains; black lines: faults *(from Ross, 1996).*

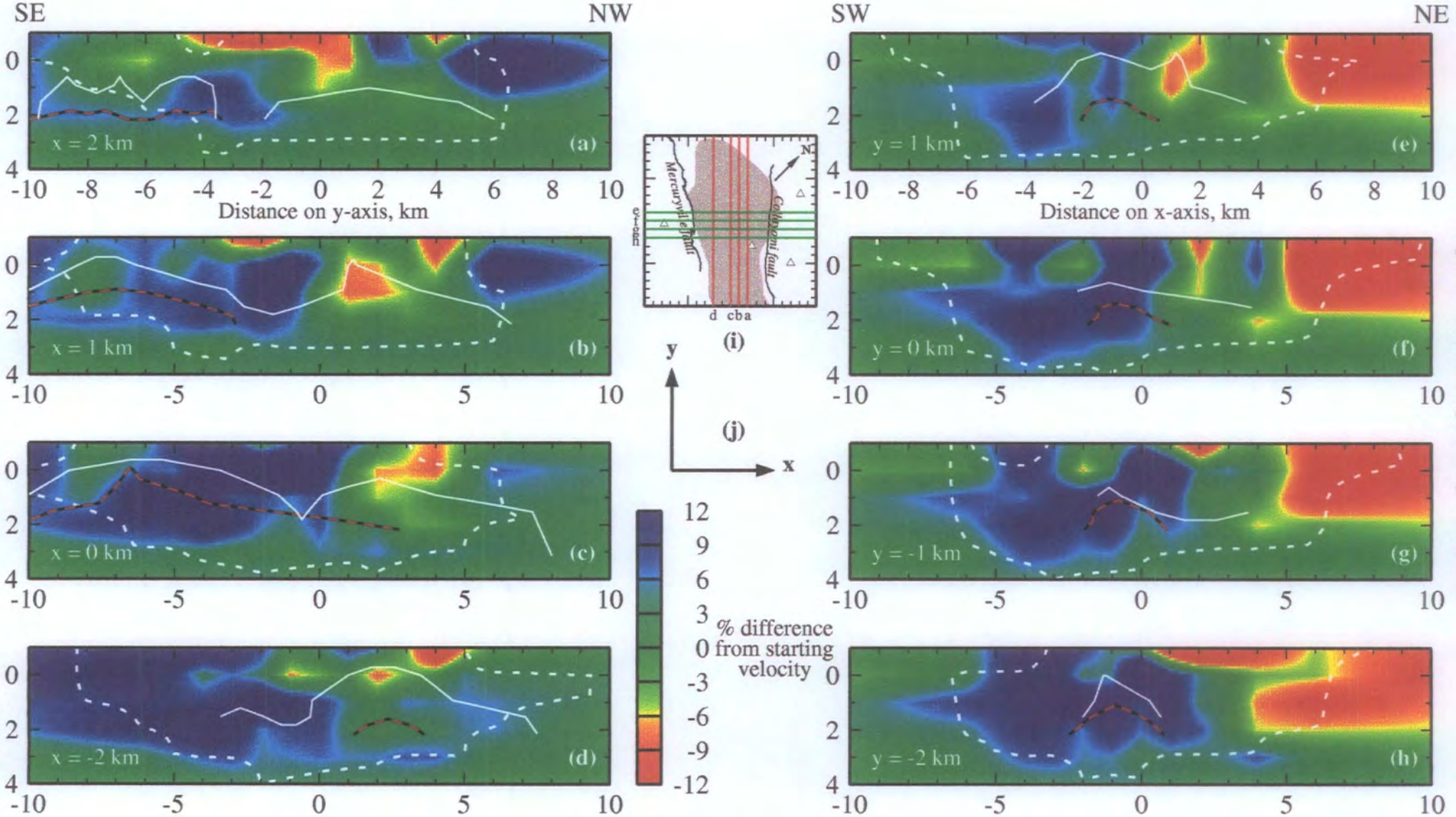

Figure 4.9b Cross-sections through the v_p model showing percentage difference from mean layer velocity. (a-d) Southeast-northwest cross-sections. (e-h) Southwest-northeast cross-sections. The same convention is adopted as in Figure 4.9a. (i) Map of the model volume showing principal surface features. Red lines: cross-sections (a-d); green lines; cross-sections (e-h)*(from Ross, 1996)*.

4.3.4.3 locate_hand

The Bourne shell script ***locate_hand*** was used to locate each earthquake using ***eloc*** (Section 4.3.4.1), calculate the magnitude using each trace and to remove traces containing multiple events where the main event on the trace had not been auto-picked (Figure 4.10; Appendix 4). The script worked as follows. First, the RMS residual time was examined. If the main event had been chosen correctly, the RMS residual would be low, say ≤ 0.3; if not, it would be much higher. Traces with high RMS residuals were discarded. The mean magnitude and its standard deviation were calculated using the magnitudes from the remaining traces. Magnitudes that were less than or greater than one standard deviation from the mean were discarded. These discarded magnitudes corresponded to traces where either the main event had not been picked or the main event signal was poor and consequently the coda length had been underestimated. Finally, the mean of the magnitudes obtained for the remaining traces was calculated.

In addition to calculating the location and final magnitude, for each event information regarding how many P-wave, noise and coda picks had been made, how many traces had been used to locate the earthquake and M_{dcount}, the number of magnitudes that had been used to calculate the final value of M_d, were written to the catalogue files. Since the operating parameters used in ***eloc*** prevented the program from locating earthquakes at or above 0 km, events located at these depths were discarded.

4.4 Results

4.4.1 Introduction

The final results, for events between 1989 and 1994, consist of hypocentral locations calculated using both the one-dimensional and the three-dimensional

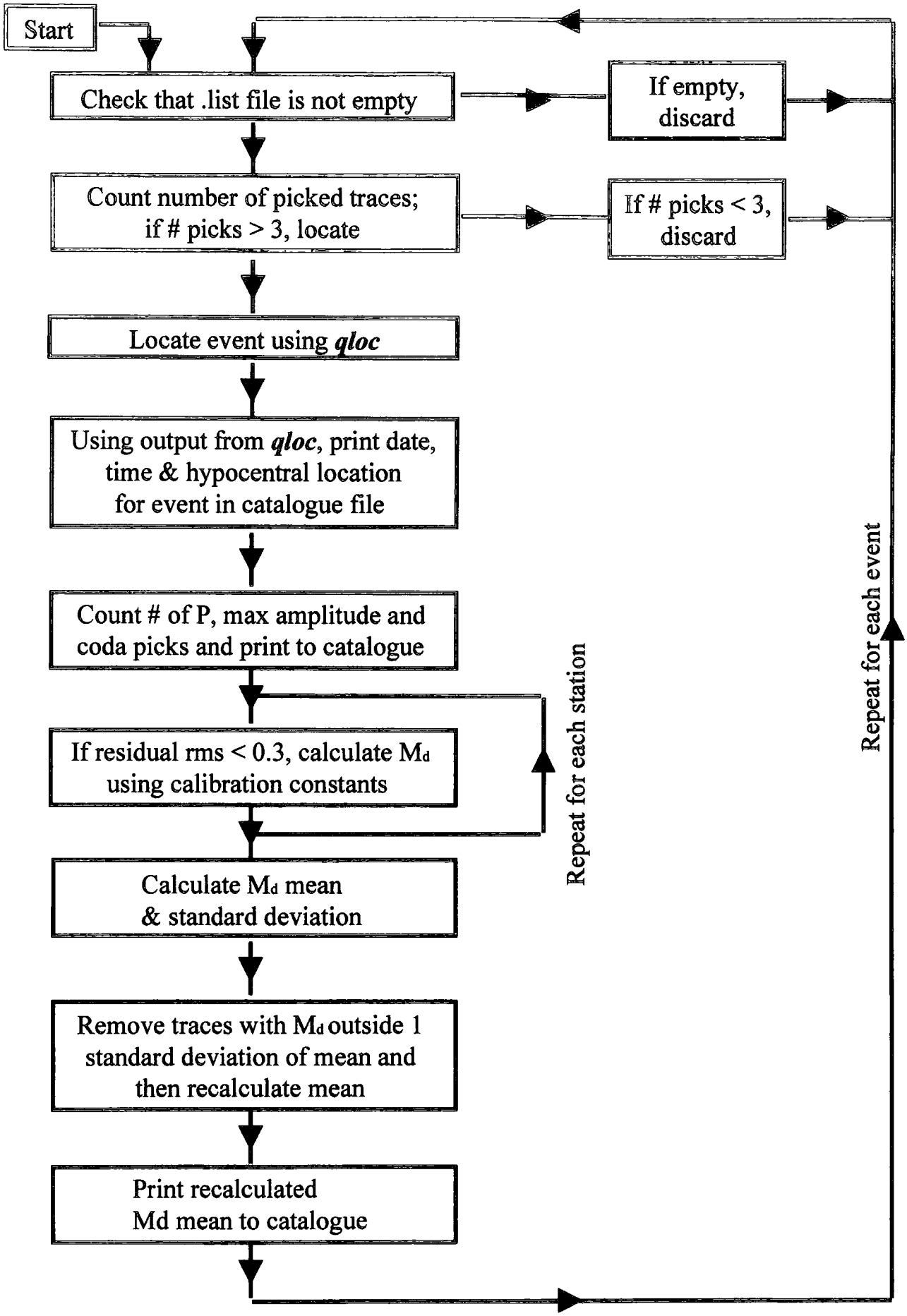

Figure 4.10 Flow diagram for program ***locate_hand***

velocity models, and magnitudes for 38,296 events. This catalogue is henceforth referred to as 'the Barton catalogue'. Before analysing the results further, it was necessary to remove events that were poorly located or with poorly determined magnitudes.

4.4.2 Location errors

This research project concerns spatial variations in the fractal dimension for which accurate locations are required. An estimate of the location errors was obtained by comparing the automatic locations, calculated as part of this project with manual locations by a fellow student using the Geysers IRIS dataset *(Ross, 1996)*. That dataset included 500 events of which 296 were used in the tomographic modelling. For the rest of this thesis, the 'IRIS dataset' refers to those 296 high-quality, manually located events.

Ross (1996) quotes event location errors for the IRIS dataset using the one-dimensional velocity model as ± 0.4 km in the horizontal and ± 0.7 km in the vertical. Figure 4.11 is a map of the relative change in hypocentral location for the 168 common events in the IRIS dataset and the Barton catalogue. The mean differences in horizontal and vertical locations were calculated ignoring the best and worst 5% (Figure 4.12). These were found to be ~ 0.26 km and ~ 0.58 km respectively.

For the three-dimensional model, *Ross (1996)* quotes the IRIS location errors at about ± 0.2 km. Figure 4.13 is a map of the relative change in hypocentral location for three-dimensional locations in the IRIS dataset and the Barton catalogue. The differences are much smaller than when using the one-dimensional model. The mean differences in locations are ~ 0.17 km and ~ 0.24 km in the horizontal and vertical respectively. The three-dimensional tomographic model was created using data from April 1991. The reservoir is known to be constantly evolving as it is changed by production activities *(Ross et al., 1998, in press)* so the

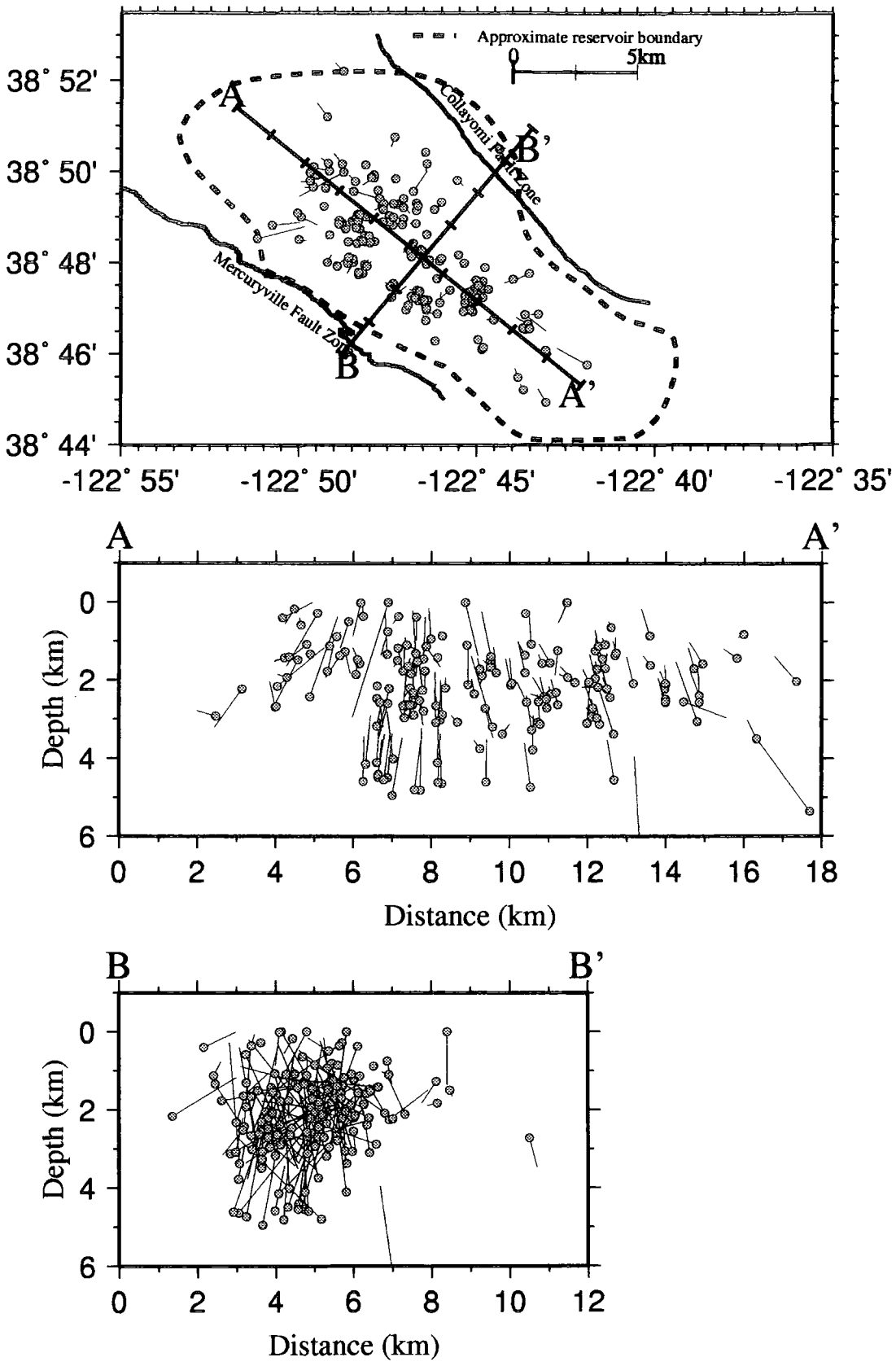

Figure 4.11 Map of The Geysers showing the differences in hypocentral location between IRIS and Barton catalogue events located using a 1-D velocity model for April 1991. Filled circles are the Barton catalogue and a vector connects them to the IRIS location.

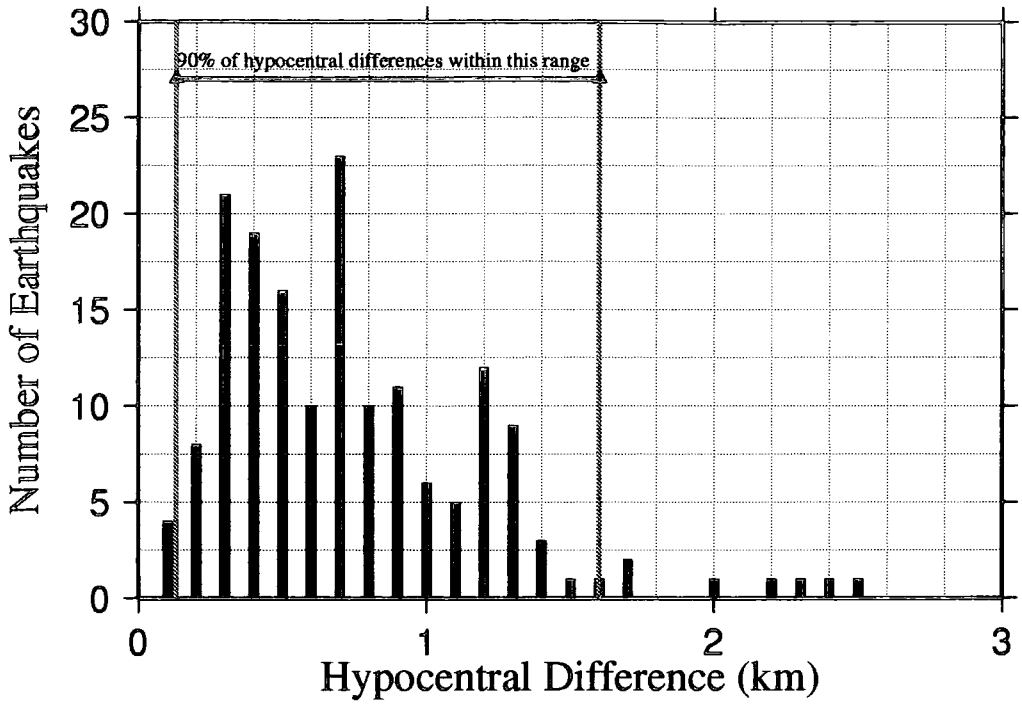

Figure 4.12a Histogram of hypocentral difference against number of earthquakes for IRIS and Barton catalogue locations when located using the one-dimensional V_p model.

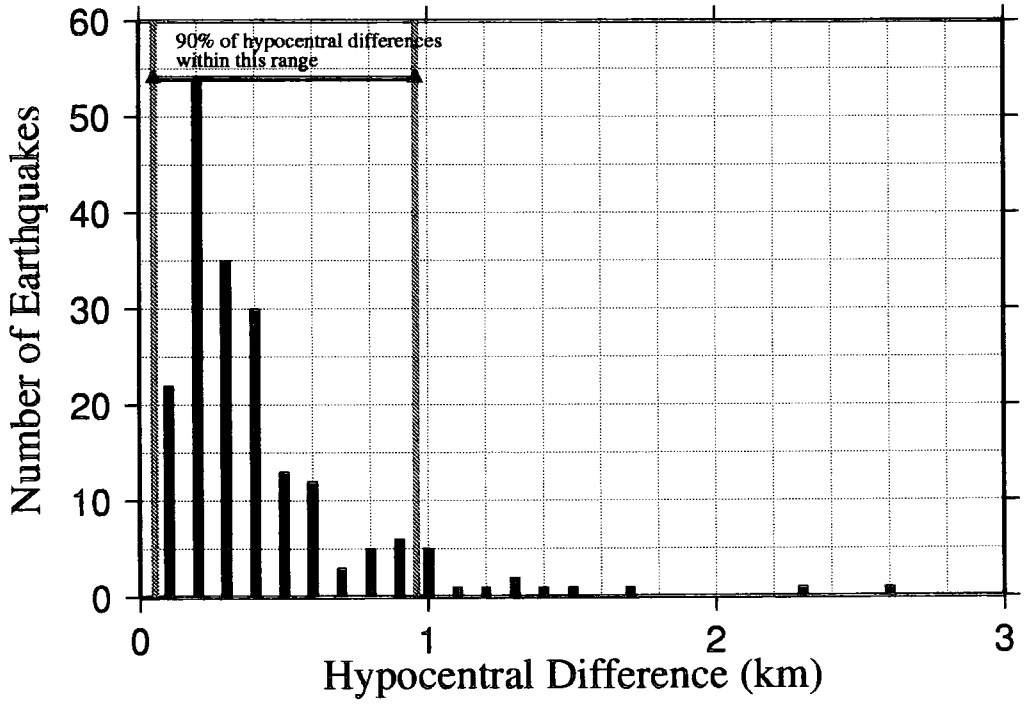

Figure 4.12b Same as Figure 4.12a except for a three dimensional V_p model.

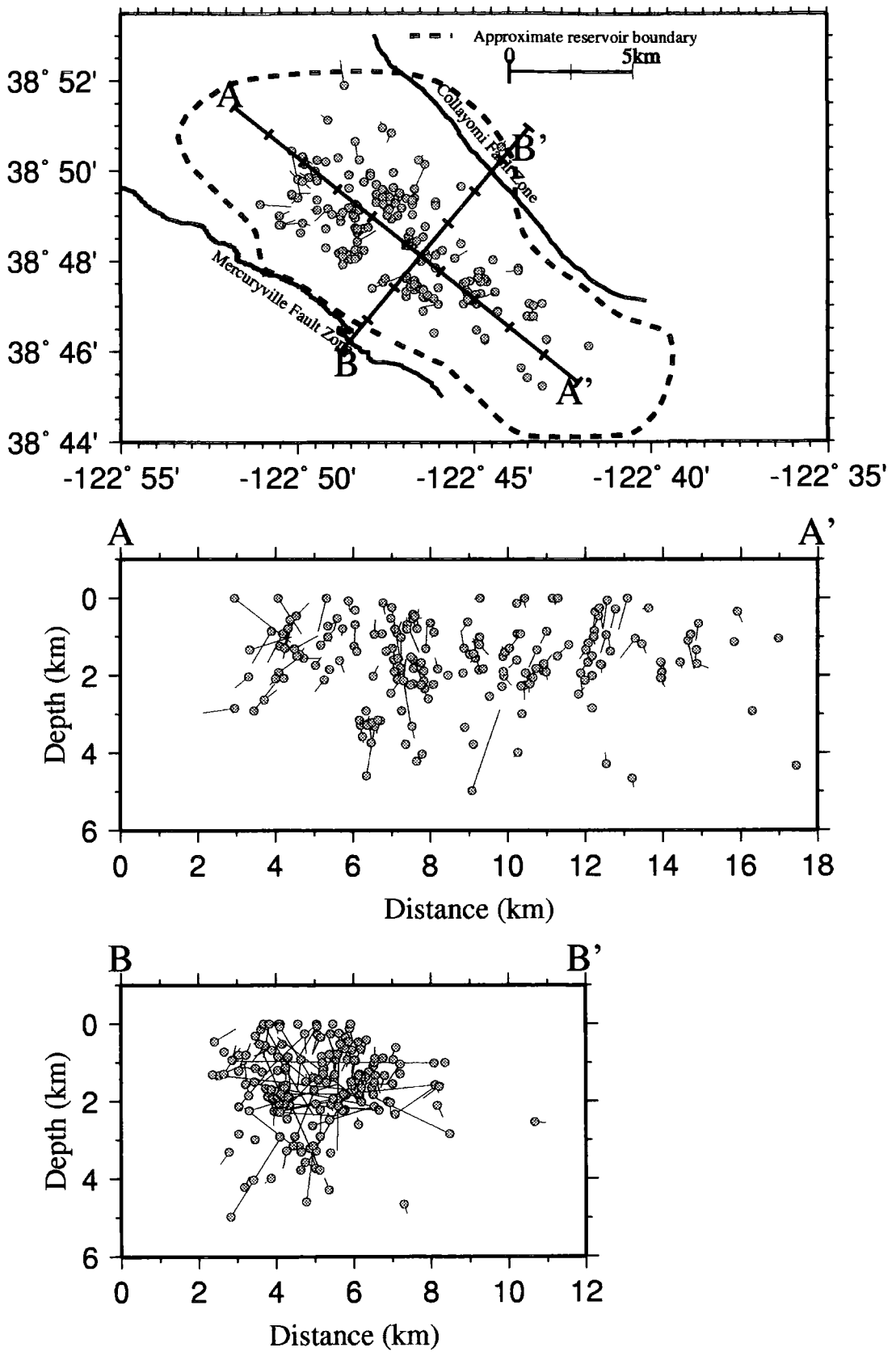

Figure 4.13 Same as Figure 4.11 except for events located using a three-dimensional velocity model.

tomographic model is only an accurate representation of the velocity structure during this month. This effect is probably insignificant, however.

Figure 4.14 shows epicentres calculated using the one-dimensional and three-dimensional models for events in the Barton catalogue where at least four P picks were available. The three-dimensional locations exhibit tighter clustering and less inter-cluster scattering than the one-dimensional locations. Consequently, the locations made using the three-dimensional velocity model were used in further analysis.

4.4.3 Magnitude and M_{dcount}

The number of traces used to calculate the final magnitude, M_{dcount}, was used as a rough guide to gauge how well an event had been located. For the vast majority of earthquakes, $2 \leq M_{dcount} \leq 6$ (Table 4.3). Figure 4.15 is a series of maps showing the epicentral distribution of earthquakes over the study period for $M_{dcount} \geq 1$, $M_{dcount} \geq 3$ and $M_{dcount} \geq 6$ using the locations made with the three-dimensional velocity model.

Table 4.3 Number of events for different values of M_{dcount}

M_{dcount}	# of events	M_{dcount}	# of events
1	1070	9	556
2	16306	10	245
3	8653	11	59
4	5756	12	9
5	3561	13	0
6	2490	14	0
7	1660	15	0
8	1065	16	0

For $M_{dcount} \geq 1$, several large clusters of earthquakes concentrated mostly in the north-western and central parts of The Geysers. There is a uniform scatter of events over the entire field obscuring this clustering, particularly in the north-west. The shape and extent of the clustering is more obvious for $M_{dcount} \geq 3$. The

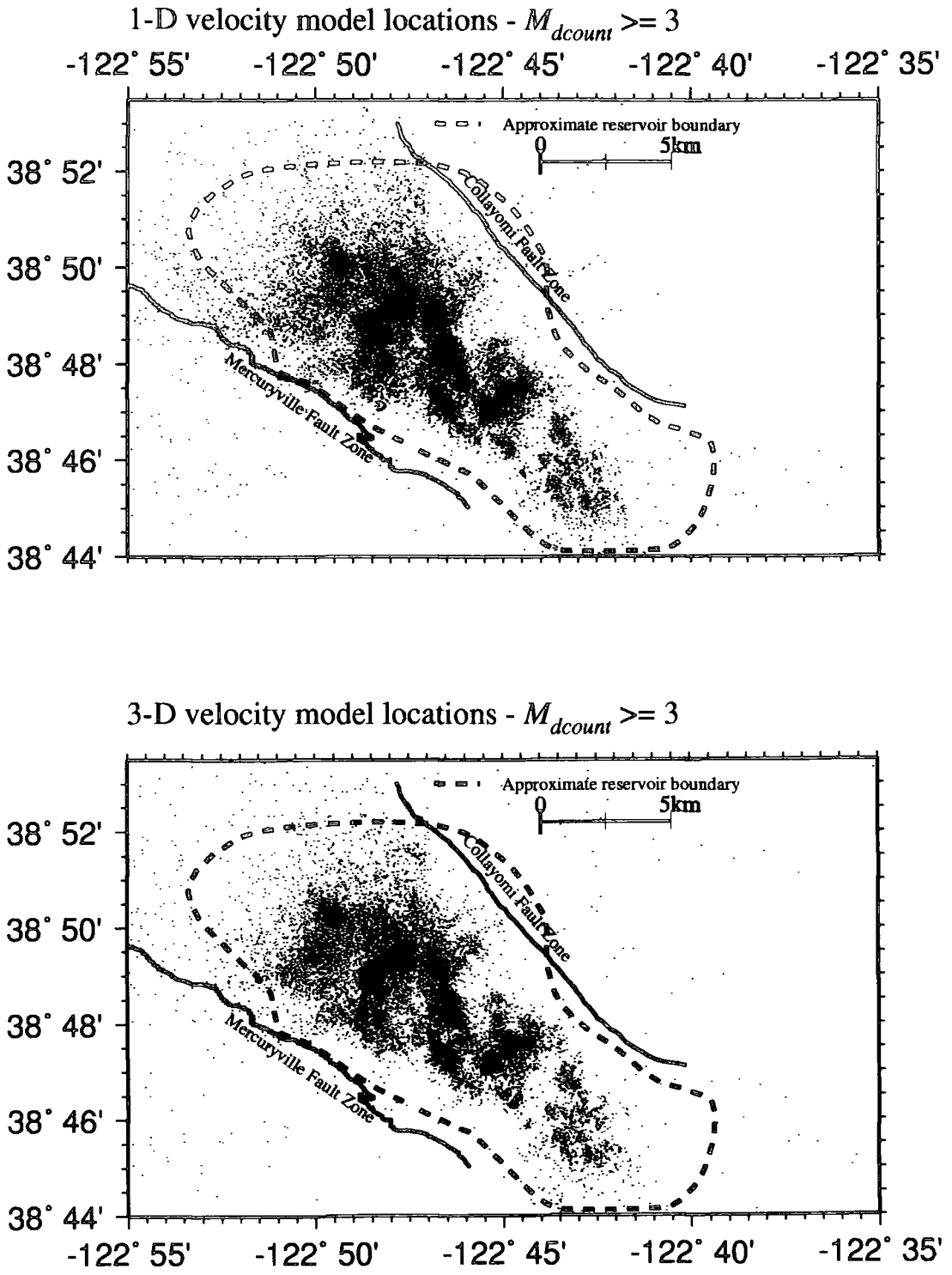

Figure 4.14 Maps of The Geysers showing the epicentral distributions of Barton catalogue earthquakes that occurred between 1989 and 1994, located using one and three dimensional velocity models.

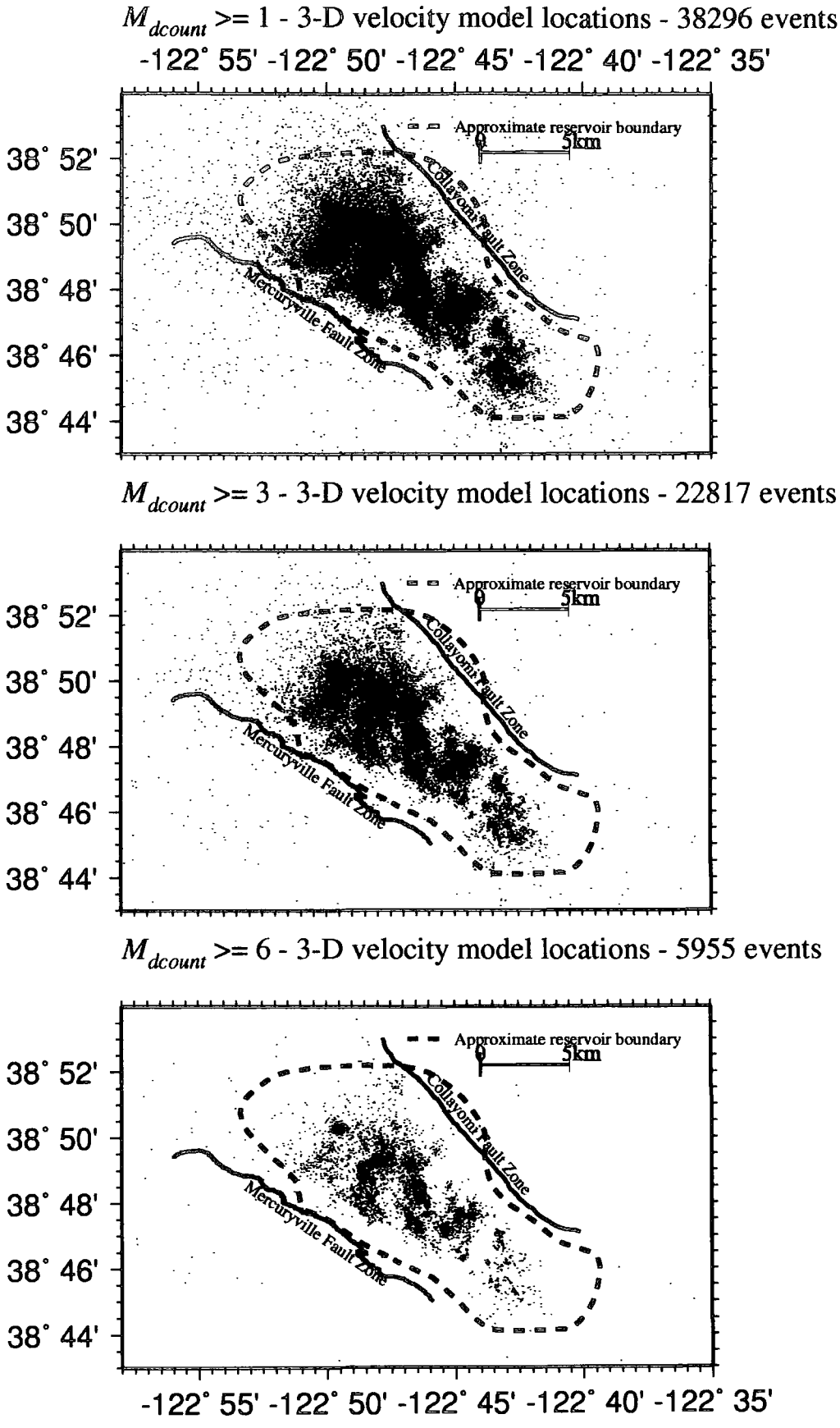

Figure 4.15 Maps of The Geysers showing the epicentral distributions of Barton catalogue earthquakes that occurred between 1989 and 1994, for different values of M_{dcount}.

majority of the scatter in the north-west of the field is not present in this subset of events and the clusters are tighter and better defined. In the southern central part of the field, sub-clusters are visible. In the case of the subset of locations where $M_{dcount} \geq 6$, clusters and sub-clusters are easily seen. However, this dataset contains only 5955 events and would be too small for a fractal and *b*-value analysis, except one encompassing the entire field. On the basis of these results, the dataset defined by $M_{dcount} \geq 3$, which contained 22,817 events, was analysed for this thesis.

4.4.4 Hypocentral distribution

Figure 4.16 shows cross-sections of the Barton catalogue events for which $M_{dcount} \geq 3$. Seismicity in The Geysers is almost exclusively confined to the area between the Mercuryville and Collayomi fault zones, with the vast majority of the earthquakes occurring between 0 and 4 km below sea level. Most of the production during the study period occurred in the north-west and central parts of the field. In the most heavily exploited parts of the field, there is more seismicity and more earthquakes at greater depths than in the less developed areas. The seismicity forms an epicentral band 6 km wide in the developed areas, but is only 3 km wide in the south-eastern area.

In the north-west Geysers there is a broad diffuse band of seismicity that marks the northernmost extent of the production area seismicity. Beyond this, there is little or no seismicity. This feature is a distributed cloud of earthquakes of approximately uniform event density which dips at an angle of 45^0 to the north-west to a depth of 3 km. In the north-eastern corner of the feature there is a cluster of events, partially obscured by more diffuse seismicity.

The central region of The Geysers has an inverted 'U' shaped band of distinct clusters of events around a large area of little or no seismicity. The aseismic zone is known as the 'deadzone' *(Ross 1996; M. A. Stark, pers. comm.)*. The epicentral

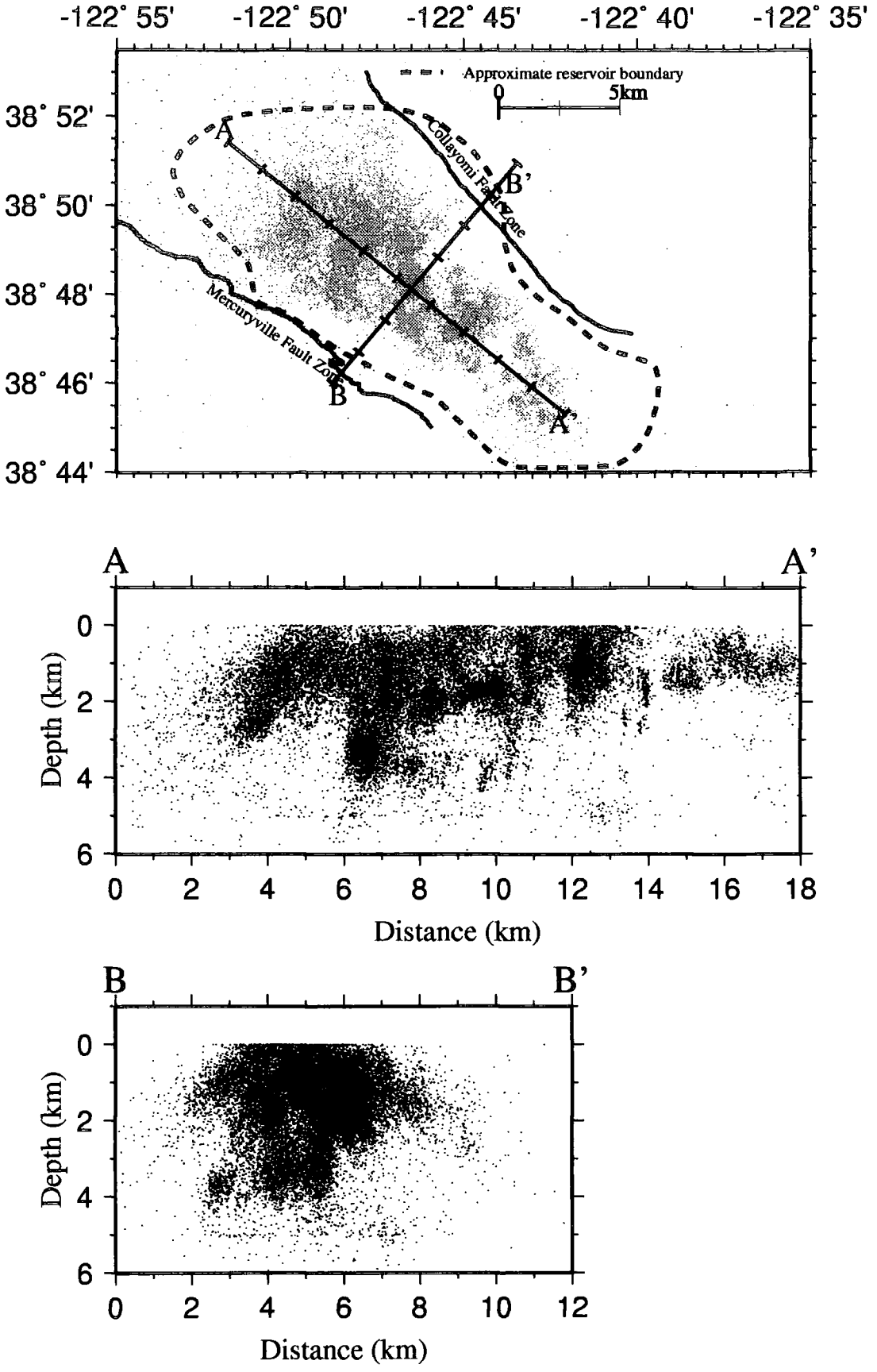

Figure 4.16 Hypocentral distribution maps for Barton catalogue earthquakes, located using the three-dimensional velocity model, that occurred between 1989 and 1994.

pattern shows that these clusters are surrounded by narrow, relatively aseismic 'haloes'. The hypocentral distribution reveals that these clusters continue near vertically at depth down to the seismic base at 2 km below sea level. The two larger 'event plumes' in the north-western part of the 'U' shaped band appear to contain many events between 0 and 2 km below sea level, few events for the 1.5 km below this, and more events again between 3.5 and 4.0 km below sea level. South of the 'deadzone' clusters, there is a second area of intense seismic clustering, exhibiting the same near-vertical distribution of events described above down to a slightly shallower base of 2 km. This seismic-base shallowing trend continues into the relatively aseismic south-east Geysers, where there are few distinct clusters. Figure 4.17 shows the major surface fault zones superimposed on a map of The Geysers seismicity. These faults are mapped to an accuracy of ± 0.5 km using the fault structure map in *McLaughlin (1981)*. The large location error accounts for the sub-surface deviation of faults from their surface locations.

4.4.5 Temporal distribution

At The Geysers there are approximately 300-350 earthquakes with $M_d \geq 0.5$ every month and the seismic rate is constantly high (Figure 4.18). Previous studies have indicated that the daily rate is about 160 earthquakes with $M_d > -0.6$ *(Ross, 1996)*, though it can vary enormously from this value. Periods of network malfunction (Figure 4.2) coincide with lower levels of earthquake detection. Also, during the interim period between the *W* and *G* networks, when the equipment failed, few earthquakes were detected. The network can only be considered reliable after May 1990.

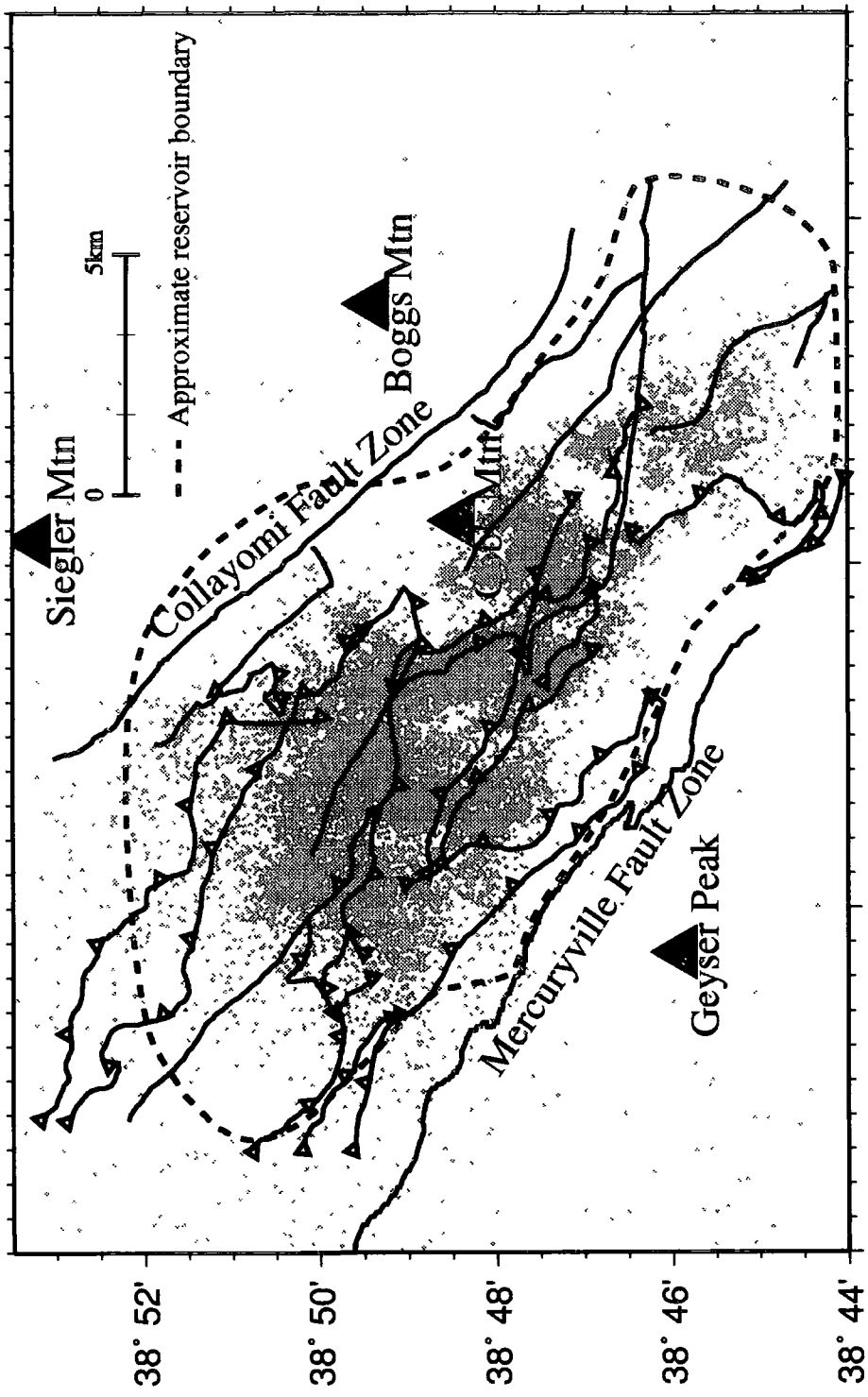

Figure 4.17 - Map of The Geysers showing the major fault zones superimposed upon Barton catalogue epicentral locations 1989-94. Fault zones from *McLaughlin (1981)*.

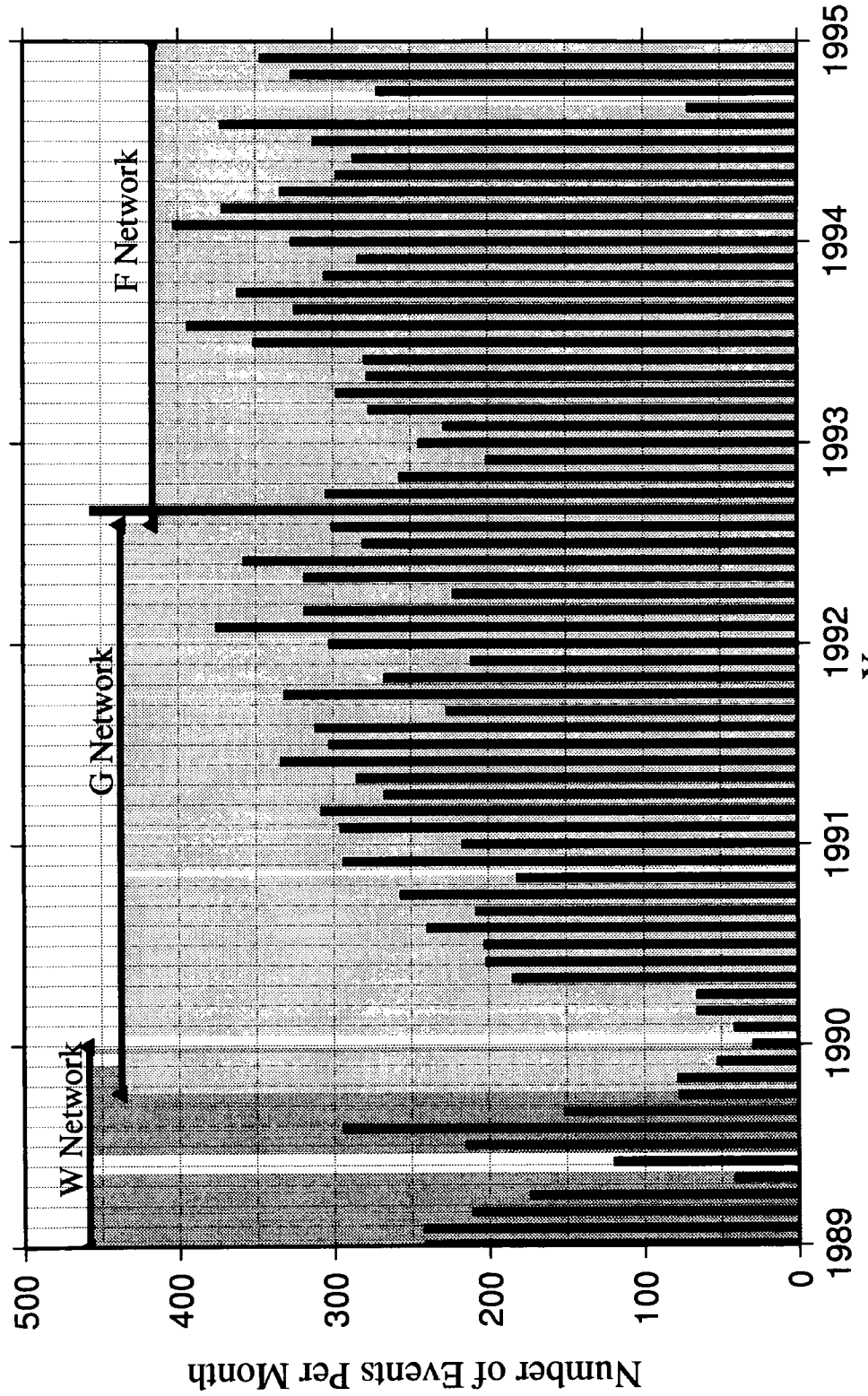

Figure 4.18 Temporal distribution of Barton catalogue events that occurred between 1989 and 1994; $M_d >= 0.5$.

4.5 Comparison with other earthquake catalogues

4.5.1 Comparison with the NCSN catalogue

4.5.1.1 Spatial comparison

A comparison of Figures 4.16 and 4.19 shows that the NCSN locations are far more diffuse than the Barton catalogue locations. The 'deadzone' is far better defined by the Barton catalogue locations and the epicentral clusters are more distinct, as are the upper and lower seismic volumes. Even so, the shapes of these features are similar in both datasets. The lower seismic volume appears to be at a shallower depth in the Barton catalogue - at about 4 km - compared to the equivalent volume revealed by the NCSN locations. The broad band of seismicity in the north-west Geysers appears to be near vertical in the NCSN dataset, whereas in the Barton catalogue locations, it dips at about 45^0. The clusters in the south-east Geysers are clearly visible in the Barton catalogue locations, but not in the NCSN dataset. The seismic base of the upper volume is at approximately the same depth in both cases. There are two lines of events in the NCSN data that are not present in the Barton catalogue at depths of 0 km and 4.5 km. These are artefacts of the regional velocity model used to locate the NCSN events.

Figure 4.20 shows the differences between the NCSN and Barton catalogue hypocentral locations for April 1991. The epicentral locations for these two datasets in the central Geysers are similar. In the north-west and south-east Geysers, there are larger differences. The cross-sections show that in general the Barton catalogue locations are shallower than the NCSN locations.

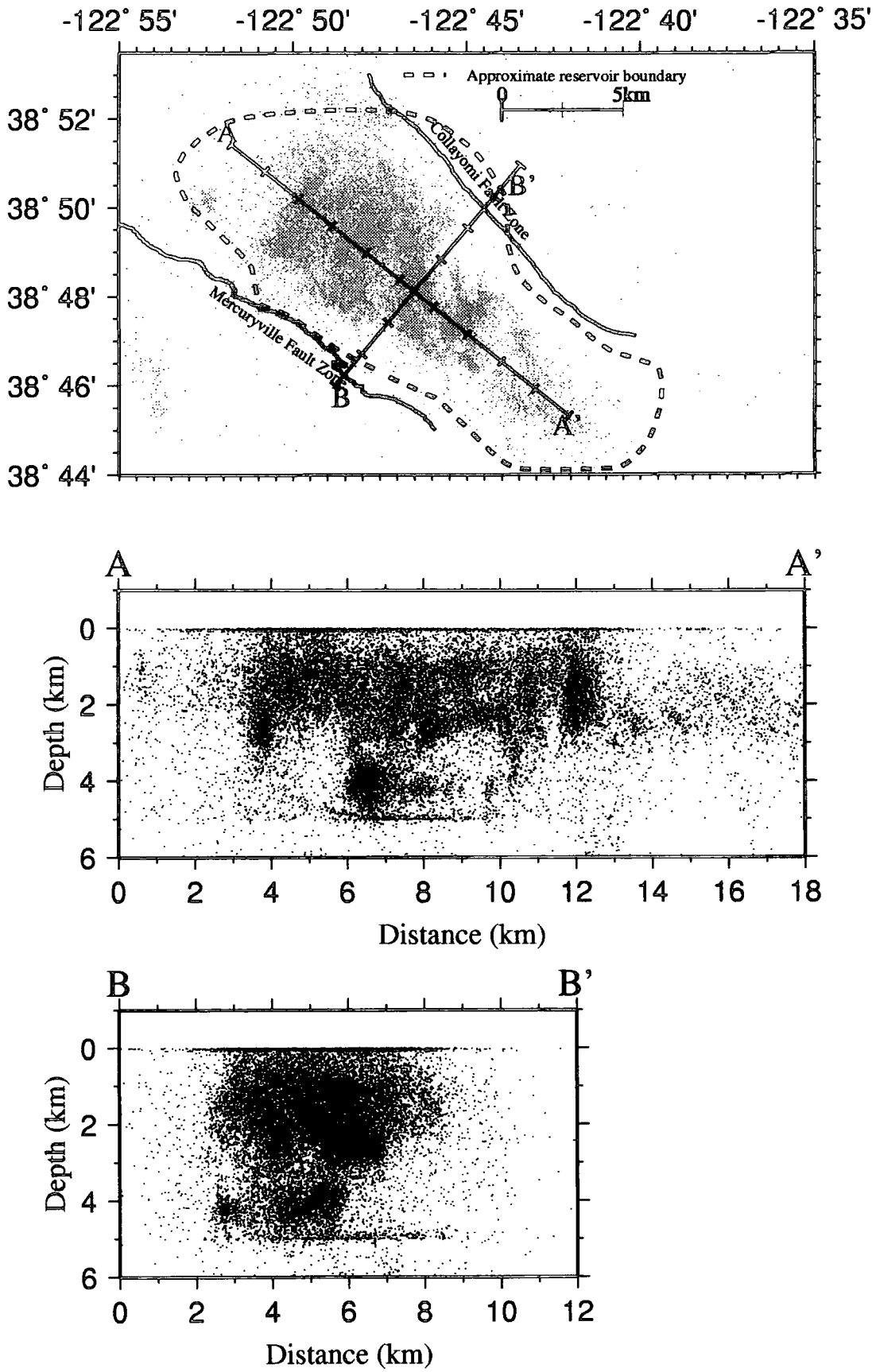

Figure 4.19 Hypocentral distribution maps for NCSN earthquakes that occurred between 1989 and 1994.

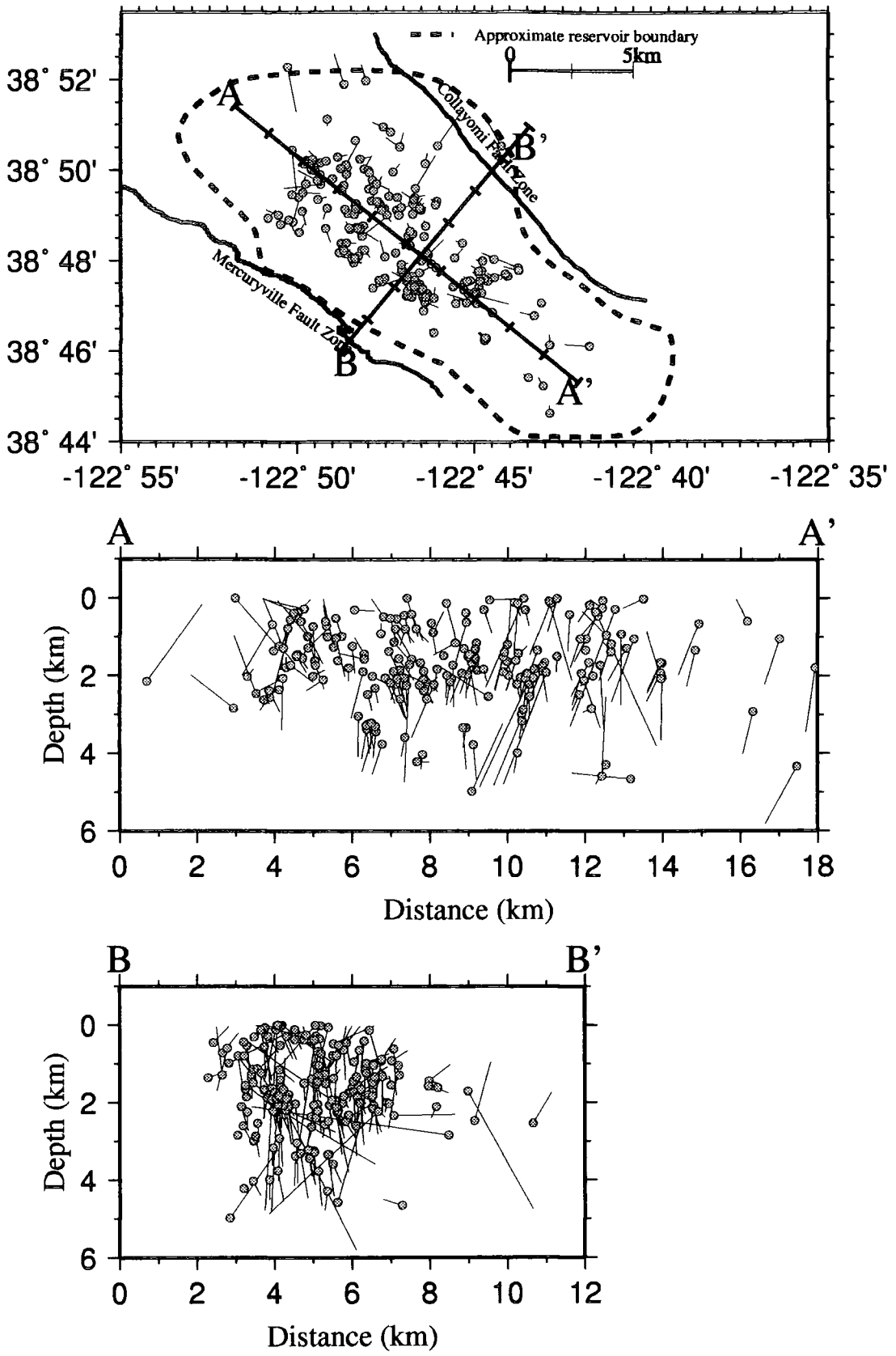

Figure 4.20 Map of The Geysers showing the differences in hypocentral location between NCSN and Barton events for April 1991. Filled circles are the Barton locations and a vector connects them to the NCSN location.

4.5.1.2 Magnitude-event occurrence comparison

Figure 4.21 shows plots of log-frequency - magnitude for (a) NCSN and (b) Barton catalogue earthquakes from April 1991. Both plots deviate from linearity above the location threshold, but this is most marked for the Barton catalogue events. Over the same magnitude range, the NCSN data form almost a straight line, with the most extreme curving for larger magnitudes, where an insignificant number of events occur. The magnitude thresholds were 0.9 for the NCSN events and 0.5 for the Barton catalogue events, yielding *b*-values of 1.2 ± 0.13 and 1.05 ± 0.11 respectively.

Figure 4.22a shows a plot of 500 earthquakes which have an 'ideal' log-frequency - magnitude distribution, i.e. a distinct threshold magnitude when $M = 0.8$ and a linear relationship over the magnitude range $M > M_{min}$. Figure 4.22b shows the same data with small, random errors within ±10 % of the magnitude of each earthquake added. The plot has a slight curvature at the threshold magnitude and non-linearity at $1.8 < M < 2.6$. When random errors of ±25 % were added to each magnitude (Figure 4.22c), the distribution clearly shows similar features to those observed in the Barton catalogue from April 1991. This suggests that random errors are a possible cause of these departures from the ideal.

4.5.2 Spatial comparison between the UNT catalogue and the Barton Catalogue for April 1991

The Barton catalogue locations obtained using the 3-D model exhibit tighter clustering, better definition of the upper seismic volume and considerably less scatter than the UNT catalogue locations obtained using a one-dimensional model (Figure 4.23). In neither case is the lower seismic volume imaged. Comparison of the two datasets shows that the UNT catalogue locations are deeper than the relocations obtained using the three-dimensional model.

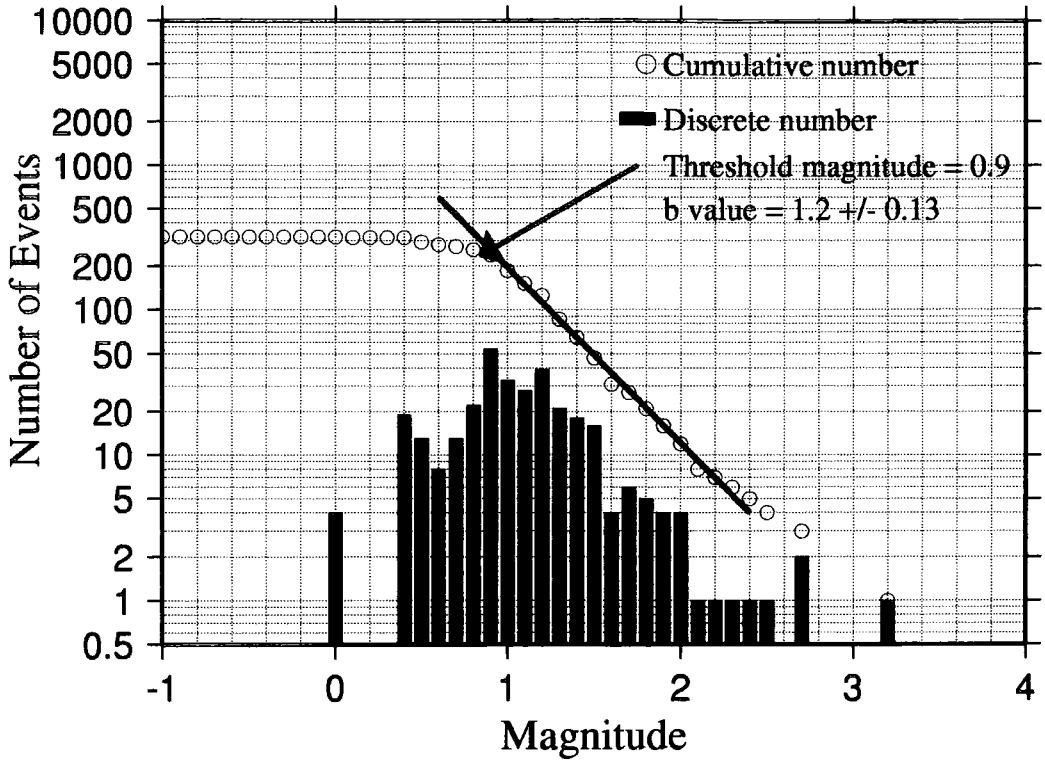

Figure 4.21a Log-frequency magnitude plot of NCSN data from April 1991.

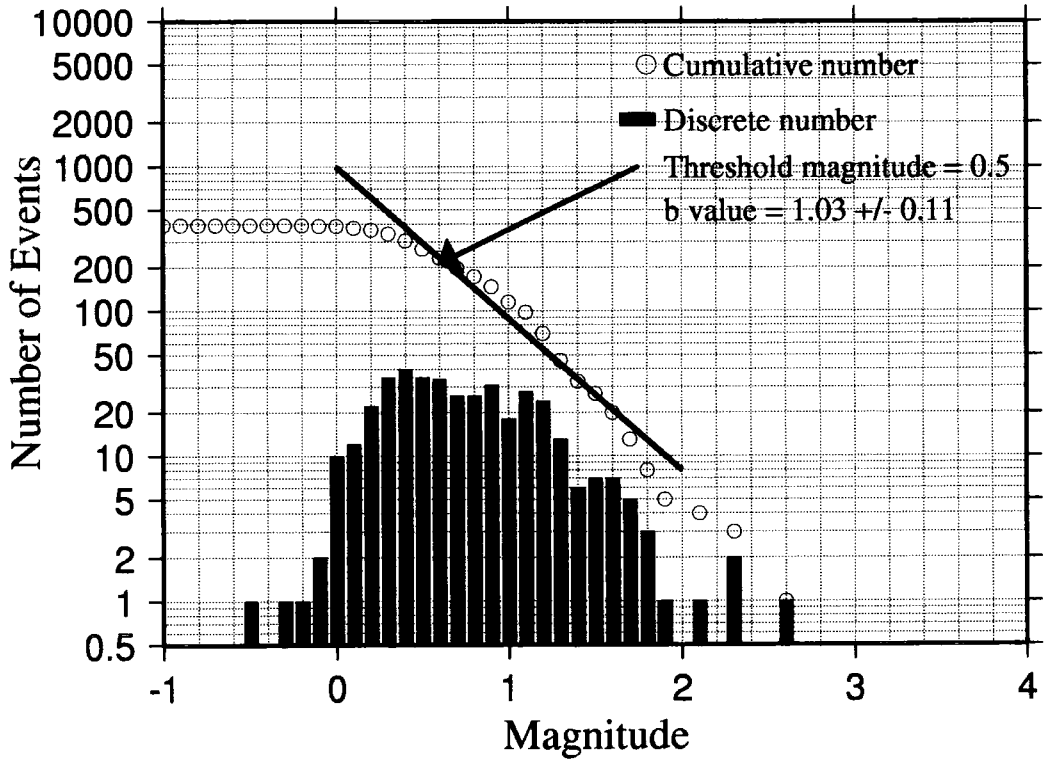

Figure 4.21b Log-frequency magnitude plot of Barton catalogue data located using the three-dimensional velocity model from April 1991.

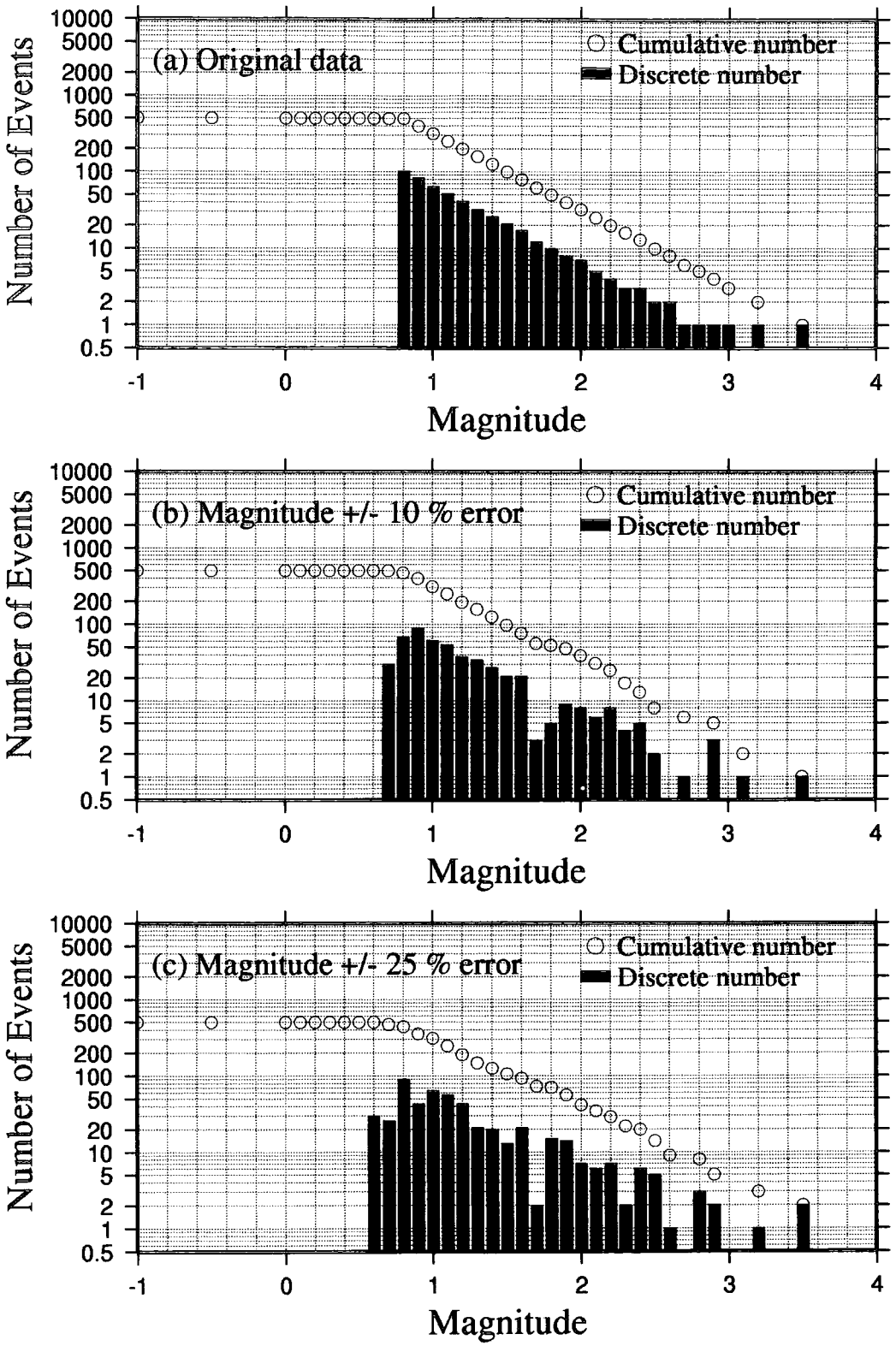

Figure 4.22 Frequency-magnitude plots showing the effect of small-magnitude errors. (a) is a plot of 500 earthquakes exhibiting an 'ideal' log-frequency magnitude distribution. (b) random errors within +/- 10% of the original earthquake magnitude added. (c) random errors of +/- 25% added.

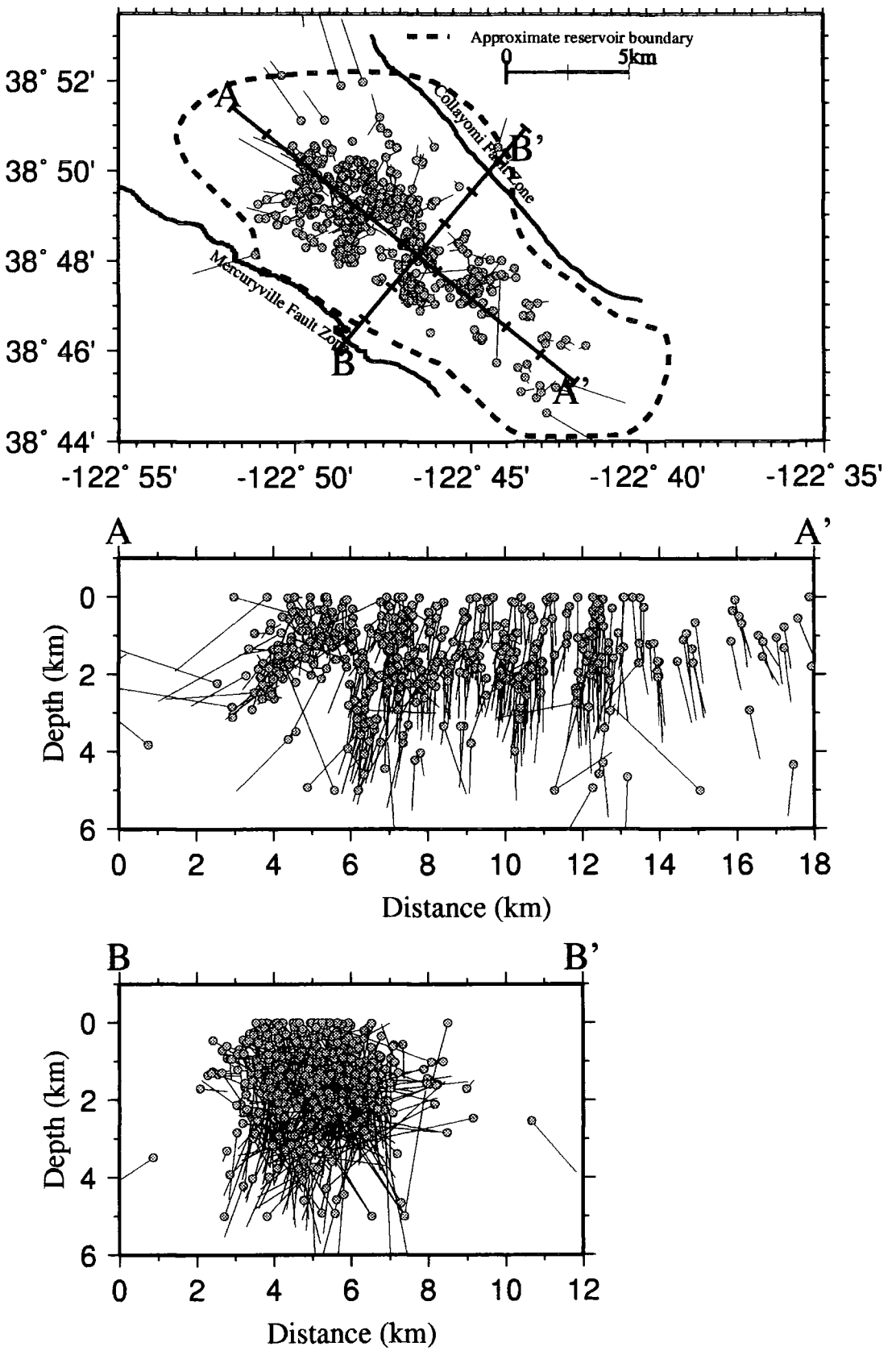

Figure 4.23 Relative differences in hypocentral location between UNT catalogue locations (ends of vectors) and Barton catalogue events relocated using the three-dimensional velocity model (dots) for April 1991.

4.6 The well data

4.6.1 Introduction

Although The Geysers has been commercially exploited for geothermal steam for 140 years, only in the last forty years has the field been developed extensively. Generating electricity at The Geysers is simple. All that is required is to drill into the fractured greywacke reservoir rock and extract the steam, which is then used to drive turbines. After extensive development in the 1980s, it was realised that the geothermal field was not a limitless resource when steam pressure fell as it began to dry out. To prolong the life of The Geysers, liquid condensate is now pumped into the reservoir in an attempt to replace the lost fluid. Some of this injection occurs down wells previously used for steam extraction, while others have been drilled specifically for injection.

4.6.2 Drilling wells in The Geysers geothermal area

The drilling equipment and methods used at The Geysers are much the same as those used for drilling for gas or oil *(Reed & Campbell, 1976)*. The first 1300 m of the well is drilled using mud as the circulating fluid. At greater depths, increasing temperature and the presence of fractures make necessary the use of compressed air as a drilling fluid. At this point, steel casing pipe is cemented to the inside of the well to support the rock walls, and all liquid is removed from the well. Flow rates of compressed air of up to 70 m^3 / minute are used when drilling penetrates the top of the steam-bearing rocks. In these conditions, attempting to drill using mud would clog or damage the steam-bearing fractures. Drilling with compressed air does not cause this problem. The drilling continues through the steam zone in the reservoir rock until an economical flow of steam is achieved or until the economically limiting depth of 3000 m is reached. Production wells are left uncased through the steam zone since the higher strength rock in this zone negates

the need for additional support. Injection wells are lined with slotted steel pipe in the steam zone to prevent caving of the rock walls during injection.

Two government agencies have direct jurisdiction over drilling activities in The Geysers. Drilling on private or state land is governed by the California Division of Oil, Gas and Geothermal Resources (D.O.G.G.R.). If the drilling is conducted on federal-owned land, or on land where the mineral rights are owned by the federal government, then the drilling activities are governed by the Conservation Division of the United States Geological Survey. When drilling permits are issued, information about the operator name, the well name, surface location and altitude are made public. Other information is made available in environmental reports. According to Californian law, state records of geothermal wells are made public five years after abandonment, or five years after the start of production or injection. If required, the operator may also apply for a further two years of confidentiality before the well histories must be made public.

4.6.3 Types of well

A complete list of well licences issued in The Geysers, provided by the D.O.G.G.R., gives details of the types of well in operation, their operational status and their current owners up until the end of 1997. There are 1571 wells split into eight categories (Tables 4.4, 4.5 and 4.6). Development steam (DST) and exploratory steam (EST) wells are used for the commercial extraction of steam, and have well temperatures in excess of 100^0C. Condensate injection is achieved using injection wells (INJ). Some of these wells are purpose-built, while others are converted DST or EST wells. In a few wells, injection and steam extraction activities are alternated month by month. Low-temperature wells provide hot water for both commercial (CLT) and domestic (NLT) purposes and operate at between 30 - 100^0C. Water wells (WW) operate at temperatures less than 30^0C. Low-temperature and water wells are not used for the generation of geothermal energy. Temperature-gradient wells (TG) are used for monitoring purposes only.

Also, 242 licences were issued but were not allocated to operating companies. These are signified by an asterisk in Table 4.4. The vast majority of production and injection wells are owned by the Union Oil Company of California (UNOCAL), Calpine Geysers Company (CGC) and the Northern California Power Agency (NCPA) (Table 4.4). Several companies, such as Chevron, Shell and Freeport McMoran Partners (FMRP), have drilled large numbers of temperature gradient wells but have no capacity for commercial steam production. The majority of these exploration wells have been either abandoned or cancelled. A complete list of wells and operating companies is given in Appendix 5.

4.6.4 Well histories

All the public well histories for DST, EST and INJ wells were obtained from the D.O.G.G.R. open record. It contained the well histories of 470 wells from 1924 to the end of 1997 - a total of ~24 Mb of data. Of these, 427 were used for production purposes (337 between 1989-1994), 34 for injection (24 between 1989-1994) and 9 were converted from production to injection or used for both purposes. The open record contained a monthly account for each well, detailing the amount of steam extraction/injection, changes in temperature and pressure, and any geochemical changes in the well (Appendix 5).

The author also wrote to each of the geothermal companies operating in The Geysers. The response was disappointing. Although NCPA and CGC provided more data than was initially available from the D.O.G.G.R., this data was contained in a later version of the open record. More data was hoped for from UNOCAL, but this failed to materialise. The other companies did not respond. According to the D.O.G.G.R. licences list, there are 172 production and 14 injection wells with confidential histories currently active in The Geysers (Table 4.7). Since the well-history database is incomplete, the available data do not give the full picture of commercial geothermal activity in The Geysers.

Table 4.4 Number of wells by type and operating company in The Geysers

	Confidential								Public								
Operator	CLT	DST	EST	INJ	NLT	TG	WW	Total	CLT	DST	EST	INJ	NLT	TG	WW	Total	Grand Total
Andar	0	0	0	0	0	0	0	0	0	0	2	0	0	38	1	41	41
CCPA	0	8	0	0	0	0	0	8	0	14	1	3	0	4	0	22	30
CGC	0	7	0	1	0	0	0	8	0	85	0	7	0	0	0	92	100
Chevron	0	0	0	0	0	0	0	0	0	0	1	0	0	22	0	23	23
DWR	0	11	0	0	0	0	0	11	0	17	0	1	0	0	0	18	29
FMRP	0	1	0	0	0	7	0	8	0	0	0	0	0	104	0	104	112
GEO	0	5	0	0	0	1	0	6	0	33	2	2	0	125	1	163	169
GEP	0	3	1	0	0	0	0	4	0	5	0	1	0	0	0	6	10
NCPA	0	84	0	6	0	0	0	90	0	1	1	0	0	0	0	2	92
Republic	0	0	2	0	0	2	0	4	0	0	2	0	0	15	0	17	21
Shell	0	0	0	0	0	12	0	12	0	0	2	0	0	25	0	27	39
Silver	0	36	0	2	0	0	0	38	0	0	0	0	0	0	0	0	38
SRGC	0	2	0	0	0	0	0	2	0	6	3	2	0	9	0	20	22
UNOCAL	0	64	0	5	0	14	0	83	0	291	1	26	0	155	0	473	556
*	0	0	0	0	0	0	0	2	0	0	0	0	0	0	0	240	242
Others	1	0	0	0	1	1	0	3	4	2	16	0	0	21	0	44	47
Totals	1	221	3	14	1	37	0	279	4	454	31	42	0	518	2	1292	1571

Table 4.5 Types of well in The Geysers

Well Type	Description	Injection / production
CLT	Commercial Low Temperature (30^{0}C to 100^{0}C)	N/A
DST	Development Steam (> 100^{0}C)	Production - some Converted to injection
EST	Exploratory Steam	Production - some converted to injection
INJ	Injection	Injection - two converted to production
NLT	Non-commercial - Low Temperature (30^{0}C to 100^{0}C)	N/A
TG	Temperature Gradient	N/A
WW	Water wells (< 30^{0}C)	N/A

Table 4.6 Major well-owning companies in The Geysers geothermal area

Operator	Full Name	Operator	Full Name
Andar	Anadarko Petroleum Corporation	NCPA	Northern California Power Agency
CCPA	Central California Power Agency	Republic	Republic Geothermal Incorporated
CGC	Calpine Geysers Company	Shell	Shell Oil Company
Chevron	Chevron Oil Company	Silver	Silverado Geothermal
DWR	Department of Water Resources	SRGC	Santa Rosa Geothermal Company
FMRP	Freeport McMoran Partners	UNOCAL	Union Oil Company of California
GEO	Geo East Mesa Limited Partnership	Others	Companies with < 10 wells
GEP	Geothermal Energy Partners	*	Planned wells

Table 4.7 Distribution of production, injection and production/injection wells in The Geysers.

Key to well codes: ACTV = active, ABDN = abandoned, CANC = cancelled, SUSP = suspended, PROP = proposed.

Operator	Production (Public)		Production (Proprietary)					Injection (Public)		Injection (Proprietary)		Combination (Public)	
	Active	Inactive	ACTV	ABDN	CANC	SUSP	PROP	Active	Inactive	ACTV	ABDN	Active	Inactive
Andar	0	0	0	2	0	0	0	0	0	0	0	0	0
CCPA	15	0	4	2	2	0	0	2	1	0	0	0	0
CGC	81	6	2	0	0	0	1	3	0	1	0	6	0
Chevron	0	0	0	1	0	0	0	0	0	0	0	0	0
DWR	9	8	0	0	9	1	1	1	0	0	0	0	0
FMRP	0	0	0	0	1	0	0	0	0	0	0	0	0
GEO	12	14	0	9	5	0	0	2	0	0	0	0	0
GEP	4	0	4	0	0	0	0	2	0	0	0	0	0
NCPA	0	0	76	8	0	0	2	0	0	6	0	0	0
Republic	0	0	0	2	0	0	2	0	0	0	0	0	0
Shell	0	0	0	2	0	0	0	0	0	0	0	0	0
Silver	0	0	35	0	0	0	1	0	0	2	0	0	0
SRGC	1	5	0	4	1	0	0	2	0	0	0	0	0
UNION	215	56	51	28	4	1	3	12	9	5	0	3	0
Others	0	1	0	14	3	0	0	0	0	0	0	0	0
Totals	337	90	172	72	25	2	10	24	10	14	0	9	0

The surface locations of every well in The Geysers was estimated using a map provided by the D.O.G.G.R.. The (usually confidential) sub-surface deviation from the surface location can be as much as several hundred metres, and this must be borne in mind when considering spatial correlations between seismicity and well activity.

4.6.5 Distribution of injection & production wells in The Geysers

In several cases clusters of seismicity occur in close proximity to injection wells. Other clusters did not, according to the available data, have adjacent well activity, but proprietary wells may have been in operation in these areas.

Figures 4.24 and 4.25 are, respectively, maps of production and injection in The Geysers 1989 to 1994 superimposed on the major fault zones *(from McLaughlin,*

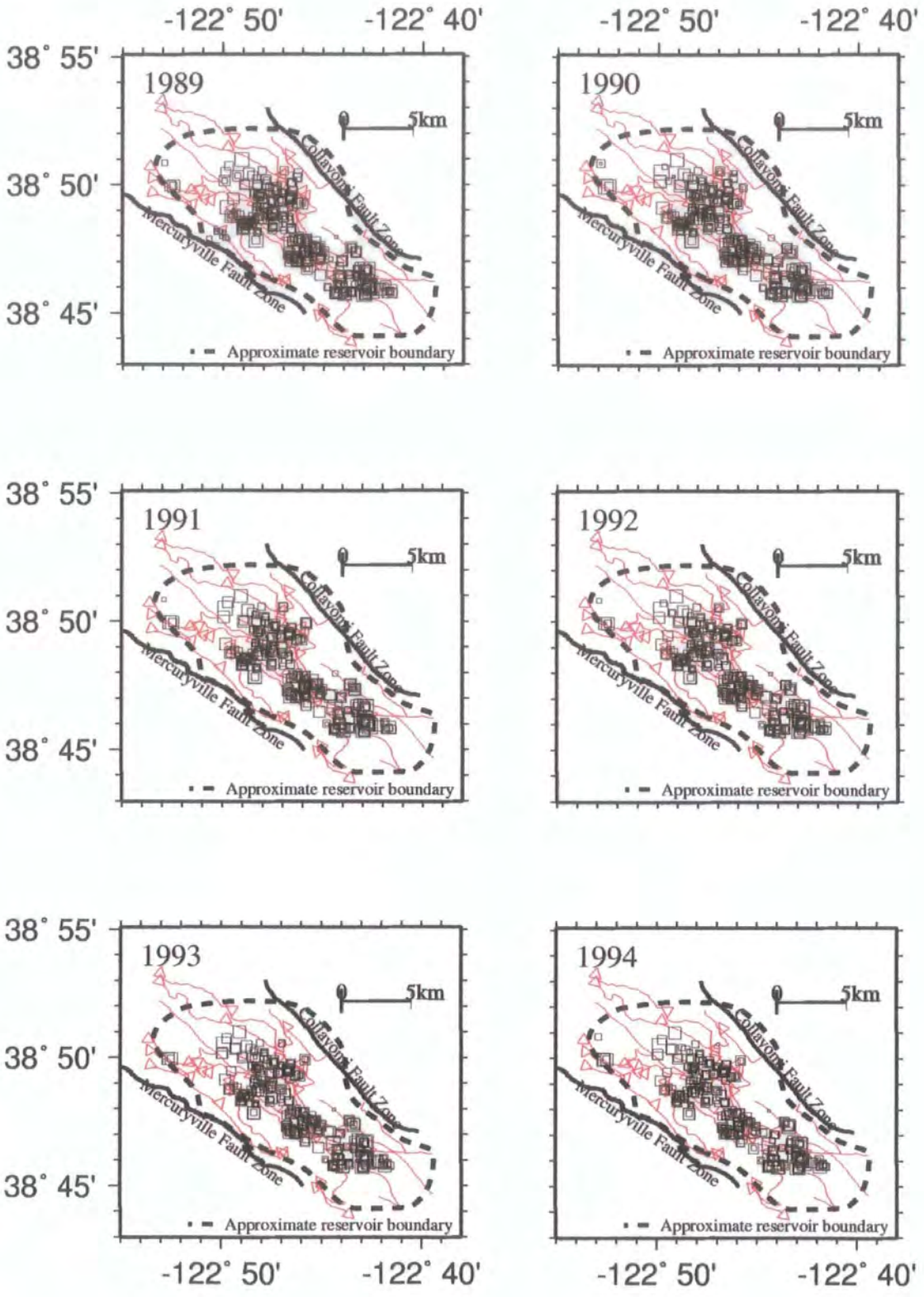

Figure 4.24 Maps of The Geysers showing amount of production from 1989 to 1994. Squares: 1 cm^2 = $1x10^{13}$ kg^2 / year of steam extracted. Red lines show the major fault zones within the reservoir boundary. (Faults from *McLaughlin, 1981*).

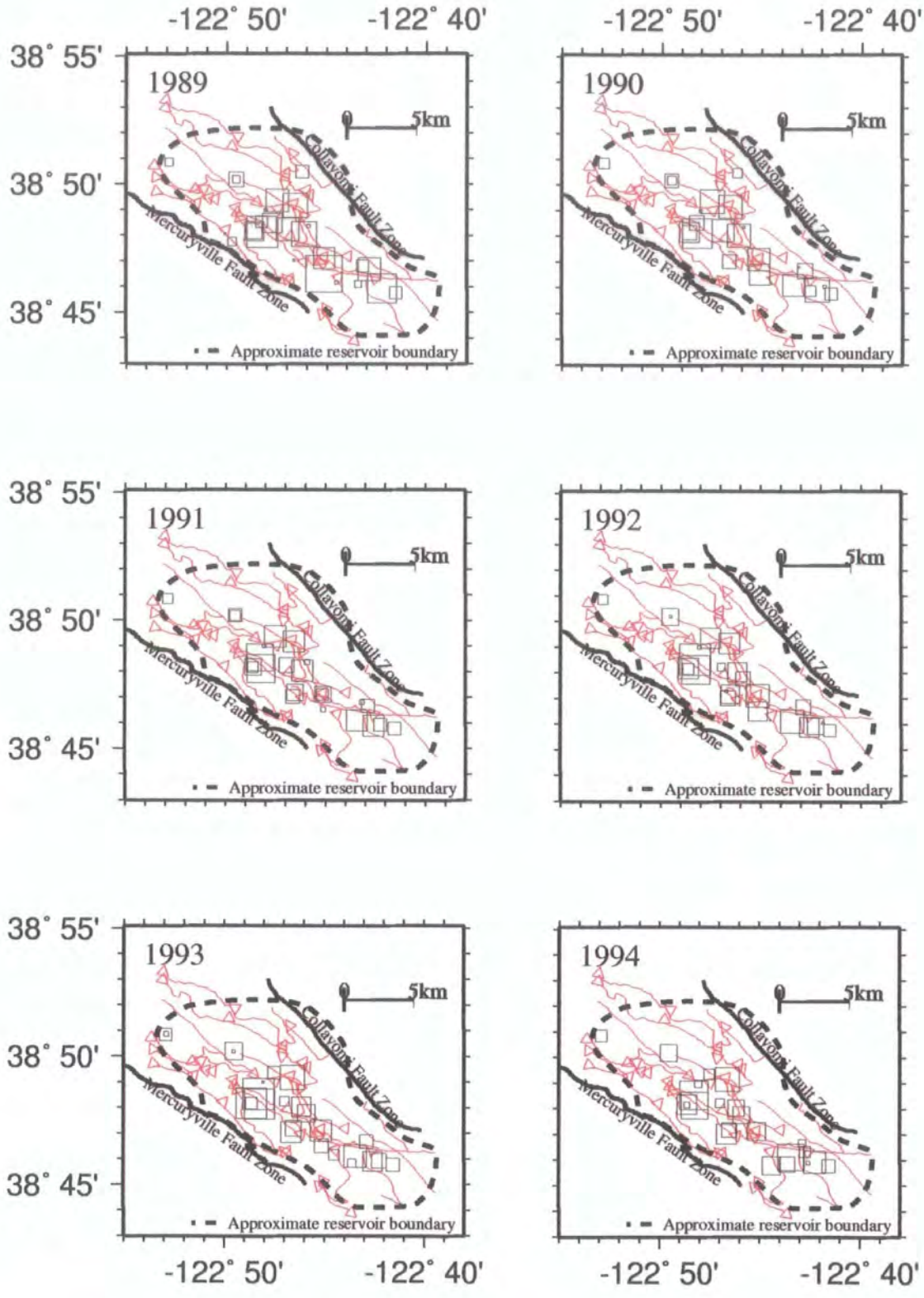

Figure 4.25 As Figure 4.24, except for injection.

1981). The majority of injection and production activity lies along fault zones. Also, the patterns of injection and especially production mirror the seismicity patterns. The 'deadzone', in the central Geysers, is clearly visible and the clusters of production activity are distributed in a similar pattern to that of the observed seismicity.

4.7 Summary

In 1985, the UNOCAL - NEC - Thermal (UNT) partnership began seismic monitoring to study the environmental impact of industrial activity in The Geysers. The mature seismic network has 8 three-component and 14 vertical-only component seismometer stations, and detects 40 - 50 $M_d \geq 0.2$ events per day.

Non-linear cumulative frequency - magnitude plots from April 1991 indicated that the UNT magnitudes are not reliable. The data were thus reprocessed, a total of about ~25,000 - 35,000 raw seismograms. Since seismogram amplitudes were often saturated, earthquake magnitude was estimated using coda lengths.

Raw seismograms were processed automatically using programs for picking P-wave arrivals, sampling noise and coda length and calculating event locations and magnitudes. Stations were calibrated by comparison with NCSN magnitudes The earthquakes were located using a three-dimensional, tomographically determined velocity model. After poorly located earthquakes were removed, the Barton catalogue contained 22,817 events, approximately 300-350 $M_d \geq 0.5$ earthquakes per month. The location error was ~ 0.2 km.

There are 1571 wells in The Geysers. Between 1989 and 1994, 337 of these were used for steam extraction, 24 for fluid injection and 9 for both purposes. Most of these wells were in the central Geysers, concentrated around the 'deadzone'. Since 172 production and 14 injection wells currently have confidential histories, the well database is not complete. Seismicity usually occurs in close proximity to

active wells and fault zones. A few seismic clusters did not appear to have known adjacent well activity.

Chapter 5

Results of analysis of data from The Geysers geothermal area

5.1 Introduction

The earthquake dataset from The Geysers was analysed as a single dataset and as subsets representing individual clusters of seismicity. A threshold magnitude of M_d = 0.5 was used, based on selection of the threshold magnitude from visual inspection of log-frequency vs. magnitude plots (Figure 5.1).

Program ***b_D_3d.c*** calculates the temporal variation in *b*-value using the equation of *Page (1968)* (Equation 2.25), and the fractal dimension using the correlation dimension method (Section 2.1.3.2) (Appendix 6). From this point on in this thesis, *D* represents the correlation dimension. A flow diagram for ***b_D_3d.c*** is in Figure 5.2. Each earthquake was defined as a five-dimensional variable: time (in decimal years), location in x, y and z co-ordinates (in kilometres relative to an arbitrary point), and magnitude. The scaling range over which *D* was calculated was estimated using the distances of depopulation, r_n, and saturation, r_s, (Equations 2.11 and 2.12). The length of the hypercube, $2R$, in the two-dimensional case was taken as the length of the longest axis of the epicentral cluster. In the three-dimensional case, the longest axis of the hypocentral cluster was used. By using the longest axis as the length of the hypercube, the seismic volume was maximised, allowing the largest possible number of earthquakes for the *b/D* analysis. Then, using the embedding dimension (2 in the two-dimensional case; 3 in the three-dimensional) and the number of points in each event window (200 or 400), the scaling limits needed to calculate *D* were obtained using Equations 2.11 and 2.12. The limit $r_n/3$ was used as the depopulation limit *(Eneva,*

1996). Examples of plots of $C(r)$ vs. r for 200-event samples of seismicity are shown in Figure 5.1.

The temporal changes in b and D were calculated using a sliding window technique. The required parameter was calculated over a pre-set window of events. The window was then moved along the data, either by a number of events or a time period, and the parameter was recalculated. As the events are input in chronological order, this technique shows how the b-value and D change over time. A set number of samples per window was generally used since the event rate was not constant. Using a set time period would have resulted in some windows having very few events. In previous work, windows containing either 50 events *(Smith, 1981)* or 100 events *(e.g. Henderson et al., 1994; Öncel et al., 1995)* were used, typically moved on by 10 or 50 samples after each calculation. For this study, an increment of 10 samples was adopted. In order to find a suitable number of events for each calculation for the data in this thesis, samples ranging from 100 to 500 events were tried (Figure 5.3). Smaller samples resulted in noisy sequences with large and frequent changes in amplitude, and large errors. Larger samples generated smoother sequences with smaller errors, but anomalies in the data were obscured. The window size adopted, 200 events, struck a balance between these two effects. The calculated values of b and D were plotted at the time-window median point. The program was tested with a fourth-order Sierpinski carpet and seventh-order Cantor dust. The results were within 5% of the deterministic (true) values (Section 2.1.2). The values of r_s and r_n used to calculate D for the whole dataset and for the individual clusters are presented in Appendix 7.

For the whole dataset and each subset three plots are shown:

1) Epicentral maps and cross-sections: Epicentral maps with north-west - south-east and south-west - north-east cross-sections were generated for each of the years 1989-1994. Also shown on each map are the surface fault zones (from *McLaughlin, 1981*) and injection and production for that year (Figure 5.4(a)).

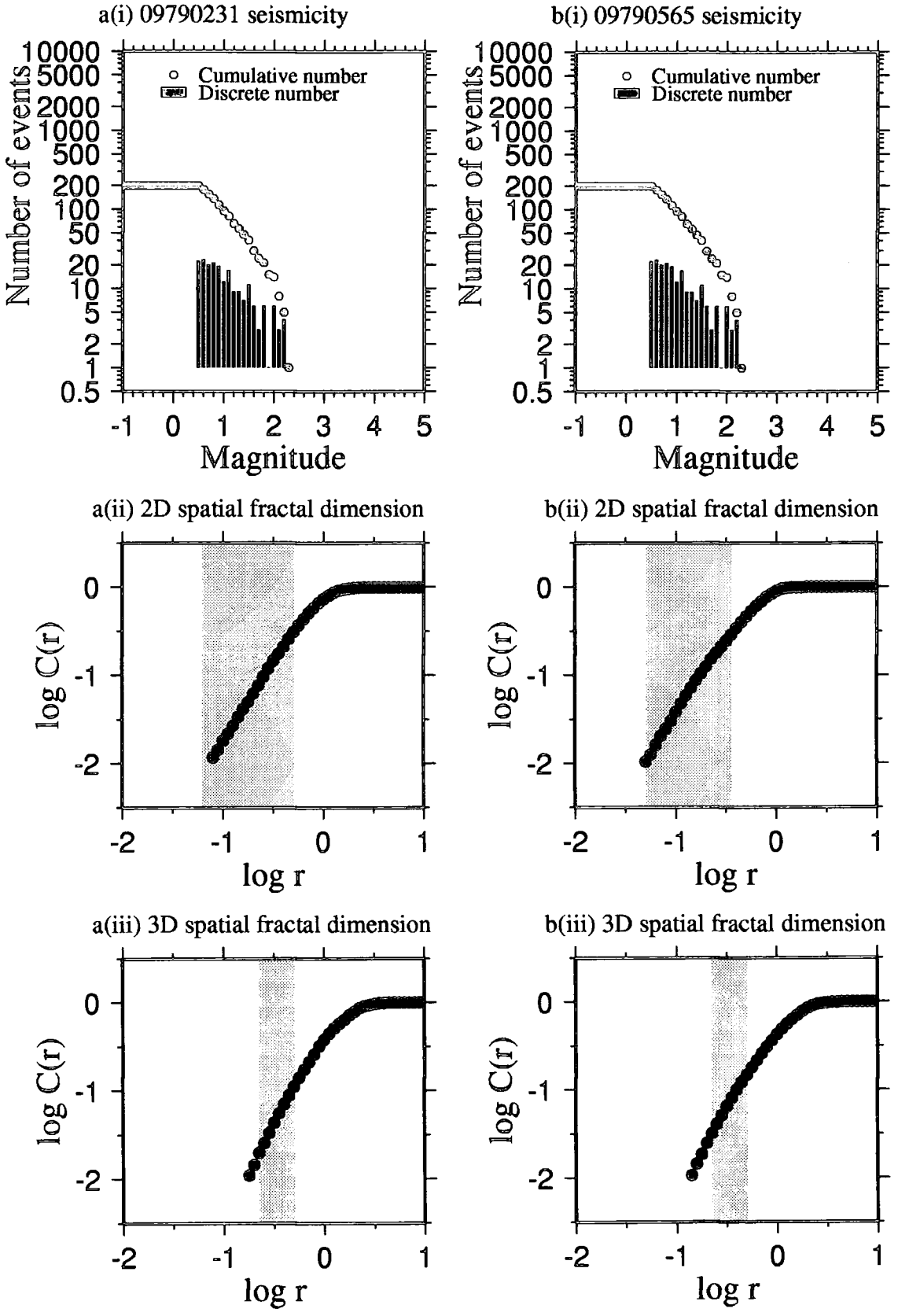

Figure 5.1(a) for a 200-event sample of seismicity with $M_d >= 0.5$ adjacent to well 09790231 (i) log-frequency vs. magnitude, (ii) $C(r)$ vs. r for epicentres, and (iii) $C(r)$ vs. r for hypocentres. The range $r_n/3 < r < r_s$ is shaded. (b) same as (a) but for seismicity adjacent to well 09790565.

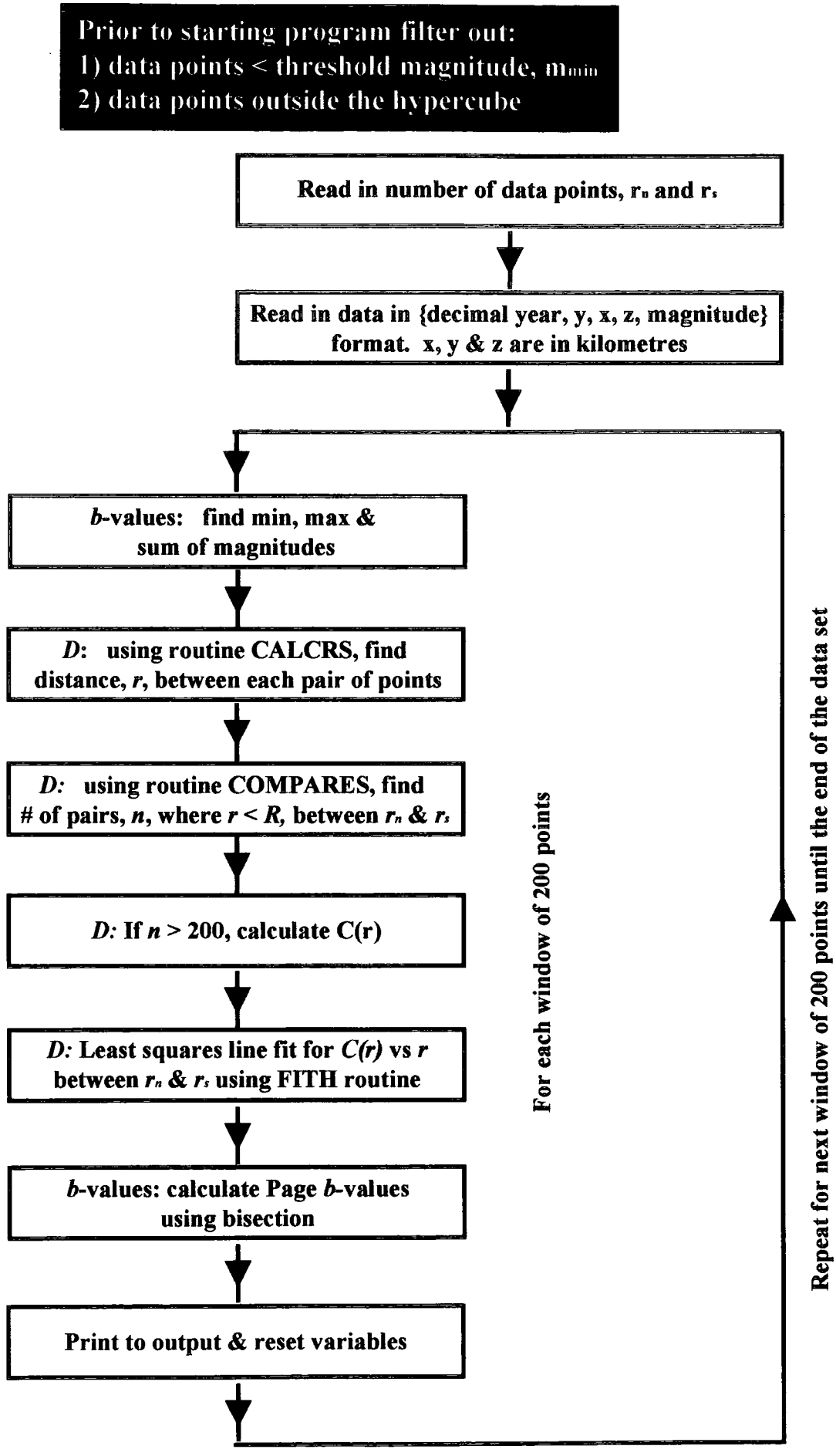

Figure 5.2 Flow diagram for program *b_D_3d.c*

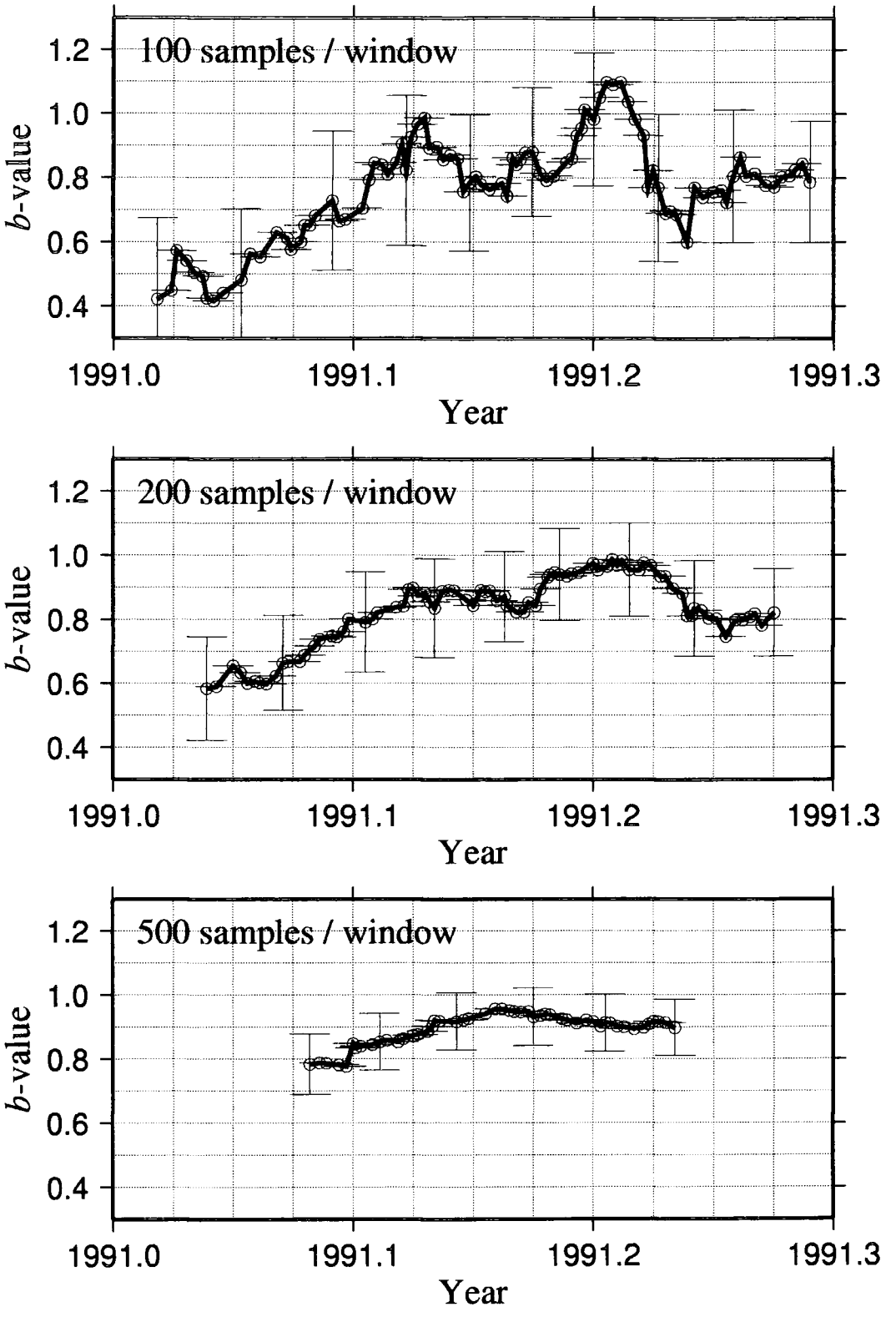

Figure 5.3 Figure showing the effect of different window sizes for *b*-value calculations. The data used are the first 1000 events from the Barton catalogue from 1991 (Chapter 4). *b*-values are plotted at the middle of each window.

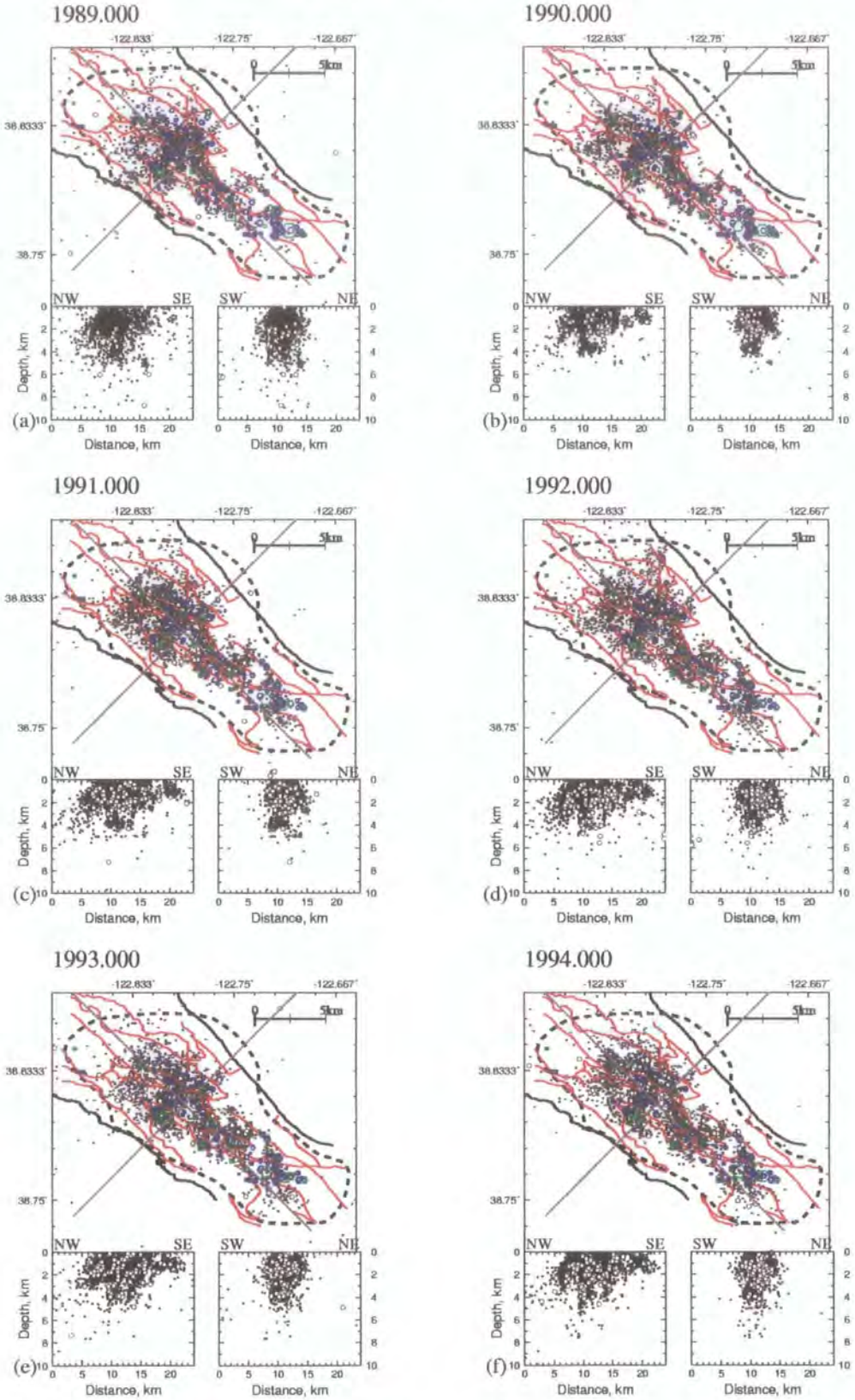

Figure 5.4(a) Epicentral maps and cross-sections for seismicity in The Geysers geothermal area 1989-1994. Dots: events with $0.5 >= M_d > 2.0$, circles: events with $M_d >= 2.0$, red lines: faults, green squares: surface locations of Sonoma County injection wells, green hexagons: surface location of Lake County injection wells, blue symbols: surface location of production wells. The size of the production and injection symbols are scaled to indicate activity: 1 cm^2 represents 5 x 10^{13} kg / year of fluid. 24-km long cross-sections are shown by grey lines. Dotted line = approximate reservoir boundary.

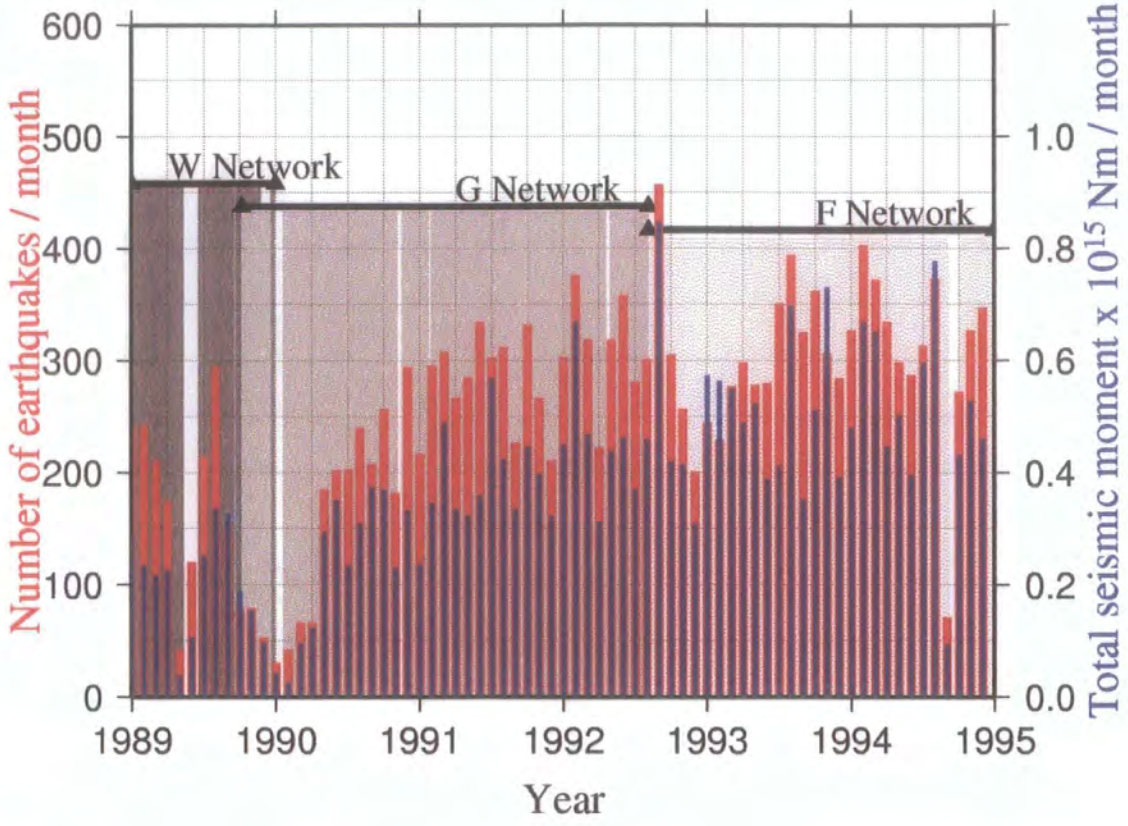

Figure 5.4(b) Temporal distribution of number of events and total seismic moment of earthquakes with $M_d >= 0.5$ for the whole of The Geysers 1989 and 1994. Shaded bars show when the networks were in operation.

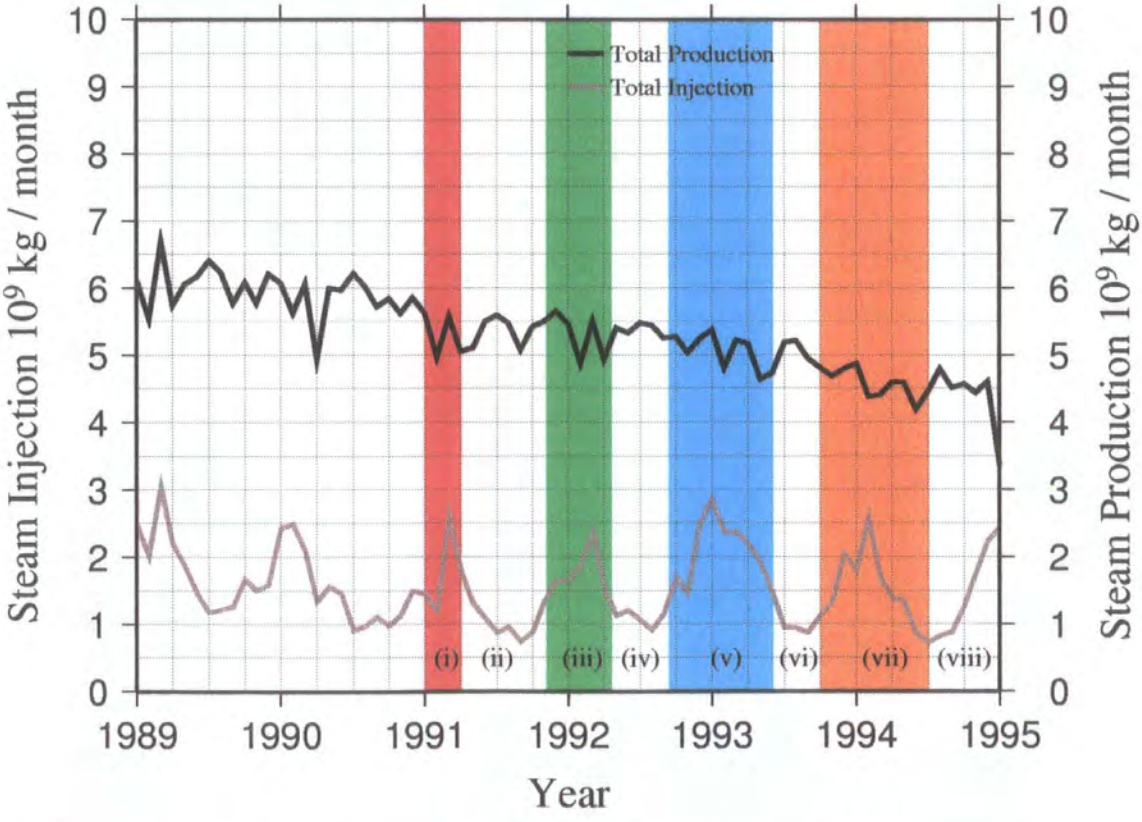

Figure 5.4(c) Well activity for the whole of The Geysers 1989-1994. Coloured bars highlight peaks in total injection after May 1990.

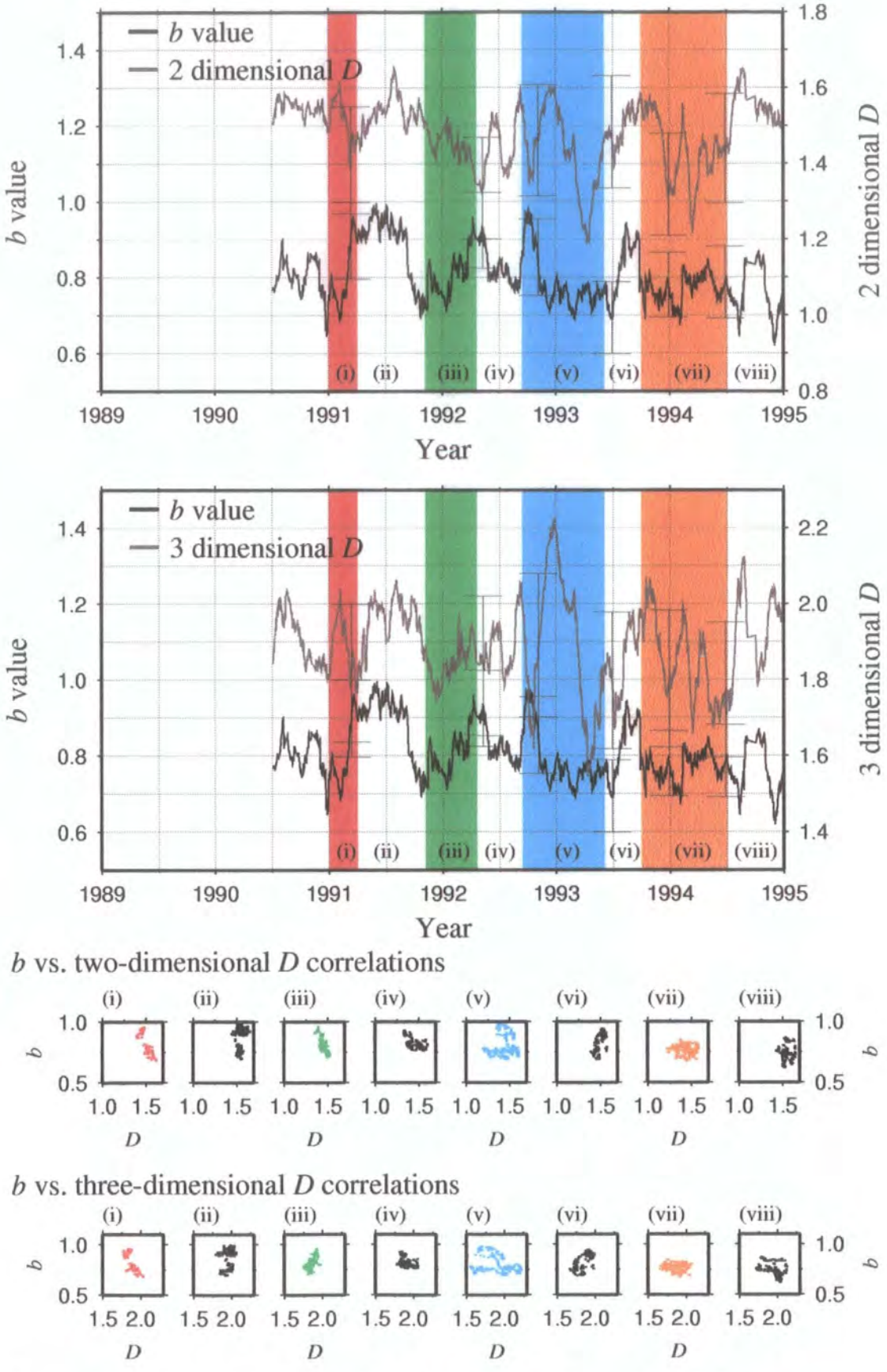

Figure 5.4(d) Plots of b value against two- and three- dimensional D for seismicity in The Geysers. Coloured bars correspond to those shown in Figure 5.4(c).

2) Event rate, seismic moment and well histories: The total number of events and the total seismic moment per month for the 6-year period 1989-1994 is shown (Figure 5.4(b)). The total injection and production over the period 1989-1994 is shown, along with the histories of important wells in the vicinity of each cluster (Figure 5.4(c)).

3) *b*-value and fractal dimension: Due to incomplete data prior to May 1990, data from before this date were not analysed (Figure 5.4(d)). Fractal dimension and *b*-value were not calculated for datasets containing fewer than 500 $M_d \geq 0.5$ events occurring after May 1990. Temporal variations in b and D were calculated using 400-event windows for the whole field and 200-event windows for the cluster subsets. Error bars shown for b are the 95% confidence limits (Equation 2.26). The error bars shown for D are ± 10% of the calculated value of D (Section 2.1.3.2). The correlations between b and both two-dimensional and three-dimensional D are also shown.

5.2 The entire dataset

Seismicity in The Geysers can be divided geographically into three regions (Section 4.4.4 & Figure 5.4(a)):

1) An area of diffuse seismicity in the NW Geysers dipping at 45^0 and extending from near the surface to a depth of 3 km below sea level.
2) A 'U'-shaped area of seismicity around the relatively aseismic 'deadzone' in the central Geysers. This area is highly active from near the surface down to a depth of 4 km below sea level, with an aseismic zone between 2 and 3.5 km.
3) The area south-east of this 'U'-shaped seismic zone.

The seismic rate in The Geysers was ~ 300 events per month for the much of the six-year period 1989-94 (Figure 5.4(b)), with a significant drop in the measured event rate between mid 1989 and mid 1990 during the switch between the W and G

networks (Section 4.1.1). This was probably due to failure of the network. The drop in the event rate in September 1994 may be attributed to the same problem.

In the period 1989 to 1994, total injection in The Geysers had an annual cyclical pattern (Figure 5.4(c)). This may be traced to wells 09790020, 09790534 (which is adjacent to 09790020) and 09790612 on the northerly branch of the 'U'-shaped seismic zone, and well 09790565 on the southerly branch (Figure 5.5). The remainder of the injection activity in The Geysers is either uniform or low-level. Production over the entire field was uniform and declining, with typically ~ 6 x 10^9 kg / month (~ 2300 kg/s) produced in 1989, decreasing to ~ 4.5 x 10^9 kg / month (~1750 kg/s) in late 1994. Due to the large number of earthquakes available, 400-event windows were used to calculate b and D for the entire Geysers dataset. Intense clustering corresponded to a decrease in D. Little in the way of changes in the correlation between b and D corresponding to the episodes of injection are discernible in the whole dataset (Figure 5.4(d)). In both the two-dimensional and three-dimensional cases most of the periods (i) - (viii) (Figure 5.4(d)) show little correlation between b and D. A negative correlation was observed in period (iv) when injection was low, but this behaviour is not exhibited during the periods of low injection (ii), (vi) and (viii). Negative correlations were also observed for period (i) when injection was high and period (iii) in the two dimensional case. Positive b/D correlations were seen for period (iii) (injection high) in the three-dimensional case and period (vi) (injection low) in both two and three dimensional cases of D.

5.3 Individual clusters within The Geysers

5.3.1 Introduction

There are two methods of dividing up seismicity into clusters. The first is subdividing events by visual inspection of hypocentral plots. This is highly

subjective, but is used traditionally *(e.g. Takeya, 1992)*. Second, data can be split into clusters using an algorithm. Although these algorithms can generate clusters that are non-user subjective, they do have drawbacks. The shape of cluster generated is dependent on the algorithm irrespective of the dataset studied. These methods also tend to overlook elongate clusters. Clusters in The Geysers are typically elongate. Additionally, to use these methods on datasets containing tens of thousands of points a large amount of computational power is required. Algorithms which can be applied to earthquake datasets, such as the 'Simple Linkage Method' *(Florek et al., 1951; Frohlich & Davis, 1990)* and the 'Nearest Centroid Sorting Method' *(Anderberg, 1973)* have other disadvantages. The 'Simple Linkage Method', in which the distance between two clusters is defined by the minimum distance between observations belonging to different clusters, tends to link clusters that are distinct to the eye on the basis of a sparse, background seismicity 'chain' between them *(Henderson et al., 1994)*. The 'Nearest Centroid Sorting Method' generates a given number of clusters, starting from a number of 'cluster seeds'. The selection of these 'seeds' is critical and subjective. Also, elongate clusters tend to be ignored in this method.

In the present study, clusters were chosen subjectively by comparing the surface locations of injection wells with the seismicity. The events in each cluster were extracted using the Macintosh PC-based three-dimensional visualisation package ***Datadesk***. Each cluster is labelled by the most active injection well associated with it. Figure 5.5 shows the locations of the clusters chosen.

5.3.2 Seismicity adjacent to well 09790016

The level of seismicity was low in this area (Figures 5.6(a) to (c), Table 5.1). Three small, distinct, clusters occurred adjacent to the surface locations of the three injection wells (Figure 5.6(a)). This seismicity extended down to ~ 2 km below sea level. Injection was either continuous and irregular (well 09790607) or occurred in short bursts (09790016 and 09790525) (Figure 5.6(c)). Production

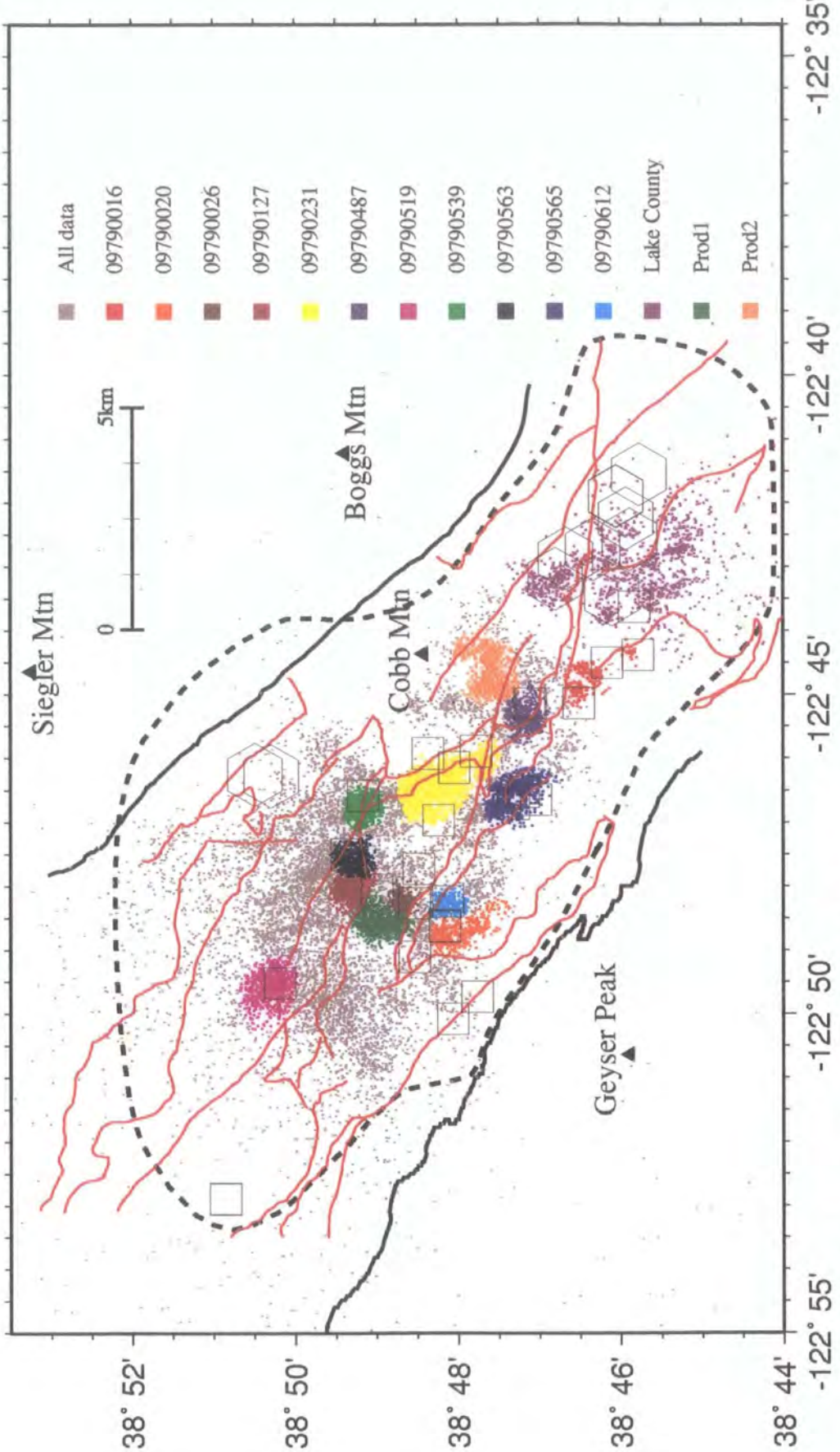

Figure 5.5 Map of The Geysers showing clusters and the surface locations of injection wells (squares = Sonoma County; hexagons = Lake County) and major fault zones (red lines). Earthquakes with M_d >= 0.5 are shown. Other symbols as for Figure 3.1.

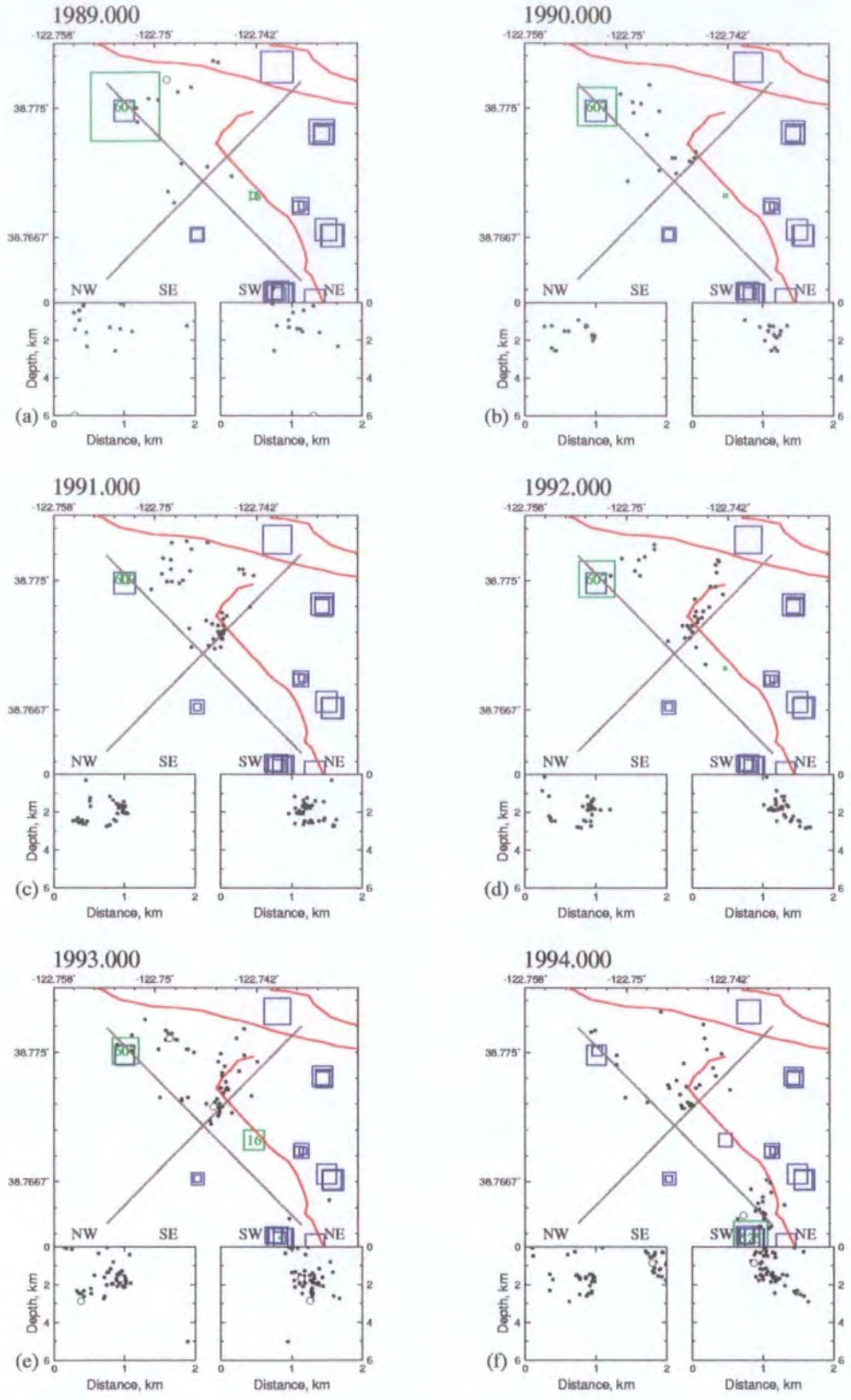

Figure 5.6(a) Epicentral maps and cross-sections for seismicity close to injection well 09790016, 1989-1994. Dots: events with $0.5 >= M_d > 2.0$, circles: events with $M_d >= 2.0$, red lines: faults, green squares: surface locations of injection wells, blue squares: surface locations of production wells. The size of the production and injection symbols are scaled to indicate activity: 1 cm^2 represents 1 x 10^{12} kg / year of fluid. 24-km long cross-sections are shown by grey lines. Dotted line = approximate reservoir boundary.

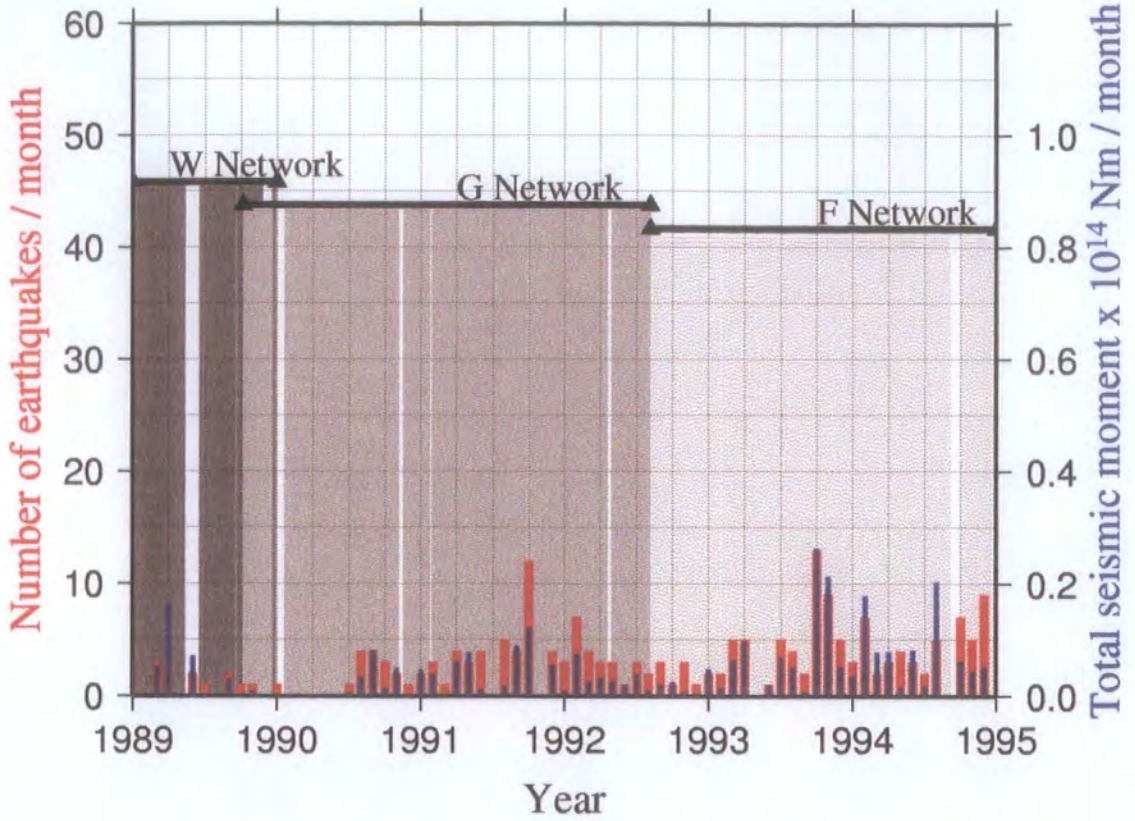

Figure 5.6(b) As Figure 5.4(b) except for earthquakes adjacent to injection well 09790016.

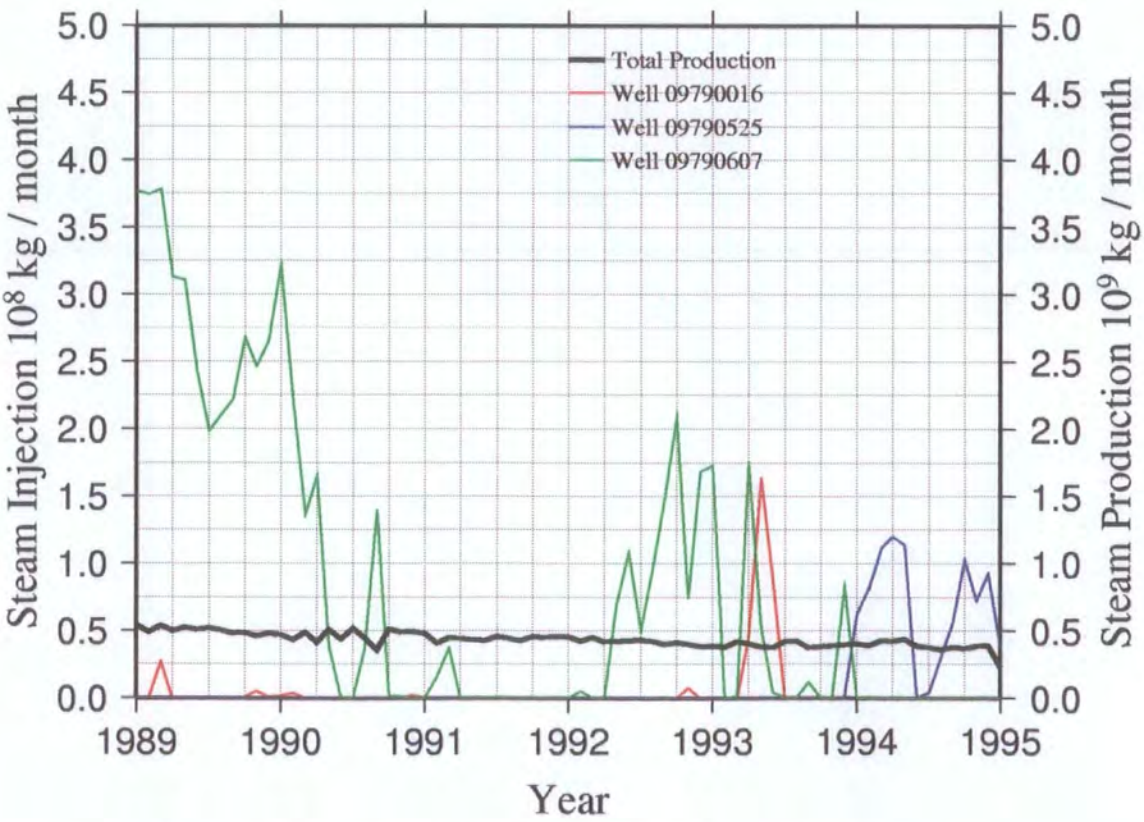

Figure 5.6(c) Well activity close to injection well 09790016 1989-1994.

was continuous and slightly declining. There were insufficient events to perform a *b/D* analysis.

Table 5.1 Summary of observations in the neighbourhood of well 09790016

Production History	Injection History	Seismicity	*b/D* correlation
Uniform decline in production. Production typically ~ 0.5 x 10^9 kg / month (~190 kg/s).	**09790016:** Peak in mid 1993. **09790525:** Small scale injection since 1994. **09790607:** variable scale, irregular injection since 1989.	Three small distinct clusters with a seismogenic base of ~ 2 km dipping to the NE. **1989 - 1990:** A little activity near 09790607. **1991 - 1993:** Activity near well 09790016 along fault. **1994:** Same level of activity (5 - 10 events / month) adjacent to 09790525, with a slight increase in the seismic moment rate.	Insufficient events for analysis.

5.3.3 Seismicity adjacent to well 09790020

The seismic activity in this area was distributed bimodally in depth with sub-clusters centred at ~ 1 km and ~ 4 km (Figures 5.7(a) to (c), Table 5.2). Injection in both wells 09790020 and 09790534 occurred in 6-month long episodes starting at the beginning of each year (Figure 5.7(c)). In early 1992 and early 1993 there were increases in the event rate and the seismic moment rate concurrent with injection (Figure 5.7(b)). Production was in steady decline between 1989 and 1994 (Figure 5.7(c)). There were insufficient events to perform a *b/D* analysis.

Table 5.2 Summary of observations in the neighbourhood of well 09790020

Production History	Injection History	Seismicity	*b/D* correlation
Uniform decline in production from ~ 2.5 to 1.0 x 10^8 kg/month (~ 96 to 39 kg/s).	**09790020:** 6-monthly injection peaks starting at beginning of each year. **09790534:** As 09790020, but with a higher injection rate.	NW - SE elongate cluster 2 km x 0.5 km in area. Bimodal depth distribution. Up to ~ 10 events/month with occasional bursts of seismicity. In February 1992, a swarm of larger events ~ 0.5 km to the south of the injection wells occurred at the same time as the injection episode. In early and late 1993 there were increases in seismic activity adjacent to the injection wells concurrent with injection episodes.	Insufficient events for analysis.

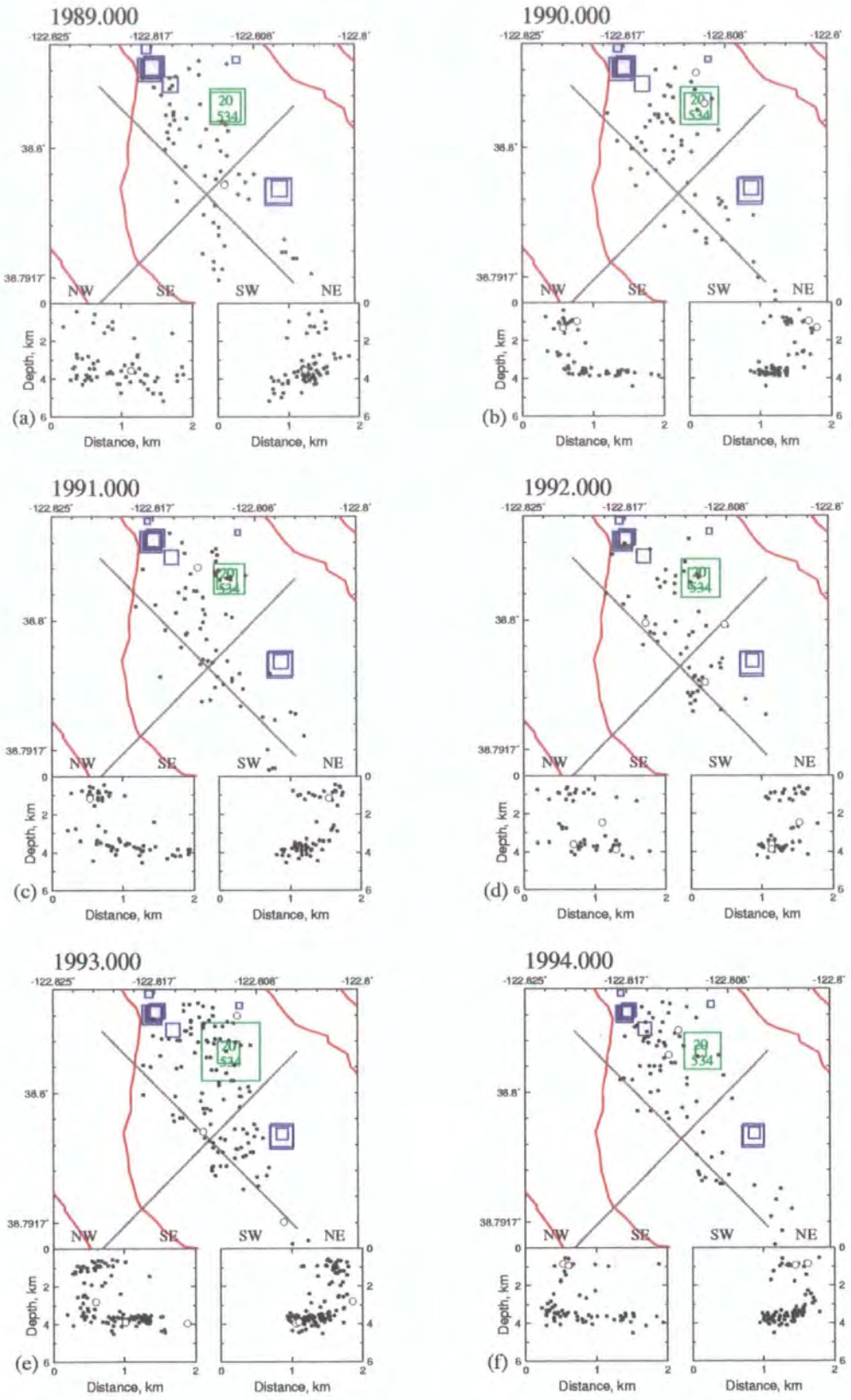

Figure 5.7(a) As Figure 5.6(a) except for earthquakes adjacent to injection well 09790020.

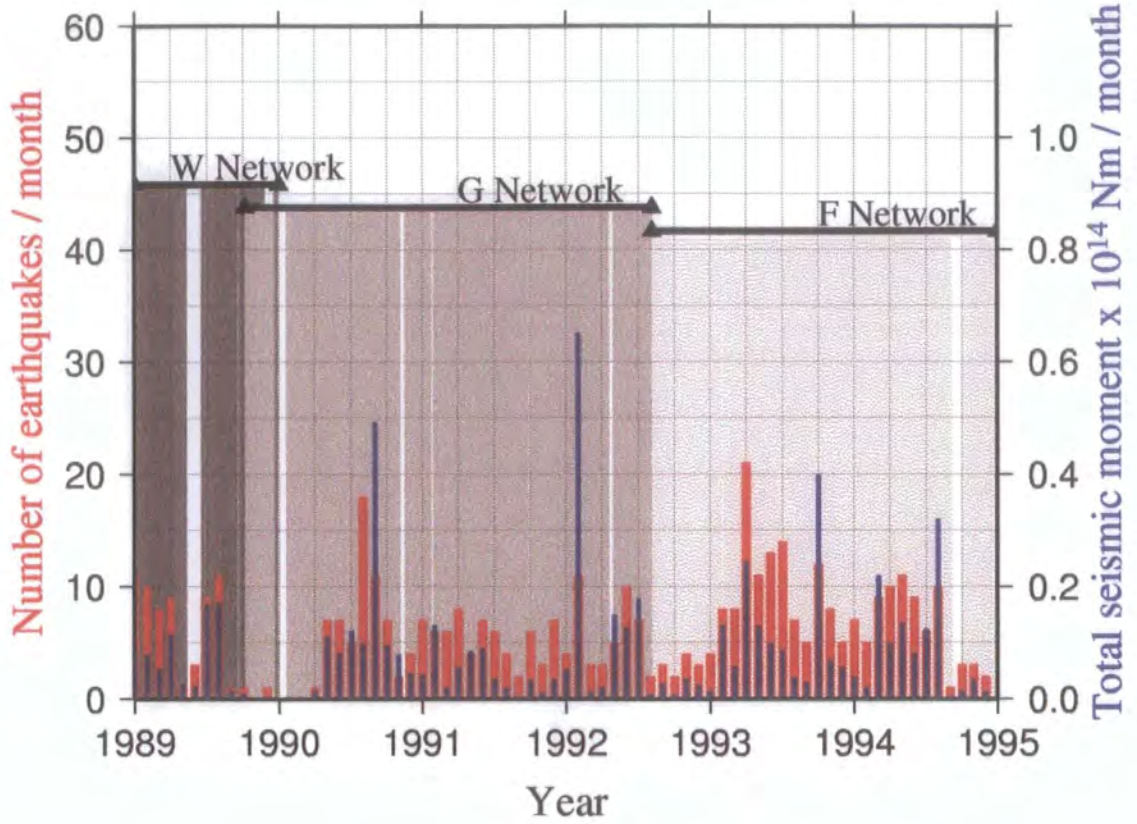

Figure 5.7(b) As Figure 5.4(b) except for earthquakes adjacent to injection well 09790020.

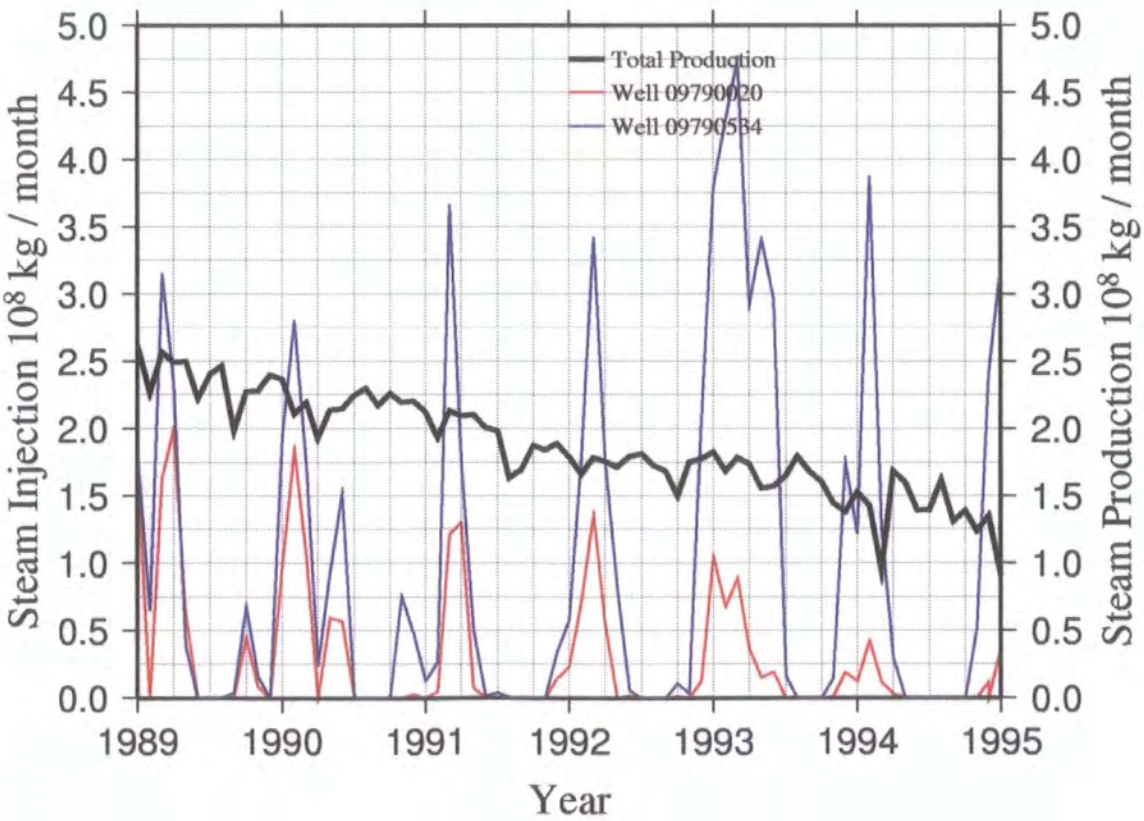

Figure 5.7(c) Well activity close to injection well 09790020 1989-1994.

5.3.4 Seismicity adjacent to well 09790026

Seismicity in this area was tightly clustered to the north of injection well 09790026 (Figure 5.8(a) to (c), Table 5.3). In early 1991, the event rate increased from ~ 2 events/month to ~ 10 events/month and remained at this level for the remainder of the study period (Figure 5.8(b)).

Table 5.3 Summary of observations in the neighbourhood of well 09790026

Production History	Injection History	Seismicity	*b/D* correlation
Very slight decline in production from 1.75 to 1.0 x 10^8 kg/month (~ 68 to 39 kg/s).	**09790026:** Variable and in pulses, increasing to constantly exceed ~ 1.25 x 10^8 kg/month (~ 48 kg/s) after 1992.	Single cluster 0.75 km x 0.75 km in area to the north of the injection well. After 1991 the seismicity rate was up to ~ 10 events / month. An increase in seismicity in early 1991 coincided with the rise in the injection rate. A further injection episode in 1992 generated a large transient increase in the seismic moment rate.	Insufficient events for analysis.

Injection increased gradually between 1989 and 1993 and remained at a level above about 1.2 x 10^8 kg / month (~ 48 kg/s) (Figure 5.8(c)). Production was uniform with a slight decline over the six-year period. There were insufficient events for a *b/D* analysis.

5.3.5 Seismicity adjacent to well 09790127

The cluster was immediately north of injection well 09790127 (Figure 5.9(a) to (d), Table 5.4). The earthquakes had a bimodal distribution with sub-clusters centred at ~ 1 km and ~ 4 km (Figure 5.9(a)). The seismicity and seismic moment rates increased sharply in early 1993 (Figure 5.9(b)), with most events concentrated in the deeper sub-cluster (Figure 5.9(a)). There was a further increase in seismic activity in early 1994. Apart from a brief pulse of injection peaking at 1.0 x 10^8 kg/month (~ 39 kg/s) in early 1994, injection in the area was very low level (Figure 5.9(c)). Production was uniform and declining. In the case

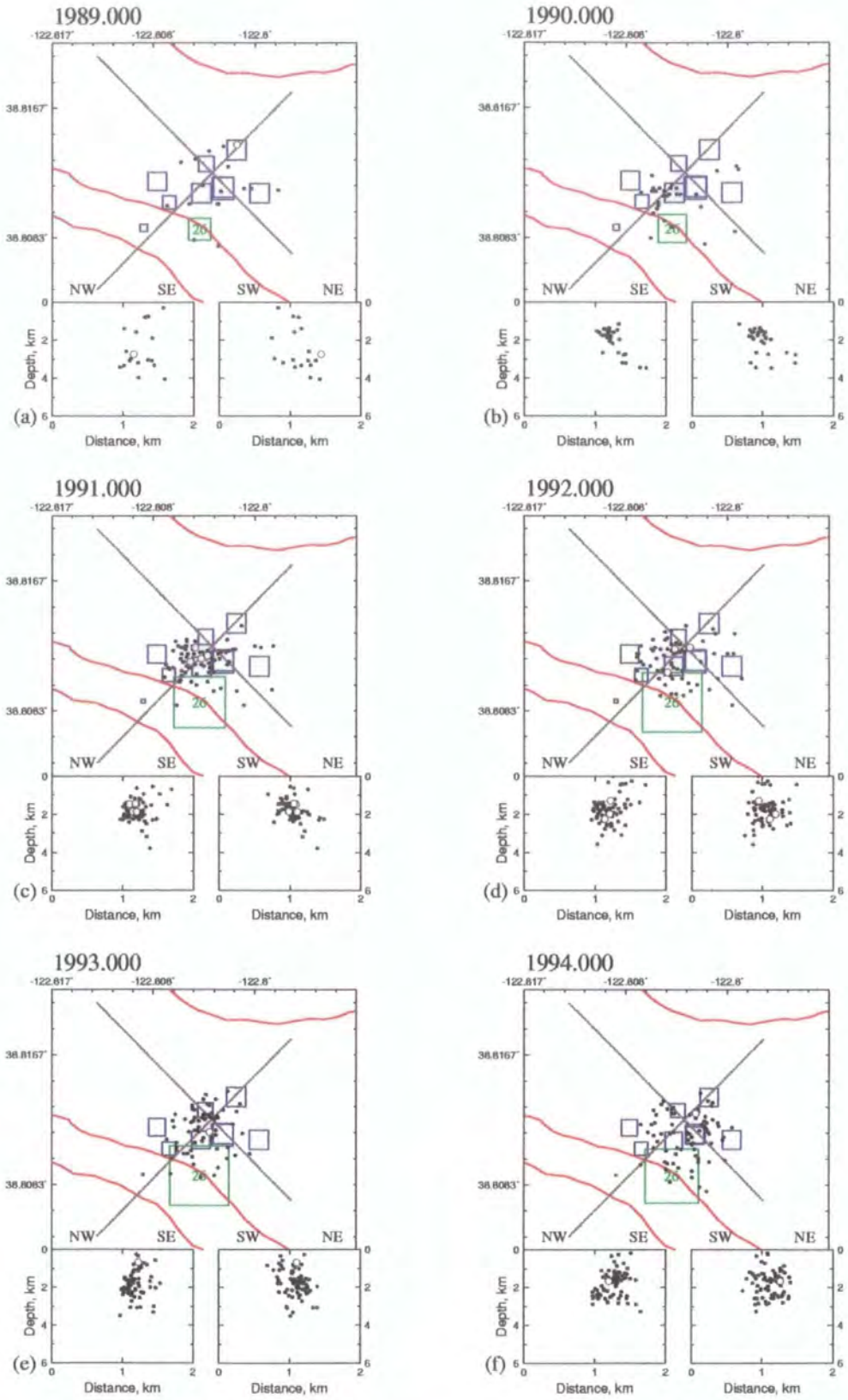

Figure 5.8(a) As Figure 5.6(a) except for earthquakes adjacent to injection well 09790026.

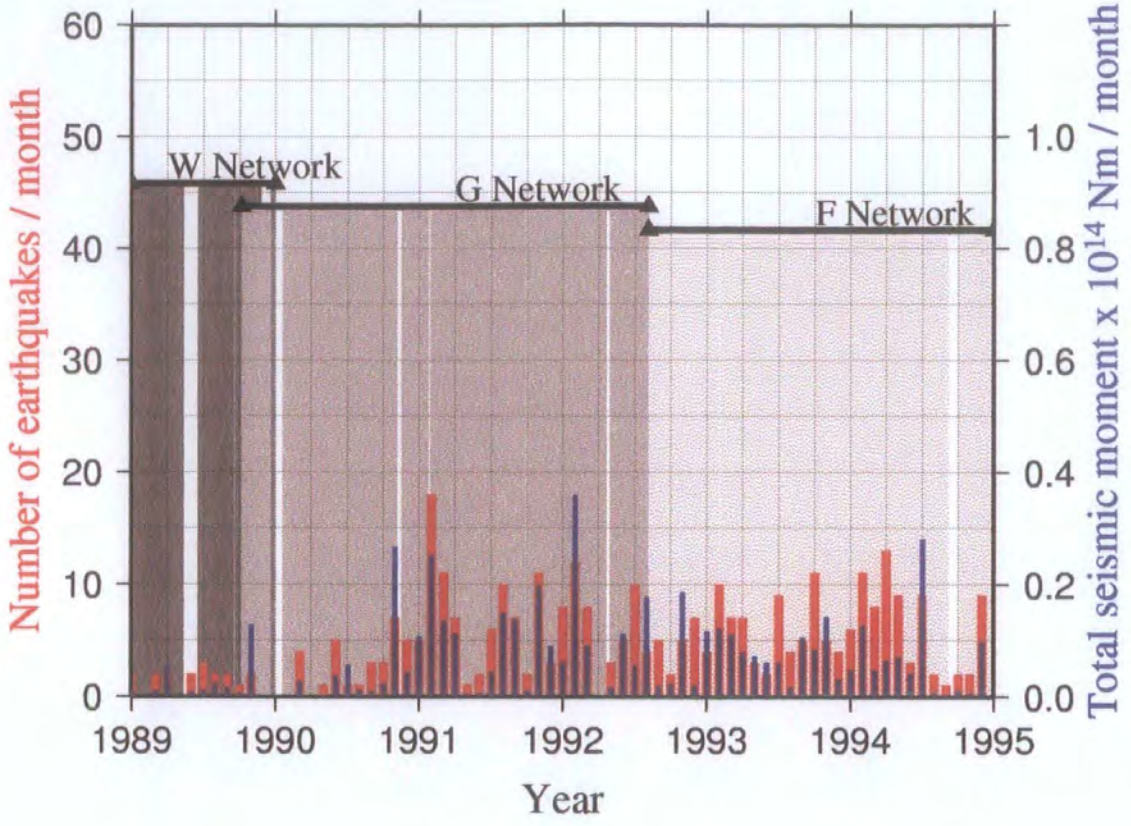

Figure 5.8(b) As Figure 5.4(b) except for earthquakes adjacent to injection well 09790026.

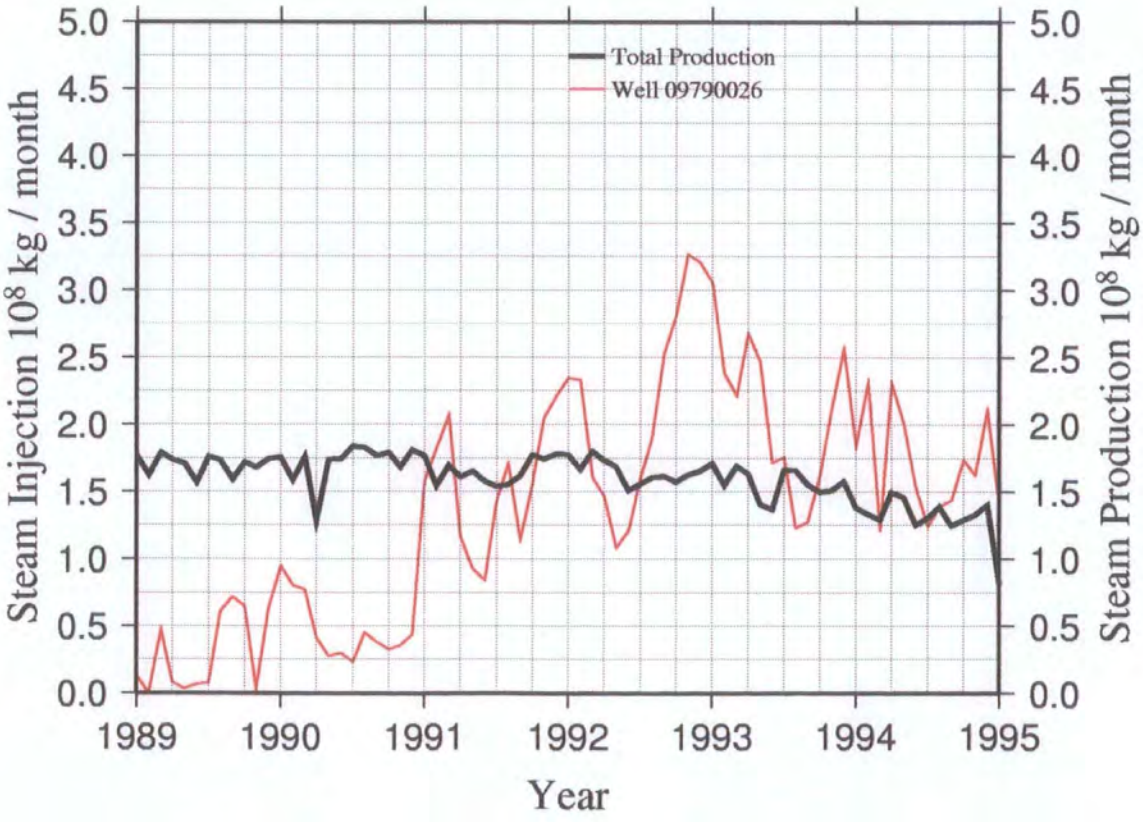

Figure 5.8(c) Well activity close to injection well 09790026 1989-1994.

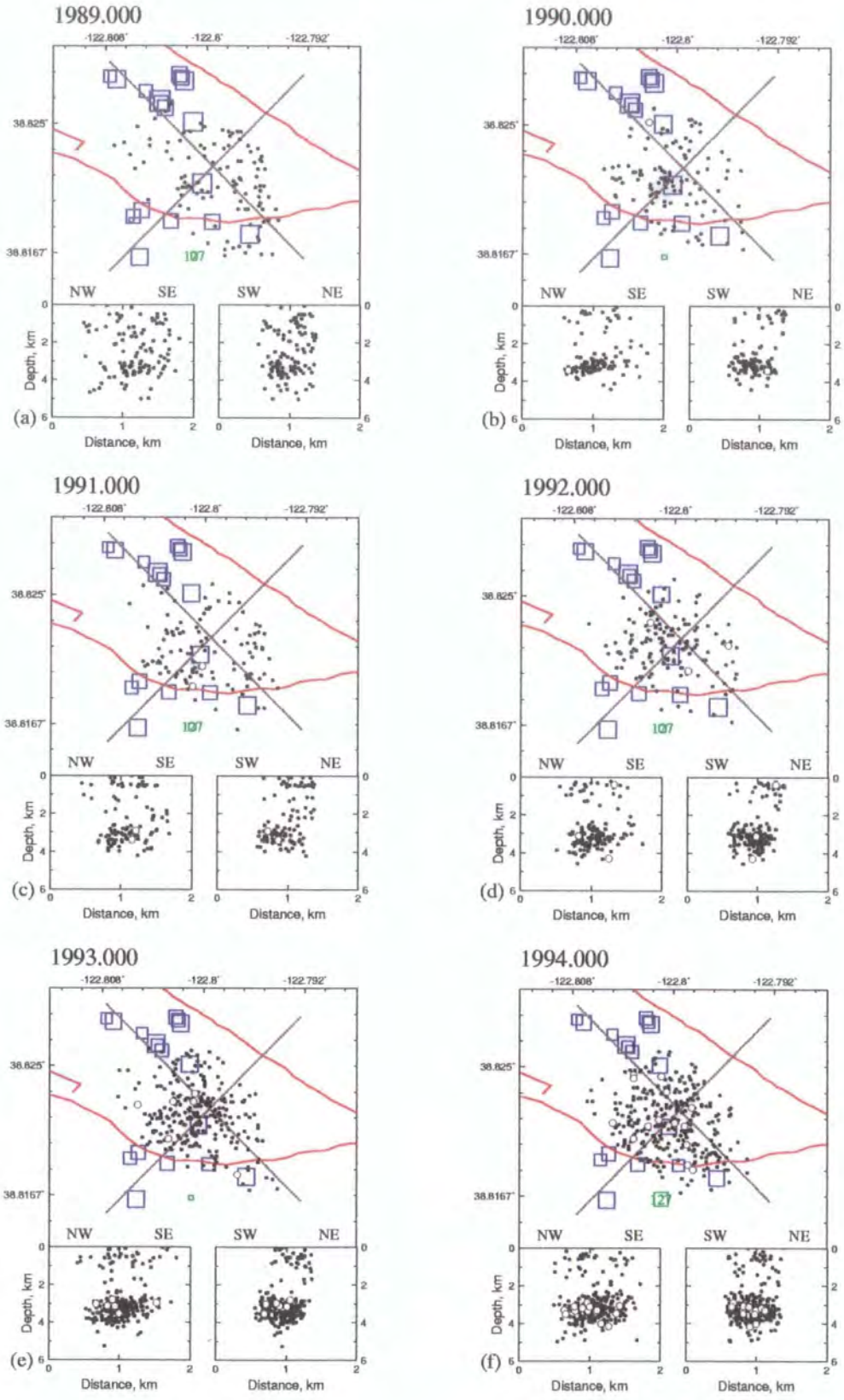

Figure 5.9(a) As Figure 5.6(a) except for earthquakes adjacent to injection well 09790127.

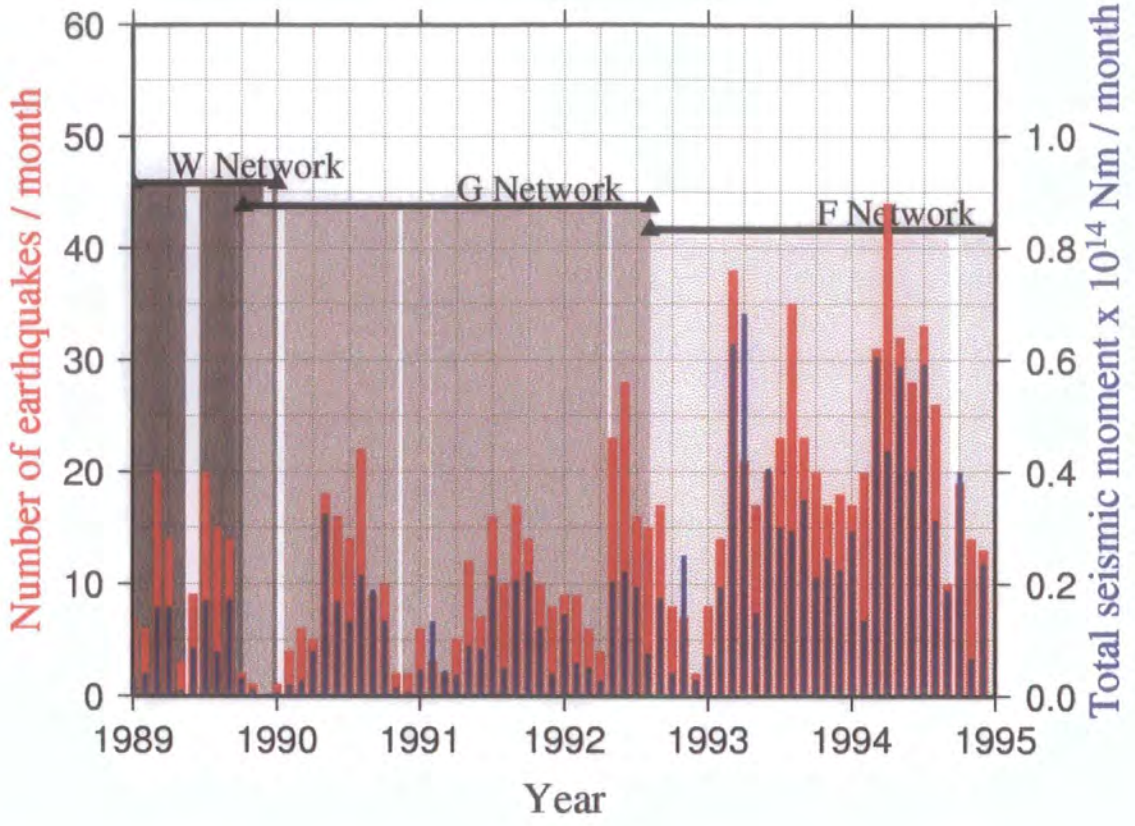

Figure 5.9(b) As Figure 5.4(b) except for earthquakes adjacent to injection well 09790127.

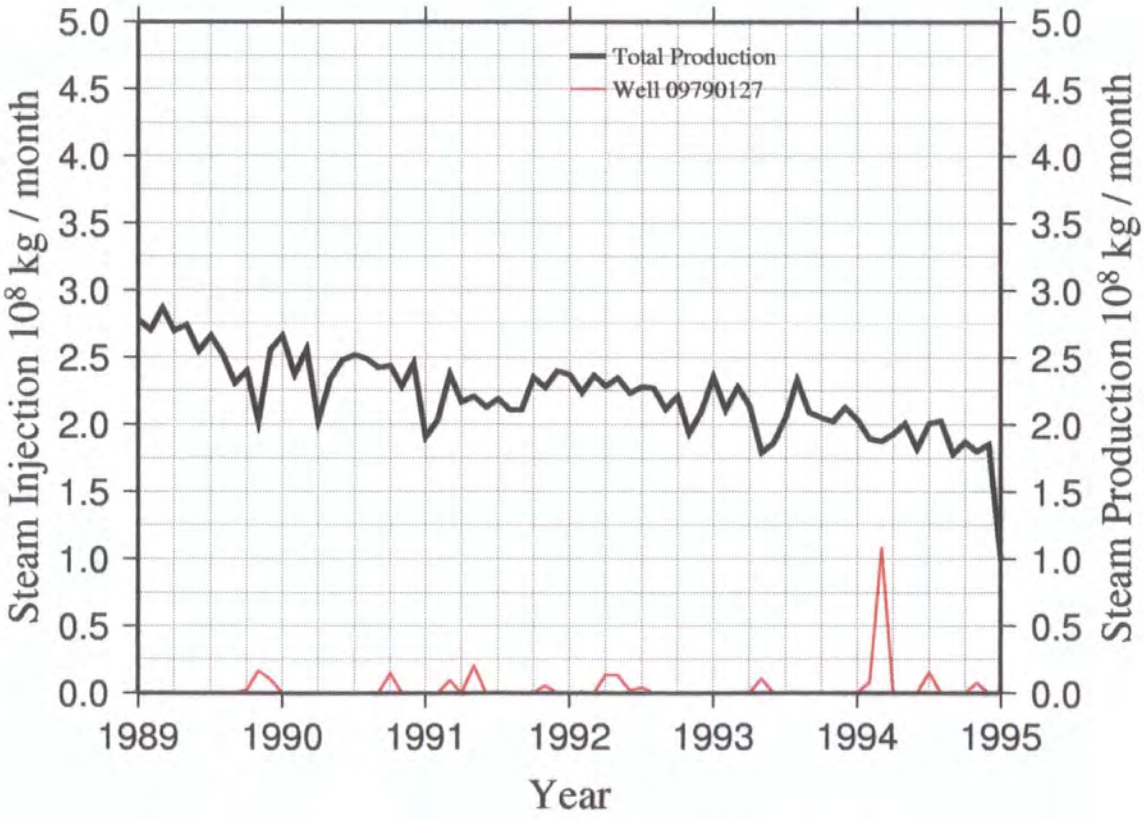

Figure 5.9(c) Well activity close to injection well 09790127 1989-1994.

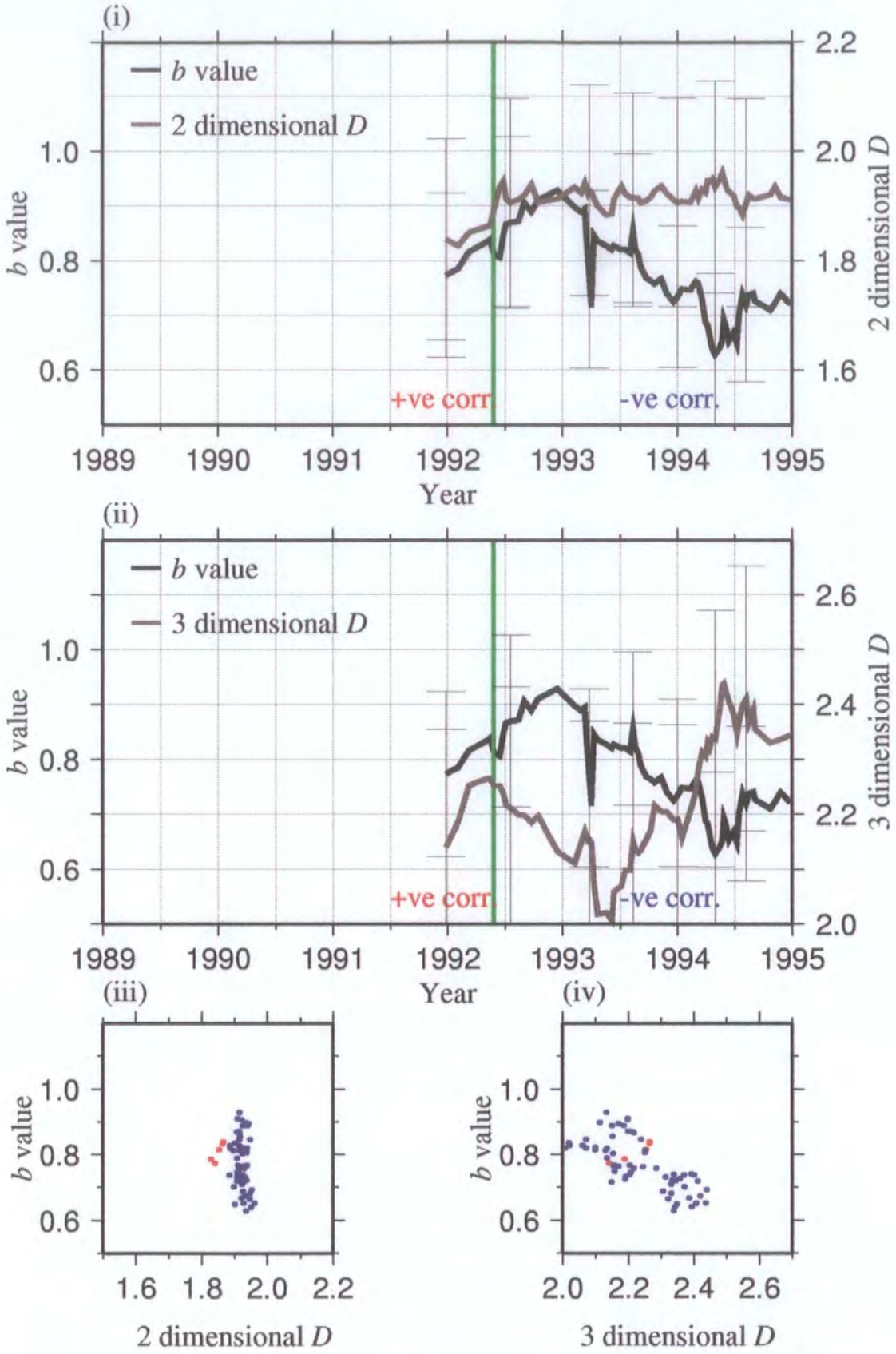

Figure 5.9(d)(i) Plot of *b* value and two-dimensional *D* for seismicity adjacent to well 09790127 1989-94. (ii) as (i) except for three-dimensional *D*. (iii) *b* / two- dimensional *D* correlation plot. (iv) as (iii) except for three-dimensional *D*. Red text and circles indicate a positive *b*/*D* correlation; blue text and circles a negative one.

of this seismic volume, clustering results in high two-dimensional D and low three-dimensional D. In mid 1992, the correlation between b and D changed from positive to negative in both the two-dimensional and three-dimensional cases of D. This change coincided with the increase in the seismic event rate. It should be noted, however, that there are very few data points prior to mid-1992.

Table 5.4 Summary of observations in the neighbourhood of well 09790127

Production History	Injection History	Seismicity	*b/D* correlation
Uniform decline in production from ~2.75 to ~ 1.0×10^8 kg / month (~ 106 to 39 kg/s).	**09790127** Very little. Brief increase to ~ 1.0×10^8 kg / month (~ 39 kg/s) in early 1994.	NW - SE elongated cluster 1.5 km x 1 km in area. Bimodal depth distribution with sub-clusters at ~ 1 km and ~ 4 km. **Pre mid 1992:** Variable seismic rate up to ~ 10 - 20 events / month. Larger events ($M_d \geq 2.0$) in both sub-clusters. **Post mid 1992:** Increase in seismic rate to occasionally exceed 35 events / month. Most events in deeper sub-cluster, with many larger events there. Further increase in 1994.	Two-dimensional case: switch from +ve to no correlation in mid 1992. Two-dimensional case: switch from +ve to -ve correlation in mid 1992. There is very little pre-1992 data.

5.3.6 Seismicity adjacent to well 09790231

The earthquakes that comprise this cluster also have a bimodal depth distribution, one sub-cluster centred at a depth of ~ 2 km and the other at ~ 1 km (Figure 5.10(a) to (d), Table 5.5). Before 1992, seismicity was uniformly distributed throughout the cluster. Injection was high and continuous, and production was low and continuous (Figure 5.10(c)). In 1992, production well 09790045 was converted into an injection well. Almost immediately a tight cluster of earthquakes appeared to the south-west of the well (Figure 5.10(a)) and the seismicity exhibited a large negative anomaly in D (Figure 5.10(d)). In this cluster, stronger clustering corresponded to low D. The time sequence was divided into three periods, before the anomaly, during and after (Figure 5.10(d)). There was a positive *b/D* correlation before and after the anomaly and a negative one during in the two-dimensional D case. In the three-dimensional D case there are weak negative *b/D* correlations before and during the anomaly, and a positive one after.

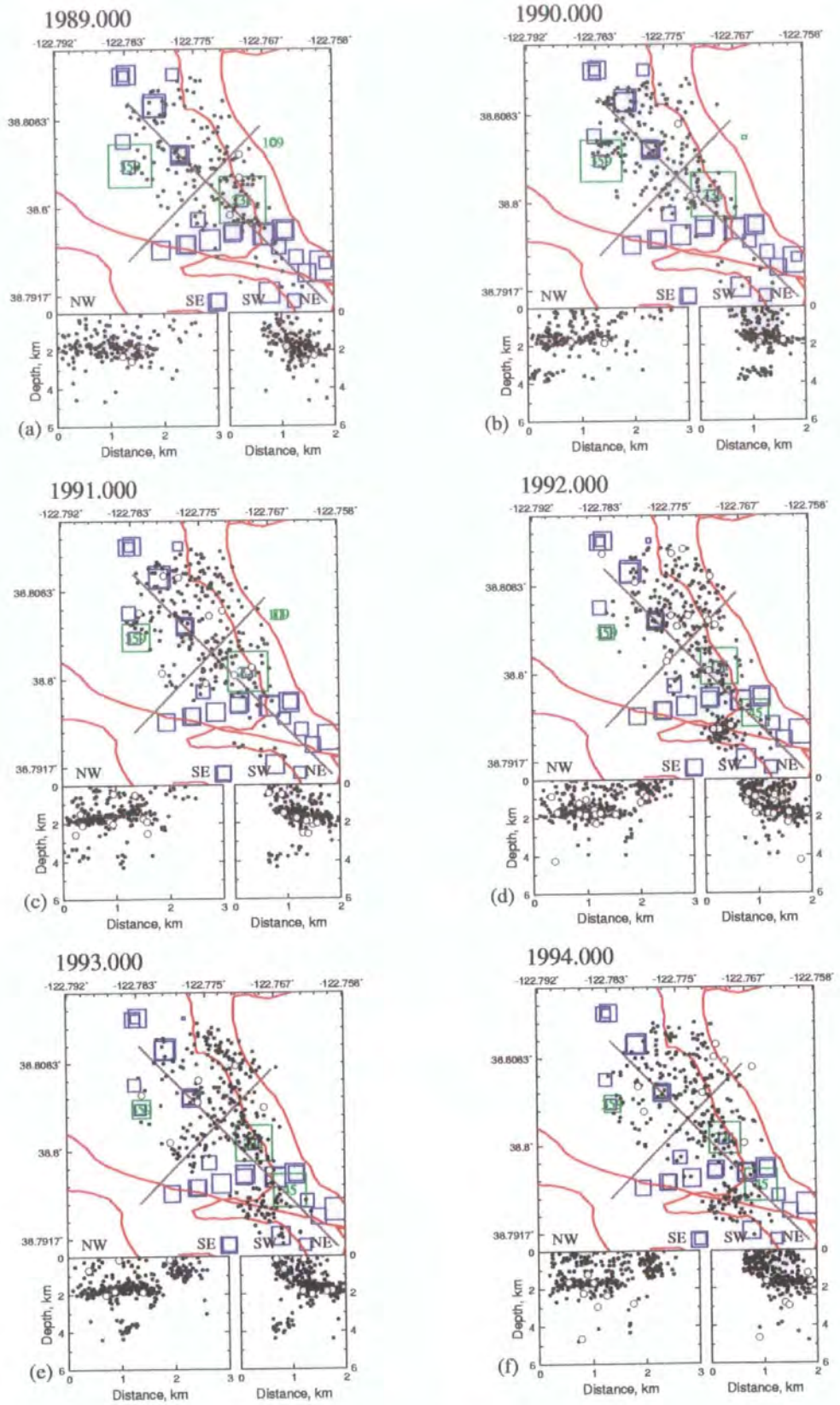

Figure 5.10(a) As Figure 5.6(a) except for earthquakes adjacent to injection well 09790231.

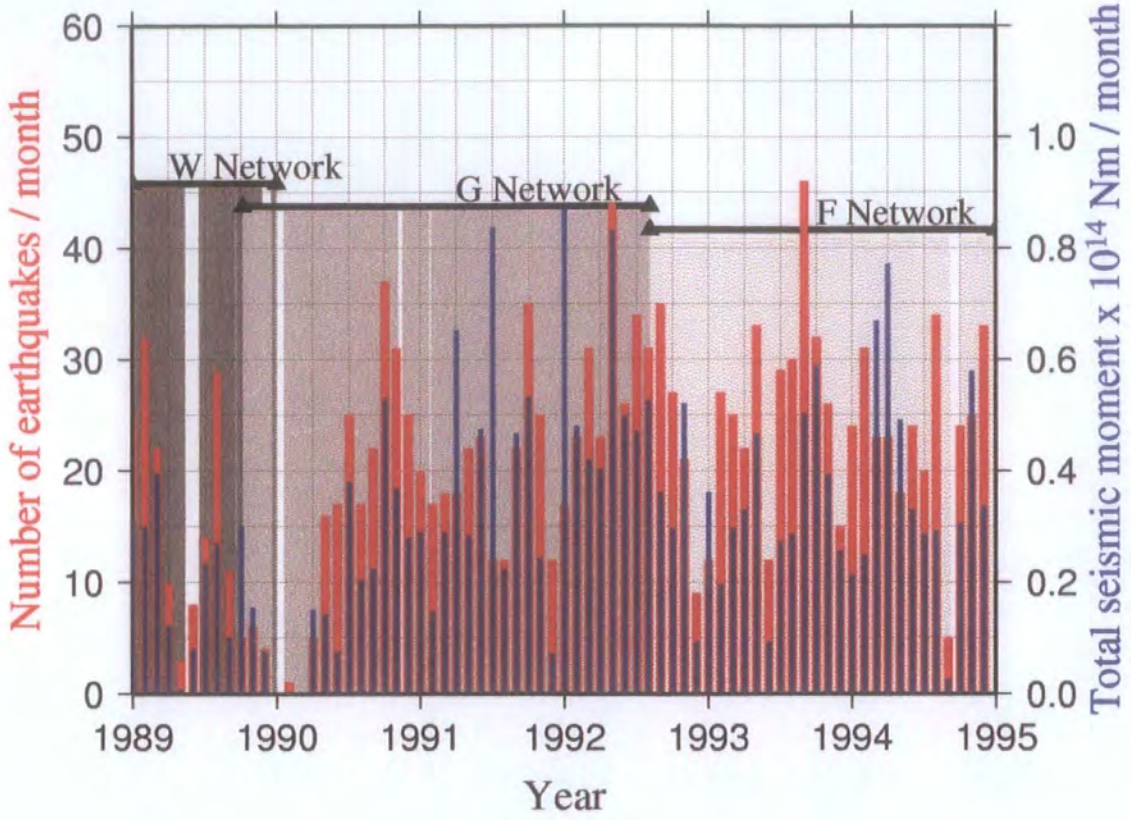

Figure 5.10(b) As Figure 5.4(b) except for earthquakes adjacent to injection well 09790231.

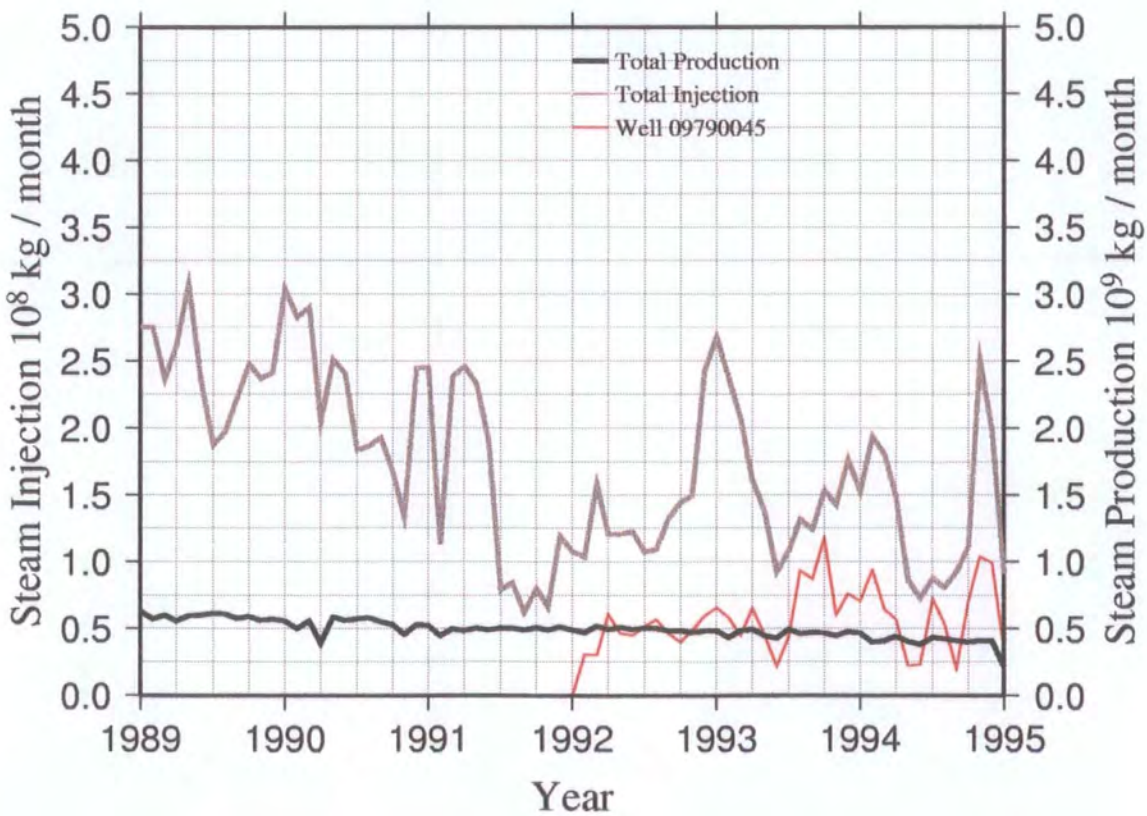

Figure 5.10(c) Well activity close to injection well 09790231, 1989-1994.

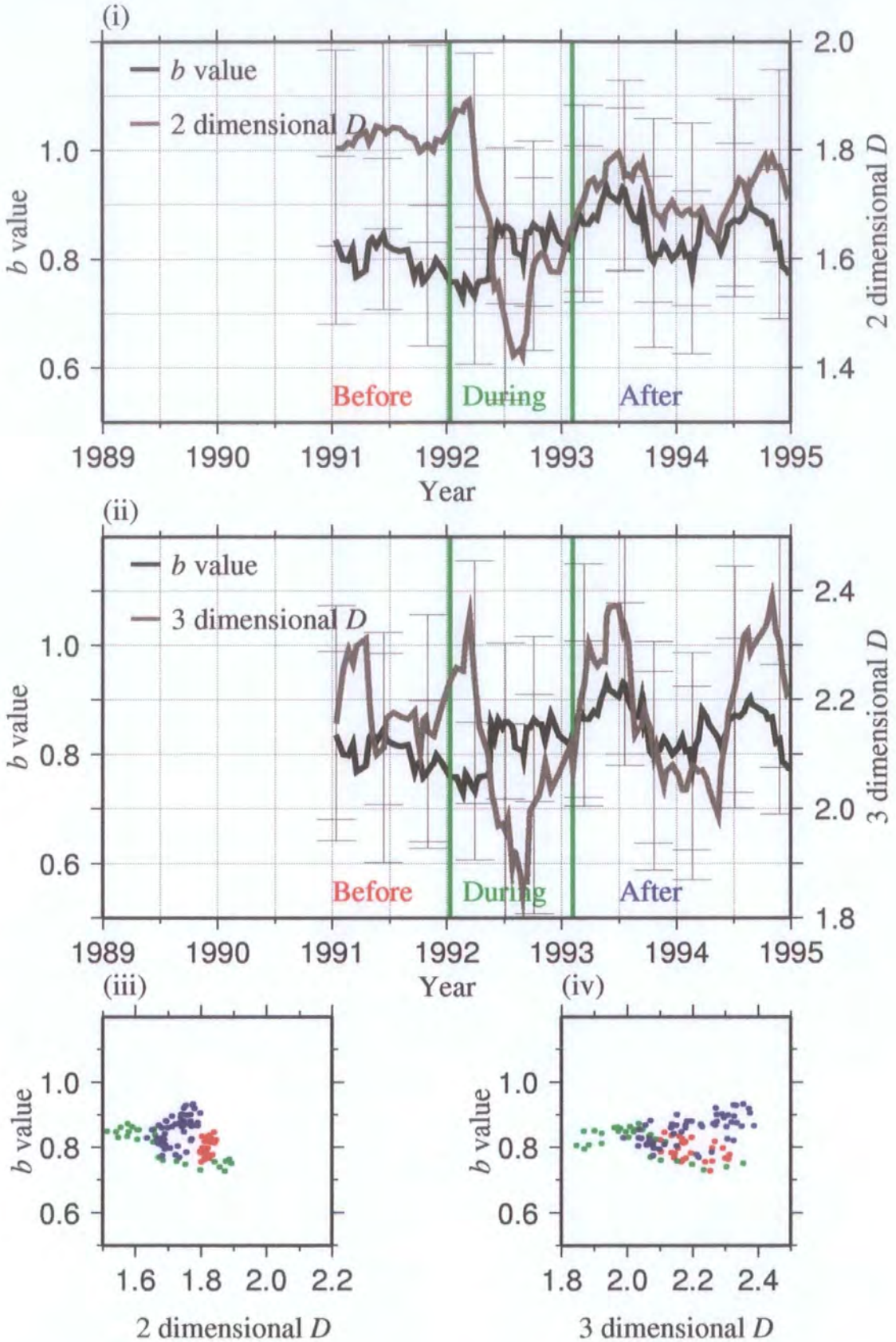

Figure 5.10(d)(i) Plot of *b* value and two-dimensional *D* for seismicity adjacent to well 09790231 1989-94. (ii) as (i) except for three-dimensional *D*. (iii) *b* / two-dimensional *D* correlation plot. (iv) as (iii) except for three-dimensional *D*. Red text and circles indicate *b* / *D* correlation before the 1992 *D* anomaly, green text and circles during, and blue text and circles after.

Table 5.5 Summary of observations in the neighbourhood of well 09790231

Production History	Injection History	Seismicity	*b/D* correlation
Production continuous and high, declining from 0.75 to 0.4 x 10^9 kg/month (290 to 154 kg/s).	Continuously high and variable. In 1992, well 09790045 was converted from production to injection with no noticeable change in production.	NW - SE trending cluster 2.75 km x 1 km in area. Sub-clusters centred at depths of ~ 1 km along entire cluster, second at ~ 2 km in the NW. This cluster is located on a fault zone. Event rate is continuously high with up to ~ 45 events/month. In 1992, a tight cluster of events adjacent to well 09790045 developed. Larger events mostly found in the deeper sub-cluster and the sub-cluster that developed close to well 09790045.	In both two-dimensional and three-dimensional cases of *D* there are large negative anomalies in *D* early 1992 to mid 1993. In the two-dimensional *D* case, before and after the anomaly there is a positive correlation, and a negative correlation during. In the three-dimensional *D* case there are weak negative correlations before and during the anomaly and a positive correlation afterwards.

5.3.7 Seismicity adjacent to well 09790487

In the neighbourhood of this well, a small cluster occurred centred at ~ 1 km depth (Figures 5.11(a) to (d), Table 5.6). Prior to mid 1991, the seismic rate was low (Figure 5.11(b)).

Table 5.6 Summary of observations in the neighbourhood of well 09790487

Production History	Injection History	Seismicity	*b/D* correlation
Production is uniform and declining with some large drops in early 1991 , 1992 and 1994. Production typically ~ 3.75 x 10^8 kg / month (~ 145 kg/s).	**09790655:** Injection continuous between 1989 and mid 1991, when it ceases. **09790487:** Injection starts mid 1991. Surge in late 1992.	NW - SE elongated cluster 1 km x 1.5 km in area, centred at a depth of 1 km. **1989 - 1990:** Very little activity, mostly near 09790665. **1991 - 1994:** Sudden increase in activity in the middle of 1991, mostly to the SW of 09790487.	There is little data before injection was transferred from well 09790655 to 09790487. There is a slight increase in *D* during 1993 (most evident in the two-dimensional *D* case) simultaneous with the concurrent injection surge. No clear *b/D* correlation.

Following the transfer of injection from well 09790655 to nearby well 09790487 in mid 1991 (Figure 5.11(c)), seismicity greatly increased. In both the two

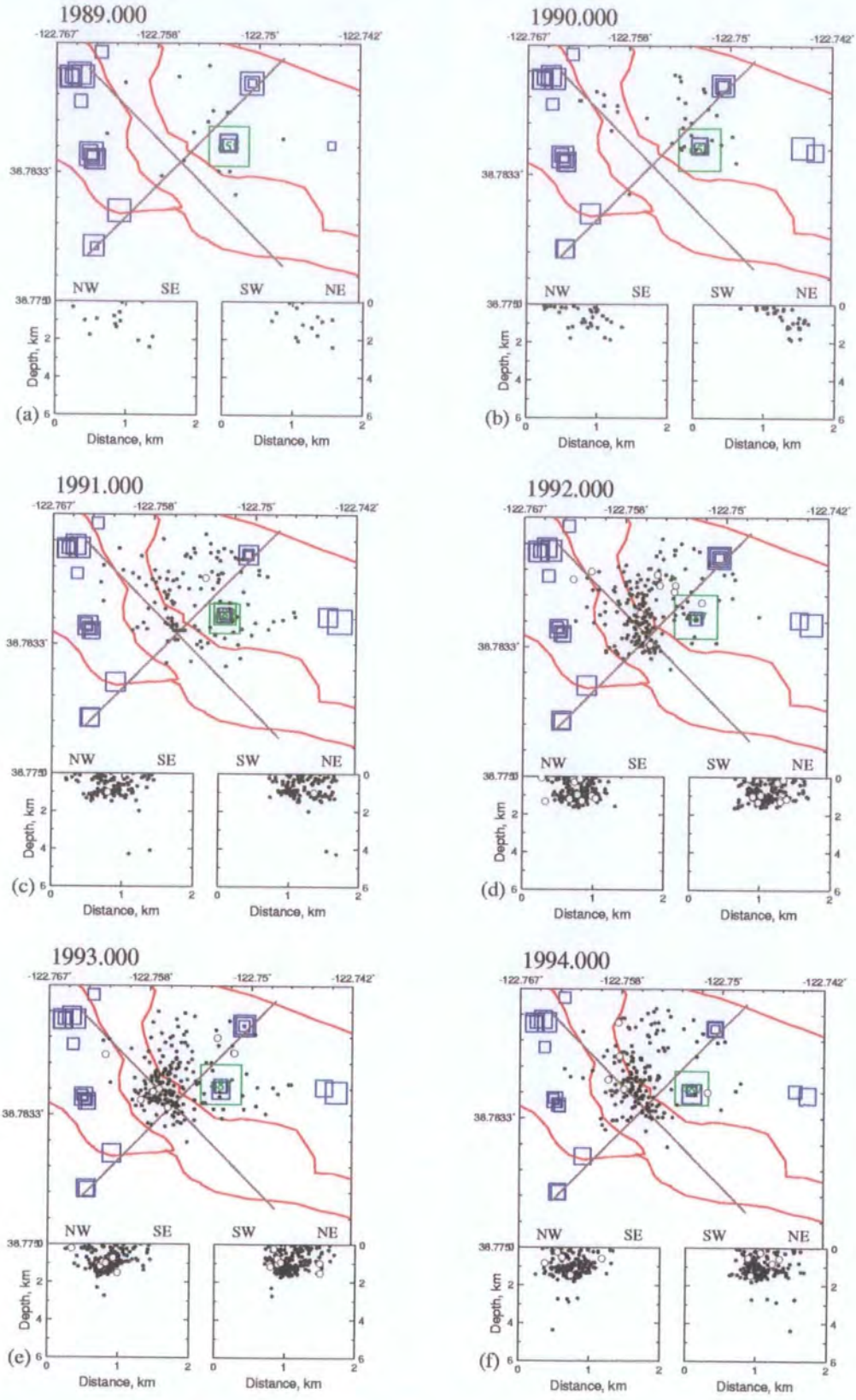

Figure 5.11(a) As Figure 5.4(a) except for earthquakes adjacent to injection well 09790487.

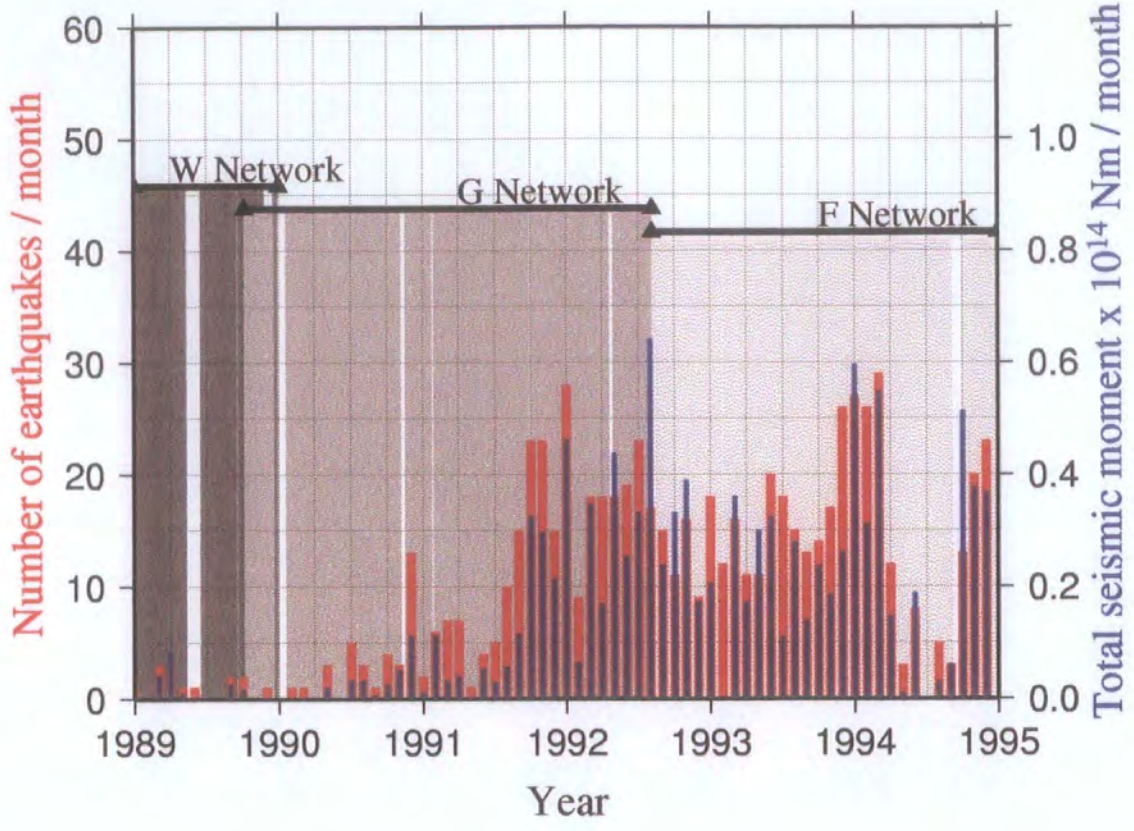

Figure 5.11(b) As Figure 5.4(b) except for earthquakes adjacent to injection well 09790487.

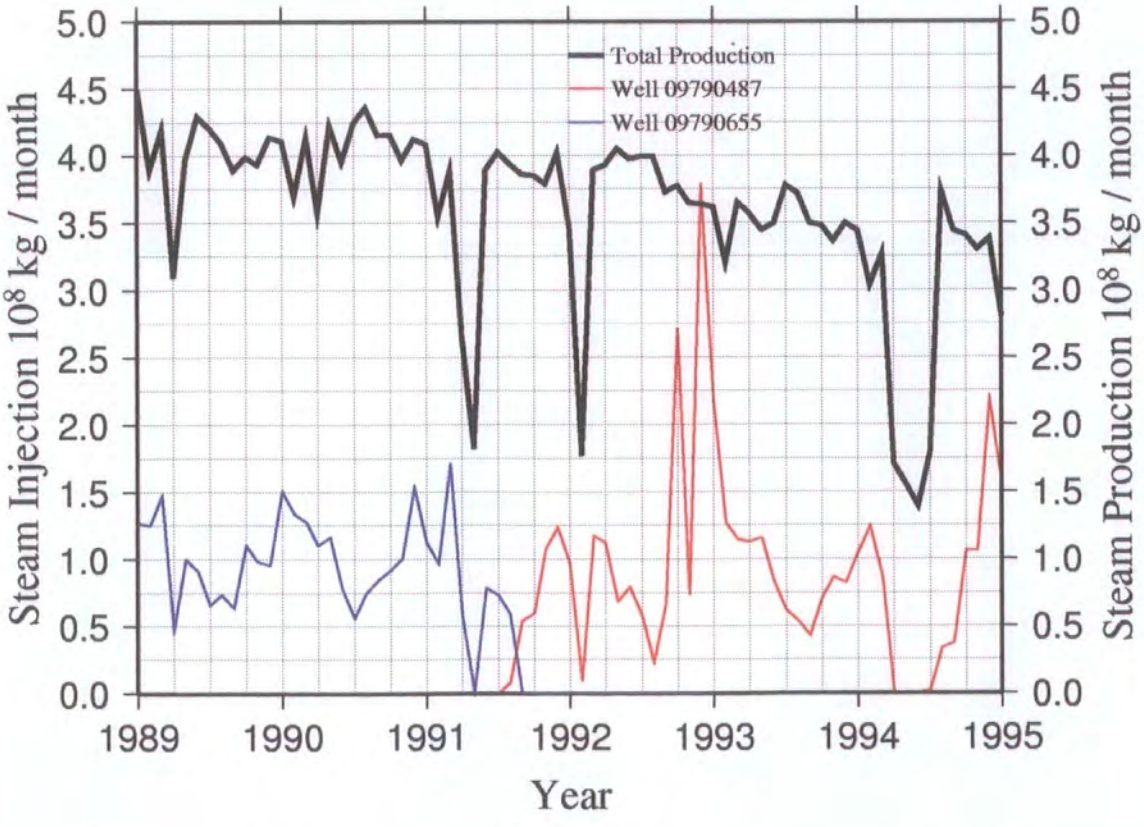

Figure 5.11(c) Well activity close to injection well 09790487 between 1989-1994.

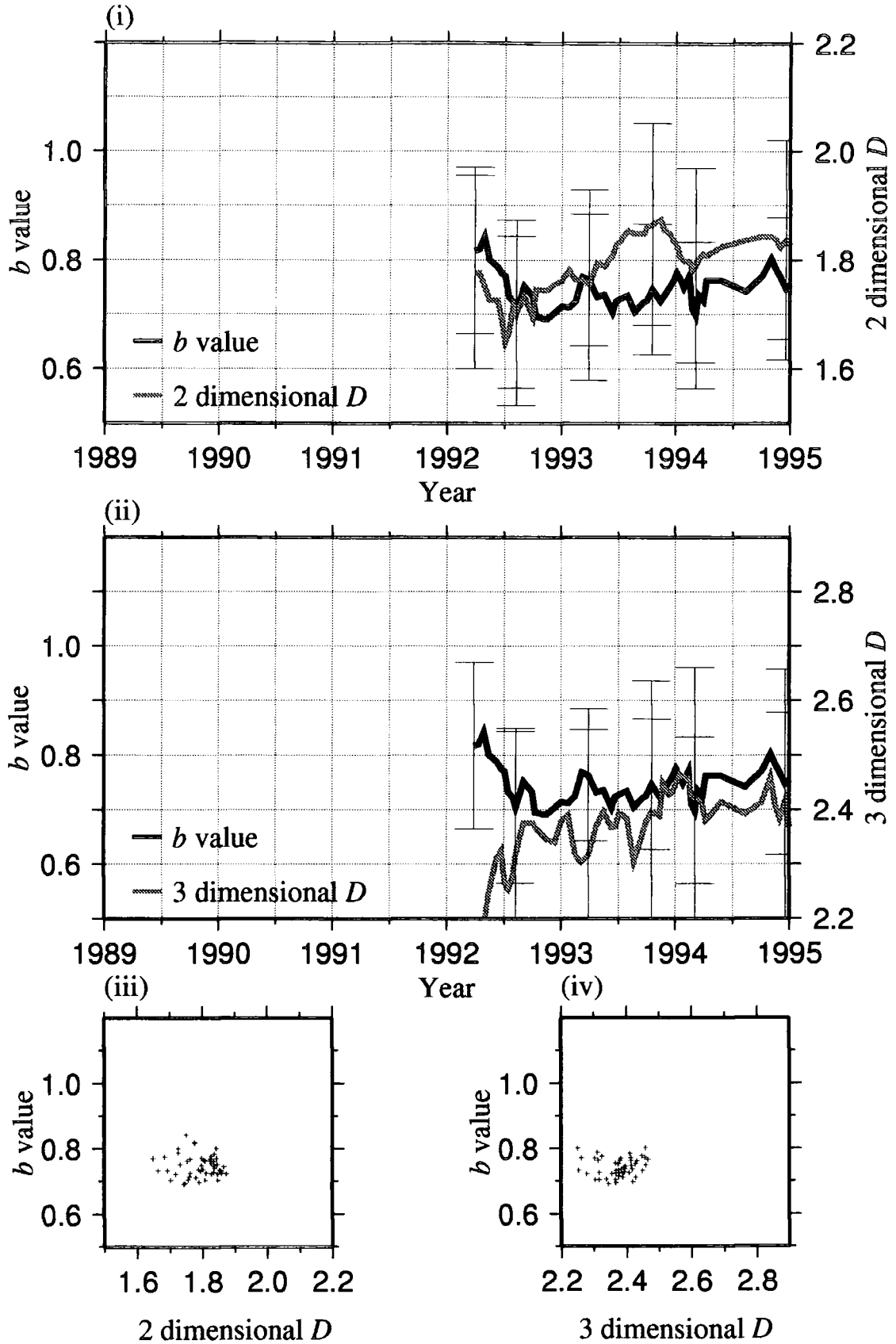

Figure 5.11(d) As Figure 5.9(d) but for seismicity adjacent to well 09790487.

-dimensional and three-dimensional cases of D greater clustering resulted in an increase in D. There were insufficient data to study the b/D correlation before and immediately after the transfer of injection to the new well. No clear correlation was apparent in the dataset.

5.3.8 Seismicity adjacent to well 09790519

Events in this cluster, in the north-west Geysers, have a bimodal depth distribution (Figure 5.12(a) to (d), Table 5.7), with events clustered at depths of ~ 1 km and ~ 4 km. Four episodes of high seismic rate occur between 1989 and 1994 (Figure 5.12(b)). In each episode the seismicity was evenly distributed throughout the cluster, apart from in the early-1994 episode when a few small sub-clusters occurred to the north of the injection wells (Figure 5.12(a)).

Table 5.7 Summary of observations in the neighbourhood of well 09790519

Production History	Injection History	Seismicity	b/D correlation
Production uniform apart from a drop in early 1989 and surges in late 1989 and late 1990. Production typically ~ 1.75 x 10^8 kg/month (~ 68 kg/s).	Injection low and cyclic with a period of ~ 1 year. Typical injection ~ 0.0 - 1.0 x 10^8 kg/month (~ 39 kg/s).	Cluster 1.5 x 2 km in area with a 1 - 4 km depth range. Activity occurs in bursts when the seismic rate may reach > 30 events / month.	Correlation changes from negative before 1993, to positive after for both two- and three-dimensional locations.

Injection was continuous and cyclic with a 1-year period (Figure 5.12(c)). Only the 1992 injection cycle coincided with an increase in seismicity. Production was continuous with an occasional surge. Greater clustering resulted in a decrease in D for both the two-dimensional and three-dimensional locations. The b/D correlation changed from negative to positive in mid 1993 (Figure 5.12(d)).

5.3.9 Seismicity adjacent to well 09790539

The seismicity had a bimodal depth distribution, with sub-clusters centred at ~ 1 km and ~ 2 km (Figure 5.13(a) to (d), Table 5.8). This cluster was most active

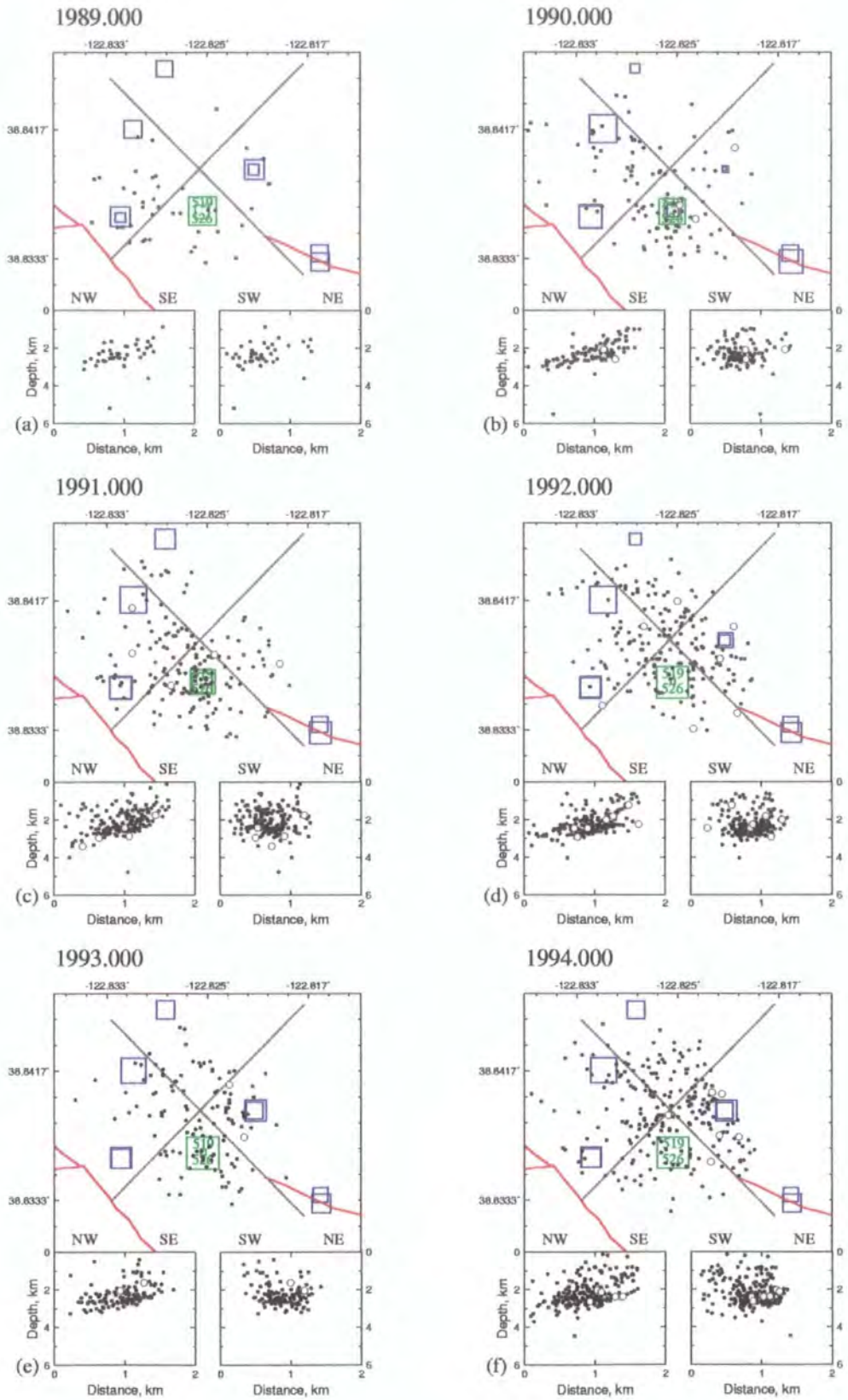

Figure 5.12(a) As Figure 5.6(a) except for earthquakes adjacent to injection well 09790519.

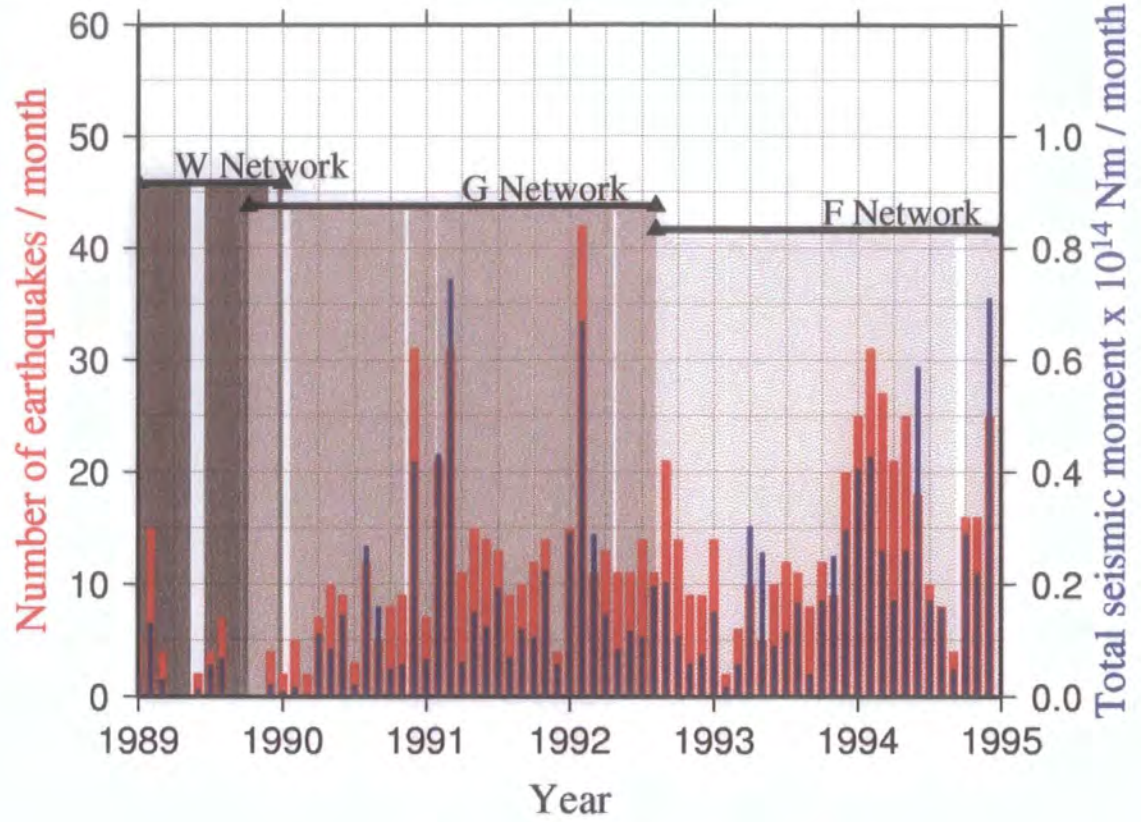

Figure 5.12(b) As Figure 5.4(b) except for earthquakes adjacent to injection well 09790519.

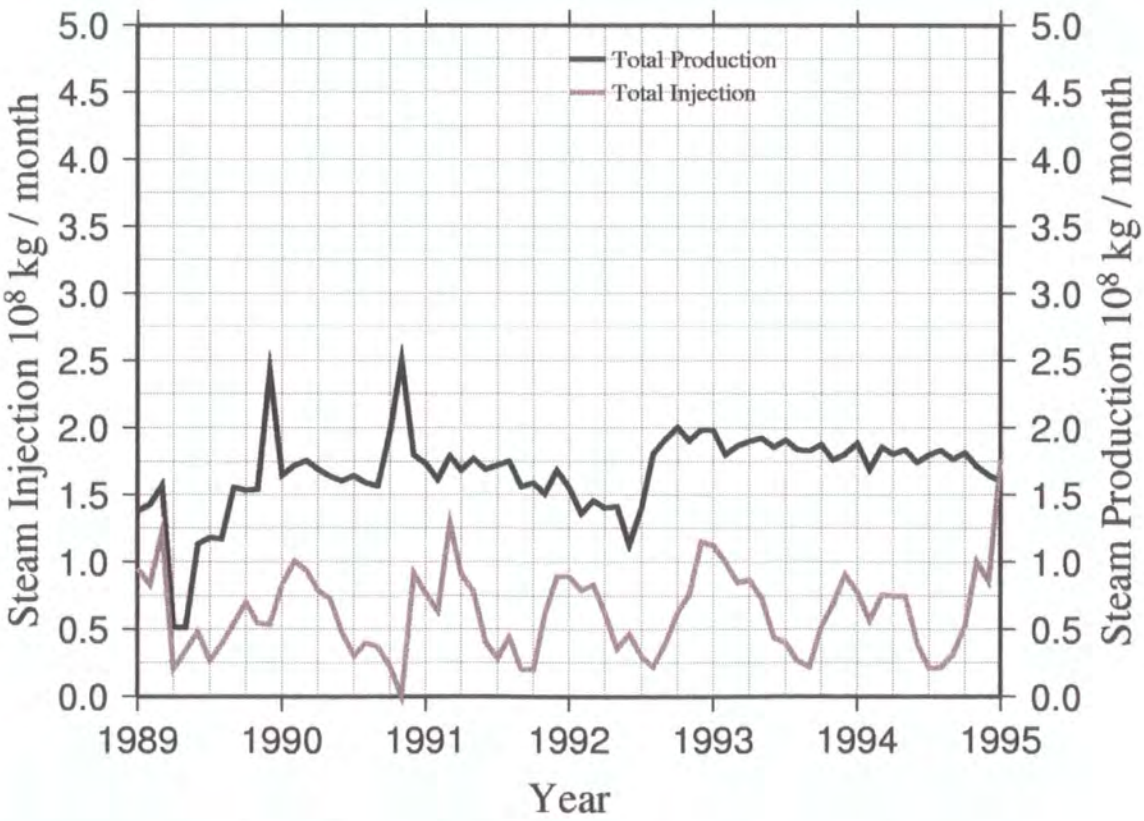

Figure 5.12(c) Well activity close to injection well 09790519 1989-1994.

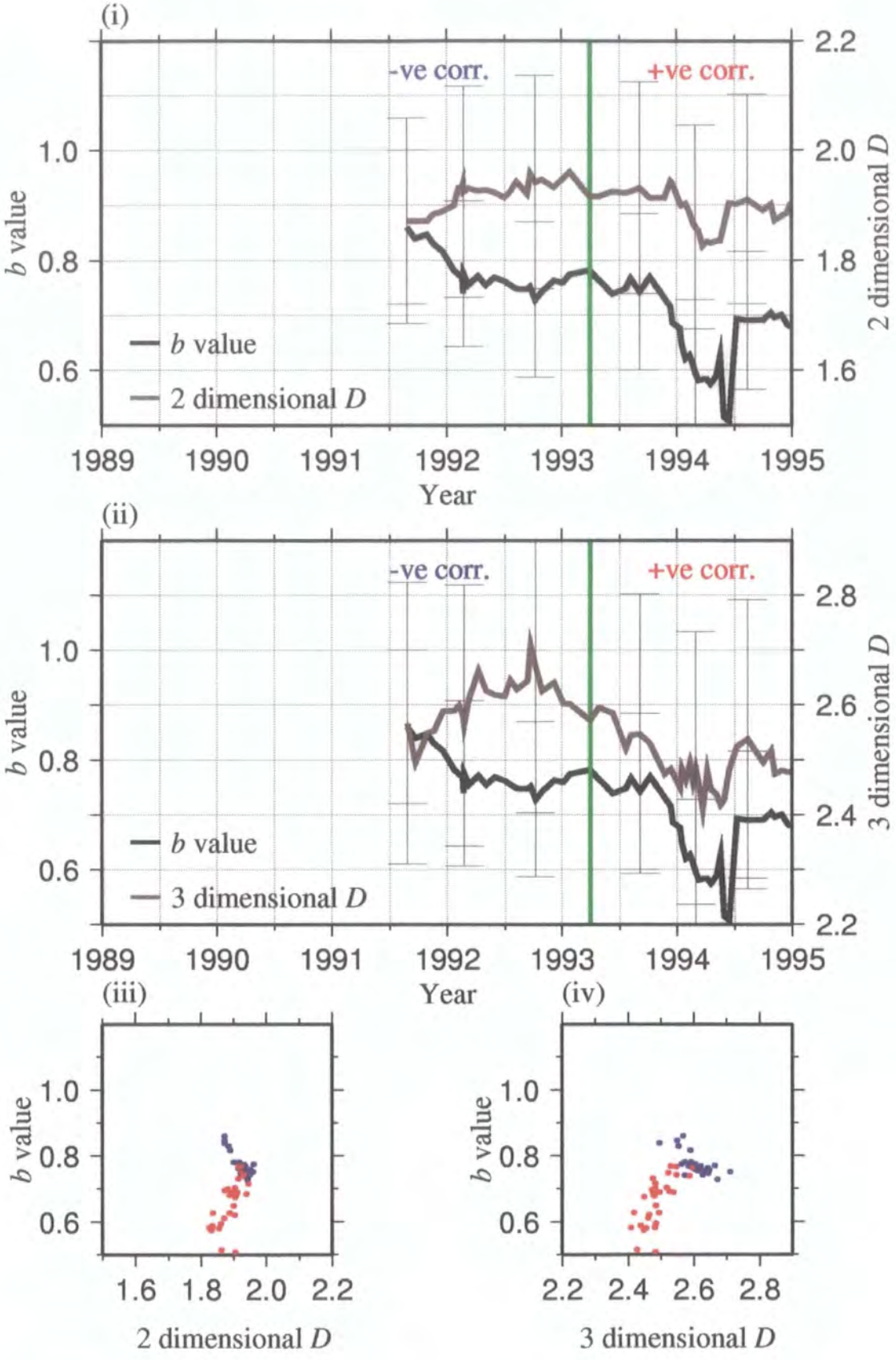

Figure 5.12(d) As Figure 5.9(d) but for seismicity adjacent to well 09790519.

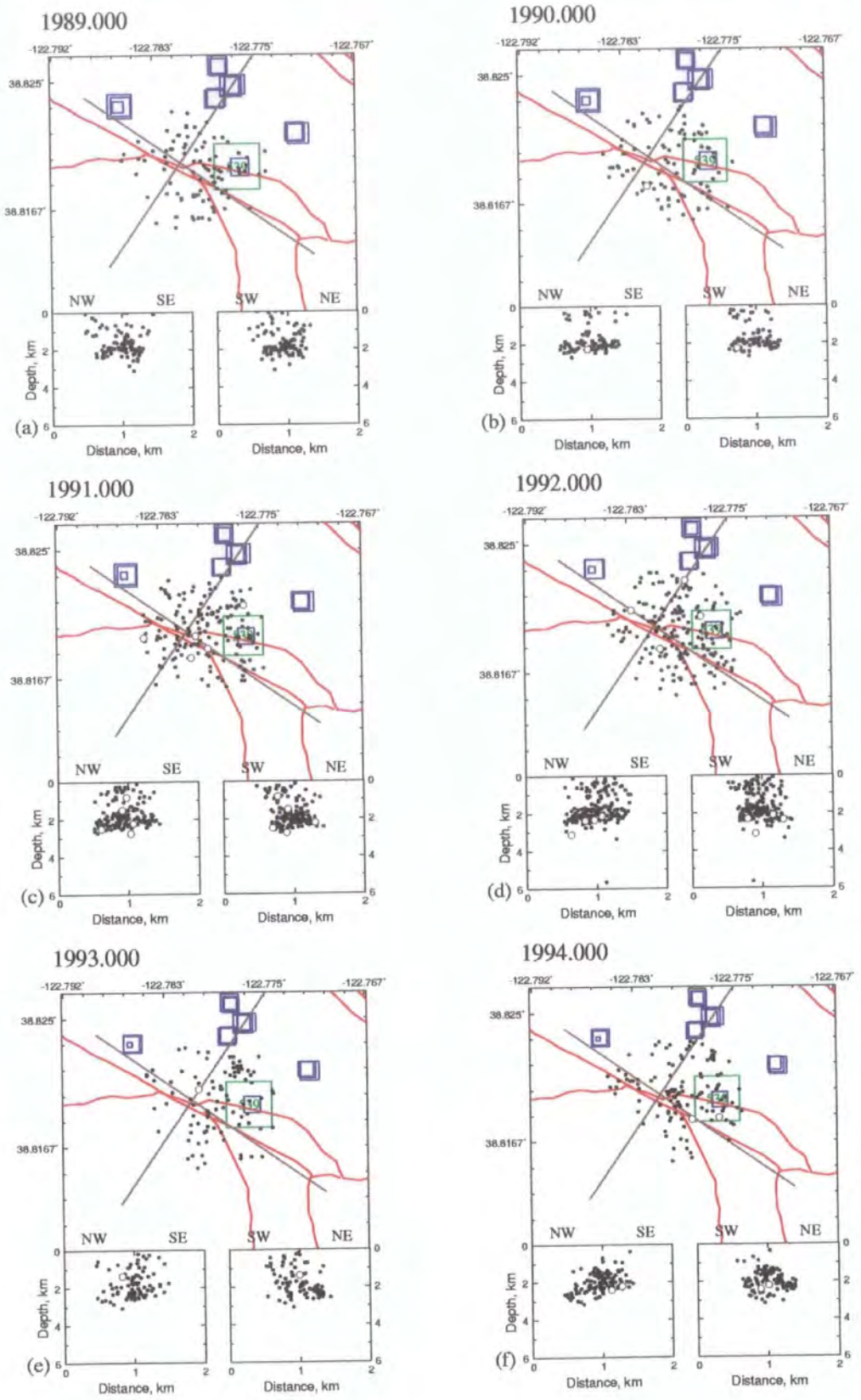

Figure 5.13(a) As Figure 5.6(a) except for earthquakes adjacent to injection well 09790539.

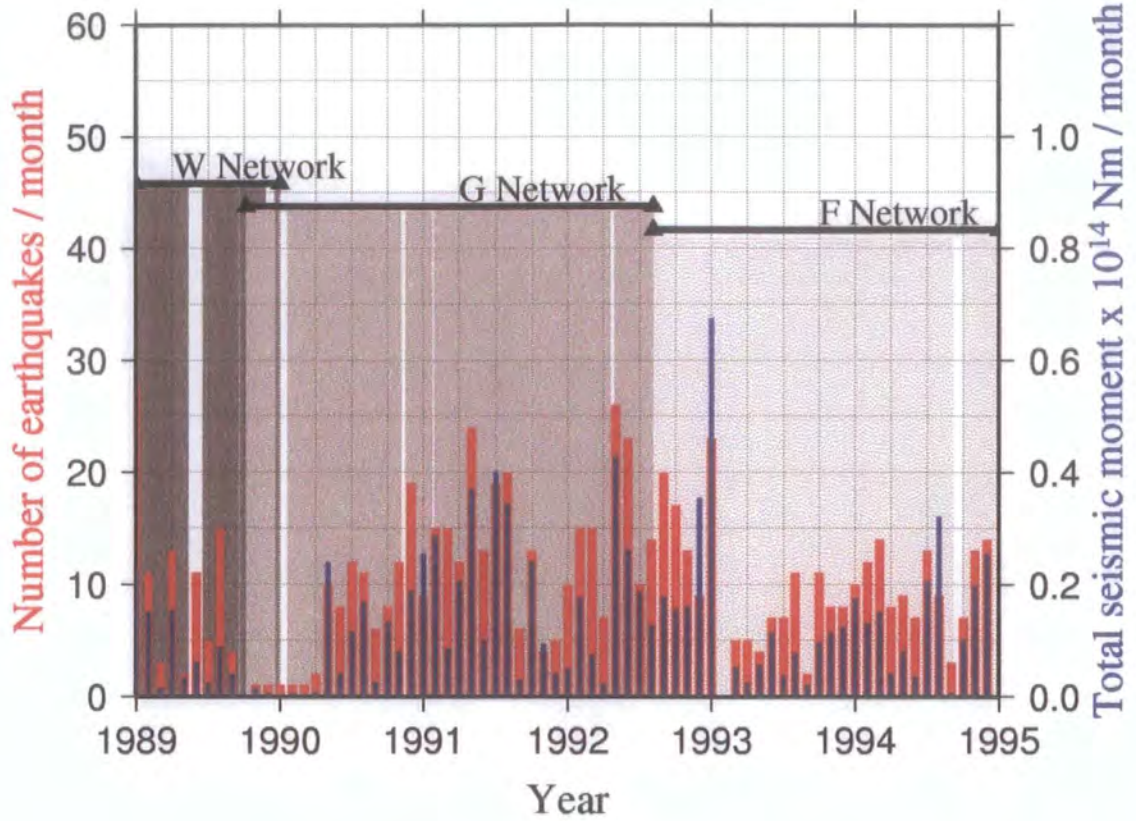

Figure 5.13(b) As Figure 5.4(b) except for earthquakes adjacent to injection well 09790539.

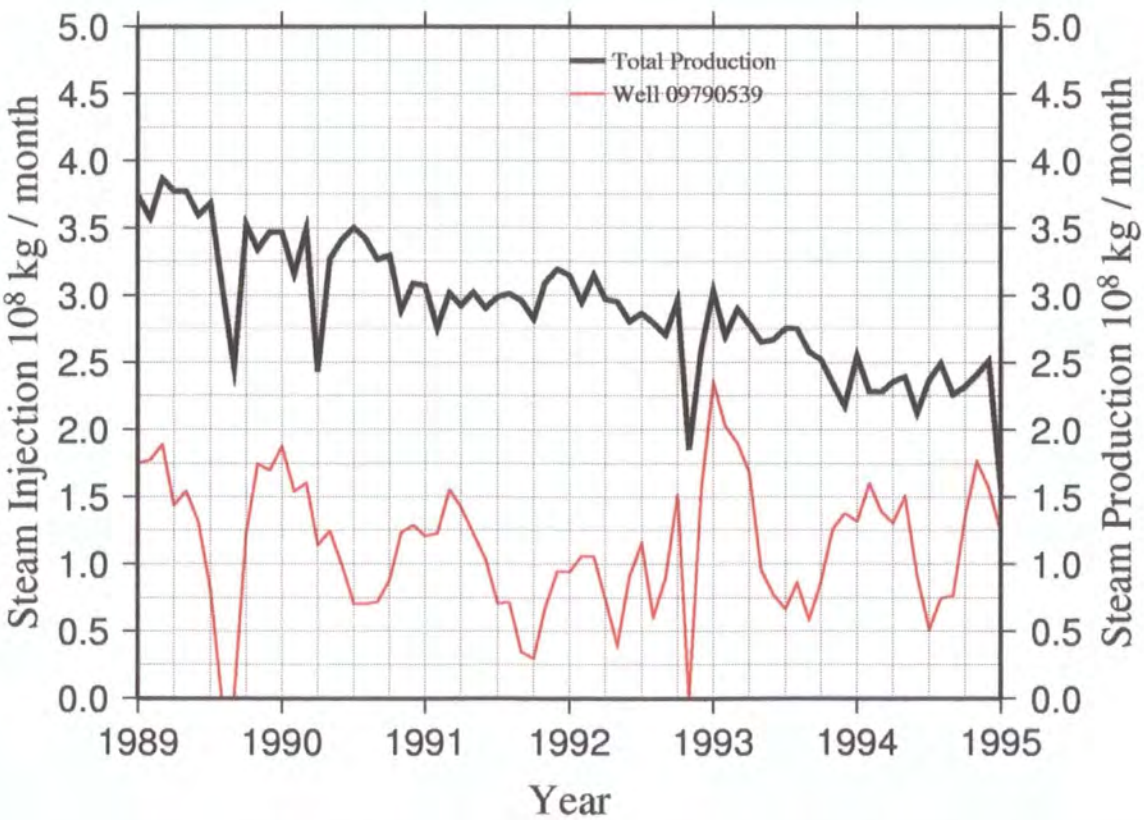

Figure 5.13(c) Well activity close to injection well 09790539 1989-1994.

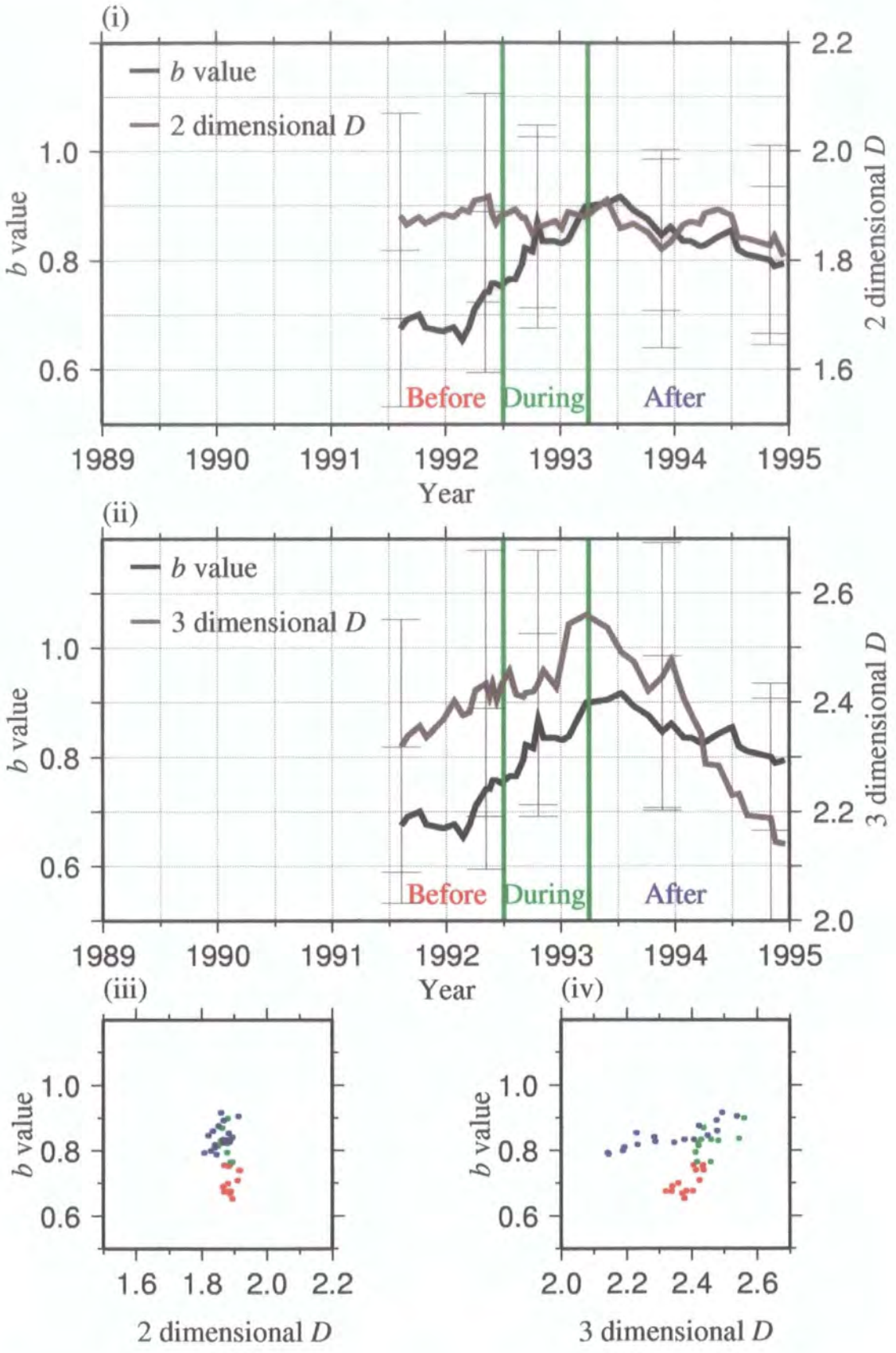

Figure 5.13(d) As Figure 5.9(d) but for seismicity adjacent to well 09790539.

1991 to 1992, with the event rate falling to zero in early 1993 (Figure 5.13(b)). Injection was continuous with a prominent high in late 1992 - early 1993 (Figure 5.13(c)). Production was continuous and declining. For the *b/D* analysis, the time sequence was split into three periods - before, during and after the injection episode in late 1992 - early 1993. In both the two-dimensional and three-dimensional data, increased clustering resulted in an increase in D. There was a positive correlation between b and D for the entire six-year period apart from a brief negative correlation in the two dimensional case of D in 1992 - 1993 (Figure 5.13(d)).

Table 5.8 Summary of observations in the neighbourhood of well 09790539

Production History	Injection History	Seismicity	*b/D* correlation
Production Continuous and declining, from ~3.75 to 2.5 x 10^8 kg/month (~145 to 96 kg/s).	**09790539**: Injection is fairly continuous with brief drops to zero in mid 1989 and late 1992, and a prominent surge in late 1992/early 1993. The injection well is on a fault zone.	A cluster 1.25 km x 1.25 km in area with sub-clusters centred at depths of ~ 1 km and ~ 2 km. Most larger events ($M_d \geq 2.0$) in the deeper sub-cluster. The event rate increases at the end of 1992 (with several larger earthquakes), before falling to zero in early 1993, and subsequently recovering.	There is a positive correlation for the entire period apart from a small negative correlation in the 2D case in 1992/1993.

5.3.10 Seismicity adjacent to well 09790563

The seismicity rate in this cluster was fairly constant (Figure 5.14(a) to (d), Table 5.9) with a slight increase between early 1991 and mid 1992. Earthquakes clustered in two seismic volumes centred at ~ 1 km and ~ 4 km, mostly to the west of the injection well (Figure 5.14(a)). Between 1989 and 1992, injection was constant at ~ 1.25 x 10^8 kg/month (48 kg/s), then falling to ~ 0.5 x 10^8 kg/month (19 kg/s) until late 1994 (Figure 5.14(c)). Production was continuous and declining. Increased clustering resulted in an increase in D. There was a positive correlation between b and D for the two-dimensional locations, and a negative correlation for the three-dimensional locations (Figure 5.14(d)).

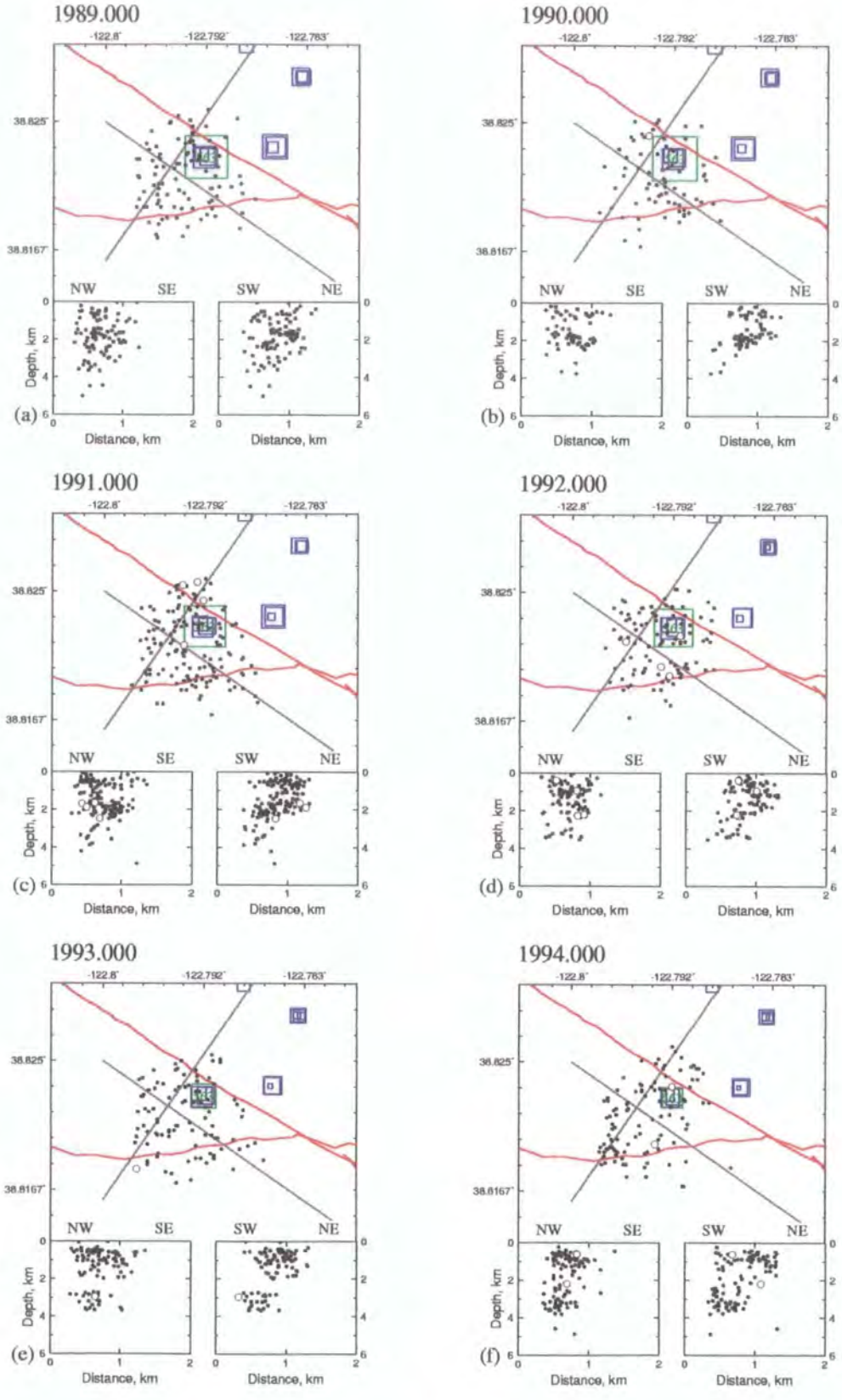

Figure 5.14(a) As Figure 5.6(a) except for earthquakes adjacent to injection well 09790563.

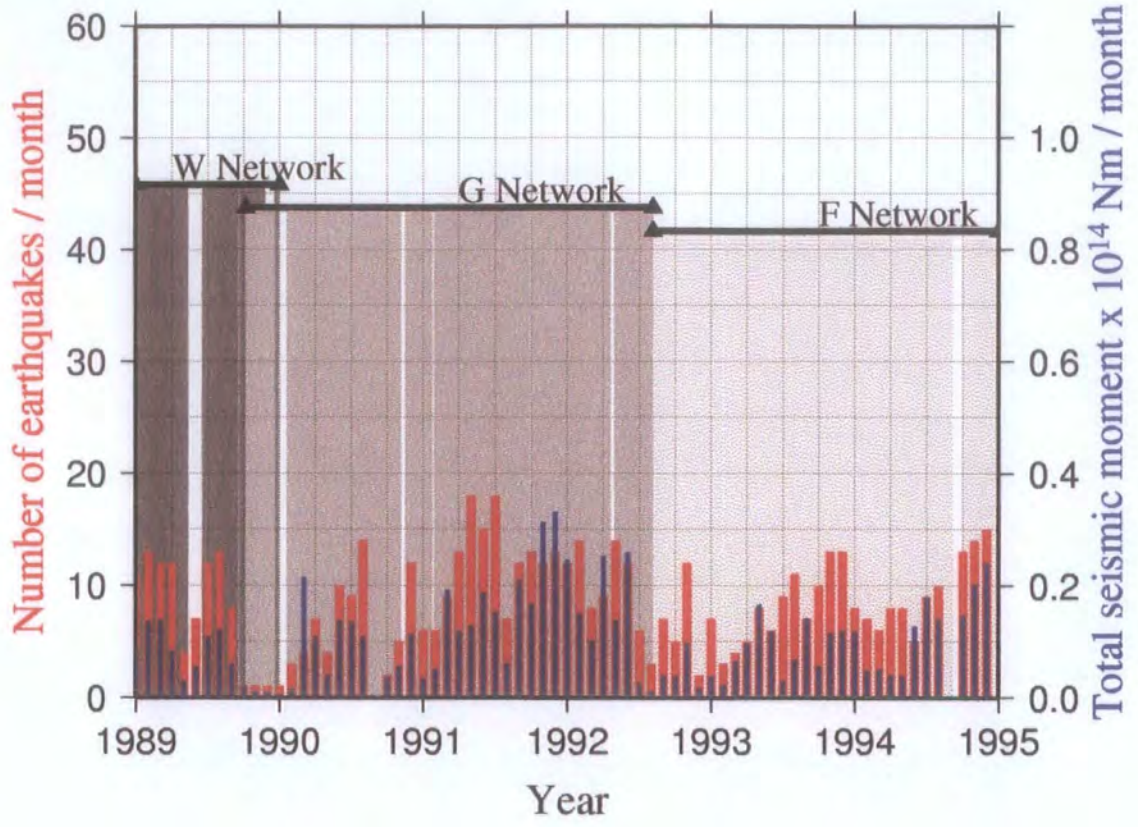

Figure 5.14(b) As Figure 5.4(b) except for earthquakes adjacent to injection well 09790563.

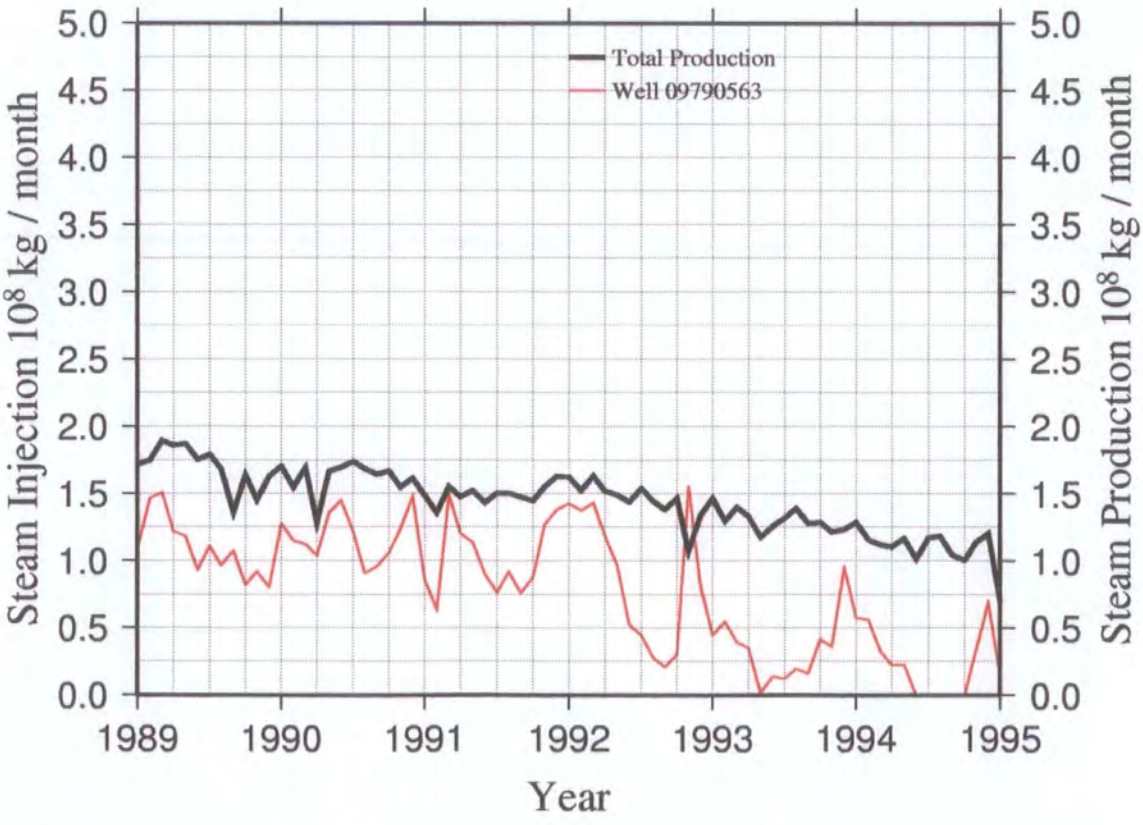

Figure 5.14(c) Well activity close to injection well 09790563 1989-1994.

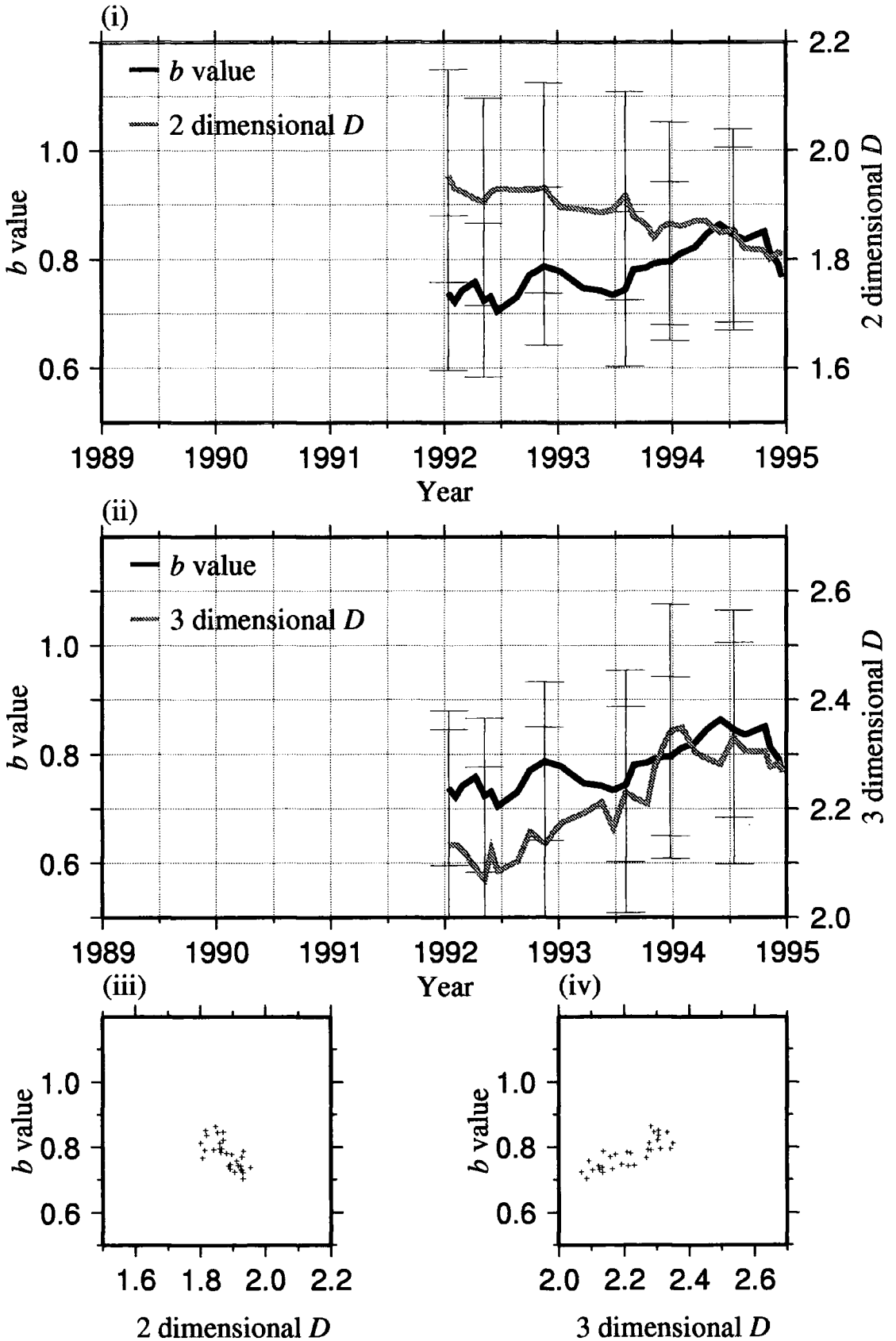

Figure 5.14(d) As Figure 5.9(d) but for seismicity adjacent to well 09790563.

Table 5.9 Summary of observations in the neighbourhood of well 09790563

Production History	Injection History	Seismicity	*b/D* correlation
Production declines at a uniform rate from ~1.75 x 10^8 kg / month (68 kg/s) in 1989 to ~ 1.0 x 10^8 kg / month (39 kg/s) in late 1994.	**09790563:** Between 1989 and 1992, the injection is constant at ~ 1.25 x 10^8 kg / month (48 kg/s). The gross injection then falls to ~ 0.5 x 10^8 kg / month (19 kg/s) until late 1994.	NE - SW elongated cluster 1.5 km x 1 km in area. Two sub-clusters, one ~ 1 km deep and the other ~ 4 km. Seismicity is constant with a slight increase between early 1991 and mid 1992. The seismicity is mostly west of the injection well with larger events ($M_d \geq 2.0$) exclusively to the west.	Negative correlation for the two-dimensional locations and positive for the three-dimensional locations.

5.3.11 Seismicity adjacent to well 09790565

This cluster represents a single seismogenic volume dipping to the north (Figure 5.15(a) to (d), Table 5.10).

Table 5.10 Summary of observations in the neighbourhood of well 09790565

Well History – Production	Well History – Injection	Seismicity	*b/D* correlation
Production declining from 3.5 to 2.5 x 10^8 kg/month (135 to 96 kg/s, with drops in early 1989, early 1990, early 1993 and late 1994.	**09790203:** Very low. **09790227:** Continuous low level injection (~ 0.75 x 10^8 kg/month (30 kg/s)). **09790565:** Changed from production to injection in early 1991. Between 1991 and 1994, four injection episodes. The most prolonged was between mid 1991 and mid 1992 (2); the largest in early 1994 (4).	The cluster is 1 km x 1.5 km in area centred at a depth of ~ 4 km in the NW and ~ 2 km in the SE. Each injection episode accompanied by an increase in the seismicity rate. The largest swarms of events (> 30 events / month) correlate with injection episodes (2) and (4) with simultaneous increases in seismic moment.	two-dimensional *D* case: negative correlations simultaneous with episodes (2) and (4); positive for episode (3). three-dimensional *D* case: negative correlation for episodes (2), (3) and (4).

Both injection in well 09790565 and total injection for the area occur in bursts (Figure 5.15(c)) which are accompanied by increases in the seismic event and the seismic moment rates (Figure 5.15(b)). Increased clustering resulted in a decrease in *D*. In the two-dimensional *D* case, there were negative *b/D* correlations for injection episodes (2) and (4) and a positive correlation for episode (3) (Figure 5.15(d)). In the three-dimensional *D* case there are negative correlations for all three episodes.

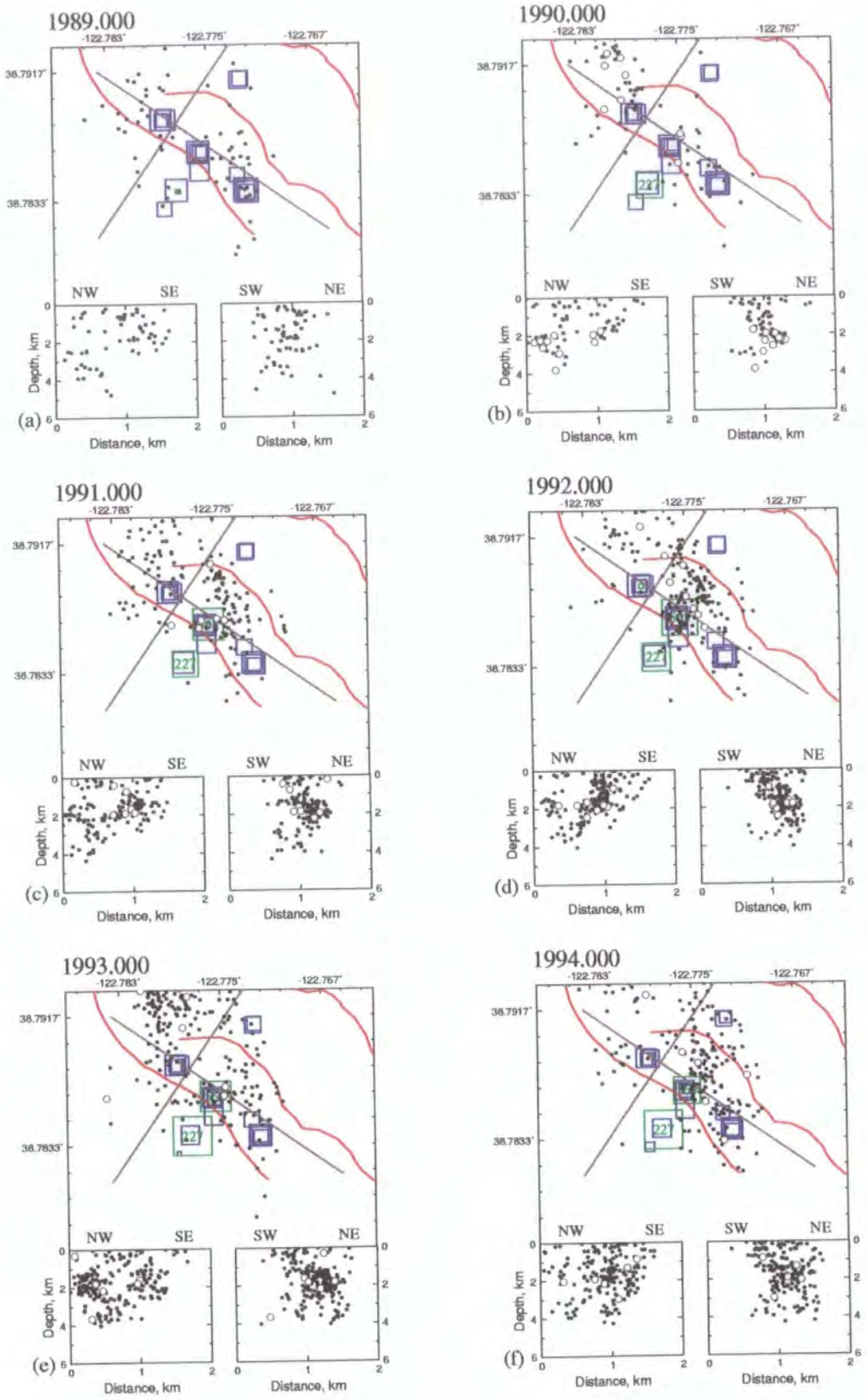

Figure 5.15(a) As Figure 5.6(a) except for earthquakes adjacent to injection well 09790565.

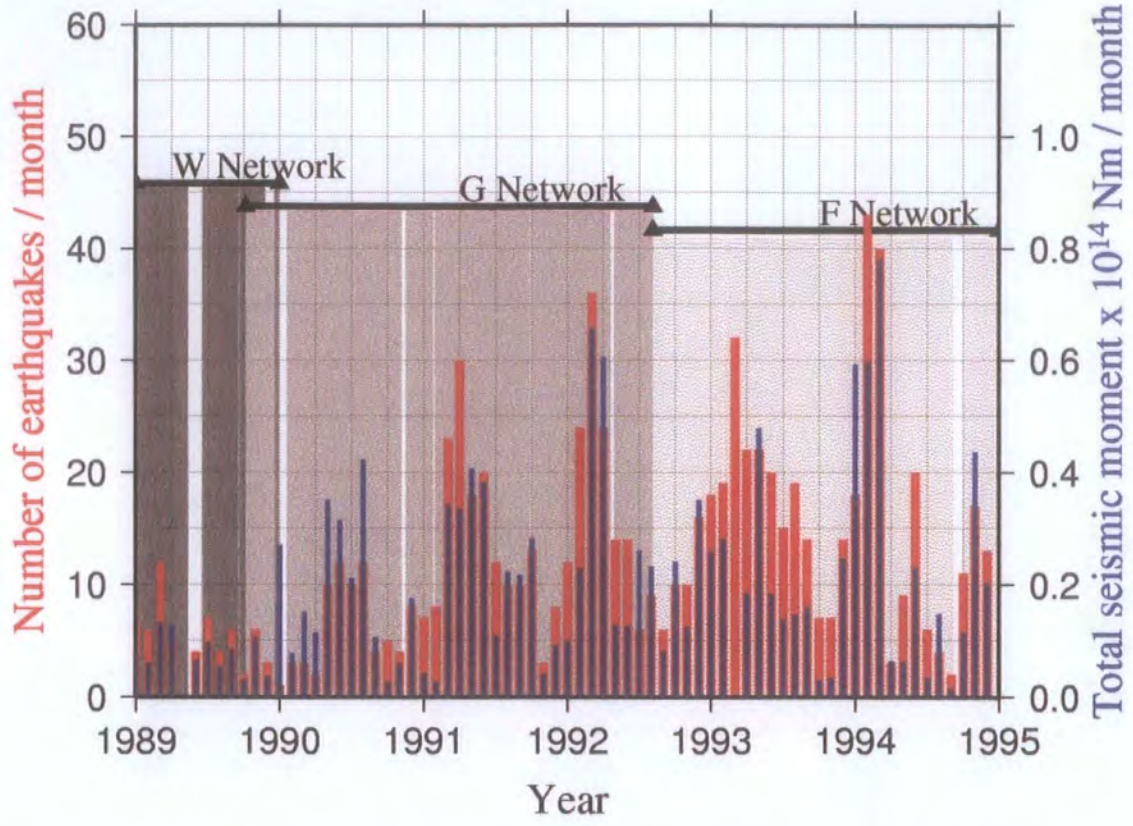

Figure 5.15(b) As Figure 5.4(b) except for earthquakes adjacent to injection well 09790565.

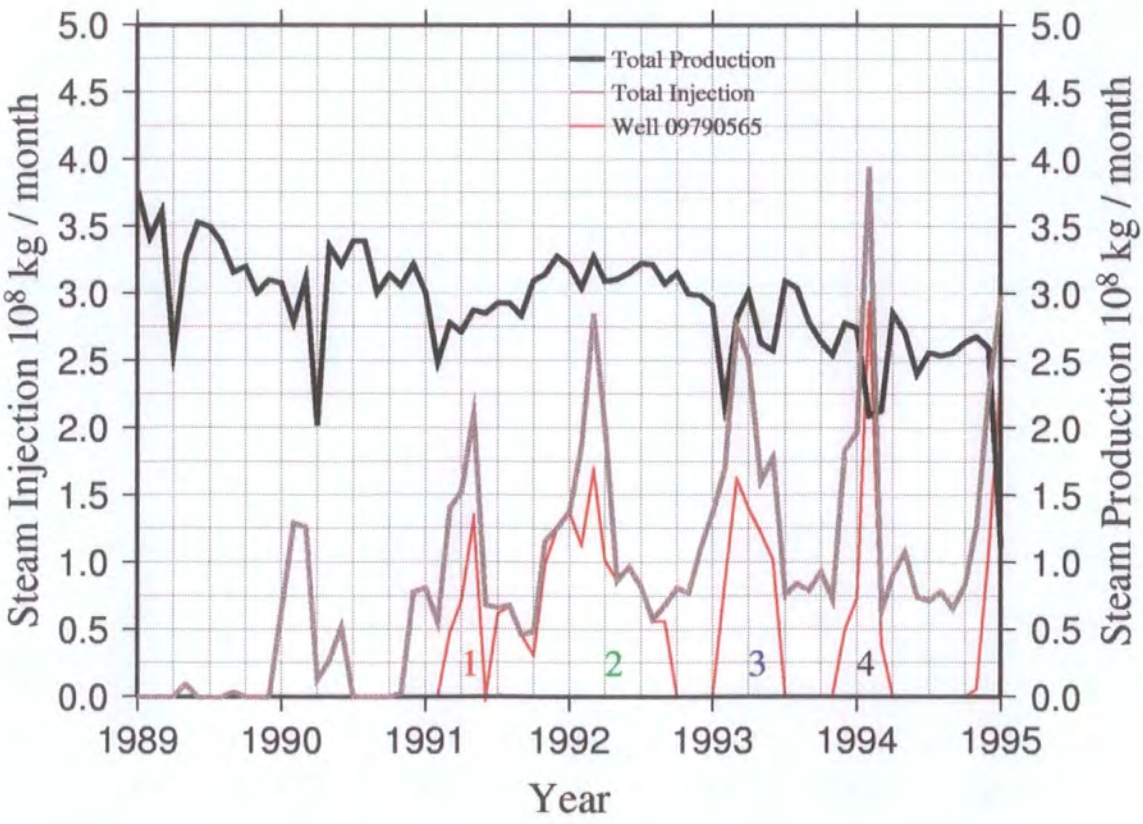

Figure 5.15(c) Well activity close to injection well 09790565 1989-1994. The injection episodes in well 09790565 are numbered 1 - 4.

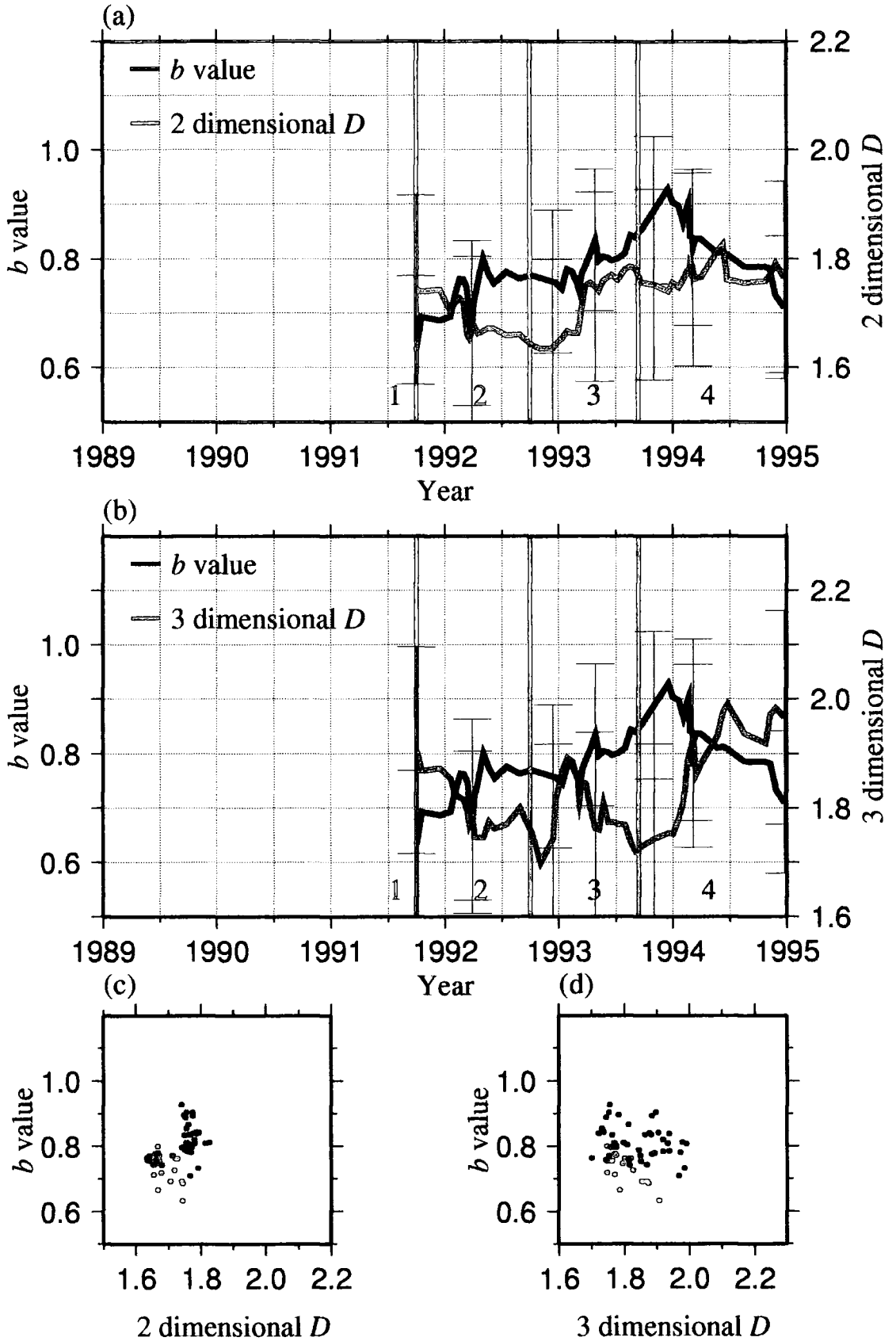

Figure 5.15(d) As Figure 5.9(d) but for seismicity adjacent to well 09790565. Numbers in red, green, blue and black correspond to periods of injection in well 09790565 (Figure 5.15(c)).

5.3.12 Seismicity adjacent to well 09790612

Seismic activity in this cluster was continuous and at a low level (Figures 5.16(a) to (c), Table 5.11). Injection occurred in yearly cycles similar to wells 09790020 and 09790534 (Section 5.3.3; Figure 5.16(c)). After 1993, with each injection episode there is an accompanying increase in the seismicity rate.

Table 5.11 Summary of observations in the neighbourhood of well 09790612

Production History	Injection History	Seismicity	*b/D* correlation
Production continuous and declining from ~ 1.5×10^8 kg/month (58 kg/s) in 1989 to ~ 1.0×10^8 kg/month (39 kg/s) in 1995.	**09790612:** Injection in yearly cycles similar to wells 09790020 and 097900534.	A cluster 0.5 km by 0.5 km in area centred at a depth of ~ 2 km. Seismic activity is continuous and low level. Between 1993 and 1994, a greater number of $M_d \geq 2.0$ events. After 1993, with each injection episode there is an accompanying increase in the seismicity rate.	Insufficient events for analysis.

Production was continuous and declining. There were insufficient events to perform a *b/D* analysis.

5.3.13 Seismicity adjacent to wells in Lake County in the SE Geysers

Seismicity in the south-east Geysers was in small isolated clusters, almost exclusively at depths between 0.5 and 1.5 km below sea level. There were peaks in the event rate in mid 1991, late 1992 and mid 1993-mid 1994, apparently unrelated to the almost constant production and injection activity (Figures 5.17(a) to (c), Table 5.12). Due to the scattered nature of the seismicity it was not possible to find a valid scaling range for this cluster. Consequently it was not possible to perform a *b/D* analysis.

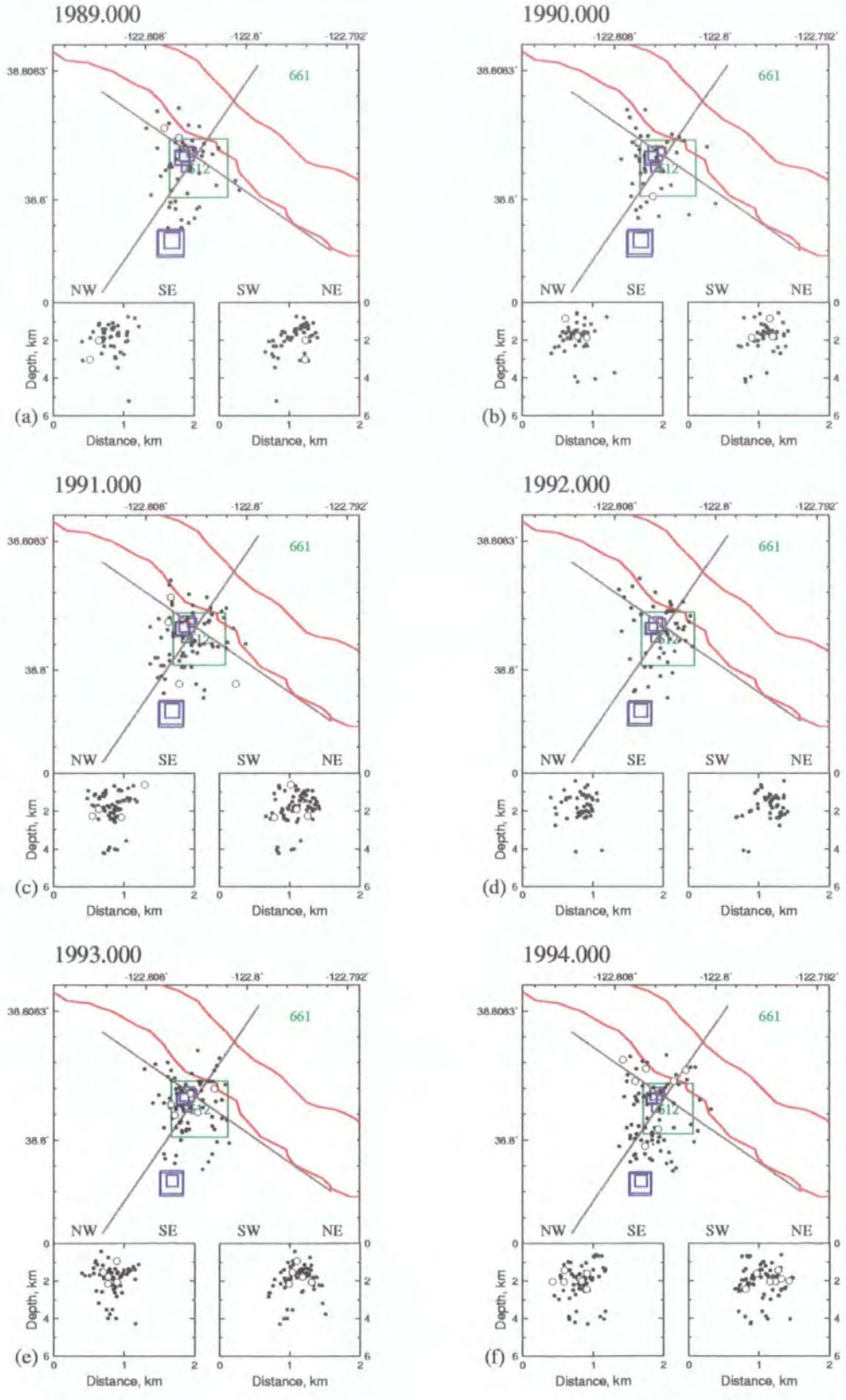

Figure 5.16(a) As Figure 5.6(a) except for earthquakes adjacent to injection well 09790612.

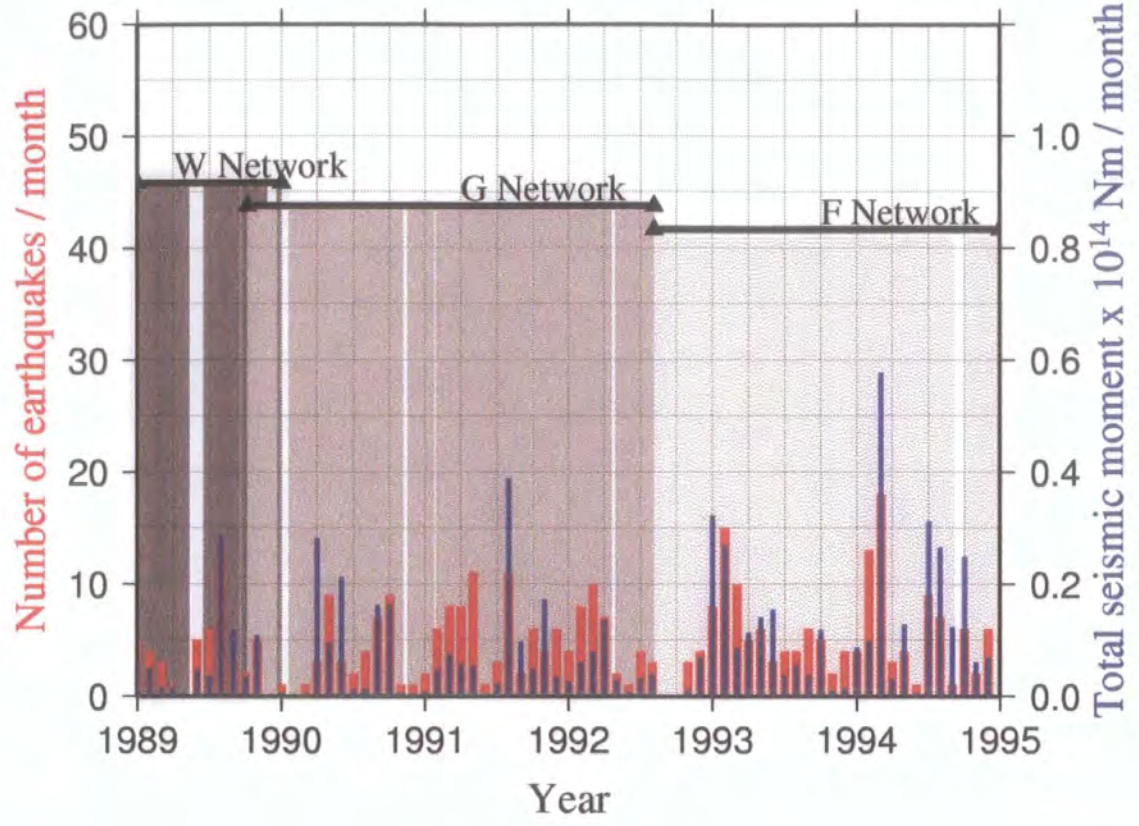

Figure 5.16(b) As Figure 5.4(b) except for earthquakes adjacent to injection well 09790612.

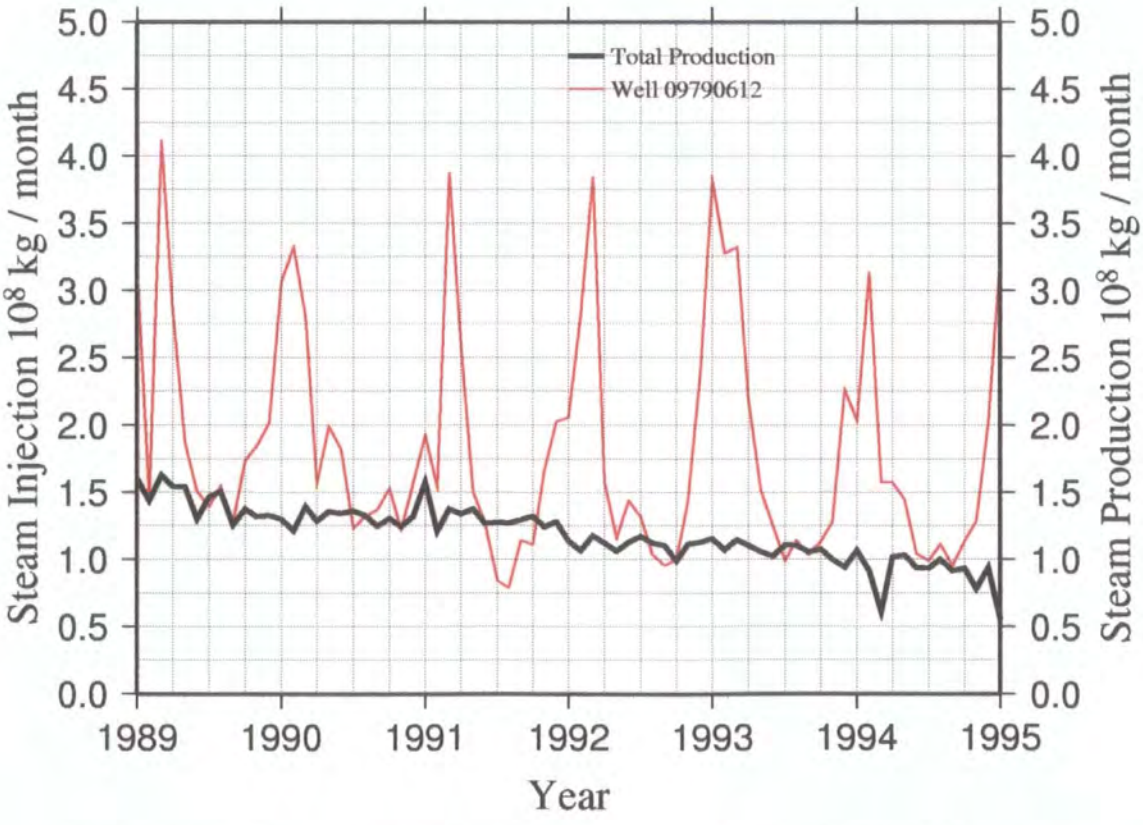

Figure 5.16(c) Well activity close to injection well 09790612 1989-1994.

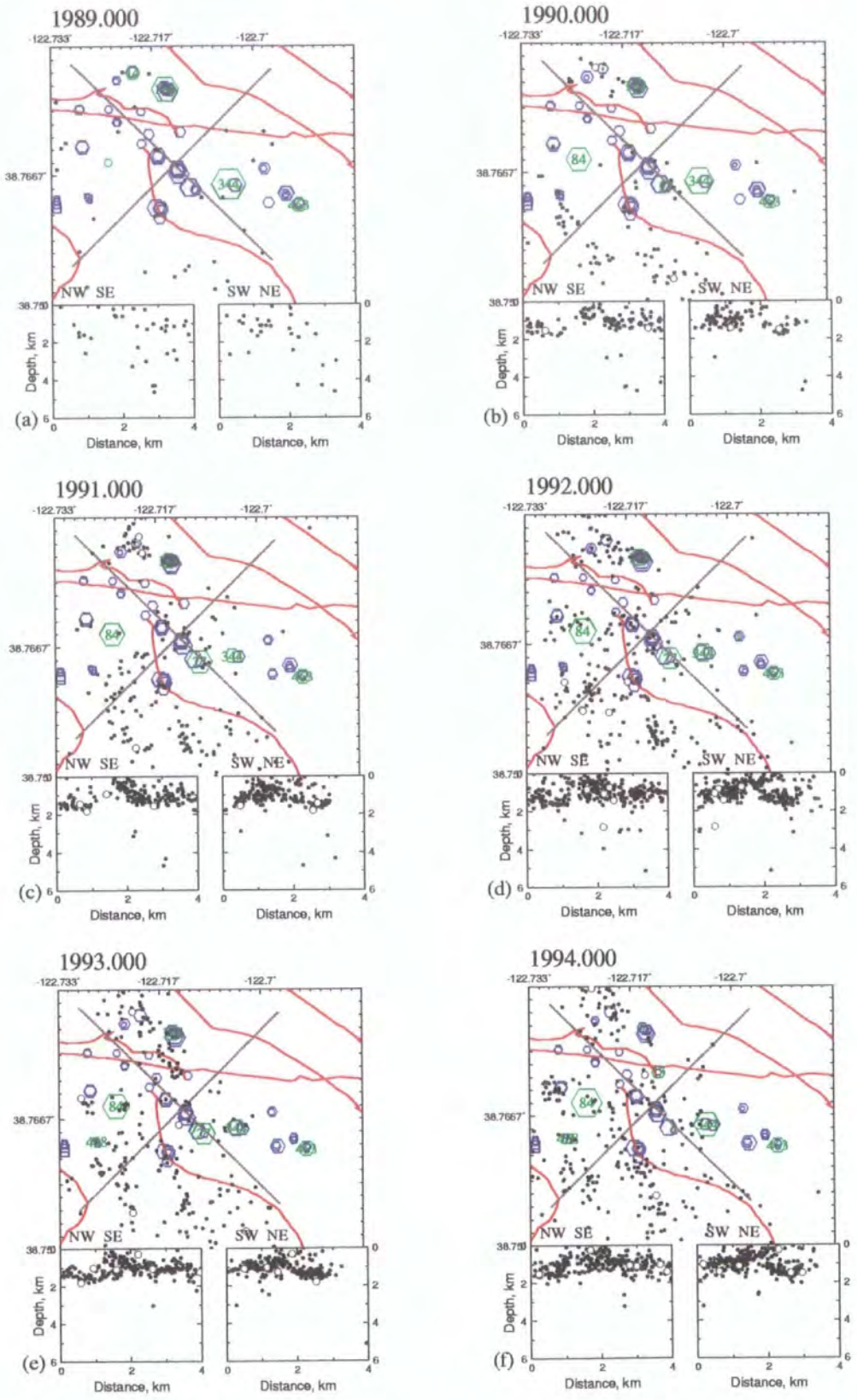

Figure 5.17(a) As Figure 5.6(a) except for earthquakes in south east Geysers in Lake County. Symbols are scaled to show quantity of fluid; 1 cm^2 represents $1x10^{13}$ kg.

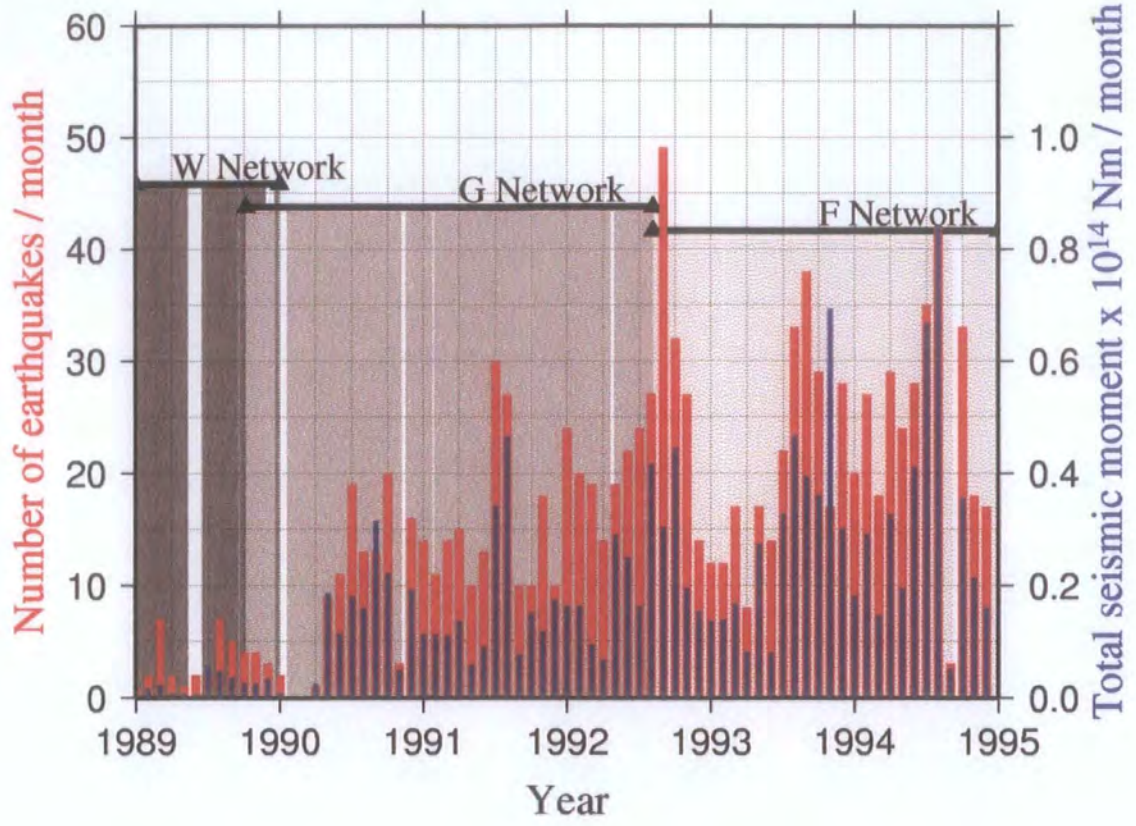

Figure 5.17(b) As Figure 5.4(b) except for earthquakes in Lake County in south east Geysers.

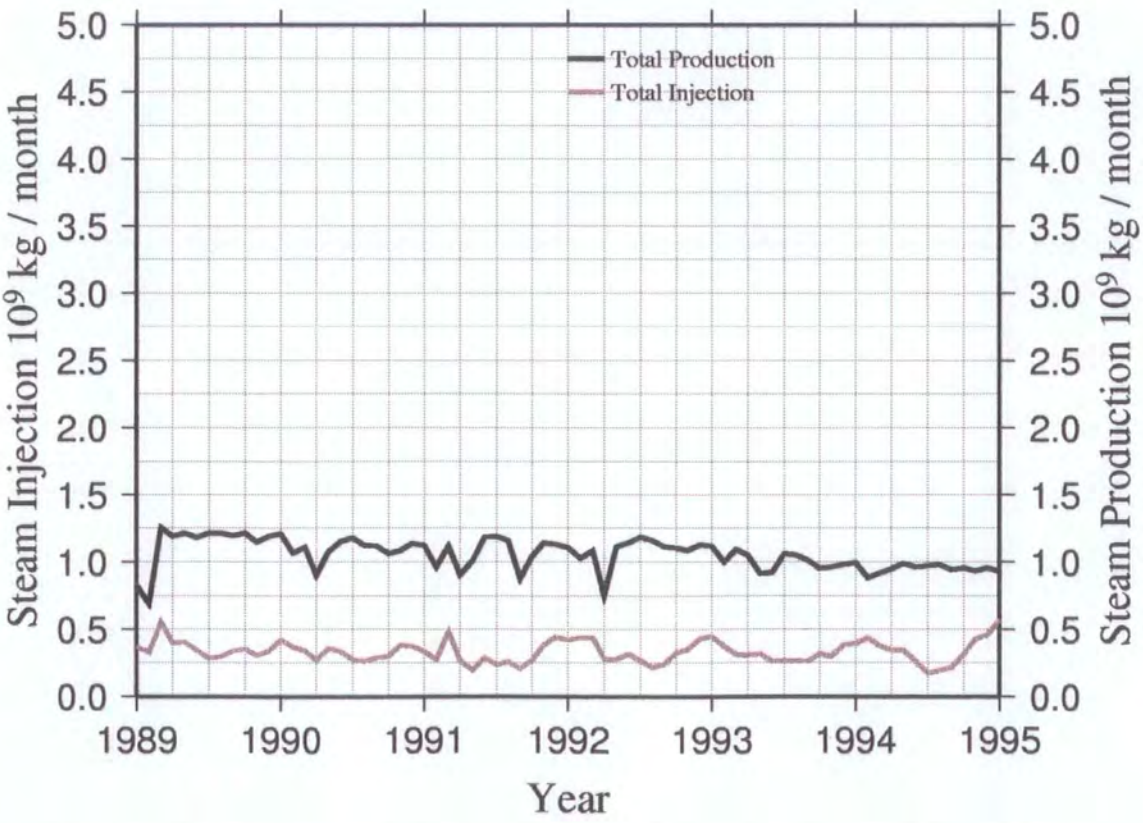

Figure 5.17(c) Well activity in Lake County in south east Geysers 1989-1994.

Table 5.12 Summary of observations in the neighbourhood of wells in Lake County in the south-east Geysers

Production History	Injection History	Seismicity	*b/D* correlation
Production high and continuous. Typical gross production is ~ 1.0×10^9 kg / month (385 kg/s).	Injection high and continuous. Typical gross injection ~ 4.0×10^8 kg / month (154 kg/s).	Small isolated clusters. A little scatter between the clusters. Seismogenic volume centred at ~ 1km. Peaks in seismicity in mid 1991, late 1992 and mid 1993-mid 1994.	Not possible to find a valid scaling range due to the scattered nature of the seismicity.

5.3.14 Seismicity adjacent to production-only area 1

This is an area of high seismic activity that has generated several $M_d \geq 2.0$ events (Figure 5.18(a) to (d), Table 5.13). It mostly comprises a single seismic volume centred at ~ 4 km. From 1991 to 1992 the seismicity formed two distinct clusters separated by a area of relative aseismicity. At the beginning of 1993 there was a dramatic increase in both the event rate and seismic moment rate (Figure 5.18(b)), and the seismicity merged into a single cluster. An increase in clustering results in an increase in D for both the two-dimensional and three-dimensional locations. The increase in activity in 1993 also coincided with a change from a negative correlation to no correlation between b and D (Figure 5.18(d)). There is little production and no injection adjacent to this cluster (Figure 5.18(c)).

Table 5.13 Summary of observations in the neighbourhood of production-only area 1

Production History	Injection History	Seismicity	*b/D* correlation
Production low and continuous ~ 0.5×10^8 kg/month (19 kg/s).	None	The cluster is 1.7 km x 1.0 km in area centred at a depth of ~ 4 km. Two distinct clusters during 1991-1992, which merge 1993-1994. Seismic activity continuous. Between 1989 and early 1993, the seismic rate was ~ 15 events / month, with swarms in early - mid 1991 and early 1992. A sharp increase to ~ 25 events / month in early 1994.	In early 1993, the correlation changes from negative to none in for both two-dimensional and three-dimensional locations.

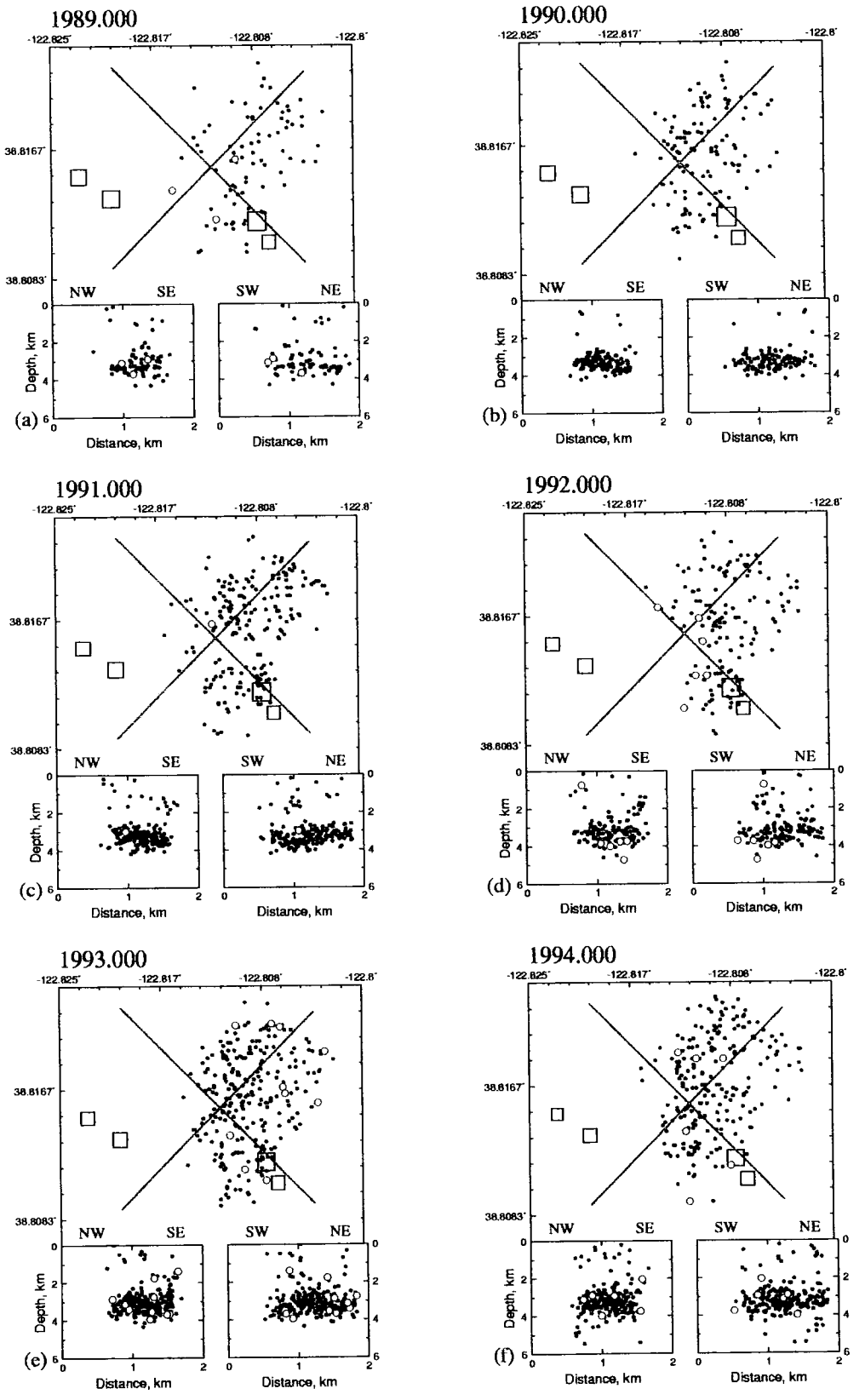

Figure 5.18(a) As Figure 5.6(a) except for earthquakes adjacent to production only area 1.

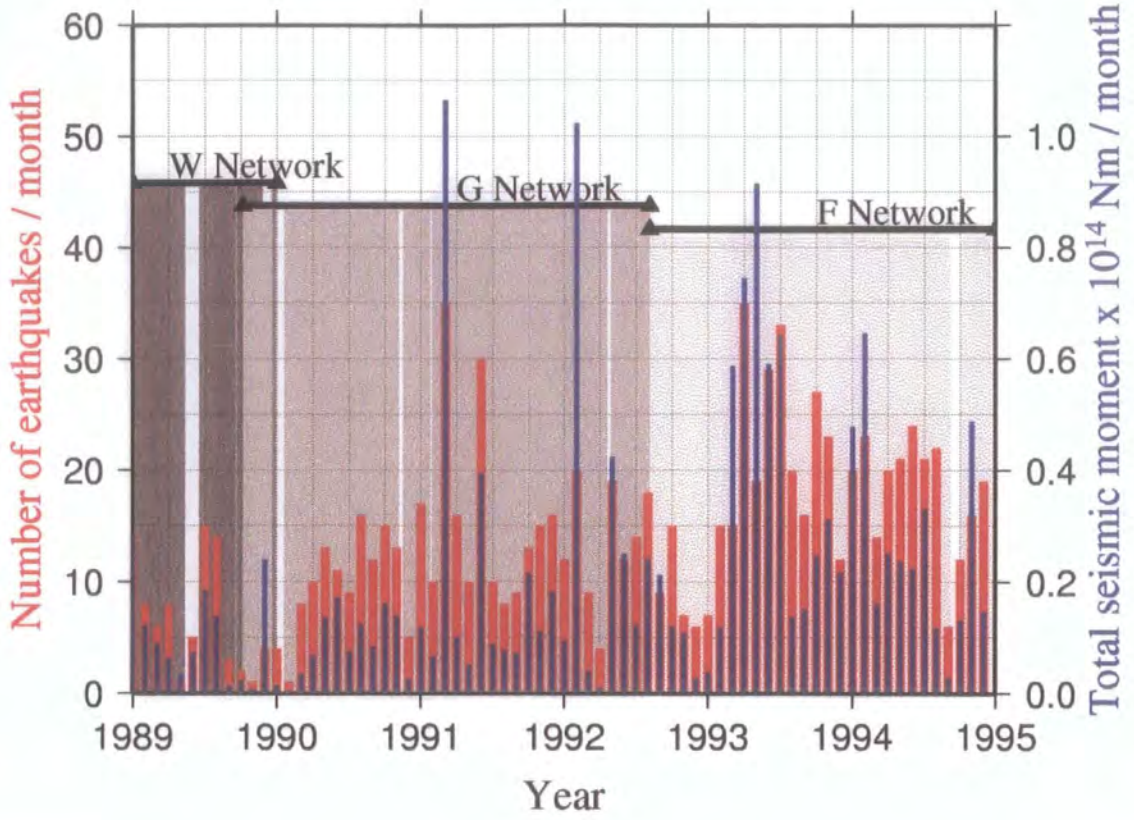

Figure 5.18(b) As Figure 5.4(b) except for earthquakes in production only area 1.

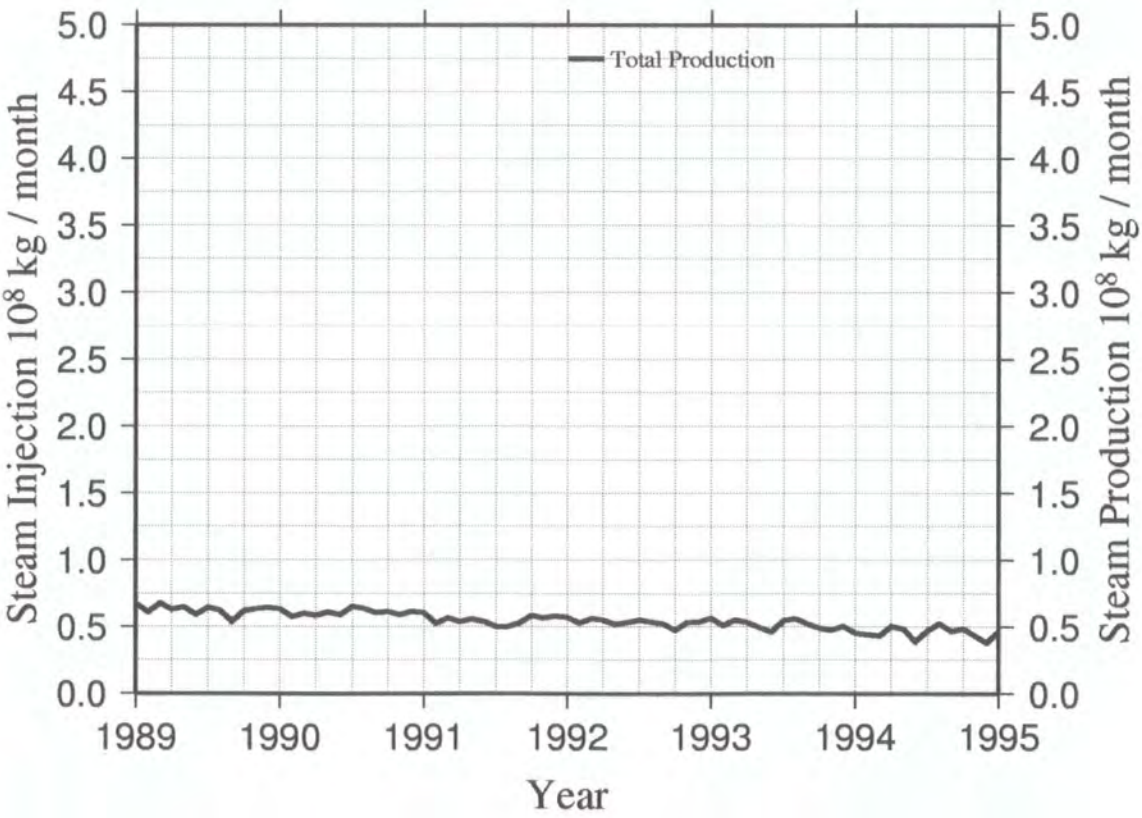

Figure 5.18(c) Well activity close to production only area 1 1989-1994.

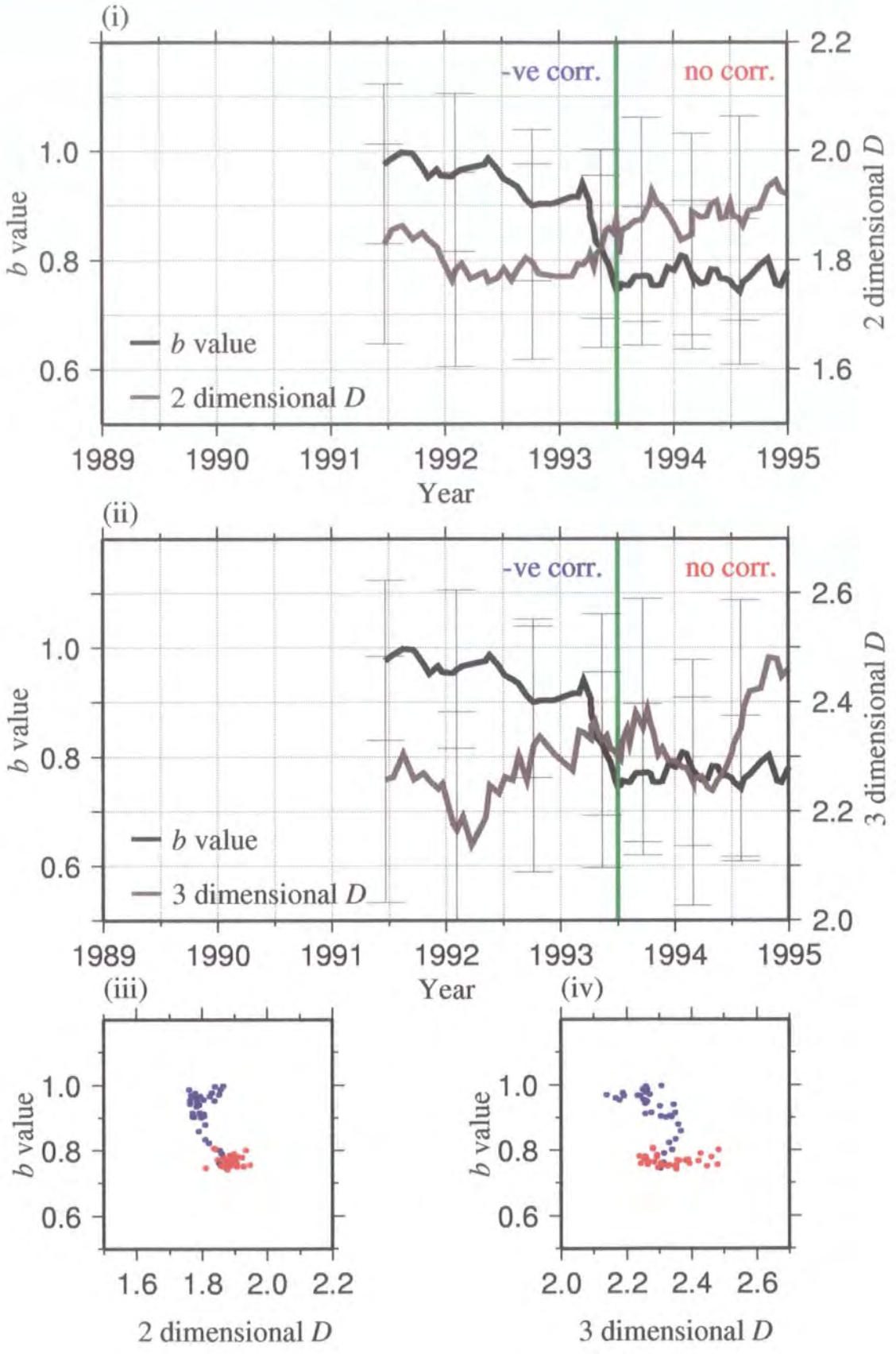

Figure 5.18(d) As Figure 5.9(d) but for seismicity adjacent to production-only area 1.

5.3.15 Seismicity adjacent to production-only area 2

This area exhibits intense seismicity with little apparent commercial activity (Figures 5.19(a) to (d), Table 5.14). The cluster is 'U' shaped and is centred at a depth of ~ 1 km. There is no injection and very little production nearby. Intense clustering produced a large negative anomaly in D 1992 - 93 (Figure 5.19(d)). In mid 1993, the b/D correlation changed from negative to positive for both two- and three-dimensional D.

Table 5.14 Summary of observations in the neighbourhood production-only area 2

Production History	Injection History	Seismicity	*b/D* correlation
Production is low and fairly continuous.	None	'U' shaped cluster 2.0 km x 1.75 km in area centred at a depth of ~ 1 km. From mid 1990, the area became seismically active with ~ 20 events / month. 1991 - 1992, a westerly cluster formed containing several larger events. During early 1993, the area became relatively quiescent.	In mid 1993, the correlation changed from negative to weak positive in both two-dimensional and three-dimensional cases.

5.4 The choice of a higher threshold magnitude to calculate b and D

As discussed in Section 4.5.1.2, in the Barton catalogue the log-frequency - magnitude curve exhibits curvature near the threshold magnitude. The choice of threshold magnitude is thus somewhat subjective. In the case of the analysis described above, as low a threshold magnitude as possible was used (M_d = 0.5) in order to maximise the number of data used.

The true threshold magnitude (i.e. the magnitude above which the dataset is essentially complete) may vary with time as a result of changes in the monitoring network, e.g. station breakdowns, and may at times be above the magnitude selected. In order to assess the effect of this on the results, where sufficient data

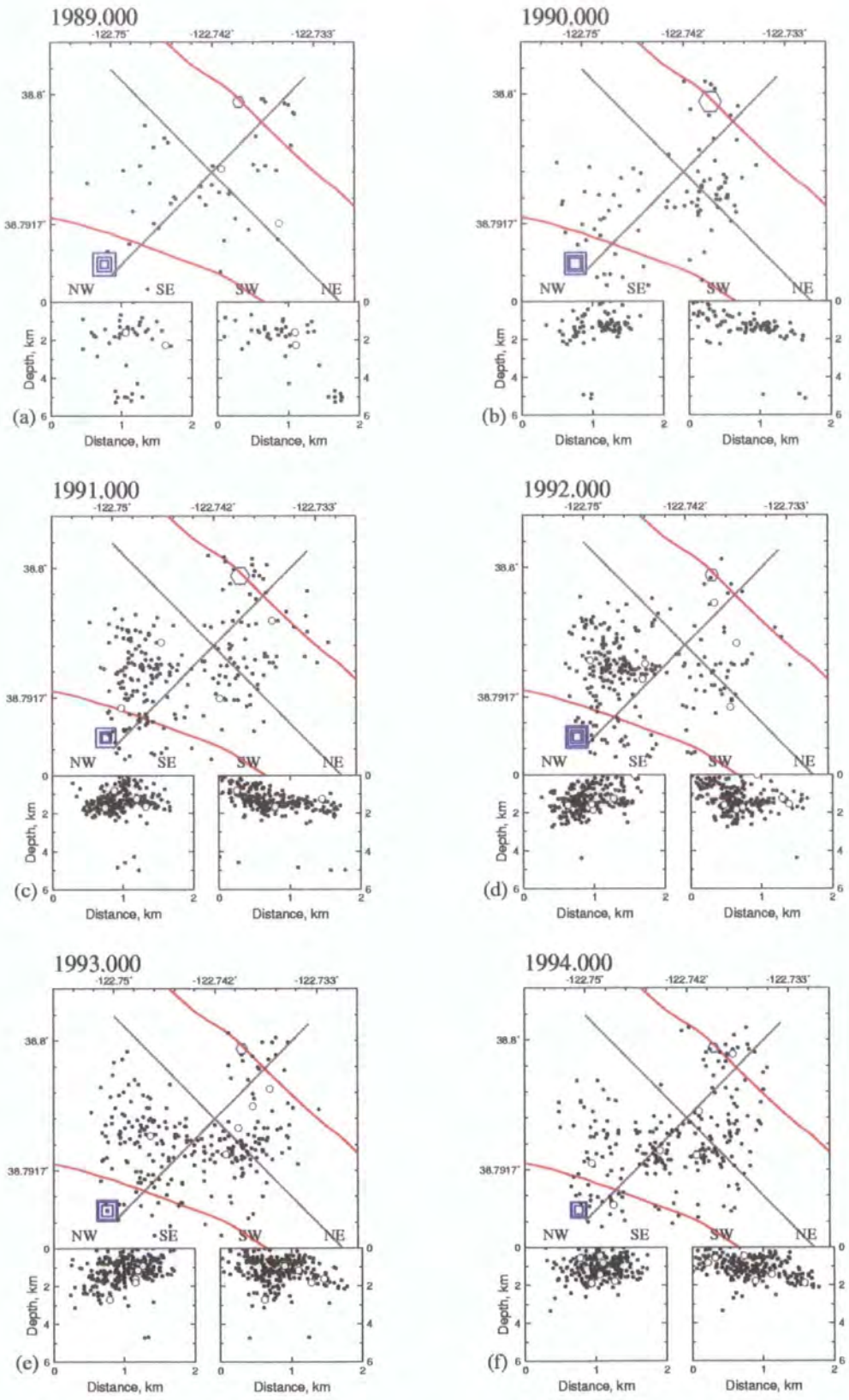

Figure 5.19(a) As Figure 5.6(a) except for earthquakes adjacent to production only area 2.

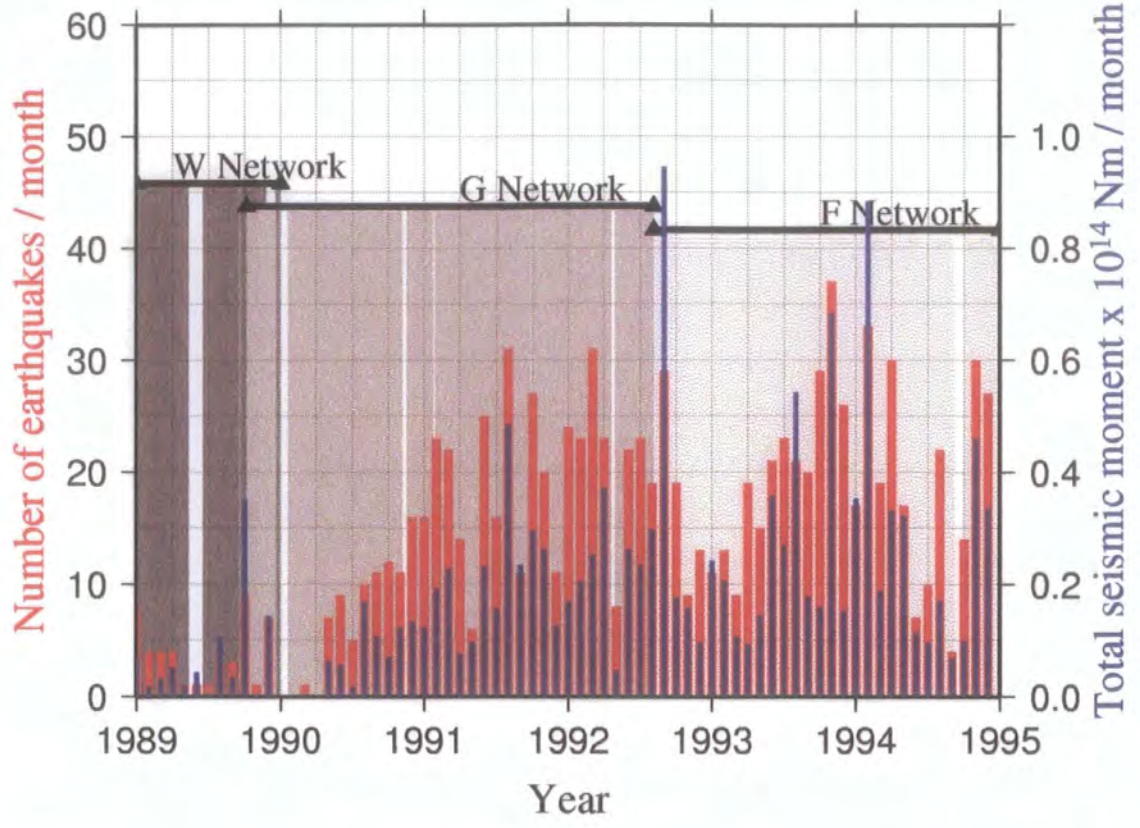

Figure 5.19(b) As Figure 5.4(b) except for earthquakes in production only area 2.

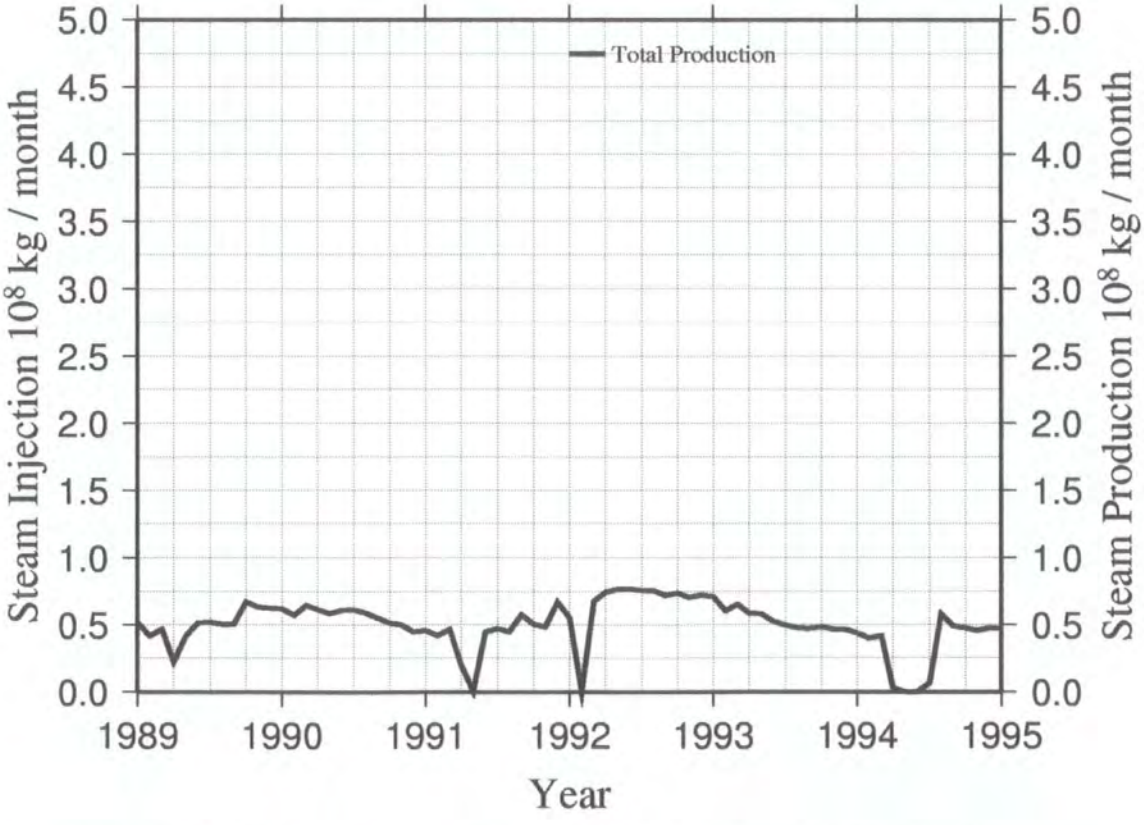

Figure 5.19(c) Well activity close to production only area 2 1989-1994.

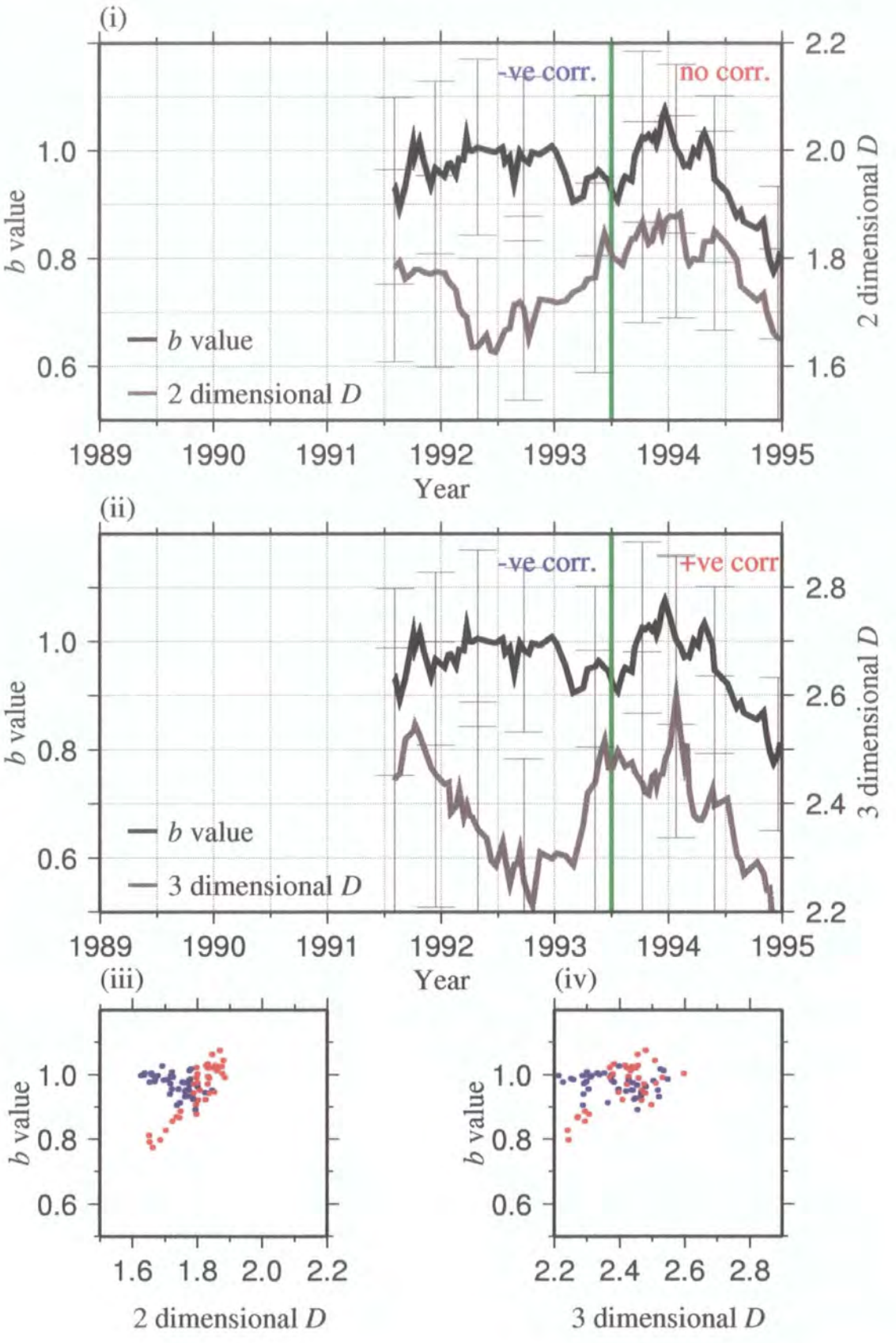

Figure 5.19(d) As Figure 5.9(d) but for seismicity adjacent to production-only area 2.

existed a second analysis was done using a higher magnitude threshold. In six of the eight cases studied, the nature of the *b/D* correlation analysis remained the same. In two cases the result was different when the higher threshold magnitude was used (Table 5.15).

Table 5.15 Comparison of *b/D* correlations using different threshold magnitudes

Well area	*b/D* correlation using $M_d \geq 0.5$	Higher threshold Magnitude used	*b/D* correlation using higher threshold magnitude
09790127	Negative after 1992	0.8	Same
09790231	Two-dimensional case: positive before and after; negative during. three-dimensional case: weak negative correlation before and strong negative during anomaly in *D*. Positive correlation after.	0.8	Same
09790487	No correlation.	-	Insufficient data for $M_d > 0.5$.
09790519	Positive after 1993	0.9	Negative after 1993
09790539	Positive correlation	0.8	Same
09790563	Two-dimensional case: negative; three-dimensional case: positive	0.9	Same
09790565	Negative correlations for ejection episodes in most cases for two-dimensional and three-dimensional	0.8	Same
Prod 1	Positive from 1993	0.8	Same
Prod 2	Switch from negative to positive in mid 1993	0.9	Change from negative to no correlation.

5.5 Summary

The relationships between seismicity, seismic *b* value and spatial fractal dimension, *D*, for commercially-induced earthquakes at The Geysers geothermal area were studied by examining locations, event rate, seismic moment rate, well histories, temporal variations in *b* and *D* and the correlation between them. These relationships were examined for the whole dataset and for clusters within it.

A program to calculate the temporal variation in *b*-value using the *Page (1968)* Equation and the correlation dimension for hypocentres was written by the author. The temporal changes in these variables were calculated using a sliding window

technique. A window size of 200 samples with an increment of 10 samples was used. As input is in chronological order, this technique shows how *b*-value and correlation dimension change over time. Tests with mathematical fractal sets show that calculated values of the correlation dimension were within 5% of their deterministic values.

For the entire dataset, total injection exhibited annual cyclicity which could be traced to a few wells in the south central Geysers. Apart from these wells, injection was uniform and fairly constant. Production was fairly uniform and declining. For all of the injection episodes, no correlation between b and D was observed. A negative correlation was seen for one of the low-injection periods, though this behaviour was not exhibited for other periods of low injection.

The earthquake dataset was divided into spatial clusters which were analysed individually. In the neighbourhood of most clusters, production was in general uniform and declining, but the injection history varied. It was sometimes fairly uniform and sometimes came in periodic bursts. Occasionally the injection rate remained constant but the injection was switched to a different well. There were several cases where injection episodes coincided with increased seismicity in nearby clusters and changes in b, D and the correlation between these two variables. In three cases a positive correlation between b/D occurred during continuous production and/or injection, changing to a negative correlation when an injection pulse onset. In two cases, there was no apparent injection, but increases in the event rate and changes in the b/D correlation occurred similar to those in clusters where there had been injection. Using a higher value for the threshold magnitude gave the same results in 75% of the cases studied.

Chapter 6

b-value and spatial fractal dimension anomalies at Long Valley caldera, California

6.1 Introduction

Long Valley is a highly active volcanic area in east-central California (Figure 6.1). After several periods of unrest during the late 1970s/early 1980s, the USGS commenced, in 1982, monitoring and studying the volcanic activity in Long Valley. Any escalation in the unrest could pose a threat to the 5,000 residents there, plus the tens of thousands of tourists who visit the area for summer and winter sports. The area also has three geothermal power plants producing a total of 40 MW of electricity. Studying and understanding the volcanic system could reduce potential hazards and possibly warn of impending volcanic eruptions.

On 22 November 1997 there was greatly increased seismic activity in the south moat of the resurgent dome (Figure 6.1), accompanied by rapid inflation of the dome. In this chapter these phenomena will be described, along with the temporal variation of the *b*-value and spatial fractal dimension of hypocentres and their correlations before, during and after this event.

6.2 The geology and magmatic bodies of the Long Valley system

Long Valley lies at the boundary between the high-heat-flow Basin and Range extensional province to the east and the cold Sierra Nevada block to the west *(Bailey et al., 1976)*. Over the past 4 Ma, the area has been subjected to persistent earthquake and volcanic activity. During this time, it has been dominated by two

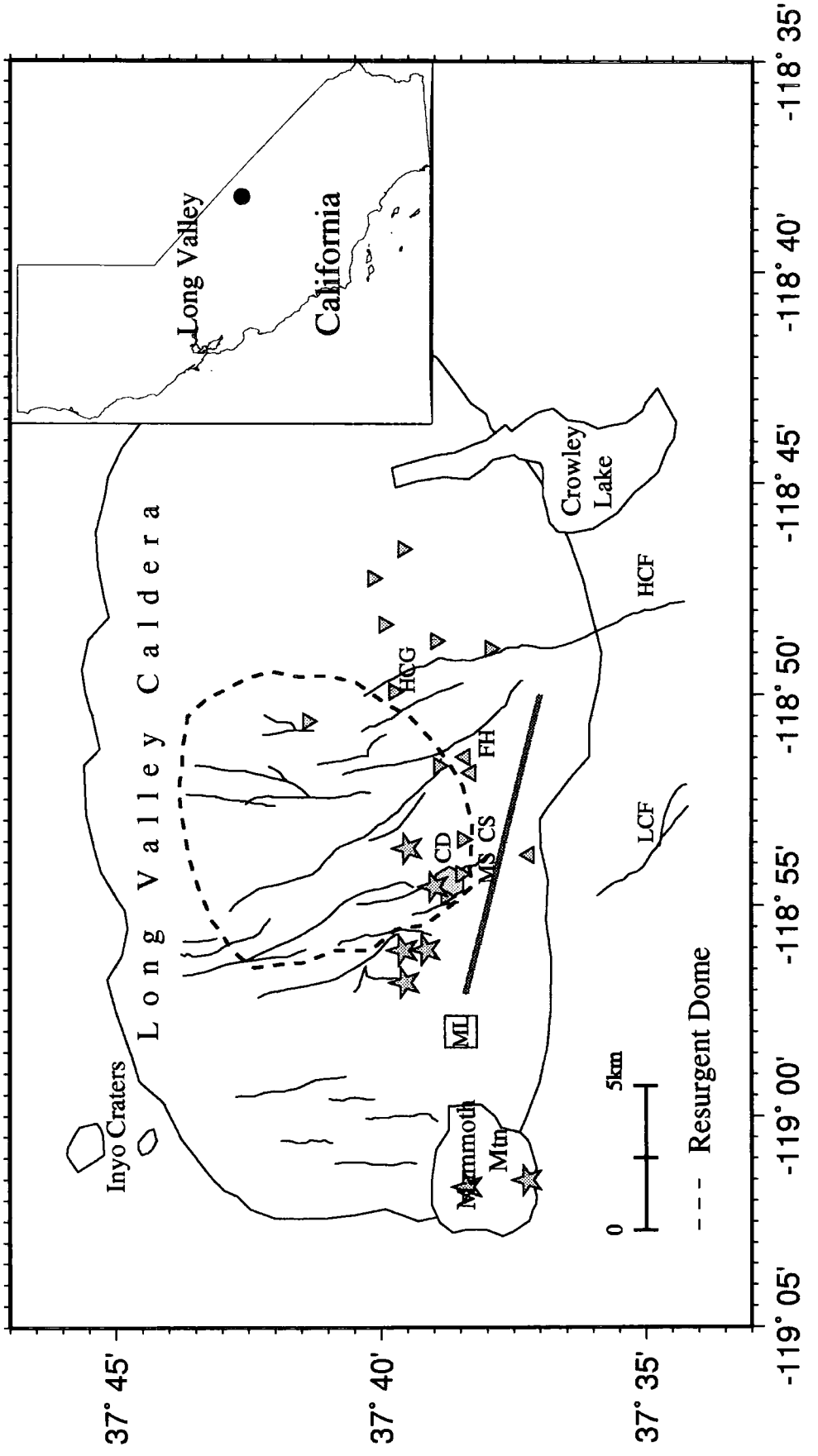

Figure 6.1 Map of Long Valley caldera. Fumaroles are shown by stars, hot springs by inverted triangles and non-thermal springs by triangles. CS = Colten Spring, FH = Hot Creek Fish Hatchery spring, HCG = Hot Creek George Spring, MS = Meadow Spring. The South Moat fault is shown by a continuous grey line. Other faults are indicated by continuous thin black lines. HCF = Hilton Creek fault. LCF = Laurel Convict fault. The Casa Diablo geothermal field (CD) is indicated by a hexagon. The location of the town of Mammoth Lakes (ML) is shown by a square. Map features from *Sorey (1985)* and *Sorey et al. (1995)*.

distinct but related silica rich magmatic systems. The older of these two magmatic systems is centred in the Long Valley caldera, covering an area of 4,000 km^2 (Figure 6.2). Between 3.8 and 2.8 Ma this system produced widespread eruptions of basalts and andesites. At about 3 Ma it experienced major uplifts of up to 1000 m. From 3.1 to 2.5 Ma the volcanic activity became concentrated on the location of the current caldera, with eruptions of rhyodacites followed by high-silica rhyolites from 2.1 to 0.8 Ma. The lavas from these latter eruptions form Glass Mountain on the north-eastern rim of the caldera (Figure 6.2).

At about 0.76 Ma, deposition of the Glass Mountain lavas culminated in a cataclysmic eruption of 600 km^3 of high-silica rhyolite, fed by a large, chemically evolving magma chamber in the shallow crust *(Bailey et al., 1976)*. This event deposited ~ 600 km^3 of material onto the surface, the majority of which now forms the Bishop tuff. The event caused a ring fault to form, and subsequently 2 - 3 km subsidence of the magma chamber roof forming a 17 x 32 km oval depression (Figure 6.3). Ensuing eruptions were confined to the caldera. Extrusions of relatively hot, crystal-free rhyolites at 0.7 to 0.6 Ma caused the caldera floor to upwarp, forming the resurgent dome, currently 10 km in diameter and rising 600 m above the caldera floor. Further eruptions of cooler, crystal-rich rhyolites starting at 0.5 Ma have occurred at 0.2 Ma intervals in clockwise succession around the resurgent dome.

The younger of the two Long Valley magmatic systems, the Mono Inyo craters system, has as its surface expression a long, narrow north-trending fissure extending from the south of Mammoth Mountain to the north shore of Mono Lake (Figure 6.2). This system, first active at 0.4 Ma, currently erupts at intervals of 250 to 700 years, generating high-silica rhyolites. The most recent eruptions were 250 years ago. Unlike the Long Valley caldera system, it is thought that these eruptions originate from small discrete magma bodies.

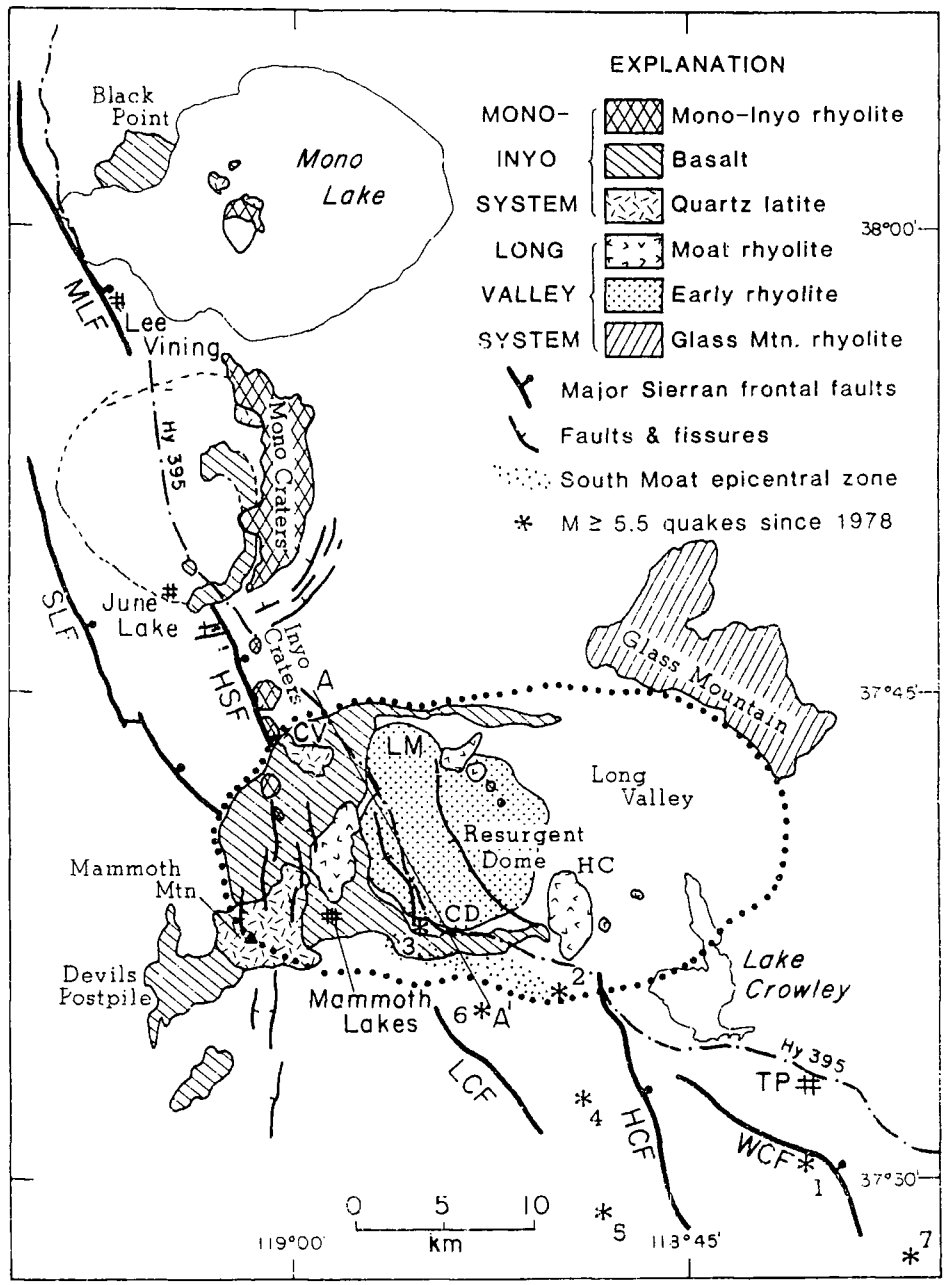

Figure 6.2 Regional and tectnic setting of Long Valley caldera. Dots indicate the boundary of the caldera. HC = Hot Creek, MLF = Mono Lake Fault, WCF = Wheeler Crest Fault, HSF = Hartley Springs Fault, SLF = Silver Lake Fault, LM = Lookout Mountain, TP = Tom's Place, CV = Crestview. Numbers refer to the following dates and magnitudes of earthquakes: (1) 4 October 1978, M = 5.7; (2) 25 May 1980, M = 6.1; (3) 25 May 1980, M = 6.0; (4) 25 May 1980, M = 6.1; (5) 27 May 1980, M = 6.2; (6) 30 September 1981, M = 5.7; (7) 23 November 1984, M = 5.8. From *Rundle & Hill, 1988.*

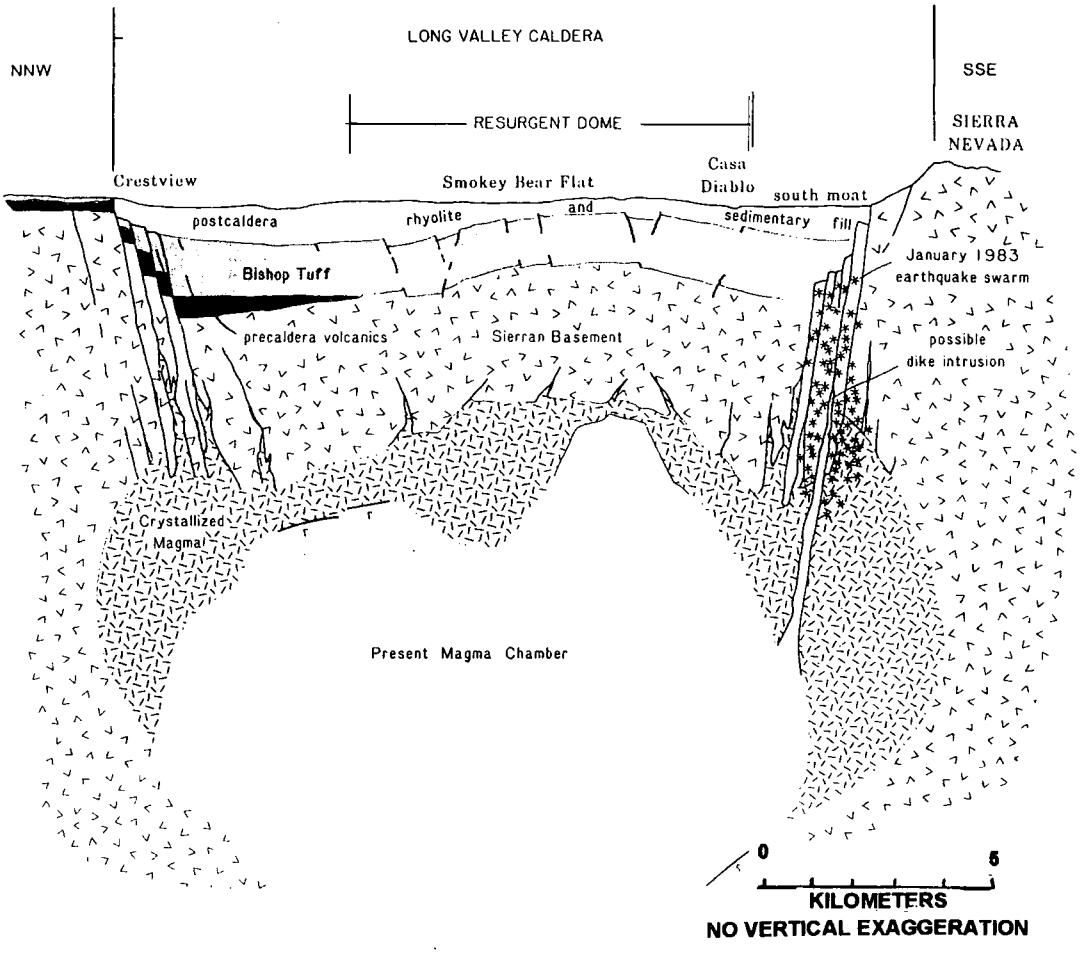

Figure 6.3 Schematic northwest - southeast cross-section through Long Valley caldera. Heavy lines represent approximate positions of reflecting boundaries indentified by *Hill et al. (1985)* and *Luetgert & Mooney (1985)*. From *Hill et al, (1985).*

6.3 Monitoring unrest in the Long Valley caldera

6.3.1 Seismic monitoring

Following the unrest in Long Valley during the late 1970s/early 1980s, seismic monitoring commenced in 1982. There are currently about fifty NCSN recording stations within 50 km of the Long Valley area (Figure 6.4).

The Long Valley NCSN catalogue contains both earthquake locations and magnitudes based on hand-picked arrival times and amplitudes (CalTech-USGS-Seismic-Processing (CUSP)) and automatic seismogram processing (Earthworm). The CUSP and Earthworm results are merged in the catalogue, with the CUSP results taking precedence where both exist.

For earthquakes at Long Valley, during periods of relatively low activity, the catalogue of CUSP locations is complete down to magnitude 1.2. During intense swarms, however, staff time is only sufficient to process the largest events and many earthquakes larger than magnitude 1.2 are processed only by Earthworm. Earthworm magnitudes are determined from coda lengths and several closely spaced events may be interpreted as a single large event. As is the case at The Geysers, this causes exaggeration of the numbers of large-magnitude events and underestimation of the number of low-magnitude events in the Earthworm results. The effect of this during intense swarms can be seen from cumulative-frequency vs. magnitude plots (Figure 6.5). During periods of low activity, a straight line distribution, following the Gutenberg-Richter equation (Equation 2.14), is exhibited. However, during intense swarms a distorted cumulative-frequency vs. magnitude plot results and a correct *b*-value cannot be calculated.

To overcome these problems, analysis was restricted to those time periods for which the CUSP data are complete down to a threshold magnitude of $M = 1.8$. By

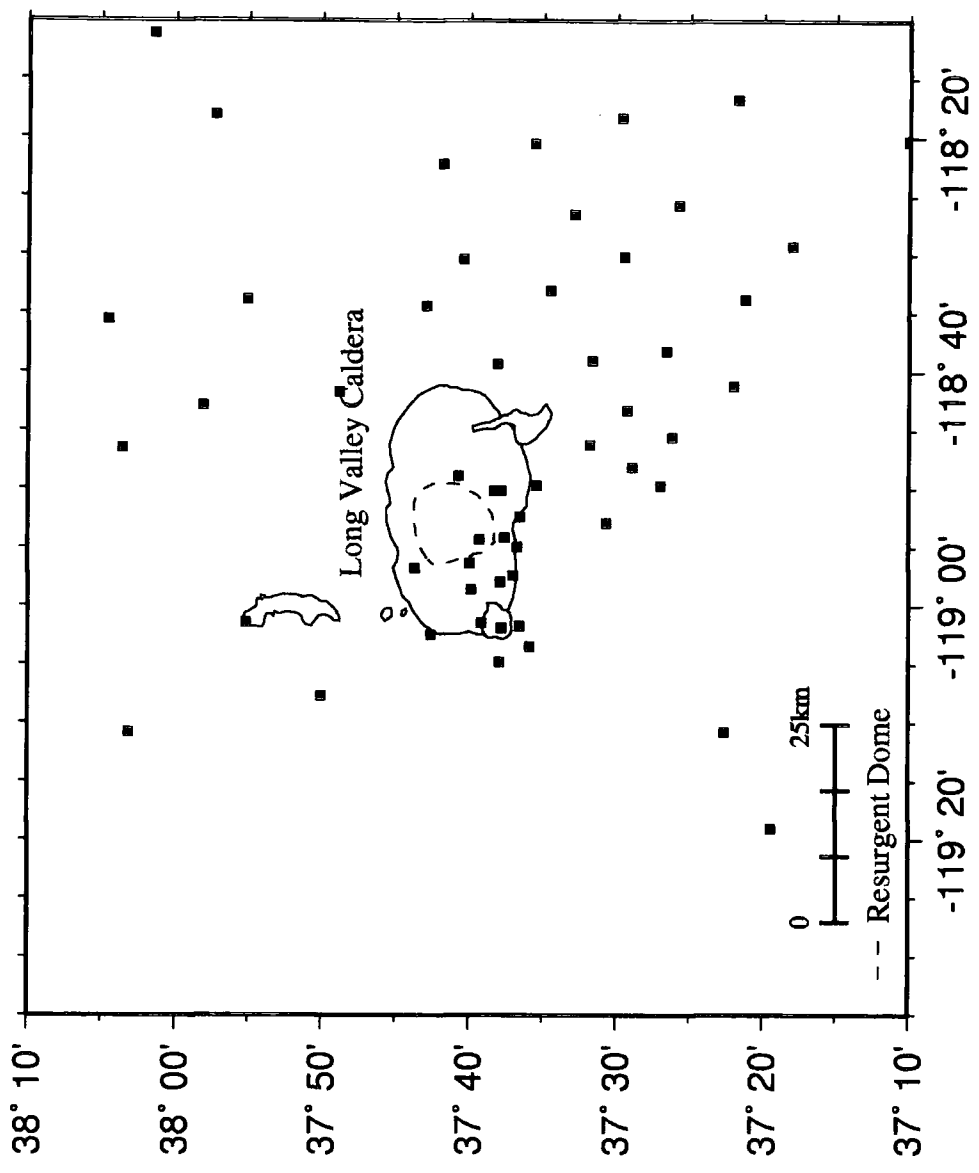

Figure 6.4 Map of NCSN seismic stations (black squares) within 50 km of Long Valley caldera that were in use 1997 - 98.

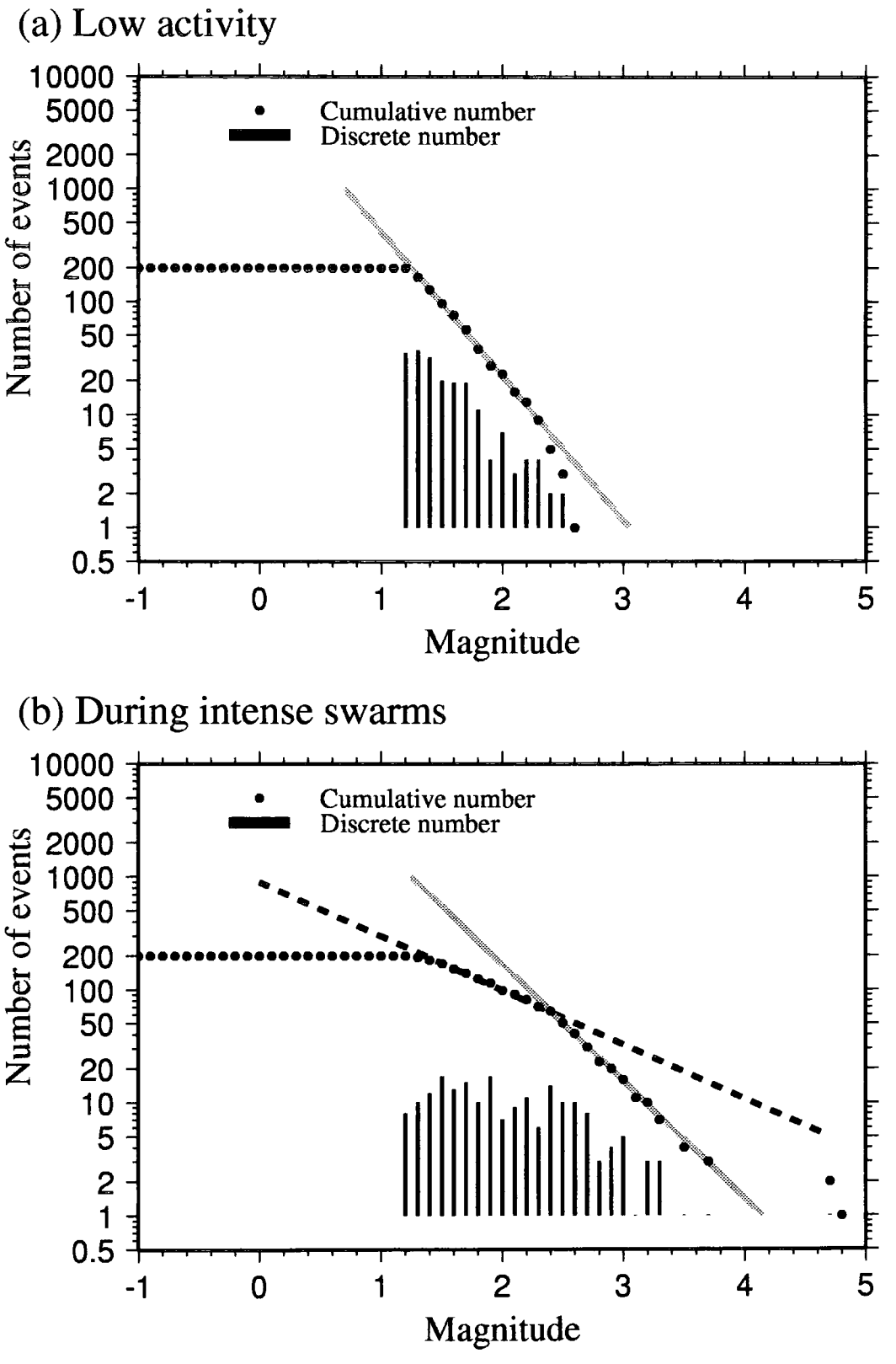

Figure 6.5 (a) Plot of log-cumulative number vs. magnitude for data from June 1997 when the CUSP (hand-picked) magnitude threshold was 1.2. There is a linear relationship above magnitude 1.2. (b) Same as (a) but for data from late November 1997 during an intense swarm. There is a linear relationship but only above a much higher threshold magnitude.

using only CUSP data, observed differences in b-value may be trusted to be real. Furthermore, this approach restricts the analysis to the most accurately located earthquakes.

6.3.2 Ground deformation monitoring using two colour geodimeters

Ground deformation at Long Valley is monitored by networks of two-colour geodimeters, tiltmeters, strainmeters and GPS stations. The geodimeter data were used in this study because it has the most comprehensive station coverage (Figure 6.6).

The two-colour geodimeter is an ultra-precise distance measuring instrument with a precision of 0.5 to 1.0 mm for ranges between 1 and 12 km. This instrument has been used to monitor deformation at Long Valley caldera since 1983, with measurements taken several times a week. The instrument measures the transit time of two colours (red and blue) of visible light through the atmosphere. The difference in travel time between the two colours is dependent on atmospheric temperature and pressure. The travel-time difference is used to calculate the average temperature and pressure, which are then used to calculate the atmospheric index of refraction. This index is used to find the distance from the travel time of one of the colours.

Unlike conventional one-colour laser electronic distance measuring devices, the two- colour geodimeter does not require precise measurement of pressure and temperature along the light path. Compared with Global Positioning System (GPS) surveying, the two-colour geodimeter method is more accurate for ranges less than 10 km. However, the system is expensive, requires a highly skilled crew and has a limited range due to the atmospheric scattering of the short-wavelength blue light.

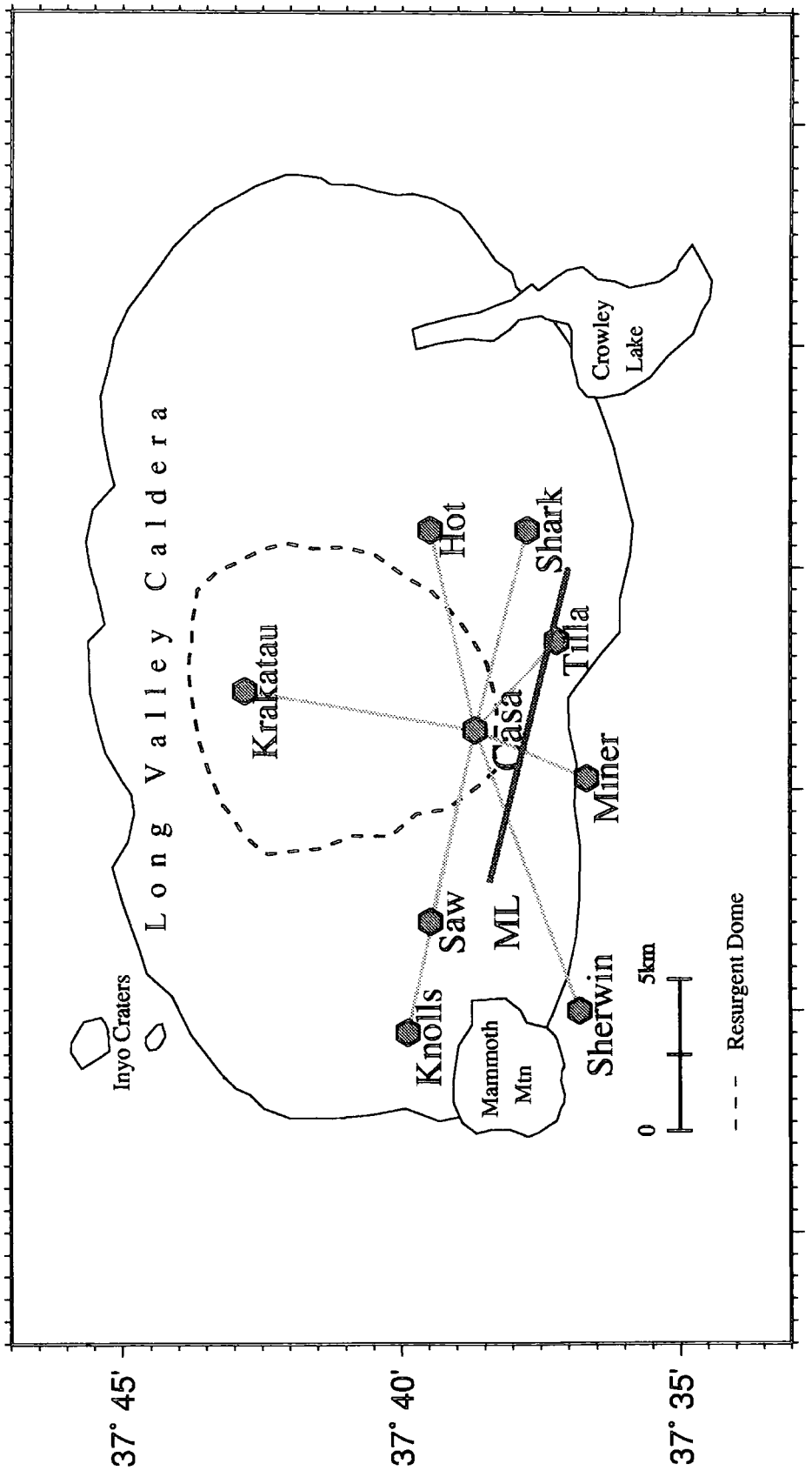

Figure 6.6 Map of Long Valley caldera showing two-colour geodimeter station locations and lines routinely measured. ML = Mammoth Lakes. Grey continuous line = South Moat fault.

6.4 The effects of magmatic unrest in Long Valley

6.4.1 Seismicity

6.4.1.1 Seismicity prior to 1997

Prior to 1978 there was little recorded seismicity in the Long Valley caldera area (Figure 6.7). However, since 4 October 1978, when a large (M = 5.7) earthquake occurred 20 km south of the caldera near the town of Bishop (Figure 6.2), Long Valley has been in a state of unrest *(Rundle and Hill, 1988)*. Over the following two years a sequence of swarms migrated towards the caldera *(Ryall & Ryall, 1980; Van Wormer & Ryall, 1980)*. This activity was precursory to larger events *(Van Wormer & Ryall, 1980)*.

In May 1980 there was an intense earthquake swarm featuring four $M > 5.0$ events. Since then Long Valley caldera has experienced continuous high level seismic activity, with several shocks as large as $M \sim 5.0$. Between May 1980 and the end of 1982, there were eight moderate swarms and a slight trend towards shallower hypocentral depths.

Since 1982, the seismicity has been mostly confined to the south-western quadrant of the caldera and to the Sierra Nevada block to the south, in four distinct clusters (Figure 6.8 and 6.9). (See Figure 6.1 for place names).

1. A cluster roughly 4 km in diameter near the south-west margin of the resurgent dome along the South Moat fault, a blind, near-vertical, right-lateral fault. This cluster contains most of the large $M > 4.0$ earthquakes.
2. A cluster located in the centre of the south moat of the resurgent dome coinciding with geothermal features.
3. A cluster on the south-western flank of Mammoth Mountain.

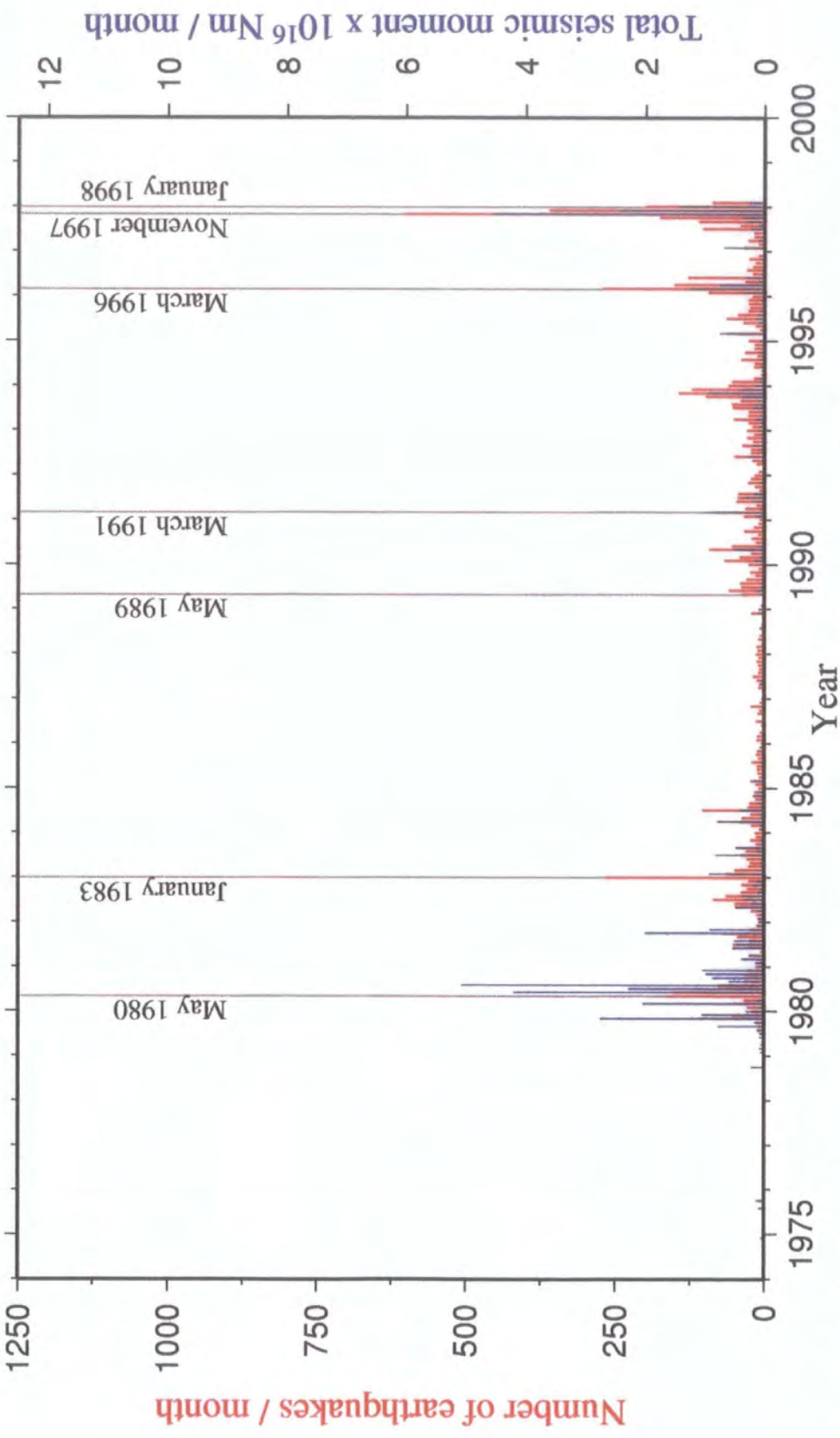

Figure 6.7 Number of events and total seismic moment per month for $M >= 1.8$ events in Long Valley caldera between 1974 and 1998. Earthworm events have not been plotted.

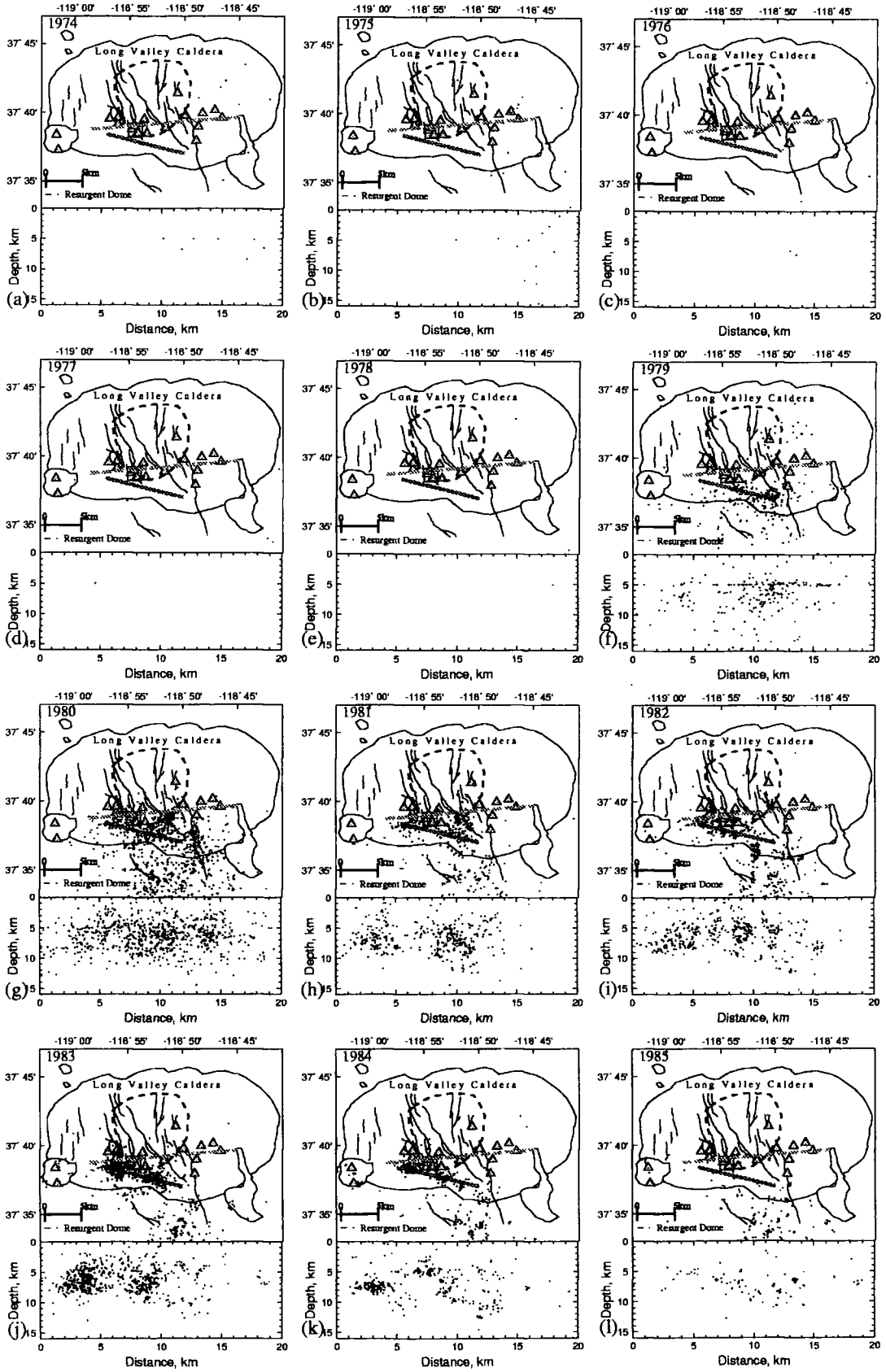

Figure 6.8 Epicentre maps and west-east cross-sections for Long Valley earthquakes within 10 km of the line of the section with $M >= 1.8$ from 1974 to 1985. Thermal springs and fumaroles are shown as triangles. The South Moat fault is shown as a grey line and other faults as black lines. The line of the cross-section is shown as a dotted grey line. The Casa Diablo geothermal field is shown as a square. The data from the NCSN catalogue are CUSP events.

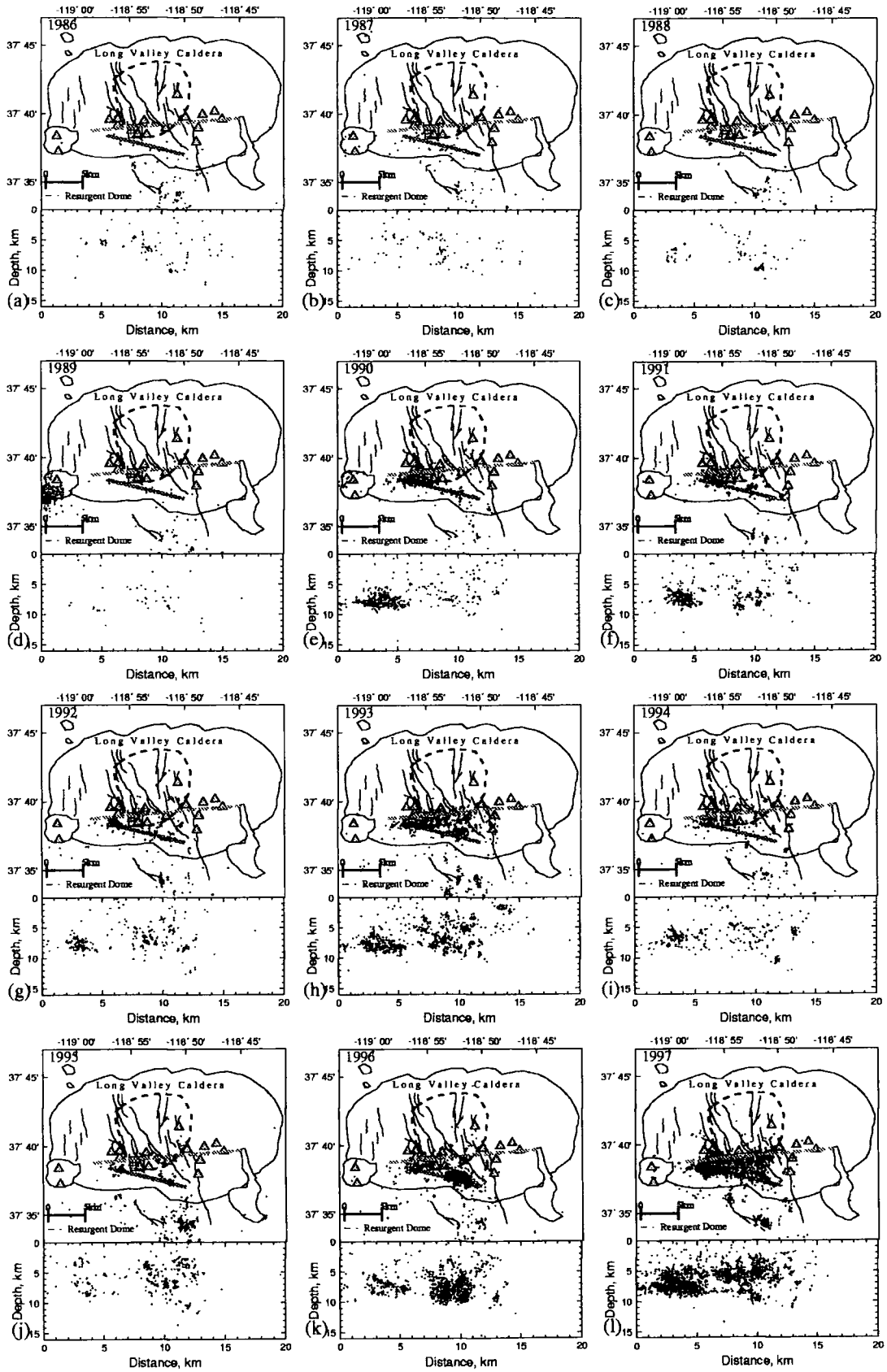

Figure 6.9 Same as Figure 6.8 except for 1986 to 1997.

4. An irregular grouping of clusters with north-south elongation defining the eastern extent of the earthquake activity within the caldera. These clusters coincide with the northern branches of the Hilton Creek fault and the hydrothermal activity at Hot Creek George Spring.

On 7 January 1983, a major swarm of over 1200 events formed an elongate zone in the south moat. The swarm contained two $M > 5.0$ earthquakes. Most events in the swarm had focal depths in the range 4 - 10 km and the overall hypocentral pattern in subsequent swarms has remained the same since then. The events were shown to be right lateral strike slip *(Rundle & Whitcomb, 1984)*. On 23 November 1984, a $M = 5.8$ earthquake near the location of the 1978 Bishop event caused a sequence of seismicity that migrated north-north-westerly up into the caldera. During the mid to late 1980s, clustering continued in the south-west moat but at a much reduced rate. In May 1989 there was an intense swarm of events on the south-west flanks of Mammoth Mountain (Figure 6.9d), followed by a rapid increase in seismicity rate in the caldera in early 1990. In March 1991 there was a large swarm of over 400 events in the south-west moat of the resurgent dome. The focal mechanisms of events in the May 1991 swarm were very similar to those of the January 1983 swarm *(Langbein et al, 1993)*.

Following the intense swarms of the early 1990s, the seismicity migrated eastwards towards the hydrothermal features on the eastern side of the resurgent dome during 1993. After a period of relative aseismicity, in March 1996 there was intense activity in the same location as the 1983 and 1991 swarms (Figure 6.9k).

6.4.1.2 Seismicity 1997 - February 1998

6.4.1.2.1 Introduction

The largest swarms between January 1997 and February 1998 took place during July and November 1997 (Figures 6.10 and 6.11). Table 6.1 is a summary of the swarm sizes and the number of large earthquakes in each swarm. The seismic activity during this period falls naturally into three time periods; 1 January - 21 November 1997, 22 November - 31 December 1997 and 1 January - 28 February 1998.

6.4.1.2.2 Seismicity 1 January - 21 November 1997

In the early part of 1997, the Long Valley caldera was relatively aseismic. Seismicity was limited to the vicinity of the Laurel Convict fault to the immediate south of the caldera (Figure 6.12). In the period 7 - 20 July, a swarm of 82 events featuring four events with $M > 3.0$ occurred to the immediate south-west of the resurgent dome (Figure 6.13). The majority of these events were around the adjacent fumaroles and hot springs.

Between 6 and 8 September a small swarm of 14 events occurred in the south-eastern corner of the resurgent dome near to the Hot Creek Fish Hatchery (Figure 6.14). None of these events were large and all were at depths of about 5 km. In late September/early October of swarm of 54 earthquakes containing seven $M >$ 3.0 events occurred to the immediate south of the north-western end of the South Moat fault.

During October, activity was concentrated in the south-western part of the moat (Figure 6.15). At the beginning of the month, events formed a halo around the

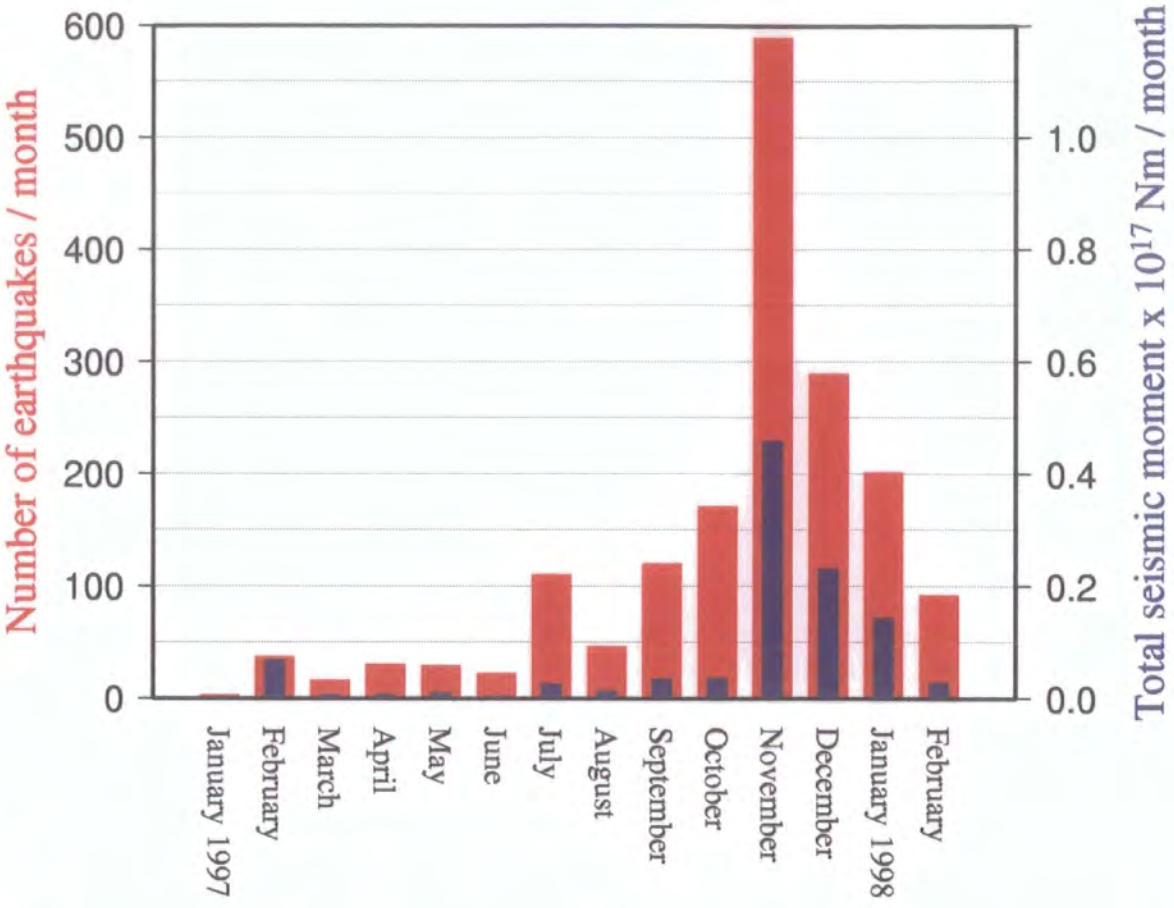

Figure 6.10 Number of events and total seismic moment per month for earthquakes with $M >= 1.8$ in Long Valley caldera between January 1997 and February 1998.

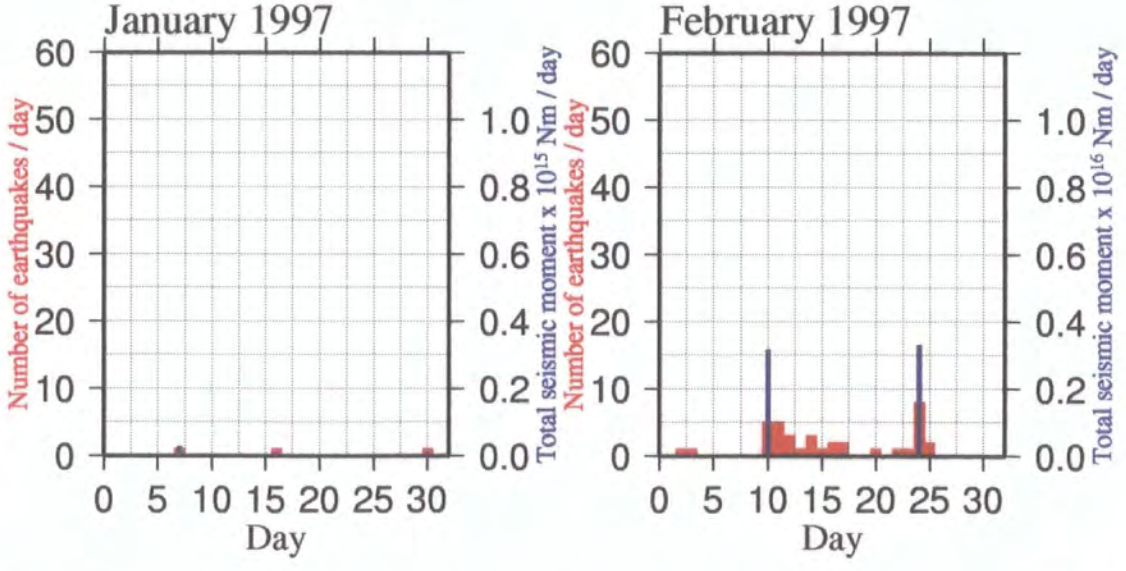

Figure 6.11(a) Number of events and total seismic moment per day for earthquakes with $M >= 1.8$ in Long Valley caldera for January and February 1997.

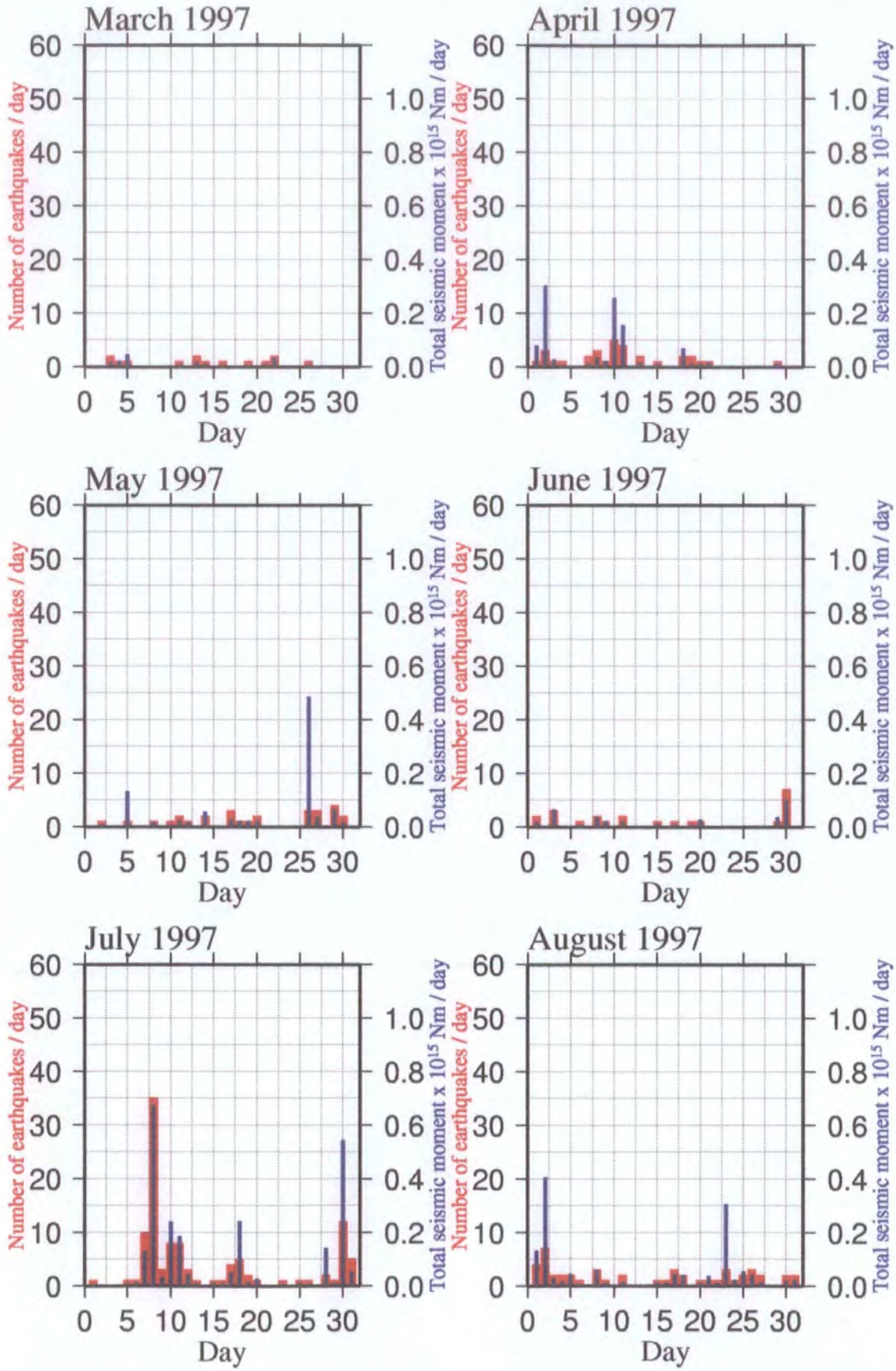

Figure 6.11(b) As Figure 6.11(a) except for the months March to August 1997.

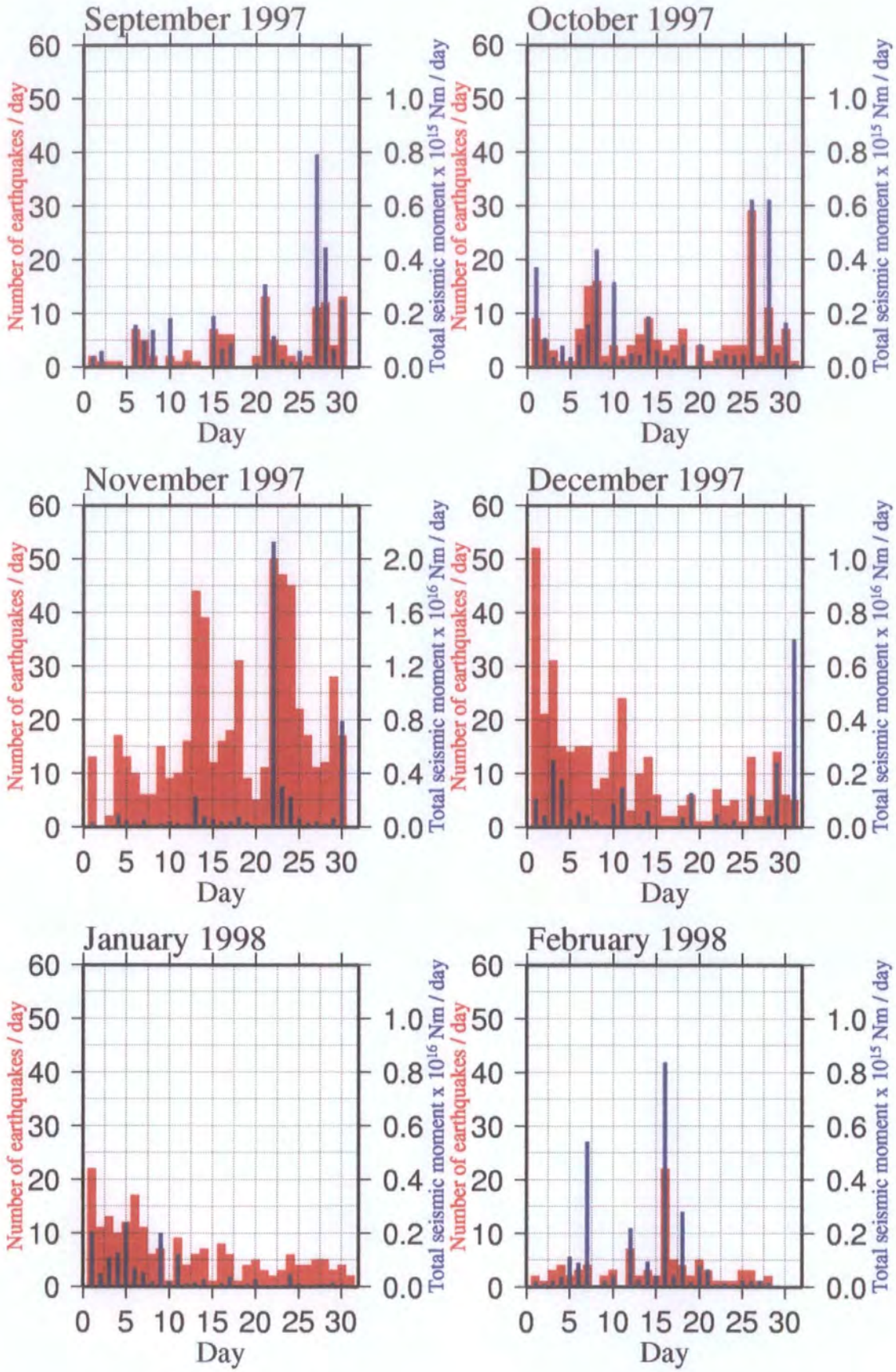

Figure 6.11(c) As Figure 6.11(a) except for the months September 1997 to February 1998.

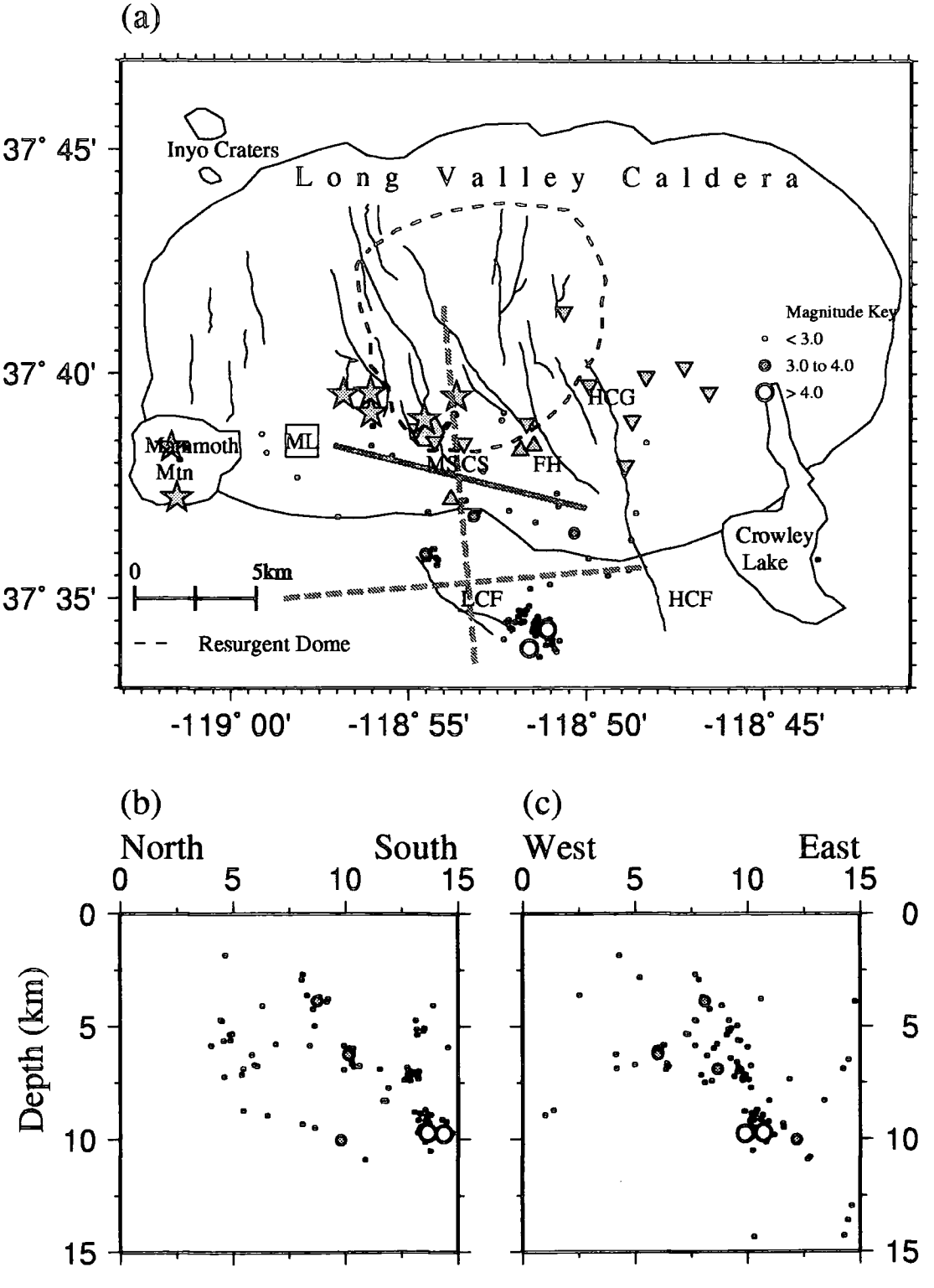

Figure 6.12 Hypocentral plot for events with $M >= 1.8$ for January to June 1997. Cross -sections include events within 10 km of the dashed line marked on the epicentral map. See Figure 6.1 for key to symbols.

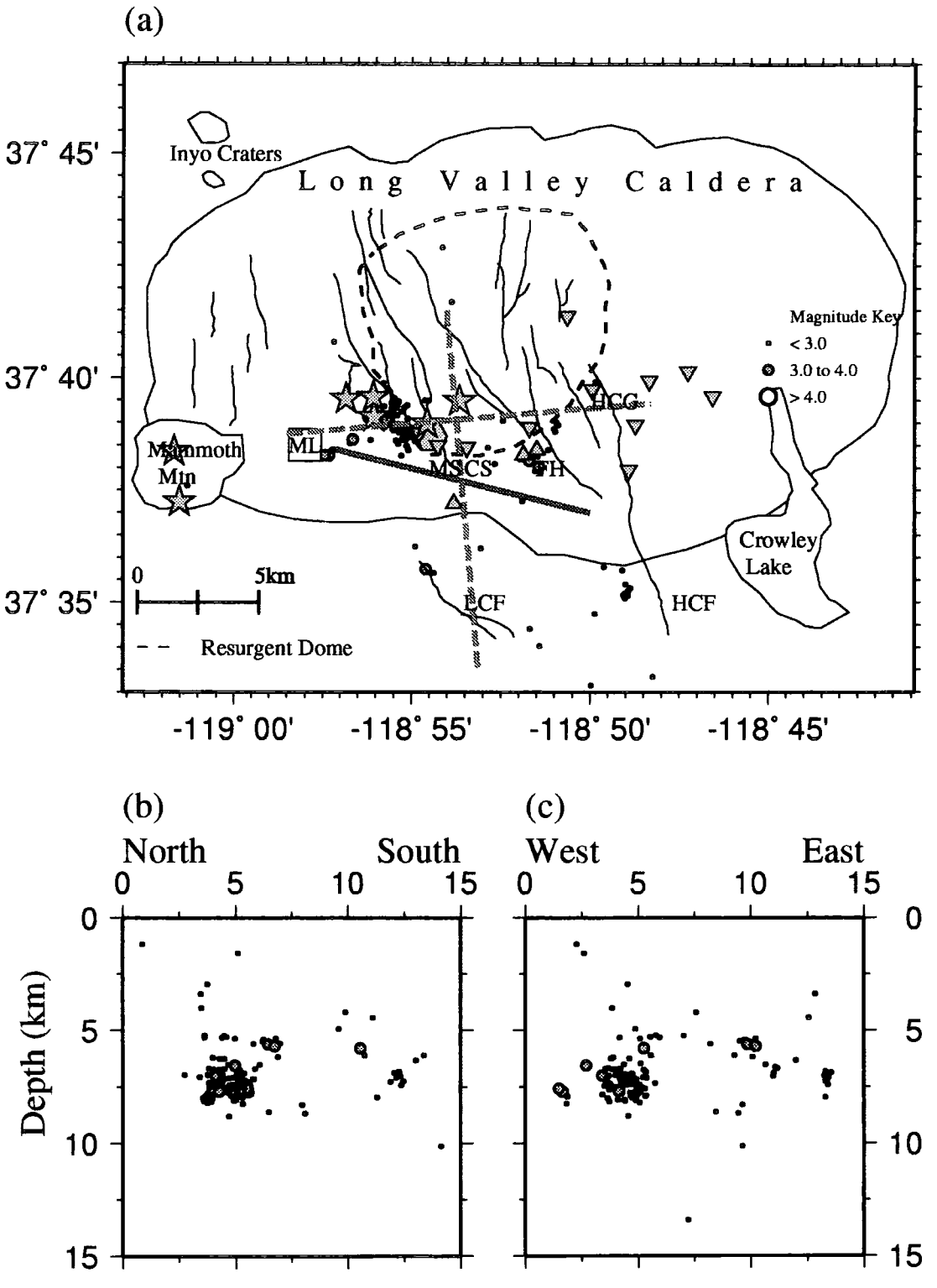

Figure 6.13 Same as Figure 6.12 except for the time period July to August 1997.

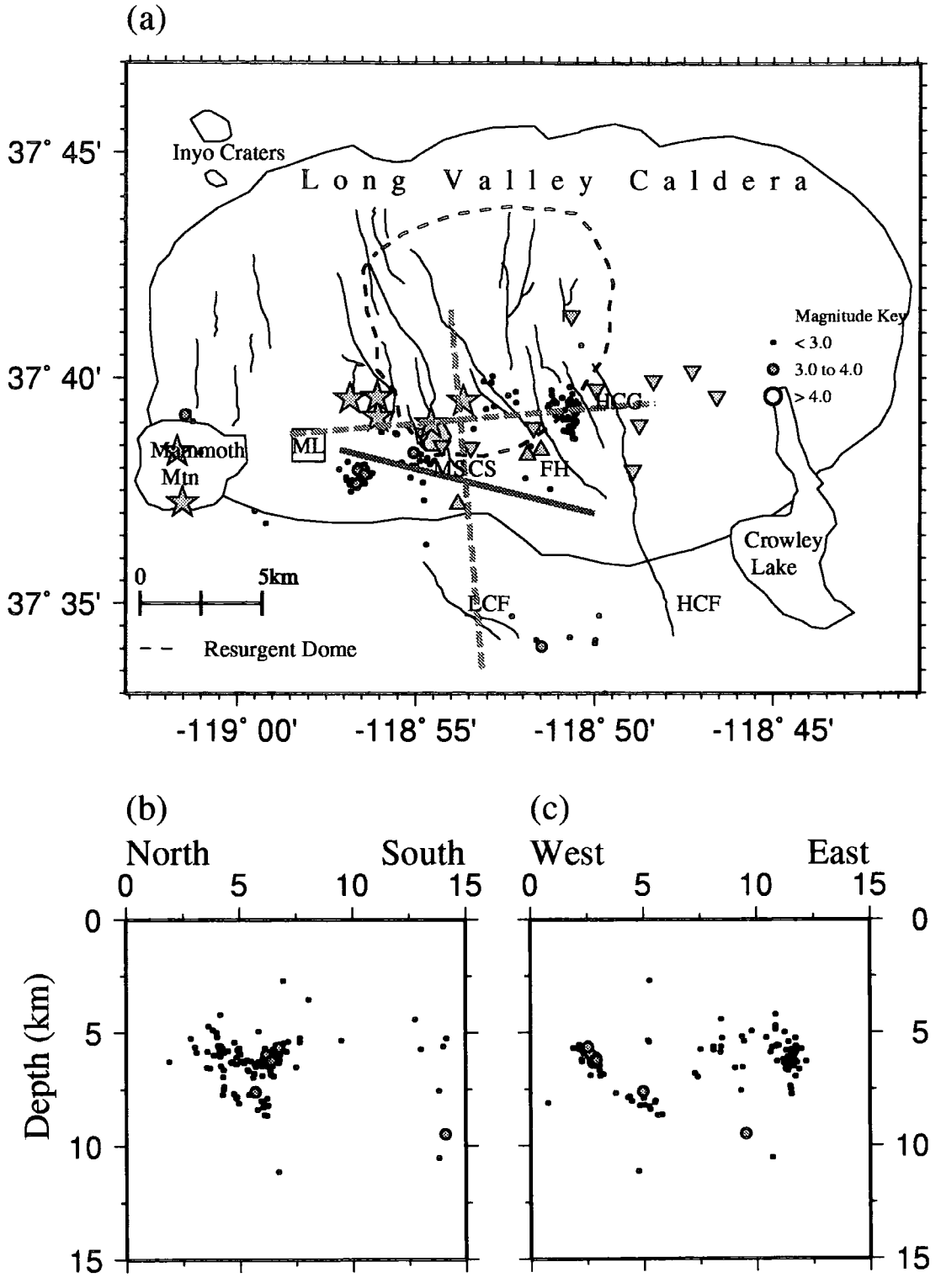

Figure 6.14 Same as Figure 6.12 except for September 1997.

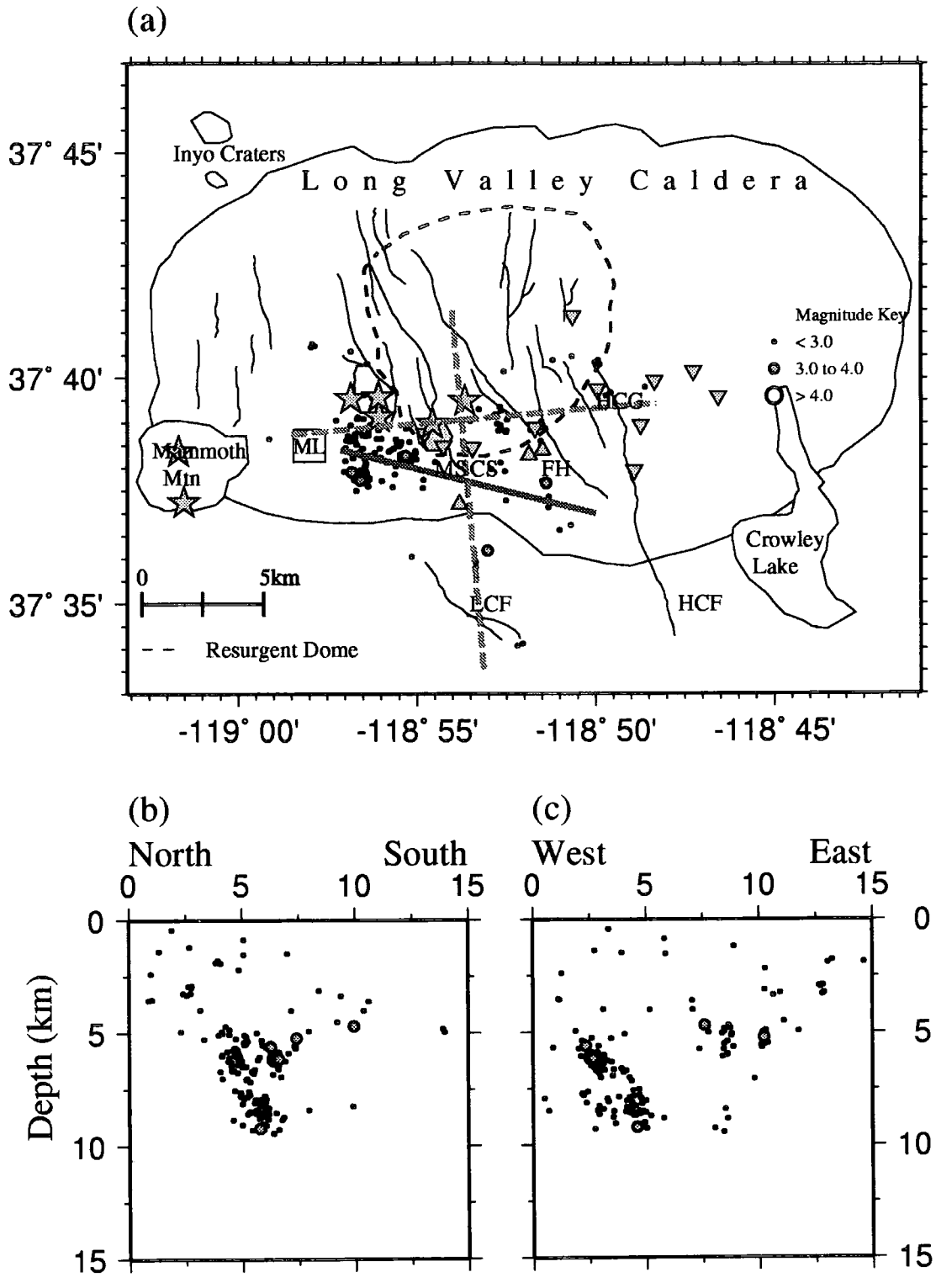

Figure 6.15 Same as Figure 6.12 except for October 1997.

Table 6.1 Earthquakes located by CUSP in Long Valley caldera, 1997 – 1998

Swarm dates	# of CUSP events with $M \geq 1.8$	# of CUSP events with $M \geq 3.0$
10 - 16 February 1997	20	1
23 - 26 February 1997	11	4
7 – 20 July 1997	82	4
30 July - 4 August 1997	32	3
6 – 8 September 1997	14	1
21 - 22 September 1997	18	0
27 September - 2 October 1997	54	7
7 – 10 October 1997	37	2
17 - 19 October 1997	11	0
25 - 27 October 1997	35	1
31 October - 2 November 1997	14	1
4 – 7 November 1997	46	4
12 - 19 November 1997	185	6
22 - 26 November 1997	181	20
29 November - 3 December 1997	104	7
1 – 3 January 1998	46	7
15 - 17 February 1998	29	2

north-western end of the South Moat fault. The seismicity then migrated into a cluster to the immediate south mid October (including two $M > 3.0$ events), forming a diffuse band along the fault. The activity became deeper (from 7.5 km to 10 km) as the month progressed. There was a swarm of 35 events near the north-western end of the South Moat fault 25 - 27 October.

At the start of November, events were clustered to the south-east of the resurgent dome to the immediate south of the early - mid September activity at the Hot Creek George Spring (Figure 6.16). By 13 - 14 November, activity had migrated westwards to the southern-most point of the resurgent dome close to the Meadow and Colten Springs, forming a dense cluster of over 100 events. On 13 November there was an $M = 3.8$ event and an $M = 3.2$ event. Most of the events were clustered at depths between 5 and 7 km. Between 15 and 18 November, the seismicity migrated further west, forming a cluster of about 30 events in the same location as the 25 - 27 October activity, and became deeper with time.

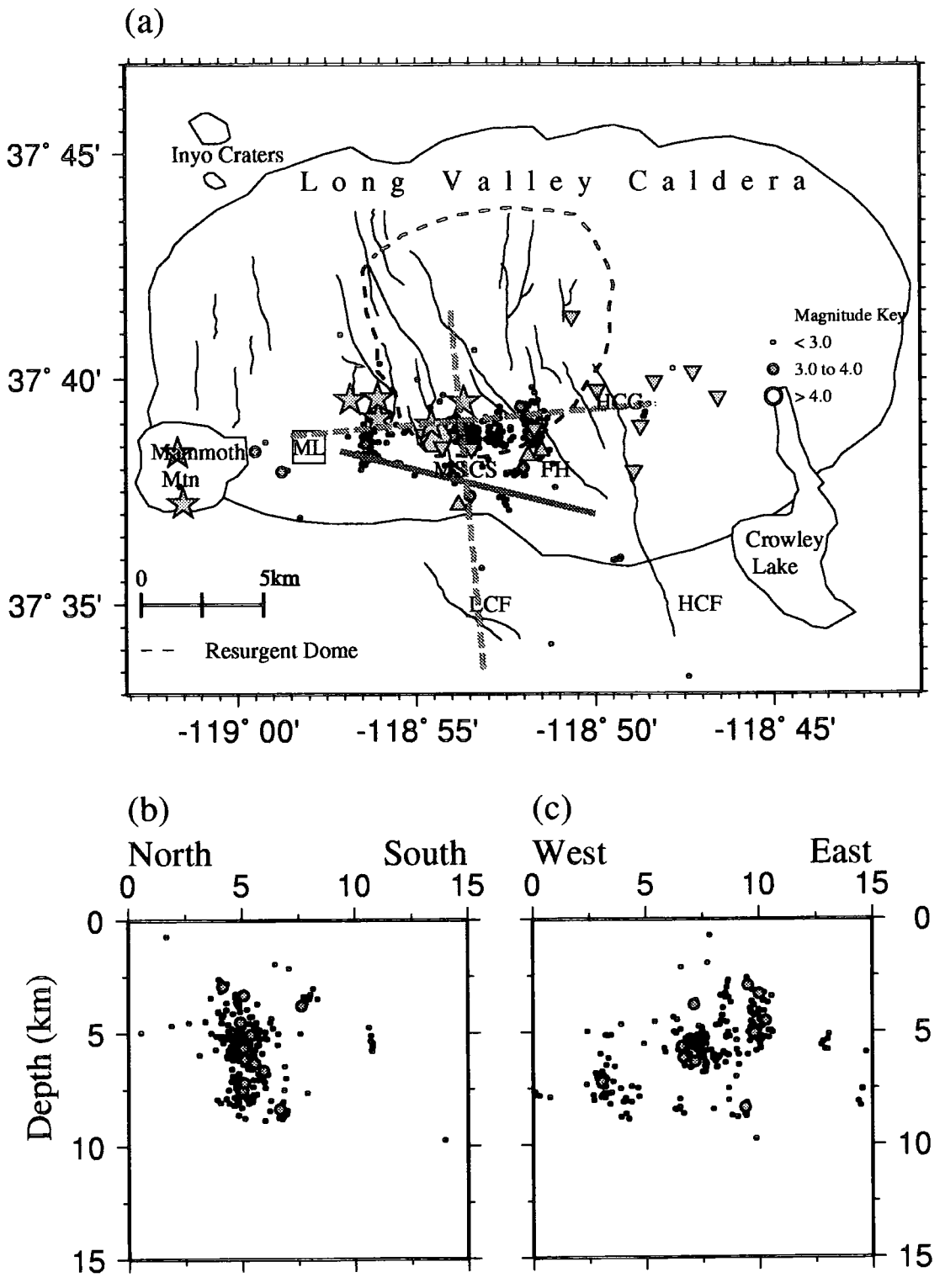

Figure 6.16 Same as Figure 6.12 except for the time period 1 - 21 November 1997.

6.4.1.2.3 Seismicity 22 November - 31 December 1997

On 22 November there was an M = 4.3 earthquake on the South Moat fault (Figure 6.17). This precipitated a massive swarm with a further two $M > 4.0$ events and seven other $M > 3.0$ events within twenty four hours of the first earthquake. Events were at depths of 5 - 10 km at the north-western end of the swarm, and gradually shallowed to 5 km at the south-eastern end. Two further swarms followed an M = 4.5 event on 30 November and an M = 3.2 event on 3 December. During the rest of December the seismicity rate dropped, but events continued to occur in the locale of the 22 November swarm. On 31 December there was an M = 4.5 event half way between the South Moat fault and the hot springs at the Hot Creek Fish Hatchery. This was followed by four further events with $M > 3.0$.

6.4.1.2.4 Seismicity 1 January - 28 February 1998

On 1 January, the area between the South Moat fault and the hot springs at the Hot Creek Fish Hatchery was even more active (Figure 6.18). There were ~ 700 $M > 1.8$ events in the NCSN catalogue for this day, though unfortunately only 22 were CUSP recorded (Figure 6.7). Most of the catalogued events were concentrated around the Hot Creek Fish Hatchery springs, with a few residual earthquakes near the location of the 22 November activity. During the rest of January, the seismicity migrated westwards towards the Meadow and Colten Springs, eventually petering out by the end of the month. There was little seismicity during February, with only minor clusters around Meadow and Colten Springs mid month.

6.4.2 Inflation of the resurgent dome

After the May 1980 earthquake swarm, it was discovered that the resurgent dome had risen by ~ 25 cm since summer 1979 *(Savage & Clark, 1982; Castle et al.,*

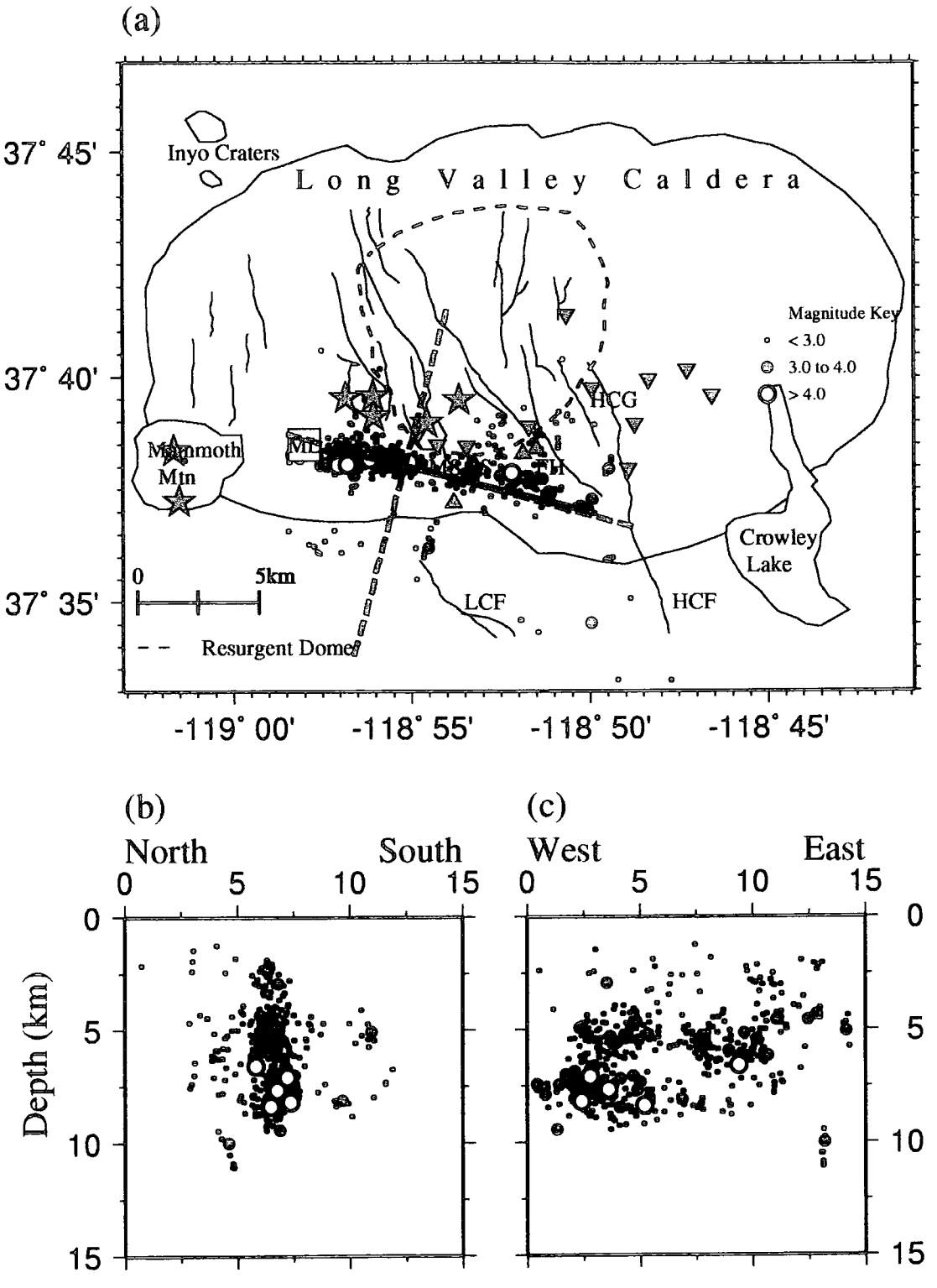

Figure 6.17 Same as Figure 6.12 except for the time period 22 November - 31 December 1997.

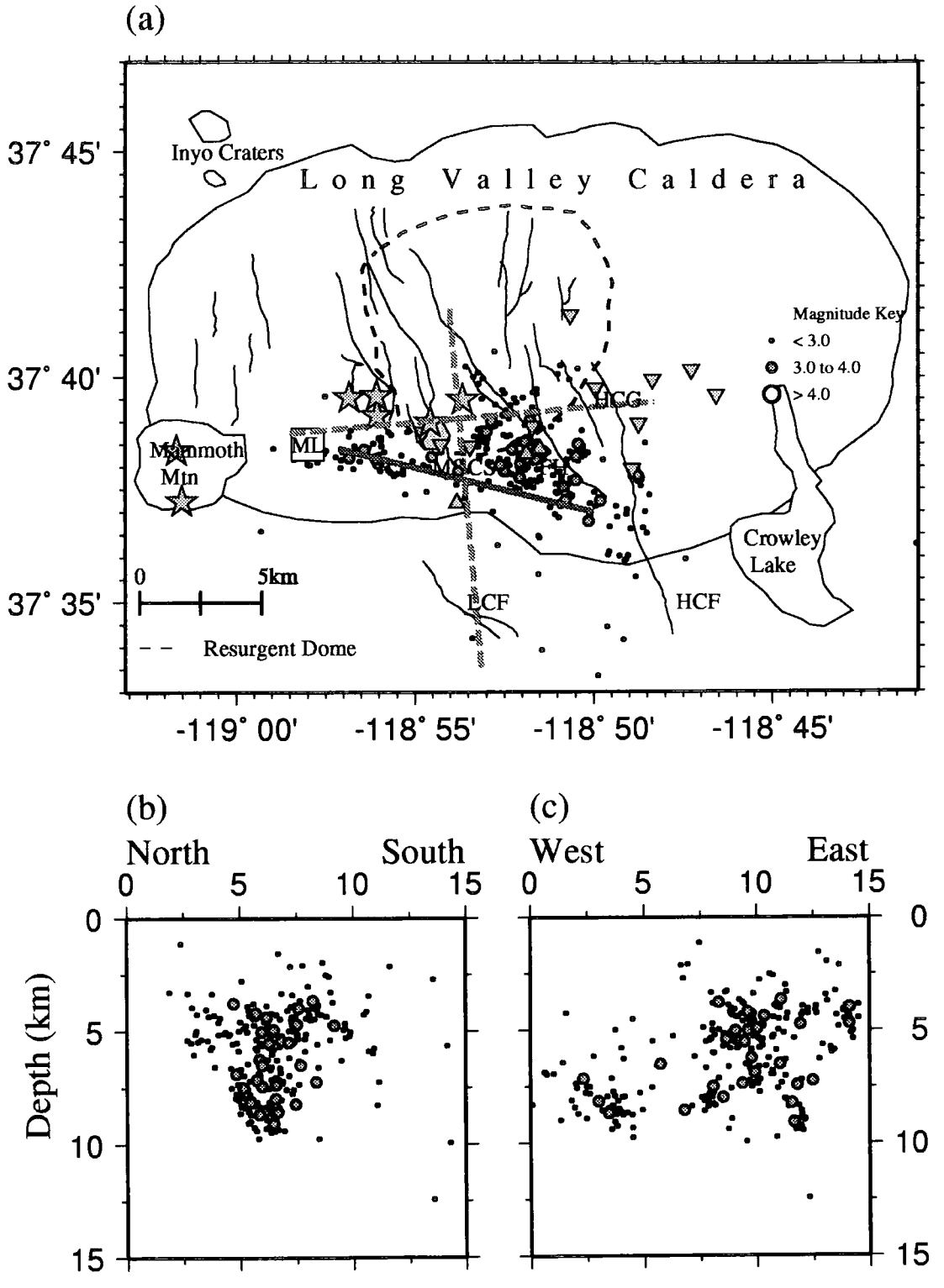

Figure 6.18 As Figure 6.12 except for the time period January to February 1998.

1984). This inflation was interpreted as new magma rising beneath the caldera. The dome has risen by variable rates ever since, with continuous inflation since 1989. There are thought to be two sources of inflation *(Langbein et al., 1993)*; a shallow (5.5 km deep) source 0.5 km north of the two colour geodimeter station Casa (Figure 6.6) and a deeper source (10 km) 6 km north-north-west of Casa. The increase in seismicity in November 1997 coincided with accelerated inflation of the resurgent dome.

6.4.3 Interpreting deformation at Long Valley

Most deformation models for Long Valley caldera have these features in common *(e.g. Rundle & Whitcomb, 1984; Denlinger et al., 1985; Langbein et al., 1993)* (Figure 6.19):

1. A primary chamber beneath the central part of the resurgent dome, centred at a depth of 7 - 10 km,
2. A secondary chamber centred beneath the southern margin of the resurgent dome at a depth of 4 - 8 km,
3. Right-lateral slip on a vertical west-north-west striking blind fault in the south moat with a depth range between 0.5 - 12 km. This South Moat fault is probably the locus of most of the large earthquakes from 1980 onwards, with the remainder occurring on the Hilton Creek fault (Figure 6.1).

During the 1980 activity, an estimated 0.05 km^3 of magma was injected into the primary chamber, with approximately 0.0045 km^3 entering the secondary chamber *(Rundle & Whitcomb, 1984)*. At this time, about 0.25 m of right-lateral strike-slip faulting occurred on the South Moat fault in the depth range 0.5 - 7 km, and 1 m in the depth range 7 - 12 km *(Rundle & Whitcomb, 1984)*. Estimates of the amount of injected magma for the 1983 episode vary from 0.0015 km^3 (primary chamber) and 0.009 km^3 (secondary chamber) *(Rundle & Whitcomb, 1984)* to 0.019 km^3 (primary) and 0.004 km^3 (secondary) *(Denlinger et al., 1985)*. The amount of

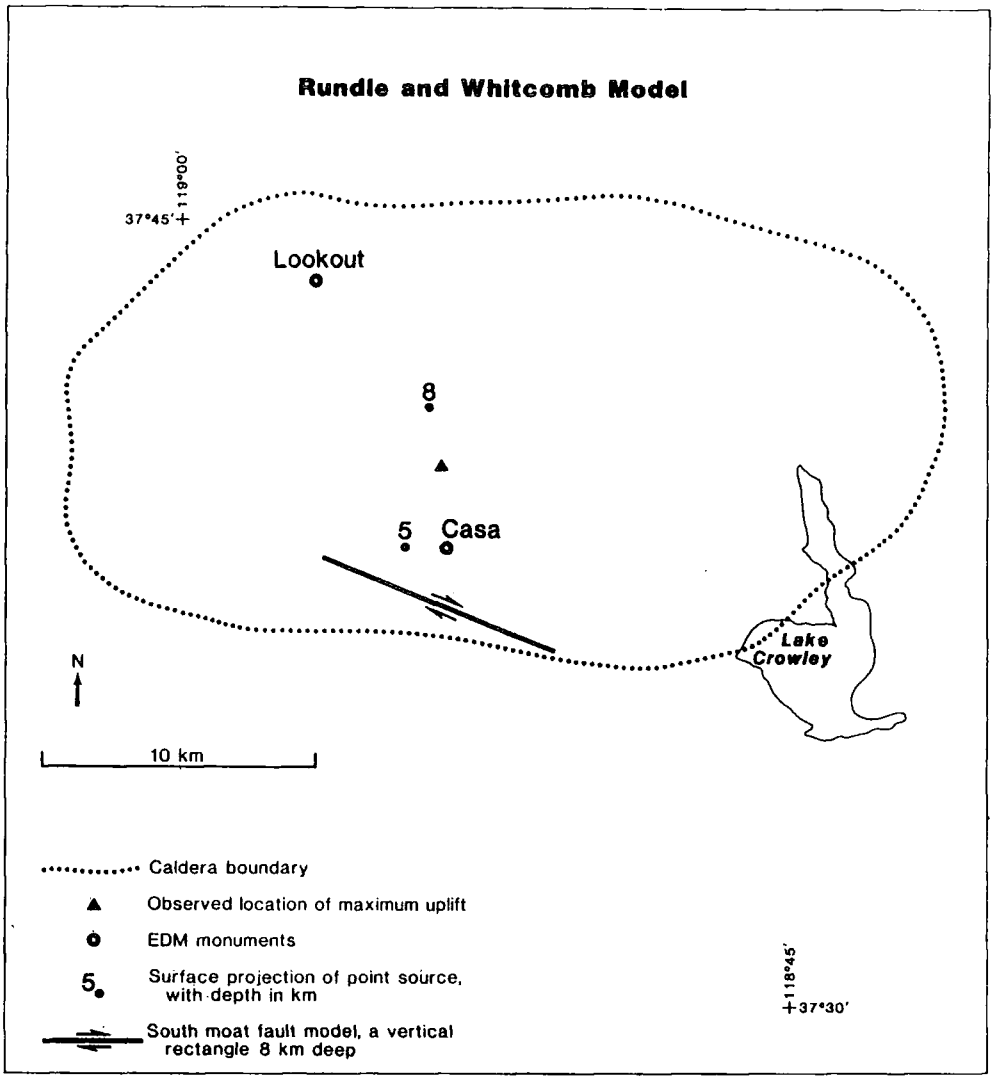

Figure 6.19 A model for the deformation of Long Valley during the swarm of January 1983. From *Denlinger et al.(1985)*.

estimated strike-slip movement on the South Moat fault varies from 0.165 m *(Rundle & Whitcomb, 1984)* to 0.25 m *(Denlinger et al., 1985)*.

Due to the paucity of deformation data prior to 1983, accurate temporal comparisons between the seismic activity and deformation cannot be made, nor can any causal relationship between them be proven. However, inflation of the primary magma chamber can explain most of the accumulated caldera deformation prior to 1983 *(Savage & Clark, 1982; Savage, 1988)*. Models for the January 1983 swarm require greater contributions from secondary chamber inflation and movement along the South Moat fault *(Langbein et al., 1993)*.

The pattern of deformation in the period 1989 - 1991 suggests that the deformation source was beneath the resurgent dome, with little or no contribution from the South Moat fault zone or from the secondary chamber *(Langbein et al., 1993)*. During this episode, an estimated 0.025 km^3 of magma was injected into the primary chamber *(Langbein et al., 1993)*. The seismicity during the 1989 - 1991 was due to magmatic processes, i.e. pressurisation of one or more magma bodies triggering adjacent brittle failure *(Langbein et al., 1993)*. If the seismicity and deformation had a tectonic origin (i.e. non-magmatic), it would be expected that the seismic activity would had been followed by the inflation. Acceleration of deformation was observed to lead the brittle failure by two months, rendering a tectonic origin for the deformation unlikely. The earlier May 1989 activity beneath Mammoth Mountain is thought to be due to dyke intrusion at depths of 2 - 15 km.

6.4.4 CO_2 emission

During the early 1990's, it was noticed that trees were dying off at several locations on Mammoth Mountain as a result of carbon dioxide poisoning. The gas was seeping up through the soil from beneath. It was postulated that as magma moved towards the surface, it released CO_2 and other volcanic gases as it degassed. The area currently vents 400-500 tonnes of CO_2 per day *(Michael Sorey, pers. comm.)*.

6.4.5 Hydrothermal activity

Current hydrothermal activity within Long Valley is primarily around the southern and south-eastern sides of the resurgent dome, and to the east of the intra-caldera extension of the Hilton Creek fault (Figure 6.1). With the exception of the latter group, most of the hot springs lie on north to north-west trending normal faults. Steam discharge by fumaroles and diffuse seepage through the soil occur along normal faults in the south moat and on the northern and southern flanks of Mammoth Mountain.

6.5 Geothermal development of Long Valley caldera

The liquid-dominated Casa Diablo geothermal field in the southern moat of the resurgent dome has been exploited for electricity production since 1985 *(Sorey et al., 1995)*. Thermal fluids migrate through fracture zones from the source reservoir in the western moat to a fractured production zone comprised of rhyolite flows and tuff at Casa Diablo. Fluid is extracted to drive turbines and then re-injected to provide pressure support for the production wells. Since the geothermal fluid does not boil as it passes through the power plant system, none of it is lost. The production zone is separated from the underlying injection zone by less fractured, less permeable rock, with normal faults near the eastern edge of the field allowing vertical pressure communication between the production and injection wells (Figure 6.20).

Geothermal development of the Casa Diablo area of the caldera commenced in January 1985 with the building of a 10 MW plant. The average total fluid extraction rate for this period was 230 kg/s. An additional two 15 MW plants were built in 1990. Since then, the average total fluid extraction rate has been 850 kg/s. The total output from Casa Diablo (40 MW) is a small fraction of The Geysers geothermal area output (2043 MW in 1989). Reservoir conditions within

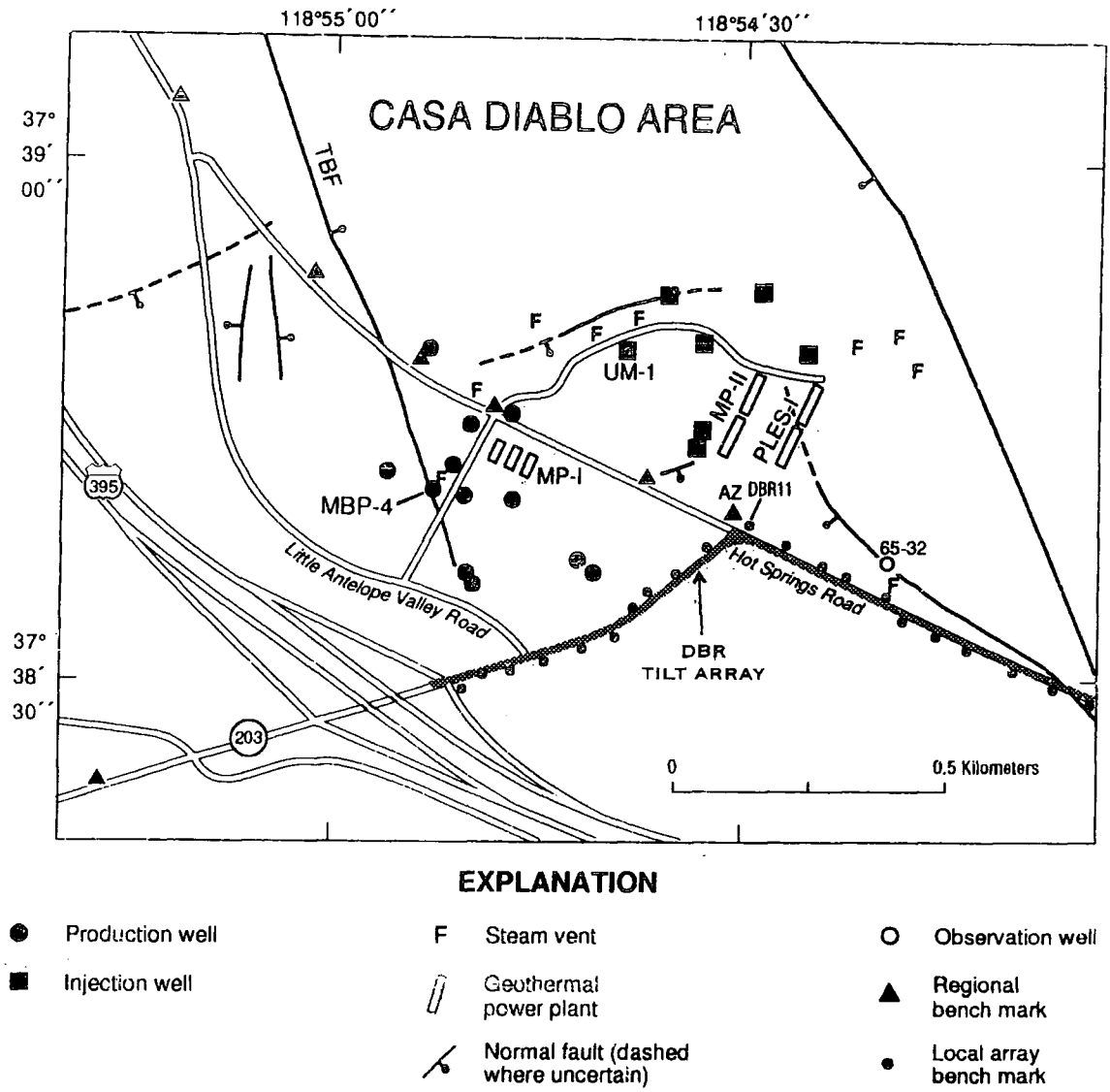

Figure 6.20 Map of the Casa Diablo area showing geothermal production and injection wells supplying three geothermal power plants. Mapped faults are from *Bailey(1989)* and unpublished mapping by J. F. Howle. TBF denotes Taylor-Bryant fault. From *Sorey et al. (1995)*.

the Casa Diablo field show a history of pressure decline in the production zone and pressure increase within the injection zone. Temperatures have declined slightly since 1985 as a result of movement of the relatively cool injectate away from the injection wells.

Since the start of commercial activity Casa Diablo has subsided relative to adjacent areas. Between 1975 and 1992, benchmarks on the north-west and south-east of the resurgent dome have risen by 0.6 m. Relative subsidence at the geothermal field between 1985 and 1992 was 0.17 m. Correlations between the deformation and pressure changes in the geothermal production zone indicate a direct relation between the level of geothermal production and the amount of subsidence *(Sorey et al., 1995)*.

Between 1985 and 1998 there has been no perceptible increase in seismicity in the Casa Diablo area (Figure 6.21). The onset of commercial activity in 1985 (Figure 6.21b) and the installation of two additional power plants in 1990 (Figure 6.21g) were not apparently accompanied by any increase in seismicity. Over the fourteen-year period of exploitation, the area around Casa Diablo has been relatively aseismic compared with the south moat and the hydrothermal areas to the east.

6.6 b-value and spatial fractal dimension analysis

Due to the deficiencies in the Earthworm data, only CUSP events were processed. Between January 1997 and February 1998, 24,511 earthquakes were catalogued, 4,820 of which had CUSP locations. Sliding windows of 200 data points were used to estimate *b* and D, with each window overlapping the next by ten events. The values of *b* and *D* were plotted at the end of each window. Since the range of observed magnitudes was small, the *b*-value was estimated using the maximum likelihood method of *Page (1968)* (Equation 2.25). The threshold magnitude was selected by examining individual plots of log frequency against magnitude. A

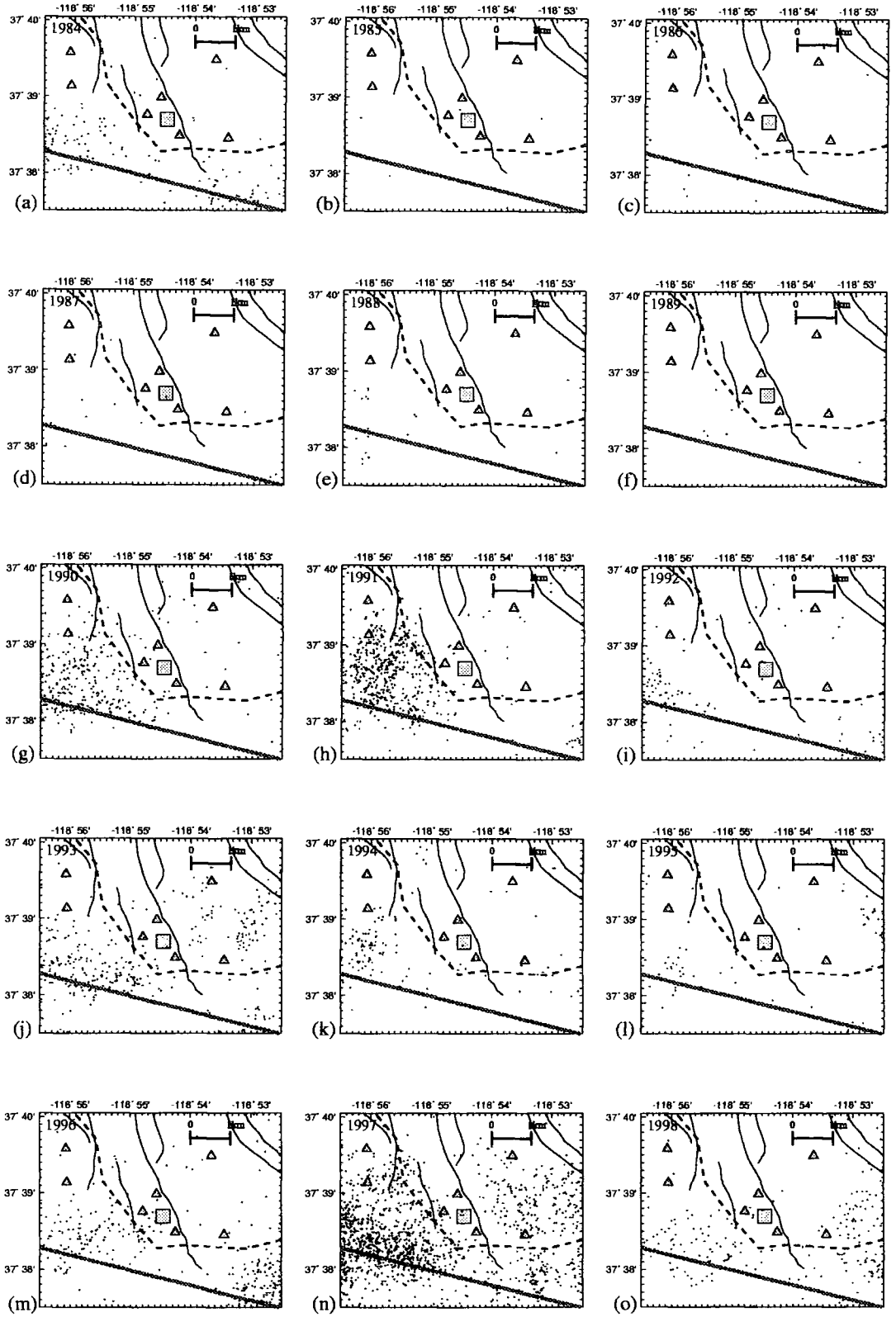

Figure 6.21 Epicentre maps for earthquakes with $M >= 1.8$ between 1984 and 1997 in the south moat of the resurgent dome. Thermal springs and fumaroles are shown as triangles. The Casa Diablo geothermal field is shown as a square. The South Moat fault is shown by a grey line and all other faults by thin black lines. The edge of the resurgent dome is shown by a dashed line. Earthquake data are CUSP events (NCSN catalogue).

threshold magnitude of 1.8 was the lowest suitable for all the data and this was thus used for the whole dataset.

The hypocentral spatial dimension of these events for 200-event windows was estimated using the correlation dimension *D* (Section 2.1.3.2). Although the distances of saturation and depopulation were calculated for this dataset, the resulting scaling range did not correspond to the straightest part of the curve (Figure 6.22), even when using the adjusted scaling range suggested by *Eneva (1996)* (Section 2.1.3.2). This was especially true during periods of low activity (Figure 6.22a). The scaling range chosen to calculate *D* corresponded to the part of the *C(r)* vs. *r* curve that was straightest (i.e. most fractal) for each 200-event window over the whole dataset. This range corresponded to small values of *r*. This implies that in this study a high value of *D* would indicate strong clustering. The range used was 0.4 km < r < 1 km. Since the seismicity fell naturally into three time periods the changes in *b* and *D* were examined for each.

6.7 Results

6.7.1 Changes in b-value and fractal dimension

6.7.1.1 1 January - 21 November 1997

About July 1997, Figure 6.23a shows a rapid increase in *D* from 1.77 ± 0.18 to 1.85 ± 0.19, followed by a slower increase in *D* from 1.95 ± 0.19 to 2.00 ± 0.20. During this period there is a decrease in *b* from 1.25 ± 0.19 to 1.10 ± 0.18.

About 27 September there is a sudden drop in *D* and *b*. This marks the end of the inclusion of the July swarm events in the 200-event windows. During this time, the 200-event windows spanned periods of about 80 days. There is also a near-simultaneous increase in *b*, since the earlier events contained a greater proportion of larger events. After 27 September, *b* increased from 1.10 ± 0.18 to 1.35 ± 0.20

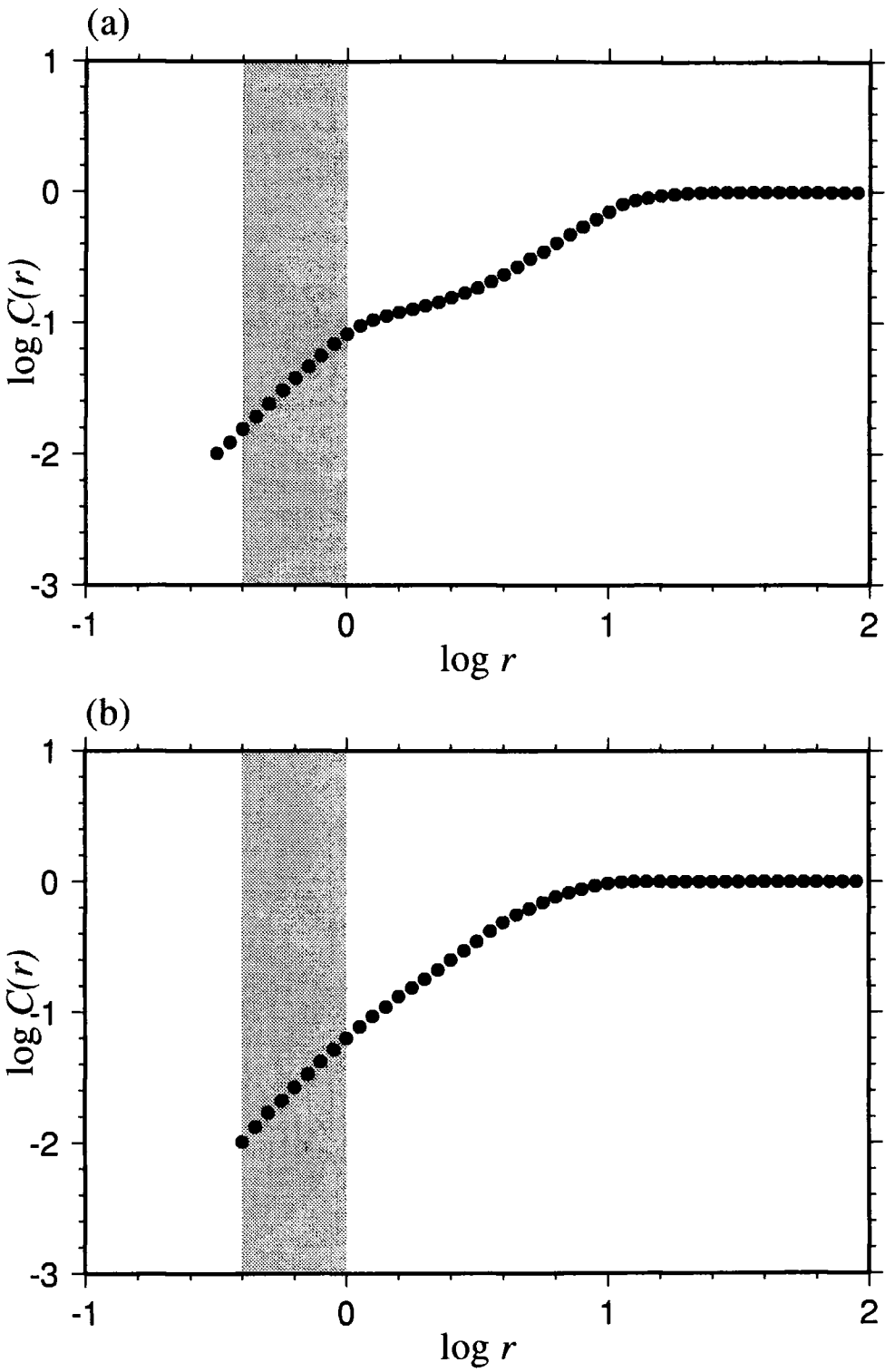

Figure 6.22 (a) Plot of log $C(r)$ vs. log r for a 200 event M_d >=1.8 sample of earthquakes from January 1997. The shaded area is the range selected for calculating D. (b) As (a) but for a typical 200 event sample from November 1997.

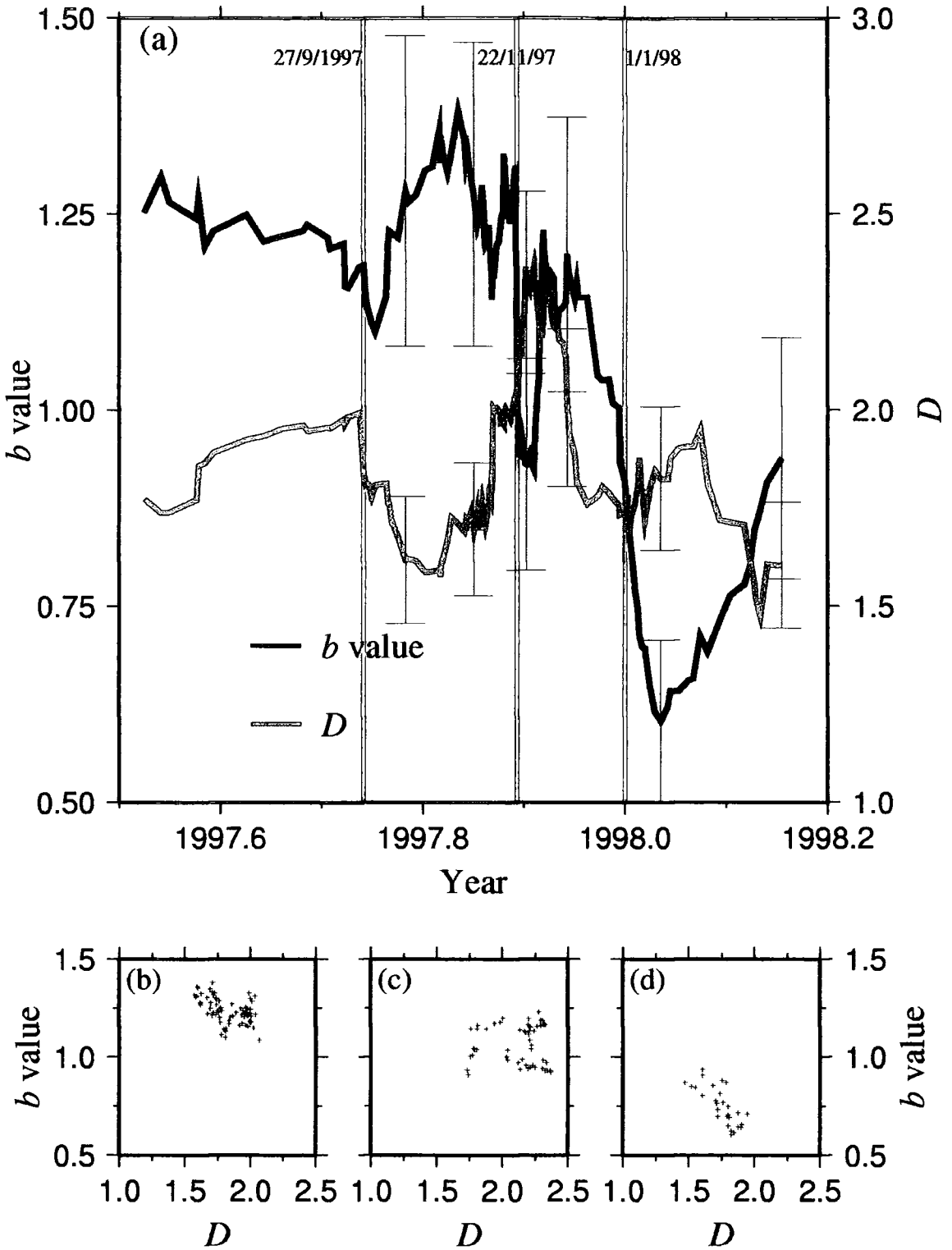

Figure 6.23 (a) Plot of *b* and *D* for the period 1 January 1997 to 28 February 1998. Error bars for *b* correspond to the 95% confidence limits. The error bars for *D* are 10% of the calculated value *(Henderson et al., 1992; Havstad & Ehlers, 1989).* (b) Plot of *b* vs. *D* for the period 1 January to 22 November 1997, (c) as (b) except for the period 22 November - 31 December 1997, (d) as (b) except for the period 1 January - 28 February 1998.

and D decreased from 2.00 ± 0.20 to 1.65 ± 0.16 by late October. With the onset of the 26 October swarm around the western end of the South Moat fault, there is a rapid increase in D to 2.00 ± 0.20 with an accompanying fall in b to 1.10 ± 0.18. During the early part of November there are high values of b (1.30 ± 0.2) and D (2.00 ± 0.20), with the 200-event windows spanning periods of 34 days. Between 1 January 1997 and 21 November 1997 there is a negative correlation between b and D (Figure 6.23b).

6.7.1.2 22 November - 31 December 1997

On 22 November there is a rapid decrease in b, from 1.30 ± 0.20 to 0.93 ± 0.13, accompanied by a continuing rise in D from 2.00 ± 0.20 to 2.4 ± 0.24. The b value returned to a high value of 1.25 ± 0.18 on 4 December. At this time, the 200-event windows spanned a period of 8 days. In mid-December both b and D decreased together until 1 January with a six-day lag in b. Between 22 November and 1 January there is no correlation between b and D (Figure 6.23c).

6.7.1.3 1 January - 28 February 1998

The most striking negative anomaly in b starts 18 December, when b dropped from 1.20 ± 0.18 to 0.60 ± 0.10 by 12 January 1998, and then rose again to 0.85 ± 0.13 in February 1998. During this time, D fell from 2.65 ± 0.27 (18 December) to 1.75 ± 0.18 (1 January 1998) and then remained at approximately this value. This anomaly coincides with another change in the relationship between b and D with clear negative correlation after 1 January 1998 (Figure 6.23d). It also marks a return to a reduced seismicity rate.

6.7.2 Two colour geodimeter data

Before July 1997 there was slow change only in length on any of the geodimeter lines in the raw geodimeter data (Figure 6.24). During the July swarms, rapid lengthening commenced on the Casa-Krakatau, Saw, Knolls and Sherwin baselines. These stations lie on and to the west of the resurgent dome (Figure 6.6).

On 22 November, the rate of lengthening of all these baselines increased rapidly. This decreased again after 1 January. Other stations to the east and south experienced no change (Casa-Miner and Shark) or slight decreases (Casa-Tilla). Casa-Hot, a station to the east of the resurgent dome adjacent to the 1 January swarm (Section 6.4.1.2.4) had a concurrent episode of rapid lengthening.

Figure 6.25 shows a plot of the data with secular rate removed. This is generated by removing the linear trend in time and average distance *(John Langbein, pers. comm.)*. On this plot, prior to 22 November, rapid dome inflation occurred with the greatest line lengthening on the two colour geodimeter lines Casa-Krakatau, Saw, Hot and Knolls. Between 22 - 26 November, accelerated lengthening occurred on the Casa-Krakatau and Saw lines, but lengthening ceased on the Casa-Hot and Casa-Knolls lines. The Casa-Tilla and Casa-Miner lines began to contract. After 26 November, accelerated lengthening for the Casa-Krakatau line decreased, and the rates of lengthening for the Casa-Knolls, Saw and Sherwin lines increased abruptly.

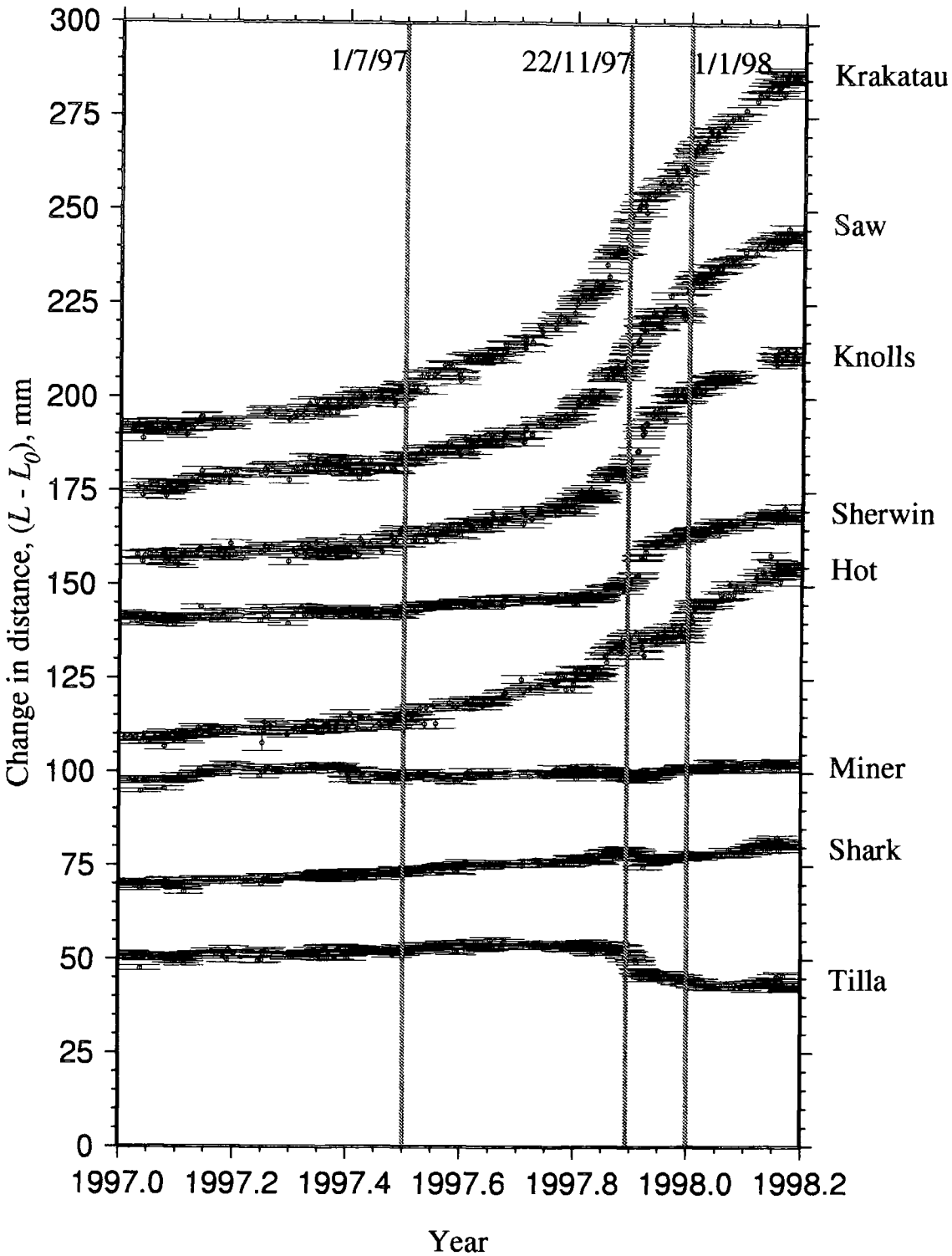

Figure 6.24 Long Valley caldera raw two-colour geodimeter line length measurements of the eight most commonly measured lines between 1 January 1997 and 28 February 1998. The 'nominal distance', L_0, has been scaled for plot clarity. Error bars are one standard deviation *(John Langbein* pers. comm.).

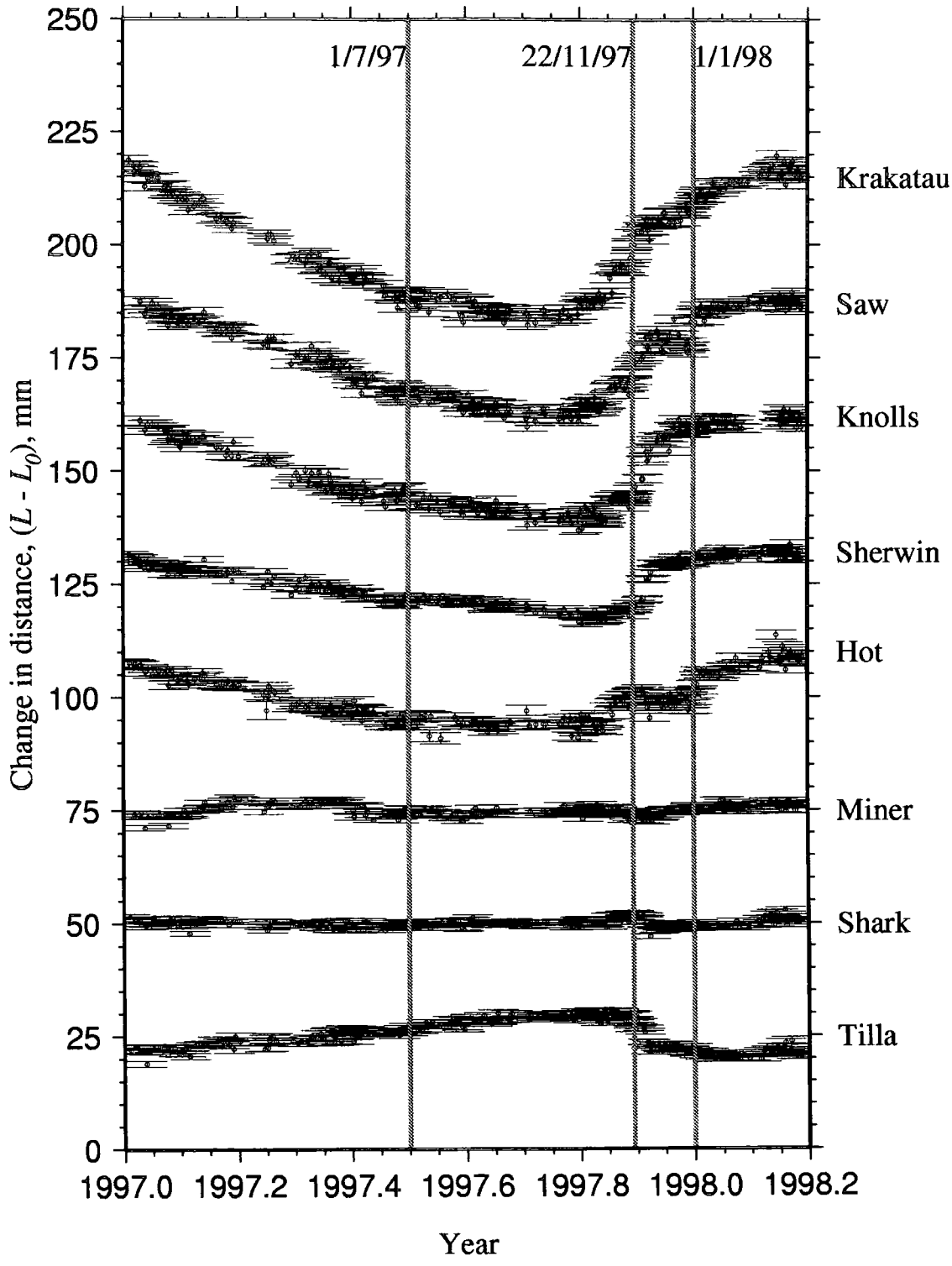

Figure 6.25 As Figure 6.24 except with the secular rate removed *(John Langbein pers. comm.)*.

6.8 Summary

Long Valley caldera is an intracontinental volcano that is currently highly seismically and volcanically active. Over the past two decades, seismic activity has accompanied inflation of the resurgent dome, which has been interpreted as indicating the flow of magma into magma chambers beneath. A major earthquake swarm in 1983 occurred in the south moat along a mature and well developed blind, right-lateral, strike-slip fault. A major swarm in the south moat in 1991 was entirely due to resurgent dome inflation and had no movement along this fault. Recently, very intense activity occurred on 22 November 1997, featuring over 2000 events, with 5 events with $M > 4.0$. The area is exploited for geothermal energy.

Long Valley is continuously monitored by the NCSN network using automatic (Earthworm) and human timed (CUSP) techniques for determining locations and magnitudes. However, during intense swarms many small events are only processed automatically. This results in an inhomogeneous catalogue regarding location accuracies and magnitudes, and distorted log-cumulative frequency vs. magnitude plots. Although 24,511 events were catalogued January 1997 - February 1998, only 4820 were hand processed. A higher magnitude threshold of 1.8 was thus imposed on the events processed, which excluded all the automatically processed results.

The temporal variation of b value and the fractal dimension of hypocentres was calculated for sliding windows of 200 events. The correlations between b and D were found before, during and after the 22 November seismic activity. There was a negative correlation between before reactivation of the South Moat fault, no correlation during the reactivation, and a return to a negative correlation on 1 January 1998. Two colour geodimeter data show significant deformation that correlate with the seismic anomalies.

Chapter 7

Discussion and conclusions

7.1 Seismicity and commercial development in The Geysers

The Geysers geothermal area is the world's largest development of geothermal steam for electrical production. During the 1980s, rapid development led to The Geysers becoming over-exploited. Developers and operators are seeking methods to prolong the useful life of the field. Condensate injection is practised, as is injection of partially treated sewage from two pipelines in the south-east Geysers.

Commercial development of The Geysers coincided with an increase in seismicity. Prior to exploitation seismicity levels were low. As development of the geothermal field expanded into new areas, seismicity followed. The Geysers was most seismically active during the rapid development of the resource in the 1980s, reaching a crescendo in 1986-7. Declining reservoir pressures, first observed in the late 1980s, have led to a reduction in commercial activity during the 1990s. Seismicity levels also declined during this period.

There is a correlation between seismicity and the locations of power plants (Figure 3.17). When a power plant started production there was usually a corresponding increase in seismic activity. Seismogenic areas became quiescent when commercial activity ceased. There is also a correlation between the average rate of steam extraction and the number of earthquakes per year (Figure 3.18). Possible mechanisms for production-induced seismicity include shear-stress response to volume changes, increases in reservoir strength, cooling due to steam extraction and fracture deflation.

Condensate injection also induces seismicity. Seismicity clusters around injection wells and closely follows well activity *(Stark, 1992)*. An analysis of seismic rates reveals that, since the start of effluent injection in the south-east Geysers pipeline, there have been 50 - 80 more earthquakes per month, mostly in the central Geysers area (Figure 3.22). Enigmatically, there was no increase in seismicity in the south-east Geysers where the effluent is injected. Without a complete dataset of well histories it is impossible to be sure that there was no change in industrial activity in the central Geysers that could explain the increased seismicity. Localised cooling, and failure due to increased pore pressures *(Hubbert & Rubey, 1959)*, have been suggested as mechanisms for injection-induced seismicity.

Operators have been reluctant to admit that their activities have been inducing seismicity. Despite assurances that the induced earthquakes do not pose a seismic hazard, there is considerable opposition to any further development of The Geysers.

The Barton catalogue was generated from raw seismograms recorded by the UNT network between 1989 and 1994. Earthquake magnitudes were calculated using coda lengths. Seismograms were processed automatically using programs for picking P- wave arrivals and coda lengths. Earthquakes were located using one-dimensional and three-dimensional velocity models. After removing poorly located earthquakes, the Barton catalogue contained approximately 300-350 $M_d \geq$ 0.5 earthquakes per month. Due to network problems the catalogue is only reliable after May 1990.

There are 1571 wells in The Geysers. Between 1989 and 1994, 337 of these were used for steam extraction, 24 for fluid injection and 9 for both purposes. Most of these wells were in the central Geysers, concentrated around the 'deadzone'. Since 172 active production and 14 active injection-wells have confidential histories, the well database is not complete. However, seismicity usually occurred

in close proximity to known active wells and fault zones. A few earthquake clusters did not appear to have adjacent well activity, but it remains a possibility that this is simply because the relevant wells are proprietary.

7.2 Discussion of results from the Geysers

7.2.1 Seismicity and well activity

Steam extraction and injection activities in The Geysers were conducted using different strategies during the study period. Steam extraction was continuous, with some decline in the extracted volume over the six-year period. Injection either came in short bursts, was continuous or was in a cyclical pattern, usually with a peak at the beginning of the year when rainfall in California is greatest.

For the entire dataset, there was little correlation between the seismicity and the cyclical pattern of injection. For sub-clusters of seismicity, the different types of seismicity/well activity behaviour may be summarised as (Table 7.1):

1) An injection pulse was followed closely by an increase in seismicity.

Observed: (i) when well 09790045 (cluster 5) (Table 7.1) was converted from a production well into an injection well in 1992, immediately afterwards a small, dense cluster of seismicity appeared in a fault zone near the well to the south-west of the main cluster. (ii) When injection started in wells 09790016 and 09790525 (cluster 1), earthquakes appeared near these wells. (iii) Injection in well 09790487 (cluster 6) from mid 1991 induced seismicity. (iv) Each of the four injection episodes in well 09790565 were accompanied by an increase in seismicity (cluster 10). In all of these cases, injection wells were near surface fault zones. (v) There is a possible link between increases in injection and seismicity in 1994 in cluster 7.

2) In wells with continuous injection punctuated by brief injection pulses, an increase in seismicity closely followed each pulse.

Observed: at the beginning of each year, injection episodes in wells 09790020 (cluster 2), 09790534 (cluster 2) and 09790612 (cluster 11) induced bursts of seismicity.

3) Seismicity bursts occurred when injection was continuous and without pulses.

Observed: (i) Around injection well 09790127 (cluster 4), (ii) around injection well 09790519 (cluster 7), (iii) large scale injection in Lake County in south-east Geysers (cluster 12).

4) Areas contained only production activity that was uncorrelated with the seismicity.

Examples: production-only area 1 (cluster 13) and production-only area 2 (cluster 14).

5) Pulses of injection did not induce seismicity.

Observed: (i) associated with injection well 09790607 (cluster 1) prior to 1993, (ii) associated with injection well 09790655 (cluster 6) prior to mid 1991.

6) Injection and steam-production activities were continuous and the seismicity rate did not change.

Observed associated with injection well 09790563 (cluster 9).

These results indicate that bursts of injection induced seismicity are most likely when a well injects in short bursts and is located on or near a fault. Injection-induced seismicity either does not occur or is continuous when an injection well injects continuously and is in an unfaulted area.

Table 7.1 Comparison between well activity and seismicity in The Geysers.

Cluster	Area	Production	Injection	Seismicity	Interpretation
-	Whole dataset	Uniform and declining	Annual cyclical pattern traceable to wells around 'deadzone'	Field-wide level of seismicity constant at ~ 300 - 350 events / month	Cyclical injection has little or no observable effect on the field-wide seismicity.
1	Adjacent to well 09790016	Low, uniform and declining	09790016: Peak in mid 1993. 09790525: Small scale injection since 1994. 09790607: Irregular since 1989.	A little seismicity adjacent to 09790607 prior to 1993. Seismicity along fault adjacent to 09790016 1991 - 1993. Increase in activity along fault zone adjacent to 09790525 in 1994.	Injection adjacent to 09790607 has little effect. Injection episodes near the other two wells (both on faults) generates earthquakes in previously aseismic areas.
2	Adjacent to well 09790020	Uniform and declining	6-monthly bursts of injection in wells 09790020 and 09790534	Increases in event and seismic moment rates at 6-monthly intervals.	Increases in event rate and seismic moment concurrent with start of injection episodes from 1992 onwards.
3	Adjacent to well 09790026	Slight decline	Variable and in pulses. Increases in injection in early 1991, early 1992 and late 1992 / early 1993.	Increases in event rate and seismic moment in early 1991 and 1992. Constant thereafter.	Injection pulses in 1991/1992 coincide with increases in seismicity. 1993 pulse has little effect.
4	Adjacent to well 09790127	Uniform and declining	Very little	Variable. Bursts of seismicity in mid 1992, early-mid 1993 and mid 1994.	No correlation between commercial activity and seismicity.
5	Adjacent to well 09790231	High and continuous with a slight decline.	Continuous, high and variable. Injection starts in well 09790045 in early 1992.	Before 1992, large uniform seismicity cluster near well 09790231. Smaller sub-cluster formed near 09790045 after 1992.	Seismic sub-cluster caused by injection in 09790045. Other seismicity possibly injection/production induced.
6	Adjacent to well 09790487	Uniform and declining, with some large drops.	Switch from 09790655 to 09790487 in mid 1991.	Before mid 1991, very little seismicity. After this date, an increase in seismicity to the SW of 09790487.	Injection activity in well 09790655 had little effect on seismicity. Well activity in well 09790487 caused increase in seismicity. The sub-surface structure of well 09790487 might lie on a fault zone; 09790655 might not.
7	Adjacent to well 09790519	Uniform and declining	Low and cyclic with a period of one year.	Bursts in activity in early 1991, early 1992 and early 1994.	Possible link between increase in production and injection in 1991 with 1991 seismicity burst. Possible correlation between injection in 1994 with seismicity (?).
8	Adjacent to well 09790539	Continuous and declining	Continuous with brief drops to zero in 1989 and late 1992. Surge in late 1992 / early 1993.	Increase in late 1992, followed by a lull in early 1993.	Increase in injection appears to be concurrent with seismicity increase. No apparent explanation for seismicity lull in early 1993 (network failure?).
9	Adjacent to well 09790563	Declining and uniform	Continuous with a slight decline.	Continuous.	-
10	Adjacent to well 09790565	Declining with several drops.	Three wells. One with very little injection and another with continuous low level activity. 09790565 started injection in early 1991 with four large bursts of injection between 1991 and 1994.	Four increases in seismic activity from 1991. Third increase to the north of the others, apparently unrelated to the injection activity in well 09790565.	Injection in 09790565 coincides with increases in seismicity.

Table 7.1 – continued.

Cluster	Area	Production	Injection	Seismicity	Interpretation
11	Adjacent to well 09790612	Continuous and declining	Injection in annual cycles.	Surges in seismic activity.	Injection is not synchronised with increases in seismicity except in 1993 and 1994. Delayed effect?
12	Lake County in south-east Geysers	Constant	Constant	Small clusters of events. Peaks in seismicity in mid 1991, late 1992 and mid 1993-mid 1994.	Small clusters of events appear to be spatially unrelated to injection wells. No apparent correlation between injection, production and seismicity
13	Production area 1	Low and continuous	None	Increases in seismicity and seismic moment in mid 1991, early 1992, mid 1993 and early 1994.	No apparent explanation.
14	Production area 2	Low and continuous, occasional drop to zero.	None	Starts in mid 1990. Denser distribution of seismicity to west of cluster in 1992, migrating east and then north during1993 – 1994.	No apparent explanation.

Plots of seismicity and surface well locations (Figures 7.1, 7.2 and 7.3) reveal that there are wells with proprietary histories in clusters 1, 5, 6, 10, 12 and 14. In clusters 1, 10, 12 and 14, there are seismicity bursts near to these proprietary wells. Hence, injection activity in these wells could be causing seismicity, though it is not possible to verify this without the well histories.

7.2.2 b value, spatial fractal dimension and well activity

When examining the changes in *b/D* correlation, it is important to note whether a high value of *D* corresponds to stronger or weaker clustering. Table 7.2 summarises possible relationships between *b*, *D* and the sign of their correlation.

Table 7.2 Types of *b/D* correlation behaviour.
(a) *b/D* correlations when high *D* corresponds to weaker clustering.

b	*D*	Type of seismicity	*b/D* correlation
high	High	small magnitude, diffuse	Positive
high	Low	small magnitude, clustered	Negative
low	High	large magnitude, diffuse	Negative
low	Low	large magnitude, clustered	Positive

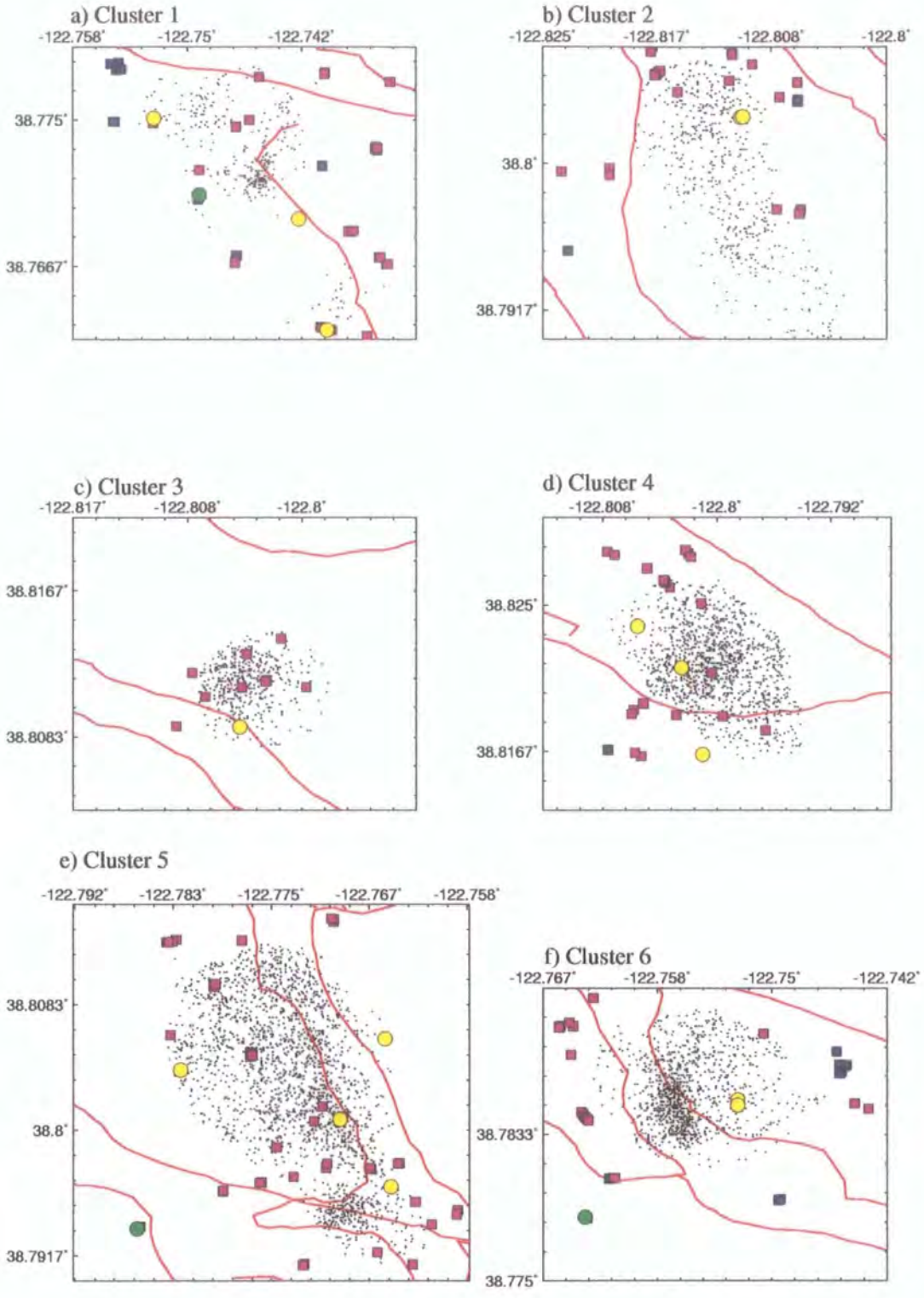

Figure 7.1 Maps of seismicity, well surface locations and surface fault zones in The Geysers for areas close to injection wells 09790016, 09790020, 09790026, 097900127, 09790231 and 09790487. Injection wells with public well histories are shown by yellow circles; those with confidential histories by green. Production wells with public histories are indicated by purple squares; those with confidential histories by blue. Red lines are surface faults.

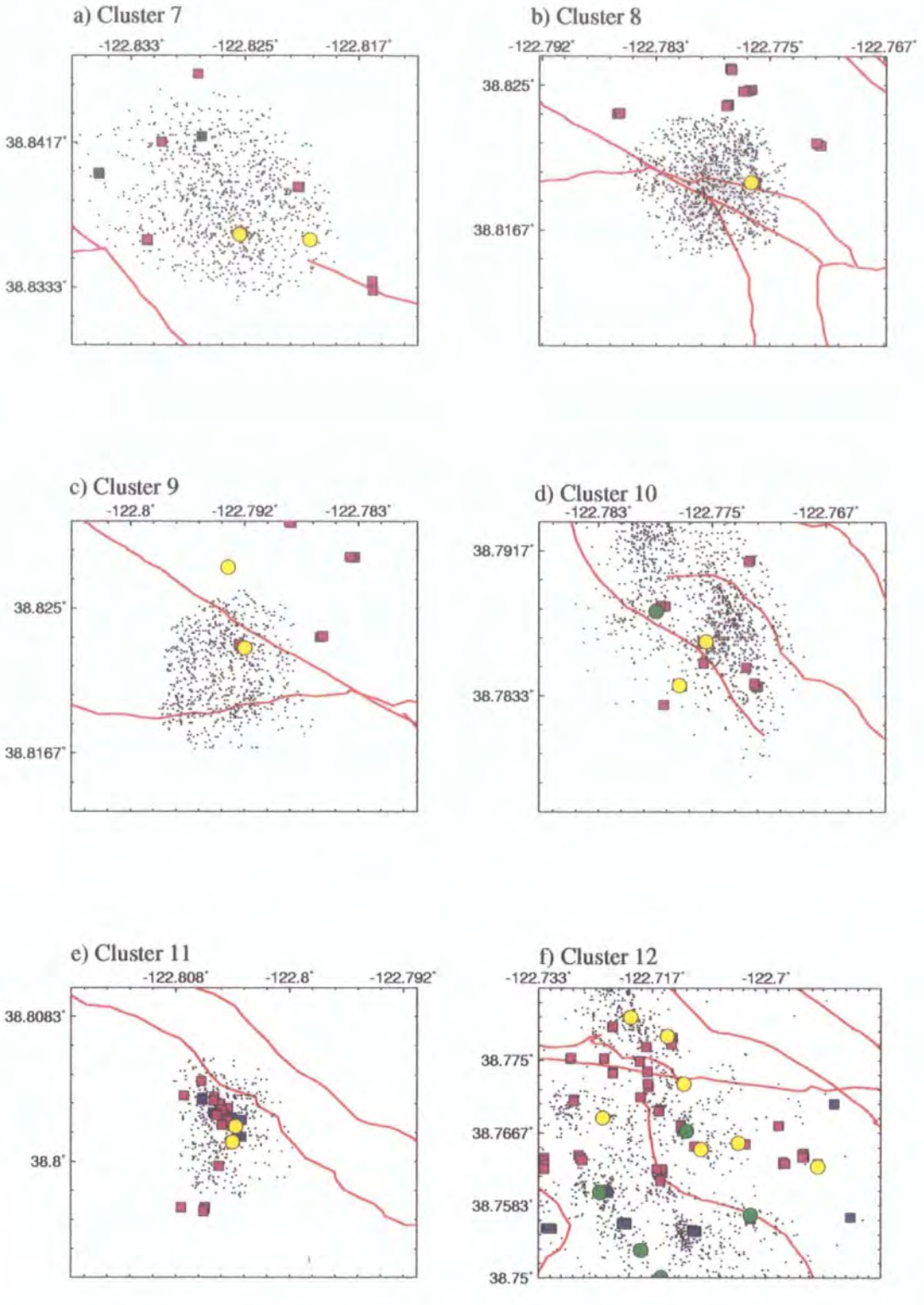

Figure 7.2 As Figure 7.1, but for areas close to injection wells 09790519, 09790539, 09790563, 09790565, 09790612, and for seismicity in Lake County in south-east Geysers.

a) Cluster 13

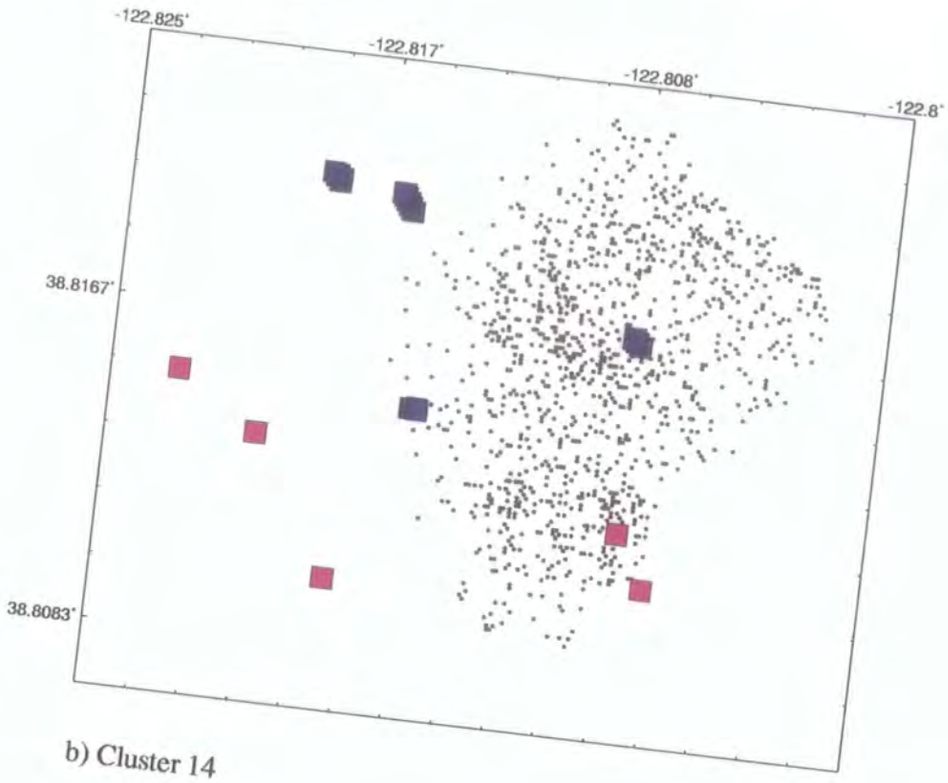

b) Cluster 14

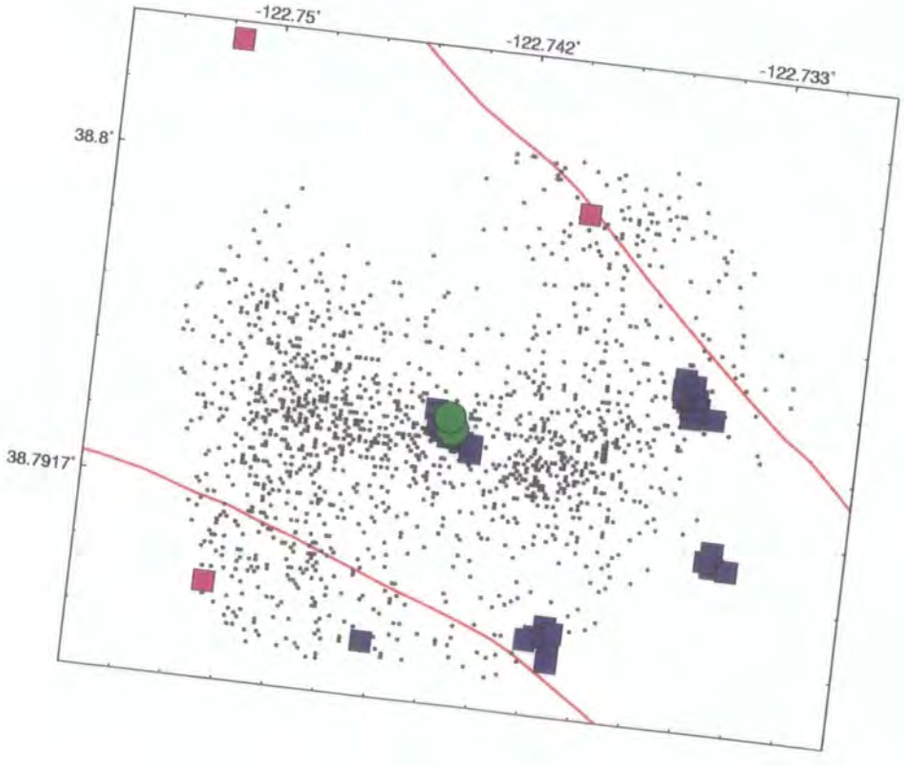

Figure 7.3 As Figure 7.1, but for production-only areas 1 and 2.

(b) *b/D* correlations when high *D* corresponds to stronger clustering.

b	*D*	Type of seismicity	*b/D* correlation
high	Low	small magnitude, diffuse	Negative
high	High	small magnitude, clustered	Positive
low	Low	large magnitude, diffuse	Positive
low	High	large magnitude, clustered	Negative

The whole Geysers dataset was too complex to show clearly what processes were in operation (Table 7.3). To see systematic changes, it was necessary to examine clusters of seismicity within the whole dataset (Table 7.3).

Table 7.3 Comparison between *b*, *D*, and *b/D* correlation for clusters in The Geysers

Cluster	Area	High *D* corresponds to:	b-value	Fractal dimension, *D*	b / *D* correlation	Summary
-	Whole dataset	Weaker clustering	Complex changes not consistently correlated with injection.	Complex changes not consistently correlated with injection.	Various positive, negative and zero correlations associated with injection pulses.	*Conclusion: The dataset is probably too complex for processes to clearly revealed.*
1	Adjacent to well 09790016	-	-	-	Insufficient events for analysis	-
2	Adjacent to well 09790020	-	-	-	Insufficient events for analysis	-
3	Adjacent to well 09790026	-	-	-	Insufficient events for analysis	-
4	Adjacent to well 09790127	2-D: Stronger clustering 3-D: Weaker clustering	Gradual decline after 1993.	Two-dimensional case: little change Three-dimensional case: small negative anomaly in mid 1993.	*b/D* change in mid 1992 from positive to negative, accompanying an increase in seismicity.	*Conclusion: Transient negative b/D correlation but not correlated with the known injection data.*
5	Adjacent to well 09790231	Weaker clustering	Little change.	Variations in two-dimensional and three-dimensional *D* are very similar. Two negative *D* anomalies; first is associated with injection pulse.	Two-dimensional *D* case: Correlations are +ve before, -ve during and +ve after the injection pulse. Three dimensional *D* case: correlations are none before, strong -ve during, and +ve after the anomaly.	*Conclusion: Injection pulse accompanied by a transient, pulse of negative b/D correlation.*
6	Adjacent to well 09790487	Stronger clustering	Little change.	Gradual increase.	No clear *b* / *D* correlation.	*Not possible to interpret switch of injection from well 09790655 to 09790487 because of too few earthquakes.*

Table 7.3 Comparison between *b*, *D*, and *b/D* correlation for clusters in The Geysers (continued)

Cluster	Area	High *D* corresponds to:	b-value	Fractal dimension, *D*	b / *D* correlation	Summary
7	Adjacent to well 09790519	Stronger clustering	Little change apart from negative anomaly in 1994.	Little change apart from negative anomaly in 1994.	For both two-dimensional and three-dimensional D, the *b/D* correlation changes from negative to positive in mid 1993.	*Conclusion: change in b/D correlation accompanies onset of (minor?) injection episode. Large b and D anomalies accompany injection activity.*
8	Adjacent to well 09790539	Stronger clustering	Increase before 1993; decrease after.	Same as for *b*-value.	No significant anomalies.	*Conclusion: injection accompanies increase in seismicity. Essentially no b/D anomalies.*
9	Adjacent to well 09790563	Stronger clustering	Gradual increase.	Two-dimensional *D*: gradual decrease Three-dimensional *D*: gradual increase	Two dimensional *D* case: negative correlation. Three dimensional *D* case: positive correlation	*Conclusion: Little variation in injection, production, seismicity, b, D, or b/D .*
10	Adjacent to well 09790565	Weaker clustering	Only gradual changes resolvable.	Transient positive or negative anomalies in *D* associated with injection pulses and bursts of seismicity.	Two-dimensional *D* case: negative correlations simultaneous with episodes (2) and (4); positive for episode (3). Three-dimensional *D* case: negative *b/D* correlation for episodes (2), (3) and (4). Insufficient data to resolve *b/D* correlations during injection episode (1).	*Conclusion: Two injection pulses accompanied by negative b/D correlations in well 09790565, where seismicity was close to the well. One injection pulse accompanied by a positive b/D correlation, where the seismicity was relatively distant from the well.*
11	Adjacent to well 09790612	-	-	-	Insufficient events for analysis	-
12	Lake County in south-east Geysers	-	-	-	Not able to find a suitable scaling range for *D* due to scattered nature of the seismicity.	-
13	Production-only area 1	Stronger clustering	Rapid drop in 1993	Increase after 1993.	In early 1993, there is a change from a negative *b/D* correlation to no correlation for both two-dimensional and three-dimensional D.	*Conclusion: A large increase in the seismicity rate is accompanied by a fall in b, an increase in D and a change from negative to positive b/D correlation. INJECTION ONSET?*
14	Production-only area 2	Weaker clustering	Minor changes.	Large negative *D* anomaly between mid 1991 and mid 1993.	Change from a negative to a positive *b/D* correlation in mid 1993.	*Conclusion: Sudden increase in seismicity accompanied by a negative b/D correlation, low D and high b. INJECTION ONSET? Fall off in seismicity accompanied by a positive b/D correlation, high b and D. INJECTION TURNED OFF?*

The following types of *b*, *D*, *b/D* correlation, injection and seismicity behaviour were observed for clusters within The Geysers data (Tables 7.3 and 7.4). The cases listed below are naturally a subset of those quoted in Section 7.2.1, since for some clusters there were insufficient events for *b/D* analysis.

1) Injection pulse accompanied by increase in seismicity, clustering, a constant b and a transient change in b/D correlation (Cases 1 and 2, Section 7.2.1).

Observed:

High D corresponds to weaker clustering: (i) In cluster 5, the onset of injection in well 09790045 is accompanied by a decrease in *D* and a transient negative *b/D* correlation. (ii) In cluster 10, two injection episodes in well 09790565 are accompanied by transient negative *b/D* correlations.

High D corresponds to stronger clustering: (i) In cluster 7, the increase in injection in well 09790519 is accompanied by a transient positive *b/D* correlation in 1994.

2) An increase in seismicity, a change in b, D and/or b/D without injection activity (Case 3, Section 7.2.1)

Observed:

High D corresponds to weaker clustering:

(i) in cluster 4 a transient negative *b/D* correlation cannot be correlated with the injection activity in well 09790127. (ii) In cluster 14 (Production-only area 2) there is a change from a positive to a negative *b/D* correlation, but there is no known injection activity associated with this cluster.

High D corresponds to stronger clustering:

(i) In cluster 13 (Production-only area 1) , there is a large increase in seismicity accompanied by a change from a negative to a positive *b/D* correlation. There is no known injection activity associated with this cluster.

3) Injection pulse associated with an increase in seismicity with no significant anomalies in b, D or b/D

Observed: In cluster 8, there is an increase in seismicity associated with injection well activity but no change in the *b/D* correlation

Table 7.4 Summary of categories of injection seismicity and *b/D* behaviour observed

Type	Injection	Seismicity	*b/D* anomaly	Number of cases
1	✓	✓	✓	3
2		✓	✓	3
3	✓	✓		1

The results suggest that some injection episodes cause negative *b/D* anomalies where a high value of *D* corresponds to weaker clustering, and positive *b/D* correlation anomalies where a high value of *D* corresponds to stronger clustering. These cases correspond to either clustered, small magnitude seismicity or diffuse, large magnitude seismicity (Table 7.2). In addition, there were four cases where similar anomalies were observed without known injection.

In cluster 10, where a high *D* corresponds to weaker clustering, there are four injection episodes in well 09790565, each accompanied by bursts in seismic activity (Figures 5.15 (a) to (d)). The first, second and fourth seismicity bursts are close to the injection well. There were insufficient data to calculate *b* and *D* for the first seismicity burst. The second and fourth seismicity bursts were accompanied by negative *b/D* correlations. The seismicity accompanying the second injection episode is small-magnitude (high *b*) and clustered (low *D*). The fourth injection episode is accompanied by seismicity that is large-magnitude (low *b*) and diffuse (high *D*). The *b/D* correlations suggest that the seismicity accompanying the second and fourth injection episodes were induced by the injection activity in well 09790565. The third seismicity burst is relatively distant from the injector and exhibits a positive *b/D* correlation. The positive *b/D* correlation and comparatively distant location of this seismicity suggests that (a) it was not injection-induced and

(b) it was probably not caused by injection in well 09790565. There is a proprietary injection well in the west of the cluster on a fault zone (Figure 7.2f), with a small cluster of seismicity adjacent to it. It is not possible to know what, if any, effect this well had on D, b and the b/D correlation without obtaining its well history.

In cluster 4, where a high D corresponds to weaker clustering for three-dimensional D, in mid 1993 there was a small negative anomaly for the three-dimensional D case accompanying an increase in seismicity (Figures 5.9(a) to (d)). This suggests that injection had started at this time. The only publicly released injection data in this area (well 09790127) does not correlate with this anomaly. Also, there are no nearby injection wells that have confidential well histories (Figure 7.1d). Since mixed injection/steam extraction wells are sometimes designated as development steam (DST) wells in the D.O.G.G.R. licences list (Section 4.6.3), not as injection wells (INJ), it is possible that the seismicity could have been induced by undeclared injection in a mixed proprietary well.

In Production-only area 1 (cluster 13), where a high D corresponded to stronger clustering, the increase in seismicity in early 1993 was accompanied by fall in b and an increase in D. The b/D correlation at this time changed from negative (b high, D low) to weak positive (b high, D high). This is similar to the behaviour observed in clusters 5 and 7 (Table 7.2), where injection pulses also occurred. This suggests that injection might be the cause of the seismicity anomalies in Production-only area 1. In this area there are no public injection wells, nor any confidential wells designated as injection (INJ) in the D.O.G.G.R. licences list (Figure 7.3a). As in cluster 4, the increase in seismicity and clustering, and change in b/D correlation, may have been caused by undeclared injection in a mixed-activity well.

Production-only area 2 (cluster 14), where a high D corresponded to weaker clustering, became seismically active in mid 1990. The event rate continued to increase until early 1993, after which the area became quiescent. Between 1990

and 1993, there was a large negative anomaly in D and a negative b/D correlation. This is identical behaviour to that observed in cluster 5, associated with injection, suggesting that the increase in seismicity may have been induced by injection activity here also. During the period of quiescence starting in late 1992, there is a positive b/D correlation (high b, high D). This is atypical b/D behaviour for the onset of injection. These b/D correlations imply that an injection well may have been turned on in 1990 and off again in 1993. There are two injection wells with confidential well histories near Production-only area 2 (Figure 7.3b). These could be the source of the hypothesised injection-induced seismicity, though this cannot be verified without the well histories.

It has been suggested that production- and injection-induced earthquakes have different source mechanisms, and this can be used to discriminate between them *(Ross et al., 1998)*. The Geysers study has shown that injection and non-injection (production?) activity are associated with changes in b-value, fractal dimension and the correlation between them, providing further evidence that these two kinds of earthquakes are associated with different physical processes.

7.2.3 A model for The Geysers results

The results for the Geysers suggest that pulses of injection induce either small-magnitude, clustered earthquakes (e.g. cluster 5) or large-magnitude, diffuse seismicity (e.g. injection episode 4 in cluster 10) (Tables 7.2 and 7.3). The former case is more common. The small magnitude / clustered seismicity can be modelled by considering the changes in pore pressure in the system. Consider a system where a high D corresponds to weaker clustering. During periods of continuous or no injection, small fluctuations in pore fluid pressure lead to seismic activity *(Henderson et al., 1998)*. This seismicity inhibits further activity, perhaps due to dilitant hardening *(Scholz et al., 1973)*. This scenario would have a greater proportion of smaller events (high b) in a less clustered seismicity pattern (high D), thus yielding a positive b/D correlation. In the fracture model presented in

Section 2.2.1, this behaviour was exhibited in the 'persistent' phase, when cracks were well ordered, diffuse (high D) and small (high b).

During an injection episode, the substantial change in pore pressure overcomes the inhibiting factor, so triggering earthquakes *(Hubbert & Rubey, 1959)* (Section 3.8). Thus, an injection episode generates a dense cluster of earthquakes adjacent to the injection well (low D). It has been proposed that where changes in the pore fluid pressure are large compared with the fault-zone permeabilities, the resulting seismicity will be dominated by smaller events (high b). Thus there would be a negative b/D correlation during an injection episode. The b/D correlations would be reversed if a high value of D corresponded to stronger clustering.

It is not obvious what mechanisms could generate earthquakes that are large (low b) and diffuse (high D). A study of this problem would be an interesting topic for future work.

7.2.4 Errors and problems

The results described above suggest that there are correlations between injection, seismicity, b-value, D and the correlation between b and D. However, these results should be viewed as preliminary since the analysis was subject to many problems and uncertainties.

Well, surface fault and earthquake locations have to be known accurately. The errors in earthquake locations in the Barton catalogue were ± 0.17 km (horizontal) and ± 0.24 km (vertical) (Section 4.4.2). The surface locations of the wells, although estimated using the D.O.G.G.R. map to the nearest 0.1 km, do not necessarily reflect the sub-surface positions as well deviations can be as much as a few hundred metres. Surface fault locations were only accurate to the nearest 0.5 km. These uncertainties may be compared with the typical diameter of clusters studied which is about 1 - 2 km.

The well database is missing the confidential histories of 172 steam extraction and 14 injection wells. It is thus unknown whether these wells were active or inactive during the study period.

It is not possible to completely separate injection-induced seismicity and production-induced seismicity. Analysing mixed seismic sequences will make anomalies more difficult to identify if associated with one kind of activity and not the other, as appears to be the case here.

The earthquakes were divided into clusters subjectively. This is a problem as it introduces operator dependency into the results. The problem is exacerbated because seismicity in The Geysers is rather spatially continuous and it is difficult to judge where one cluster stops and the next starts. Given the errors in the well locations, faults and earthquake locations, this problem is serious.

The log-frequency - magnitude distributions near the threshold magnitude exhibited curvature. This made fitting a linear relationship to the distribution to find b problematic, and would cause systematic underestimation of b if too low a threshold magnitude were used. However, very large numbers of earthquakes were needed for this type of analysis, where many estimates of b are necessary. In the case of this study, a massive dataset of 22,817 earthquakes was available so the effect on the calculated b/D correlations was minimal (Section 5.4). However, such a large dataset is exceptional and the requirement for so many earthquakes must limit the applicability of this method.

b and D have small dynamic ranges and large errors. Although systematic behaviour was observed in The Geysers data, changes in b and D were mostly within these errors and consequently statistically insignificant. For this reason the results must be viewed as an intriguing hint at a seismic phenomenon and confirmation must await the analysis of an even bigger and better dataset.

Even though The Geysers dataset was high quality and contains tens of thousands of events, anomalies in it were hard to find. A huge dataset with a much lower threshold magnitude would be required to study exhaustively all the changes in injection in The Geysers using the *b/D* method.

7.3 Long Valley caldera

7.3.1 Introduction

Long Valley caldera is an intra-continental volcano in east-central California that has been in a state of volcanic unrest since 1978. Seismicity is concentrated in four areas: (1) in an elongate zone in the south moat of the resurgent dome along the blind, near-vertical, right-lateral South Moat fault, (2) around geothermal features on the southern margin of the resurgent dome, (3) on the south-west flank of Mammoth Mountain and (4) easterly within the caldera. Major swarms in the south moat have been interpreted as reactivation of the South Moat fault *(Rundle & Whitcomb, 1984)*. Ground deformation is continuous and irregular. Models for this deformation have three features in common: (1) a primary deforming chamber centred at a depth of 7 -10 km, (2) a secondary chamber beneath the southern margin of the resurgent dome at a depth of 4 - 8 km, and (3) right-lateral slip along the South Moat fault. The relative importance of these components varies with time. On 22 November 1997, there was a great increase in seismicity in south moat accompanied by rapid inflation of the resurgent dome, and a large earthquake dataset was available for *b/D* analysis.

The liquid-dominated Casa Diablo geothermal field has been exploited since 1985 *(Sorey et al., 1995)*. The total installed capacity is 40 MW, a small fraction of the 2043 MW capacity of The Geysers. Casa Diablo has subsided relative to adjacent areas since the start of commercial activity. A relationship between deformation

and pressure changes in the production zone indicate a link between the level of geothermal production and the amount of subsidence *(Sorey et al., 1995)*. There has been no perceptible increase in seismicity in the Casa Diablo area since the start of commercial activity.

7.3.2 Results of the Long Valley analysis

Prior to 22 November 1997, clusters of events formed an easterly-trending zone in the south moat of the resurgent dome. This zone coincided with thermal springs and fumaroles which occur where north-north-westerly faults cross the southern edge of the resurgent dome. The hydrothermal area is likely to be an immature fault zone, lacking a well-developed fault plane. This seismicity is thought to be due to accelerated resurgent-dome uplift, causing extension and allowing upward migration of hot fluids *(Foulger et al., 1998)*.

The linear seismic feature activated on and after 22 November coincides with the South Moat fault (Section 6.4.3). Motion on this fault may have been caused by the same processes that generated the adjacent pre-22 November activity, or have been triggered by that activity or stress changes caused by it. After 1 January 1998, the seismicity migrated from the South Moat fault area to areas of hydrothermal activity in the eastern part of the caldera.

Although detailed modelling has yet to be done, ground deformation data suggest that, in association with this seismic episode, the area of greatest deformation moved from beneath the resurgent dome to an area immediately to the south-west. This is also the site of the intense seismicity 22 November 1997 to 1 January 1998.

In the Long Valley *b/D* analysis, a high value of *D* corresponded to greater clustering. Prior to the failure of the South Moat fault on 22 November, *b* is high, *D* is low and there is a negative *b/D* correlation. During the failure of the fault, both *b* and *D* are high. These observations could be explained by the following

model. In the hydrothermal zones that were seismically active prior to 22 November, there was a highly heterogeneous, high permeability environment comprised of numerous small faults and structures. This was possibly a result of long-term cracking. The high permeability of the rocks and corresponding rich supply of pore fluids resulted in low effective stress in this zone. Thus earthquakes within this zone were caused by the failure of small, isolated asperities and were small (i.e. resulting in high b) and diffuse (low D). This is consistent with the negative b/D anomaly prior to 22 November shown in Figure 6.23b.

From 22 November, seismic activity was transferred to the South Moat fault. This fault had failed in the recent past, and has a mature, well developed, coherent fault plane. Highly stressed asperities are widely spaced along it. Consequently, when the South Moat fault failed, large magnitude earthquakes were generated causing a low b-value. These were followed by numerous smaller-magnitude aftershocks, and thus the increase in b immediately after failure of the fault. The intense clustering of earthquakes along the fault generated a high value of spatial fractal dimension, D. This behaviour of b and D is similar to that reported for the tectonic cluster in the Joâo Câmara dataset *(Henderson et al., 1994)*, and in Parkfield, California following the Coalinga earthquake *(Henderson & Main, 1992)* (Section 2.3).

The behaviour of the South Moat fault during the 1997-98 period shows that, in contrast to the hydrothermal zone to the immediate north, it is capable of generating large earthquakes. The area of the fault plane, estimated from the distribution of hypocentres, is about 85 km^2. If the whole fault were to slip in one event, an earthquake of $\sim M = 6$ would be generated. Apart from the danger of a volcanic eruption at Long Valley (tremor was observed there in September 1998), further reactivation of the South Moat fault may be the most serious threat to the town of Mammoth Lakes.

7.3.3 Problems and errors

The events used in the Long Valley analysis were hand-picked and well located, and there were sufficient estimates of b and D to resolve the reactivation of the South Moat fault. The changes in b-value and D were not due to temporal changes within the same structure, but changes resulted from processes in different structures. Due to the lack of $M \geq 1.8$ CUSP data, it was not possible to perform separate b/D analyses on the seismicity close to the southern edge of the resurgent dome, that near the South Moat fault and the post 1 January seismicity east of the resurgent dome. Problems arising from the small dynamic range of b and D and their large errors that plagued The Geysers data also made the Long Valley study difficult.

7.4 Comparison between The Geysers and Long Valley caldera

Both The Geysers and Long Valley are exploited for geothermal power. The Geysers reservoir is fractured vapour-filled greywacke. Steam extraction and injection activity is conducted on a massive scale and the intense seismicity is almost entirely industrially induced. In Long Valley, the seismicity is of volcanic origin, apparently largely the response of the crust to upwarp of the caldera floor caused by magma-chamber inflation.

The most remarkable anomalies in b and D at The Geysers were associated with injection pulses or the onset of injection. Injection-induced earthquakes are probably induced by pore-pressure increases or by cooling. Steam-extraction related seismicity, on the other hand, is caused by shear-stress response to volume change, increases in reservoir strength or by cooling. The seismicity in Long Valley is probably all the result of the same process, pore-fluid changes (hydrothermal activity) or magmatic movement within a perturbed stress field (tectonic activity). There, variations in b and D are associated with contrasting structures in the

different areas activated. There is a small geothermal development at Long Valley, but there is no evidence that it is associated with enhanced seismic activity. On the contrary, it appears to be associated with relatively low seismicity, and it is possible that extraction of geothermal fluids here is actually lowering the pore pressures and surpressing earthquake activity.

7.5 Future work

7.5.1 The Geysers

In order to refine the results presented in this thesis, improvements in the earthquake catalogue, the well dataset and fault locations are needed. Reprocessing of the raw seismogram data would be desirable, using an improved method for resolving multiple seismic events on a single trace. This reprocessing would need to be done automatically due to the large size of the raw seismogram dataset (about 20 Gbytes) though advances in disk capacities would mean that now all the data could be kept on line at once, making processing easier. If smaller events could be resolved the threshold magnitude could be reduced, so providing a larger catalogue for *b/D* analysis. Reprocessing of The Geysers data could also show whether the curvature near the threshold magnitude exhibited in the log-frequency - magnitude plots is real, due to magnitude errors or due to deviation from the Gutenberg - Richter relationship. Using velocity models that take into account the evolution of the reservoir in time, or perhaps using relative relocation methods, better earthquake locations could be determined.

Obtaining the currently proprietary well data would make a true comparison between the well activity and seismicity possible. Acquiring the sub-surface deviation of each well would allow the unique allocation of wells to specific seismic clusters to be made with a greater degree of confidence. If areas of The Geysers could be identified that contain only production or injection wells, more confidence could be placed in deductions of the relationship between seismicity, *b*,

D and *b/D* correlations. The effect of different types of commercial activity could be studied, e.g. continuous, episodes of varying lengths, and episodes of different magnitudes. The effect of large-scale injection in the south-east Geysers by the effluent pipelines should be carefully examined. Such a study should examine the effect of the injection on the production rates of steam wells and the amount of seismicity generated to assess the environmental impact of pumping large quantities of sewage into the reservoir.

The approximate surface locations of major faults correlated poorly with the well locations and the seismicity. A correlation might have appeared had the surface faults been located more accurately. Since seismicity is expected to occur along fault planes, the earthquakes could be used to map the sub-surface fault structure. It is likely that relative relocation methods are necessary for this.

7.5.2 Long Valley caldera

The Long Valley caldera earthquake dataset contained 24,511 earthquakes between January 1997 and February 1998. Only 4,820 of these were CUSP located. An increase in the number of smaller earthquakes CUSP located during intense swarms would expand the dataset and permit an improved analysis of the changes in seismicity, *b*-value and fractal dimension. Modelling of the geophysical data constraining the seismic deformation crisis needs to be improved to clarify the processes at work and to help test the seismicity model presented in this thesis. The South Moat fault has been repeatedly active in recent years. By improving the coverage of seismometers and other geophysical instruments adjacent to this feature, the next period of reactivation could be more carefully studied. Detailed analysis of the geothermal activity in Casa Diablo is required. This could be done using a high-density seismometer network and by obtaining the well histories.

7.5.3 The broader picture

Recent work has shown that the spatial distribution of earthquakes cannot be adequately described by a single fractal dimension *(e.g. Hirata & Imoto, 1991; Dongsheng et al, 1994)*. Some earthquake clusters feature clusters within clusters, which require a infinite spectrum of fractal dimensions to adequately describe their complex structure. Multi-fractal behaviour has also been observed in oil-pumping-induced seismicity *(Volant, 1993)*. Multifractal analysis should be applied to both The Geysers and Long Valley catalogues. Another method that could be applied to these areas is mapping high stress levels at asperities using changes in *b*-value. This method was used in Long Valley and was successful in mapping significant variations in *b*-value near the resurgent dome *(Weimer & Wyss, 1997)*. Finally, the methods described in this thesis could be applied to other geothermal fields around the world.

7.6 Conclusions

7.6.1 The Geysers geothermal area

1) The UNT earthquake catalogue was unreliable. Reprocessing of the data from the raw seismograms resulted in a considerable improvement in location accuracy and magnitude estimates.
2) In several cases, pulses of injection caused bursts of seismicity. However, bursts of seismicity also occurred in the apparent absence of injection, and pulses of injection occurred without inducing a clear burst of seismicity.
3) For the whole field, it was not possible to correlate changes in seismicity, *b*, *D*, and *b/D* correlations with the production and injection histories. Clear behaviour could only be detected for clusters of seismicity within the whole dataset.

4) Episodes of fluid injection induced clusters of seismicity in a number of cases, especially when injection wells were on or near fault zones.
5) Pulses of injection were often accompanied by changes in the correlation in *b* and *D*, that corresponded to either clustered, small-magnitude activity or diffuse large magnitude activity. There were also cases of *b/D* anomalies without injection pulses and a single case of an injection pulse without a *b/D* anomaly.
6) Clear *b/D* anomalies in areas where no injection is publicly declared suggest that there may have been proprietary injection activity. However, without the well data this cannot at present be proven or disproven and the possibility remains that *b/D* anomalies are not a 100% reliable indication of injection processes at The Geysers.
7) Production- and injection-induced events probably result from different physical processes.

7.6.2 Long Valley caldera

1. On 22 November 1997, seismicity induced by accelerated magmatic activity at Long Valley caldera migrated from the hydrothermal zone near the southern edge of the resurgent dome to the South Moat fault area to the immediate south-west.
2. Major anomalies in *b*-value and fractal dimension, *D*, were associated with the seismic sequence. Before reactivation of the fault, *b* fell (larger events) and *D* rose (greater clustering). After the reactivation, both *b* and *D* were high.
3. In the hydrothermal zone, earthquakes were probably caused by the failure of small, isolated asperities. Earthquakes in the South Moat fault were the result of the failure of widely spaced, highly stressed asperities.
4. The hydrothermal zone is an inhomogeneous zone containing numerous fault planes. The South Moat fault, on the otherhand, is a mature structure that has probably failed before repeatedly, and has developed a single, coherent fault plane. This fault is capable of generating earthquakes up to $M = 6$ in the

future, but the seismicity in the hydrothermal zone is likely to be limited to more modest magnitudes.

Bibliography

Akaike, H., Information theory and an extension of the maximum likelihood principle, *2nd International Symposium on Information Theory*, ed. B.N. Petrov and F. Csaki, p 267-281, Akademiai Kiado, Budapest, 1973

Aki, K., A probabilistic synthesis of precursory phenomena, *in Earthquake Prediction: an international Review, M. Ewing Ser. 4(editors D. Simpson and P. Richards) AGU, Washington, DC*, p 566-574, 1981

Aki, K., Maximum likelihood estimate of b in the formula log N = a-bm, *Bulletin of the Earthquake Research Institute of Tokyo University*, **43**, p 237-239, 1965

Allis, R. G., Mechanism for induced seismicity at The Geysers geothermal reservoir, California, *Geophys. Res. Lett.*, **9**, p 629-632, 1982

Anderberg, M. R., Cluster analysis for applications, *Academic Press, New York*, 1973

Asada, T., Suzuki, Z. & Tomoda, Y., Notes on the energy and frequency of earthquakes, *Bull. Earthq. Res. Inst.*, **29**, p 289-293, 1951

Atkinson, P., The continuing evolution of The Geysers project, *draft manuscript, UNOCAL Exploration & Production Technology, Sugar Land, Texas*, 1998

Aviles, C.A., Scholtz, C.H. & Boatwright, J., Fractal analysis applied to characteristic segments of the San Andreas Fault, *J. geophys. Res.* **92**, p 331-334, 1987

Bai-Lin, H., Chaos, (Editor), *World Scientific*, Singapore, 1984

Bailey, E. H., Blake, M. C., Jr & Jones, D. L., On-land Mesozoic oceanic crust in the Californian Coast Ranges, *U.S. Geological Survey Professional Paper 700-C*, C70-C81, 1970

Bailey, R.A., Geological map of Long Valley caldera, Mono-Inyo craters volcanic chain, and vicinity, eastern California, *USGS Map, 1-1933*, 2 sheets, 11 pp, 1989

Bailey, R.A., G.D. Dalrymple and M.A. Lanphere, Volcanism, structure and geochronology of Long Valley Caldera, Mono County, California , *J. Geophys. Res.*, **81**, p 725-744, 1976

Bakun, W. H. & Lindh, A. G., Local magnitudes, seismic moments and coda durations for earthquakes near Oroville, California, *Bull. Seism. Soc. Am.*, **67**, p 615-629, 1977

Barker, B. J., Gulati, M. S., Bryan, M. A. & Riedel, K. L., Geysers reservoir performance, *in Stone, C., ed., Geothermal Resources Council Special Report*, **17**, p 167-177, 1992

Barton, C. C. & Larsen, E., Fractal geometry of two dimensional fracture networks at Yucca Mountain, South-western Nevada, *In Proc. Int. Symp. on Fundamentals of Rock Joints, (Editor O. Stephanson)*, p 77-84, 1985

Batini, F., Console, R. & Luongo, G., Seismological study of Larderello-Travale Geothermal area, *Geothermics*, **14**, p 255-272, 1985

Benz, H. M., Zandt G. & Oppenheimer, D. H., Lithospheric structure of Northern California from teleseismic images of the upper mantle, *J. Geophys. Res.*, **97**, p 4791-4807, 1992

Blakely, R. J. & Stanley, W. D., The Geysers Magma Chamber, California: constraints from gravity data, density measurements, and well information, *Geothermal Resources Council Transactions*, **17**, p 227-233, 1993

Bromley, C. J., Pearson,C. F. & Rigor, D. M., Microearthquakes at the Puhagan Geothermal Field, Philippines – A case of induced seismicity, *J. Geophys. Res.*, in press, pre-print in Santa Rosa central files, 1986

Brune, J., Seismic moment, seismicity and rate of slip along major fault zones, *J. Geophys. Res.*, **73**, p 777-784, 1968

Brune, J., Implications of earthquake triggering and rupture propagation for earthquake prediction based on premonitory phenomena, *J. Geophys. Res.*, **84**, p 2195-2198, 1979

Bufe, C.G., Marks, S.M., Lester, F.W., Ludwin, R.S. & Stickney, M.C. Seismicity of the Geysers-Clear Lake Region, *Geological Survey Professional Paper 1141*, edited by R. McLaughlin & J. M. Donnelly-Nolan, 1981

Byerlee, J. D. & Brace, W. F., Fault stability and pore pressure, *Bull. Seismol. Soc. Am.*, **62**, p 657-660, 1972

Castillo, D. A. & Ellsworth, W. L., Seismotectonics of the San Andreas fault system between Point Arena and Cape Mendocino in northern California; Implications for the development and evolution of a young transform, *J. Geophys. Res.*, **98**, p 6543-6560, 1993

Castle, R.O., Estrem, J.E. & Savage, J.C., Uplift across the Long Valley caldera, California, *J. Geophys. Res.*, **89**, 11507-1116, 1984

Chapman, R. H., Gravity map of The Geysers area, California, *California Division of Mines and Geology Mineral Information Service*, **v. 19**, p 148-149, 1966

Cockenham, R. S., Evidence for a 180-km-long subducted slab beneath Northern California, *Bull. Seismol. Soc. Am.*, **74**, p 569-576, 1984

Costin, L. S., A microcrack model for the deformation and failure of brittle rock, *J. Geophys. Res.*, **88**, p 9485 - 9492, 1983

Costin, L. S., Deformation and failure. In: *Fracture Mechanics of Rock* (edited by Atkinson, B.K.), Academic Press, London, 1987

Dalrymple, G. B., Preliminary report on $^{40}Ar/^{39}Ar$ incremental heating experiments on feldspar samples from the felsite unit, Geysers geothermal area, California, *U.S.G.S. Open-File Report 92-407*, 1992

De Rubeis, V., Dimitriu, P., Papadimitriou, E. & Tosi, P.,Recurrent patterns in the spatial behaviour of Italian seismicity revealed by the fractal approach, *Geophys. Res. Lett.*, **20**, p 1911-1914, 1993

Denlinger, R. P., Seismicity induced by steam production at The Geysers steam field in Northern California (abstract), *EOS Trans. AGU*, **61**, p 1051, 1980

Denlinger, R. P. & Bufe, C. G., Reservoir conditions related to induced seismicity at The Geysers steam reservoir, northern California, *Bull. Seismol. Soc. Am.*, **72**, p 1317-1327, 1982

Denlinger, R. P. & Kovach, R. L., Three dimensional gravity modelling of The Geysers hydrothermal system and vicinity, Northern California, *Geological Society of America Bulletin*, Part 1, **92**, no. 6, p 404-410, 1981

Denlinger, R.P., Riley, F.S., Boling, J.K. & Carpenter, M.C., Deformation of Long Valley Caldera between August 1982 and August 1983, *J. Geophys. Res.*, **90**, p 11,199 - 11,209, 1985

Dongsheng, L., Zhaobi, Z. & Binghong, W., Research into the multifractal of earthquake spatial distribution, *Tectonophysics*, **233**, p 91-97, 1994

Eaton, J. P., Lee, W. H. K. & Pakiser, L. C., Use of micro-earthquakes in the study of the mechanics of earthquake generation along the San Andreas fault in central California, *Techtonophysics*, **9**, p 259-282, 1970

Eberhart-Phillips, D. Local earthquake tomography: earthquake source regions, in Seismic tomography: theory and practice, (Editors Iyer, H., M, and K. Hirahara), 613-643, Chapman and Hall, London., 1993

Eberhart-Phillips, D. M., Three-dimensional velocity structure in Northern California Coast ranges from inversion of local earthquake arrival-times, *Bull. Seis. Soc. Am.*, **76**, p 1025-1052, 1986.

Eberhart-Phillips, D. M. & Oppenheimer, D. H., Induced seismicity in The Geysers geothermal area, California, *J. Geophys. Res.*, **89**, p 1191-1207, 1984

Eneva, M., Effect of limited data sets in evaluating the scaling properties of spatially distributed data: an example from mining induced seismic activity, *Geophys. J. Int.*, **124**, p 773-786, 1996

Evenden, J. F., Study of regional seismicity and associated problems, *Bull. Seis. Soc. Amer*, **60**, p 393-446, 1970

Farmer, J. D., Dimension, fractal measures, and chaotic dynamics, *in Evolution of order and chaos (Editor: H. Haken), Springer, Berlin*, p 228-248, 1982

Feder, J., Fractals, *Plenum Press, New York*, 1989

Fieldler, G., Local *b*-values related to seismicity, *Tectonophysics*, **23**, p 277-282, 1974

Florek, K. J., Lukaszewicz, J., Perkal, J. & Zubrzycki, S., Sur la liaison et la division des points d'un ensemble fini, *Colloquium Mathematicae*, **2**, p 282-285, 1951

Forrest, S. R. & Witten, T. A., Jr., Long range correlation in smoke particle aggregates, *J. Phys., A*, **12**, p L109-L117, 1979

Foulger, G., The Hengill triple junction, SW Iceland: 1. Tectonic structure and the spatial and temporal distribution of local earthquakes, *J. Geophys. Res.*, **93**, p 13,493-13,506, 1988

Foulger, G.R., Malin, P.E., Julian, B., Shalev, E. & Hill, D.P., The Mammoth 97 seismic experiment, *EOS, Trans AGU*, **79**, p 357-363, 1998

Frolich, C. & Davis, S. D., Single-link cluster analysis as a method to evaluate spatial and temporal properties of earthquake catalogues, *Geophys. J. Int.*, **100**, p 19-32, 1990

Frye, G., The team Geysers solution, *Geothermal Resources Council Bulletin*, p 197-199, 1997

Furlong, K. P., Thermal-rheologic evolution of the upper mantle and the development of the San Andreas fault system, *Tectonophysics*, **223**, p 149-164, 1993

Furlong, K. P., Hugo, W. D. & Zandt, G., Geometry and evolution of the San Andreas fault zone in Northern California, *J. Geophys. Res.*, **94**, p 3100-3110, 1989

Gibowicz, S. J., Variation of the frequency-magnitude relation during earthquake sequences in New Zealand, *Bull. Seis. Soc. Amer*, **63**, p 517-528, 1973

Gibowicz, S. J., Frequency-magnitude, depth and time relations for earthquakes in an island arc: North Island, New Zealand, *Tectonophysics*, **23**, p 283-297, 1974

Goff, F. E., Donnelly, J. M., Thompson, J.M. & Hearn, B. C. Jr, Geothermal prospecting in The Geysers-Clear Lake area, Northern California, *Geology*, **5**, p 509-515, 1977

Grassberger, P. & Procaccia, I., Measuring the strangeness of strange attractors, *Physica*, **9D**, p 189-208, 1983a

Greenside, H. S., Wolf, A., Swift, J., & Pignataro, T., Impracticality of a box counting algorithm for calculating the dimensionality of strange attractors, *Phys. Rev.*, A, **25**, p 3453-3456, 1982

Gunderson, R. P., Porosity of Reservoir Graywacke at The Geysers, *Geothermal Resources Council Special Report*, **17**, p 89-93, 1992

Gutenberg, B., Amplitude of surface waves and magnitudes of shallow earthquakes, *Bull. Seismol. Soc. Am.*, **35**, p 3-12, 1945

Gutenberg, B & Richter, C.F. Earthquake magnitude, intensity, energy and acceleration, *Bull. Seism. Soc. Amer.*, **32**, p 163-191, 1942

Gutenberg, B. & Richter, C. F., Magnitude and energy of earthquakes, *Ann. Geophys.*, **9**, pp1-15, 1956

Hamilton, R. M. & Muffler, L. J. P., Microearthquakes at the Geysers geothermal area, California, *J. Geophys. Res.*, **v. 77**, p 2081-2086, 1972

Hanks, T. C. & Kanamori, H., A moment-magnitude scale, *J. Geophys. Res.*, **84**, p 2348-2350, 1979

Hatton, C. G., Main, I. G. & Meredith, P. G., A comparison of seismic and structural measurements of scaling exponents during tensile subcritical crack growth, *J. Struct. Geol.*, **15**, p 1485-1495, 1993

Havstad, J.W. & Ehlers, C. L., Attractor dimension of non-stationary dynamical systems from small data sets, *Phys. Rev. A*, **39**, p 845-853, 1989

Hearn, B. C., Donnelly-Nolan, J. M. & Goff, F. E., Geology and chronology of the Clear Lake Volcanics, California, *U.N. Symposium on the development and use of geothermal resources*, San Francisco, Proceedings, **1**, p 423-428, 1976b

Hearn, B. C., Donnelly-Nolan, J. M. & Goff, F. E., The Clear Lake volcanics: Tectonic setting & magma sources, *U.S. Professional Paper 1141*, p 25-45, Research in The Geysers-Clear Lake Geothermal Area, Northern California, edited by R. McLaughlin & J. M. Donnelly-Nolan, 1981

Henderson, J. R., Barton, D. J. & Foulger, G. R., Fractal clustering of induced seismicity in The Geysers geothermal area, California, *In Press*, 1998

Henderson J. R. & Main, I. G., Riverside: the evolution of seismicity - an example from Riverside, California and a fracture-mechanical interpretation, *paper presented at the annual meeting of the European Geophysical Society, Edinburgh*, 1992

Henderson, J. R., Main, I. G., Pearce, R.G. & Takeya, M Seismicity in north-eastern Brazil: fractal clustering and the evolution of the *b*-value. *Geophys. J. Int.*, **116**, p 217-226, 1994

Hill, D. P., Bailey, R. A. & Ryall, A. S., Active tectonic and magmatic processes beneath Long Valley caldera, Eastern California: an overview, *J. Geophys. Res.*, **90**, p 11,111-11,120, 1985

Hill, D. P., Eaton, J. P. & Jones, L.M., Seismicity, 1980-86, *U.S. Geological Survey Professional Paper*, 1515, in The San Andreas Fault System, California, edited by R. E. Wallace, p 115-151, 1990

Hirata, T., A correlation between the *b*-value and fractal dimension of earthquakes, *Journal of Geophysical Research*, **94**, B6 p 7507-7514, 1989

Hirata, T. & Imoto, M., Multifractal analysis of spatial distribution of microearthquakes in the Kanto region, *Geophys. J. Int.*, **107**, p 155-162, 1991

Hirata, T., Satoh, T. & Ito, K., Fractal structure of spatial distribution of microfracturing in rock, *Geophys. J. R. Astron. Soc.*, **90**, p 369-374, 1987

Hubbert, M. K. & Rubey, W. W., Role of fluid pressure in mechanics of overthrust faulting, *Geol. Soc. Am. Bull.*, **70**, p 115 - 166, 1959

Hulen, J. B. & Nielson, D.L., Interim report on geology of The Geysers felsite, northwestern California, *Geothermal Resources Council Transactions*, **17**, p 249 – 258, 1993

Imoto, M. & Ishiguro, M., A Bayesian approach to the detection of changes in the magnitude-frequency relation of earthquakes, *J. Phys. Earth*, **34**, p 441-455, 1986

Isherwood, W. F., Gravity and magnetic studies of The Geysers-Clear Lake geothermal region, California, *Ph.D. thesis, Boulder, University of Colorado*, p 109, 1975

Isherwood, W. F., Gravity and magnetic studies of The Geysers - Clear Lake geothermal region, California, *Second United Nations Symposium on Development and Use of Geothermal Resources, San Francisco, CA, Proceedings*, **v. 2**, p 1065-1073, 1976

Isherwood, W. F., Geophysical overview of The Geysers: in *U.S. Professional Paper 1141, Research in The Geysers-Clear Lake Geothermal Area, Northern California*, p 83 – 96, 1981

Ishimoto, M. & Iida, K., Observations of earthquakes registered with the microseismograph constructed recently (I) *Bull. Earthq. Res. Inst.*, **17**, p 443-478, 1939

Iyer, H. M., Oppenheimer, D. H., Hitchcock, T., Roloff, J. N. & Coakley, J. M., Large P-wave delays in The Geysers-Clear Lake geothermal area, *U.S. Professional Paper 1141*, Research in The Geysers-Clear Lake Geothermal Area, Northern California, p 97-116, 1981

Julian, B. R., Ross, A., Foulger, G.R., Evans, J.R., Three-dimensional seismic image of a geothermal reservoir: The Geysers, California, *Geophys. Res. Let.*, **23**, p 685-688, 1996

Kagan, Y., Observational evidence for earthquakes as a non-linear dynamic process, *Physica D*, 77, p 160-192, 1994

Kagan, Y. & Knopoff, L., A stochastic model of earthquake occurrence , *Proc. 8th Int. Conf. Earthq. Eng*, **1**, p 295-302, 1981

Kanamori, H., Quantification of earthquakes, *Nature*, **271**, p 411-414, 1978

Kanamori, H. & Anderson, D. L., Theoretical basis of some empirical relations in seismology, *Seis. Soc. Seism. Amer.*, **65**, p 1073-96, 1975

Kennedy, B. M. & Truesdale, A. H., Active degassing in the NW Geysers High-temperature reservoir, *Geothermal Resources Council Transactions*, **18**, p 325-330, 1994

Kerr, R. A., Geothermal tragedy of the commons, *Science*, **253**, p 134-135, 1991

Kirkpatrick, A., Peterson, J. E. & Majer, E. L., Microearthquake monitoring at the south-east Geysers using a high-resolution digital array, *Proc. 20th Workshop in Geotherm. Reservoir Engineering, Stanford University*, p 79-89, 1995

Kissling, E., Ellsworth, W. L., Eberhart-Phillips, D. M., Kradolfer, U., Initial reference models in local earthquake tomography, *J. Geophys. Res.*, **99**, p 19,635-19,646, 1994

Langbein, J., Hill, D.P., Parker, T.N., Wilkinson, S.K., An episode of reinflation of the Long Valley Caldera, Eastern California: 1989-1991, J. Geophys. Res., 98, 15851-15870, 1993

Lange, A. L. & Westphal, W. H., Microearthquakes near The Geysers, Sonoma County, California, *J. Geophys. Res.*, **74**, p 4377-4378, 1969

Lee, W. H. K. (editor), Toolbox for seismic data acquisition, processing and analysis, IASPEI Software Library, *Seismological Society of America*, **1**, 1992

Lee, W. H. K., Bennett, R. E., & Meagher, K. L., A method of estimating magnitude of local earthquakes from signal duration, *U.S. Geological Survey Open File Report*, 1972

Lee, W. H. K. & Lahr, J. C., HYPO71 (revised): a computer program for determining hypocentre, magnitude and first motion pattern of local earthquakes, *U.S. Geological Survey Open-File Report 75-311*, 113 pp, 1975

Lee, W. H. K. & Wetmiller, R. J., A survey of practice in determining magnitude of near earthquakes: summary report for networks in North, Central and South America, *U.S. Geological Survey Open File Report 76-677*, 1976

Legrand, D., Cisternas, A. & Dorbath, L., Multifractal analysis of the 1992 Erzincan aftershock sequence, *Geophys. Res. Lett.*, **23**, p 933-938, 1996

Lockner, D. A., Byerlee, J. D., Kuksenko, V., Ponomarev, A. & Sidorin, A., Quasi-static fault growth and shear fracture energy in granite, *Nature*, **350**, p 39-42, 1991

Lofgren, B. E., Monitoring crustal deformation in The Geysers-Clear Lake region, *U.S Geological Survey Professional Paper 1141*, Research in The Geysers-Clear Lake Geothermal Area, Northern California, p 139 - 148, 1981

Ludwin, R. S. & Bufe, C. G., Continued seismic monitoring of The Geysers, California, geothermal area, *U.S. Geological Survey Open File Report*, 80-1060, 50 p, 1980

Ludwin, R. S., Cagnetti, V. & Bufe, C. G., Comparison of seismicity in The Geysers geothermal area with the surrounding region, *Bull. Seismol. Soc. Am.*, **72**, p 863-871, 1982

Luetgert, J.H. & Mooney, W. D., Crustal refraction profile of the Long Valley caldera, California, from the January 1983 Mammoth Lakes earthquake swarm, *Bull. Seism. Soc. Amer.*, **75**, p 11-21, 1985

Ma, H-C, High b-value before Tangshan and Haicheng earthquakes, *Acta Seism. Sin.*, **21**, p 126-141, 1978

Majer, E. L. & McEvilly, T. V., Seismological investigations at The Geysers geothermal field, *Geophysics*, **44**, p 246 - 268, 1979

Majer, E. L., McEvilly, T. V., Eastwood, F. S. & Myer, L. R., Fracture detecting using P-wave and S-wave Vertical Seismic Profiling at The Geysers, *Geophysics*, **53(1)**, p 76-84, 1988

Mandelbrot, B. B., How long is the coast of Britain? Statistical self-similarity and fractional dimension, *Science* **156**, 636-8, 1967

Marks, S. M., Ludwin, R. S., Louie, K. B. & Bufe, C. G., Seismic monitoring at The Geysers geothermal field, California, *U.S. Geological Survey Open File Report*, 78-798, 26 pp., 1978

McLaughlin, R. J. Tectonic Setting of Pre-Tertiary rocks and its relation to geothermal resources in the Geysers-Clear Lake area, *U.S. Professional Paper 1141, p* 3-23, Research in The Geysers-Clear Lake Geothermal Area, Northern California, edited by R. McLaughlin & J. M. Donnelly-Nolan, 1981

Merceron, T. & Velde, B. Application of Cantors method for fractal analysis of fractures in the Toyota Mine, Hokkaido, Japan *J. geophys. Res.*, **96**, 16,641-16,650, 1991

Meredith, P.G. & Atkinson, B.K., Stress corrosion and acoustic emission during tensile crack propagation in Whin Sill dolerite and other basic rocks *Geophys. J. R. Astron. Soc.*, **75**, p 1-21, 1983

Meredith, P. G., Main, I. G. & Jones, C., Temporal variations in seismicity during quasi-static and dynamic rock failure, *Tectonophysics*, **175**, p 249-268, 1990

Miller, A., Seismic structure and earthquake focal mechanisms of the Hengill volcanic complex, south-west Iceland, PhD Thesis, *University of Durham, UK*, 1996

Mogi, K., Magnitude frequency relation for elastic shocks accompanying fractures of various materials and some related problems in earthquakes, *Bull. Earthq. Res. Inst. Univ. of Tokyo*, **40**, 831-853, 1962

Mossop, A. & Segall, P., Subsidence at the Geysers geothermal field, N. California from a comparison of GPS and levelling surveys, *Geophysical Research Letters*, **24**, p 1839-1842, 1997

Nerenberg, M. A. H. & Essex, C., Correlation dimension and systematic geometric effects, *Phys. Rev. A.*, **42**, p 7065-7074, 1990

O'Connell, D. R. H., Seismic velocity structure and micro-earthquake source properties at The Geysers geothermal area, California, Ph.D. Thesis, *University of California, Berkeley, California*, 1986

Okubo, P.G. & Aki, K. Fractal geometry in the San Andreas fault system *J. geophys. Res.* **92**, p 345-355, 1987

Omori, F., Macroseismic measurements in Tokyo, II and III, *Pub. Earthq. Invest. Com.*, **11**, p 1-95, 1902

Öncel, A. O., Alptekin, O. & Main, I., Temporal variations of the fractal properties of seismicity in the western part of the north Anatolian Fault Zone: possible artifacts due to improvements in station coverage, *Nonlinear Processes in Geophysics*, **2**, p 147-157,1995

Oppenheimer, D. H., Extensional tectonics at The Geysers geothermal area, California, *J. Geophys. Res.*, **91**, p 11,463- 11,476, 1986

Oppenheimer, D. H. & Herkenhoff, K. E., Velocity-density properties of the lithosphere from three-dimensional modelling at The Geysers-Clear Lake region, California, *J. Geophys. Res.*, **86**, p 6057-6065, 1981

Page, R., Aftershocks and micro-aftershocks of the Great Alaska Earthquake of 1964, Bull. Seism. Soc. Amer., 58, p 1131-1168, 1968

Press, W. H., Flannery, B. P., Teukolsky, S. A. & Vetterling, W.T., Numerical Recipes - the art of computing languages in C, *Cambridge University Press*, 1988

Real, C. R., & Teng, T. L., Local Richter magnitude and total signal duration in Southern California, *Bull. Seism. Soc. Am.*, **63**, p 1809-1827, 1973

Reed, M. J. & Campbell, G. E., Environmental impact of development in The Geysers Geothermal Field, *USA: Proceedings, Second United Nations Symposium on the Development and Use of Geothermal Resources*, San Francisco, California, **2**, p 1399 - 1410, 1976

Richter, C. F., Elementary Seismology, Freeman, San Francisco, 768 pp, 1958

Romero, A. E., Kirkpatrick, A., Majer, E. L. & Peterson, J. E., Seismic monitoring at The Geysers geothermal field, *Geothermal Resources Council Transactions*, **18**, p 331-338, 1994

Romero A. E., McEvilly, T. V., Majer & E.L., Vasco, D., Characterization of the geothermalsystem beneath the northwest Geysers steam field, California, from seismicity and velocity patterns, *Geothermics*, **24**, p 471-487, 1995

Ross, A. C., The Geysers geothermal area, California: Tomographic images of the depleted steam reservoir and non-double-couple earthquakes, Ph.D. Thesis, University of Durham, United Kingdom, 1996

Ross, A., Foulger, G. R. and Julian, B. R., Source processes of industrially-induced earthquakes at The Geysers geothermal area, California, *Geophysics*, in press, 1998.

Rundle, J.B. and Hill, D.P., The geophysics of a restless caldera - Long Valley, California, Ann. Rev. Earth Planet. Sci., 16, p 251-271, 1988.

Rundle, J.B. & Whitcomb, J.H., A model for deformation in Long Valley, California, 1980-83, J. Geophys. Res., 89, 9371-80, 1984

Ryall, A. & Ryall, F., Spatial-temporal variations in the seismicity preceding the May 1980, Mammoth Lakes, California, earthquakes, In special report 150, Mammoth Lakes, California Earthquakes of May 1980, ed. R.W. Sherburne, p. 27-40, Sacramento: Calif. Div. Mines Geol., 141 pp, 1980

Sadowiskiy, M.A., Golubeva, T.V., Pisarenko, V.F. & Shnirman, M.G., Characteristic dimensions of rocks and hierarchical properties of seismicity, *Phys. Solid Earth*, **20**, p 87-95, 1984

Sammonds. P. R., Meredith, P. G. & Main, I.G., Role of pore fluids in the generation of seismic precursors to shear fracture, *Nature*, **359**, p 228-230, 1992

Sarmiento, Z.F., Wastewater reinjection at Tongonan Geothermal Field: Results and implications, *Geothermics*, **15**, p 295-308, 1986

Savage, J. C., Principal component analysis of geodetically measured deformation in the Long Valley caldera, eastern California, *J. Geophys. Res.*, **93**, p 13927-13,306, 1988

Savage, J.C. & Clark, M., Magmatic resurgence in Long Valley caldera, California - possible cause of the 1980 Mammoth Lakes earthquakes, *Science*, **217**, p 531-533, 1982.

Scholz, C. H., The frequency-magnitude relation of microfracturing in rock and its relation to earthquakes, *Bull. Seism. Soc. Amer.*, **58**, p 399-415, 1968

Scholz, C. H., Sykes L. R., Aggarwal, Y. P., Earthquake predictions: A physical basis, *Science*, **181**, p 803-810, 1973

S.E. Geysers Wastewater Recycling System Website, http://www.geysers-pipeline.com/

Sherburn S., Seismic monitoring during a cold water injection experiment, Wairakei geothermal field – Preliminary results, *Proceedings, 6th New Zealand Geothermal Workshop, p* 129-133, 1984

Smalley, R.F., Chatelain, J.L., Turcotte, D.L. & Prevot, R., A fractal approach to the clustering of earthquakes: Applications to the seismicity of the New Hebrides, *Seis. Soc. Am. Bull.* 77, p 1368-81, 1987

Smith, L.A. Intrinsic Limits on dimension calculations. *Physics Letters A*, **113**, pp283-288, 1988

Smith, W. D., The *b*-value as an earthquake precursor, *Nature*, **289**, p 136-139, 1981

Smith, W. D., Evidence for precursory changes in the frequency-magnitude *b*-value, *Geophys. Jour. Roy. Astr. Soc.*, **86**, p 815-838, 1986

Sorey, M.L., Farrar, C.D., Marshall, G.A. & Howle, J.F.,Effects of geothermal development on deformation in the Long Valley caldera, eastern California, 1985-1994, *J. Geophys. Res.*, **100**, p 12,475-12,486, 1995

Sornette, D., Vanneste, C. & Sornette, A., Dispersion of *b*-values in the Gutenberg-Richter law as a consequence of a proposed fractal nature of continental faulting, *Geophys. Res. Lett.*, **18**, p 897-900, 1991

Stanley, W. D. & Blakely, R. J., The Geysers-Clear Lake geothermal area, California - An updated geophysical perspective of heat sources, *Geothermics*, 24, p 187-221, 1995

Stark, M. A. & Davis, S. D., Remotely triggered microearthquakes at The Geysers geothermal field, California, *Geophys. Res. Letts.*, **23**, p 945-948, 1996

Stark, M. A., Imaging injected water in The Geysers reservoir using micro-earthquake data, *Geothermal Resources Council Transactions*, **14**, p 1-8, 1990

Stark, M. A., Micro-earthquakes - A tool to track injected water in The Geysers reservoir, *Geothermal Resources Council Special Report*, **17**, p 111-117, 1992

Stetsky, R. M., W. F. Brace, D. W. Riley & P.-Y. F. Robin, Friction in faulted rock at high temperature and pressure, *Tectonophysics*, **23**, p 177-203, 1974

Takens, F., On the numerical determination of the dimension of an attractor, *in (Editors: B. L. J. Braaksma, H. W. Broer & F. Takens) Dynamical systems and bifurcations, Springer, Berlin-Heidelberg-New York-Tokyo*, p 99-106, 1984

Takeya, M., High precision studies of an intraplate earthquake sequence in northeastern Brazil, *Ph.D. Thesis*, Edinburgh University, 1992

Takeya, M., Ferreira, J. M. Pearce, R.G., Assumpção, M., Costa, J. M. & Sophia, C. M., The 1986-1988 intraplate earthquake sequence near João Câmara, northeast Brazil - evolution of seismicity, *Tectonophysics*, 1989

Theiler, J., Estimating the fractal dimension of a chaotic time series, *Lincoln Lab Journal*, **3**, 63-85, 1990

Trifu, C. I., Urbancic, T. I. & Young, R. P., Non-similar frequency magnitude distribution for M < 1 seismicity, *Geophys. Res. Lett.*, **20**, p 427-430, 1993

Truesdale, A. H., Walters, M., Kennedy, M. & Lippmann, M., An integrated model for the origin of the Geysers Geothermal Field, *Geothermal Resources Council Transactions*, **17**, p 273-280, 1993

Truesdale, A. H. & White D. E., Production of superheated steam from vapour dominated geothermal systems, *Geothermics 2*, **3-4**, p 154-173, 1973

Turcotte, D. L.,Fractals and chaos in geology and geophysics, *Cambridge University Press, Cambridge*, 1992

Van Wormer, J.D. & Ryall, A.S., Sierra Nevada - Great Basin boundary zone: earthquake hazard related structure, active tectonic processes, and anomalous patterns of earthquake occurrence, Bull. Seism. Soc. Amer., 70, 1557-72, 1980

Volant, Ph., Mécanisme des déformations et aspect fractal de la sismicité induite par l'exploitation d'un gisement d'hydrocarbures (Lacq, France). *Thèse de Doctorat,* Université Joseph Fourier, Grenoble, France, 1993

Volant, Ph. & Grasso, J.-R., The finite extension of fractal geometry and power law distribution of shallow earthquakes: a geomechanical effect, *J. Geophys, Res.*, **99**, p 21879-21889, 1994

Wadati, K., On travel time of earthquake waves, Part II, Geophys. Mag, 7, 101-111, 1933

Walter, S. R., Intermediate-focus earthquakes associated with Gorda plate subduction in Northern California, *Bull. Seismol. Soc. Am.*, **76**, p 583-588, 1986

Walters, M. A., Sternfield, J. N., Haizlip, J. R., Drenick, A. F. & Combs, J, A vapour dominated reservoir at The Geysers, California, *Geothermal Resources Council Special Report*, **17**, p 121-132, 1992

Wannamaker, P. E., Electrical conductivity of water-undersaturated crustal melting, *J. Geophys. Res.*, **91**, p 6321-6328, 1986

Warren, N.W. & Latham, G.V., An experimental study of thermally induced microfracturing and its relation to volcanic seismicity, *J. Geophys Res.I*, **75**, 4455-4464, 1970

Weeks, J., Lockner, D. & Byerlee, J., Change in *b*-values during movement on cut surfaces in granite, *Bull. Seis. Soc. Amer.*, **68**, p 333-341, 1978

Weimer, S. & McNutt, S., Variations in frequency-magnitude distribution with depth in two volcanic areas: Mount St. Helens, Washington, and Mt. Spurr, Alaska, *Geophys. Res. Lett.*, **24**, 189-192, 1998

Weimer, S. & Wyss, S., Mapping the frequency-magnitude distribution in asperities: An improved technique to recalculate recurrence times, *J. Geophys. Res*, **102**, p 15,515-15,128, 1997

Wyss, M., Towards a more physical meaning of the earthquake frequency distribution, *Geophys. J. Royal Astr. Soc.*, **31**, 341-359, 1973

Wyss, M., Evaluation of proposed earthquake precursors (Editor), *AGU, Washington D.C.*, 1991

Wyss, M., Bodin, P. & Habermann, R.E. Seismic quiescence at Parkfield: an independent indication of an imminent earthquake. *Nature*, **345**, p 426-428, 1990

Wyss, M. & Lee, W. H. K., Time variation of the average earthquake magnitude in Central California, *in Proc. Conf. Tectonic Problems of the San Andreas Fault System, School of Earth Science, Stanford University*, p 24 - 42, 1973

Xie, H. & Pariseau, W. G., Fractal character and mechanism of rock bursts, *Int. J. Rock. Mech. Min. Sci. & Geomech. Abstr.*, **30**, p 343-350, 1993

Zhang, J.Z. & Song, L.-Y. On the method of estimating b-value and its standard error, *Acta Seism. Sin.*, **3**, p 292-301, 1981

Zucca, J. J., Hutchings, L. J. & Kasameyer, P. W., Velocity and attenuation structure of The Geysers geothermal field, California, *submitted to J. Geophys.Res.*, 1994

Appendix 1

Listing for program pcql2ah_script

This script was used to convert seismograms from UNOCAL Corporation PCQL trace file (standard input default) format into XDR (External Data Representation) version of Lamont's AH (AdHoc) format. It uses the program ***pcql2ah***, *(B. Julian, pers. comm.)* to achieve this.

```
#! /bin/sh

# Version 1.1: sept 1995 djb

# starting with pcql files:
# 1) convert into .ah files and place in a directory of the type:
#           /usr/local/seismic/barton/geysers{year}/unocal/{f|g|w}{year}{day}/
# 2) compress pcql files in current place

year=$1                 # year
st=$2                   # station type : f, g or w
ls -1 $SROOT/19$year | sed 's/^....././/' > $SROOT/$year.day_cat.pcql2ah

mkdir $SROOT/geysers$year
mkdir $SROOT/geysers$year/unocal
mkdir $SROOT/geysers$year/unocal/$st

for day in `cat $SROOT/$year.day_cat.pcql2ah`
do
        echo 1: $SROOT/geysers$year/unocal/$st/$st$year$day
        mkdir $SROOT/geysers$year/unocal/$st/$st$year$day
#       gunzip -q $SROOT/19$year/19$year.$day/*$st*
        ls -1 $SROOT/19$year/19$year.$day/*.$st* |
        sed 's/^.....//' |
        sed 's/....$//' > $SROOT/E$year.$day.catalog.$st.pcql2ah

for fl in `cat $SROOT/E$year.$day.catalog.$st.pcql2ah`
do
        pcql2ah -stafile $SROOT/bin/$st.stn $SROOT/19$year/19$year.$day/$fl.$st$year >
$SROOT/geysers$year/unocal/$st/$st$year$day/$year$fl.ah

        gzip -q $SROOT/geysers$year/unocal/$st/$st$year$day/$year$fl.ah
        rm $SROOT/19$year/19$year.$day/$fl.$st$year
done
        rm $SROOT/E$year.$day.catalog.$st.pcql2ah
        rmdir $SROOT/19$year/19$year.$day
done
rmdir $SROOT/19$year
rm $SROOT/$year.day_cat.pcql2ah
```

Appendix 2

Listing for program codapick

This *C* program was used to pick codalengths. It is based on the program ***autopick*** (*R. Crosson, Mary O'Neill and Angus Miller, pers. comm.*) and uses a modified version of the algorithm by *Lee et al. (1972)* (see text).

codalength.c

```
#include <stdio.h>
#include <string.h>
#include <local/local.h>
#include <local/stdtyp.h>
#include "results.h"
#include "control.h"

        FILE    *efopen();
        char    *emalloc();

/*
 * Calculate coda length of seismogram.
 */
int
codalength(stanam, rate, start, end, seis, noise, results)
        char    *stanam;        /* Station name                                 */
        float   rate;                   /* Sampling rate                        */
        float   start;                  /* Start of window (in secs.)           */
        float   end;                    /* End of window (in secs.)             */
        float   *seis;                  /* Values of seismogram                         */
        float  noise;                   /* Amount of ambient noise              */
        RESULTS *results;
{
        int     stind;                  /* Index of start trace         */
        int     endind;                 /* Index of end of trace        */
        int     g;                      /* counter                              */
        int     i;                      /* counter                              */
        float   cwin = 50.0;            /* window for coda length = 50 samples  */
        float   maxnoise = 10.75;   /* max noise level - rms from noisepick */
        float   cthresh = 200.0;    /* coda pick threshold - cthresh = 100.0 for w network produces magnitudes ~
                                        CALNET
                                        thresh = 200.0 for g network produces magnitudes ~ CALNET
                                          i.e. gain for g network is twice the w network  */
        float   junk;
        stind = (int) (start*rate);
        endind = (int) (end*rate);

        /* Verify that : 1) max signal strength is five times greater than background noise
                         2) noise is less than for 80% of traces ( = maxnoise) */

        if ((results->Maxamp >= cthresh) && (noise <= maxnoise)) {
                for (g = ((results->Maxtime)*rate) ; g < endind ; g++) {
                junk = g / rate;
                        for (i = g; i < g + cwin; i++) {
                                if (fabs(-seis[i] + seis[i-1]) > cthresh) {
                                        break;
                                }
                                if ((fabs(-seis[i] + seis[i-1]) <= cthresh) && (i + 1 == g + cwin)) {
                                results->Codatime = (float) g/rate;
                                results->Codalen  = ((float) g/rate) - ((float)stind/rate);
            results->Cflg = TRUE;
                                return SUCCEED; }

                        }
```

```
                }
                return FAIL;
        }
}
```

codapickg_new.c

```
/*
 * Calculates 1) The max amplitude in a seismogram.
 *          2) Coda length
 * Output (to stdout) in epick PICK format, with max amplitude picks labelled "max".
 *                                  coda length picks labelled "coda".
 */
#include <stdio.h>
#include <rpc/rpc.h>
#include <string.h>
#include "local.h"
#include "cmd_opt.h"
#include "ahhead.h"
#include "stdtyp.h"
#include "date_time.h"
#include "control.h"
#include "results.h"
#include "pick_struct.h"

#define index   strchr  /* Gratuitously renamed by some committee      */

#define SUCCEED      0
#define strneq       !strncmp

        CONTROL         control;
        double  atof();                 /* Unix C library                       */
        FILE    *efopen();  /* -lq (efopen.c)                       */
        char    *emalloc();/* -lq (emalloc.c)                       */
        void    error();    /* -lq (error.c)                        */
        void    exit();                 /* Unix C library                       */
        char    *index();   /* Unix C library                       */
static  int     read_ptime();           /* Defined below                        */
static  int     read_stime();           /* Defined below                        */
static  void    one_file(); /* Defined below                        */
        char    *strncpy(); /* Unix C library                       */
        void    writepik(); /* pfutils.c                            */
static  char    *epfile;    /* ep file name                         */

/*— COMMAND-LINE ARGUMENT PROCESSING —*/

qhelp       (){ if(eargc>2) prt_help(); else prt_doc("[ah_file...]"); }
qepfile (){ epfile = aarg(); }
qplead  (){ control.plead = narg(); }
qspfrac (){ control.spf = narg(); }
qverb       (){ control.verbose = TRUE; }

struct command cmd[] = {
  qhelp  , "-help"    , "[opt...]" , "Documentation help",
  qepfile, "-epfile"  , "name"     , "input epfile (required)",
  qplead , "-plead"   , "seconds"  , "time before P-pick to use for vertical channel",
  qspfrac, "-spfrac"  , "value"    , "fraction of S-P time to use for horizontal channels",
  qverb  , "-verbose" , ""         , "Print picks to stderr",
};

main(argc,argv)
        int     argc;
        char    *argv[];
{
        FILE    *fin;                   /* Input unit                                   */

        /* Set defaults and process command-line options */
        epfile = (char *)NULL;
        control.plead = 1.0;
        control.spf = 0.5;
        control.verbose = FALSE;
```

```
        PROCESS_OPTS;
        if (epfile == (char *)NULL)
                error("Input ep file required");

        /* Process named files (standard input default) */
        if (iarg >= argc)
                one_file(stdin, stdout, &control);
        else
                for (; iarg<argc; iarg++) {
                        (void)fprintf(stderr, "Process file %s\n", argv[iarg]);
                        fin = efopen(argv[iarg], "r");
                        one_file(fin, stdout, &control);
                        (void)fclose(fin);
                }

        return 0;
}

/*
 * Process one input file
 */
static void
one_file(fin, fout, control)
        FILE    *fin, *fout;
        CONTROL         *control;
{
        RESULTS results;
        int     tralen;
        char    *staname;
        char    *stachan;
        float   srate;
        TIME    starttime;  /* trace start time                          */
        TIME    ptime;              /* P-pick time                                  */
        TIME    stime;              /* S-pick time                                  */
        float   noise;              /* ambient noise level for a trace   */
        float   sec1;               /* Pick window end (in seconds)              */
        ahhed   hd;                 /* AH trace header                           */
        float   *wf;                /* [0..ndata-1]                              */
        XDR     xdrin;              /* XDR input stream                          */
        PMAIN   p;
        PMAIN   c;
        FILE    *fep;

        /* Check for binary I/O on a terminal */
        if (isatty(fileno(fin)))
                error("Can't get binary input from a terminal.");
        if (isatty(fileno(fout)))
                error("Can't send binary output to a terminal.");

        /* Create XDR streams */
        xdrstdio_create(&xdrin, fin, XDR_DECODE);

        /* Open ep file */
        fep = efopen(epfile, "r");

        /* Loop over traces */
        while (xdr_gethead(&hd, &xdrin) == 1) {

                /* Get header information */
                tralen = (int)hd.record.ndata;
                staname = hd.station.code;
                stachan = hd.station.chan;
                srate = 1.0/hd.record.delta;
                starttime = timvar((int)hd.record.abstime.yr,
                                   (int)hd.record.abstime.mo,
                                   (int)hd.record.abstime.day,
                                   (int)hd.record.abstime.hr,
                                   (int)hd.record.abstime.mn,
                                   hd.record.abstime.sec,
                                   GREGORIAN);

                /* Read trace */
                wf = (float*)emalloc((unsigned)hd.record.ndata*sizeof(float));
```

```
                if ((xdr_getdata(&hd, (char*)wf, &xdrin)) <= 0)
                        error("Error reading data");

                /* Read P-pick time from epfile */
                ptime = starttime;
                rewind(fep);
                if ((read_ptime(fep, staname, &ptime)) == FAIL) {
                        if (control->verbose) {
                                (void)fprintf(stderr,
                                        "%s %s : No P pick\n", staname, stachan);
                        }
                        free((char*)wf);
                        continue;
                }

        /* Use P time as end of window */
        sec1 = ptime-starttime;

        /* look for noise pick for this channel */
        noise = 0.0;
        rewind(fep);
        if ((read_noise(fep, staname, &noise)) == FAIL) {
                        if (control->verbose) {
                    (void)fprintf(stderr,
                    "%s %s : No Noise pick\n", staname, stachan);
                        }
            free((char*)wf);
            continue;
        }

                /* Pick max amplitude */
                (void)dopick(staname, srate, sec1, (tralen/srate), wf, &results);

                /* print out seismogram */
/*          (void)seislook(staname, srate, sec1, (tralen/srate), wf, noise, &results); */

        /* pick coda length */
        (void)codalength(staname, srate, sec1, (tralen/srate), wf, noise, &results);

                /* Output pick details to standard error */
                if ((control->verbose) && (results.Pflg)) {
                        (void)fprintf(stderr, "%s %s  max: %6.2f  %6.2f\n",
                                staname, stachan, results.Maxtime, results.Maxamp);}
        if ((control->verbose) && (results.Cflg)) {
            (void)fprintf(stderr, "%s %s coda: %6.2f  %6.2f  %6.2f\n",
                staname, stachan, results.Ptim, results.Codatime, results.Codalen);
                } else if (control->verbose) {
                (void)fprintf(stderr, "%s %s - no coda pick\n",staname, stachan); }

                /* Put common and default info. in PMAIN structure      */
        /* max amp values */
        if (results.Pflg) {
                (void)strncpy(p.stcode, hd.station.code, sizeof(p.stcode));
                (void)strncpy(p.chan, hd.station.chan, sizeof(p.chan));
                p.onset = ' ';
                p.pol = ' ';
                p.qual = '0';

                /* Copy pickinfo. from results to PMAIN and write       */
                p.t = starttime + results.Maxtime;
                (void)strncpy(p.phcode, "max", sizeof(p.phcode));
                p.setime = 0.0;
                p.amp = results.Maxamp;
                p.freq = 0.0;
                if (fwrite((char *)&(p), sizeof(p), 1, fout) != 1)
                                        error("Can't write pick");
                }
        /* coda length values */
        if (results.Cflg) {
        (void)strncpy(c.stcode, hd.station.code, sizeof(c.stcode));
        (void)strncpy(c.chan, hd.station.chan, sizeof(c.chan));
        c.onset = ' ';
        c.pol = ' ';
```

```
        c.qual = '0';

        /* Copy coda pickinfo. from results to PMAIN and write      */
        c.t = starttime + results.Codatime;
        (void)strncpy(c.phcode, "coda", sizeof(c.phcode));
        c.setime = 0.0;
        c.freq = 0.0;
        if (fwrite((char *)&(c), sizeof(c), 1, fout) != 1)
                error("Can't write coda pick");
        }

                /* Release allocated space */
                free((char*)wf);
        }

        /* Close ep file */
        (void)fclose(fep);

        /* Destroy XDR streams */
        xdr_destroy(&xdrin);
}

/*
 * Find P pick time
 */
static int
read_ptime(f, sta, time)
        FILE    *f;     /* Open ep file                                 */
        char    *sta;   /* Station code to search for       */
        TIME    *time;  /* P pick time                                  */
{
        PICK    pk;

        while (fread((char*)&(pk.pm), sizeof(pk.pm), 1, f) == 1) {
                if (strneq(pk.pm.stcode, sta, sizeof(sta))
                        && strneq(pk.pm.phcode, "P", 1)) {
                        *time = pk.pm.t;
                        return SUCCEED;
                }
        }
        return FAIL;
}

/*
 * Find Noise pick
 */
static int
read_noise(f, sta, noise)
    FILE   *f;    /* Open ep file             */
    char   *sta;  /* Station code to search for  */
    float  *noise; /* noise pick               */
{
    PICK   pk;

    while (fread((char*)&(pk.pm), sizeof(pk.pm), 1, f) == 1) {
        if (strneq(pk.pm.stcode, sta, sizeof(sta))
            && strneq(pk.pm.phcode, "N", 1)) {
/*            fprintf(stderr,"station code %s phase code %s \n", pk.pm.stcode, pk.pm.phcode); */
            *noise = pk.pm.amp;
            return SUCCEED;
        }
    }
    return FAIL;
}
```

control.h

```
typedef struct {
        float   plead;          /* Time window before P-time for vert. channel*/
        float   spf;            /* fraction of S-P time for horiz. channels */
        bool    verbose;    /* Produce verbose output to stderr?        */
```

```
} CONTROL;
```

dopick.c

```
#include <stdio.h>
#include <string.h>
#include <math.h>
#include <local/local.h>
#include <local/stdtyp.h>
#include "results.h"
#include "control.h"

        FILE    *efopen();
        char    *emalloc();

/*
 * Calculate max amplitude in seismogram
 */
int
dopick(stanam, rate, start, end, seis, results)
        char    *stanam;   /* Station name                                  */
        float   rate;              /* Sampling rate                         */
        float   start;             /* Start of window (in secs.)            */
        float   end;               /* End of window (in secs.)              */
        float   *seis;
        RESULTS *results;
{
        int     stind;                  /* Index of start of trace                  */
        int     endind;                 /* Index of end of trace            */
        int     k;                      /* counter                                  */
        int     i;                      /* another counter                          */
        int     maxind = 0;             /* Index of max amplitude value             */
        float   maxamp = 0.0;           /* Max amplitude value
        */
        float  maxnoise = 10.75;        /* max noise level - rms from noisepick     */
    float  cwin = 50.0;             /* window length = 50 samples               */
        float   cutoff;                 /* cut off amplitude to stop scanning       */
        results->Cflg = FALSE;
    results->Pflg = FALSE;
        stind = (int) (start*rate);
        endind = (int) (end*rate);

        /* read in data - convert to absolutes */
/*      (void)fprintf(stderr,"stind = %d : endind = %d\n", stind, endind);*/
    for (k = stind ; k < endind ; k++) {
        if (fabs(-seis[k] + seis[k-1]) > maxamp) {
        maxamp = fabs(-seis[k] + seis[k-1]);
        maxind = k;
                cutoff = maxamp / 4.0;
/*              (void)fprintf(stderr, "maxamp = %f : maxind = %d\n",maxamp,maxind);*/
                }
        if (fabs(-seis[k] + seis[k-1]) < cutoff) {
            for (i = k; i < k + cwin; i++) {
/*(void)fprintf(stderr,"amps < maxnoise k = %d : cutoff = %f : amp[%d] = %f : amp[%d] = %f : fabamp =
%f\n",k,cutoff,i,seis[i],i-1,seis[i-1],fabs(-seis[i] + seis[i-1]));*/
                if ( fabs(-seis[i] + seis[i-1]) > cutoff) {
/*(void)fprintf(stderr,"amps > maxnoise k = %d : cutoff = %f : amp[%d] = %f : amp[%d] = %f : fabamp =
%f\n",k,cutoff,i,seis[i],i-1,seis[i-1],fabs(-seis[i] + seis[i-1]));*/
/*                      (void)fprintf(stderr,"\n");*/
                    break; }
                if (i == k + cwin - 1) {
/*                      (void)fprintf(stderr,"k = %d : i = %d\n", k,i);
                                (void)fprintf(stderr, "END: maxamp = %f : maxind =
%d\n",maxamp,maxind);*/
                                    /* Put pick info. in results structure */
                                results->Maxtime = (float) maxind/rate;
                                results->Maxamp = maxamp;
                                results->Ptim = stind/rate;
                                results->Pflg = TRUE;
                                return SUCCEED;
                                }
                        }
```

```
                }
        }
}
```

pick_struct.h

```
#define STCSIZE     4               /* Length of station code          */
#define CHANSIZE    6               /* Length of channel code          */
#define PHCSIZE             8               /* Length of phase code                    */
#define NULL_TIME 1.0e10

/* Indespensable part of a PICK */
typedef struct {
        char    stcode[STCSIZE];/* Station code                                    */
        char    chan[CHANSIZE]; /* Channel code                                    */
        char    phcode[PHCSIZE];/* Phase code                                      */
        TIME    t;              /* Arrival time                                   */
        float   setime;         /* Standard error of arrival time  */
        char    onset;          /* 'e' or 'i'                                     */
        char    pol;            /* Polarity:  'u' or 'd'           */
        char    qual;           /* Pick quality                                   */
        float   amp;            /* Amplitude                                      */
        float   freq;           /* Frequency                                      */
} PMAIN;

/* Alternate version of time, e.g. from clock or radio time channel */
typedef struct {
        TIME    at;
} PAT;

/* Related things measured from a trace */
typedef struct {
        PMAIN   pm;             /* Required                                       */
        PAT     *pat;           /* Optional                                       */
} PICK;
```

results.h

```
/* Results of picking operation */

typedef struct {
        float   Ptim;           /* P Pick time (sec after start of trace)         */
        float   Amp;            /* Picked amplitude                               */
        float   Maxtime;  /* Pick time of max amplitude                           */
        float   Maxamp;         /* max amplitude                                  */
        float   Codatime;  /* time of coda pick                                   */
        float   Codalen;   /* time (secs) between p pick & coda pick  */
        int     Cflg;           /* true if coda pick is made                      */
        int     Pflg;           /* true if max amp pick is made                   */
} RESULTS;
```

seislook.c

```
#include <stdio.h>
#include <string.h>
#include <math.h>
#include <local/local.h>
#include <local/stdtyp.h>
#include "results.h"
#include "control.h"

        FILE    *efopen();
        char    *emalloc();

/*
 * Calculate coda length of seismogram.
 */
int
seislook(stanam, rate, start, end, seis, noise, results)
```

```
        char    *stanam;    /* Station name                                  */
        float   rate;               /* Sampling rate                         */
        float   start;              /* Start of window (in secs.)            */
        float   end;                /* End of window (in secs.)              */
        float   *seis;              /* Values of seismogram                          */
        float  noise;               /* Amount of ambient noise               */
        RESULTS *results;
{
        int     stind;              /* Index of start trace        */
        int     endind;             /* Index of end of trace       */
        int     g;                  /* counter                               */
        float   junk;
        stind = (int) (start*rate);
        endind = (int) (end*rate);

                for (g = stind ; g < endind ; g++) {
                junk = g / rate;
                        (void)fprintf(stderr, "time = %6.2f  :  amplitude = %6.2f  :  | amplitude | = %6.2f \n",
                                                junk, seis[g], (fabs(seis[g])));
                        }
}
```

Appendix 3

Listing for program ah2codapick

This program controls the autopick, noisepick and codapick programs to pick P-wave, noise and coda lengths and then locates earthquakes using the locate_hand script. The processed UNT earthquakes are then written to a file, forming the Barton catalogue

```
#! /bin/sh

# ah2codapick.test jan 1996 djb

# starting with .ah files:
# 1) create catalog file of all files for days listed in a file
# 2) create list files for each day
# 3) p picks -> write to E$day_picks.ap file
# 4) noise sampling -> write to E$day_picks.ap file
# 5) coda picking -> write to E$day_picks.ap file

#       start process in  /usr/local/seismic/barton on alice
# format ah2codapick year station-type

year=$1                 # year
st=$2   # station type : f, g or w

mkdir $SROOT/geysers$year/$st

#       ls -1 $SROOT/geysers$year/unocal/$st |
#       sed 's/^.../' > $SROOT/geysers$year/$st/$year.day_cat.$st

for day in `cat $SROOT/geysers$year/$st/$year.day_cat.$st`

do
        echo
        echo "Year = $year : Day = $day"
        echo "----------"

#       create catalog file for day
        gunzip -q $SROOT/geysers$year/unocal/$st/$st$year$day/*
    ls -1 $SROOT/geysers$year/unocal/$st/$st$year$day |
    sed 's/^...../' | sed 's/.ah//' > $SROOT/geysers$year/$st/E$year.$day.$st.catalog_uno
        rm $SROOT/geysers$year/$st/xh.$st.* $SROOT/geysers$year/$st/yh.$st.* $SROOT/geysers$year/$st/zh.$st.*

for fl in `cat $SROOT/geysers$year/$st/E$year.$day.$st.catalog_uno`
do

#       create list file for day catalog
        mkahlist $SROOT/geysers$year/unocal/$st/$st$year$day/$year$day$fl.ah >
$SROOT/geysers$year/$st/E$year.$day.$fl.$st.1.list

#       make p, noise & coda picks
        echo
        echo "P picks for: E$year.$day.$fl.$st.1.list "
        pick.ap.$st $SROOT/geysers$year/$st/E$year.$day.$fl.$st.1.list >
$SROOT/geysers$year/$st/E$year.$day.$fl.$st.1.ap
        echo
        echo "Noise picks for: E$year.$day.$fl.$st.1.list "
        pick.np.$st $SROOT/geysers$year/$st/E$year.$day.$fl.$st.1.list >>
$SROOT/geysers$year/$st/E$year.$day.$fl.$st.1.ap
        echo
        echo "Coda picks for: E$year.$day.$fl.$st.1.list "
```

```
        pick.cp.$st $SROOT/geysers$year/$st/E$year.$day.$fl.$st.1.list >>
$SROOT/geysers$year/$st/E$year.$day.$fl.$st.1.ap

#       locate earthquake position & calculate magnitudes
        echo
        locate_hand -y $year -s $st -1d -t 3 $SROOT/geysers$year/$st/E$year.$day.$fl.$st.1.ap
        locate_hand -y $year -s $st -3d -t 3 $SROOT/geysers$year/$st/E$year.$day.$fl.$st.1.ap

#       remove unwanted files
        rm $SROOT/geysers$year/$st/E$year.$day.$fl.$st.1.list
        rm $SROOT/geysers$year/$st/E$year.$day.$fl.$st.1.ap
done
        rm $SROOT/geysers$year/$st/E$year.$day.$st.catalog_uno
        cat $SROOT/geysers$year/$st/xh.$st.* >> $SROOT/geysers$year/$st/E$year.$st.max_codas
        gzip -q $SROOT/geysers$year/unocal/$st/$st$year$day/*
        rm $SROOT/geysers$year/$st/xh.$st.* $SROOT/geysers$year/$st/yh.$st.*
done

rm $SROOT/geysers$year/$st/$year.day_cat.$st
gzip $SROOT/geysers$year/$st/*
```

Appendix 4

Listing for program locate_hand

Locate_hand used the eloc script to locate earthquakes in the Barton catalogue.

```
#! /bin/sh
# locate djb feb, march, may 1996
# 1) Examines .ap file
#       if there are more than thresh coda picks, the earthquake is located
# 2) Calculates magnitude, mean of magnitude and standard deviation
#       rejects magnitudes if they are outside of 1 stdev of mean for an event

usage="Usage: $0 [-y year][-s station network][-1d|-3d] [-t number of coda picks required to locate an earthquake] [ep_file]"

cmd="eloc"
while test "$1" != ""
do
        case "$1" in
                -y*) year=$2; shift 2;;
                -s*) st=$2; shift 2;;
                -1*) cat_file=$SROOT/geysers$year/$st/$year.catalog_hand.$st.1d; shift ;;
                -3*) cmd="eloc3d"; cat_file=$SROOT/geysers$year/$st/$year.catalog_hand.$st.3d; shift ;;
                -t*) thresh=$2;  shift 2;;
                -*) echo $usage 1>&2; exit 1 ;;
                *) break ;;
        esac
done

for file in $*
do
        name=`echo $file | sed -e 's,.ap,,'`
    list=`ls -1 $file | nawk '{print $5}'`
    if [ $list -ne 0 ]
    then
        stuff=`ep2asc < $file | coda_count`
        if [ $stuff -ge $thresh ]
                then
                        echo "locate_hand: $file: # of coda picks = $stuff picks  => $thresh  locate"
                        $cmd $file |
                        nawk '
                                NR==1 { yy = $1; mm = $2; dd = $3; ptime = $4;
                                        printf "%4d %4s %2d\t%15s\t",yy,mm,dd,ptime >> "'$cat_file'" }
                                NR==2 { printf "%6.4f\t%6.4f\t%4.3f\t", $2, $4, $6  >> "'$cat_file'" }

                                $8 == "P" {             p++
                                                        psum2 = psum2 + ($10*$10)
                                printf "%s\t%s\t%s\t%s\n",$1,$8,$9,$10 >>
"'$SROOT/geysers$year/$st/yh.$st.$$'"}
                                $8 == "coda" {          coda++
                                printf "%s\t%s\t%s\t%s\n",$1,$8,$9,$10 >>
"'$SROOT/geysers$year/$st/yh.$st.$$'"}
                                $8 == "max" && $15 !~/NaN/ {
                                                        max++
                                printf "%s\t%s\t%s\t%s\n",$1,$8,$9,$15 >>
"'$SROOT/geysers$year/$st/yh.$st.$$'"}
                                END {
                                        printf "P %2d\t", p >> "'$cat_file'"
                                        printf "%5.3f\t", sqrt(psum2/p) >> "'$cat_file'"
                                        printf "max %2d\t", max >> "'$cat_file'"
                                        printf "C %2d\t", coda >> "'$cat_file'"
                                        cmd = sprintf ("sort +1 -1 '$SROOT/geysers$year/$st/yh.$st.$$'")
                                        count = 0
                                        for (i=1; i<=p+coda+max; i++) {
                                                cmd | getline
```

```
                                                                stat[i]=$1; ph[i]=$2; time[i]=$3; res[i]=$4

if ((stat[i] == stat[i-1]) && (stat[i] == stat[i-2]) && (ph[i] ~/max/)  && (ph[i-1] ~/coda/) && (ph[i-2] ~/P/)
                        && ((sqrt(res[i-2]*res[i-2])) <= 0.3)) {
                                if          (stat[i] ~/ACR/)        { m =  1.710552 ; c =  0.206500 ;               count++ ;)
                                else if (stat[i] ~/ANG/) { m =  1.905554 ; c =  0.235788 ;              count++ ;)
                                else if (stat[i] ~/BUC/) { m =  1.893087 ; c =  0.362146 ;              count++ ; }
                                else if (stat[i] ~/CAP/) { m =  2.009503 ; c =  -0.049210 ;             count++ ; }
                                else if (stat[i] ~/CLV/) { m =  1.872942 ; c =  0.225319 ;              count++ ; }
                                else if (stat[i] ~/DES/) { m =  1.920600 ; c =  0.144974 ;              count++ ; }
                                else if (stat[i] ~/DRK/) { m =  1.706079 ; c =  0.189482 ;              count++ ; }
                                else if (stat[i] ~/DVB/) { m =  1.941633 ; c =  0.223597 ;              count++ ; }
                                else if (stat[i] ~/DXR/) { m =  1.808221 ; c =  0.229538 ;              count++ ; }
                                else if (stat[i] ~/FNF/) { m =  1.873438 ; c =  0.335594 ;              count++ ; }
                                else if (stat[i] ~/FUM/) { m =  1.724657 ; c =  0.210134 ;              count++ ; }
                                else if (stat[i] ~/LCK/) { m =  2.006317 ; c =  -0.083078 ;             count++ ; }
                                else if (stat[i] ~/PFR/) { m =  2.005973 ; c =  0.480328 ;              count++ ; }
                                else if (stat[i] ~/SB4B/)               { m =  1.791232 ; c =  0.306041 ;               count++ ; }
                                else if (stat[i] ~/SSR/) { m =  2.091199 ; c =  0.257708 ;              count++ ; }
                                else if (stat[i] ~/STY/) { m =  1.928002 ; c =  0.376398 ;              count++ ; }
                                else { m = 0 ; c = 0; }
                                                mag[count] = (m*(log(time[i-1]-time[i-2]))/log(10))+c
                                                residual[count] = res[i-2]
                                                station[count] = stat[i]
                                                magsum += (m*(log(time[i-1]-time[i-2]))/log(10))+c;
printf "%s\tcoda\t%f\tmax\t%f\n",station[count],(time[i-1]-time[i-2]),res[i] >> "'$SROOT/geysers$year/$st/xh.$st.$$"'
                                                        }
                                                }
                                                if ( (count > 1) ) {
                                                        ave = magsum/count
                                                        for (si = 1; si<=count;si++) {
                                                                svar = svar + ((mag[si] - ave)*(mag[si] - ave))
}
                                                        svar /= (count-1)
                                                        sdev = sqrt(svar)
                                                        for (chuck = 1; chuck <= count ; chuck++) {
                                                if ( (mag[chuck] > ave - sdev) && (mag[chuck] < ave + sdev )) {
                                                                new_magsum += mag[chuck]
                                                                ccount++
printf "%s\t%s\t%s\t%s\t%s\t%s\t%s\t%2.1f\n",chuck,station[chuck],yy,mm,dd,ptime,residual[chuck],mag[chuck] >>
"'$SROOT/geysers$year/$st/zh.$st.$$"'
                                                                        }
                                                        }
                                if (ccount != 0) {printf "# = %d\t%2.1f\n",ccount,new_magsum/ccount >> "'$cat_file"'}
                                if (ccount == 0) {printf "No mag - statistics failed\n" >> "'$cat_file"'}
                                                }
                                                else if (count == 1) {
printf "%s\t%s\t%s\t%s\t%s\t%s\t%s\t%s\t%2.1f\n",count,station[count],yy,mm,dd,ptime,residual[count],mag[count] >>
"'$SROOT/geysers$year/$st/zh.$st.$$"'
                                        printf "# = %d\t%2.1f\n",count, magsum/count >> "'$cat_file"'
                                                }
                                                else if (count == 0) {printf "No mag - high residuals\n" >>
"'$cat_file"'
                                                }
                                                close(cmd)
                                }
                        '
                        elif    [ $stuff -lt $thresh ] &&
                                [ $stuff -gt 0 ]
                        then
                                echo "locate_hand: $file: # of coda picks = $stuff 0 < # coda picks < $thresh   do nothing"
                        else
                                echo "locate_hand: $file: # of coda picks = $stuff do nothing"
                        fi
                else
                        echo "locate_hand: $file:  empty .ap file"
                fi
done
```

Appendix 5

Well data

Appendix 5.1 Well owning companies in The Geysers geothermal area

Operator	Full Name	Operator	Full Name
Amax	AMAX Exploration Co.	NCPA	Northern California Power Agency
Andar	Anadarko Petroleum Corporation	OXY	Occidental Geothermal Inc.
CCPA	Central California Power Agency	Republic	Republic Geothermal Incorporated
CGC	Calpine Geysers Company	RESFL	Resources Funding Ltd.
Chevron	Chevron Oil Company	SANFE	Santa Fe Geothermal, Inc.
DWR	Department of Water Resources	SBGPC	Sulphur Bank Geothermal Power Company
Earth	Earth Energy Inc.	SCPD	Sonoma Local Agency Formation Commission
EEI	Exploration Engineering Inc.	Shell	Shell Oil Company
FMRP	Freeport McMoran Partners	Silver	Silverado Geothermal
GEO	Geo East Mesa Limited Partnership	SMI	Sonoma Mission Inn
GEP	Geothermal Energy Partners	SOUPC	Southern Union Production Company
Getty	Getty Oil Company	SRGC	Santa Rosa Geothermal Company
GKI	Geothermal Kinetics Inc.	SUNED	Sunoco Energy Development Co.
Grace	Grace Geothermal Corporation	Therm	ThermaSource, Inc.
Hawaii	Hawaii Thermal Power Company	Towne	E.B. Towne
Lake	Lake City Geothermal I, L.P.	TRMOG	Thermogenics Inc.
Leisk	Joseph A. Leisek	UNION	Union Oil Company of California
Magpo	Magma Power Company	USGS	United States Geological Survey
MSR	MSR Public Power Agency	*	Planned wells

Appendix 5.2 Distribution of wells by type and operating company in The Geysers

Key: CLT = Commercial Low Temperature (30°C to 100°C), DST = Development Steam (> 100°C), EST = Exploratory Steam, INJ = injection, NLT = Non-commercial - Low Temperature (30°C to 100°C), TG = Temperature gradient, WW = water wells.

	Confidential								Unconfidential								
Operator	CLT	DST	EST	INJ	NLT	TG	WW	Total	CLT	DST	EST	INJ	NLT	TG	WW	Total	Grand Total
Amax	0	0	0	0	0	0	0	0	0	0	0	0	0	1	0	1	1
Andar	0	0	0	0	0	0	0	0	0	0	2	0	0	38	1	41	41
CCPA	0	8	0	0	0	0	0	8	0	14	1	3	0	4	0	22	30
CGC	0	7	0	1	0	0	0	8	0	85	0	7	0	0	0	92	100
Chevron	0	0	0	0	0	0	0	0	0	0	1	0	0	22	0	23	23
DWR	0	11	0	0	0	0	0	11	0	17	0	1	0	0	0	18	29
Earth	0	0	0	0	0	0	0	0	0	0	2	0	0	0	0	2	2
EEI	0	0	0	0	0	0	0	0	1	0	0	0	0	0	0	1	1
FMRP	0	1	0	0	0	7	0	8	0	0	0	0	0	104	0	104	112
GEO	0	5	0	0	0	1	0	6	0	33	2	2	0	125	1	163	169
GEP	0	3	1	0	0	0	0	4	0	5	0	1	0	0	0	6	10
Getty	0	0	0	0	0	0	0	0	0	0	1	0	0	0	0	1	1
GKI	0	0	0	0	0	0	0	0	0	0	1	0	0	0	0	1	1
Grace	0	0	0	0	0	0	0	0	0	0	0	0	0	2	0	2	2
Hawaii	0	0	0	0	0	0	0	0	0	0	1	0	0	0	0	1	1
Lake	0	0	0	0	0	0	0	0	3	0	0	0	0	0	0	4	4
Leisk	0	0	0	0	0	0	0	0	0	0	0	0	0	4	0	4	4
Magpo	0	0	0	0	0	0	0	0	0	0	1	0	0	0	0	1	1
MCR	0	0	0	0	0	0	0	0	0	1	2	0	0	0	0	3	3
MSR	0	0	0	0	0	0	0	0	0	0	1	0	0	0	0	1	1
NCPA	0	84	0	6	0	0	0	90	0	1	1	0	0	0	0	2	92
OXY	0	0	0	0	0	0	0	0	0	0	4	0	0	0	0	4	4
Republic	0	0	2	0	0	2	0	4	0	0	2	0	0	15	0	17	21
RESFL	0	0	0	0	0	0	0	0	0	0	0	0	0	7	0	7	7
SANFE	0	0	0	0	0	0	0	0	0	0	0	0	0	3	0	3	3
SBGPC	0	0	0	0	0	0	0	0	0	0	1	0	0	0	0	1	1
SCPD	0	0	0	0	1	0	0	1	0	0	0	0	0	0	0	0	1
Shell	0	0	0	0	0	12	0	12	0	0	2	0	0	25	0	27	39
Silver	0	36	0	2	0	0	0	38	0	0	0	0	0	0	0	0	38
SMI	1	0	0	0	0	0	0	1	0	0	0	0	0	0	0	0	1
SOUPC	0	0	0	0	0	0	0	0	0	0	1	0	0	0	0	1	1
SRGC	0	2	0	0	0	0	0	2	0	6	3	2	0	9	0	20	22
SUNED	0	0	0	0	0	0	0	0	0	0	0	0	0	3	0	3	3
Therm	0	0	0	0	0	0	0	0	0	0	0	0	0	1	0	1	1
Towne	0	0	0	0	0	0	0	0	0	0	1	0	0	0	0	1	1
TRMOG	0	0	0	0	0	0	0	0	0	1	0	0	0	0	0	1	1
UNION	0	64	0	5	0	14	0	83	0	291	1	26	0	155	0	473	556
USGS	0	0	0	0	0	1	0	1	0	0	0	0	0	0	0	0	1
*	0	0	0	0	0	0	0	2	0	0	0	0	0	0	0	240	242
Totals	1	221	3	14	1	37	0	279	4	454	31	42	0	518	2	1292	1571

Appendix 5.3 Distribution of production, injection and production/injection wells in The Geysers

Key to well codes: ACTV = active, ABDN = abandoned, CANC = cancelled, SUSP = suspended, PROP = proposed.

Operator	Production (Got Histories)		Production (Missing Histories)					Injection (Got Histories)		Injection (Missing Histories)		Combination (Got histories)	
	Active	Inactive	ACTV	ABDN	CANC	SUSP	PROP	Active	Inactive	ACTV	ABDN	Active	Inactive
Amax	0	0	0	0	0	0	0	0	0	0	0	0	0
Andar	0	0	0	2	0	0	0	0	0	0	0	0	0
CCPA	15	0	4	2	2	0	0	2	1	0	0	0	0
CGC	81	6	2	0	0	0	1	3	0	1	0	6	0
Chevron	0	0	0	1	0	0	0	0	0	0	0	0	0
DWR	9	8	0	0	9	1	1	1	0	0	0	0	0
Earth	0	0	0	2	0	0	0	0	0	0	0	0	0
EEI	0	0	0	0	0	0	0	0	0	0	0	0	0
FMRP	0	0	0	0	1	0	0	0	0	0	0	0	0
GEO	12	14	0	9	5	0	0	2	0	0	0	0	0
GEP	4	0	4	0	0	0	0	2	0	0	0	0	0
Getty	0	0	0	1	0	0	0	0	0	0	0	0	0
GKI	0	0	0	1	0	0	0	0	0	0	0	0	0
Grace	0	0	0	0	0	0	0	0	0	0	0	0	0
Hawaii	0	0	0	1	0	0	0	0	0	0	0	0	0
Lake	0	0	0	0	0	0	0	0	0	0	0	0	0
Leisk	0	0	0	0	0	0	0	0	0	0	0	0	0
Magpo	0	0	0	1	0	0	0	0	0	0	0	0	0
MCR	0	1	0	2	0	0	0	0	0	0	0	0	0
MSR	0	0	0	1	0	0	0	0	0	0	0	0	0
NCPA	0	0	76	8	0	0	2	0	0	6	0	0	0
OXY	0	0	0	1	3	0	0	0	0	0	0	0	0
Republic	0	0	0	2	0	0	2	0	0	0	0	0	0
RESFL	0	0	0	0	0	0	0	0	0	0	0	0	0
SANFE	0	0	0	0	0	0	0	0	0	0	0	0	0
SBGPC	0	0	0	1	0	0	0	0	0	0	0	0	0
SCPD	0	0	0	0	0	0	0	0	0	0	0	0	0
Shell	0	0	0	2	0	0	0	0	0	0	0	0	0
Silver	0	0	35	0	0	0	1	0	0	2	0	0	0
SMI	0	0	0	0	0	0	0	0	0	0	0	0	0
SOUPC	0	0	0	1	0	0	0	0	0	0	0	0	0
SRGC	1	5	0	4	1	0	0	2	0	0	0	0	0
SUNED	0	0	0	0	0	0	0	0	0	0	0	0	0
Therm	0	0	0	0	0	0	0	0	0	0	0	0	0
Towne	0	0	0	1	0	0	0	0	0	0	0	0	0
TRMOG	0	0	0	1	0	0	0	0	0	0	0	0	0
UNION	215	56	51	28	4	1	3	12	9	5	0	3	0
USGS	0	0	0	0	0	0	0	0	0	0	0	0	0
*	0	0	0	0	0	0	0	0	0	0	0	0	0
Totals	337	90	172	72	25	2	10	24	10	14	0	9	0

Appendix 5.4 Column codes for the D.O.G.G.R. data

Column #	Column data	Description
1	Segment ID (API Number)	Unique 8 digit number assigned by the D.O.G.G.R. for the well
2	Operator Code	Code for the company operating the well
3	Pool Code	Which pool the well is situated; in this case GEYSR, for The Geysers
4	District	District code; typically = 3
5	Confidential	Is this well history confidential? Yes / No
6	Mineral Rights	Either P (private) or S (state)
7	Year Original Hole Drilled	
8	Section Number	Location
9	Township Number	Location
10	Township Base	
11	Range Number	Location
12	Range Base	
13	Base Meridian	
14	Lease Name	Name of the well
15	Well Number	
16	Redrill Number	
17	Year	Report year.
18	Month	Report month
19	Status	ABDN = abandoned; CONV = converted from a producing well to an injection well or vice versa; TEST = well tested for production; BLOW = well was flowed for mechanical purposes; SHTN = well did not produce commercial steam; PROD = well produced commercial steam.
20	Well Type	DI = injection & production well (dual purpose); ST= steam well; SW = steam well with minor associated water; GS = groundwater source well
21	Days	Number of calendar days when the well was producing commercial quantities of steam
22	Gross Steam	Total mass in 10^3 kg of steam produced during the report month.
23	Gross Water	Total mass in 10^3 kg of water produced during the report month.
24	Gross Inject	Total mass in 10^3 kg of fluid injected during the report month.
25	TDS	Total dissolved solids in 10^3 parts per million (injection fluids only)
26	Density	Density of injected fluids in 10^3 kg / m^3
27	Stability Test	T = one or more tests during the month S = well produced steam / water or was injected water for 15 days or more during the report month N = well was shut down for 15 days or more during the report month & not tested
28	Steam Rate	Instantaneous steam production rate recorded during a period of stable conditions in 10^3 kg / hour
29	Water Rate	Instantaneous water production rate recorded during a period of stable conditions in 10^3 kg / hour
30	Injection Rate	Instantaneous water injection rate recorded during a period of stable conditions in 10^3 kg / hour
31	Temperature	Instantaneous wellhead temperature recorded during a period of stable conditions in ^{0}C
32	Pressure	Instantaneous wellhead pressure recorded during a period of stable conditions in Bars
33	Designate	Designated power station for the well
34	Total Steam	Total steam to the power station in 10^3 kg for the report month
35	Total Fluid	Total fluid to the power station in 10^3 kg for the report month
36	Non-condensible	Total weight % of non-condensible gases of the combined fluids in 10^3 kg / m^3

Appendix 5.5 Well database based on D.O.G.G.R. licences list and open record.

Key: API number = Unique 8 digit number assigned by the D.O.G.G.R. for the well, Operator Company = owner of the well, Confidential = is the well confidential ? (yes/no). Well status; ACTV = active, ABDN = abandoned, BLOW = blowout, PROP = Proposed, CANC = cancelled, SUSP = suspended. Activity 1989-94; PROD = production well, INJ = injection well, NA = not active, SUSP = suspended, BLOW = blowout, SHTN = shut down.

Surface locations of wells are given in latitude and longitude. Only DST, EST and INJ wells within the geothermal field have been located using the D.O.G.G.R. map.

API number	Operator Company	Confid -ential?	Lease Name	Well Number	Well Status	Well Type	Latitude	Longitude	Got History?	Activity 1989-1994
03390001	CGC	N	McKinley	1	ACTV	DST	38.774905	-122.718484	Yes	PROD
03390002	SRGC	N	McKinley	2	ABDN	DST	38.773712	-122.717401	Yes	NA
03390003	CGC	N	McKinley	3	ACTV	DST	38.771984	-122.717260	Yes	PROD
03390004	CGC	N	McKinley	4	ACTV	DST	38.770763	-122.718424	Yes	PROD
03390005	CGC	N	Thorne	1	ACTV	DST	38.773595	-122.722492	Yes	PROD
03390006	EARTH	N	Bradley Mining	1	ABDN	EST	0.000000	0.000000		
03390007	EARTH	N	Bradley Mining	2	ABDN	EST	0.000000	0.000000		
03390008	HAWAI	N	Clear Lake	1	ABDN	EST	0.000000	0.000000		
03390009	SRGC	N	Bianchi	1	ABDN	DST	38.786782	-122.709751	Yes	NA
03390010	SOUPC	N	Davies	1	ABDN	EST	38.770000	-122.690100		
03390011	SBGPC	N	Sulphur Bank	1	ABDN	EST	0.000000	0.000000		
03390012	TOWNE	N	Sullivan	1	ABDN	EST	0.000000	0.000000		
03390013	GETTY	N	Kettenhofen	1	ABDN	EST	0.000000	0.000000		
03390014	SRGC	N	McKinley	5	ABDN	INJ	38.779956	-122.719860	Yes	INJ; ABDN 2/93
03390015	CGC	N	MLM	1	ACTV	INJ	38.772278	-122.712085	Yes	PROD 1/89-6/94; INJ 8/94-1/95
03390016	SRGC	N	McKinley	6	ABDN	DST	38.772334	-122.717375	Yes	NA
03390017	CGC	N	D & V	A-1	ACTV	DST	38.773496	-122.722500	Yes	PROD
03390018	CGC	N	Abel	1	ACTV	DST	38.778040	-122.714629	Yes	PROD
03390019	UNION	Y	NE Geysers Unit	1	SUSP	DST	38.823656	-122.756039		
03390020	UNION	N	Horner St 4596	1	ABDN	DST	38.831458	-122.783535	Yes	NA
03390021	CGC	N	Thorne	3	ACTV	DST	38.775240	-122.723812	Yes	PROD
03390022	SRGC	N	McKinley	8	ABDN	DST	38.776574	-122.717578	Yes	NA
03390023	CGC	N	Davies Estate	1	ACTV	DST	38.767479	-122.698237	Yes	SHTN
03390024	CGC	N	Thorne	5	ACTV	DST	38.778875	-122.722580	Yes	PROD
03390025	CGC	N	Thorne	6	ACTV	DST	38.780041	-122.719869	Yes	PROD
03390026	*	N	*	*	CANC	*	0.000000	0.000000		
03390027	CGC	N	Barrows	1	ABDN	INJ	38.764787	-122.709567	Yes	PROD 1/89-9/90; INJ 10/90 - 10/94)
03390028	*	N	*	*	CANC	*	0.000000	0.000000		
03390029	SHELL	N	Bounsall	1	ABDN	EST	0.000000	0.000000		
03390030	SRGC	N	Davies Estate	2	ABDN	DST	38.762395	-122.673817	Yes	NA
03390031	*	N	*	*	CANC	*	0.000000	0.000000		
03390032	*	N	*	*	CANC	*	0.000000	0.000000		
03390033	DWR	Y	Francisco	1-5	SUSP	DST	38.841802	-122.771350		
03390034	CGC	N	CA-958	76-35	ACTV	DST	38.764745	-122.709472	Yes	PROD
03390035	MAGPO	N	Magma-Watson	1	ABDN	EST	0.000000	0.000000		
03390036	CGC	Y	Davies Estate	3	ACTV	DST	38.765980	-122.682363	Yes	NA

Appendix 5 - well data

API number	Operator Company	Confid -ential?	Lease Name	Well Number	Well Status	Well Type	Latitude	Longitude	Got History?	Activity 1989-1994
03390037	GEO	N	BJ	1	ABDN	EST	0.000000	0.000000	Yes	NA
03390038	UNION	N	Jorgensen	1	ABDN	DST	38.930284	-122.694837	Yes	NA
03390039	CHEV	N	RM	8A	ABDN	TG	0.000000	0.000000		
03390040	FMRP	N	NG	1	ABDN	TG	0.000000	0.000000		
03390041	FMRP	N	NG	5	ABDN	TG	0.000000	0.000000		
03390042	GEO	N	NG	9	ABDN	TG	0.000000	0.000000		
03390043	FMRP	N	NG	2	ABDN	TG	0.000000	0.000000		
03390044	FMRP	N	NG	3	ABDN	TG	0.000000	0.000000		
03390045	GEO	N	NG	4	ABDN	TG	0.000000	0.000000		
03390046	CHEV	N	Dry Creek	1	ABDN	EST	38.737348	-122.662404		
03390047	*	N	*	*	CANC	*	0.000000	0.000000		
03390048	CGC	N	PDC	1	ACTV	DST	38.792291	-122.726775	Yes	PROD
03390049	DWR	N	Francisco	2-5	ACTV	DST	38.841300	-122.770755	Yes	PROD; SHTN 2/91
03390050	FMRP	N	HS	11	ABDN	TG	0.000000	0.000000		
03390051	FMRP	N	HS	12	ABDN	TG	0.000000	0.000000		
03390052	FMRP	N	HS	13	ABDN	TG	0.000000	0.000000		
03390053	FMRP	N	HS	14	ABDN	TG	0.000000	0.000000		
03390054	FMRP	N	HS	15	ABDN	TG	0.000000	0.000000		
03390055	FMRP	N	HS	16	ABDN	TG	0.000000	0.000000		
03390056	FMRP	N	NG	32	ABDN	TG	0.000000	0.000000		
03390057	*	N	*	*	CANC	*	0.000000	0.000000		
03390058	SRGC	Y	Bianchi	2	ABDN	DST	38.790727	-122.709938		
03390059	CGC	N	MLM	2	ACTV	DST	38.777746	-122.714420	Yes	PROD
03390060	NCPA	Y	CA-949	17A-1	ACTV	DST	38.749128	-122.703694		
03390061	*	N	*	*	CANC	*	0.000000	0.000000		
03390062	*	N	*	*	CANC	*	0.000000	0.000000		
03390063	CGC	N	CA-1862	26-27	ACTV	DST	38.777173	-122.735225	Yes	SHTN
03390064	*	N	*	*	CANC	*	0.000000	0.000000		
03390065	*	N	*	*	CANC	*	0.000000	0.000000		
03390066	ANDAR	N	TG	52	ABDN	TG	0.000000	0.000000		
03390067	ANDAR	N	TG	53	ABDN	TG	0.000000	0.000000		
03390068	*	N	*	*	CANC	*	0.000000	0.000000		
03390069	*	N	*	*	CANC	*	0.000000	0.000000		
03390070	*	N	*	*	CANC	*	0.000000	0.000000		
03390071	*	N	*	*	CANC	*	0.000000	0.000000		
03390072	*	N	*	*	CANC	*	0.000000	0.000000		
03390073	*	N	*	*	CANC	*	0.000000	0.000000		
03390074	ANDAR	N	TG	60	ABDN	TG	0.000000	0.000000		
03390075	ANDAR	N	TG	61	ABDN	TG	0.000000	0.000000		
03390076	ANDAR	N	TG	62	ABDN	TG	0.000000	0.000000		
03390077	ANDAR	N	TG	63	ABDN	TG	0.000000	0.000000		
03390078	ANDAR	N	TG	64	ABDN	TG	0.000000	0.000000		
03390079	REPUB	N	HU	1	ABDN	TG	0.000000	0.000000		
03390080	REPUB	N	HU	2	ABDN	TG	0.000000	0.000000		
03390081	REPUB	N	HU	3	ABDN	TG	0.000000	0.000000		
03390082	REPUB	N	HU	4	ABDN	TG	0.000000	0.000000		
03390083	REPUB	N	HU	5	ABDN	TG	0.000000	0.000000		
03390084	CGC	N	CA-956A	73-34	ACTV	INJ	38.768392	-122.723964	Yes	PROD 1/89-9/89; INJ 10/89-12/94

Appendix 5 - well data

API number	Operator Company	Confid -ential?	Lease Name	Well Number	Well Status	Well Type	Latitude	Longitude	Got History?	Activity 1989-1994
03390085	RESFL	N		1	ABDN	TG	0.000000	0.000000		
03390086	RESFL	N		2	ABDN	TG	0.000000	0.000000		
03390087	RESFL	N		3	ABDN	TG	0.000000	0.000000		
03390088	RESFL	N		3A	ABDN	TG	0.000000	0.000000		
03390089	*	N	*	*	CANC	*	0.000000	0.000000		
03390090	RESFL	N		4A	ABDN	TG	0.000000	0.000000		
03390091	RESFL	N		5	ABDN	TG	0.000000	0.000000		
03390092	RESFL	N		6	ABDN	TG	0.000000	0.000000		
03390093	*	N	*	*	CANC	*	0.000000	0.000000		
03390094	SUNED	N		237611	ABDN	TG	0.000000	0.000000		
03390095	SUNED	N		237612	ABDN	TG	0.000000	0.000000		
03390096	SUNED	N		237613	ABDN	TG	0.000000	0.000000		
03390097	REPUB	N	Bouscal	1A	ABDN	EST	0.000000	0.000000		
03390098	CGC	N	D & V	A-2	ACTV	DST	38.770500	-122.728200	Yes	PROD
03390099	CGC	Y	Sullivan & Lodge	1	ACTV	DST	38.794262	-122.719971	Yes	NA
03390100	NCPA	Y	CA-949	17-1	ACTV	DST	38.749230	-122.703807		
03390101	NCPA	Y	CA-949	38-1	ABDN	DST	38.747553	-122.698739		
03390102	GEO	N	H	1	ABDN	TG	0.000000	0.000000		
03390103	FMRP	N	H	2	ABDN	TG	0.000000	0.000000		
03390104	GEO	N	H	3	ABDN	TG	0.000000	0.000000		
03390105	GEO	N	H	4	ABDN	TG	0.000000	0.000000		
03390106	GEO	N	H	5	ABDN	TG	0.000000	0.000000		
03390107	GEO	N	H	6	ABDN	TG	0.000000	0.000000		
03390108	GEO	N	H	7	ABDN	TG	0.000000	0.000000		
03390109	GEO	N	H	8	ABDN	TG	0.000000	0.000000		
03390110	GEO	N	H	9	ABDN	TG	0.000000	0.000000		
03390111	GEO	N	H	10	ABDN	TG	0.000000	0.000000		
03390112	GEO	N	H	11	ABDN	TG	0.000000	0.000000		
03390113	GEO	N	H	12	ABDN	TG	0.000000	0.000000		
03390114	GEO	N	H	13	ABDN	TG	0.000000	0.000000		
03390115	GEO	N	H	14	ABDN	TG	0.000000	0.000000		
03390116	GEO	N	H	15	ABDN	TG	0.000000	0.000000		
03390117	GEO	N	H	16	ABDN	TG	0.000000	0.000000		
03390118	*	N	*	*	CANC	*	0.000000	0.000000		
03390119	GEO	N	HS	1	ABDN	TG	0.000000	0.000000		
03390120	GEO	N	HS	2	ABDN	TG	0.000000	0.000000		
03390121	GEO	N	HS	3	ABDN	TG	0.000000	0.000000		
03390122	GEO	N	HS	4	ABDN	TG	0.000000	0.000000		
03390123	GEO	N	HS	5	ABDN	TG	0.000000	0.000000		
03390124	GEO	N	HS	6	ABDN	TG	0.000000	0.000000		
03390125	GEO	N	HS	7	ABDN	TG	0.000000	0.000000		
03390126	FMRP	N	HS	8	ABDN	TG	0.000000	0.000000		
03390127	GEO	N	HS	9	ABDN	TG	0.000000	0.000000		
03390128	GEO	N	HS	10	ABDN	TG	0.000000	0.000000		
03390129	FMRP	N	T	1	ABDN	TG	0.000000	0.000000		
03390130	FMRP	N	T	2	ABDN	TG	0.000000	0.000000		
03390131	FMRP	N	T	3	ABDN	TG	0.000000	0.000000		
03390132	FMRP	N	T	4	ABDN	TG	0.000000	0.000000		

Appendix 5 - well data

API number	Operator Company	Confid -ential?	Lease Name	Well Number	Well Status	Well Type	Latitude	Longitude	Got History?	Activity 1989-1994
03390133	FMRP	N	T	5	ABDN	TG	0.000000	0.000000		
03390134	FMRP	N	T	6	ABDN	TG	0.000000	0.000000		
03390135	FMRP	N	T	7	ABDN	TG	0.000000	0.000000		
03390136	FMRP	N	T	8	ABDN	TG	0.000000	0.000000		
03390137	CHEV	N	MSH	1	ABDN	TG	0.000000	0.000000		
03390138	CHEV	N	MSH	3	ABDN	TG	0.000000	0.000000		
03390139	CHEV	N	MSH	4	ABDN	TG	0.000000	0.000000		
03390140	CHEV	N	MSH	5	ABDN	TG	0.000000	0.000000		
03390141	CHEV	N	MSH	6	ABDN	TG	0.000000	0.000000		
03390142	CHEV	N	MSH	7	ABDN	TG	0.000000	0.000000		
03390143	CHEV	N	MSH	8	ABDN	TG	0.000000	0.000000		
03390144	REPUB	N	Boggs	77-1	ABDN	TG	0.000000	0.000000		
03390145	*	N	*	*	CANC	*	0.000000	0.000000		
03390146	*	N	*	*	CANC	*	0.000000	0.000000		
03390147	MCR	N	Newfield	1-33	ABDN	EST	38.852642	-122.747261		
03390148	SHELL	N	Heat Hole	5	ABDN	TG	0.000000	0.000000		
03390149	SHELL	N	Heat Hole	6	ABDN	TG	0.000000	0.000000		
03390150	SHELL	N	Heat Hole	8	ABDN	TG	0.000000	0.000000		
03390151	SHELL	N	Heat Hole	9	ABDN	TG	0.000000	0.000000		
03390152	SHELL	Y	Heat Hole	25	ABDN	TG	0.000000	0.000000		
03390153	UNION	N	LC	75-6	ABDN	TG	0.000000	0.000000		
03390154	UNION	N	LC	75-7	ABDN	TG	0.000000	0.000000		
03390155	UNION	N	LC	75-8A	ABDN	TG	0.000000	0.000000		
03390156	UNION	N	LC	75-9	ABDN	TG	0.000000	0.000000		
03390157	UNION	N	LC	75-11	ABDN	TG	0.000000	0.000000		
03390158	UNION	N	LC	75-13	ABDN	TG	0.000000	0.000000		
03390159	UNION	N	LC	75-15	ABDN	TG	0.000000	0.000000		
03390160	UNION	N	LC	75-17	ABDN	TG	0.000000	0.000000		
03390161	AMAX	N	L	1	ABDN	TG	0.000000	0.000000		
03390162	SRGC	N	Borax Lake	7-1	ABDN	EST	0.000000	0.000000		
03390163	NCPA	Y	CA-949	38A-1	ABDN	DST	38.747561	-122.698863		
03390164	*	N	*	*	CANC	*	0.000000	0.000000		
03390165	*	N	*	*	CANC	*	0.000000	0.000000		
03390166	REPUB	Y	Giusti	1	CANC		0.000000	0.000000		
03390167	ANDAR	N	TG	17	ACTV	WW	0.000000	0.000000		
03390168	ANDAR	N	Klau Mines	K-1A	ABDN	EST	38.747300	-122.698500		
03390169	*	N	*	*	CANC	*	0.000000	0.000000		
03390170	*	N	*	*	CANC	*	0.000000	0.000000		
03390171	UNION	N	Binkley Rch Unit	1	ACTV	DST	38.842764	-122.801049	Yes	PROD
03390172	ANDAR	N	TG	65	ACTV	TG	0.000000	0.000000		
03390173	FMRP	N	K	1	ABDN	TG	0.000000	0.000000		
03390174	FMRP	N	K	2	ABDN	TG	0.000000	0.000000		
03390175	FMRP	N	K	3	ABDN	TG	0.000000	0.000000		
03390176	FMRP	N	K	4	ABDN	TG	0.000000	0.000000		
03390177	*	N	*	*	CANC	*	0.000000	0.000000		
03390178	*	N	*	*	CANC	*	0.000000	0.000000		
03390179	FMRP	N	K	7	ABDN	TG	0.000000	0.000000		
03390180	FMRP	N	K	8	ABDN	TG	0.000000	0.000000		

Appendix 5 - well data

API number	Operator Company	Confid -ential?	Lease Name	Well Number	Well Status	Well Type	Latitude	Longitude	Got History?	Activity 1989-1994
03390181	FMRP	N	K	9	ABDN	TG	0.000000	0.000000		
03390182	FMRP	N	K	10	ABDN	TG	0.000000	0.000000		
03390183	*	N	*	*	CANC	*	0.000000	0.000000		
03390184	*	N	*	*	CANC	*	0.000000	0.000000		
03390185	*	N	*	*	CANC	*	0.000000	0.000000		
03390186	UNION	N	NE Geysers Unit	2	ABDN	DST	38.816148	-122.746821	Yes	NA
03390187	*	N	*	*	CANC	*	0.000000	0.000000		
03390188	CGC	N	Thorne	7	ABDN	INJ	38.777800	-122.714500	Yes	INJ
03390189	ANDAR	N	TG	17B	ABDN	TG	0.000000	0.000000		
03390190	REPUB	N	Robbins	78-1	ABDN	TG	0.000000	0.000000		
03390191	REPUB	N	Barceloux	78-2	ABDN	TG	0.000000	0.000000		
03390192	REPUB	N	Barceloux	78-3	ABDN	TG	0.000000	0.000000		
03390193	REPUB	N	Barceloux	78-4	ABDN	TG	0.000000	0.000000		
03390194	CGC	N	Davies St 5206	1	ACTV	DST	38.763100	-122.692510	Yes	PROD
03390195	REPUB	N	Bouscal	1	ABDN	EST	0.000000	0.000000		
03390196	FMRP	N	KX	8	ABDN	TG	0.000000	0.000000		
03390197	FMRP	N	KX	9	ABDN	TG	0.000000	0.000000		
03390198	FMRP	N	KX	10	ABDN	TG	0.000000	0.000000		
03390199	*	N	*	*	CANC	*	0.000000	0.000000		
03390200	*	N	*	*	CANC	*	0.000000	0.000000		
03390201	MCR	N	Coleman	1-5	ABDN	DST	38.838113	-122.771000	Yes	NA
03390202	FMRP	N	Hannah Strat	1	ABDN	TG	0.000000	0.000000		
03390203	FMRP	N	PB	1	ABDN	TG	0.000000	0.000000		
03390204	FMRP	N	PB	2	ABDN	TG	0.000000	0.000000		
03390205	FMRP	N	PB	3	ABDN	TG	0.000000	0.000000		
03390206	*	N	*	*	CANC	*	0.000000	0.000000		
03390207	UNION	N	BG	73-18A	ABDN	TG	0.000000	0.000000		
03390208	UNION	N	BG	73-29	ABDN	TG	0.000000	0.000000		
03390209	UNION	N	BG	73-30	ABDN	TG	0.000000	0.000000		
03390210	UNION	N	LC	74-12	ABDN	TG	0.000000	0.000000		
03390211	UNION	N	LC	75-1	ABDN	TG	0.000000	0.000000		
03390212	UNION	N	LC	75-4	ABDN	TG	0.000000	0.000000		
03390213	FMRP	Y	CRS	7	ACTV	TG	0.000000	0.000000		
03390214	FMRP	Y	CRS	8	ACTV	TG	0.000000	0.000000		
03390215	*	N	*	*	CANC	*	0.000000	0.000000		
03390216	FMRP	N	DE	1	ABDN	TG	0.000000	0.000000		
03390217	FMRP	N	DE	2	ABDN	TG	0.000000	0.000000		
03390218	FMRP	N	DE	3	ABDN	TG	0.000000	0.000000		
03390219	SRGC	N	DE	4	ABDN	TG	0.000000	0.000000		
03390220	FMRP	N	DE	5	ABDN	TG	0.000000	0.000000		
03390221	FMRP	N	CRS	9	ABDN	TG	0.000000	0.000000		
03390222	FMRP	N	BL	1	ABDN	TG	0.000000	0.000000		
03390223	FMRP	N	BL	2	ABDN	TG	0.000000	0.000000		
03390224	FMRP	N	BL	3	ABDN	TG	0.000000	0.000000		
03390225	SHELL	N	Heat Hole	15	ABDN	TG	0.000000	0.000000		
03390226	SHELL	N	Heat Hole	3	ABDN	TG	0.000000	0.000000		
03390227	SHELL	N	Heat Hole	4	ABDN	TG	0.000000	0.000000		
03390228	SHELL	N	Heat Hole	31	ABDN	TG	0.000000	0.000000		

Appendix 5 - well data

API number	Operator Company	Confid -ential?	Lease Name	Well Number	Well Status	Well Type	Latitude	Longitude	Got History?	Activity 1989-1994
03390229	SHELL	Y	Heat Hole	29	ABDN	TG	0.000000	0.000000		
03390230	SHELL	Y	Heat Hole	33	ABDN	TG	0.000000	0.000000		
03390231	SHELL	Y	Heat Hole	47	ABDN	TG	0.000000	0.000000		
03390232	*	N	*	*	CANC	*	0.000000	0.000000		
03390233	CGC	N	D & V	A-3	ACTV	DST	38.775200	-122.728700	Yes	PROD
03390234	CGC	N	CA-1862	57-27	ACTV	DST	38.775300	-122.728600	Yes	PROD
03390235	FMRP	N	Big Canyon Test	1	ABDN	TG	0.000000	0.000000		
03390236	*	N	*	*	CANC	*	0.000000	0.000000		
03390237	*	N	*	*	CANC	*	0.000000	0.000000		
03390238	*	N	*	*	CANC	*	0.000000	0.000000		
03390239	*	N	*	*	CANC	*	0.000000	0.000000		
03390240	UNION	N	NW Geysers	5	ABDN	TG	0.000000	0.000000		
03390241	*	N	*	*	CANC	*	0.000000	0.000000		
03390242	FMRP	Y	120909	1	ABDN	TG	0.000000	0.000000		
03390243	FMRP	Y	120925	1	ABDN	TG	0.000000	0.000000		
03390244	FMRP	N	Hannah Strat	2	ABDN	TG	0.000000	0.000000		
03390245	FMRP	Y	131010	1	ABDN	TG	0.000000	0.000000		
03390246	*	N	*	*	CANC	*	0.000000	0.000000		
03390247	FMRP	N	130708	1	ABDN	TG	0.000000	0.000000		
03390248	FMRP	N	130709	1	ABDN	TG	0.000000	0.000000		
03390249	CGC	N	Barrows	3	ACTV	DST	38.763100	-122.697500	Yes	PROD
03390250	NCPA	N	Cobb Valley	1	ABDN	EST	38.857605	-122.774109		
03390251	CGC	N	CA-956A	86-34	ACTV	DST	38.762100	-122.715200	Yes	PROD
03390252	OXY	N	McLeskey	1	CANC	EST	0.000000	0.000000		
03390253	OXY	N	McLeskey	2	CANC	EST	0.000000	0.000000		
03390254	OXY	N	Neasham	1	ABDN	EST	0.000000	0.000000		
03390255	OXY	N	Neasham	2	CANC	EST	0.000000	0.000000		
03390256	SRGC	N	Wilson	1	ABDN	EST	0.000000	0.000000		
03390257	REPUB	Y	Wilson	2	PROP	EST	0.000000	0.000000		
03390258	GKI	N	GKI-Boggs Mtn.	1	ABDN	EST	0.000000	0.000000		
03390259	*	N	*	*	CANC	*	0.000000	0.000000		
03390260	*	N	*	*	CANC	*	0.000000	0.000000		
03390261	GEO	N	GR	1	ABDN	TG	0.000000	0.000000		
03390262	GEO	N	GR	2	ACTV	WW	0.000000	0.000000		
03390263	GEO	N	GR	4	ABDN	TG	0.000000	0.000000		
03390264	GEO	N	GR	6	ABDN	TG	0.000000	0.000000		
03390265	GEO	N	GR	8	ABDN	TG	0.000000	0.000000		
03390266	GEO	N	GR	9	ABDN	TG	0.000000	0.000000		
03390267	GEO	N	GR	10	ABDN	TG	0.000000	0.000000		
03390268	GEO	N	GR	11	ABDN	TG	0.000000	0.000000		
03390269	GEO	N	GR	12	ABDN	TG	0.000000	0.000000		
03390270	GEO	N	GR	14	ABDN	TG	0.000000	0.000000		
03390271	FMRP	N	GR	16	ABDN	TG	0.000000	0.000000		
03390272	*	N	*	*	CANC	*	0.000000	0.000000		
03390273	DWR	N	Francisco	3-5	ACTV	INJ	38.841463	-122.770800	Yes	INJ
03390274	NCPA	Y	CA-949	53-2	ACTV	DST	38.755402	-122.710309		
03390275	*	N	*	*	CANC	*	0.000000	0.000000		
03390276	*	N	*	*	CANC	*	0.000000	0.000000		

Appendix 5 - well data

API number	Operator Company	Confid -ential?	Lease Name	Well Number	Well Status	Well Type	Latitude	Longitude	Got History?	Activity 1989-1994
03390277	UNION	N	NE Geysers Unit	7	ABDN	EST	38.829880	-122.748736		
03390278	UNION	N	NE Geysers Unit	8	ACTV	DST	38.835621	-122.760838	Yes	SHTN
03390279	*	N	*	*	CANC	*	0.000000	0.000000		
03390280	*	N	*	*	CANC	*	0.000000	0.000000		
03390281	*	N	*	*	CANC	*	0.000000	0.000000		
03390282	*	N	*	*	CANC	*	38.756217	-122.709741		NA
03390283	*	N	*	*	CANC	*	0.000000	0.000000		
03390284	SILVR	Y	CA-5637	68-21	ACTV	DST	38.786934	-122.744949		
03390285	CGC	N	CA-1862	82-28	ACTV	DST	38.799500	-122.739500	Yes	PROD
03390286	NCPA	Y	CA-949	53A-2	ACTV	DST	38.755364	-122.710422		
03390287	SRGC	N	Audrey A	1	ABDN	EST	0.000000	0.000000		
03390288	*	N	*	*	CANC	*	0.000000	0.000000		
03390289	*	N	*	*	CANC	*	0.000000	0.000000		
03390290	SILVR	Y	CA-5636	68A-21	ACTV	DST	38.787273	-122.744576		
03390291	CGC	N	Moody Unit	1	ACTV	DST	38.789100	-122.723100	Yes	PROD
03390292	*	N	*	*	CANC	*	0.000000	0.000000		
03390293	*	N	*	*	CANC	*	0.000000	0.000000		
03390294	*	N	*	*	CANC	*	0.000000	0.000000		
03390295	*	N	*	*	CANC	*	0.000000	0.000000		
03390296	*	N	*	*	CANC	*	0.000000	0.000000		
03390297	*	N	*	*	CANC	*	0.000000	0.000000		
03390298	*	N	*	*	CANC	*	0.000000	0.000000		
03390299	*	N	*	*	CANC	*	0.000000	0.000000		
03390300	*	N	*	*	CANC	*	0.000000	0.000000		
03390301	*	N	*	*	CANC	*	0.000000	0.000000		
03390302	CGC	N	CA-958	43-35	ACTV	DST	38.767300	-122.712500	Yes	PROD
03390303	*	N	*	*	CANC	*	0.000000	0.000000		
03390304	FMRP	N	140712	1	ABDN	TG	0.000000	0.000000		
03390305	NCPA	Y	CA-949	72-1	ACTV	DST	38.757013	-122.687733		
03390306	*	N	*	*	CANC	*	0.000000	0.000000		
03390307	*	N	*	*	CANC	*	0.000000	0.000000		
03390308	*	N	*	*	CANC	*	0.000000	0.000000		
03390309	GEO	N	GR	19	ABDN	TG	0.000000	0.000000		
03390310	GEO	N	GR	20	ABDN	TG	0.000000	0.000000		
03390311	*	N	*	*	CANC	*	0.000000	0.000000		
03390312	*	N	*	*	CANC	*	0.000000	0.000000		
03390313	GEO	N	GR	23	ABDN	TG	0.000000	0.000000		
03390314	GEO	N	GR	24	ABDN	TG	0.000000	0.000000		
03390315	*	N	*	*	CANC	*	0.000000	0.000000		
03390316	GEO	N	GR	26	ABDN	TG	0.000000	0.000000		
03390317	*	N	*	*	CANC	*	0.000000	0.000000		
03390318	GEO	N	GR	29	ABDN	TG	0.000000	0.000000		
03390319	GEO	N	GR	30	ABDN	TG	0.000000	0.000000		
03390320	GEO	N	GR	31	ABDN	TG	0.000000	0.000000		
03390321	*	N	*	*	CANC	*	0.000000	0.000000		
03390322	GEO	N	GR	33	ABDN	TG	0.000000	0.000000		
03390323	*	N	*	*	CANC	*	0.000000	0.000000		
03390324	*	N	*	*	CANC	*	0.000000	0.000000		

Appendix 5 - well data

API number	Operator Company	Confid -ential?	Lease Name	Well Number	Well Status	Well Type	Latitude	Longitude	Got History?	Activity 1989-1994
03390325	GEO	N	GR	36	ABDN	TG	0.000000	0.000000		
03390326	*	N	*	*	CANC	*	0.000000	0.000000		
03390327	*	N	*	*	CANC	*	0.000000	0.000000		
03390328	*	N	*	*	CANC	*	0.000000	0.000000		
03390329	GEO	N	GR	40	ABDN	TG	0.000000	0.000000		
03390330	*	N	*	*	CANC	*	0.000000	0.000000		
03390331	*	N	*	*	CANC	*	0.000000	0.000000		
03390332	GEO	N	GR	43	ABDN	TG	0.000000	0.000000		
03390333	GEO	N	GR	44	ABDN	TG	0.000000	0.000000		
03390334	*	N	*	*	CANC	*	0.000000	0.000000		
03390335	GEO	N	GR	46	ABDN	TG	0.000000	0.000000		
03390336	GEO	N	GR	47	ABDN	TG	0.000000	0.000000		
03390337	GEO	N	GR	48	ABDN	TG	0.000000	0.000000		
03390338	*	N	*	*	CANC	*	0.000000	0.000000		
03390339	CGC	N	CA-958	86A-34	ACTV	DST	38.761200	-122.715500	Yes	PROD
03390340	*	N	*	*	CANC	*	0.000000	0.000000		
03390341	*	N	*	*	CANC	*	0.000000	0.000000		
03390342	GEO	N	HS	11A	ABDN	TG	0.000000	0.000000		
03390343	GEO	N	HS	12A	ABDN	TG	0.000000	0.000000		
03390344	CGC	N	CA-958	84-35	ACTV	INJ	38.765500	-122.704100	Yes	INJ
03390345	GEO	N	HS	19	ABDN	TG	0.000000	0.000000		
03390346	GEO	N	HS	20	ABDN	TG	0.000000	0.000000		
03390347	GEO	N	HS	21	ABDN	TG	0.000000	0.000000		
03390348	GEO	N	HS	22	ABDN	TG	0.000000	0.000000		
03390349	*	N	*	*	CANC	*	0.000000	0.000000		
03390350	GEO	N	HS	24	ABDN	TG	0.000000	0.000000		
03390351	GEO	N	HS	25	ABDN	TG	0.000000	0.000000		
03390352	GEO	N	HS	26	ABDN	TG	0.000000	0.000000		
03390353	GEO	N	HS	27	ABDN	TG	0.000000	0.000000		
03390354	GEO	N	HS	28	ABDN	TG	0.000000	0.000000		
03390355	GEO	N	HS	29	ABDN	TG	0.000000	0.000000		
03390356	GEO	N	HS	30	ABDN	TG	0.000000	0.000000		
03390357	GEO	N	HS	31	ABDN	TG	0.000000	0.000000		
03390358	GEO	N	HS	32	ABDN	TG	0.000000	0.000000		
03390359	GEO	N	HS	33	ABDN	TG	0.000000	0.000000		
03390360	*	N	*	*	CANC	*	0.000000	0.000000		
03390361	GEO	N	HS	35	ABDN	TG	0.000000	0.000000		
03390362	*	N	*	*	CANC	*	0.000000	0.000000		
03390363	*	N	*	*	CANC	*	0.000000	0.000000		
03390364	*	N	*	*	CANC	*	0.000000	0.000000		
03390365	GEO	N	LR	3	ABDN	TG	0.000000	0.000000		
03390366	GEO	N	LR	4	ABDN	TG	0.000000	0.000000		
03390367	GEO	N	LR	5	ABDN	TG	0.000000	0.000000		
03390368	GEO	N	LR	6	ABDN	TG	0.000000	0.000000		
03390369	GEO	N	LR	7	ABDN	TG	0.000000	0.000000		
03390370	GEO	N	LR	8	ABDN	TG	0.000000	0.000000		
03390371	GEO	N	LR	9	ABDN	TG	0.000000	0.000000		
03390372	*	N	*	*	CANC	*	0.000000	0.000000		

Appendix 5 - well data

API number	Operator Company	Confid -ential?	Lease Name	Well Number	Well Status	Well Type	Latitude	Longitude	Got History?	Activity 1989-1994
03390373	GEO	N	SEG	2	ABDN	TG	0.000000	0.000000		
03390374	GEO	N	SEG	3	ABDN	TG	0.000000	0.000000		
03390375	GEO	N	SEG	4	ABDN	TG	0.000000	0.000000		
03390376	*	N	*	*	CANC	*	0.000000	0.000000		
03390377	GEO	N	SEG	6	ABDN	TG	0.000000	0.000000		
03390378	*	N	*	*	CANC	*	0.000000	0.000000		
03390379	GEO	N	SEG	8	ABDN	TG	0.000000	0.000000		
03390380	*	N	*	*	CANC	*	0.000000	0.000000		
03390381	GEO	N	SEG	10	ABDN	TG	0.000000	0.000000		
03390382	*	N	*	*	CANC	*	0.000000	0.000000		
03390383	SILVR	Y	CA-5636	74-21	ACTV	INJ	38.793648	-122.743141		
03390384	MCR	N	Tellyer	1-24	ABDN	EST	38.790104	-122.687233		
03390385	*	N	*	*	CANC	*	0.000000	0.000000		
03390386	*	N	*	*	CANC	*	0.000000	0.000000		
03390387	*	N	*	*	CANC	*	0.000000	0.000000		
03390388	*	N	*	*	CANC	*	0.000000	0.000000		
03390389	*	N	*	*	CANC	*	0.000000	0.000000		
03390390	GEO	N	HS	44	ABDN	TG	0.000000	0.000000		
03390391	SILVR	Y	CA-5636	23-22	ACTV	DST	38.795120	-122.735756		
03390392	CGC	N	Barrows	2	ACTV	DST	38.765397	-122.703066	Yes	PROD
03390393	UNION	N	BG	73-12	ABDN	TG	0.000000	0.000000		
03390394	*	N	*	*	CANC	*	0.000000	0.000000		
03390395	*	N	*	*	CANC	*	0.000000	0.000000		
03390396	*	N	*	*	CANC	*	0.000000	0.000000		
03390397	*	N	*	*	CANC	*	0.000000	0.000000		
03390398	*	N	*	*	CANC	*	0.000000	0.000000		
03390399	*	N	*	*	CANC	*	0.000000	0.000000		
03390400	*	N	*	*	CANC	*	0.000000	0.000000		
03390401	*	N	*	*	CANC	*	0.000000	0.000000		
03390402	*	N	*	*	CANC	*	0.000000	0.000000		
03390403	*	N	*	*	CANC	*	0.000000	0.000000		
03390404	*	N	*	*	CANC	*	0.000000	0.000000		
03390405	*	N	*	*	CANC	*	0.000000	0.000000		
03390406	*	N	*	*	CANC	*	0.000000	0.000000		
03390407	*	N	*	*	CANC	*	0.000000	0.000000		
03390408	*	N	*	*	CANC	*	0.000000	0.000000		
03390409	*	N	*	*	CANC	*	0.000000	0.000000		
03390410	*	N	*	*	CANC	*	0.000000	0.000000		
03390411	*	N	*	*	CANC	*	0.000000	0.000000		
03390412	*	N	*	*	CANC	*	0.000000	0.000000		
03390413	*	N	*	*	CANC	*	0.000000	0.000000		
03390414	*	N	*	*	CANC	*	0.000000	0.000000		
03390415	*	N	*	*	CANC	*	0.000000	0.000000		
03390416	*	N	*	*	CANC	*	0.000000	0.000000		
03390417	*	N	*	*	CANC	*	0.000000	0.000000		
03390418	*	N	*	*	CANC	*	0.000000	0.000000		
03390419	*	N	*	*	CANC	*	0.000000	0.000000		
03390420	NCPA	N	Cobb Valley	2	ABDN	DST	38.857128	-122.774757		

Appendix 5 - well data

API number	Operator Company	Confid -ential?	Lease Name	Well Number	Well Status	Well Type	Latitude	Longitude	Got History?	Activity 1989-1994
03390421	UNION	N	NE Geysers Unit	7A	ACTV	DST	38.830012	-122.748704	Yes	SHTN
03390422	CGC	N	MLM	5	ACTV	DST	38.777611	-122.713703	Yes	PROD
03390423	CGC	N	McKinley	9	ACTV	DST	38.777642	-122.713781	Yes	PROD
03390424	UNION	N	High Valley St	39-30	ABDN	DST	38.854439	-122.791863	Yes	NA
03390425	DWR	N	Coleman	1-6	SUSP	DST	38.834765	-122.776562	Yes	SUSP 3/91
03390426	UNION	Y	High Valley St	99-25	ABDN	DST	38.854683	-122.799784		
03390427	SILVR	Y	CA-5636	74A-21	ACTV	INJ	38.783953	-122.743263		
03390428	UNION	N	Tocher	2	ACTV	DST	38.783638	-122.734995	Yes	PROD
03390429	DWR	N	Coleman	2-6	ABDN	DST	38.834726	-122.776703	Yes	PROD; SUSP 3/91
03390430	UNION	N	Tocher	3	ACTV	DST	38.783718	-122.734853	Yes	PROD
03390431	*	N	*	*	CANC	*	0.000000	0.000000		
03390432	*	N	*	*	CANC	*	0.000000	0.000000		
03390433	*	N	*	*	CANC	*	0.000000	0.000000		
03390434	UNION	N	BG	73-12	ABDN	TG	0.000000	0.000000		
03390435	SILVR	Y	CA-5636	23A-22	ACTV	DST	38.794868	-122.735497		
03390436	DWR	N	Coleman	2-5	ABDN	DST	38.838113	-122.771400	Yes	NA
03390437	DWR	N	Coleman	3-6	SUSP	DST	38.834828	-122.776636	Yes	PROD; SUSP 3/91
03390438	ANDAR	N	TG	29	ABDN	TG	0.000000	0.000000		
03390439	SILVR	Y	CA-5636	23B-22	ACTV	DST	38.794628	-122.735474		
03390440	UNION	N	Kelsey Creek St	97-11	ABDN	DST	0.000000	0.000000	Yes	NA
03390441	SILVR	Y	CA-5636	87-21	ACTV	DST	38.788803	-122.739182		
03390442	DWR	N	Coleman	3-5	SUSP	DST	38.838113	-122.771319	Yes	PROD; SUSP 3/91
03390443	DWR	N	Coleman	4-6	SUSP	DST	38.834704	-122.776494	Yes	PROD; SUSP 3/91
03390444	CGC	N	Bianchi	3	ACTV	DST	38.778948	-122.722478	Yes	PROD
03390445	REPUB	Y	McLeskey	1	PROP	EST	0.000000	0.000000		
03390446	SILVR	Y	CA-5636	87A-21	ACTV	DST	38.788948	-122.739433		
03390447	DWR	N	Coleman	4-5	ABDN	DST	38.838176	-122.771514	Yes	PROD; ABDN 4/90
03390448	UNION	N	DX State 4596	52	ACTV	DST	38.821496	-122.767321	Yes	PROD
03390449	CGC	Y	Sprouse	A-1	ACTV	DST	38.775000	-122.745500	Yes	NA
03390450	*	N	*	*	CANC	*	0.000000	0.000000		
03390451	UNION	Y	High Valley St	94-25	ABDN	DST	38.863965	-122.800472		
03390452	UNION	N	71	9	ABDN	TG	0.000000	0.000000		
03390453	UNION	N	71	11	ABDN	TG	0.000000	0.000000		
03390454	UNION	N	71	26	ABDN	TG	0.000000	0.000000		
03390455	UNION	N	71	27	ABDN	TG	0.000000	0.000000		
03390456	UNION	N	71	28	ABDN	TG	0.000000	0.000000		
03390457	UNION	N	71	33	ABDN	TG	0.000000	0.000000		
03390458	UNION	N	71	34	ABDN	TG	0.000000	0.000000		
03390459	SILVR	Y	CA-5636	68B-21	ACTV	DST	38.787231	-122.744751		
03390460	UNION	Y	High Valley St	39A-30	ABDN	DST	38.854387	-122.791803		
03390461	SILVR	Y	CA-5636	68C-21	ACTV	DST	38.787323	-122.745079		
03390462	DWR	N	Coleman	5-6	SUSP	DST	38.834976	-122.775937	Yes	PROD; SUSP 3/91
03390463	CGC	N	Davies Estate	4	ACTV	INJ	38.762800	-122.692510	Yes	INJ
03390464	SILVR	Y	CA-5636	87B-21	ACTV	DST	38.788570	-122.739235		
03390465	UNION	N	DX State 4596	53	ABDN	DST	38.821389	-122.767429		
03390466	SILVR	Y	CA-5636	87C-21	ACTV	DST	38.788803	-122.739182		
03390467	UNION	N	Kelsey Creek St	88-24	ABDN	DST	38.870068	-122.798705	Yes	NA

Appendix 5 - well data

API number	Operator Company	Confid -ential?	Lease Name	Well Number	Well Status	Well Type	Latitude	Longitude	Got History?	Activity 1989-1994
03390468	UNION	N	Kelsey Creek St	82-15	ABDN	DST	38.893823	-122.836626		
03390469	CGC	N	CA-958	43A-35	ACTV	DST	38.767400	-122.712500	Yes	PROD
03390470	*	N	*	*	CANC	*	0.000000	0.000000		
03390471	*	N	*	*	CANC	*	0.000000	0.000000		
03390472	GRACE	N	PR	3	ABDN	TG	0.000000	0.000000		
03390473	GRACE	N	PR	4	ABDN	TG	0.000000	0.000000		
03390474	SILVR	Y	CA-5636	74B-21	ACTV	DST	38.793365	-122.742813		
03390475	*	N	*	*	CANC	*	0.000000	0.000000		
03390476	CGC	N	MLM	4	ACTV	DST	38.766859	-122.712291	Yes	PROD
03390477	UNION	N	NE Geysers Unit	13	ACTV	DST	38.821441	-122.767375	Yes	PROD
03390478	SILVR	Y	CA-5636	74C-21	ACTV	DST	38.793579	-122.743448		
03390479	UNION	N	L'Esperance	1	ABDN	DST	38.842446	-122.782702	Yes	SHTN
03390480	CGC	N	CA-958	43B-35	ACTV	DST	38.767300	-122.712500	Yes	PROD
03390481	*	N	*	*	CANC	*	0.000000	0.000000		
03390482	GEO	N	NWG	2	ABDN	TG	0.000000	0.000000		
03390483	GEO	N	NWG	5	ABDN	TG	0.000000	0.000000		
03390484	UNION	N	California St	92-6	ABDN	DST	38.842586	-122.782711	Yes	PROD
03390485	CGC	N	CA-956A	35-35	ACTV	DST	38.762400	-122.715500	Yes	PROD
03390486	NCPA	Y	CA-949	53B-2	ACTV	DST	38.755339	-122.710227		
03390487	NCPA	Y	CA-949	53C-2	ACTV	DST	38.755306	-122.710327		
03390488	CGC	N	CA-958	35A-35	ACTV	DST	38.762500	-122.715300	Yes	PROD
03390489	*	N	*	*	CANC	*	0.000000	0.000000		
03390490	GEO	N	H	20	ABDN	TG	0.000000	0.000000		
03390491	GEO	N	H	22	ABDN	TG	0.000000	0.000000		
03390492	CGC	N	Barrows	5	ACTV	DST	38.767523	-122.698160	Yes	PROD
03390493	GEO	N	H	21	ABDN	TG	0.000000	0.000000		
03390494	UNION	N	Binkley State	1	ABDN	DST	38.863677	-122.814081	Yes	NA
03390495	CGC	N	Barrows	4	ACTV	DST	38.767507	-122.698252	Yes	PROD; INJ 2/90
03390496	DWR	N	Coleman	5-5	SUSP	DST	38.838209	-122.771613	Yes	PROD; SUSP 3/91
03390497	CGC	N	McKinley	10	ACTV	DST	38.769266	-122.715746	Yes	PROD
03390498	UNION	N	L'Esperance	2	ABDN	DST	38.842723	-122.782719	Yes	PROD
03390499	*	N	*	*	CANC	*	0.000000	0.000000		
03390500	CGC	N	McKinley	11	ACTV	DST	38.769211	-122.715735	Yes	PROD
03390501	DWR	N	Coleman	1A-5	SUSP	DST	38.838113	-122.771500	Yes	SUSP 3/91
03390502	DWR	Y	Coleman	6-6	PROP	DST	38.834900	-122.776636		
03390503	CGC	N	McKinley	12	ACTV	DST	38.769159	-122.715724	Yes	PROD
03390504	*	N	*	*	CANC	*	0.000000	0.000000		
03390505	FMRP	Y	CA-956A	56C-34	CANC	DST	38.762700	-122.736900		
03390506	NCPA	Y	CA-949	22-1	ACTV	DST	38.757103	-122.702300		
03390507	SILVR	Y	CA-5636	87D-21	ACTV	DST	38.782894	-122.739563		
03390508	NCPA	Y	CA-949	22A-1	ACTV	DST	38.757186	-122.702300		
03390509	CGC	N	D & V	A-4	ACTV	DST	38.770306	-122.728234	Yes	PROD
03390510	SILVR	Y	CA-5636	68D-21	ACTV	DST	38.787189	-122.745102		
03390511	NCPA	Y	CA-949	38B-1	ACTV	DST	38.747545	-122.698636		
03390512	DWR	N	Francisco	4-5	SUSP	DST	38.841463	-122.770755	Yes	PROD; SUSP 3/91
03390513	NCPA	Y	CA-949	22B-1	ACTV	INJ	38.757268	-122.702300		
03390514	*	N	*	*	CANC	*	0.000000	0.000000		
03390515	*	N	*	*	CANC	*	0.000000	0.000000		

Appendix 5 - well data

API number	Operator Company	Confid -ential?	Lease Name	Well Number	Well Status	Well Type	Latitude	Longitude	Got History?	Activity 1989-1994
03390516	*	N	*	*	CANC	*	0.000000	0.000000		
03390517	LAKE	N	Ag Park	1	ACTV	CLT	0.000000	0.000000		
03390518	UNION	N	NE Geysers Unit	15	ACTV	DST	38.832083	-122.763455	Yes	PROD
03390519	UNION	N	GD Horner State	9	ACTV	DST	38.832050	-122.763455	Yes	PROD
03390520	DWR	N	Francisco	5-5	SUSP	DST	38.841463	-122.770755	Yes	SUSP 3/91
03390521	UNION	N	NE Geysers Unit	17	ACTV	DST	38.832100	-122.763300	Yes	PROD
03390522	NCPA	Y	CA-949	17B-1	ACTV	DST	38.749370	-122.703978		
03390523	NCPA	Y	CA-949	38C-1	ACTV	DST	38.747553	-122.698760		
03390524	NCPA	Y	CA-949	38D-1	ACTV	DST	38.747561	-122.698884		
03390525	NCPA	Y	CA-949	17C-1	ACTV	DST	38.749425	-122.704084		
03390526	NCPA	Y	CA-949	17D-1	ACTV	DST	38.749463	-122.704183		
03390527	NCPA	Y	CA-949	38E-1	ACTV	DST	38.747570	-122.699008		
03390528	CGC	N	Barrows	6	ACTV	DST	38.765100	-122.710500	Yes	PROD
03390529	NCPA	Y	CA-949	38F-1	ACTV	DST	38.747537	-122.699083		
03390530	NCPA	Y	CA-949	17E-1	PROP	DST	38.749496	-122.704258		
03390531	SRGC	N	CRS	1A	ABDN	TG	0.000000	0.000000		
03390532	SRGC	N	CRS	1B	ABDN	TG	0.000000	0.000000		
03390533	SRGC	N	CRS	2	ABDN	TG	0.000000	0.000000		
03390534	SRGC	N	CRS	3B	ABDN	TG	0.000000	0.000000		
03390535	SRGC	N	CRS	5	ABDN	TG	0.000000	0.000000		
03390536	SRGC	N	CRS	6	ABDN	TG	0.000000	0.000000		
03390537	FMRP	N	BG	3	ABDN	TG	0.000000	0.000000		
03390538	FMRP	N	BG	4	ABDN	TG	0.000000	0.000000		
03390539	FMRP	N	BG	5	ABDN	TG	0.000000	0.000000		
03390540	FMRP	N	BG	6	ABDN	TG	0.000000	0.000000		
03390541	FMRP	N	BG	7	ABDN	TG	0.000000	0.000000		
03390542	FMRP	N	BG	8	ABDN	TG	0.000000	0.000000		
03390543	FMRP	N	BG	9	ABDN	TG	0.000000	0.000000		
03390544	GEO	N	GR	41	ABDN	TG	0.000000	0.000000		
03390545	UNION	N	DX State 4596	87	ACTV	DST	38.821284	-122.767548	Yes	PROD
03390546	NCPA	Y	CA-949	53D-2	ACTV	DST	38.755580	-122.710781		
03390547	NCPA	Y	CA-949	38G-1	ACTV	DST	38.747509	-122.699165		
03390548	LAKE	N	Ag Park	2	ACTV	CLT	0.000000	0.000000		
03390549	NCPA	Y	CA-949	53E-2	ACTV	DST	38.755512	-122.710759		
03390550	GEO	N	LR	10	ABDN	TG	0.000000	0.000000		
03390551	GEO	N	HS	39A	ABDN	TG	0.000000	0.000000		
03390552	NCPA	Y	CA-949	53F-2	ACTV	DST	38.755446	-122.710735		
03390553	LEISK	N	Clearlake	1	ABDN	TG	0.000000	0.000000		
03390554	LEISK	N	Clearlake	2	ABDN	TG	0.000000	0.000000		
03390555	NCPA	Y	CA-949	53G-2	ACTV	DST	38.755377	-122.710713		
03390556	LEISK	N	Clearlake	3	ABDN	TG	0.000000	0.000000		
03390557	LEISK	N	Clearlake	4	ABDN	TG	0.000000	0.000000		
03390558	CGC	N	Davies St 5206	2	ACTV	DST	38.762900	-122.692510	Yes	PROD
03390559	LAKE	N	Ag Park	3	ACTV	CLT	0.000000	0.000000		
03390560	NCPA	Y	CA-949	53H-2	ACTV	DST	38.755309	-122.710692		
03390561	SILVR	Y	CA-5636	23C-22	ACTV	DST	38.794926	-122.735275		
03390562	CGC	N	CA-958	35B-35	ACTV	DST	38.762500	-122.716100	Yes	PROD
03390563	CHEV	N	RM	2	ABDN	TG	0.000000	0.000000		

Appendix 5 - well data

API number	Operator Company	Confid -ential?	Lease Name	Well Number	Well Status	Well Type	Latitude	Longitude	Got History?	Activity 1989-1994
03390564	CHEV	N	RM	5	ABDN	TG	0.000000	0.000000		
03390565	CHEV	N	RM	6	ABDN	TG	0.000000	0.000000		
03390566	CHEV	N	RM	7	ABDN	TG	0.000000	0.000000		
03390567	CHEV	N	RM	8	ABDN	TG	0.000000	0.000000		
03390568	CHEV	N	RM	9	ABDN	TG	0.000000	0.000000		
03390569	CHEV	N	RM	10	ABDN	TG	0.000000	0.000000		
03390570	CHEV	N	RM	10A	ABDN	TG	0.000000	0.000000		
03390571	CHEV	N	RM	11	ABDN	TG	0.000000	0.000000		
03390572	CHEV	N	RM	13	ABDN	TG	0.000000	0.000000		
03390573	CHEV	N	RM	14	ABDN	TG	0.000000	0.000000		
03390574	CHEV	N	RM	16	ABDN	TG	0.000000	0.000000		
03390575	CHEV	N	RM	19	ABDN	TG	0.000000	0.000000		
03390576	CHEV	N	RM	20	ABDN	TG	0.000000	0.000000		
03390577	FMRP	Y	BR	1	ABDN	TG	0.000000	0.000000		
03390578	FMRP	Y	BR	2	ABDN	TG	0.000000	0.000000		
03390579	UNION	N	71	10	ABDN	TG	0.000000	0.000000		
03390580	FMRP	N	SBM	1	ABDN	TG	0.000000	0.000000		
03390581	FMRP	N	SBM	2	ABDN	TG	0.000000	0.000000		
03390582	FMRP	N	SBM	3	ABDN	TG	0.000000	0.000000		
03390583	FMRP	N	SBM	4	ABDN	TG	0.000000	0.000000		
03390584	FMRP	N	SBM	5	ABDN	TG	0.000000	0.000000		
03390585	FMRP	N	SBM	6	ABDN	TG	0.000000	0.000000		
03390586	FMRP	N	SBM	7	ABDN	TG	0.000000	0.000000		
03390587	FMRP	N	SBM	8	ABDN	TG	0.000000	0.000000		
03390588	FMRP	N	SBM	9	ABDN	TG	0.000000	0.000000		
03390589	FMRP	N	SBM	10	ABDN	TG	0.000000	0.000000		
03390590	FMRP	N	SBM	11	ABDN	TG	0.000000	0.000000		
03390591	FMRP	N	SBM	12	ABDN	TG	0.000000	0.000000		
03390592	FMRP	N	SBM	13	ABDN	TG	0.000000	0.000000		
03390593	FMRP	N	SBM	14	ABDN	TG	0.000000	0.000000		
03390594	FMRP	N	SBM	15	ABDN	TG	0.000000	0.000000		
03390595	UNION	N	BG	73-10	ABDN	TG	0.000000	0.000000		
03390596	UNION	N	BG	73-11	ABDN	TG	0.000000	0.000000		
03390597	UNION	N	BG	73-13	ABDN	TG	0.000000	0.000000		
03390598	UNION	N	BG	73-14	ABDN	TG	0.000000	0.000000		
03390599	UNION	N	BG	73-14A	ABDN	TG	0.000000	0.000000		
03390600	UNION	N	BG	73-15	ABDN	TG	0.000000	0.000000		
03390601	UNION	N	BG	73-16	ABDN	TG	0.000000	0.000000		
03390602	UNION	N	BG	73-17	ABDN	TG	0.000000	0.000000		
03390603	UNION	N	BG	73-18	ABDN	TG	0.000000	0.000000		
03390604	UNION	N	BG	73-19	ABDN	TG	0.000000	0.000000		
03390605	UNION	N	BG	73-20	ABDN	TG	0.000000	0.000000		
03390606	UNION	N	BG	73-21	ABDN	TG	0.000000	0.000000		
03390607	UNION	N	BG	73-22	ABDN	TG	0.000000	0.000000		
03390608	UNION	N	BG	73-23	ABDN	TG	0.000000	0.000000		
03390609	UNION	N	71	35	ABDN	TG	0.000000	0.000000		
03390610	UNION	N	71	37	ABDN	TG	0.000000	0.000000		
03390611	UNION	N	71	38	ABDN	TG	0.000000	0.000000		

Appendix 5 - well data

API number	Operator Company	Confid -ential?	Lease Name	Well Number	Well Status	Well Type	Latitude	Longitude	Got History?	Activity 1989-1994
03390612	UNION	N	71	39	ABDN	TG	0.000000	0.000000		
03390613	UNION	N	BG	72-4	ABDN	TG	0.000000	0.000000		
03390614	UNION	N	BG	72-5	ABDN	TG	0.000000	0.000000		
03390615	UNION	N	BG	72-6	ABDN	TG	0.000000	0.000000		
03390616	UNION	N	BG	72-7	ABDN	TG	0.000000	0.000000		
03390617	UNION	N	BG	72-8	ABDN	TG	0.000000	0.000000		
03390618	UNION	N	BG	72-9	ABDN	TG	0.000000	0.000000		
03390619	UNION	N	BG	72-12	ABDN	TG	0.000000	0.000000		
03390620	UNION	N	BG	72-13	ABDN	TG	0.000000	0.000000		
03390621	UNION	N	BG	72-14	ABDN	TG	0.000000	0.000000		
03390622	UNION	N	BG	72-15	ABDN	TG	0.000000	0.000000		
03390623	UNION	N	BG	72-19	ABDN	TG	0.000000	0.000000		
03390624	UNION	N	BG	72-20	ABDN	TG	0.000000	0.000000		
03390625	UNION	N	LC	74-1	ABDN	TG	0.000000	0.000000		
03390626	UNION	N	LC	74-2	ABDN	TG	0.000000	0.000000		
03390627	UNION	N	LC	74-3	ABDN	TG	0.000000	0.000000		
03390628	UNION	N	LC	74-4	ABDN	TG	0.000000	0.000000		
03390629	UNION	N	LC	74-5	ABDN	TG	0.000000	0.000000		
03390630	UNION	N	LC	74-6	ABDN	TG	0.000000	0.000000		
03390631	UNION	N	LC	74-7	ABDN	TG	0.000000	0.000000		
03390632	UNION	N	LC	74-8	ABDN	TG	0.000000	0.000000		
03390633	UNION	N	LC	74-9	ABDN	TG	0.000000	0.000000		
03390634	UNION	N	LC	74-10	ABDN	TG	0.000000	0.000000		
03390635	SILVR	Y	CA-5636	74D-21	ACTV	DST	38.794113	-122.743721		
03390636	UNION	N	LC	74-23	ABDN	TG	0.000000	0.000000		
03390637	UNION	N	LC	74-24	ABDN	TG	0.000000	0.000000		
03390638	UNION	N	LC	74-25	ABDN	TG	0.000000	0.000000		
03390639	UNION	N	LC	74-26	ABDN	TG	0.000000	0.000000		
03390640	UNION	N	LC	74-27	ABDN	TG	0.000000	0.000000		
03390641	UNION	N	BG	73-24	ABDN	TG	0.000000	0.000000		
03390642	UNION	N	BG	73-25	ABDN	TG	0.000000	0.000000		
03390643	UNION	N	BG	73-26	ABDN	TG	0.000000	0.000000		
03390644	UNION	N	LC	74-11	ABDN	TG	0.000000	0.000000		
03390645	UNION	N	LC	74-13	ABDN	TG	0.000000	0.000000		
03390646	UNION	N	LC	74-14	ABDN	TG	0.000000	0.000000		
03390647	UNION	N	LC	74-15	ABDN	TG	0.000000	0.000000		
03390648	UNION	N	LC	74-16	ABDN	TG	0.000000	0.000000		
03390649	UNION	N	LC	74-17	ABDN	TG	0.000000	0.000000		
03390650	UNION	N	LC	74-18	ABDN	TG	0.000000	0.000000		
03390651	UNION	N	LC	74-19	ABDN	TG	0.000000	0.000000		
03390652	UNION	N	LC	74-20	ABDN	TG	0.000000	0.000000		
03390653	UNION	N	LC	74-21	ABDN	TG	0.000000	0.000000		
03390654	UNION	N	LC	74-22	ABDN	TG	0.000000	0.000000		
03390655	UNION	N	LC	74-28	ABDN	TG	0.000000	0.000000		
03390656	UNION	N	LC	74-29	ABDN	TG	0.000000	0.000000		
03390657	UNION	N	LC	74-30	ABDN	TG	0.000000	0.000000		
03390658	UNION	N	LC	74-31	ABDN	TG	0.000000	0.000000		
03390659	UNION	N	LC	74-32	ABDN	TG	0.000000	0.000000		

Appendix 5 - well data

API number	Operator Company	Confid -ential?	Lease Name	Well Number	Well Status	Well Type	Latitude	Longitude	Got History?	Activity 1989-1994
03390660	UNION	N	LC	74-33	ABDN	TG	0.000000	0.000000		
03390661	UNION	N	LC	74-34	ABDN	TG	0.000000	0.000000		
03390662	UNION	N	LC	74-35	ABDN	TG	0.000000	0.000000		
03390663	UNION	N	LC	74-36	ABDN	TG	0.000000	0.000000		
03390664	UNION	N	LC	74-37	ABDN	TG	0.000000	0.000000		
03390665	UNION	N	LC	74-38	ABDN	TG	0.000000	0.000000		
03390666	UNION	N	LC	74-39	ABDN	TG	0.000000	0.000000		
03390667	UNION	N	LC	75-2	ABDN	TG	0.000000	0.000000		
03390668	UNION	N	LC	75-3	ABDN	TG	0.000000	0.000000		
03390669	UNION	N	LC	75-5	ABDN	TG	0.000000	0.000000		
03390670	UNION	N	LC	75-10	ABDN	TG	0.000000	0.000000		
03390671	UNION	N	LC	75-12	ABDN	TG	0.000000	0.000000		
03390672	UNION	N	LC	75-14	ABDN	TG	0.000000	0.000000		
03390673	UNION	N	LC	75-16	ABDN	TG	0.000000	0.000000		
03390674	USGS	Y	Mt Hannah	1	ACTV	TG	0.000000	0.000000		
03390675	SRGC	N	CRS	3A	ABDN	TG	0.000000	0.000000		
03390676	SRGC	N	CRS	4	ABDN	TG	0.000000	0.000000		
03390677	NCPA	Y	CA-949	22C-1	ACTV	DST	38.757350	-122.702300		
03390678	CGC	N	Davies Estate	5	ACTV	DST	38.763900	-122.694500	Yes	PROD
03390679	CGC	N	McKinley	13	ACTV	DST	38.767600	-122.712500	Yes	PROD
03390680	UNION	N	GD Horner State	7	ACTV	DST	38.829300	-122.775600	Yes	PROD
03390681	UNION	Y	CM	1	CANC	TG	0.000000	0.000000		
03390682	UNION	Y	CM	2	CANC	TG	0.000000	0.000000		
03390683	UNION	Y	CM	5	CANC	TG	0.000000	0.000000		
03390684	CGC	N	Davies Estate	6	ACTV	DST	38.764300	-122.694600	Yes	PROD
03390685	CGC	N	Thorne	10	ACTV	DST	38.777600	-122.714300	Yes	PROD
03390686	UNION	N	GD Horner State	8	ACTV	DST	38.829100	-122.775600	Yes	PROD
03390687	NCPA	Y	CA-949	22D-1	ACTV	DST	38.757035	-122.702300		
03390688	CGC	N	Davies Estate	7	ACTV	DST	38.764200	-122.694700	Yes	PROD
03390689	CGC	N	MLM	7	ACTV	DST	38.777400	-122.714100	Yes	PROD
03390690	NCPA	Y	CA-949	22E-1	ACTV	DST	38.756966	-122.702296		
03390691	CGC	N	McKinley	15	ACTV	DST	38.767400	-122.712500	Yes	PROD
03390692	UNION	N	G	28	ACTV	TG	0.000000	0.000000		
03390693	UNION	N	G	30	ACTV	TG	0.000000	0.000000		
03390694	NCPA	Y	CA-949	22F-1	ACTV	DST	38.756832	-122.702296		
03390695	CGC	N	PDC	2	ACTV	DST	38.792291	-122.726900	Yes	PROD
03390696	CGC	N	Moody Unit	2	ACTV	DST	38.789900	-122.723100	Yes	PROD
03390697	CGC	N	PDC	3	ACTV	DST	38.792291	-122.727100	Yes	PROD
03390698	CGC	N	Moody Unit	3	ACTV	DST	38.789700	-122.723100	Yes	PROD
03390699	SILVR	Y	CA-5636	36-22	ACTV	DST	38.780916	-122.734268		
03390700	SILVR	Y	CA-5636	36A-22	ACTV	DST	38.780874	-122.733757		
03390701	NCPA	Y	CA-949	22G-1	ACTV	DST	38.757389	-122.702300		
03390702	UNION	N	Tocher	4	ACTV	DST	38.783764	-122.734775	Yes	PROD
03390703	NCPA	Y	CA-949	38H-1	ACTV	DST	38.747051	-122.697916		
03390704	*	Y	*	*	CANC	*	0.000000	0.000000		
03390705	*	Y	*	*	CANC	*	0.000000	0.000000		
03390706	CGC	N	Moody Unit	4	ACTV	DST	38.789400	-122.723100	Yes	PROD
03390707	SRGC	Y	CA-956A	86B-34	CANC	DST	38.762100	-122.715200		

Appendix 5 - well data

API number	Operator Company	Confid -ential?	Lease Name	Well Number	Well Status	Well Type	Latitude	Longitude	Got History?	Activity 1989-1994
03390708	CGC	N	Davies Estate	8	ACTV	DST	38.763900	-122.694700	Yes	PROD
03390709	FMRP	N	NG	28	ABDN	TG	0.000000	0.000000		
03390710	SILVR	Y	CA-5636	36B-22	ACTV	DST	38.791046	-122.734489		
03390711	SILVR	Y	CA-5636	68E-21	ACTV	DST	38.786800	-122.745079		
03390712	FMRP	N	NG	27A	ABDN	TG	0.000000	0.000000		
03390713	FMRP	N	NG	27	ABDN	TG	0.000000	0.000000		
03390714	FMRP	N	NG	29	ABDN	TG	0.000000	0.000000		
03390715	FMRP	N	NG	30	ABDN	TG	0.000000	0.000000		
03390716	FMRP	N	NG	31	ABDN	TG	0.000000	0.000000		
03390717	FMRP	N	HS	17	ABDN	TG	0.000000	0.000000		
03390718	FMRP	N	HS	18	ABDN	TG	0.000000	0.000000		
03390719	NCPA	Y	CA-949	22H-1	ACTV	DST	38.757427	-122.702300		
03390720	SILVR	Y	CA-5636	87E-21	ACTV	DST	38.788677	-122.739754		
03390721	SILVR	Y	CA-5636	87F-21	ACTV	DST	38.788567	-122.740013		
03390722	SILVR	Y	CA-5636	23D-22	ACTV	DST	38.795135	-122.735359		
03390723	SILVR	Y	CA-5636	23E-22	ACTV	DST	38.795330	-122.735817		
03390724	UNION	N	GD Horner State	6	ACTV	DST	38.829300	-122.775500	Yes	PROD
03390725	SILVR	Y	CA-5636	68F-21	ACTV	DST	38.788052	-122.745300		
03390726	CGC	N	Davies Estate	9	ACTV	DST	38.763300	-122.697500	Yes	PROD
03390727	CGC	N	Wolfe	1	ACTV	DST	38.777900	-122.714400	Yes	PROD
03390728	SILVR	Y	CA-5636	36C-22	ACTV	DST	38.791286	-122.734314		
03390729	SILVR	Y	CA-5636	68G-21	ACTV	DST	38.788052	-122.739243		
03390730	SILVR	Y	CA-5636	87G-21	ACTV	DST	38.788052	-122.739243		
03390731	CGC	N	CA-958	76A-35	ACTV	DST	38.765500	-122.704300	Yes	PROD
03390732	SILVR	Y	CA-5636	23F-22	ACTV	DST	38.795605	-122.735794		
03390733	SILVR	Y	CA-5636	74E-21	ACTV	DST	38.793697	-122.743607		
03390734	CGC	N	Davies St 5206	4	ACTV	DST	38.763100	-122.697300	Yes	PROD
03390735	SILVR	Y	CA-5636	74F-21	ACTV	DST	38.793438	-122.743210		
03390736	CGC	Y	East Ford Flat	1	ACTV	DST	38.776900	-122.713900	Yes	NA
03390737	SILVR	Y	CA-5636	74G-21	ACTV	DST	38.793114	-122.742485		
03390738	SILVR	Y	CA-5636	74H-21	PROP	DST	38.793324	-122.742493		
03390739	SILVR	Y	CA-5636	23G-22	ACTV	DST	38.794671	-122.734744		
03390740	SILVR	Y	CA-5636	23H-22	ACTV	DST	38.795467	-122.735481		
03390741	CGC	Y	Davies St 5206	5	ACTV	DST	38.764200	-122.694700		
03390742	CGC	Y	Moody Unit	5	ACTV	DST	38.788998	-122.723259		
03390743	CGC	Y	Barrows	7	ACTV	INJ	38.766900	-122.711700		
03390744	CGC	Y	PDC	4	PROP	DST	38.788998	-122.723259		
09790001	GEO	N	Rorabaugh	1	ABDN	DST	38.804382	-122.831758	Yes	SHTN 7/91
09790002	GEO	N	Rorabaugh	2	ABDN	DST	38.805103	-122.833954	Yes	NA
09790003	GEO	N	Rorabaugh	5	ABDN	DST	38.805852	-122.836141		
09790004	GEO	N	Rorabaugh	6	ABDN	DST	38.802544	-122.836156		
09790005	GEO	N	Rorabaugh	7	ABDN	DST	38.805974	-122.836377		
09790006	UNION	Y	CA-1863	56-18	ACTV	DST	38.804591	-122.792825		
09790007	UNION	N	CMHC	65-18	ACTV	DST	38.806306	-122.783570	Yes	PROD
09790008	UNION	N	Curry	85-13	ACTV	DST	38.799736	-122.805192	Yes	SHTN; BLOW 10/94
09790009	UNION	N	DX State 4596	1	ABDN	DST	38.814581	-122.791647	Yes	NA
09790010	UNION	N	DX State 4596	2	ACTV	DST	38.812409	-122.794342	Yes	PROD
09790011	UNION	N	DX State 4596	3	ACTV	DST	38.814253	-122.796495	Yes	PROD

Appendix 5 - well data

API number	Operator Company	Confid -ential?	Lease Name	Well Number	Well Status	Well Type	Latitude	Longitude	Got History?	Activity 1989-1994
09790012	UNION	N	DX State 4596	5	ACTV	DST	38.817763	-122.790912	Yes	PROD
09790013	UNION	N	DX State 4596	7	ABDN	INJ	38.827372	-122.792874	Yes	NA
09790014	UNION	N	DX State 4596	8	ABDN	INJ	38.809523	-122.795439	Yes	NA
09790015	UNION	N	DX State 4596	10	ACTV	DST	38.815686	-122.793409	Yes	PROD
09790016	UNION	N	D & V	73-33	ACTV	INJ	38.769357	-122.741897	Yes	INJ
09790017	UNION	Y	GDC	17-28	ACTV	DST	38.774911	-122.755390		
09790018	UNION	N	GDC	32-13	ABDN	DST	38.804075	-122.815162		
09790019	UNION	N	GDC	32A-13	ACTV	DST	38.804075	-122.815162	Yes	PROD
09790020	UNION	N	GDC	53-13	ACTV	INJ	38.802648	-122.810587	Yes	INJ; BLOW 12/94
09790021	UNION	N	GDC	65-28	ABDN	DST	38.777458	-122.744796	Yes	NA
09790022	UNION	N	GDC	66-12	ACTV	DST	38.811978	-122.808033	Yes	PROD
09790023	UNION	N	GDC	77-12	ACTV	DST	38.810634	-122.807050	Yes	PROD
09790024	UNION	N	GDC	85-12	ACTV	DST	38.813082	-122.804039	Yes	PROD
09790025	UNION	N	GDC	86-12	ACTV	DST	38.811172	-122.804387	Yes	PROD
09790026	UNION	N	GDC	88-12	ACTV	INJ	38.808886	-122.804560	Yes	INJ
09790027	UNION	N	Geysers	I	ABDN	DST	38.803653	-122.806399		
09790028	UNION	N	Geysers	II	ABDN	DST	38.803521	-122.806416		
09790029	UNION	N	Geysers	VI	ABDN	DST	38.802215	-122.804540		
09790030	UNION	N	Geysers	VIII	ABDN	DST	38.801430	-122.803550		
09790031	UNION	N	Geyser Gun Club	1	ABDN	DST	38.813502	-122.825715	Yes	NA
09790032	UNION	N	Geyser Gun Club	2	ACTV	DST	38.813480	-122.820075	Yes	PROD
09790033	UNION	N	Happy Jack	1	ACTV	DST	38.805658	-122.809725	Yes	PROD
09790034	UNION	N	Happy Jack	2	ABDN	DST	38.806318	-122.811215	Yes	NA
09790035	UNION	N	Happy Jack	3	ABDN	DST	38.806197	-122.811173	Yes	NA
09790036	UNION	N	Happy Jack	4	ACTV	DST	38.808960	-122.809161	Yes	PROD
09790037	UNION	N	Happy Jack	5	ACTV	DST	38.809772	-122.813584	Yes	PROD
09790038	UNION	N	Happy Jack	6	ABDN	DST	38.808820	-122.811191	Yes	NA
09790039	UNION	N	Happy Jack	7A	ABDN	DST	38.804728	-122.811410		
09790040	UNION	N	Happy Jack	8	ABDN	DST	38.807928	-122.809531	Yes	NA
09790041	UNION	N	Happy Jack	9	ABDN	INJ	38.808175	-122.809662	Yes	NA
09790042	UNION	N	Little Geysers	1	ABDN	DST	38.772140	-122.749130	Yes	NA
09790043	UNION	N	Little Geysers	2	ABDN	DST	38.774615	-122.746466	Yes	NA
09790044	UNION	N	LF State 4597	1	ACTV	DST	38.789514	-122.765413	Yes	PROD
09790045	UNION	N	LF State 4597	2	ACTV	INJ	38.796226	-122.764842	Yes	PROD 1/89-12/91; INJ 2/92
09790046	UNION	N	LF State 4597	5	ACTV	DST	38.796901	-122.773149	Yes	PROD
09790047	UNION	N	LF State 4597	7	ABDN	DST	38.809627	-122.779853	Yes	NA
09790048	UNION	N	LF State 4597	8	ACTV	DST	38.791094	-122.763008	Yes	PROD
09790049	UNION	N	LF State 4597	9	ACTV	DST	38.793737	-122.761380	Yes	PROD
09790050	UNION	N	Magma	1	ACTV	DST	38.803073	-122.804525	Yes	PROD
09790051	UNION	N	Ottoboni St 4596	1	ACTV	DST	38.811188	-122.799655	Yes	PROD
09790052	UNION	N	Ottoboni St 4596	2	ACTV	DST	38.819413	-122.805358	Yes	PROD
09790053	UNION	N	Ottoboni St 4596	4	ACTV	DST	38.816413	-122.805518	Yes	PROD
09790054	UNION	N	Ottoboni St 4596	5	ACTV	DST	38.818666	-122.799573	Yes	PROD
09790055	UNION	N	Ottoboni St 4596	6	ACTV	DST	38.818718	-122.802968	Yes	PROD
09790056	UNION	N	Ottoboni St 4596	7	ACTV	DST	38.813954	-122.801531	Yes	PROD
09790057	UNION	N	Ottoboni St 4596	8	ACTV	DST	38.821153	-122.800386	Yes	PROD
09790058	UNION	N	Sulphur Bank	1	ABDN	INJ	38.807797	-122.812936	Yes	NA
09790059	UNION	N	Sulphur Bank	2	ABDN	DST	38.807723	-122.822328	Yes	NA

Appendix 5 - well data

API number	Operator Company	Confid -ential?	Lease Name	Well Number	Well Status	Well Type	Latitude	Longitude	Got History?	Activity 1989-1994
09790060	UNION	N	Sulphur Bank	3	ABDN	DST	38.808480	-122.823179	Yes	NA
09790061	UNION	N	Sulphur Bank	4	ABDN	DST	38.808905	-122.825644		
09790062	UNION	N	Sulphur Bank	5	ABDN	DST	38.808439	-122.824350		
09790063	UNION	N	Sulphur Bank	6	ABDN	DST	38.808211	-122.821512	Yes	NA
09790064	UNION	N	Sulphur Bank	7	ACTV	DST	38.807977	-122.819429	Yes	PROD
09790065	UNION	N	Sulphur Bank	8	ACTV	DST	38.807195	-122.818326	Yes	PROD
09790066	UNION	N	Sulphur Bank	9	ACTV	DST	38.806383	-122.817131	Yes	PROD
09790067	UNION	N	Sulphur Bank	13	ABDN	DST	38.809693	-122.820466	Yes	NA
09790068	UNION	N	Sulphur Bank	14	ACTV	DST	38.807159	-122.816106	Yes	PROD
09790069	UNION	N	Sulphur Bank	15	ACTV	INJ	38.808853	-122.818475	Yes	PROD
09790070	UNION	N	Sulphur Bank	16	ABDN	DST	38.808093	-122.816341	Yes	NA
09790071	UNION	N	Sulphur Bank	17	ACTV	DST	38.808894	-122.817074	Yes	PROD
09790072	UNION	N	Sulphur Bank	18	ABDN	DST	38.810009	-122.817380	Yes	NA
09790073	UNION	N	Sulphur Bank	19	ACTV	DST	38.808208	-122.814591	Yes	PROD
09790074	UNION	N	Thermal	1	ABDN	DST	38.803699	-122.805533	Yes	NA
09790075	UNION	N	Thermal	2	ABDN	DST	38.802654	-122.804834	Yes	NA
09790076	UNION	N	Thermal	3	ABDN	DST	38.802393	-122.803515		
09790077	UNION	N	Thermal	5	ABDN	DST	38.803315	-122.805104	Yes	NA
09790078	UNION	N	Thermal	6	ABDN	DST	38.802330	-122.804466	Yes	NA
09790079	UNION	N	Thermal	7	ACTV	DST	38.802099	-122.804972	Yes	PROD
09790080	UNION	N	Thermal	8	ABDN	DST	38.802080	-122.804051	Yes	NA
09790081	UNION	N	Thermal	9	ABDN	DST	38.803510	-122.805583	Yes	NA
09790082	UNION	N	Thermal	10	ACTV	DST	38.802985	-122.804983	Yes	PROD
09790083	UNION	N	Thermal	11	ACTV	DST	38.802722	-122.805327	Yes	PROD
09790084	UNION	N	Sulphur Bank	12A	ABDN	DST	38.806787	-122.819384		
09790085	UNION	N	Sulphur Bank	10	ACTV	DST	38.807703	-122.818596	Yes	PROD
09790086	UNION	N	Sulphur Bank	11	ACTV	DST	38.807708	-122.817187	Yes	PROD
09790087	UNION	N	Sulphur Bank	12	ABDN	DST	38.806787	-122.818852	Yes	NA
09790088	GEO	N	Rorabaugh	A-7	ABDN	DST	38.799125	-122.831724	Yes	PROD; SHTN 6/91
09790089	UNION	N	Ottoboni St 4596	10	ABDN	INJ	38.823796	-122.805789	Yes	NA
09790090	UNION	N	GDC	58I-11	ABDN	DST	38.808697	-122.830738		
09790091	UNION	N	Ottoboni St 4596	9	ABDN	INJ	38.821433	-122.802579	Yes	NA
09790092	UNION	N	DX State 4596	9	ABDN	DST	38.832314	-122.795031	Yes	NA
09790093	UNION	N	LF State 4597	15	ACTV	DST	38.794681	-122.759171	Yes	PROD
09790094	GEO	N	Rorabaugh	A-1	ABDN	DST	38.802376	-122.836052	Yes	SHTN
09790095	GEO	N	Rorabaugh	A-2	ACTV	DST	38.802999	-122.833075	Yes	SHTN 6/91
09790096	GEO	N	Rorabaugh	A-3	ACTV	DST	38.803113	-122.835236	Yes	PROD; SHTN 6/91
09790097	GEO	N	Rorabaugh	A-4	ACTV	DST	38.798497	-122.829535	Yes	PROD; SHTN 6/91
09790098	GEO	N	Rorabaugh	A-5	ABDN	INJ	38.801096	-122.834662	Yes	INJ; SHTN 6/91
09790099	UNION	N	DX State 4596	4	ACTV	DST	38.817865	-122.796463	Yes	PROD
09790100	UNION	N	LF State 4597	6	ACTV	DST	38.788685	-122.767470	Yes	PROD
09790101	UNION	N	LF State 4597	11	ABDN	DST	38.800582	-122.771355	Yes	NA
09790102	UNION	N	GDC	38I-11	ABDN	DST	38.808469	-122.834263		
09790103	UNION	N	Thermal	13	ABDN	DST	38.804621	-122.806459	Yes	NA
09790104	UNION	N	Thermal	14	ABDN	DST	38.803784	-122.807746	Yes	NA
09790105	UNION	N	Thermal Power	1A	CANC	DST	0.000000	0.000000		
09790106	*	N	*	*	CANC	*	0.000000	0.000000		

Appendix 5 - well data

API number	Operator Company	Confid -ential?	Lease Name	Well Number	Well Status	Well Type	Latitude	Longitude	Got History?	Activity 1989-1994
09790107	*	N	*	*	CANC	*	0.000000	0.000000		
09790108	*	N	*	*	CANC	*	0.000000	0.000000		
09790109	UNION	N	LF State 4597	3	ACTV	INJ	38.806086	-122.765349	Yes	SHTN 3/94
09790110	UNION	N	LFH State 4597	1	ABDN	DST	38.813864	-122.769716	Yes	NA
09790111	GEO	N	Wildhorse	1	ABDN	DST	38.842027	-122.828166		
09790112	CCPA	Y	Wildhorse	2	ABDN	DST	38.816493	-122.854633		
09790113	UNION	N	Ottoboni St 4596	11	ACTV	DST	38.816578	-122.805977	Yes	SHTN
09790114	UNION	N	LF State 4597	18	ACTV	DST	38.798858	-122.774582	Yes	PROD
09790115	UNION	N	LF State 4597	10	ACTV	DST	38.795230	-122.762735	Yes	PROD
09790116	UNION	N	LF State 4597	12	ACTV	DST	38.796522	-122.775877	Yes	PROD
09790117	UNION	N	LF State 4597	19	ABDN	DST	38.801556	-122.770639	Yes	NA
09790118	UNION	N	GDC	20-29	ACTV	DST	38.784955	-122.772503	Yes	PROD
09790119	UNION	N	LF State 4597	17	ACTV	DST	38.792557	-122.757929	Yes	PROD
09790120	UNION	N	DX State 4596	12	ACTV	DST	38.812637	-122.783109	Yes	PROD
09790121	UNION	N	DX State 4596	11	ACTV	DST	38.830423	-122.789426	Yes	PROD
09790122	UNION	N	LF State 4597	16	ACTV	DST	38.787881	-122.764661	Yes	PROD
09790123	GEO	N	Rorabaugh	A-6	ACTV	INJ	38.796066	-122.828886	Yes	INJ; SHTN 6/91
09790124	UNION	N	Thermal	12	ABDN	INJ	38.801122	-122.804192	Yes	NA
09790125	UNION	N	LF State 4597	13	ACTV	DST	38.797804	-122.764087	Yes	PROD
09790126	UNION	N	LF State 4597	14	ACTV	DST	38.797508	-122.770365	Yes	PROD
09790127	UNION	N	Ottoboni St 4596	3	ACTV	INJ	38.816490	-122.801028	Yes	INJ
09790128	UNION	N	Geyser Gun Club	3	ABDN	DST	38.814882	-122.822756	Yes	PROD
09790129	UNION	N	Happy Jack	7	ABDN	DST	38.804728	-122.811410	Yes	NA
09790130	*	N	*	*	CANC	*	0.000000	0.000000		
09790131	UNION	Y	CA-5634	35-12	ABDN	DST	38.814528	-122.815177		
09790132	UNION	Y	Thermal	4	ACTV	DST	38.802818	-122.805586		
09790133	DWR	N	Rorabaugh	1	ABDN	DST	38.799540	-122.823652	Yes	SHTN 1/92
09790134	GEO	N	Rorabaugh	3	ABDN	DST	38.802219	-122.832685		
09790135	GEO	N	Rorabaugh	4	ABDN	DST	38.801498	-122.832255		
09790136	UNION	N	LF State 4597	4	ACTV	DST	38.797768	-122.770237	Yes	PROD
09790137	UNION	N	Geysers	IV	ABDN	DST	38.802731	-122.805221		
09790138	UNION	N	Geysers	V	ABDN	DST	38.801693	-122.803863		
09790139	UNION	N	Ottoboni St 4596	12	ACTV	DST	38.827094	-122.805075	Yes	PROD
09790140	UNION	N	DX State 4596	13	ACTV	DST	38.830118	-122.788649	Yes	PROD
09790141	UNION	N	GDC	72-30	ACTV	DST	38.782812	-122.778526	Yes	PROD
09790142	TRMOG	N	Bruno	1	ABDN	DST	38.795060	-122.823197		
09790143	UNION	N	Ottoboni St 4596	17	ACTV	DST	38.827928	-122.802113	Yes	PROD
09790144	UNION	N	DX State 4596	21	ACTV	DST	38.812733	-122.792919	Yes	PROD
09790145	UNION	N	Ottoboni St 4596	13	ACTV	DST	38.825991	-122.803440	Yes	PROD
09790146	UNION	N	DX State 4596	14	ACTV	DST	38.832081	-122.795044	Yes	PROD
09790147	UNION	N	Ottoboni St 4596	14	ACTV	DST	38.825102	-122.801155	Yes	PROD
09790148	DWR	N	Rorabaugh	2	ABDN	DST	38.799728	-122.820129	Yes	SHTN 3/92
09790149	GEO	N	Filley	1	ABDN	DST	38.805505	-122.839611	Yes	PROD; SHTN 6/91
09790150	GEO	N	Rorabaugh	A-8	ABDN	DST	38.794601	-122.833556	Yes	NA
09790151	UNION	N	Ottoboni St 4596	19	ACTV	DST	38.828134	-122.802305	Yes	PROD
09790152	UNION	N	Ottoboni St 4596	18	ACTV	DST	38.827736	-122.801890	Yes	PROD
09790153	UNION	N	Ottoboni St 4596	15	ACTV	DST	38.828049	-122.807980	Yes	PROD
09790154	UNION	N	DX State 4596	15	ACTV	DST	38.831814	-122.795172	Yes	PROD

Appendix 5 - well data

API number	Operator Company	Confid -ential?	Lease Name	Well Number	Well Status	Well Type	Latitude	Longitude	Got History?	Activity 1989-1994
09790155	UNION	N	Ottoboni St 4596	16	ACTV	DST	38.827857	-122.807437	Yes	PROD
09790156	UNION	N	DX State 4596	18	ABDN	DST	38.836637	-122.797794		
09790157	GEO	N	Rorabaugh	A-9	ABDN	DST	38.802973	-122.838028	Yes	PROD
09790158	GEO	N	Rorabaugh	A-10	ACTV	DST	38.799356	-122.834503	Yes	PROD; SHTN 6/91
09790159	*	N	*	*	CANC	*	0.000000	0.000000		
09790160	*	N	*	*	CANC	*	0.000000	0.000000		
09790161	UNION	N	Ottoboni St 4596	20	ABDN	DST	38.826269	-122.803738	Yes	NA
09790162	NCPA	Y	CA-950	86-3	ABDN	DST	38.749858	-122.725454		
09790163	UNION	N	Ottoboni St 4596	21	ACTV	DST	38.819023	-122.806036	Yes	PROD
09790164	GEO	N	Filley	2	ABDN	DST	38.805023	-122.842512	Yes	SHTN 8/91
09790165	GEO	N	Filley	3	ABDN	DST	38.807232	-122.842339		
09790166	UNION	N	DX State 4596	24	ACTV	DST	38.812564	-122.783418	Yes	PROD
09790167	UNION	N	Ottoboni St 4596	22	ACTV	DST	38.818801	-122.806206	Yes	PROD
09790168	UNION	N	CMHC	2	ACTV	DST	38.806045	-122.792260	Yes	PROD
09790169	UNION	N	CMHC	3	ABDN	DST	38.806207	-122.792004	Yes	PROD
09790170	UNION	N	CMHC	4	ACTV	DST	38.806369	-122.791745	Yes	PROD
09790171	*	N	*	*	CANC	*	0.000000	0.000000		
09790172	UNION	N	DX State 4596	22	ABDN	DST	38.823909	-122.778009		
09790173	*	N	*	*	CANC	*	0.000000	0.000000		
09790174	UNION	N	DX State 4596	25	ACTV	DST	38.812500	-122.783733	Yes	PROD
09790175	UNION	N	DX State 4596	26	ACTV	DST	38.806713	-122.791218	Yes	PROD
09790176	UNION	N	DX State 4596	27	ACTV	DST	38.806542	-122.791484	Yes	PROD
09790177	UNION	N	GDC	36-18	ACTV	INJ	38.804531	-122.792917	Yes	SHTN
09790178	UNION	N	CMHC	5	ACTV	DST	38.804715	-122.792637	Yes	PROD
09790179	UNION	N	Happy Jack	10	ACTV	DST	38.807975	-122.809935	Yes	PROD
09790180	UNION	N	Happy Jack	11	ACTV	DST	38.807887	-122.810009	Yes	PROD
09790181	UNION	N	DX State 4596	19	ACTV	DST	38.836236	-122.797443	Yes	PROD
09790182	CCPA	N	Wildhorse	5	ACTV	INJ	38.836088	-122.820246	Yes	SHTN
09790183	GEO	N	Squaw Creek St	1	ABDN	EST	38.847351	-122.866980		
09790184	UNION	N	DX State 4596	28	ACTV	DST	38.821584	-122.771440	Yes	PROD
09790185	GEO	N	Rorabaugh	A-11	ACTV	DST	38.802195	-122.832684	Yes	SHTN 6/91
09790186	*	N	*	*	CANC	*	0.000000	0.000000		
09790187	*	N	*	*	CANC	*	0.000000	0.000000		
09790188	*	N	*	*	CANC	*	0.000000	0.000000		
09790189	*	N	*	*	CANC	*	0.000000	0.000000		
09790190	*	N	*	*	CANC	*	0.000000	0.000000		
09790191	*	N	*	*	CANC	*	0.000000	0.000000		
09790192	UNION	N	DX State 4596	22A	ACTV	DST	38.823909	-122.778009	Yes	PROD
09790193	UNION	N	LF State 4597	20	ACTV	DST	38.796493	-122.776051	Yes	PROD
09790194	UNION	N	Sulphur Bank	20	ACTV	DST	38.805080	-122.816795	Yes	PROD
09790195	UNION	N	Sulphur Bank	21	ACTV	DST	38.805151	-122.816681	Yes	PROD
09790196	UNION	N	Sulphur Bank	22	ACTV	DST	38.805225	-122.816561	Yes	PROD
09790197	UNION	N	Sulphur Bank	23	ACTV	DST	38.805297	-122.816447	Yes	PROD
09790198	UNION	N	DX State 4596	29	ACTV	DST	38.814803	-122.797879	Yes	PROD
09790199	*	N	*	*	CANC	*	0.000000	0.000000		
09790200	UNION	N	D & V	1	ACTV	DST	38.763231	-122.740312	Yes	PROD
09790201	UNION	N	DX State 4596	30	ABDN	DST	38.829894	-122.788270	Yes	NA
09790202	UNION	N	DX State 4596	31	ACTV	DST	38.829956	-122.788397	Yes	PROD

Appendix 5 - well data

API number	Operator Company	Confid -ential?	Lease Name	Well Number	Well Status	Well Type	Latitude	Longitude	Got History?	Activity 1989-1994
09790203	UNION	N	GDC	1	ACTV	DST	38.788490	-122.778554	Yes	PROD
09790204	UNION	N	LFH State 4597	2	ABDN	DST	38.814040	-122.769695	Yes	NA
09790205	UNION	N	GDC	2	ACTV	DST	38.788473	-122.778732	Yes	PROD
09790206	ANDAR	N	TG	30	ABDN	TG	0.000000	0.000000		
09790207	ANDAR	N	TG	31	ABDN	TG	0.000000	0.000000		
09790208	ANDAR	N	TG	32	ABDN	TG	0.000000	0.000000		
09790209	ANDAR	N	TG	33	ABDN	TG	0.000000	0.000000		
09790210	ANDAR	N	TG	34	ABDN	TG	0.000000	0.000000		
09790211	ANDAR	N	TG	35	ABDN	TG	0.000000	0.000000		
09790212	ANDAR	N	TG	36	ABDN	TG	0.000000	0.000000		
09790213	ANDAR	N	TG	37	ABDN	TG	0.000000	0.000000		
09790214	ANDAR	N	TG	38	ABDN	TG	0.000000	0.000000		
09790215	ANDAR	N	TG	39	ABDN	TG	0.000000	0.000000		
09790216	ANDAR	N	TG	40	ABDN	TG	0.000000	0.000000		
09790217	ANDAR	N	TG	41	ABDN	TG	0.000000	0.000000		
09790218	ANDAR	N	TG	42	ABDN	TG	0.000000	0.000000		
09790219	ANDAR	N	TG	43	ABDN	TG	0.000000	0.000000		
09790220	ANDAR	N	TG	44	ABDN	TG	0.000000	0.000000		
09790221	*	N	*	*	CANC	*	0.000000	0.000000		
09790222	*	N	*	*	CANC	*	0.000000	0.000000		
09790223	ANDAR	N	TG	47	ABDN	TG	0.000000	0.000000		
09790224	ANDAR	N	TG	48	ABDN	TG	0.000000	0.000000		
09790225	ANDAR	N	TG	49	ABDN	TG	0.000000	0.000000		
09790226	SHELL	N	Hilary Farms	1	ABDN	EST	38.839135	-122.930883		
09790227	UNION	N	GDC	5	ACTV	INJ	38.783926	-122.777395	Yes	PROD 1-12/89; INJ 1/90-12/94
09790228	UNION	N	GDC	6	ACTV	DST	38.784003	-122.777544	Yes	PROD
09790229	UNION	N	LF State 4597	21	ABDN	DST	38.800914	-122.768954	Yes	NA
09790230	*	N	*	*	CANC	*	0.000000	0.000000		
09790231	UNION	N	LF State 4597	23	ACTV	INJ	38.800697	-122.769152	Yes	INJ
09790232	UNION	N	LF State 4597	24	ACTV	DST	38.800590	-122.769254	Yes	PROD
09790233	REPUB	N	MM	1	ABDN	TG	0.000000	0.000000		
09790234	REPUB	N	MM	2	ABDN	TG	0.000000	0.000000		
09790235	REPUB	N	MM	3	ABDN	TG	0.000000	0.000000		
09790236	REPUB	N	MM	4	ABDN	TG	0.000000	0.000000		
09790237	REPUB	N	MM	5	ABDN	TG	0.000000	0.000000		
09790238	GEO	N	NG	15	ABDN	TG	0.000000	0.000000		
09790239	UNION	N	Ottoboni St 4596	23	ACTV	DST	38.811591	-122.802620	Yes	PROD
09790240	UNION	N	Ottoboni St 4596	24	ACTV	DST	38.811487	-122.802681	Yes	PROD
09790241	GEP	N	Aidlin	1	ACTV	DST	38.832553	-122.874552	Yes	PROD
09790242	UNION	N	DX State 4596	32	ABDN	DST	38.812465	-122.783886		
09790243	NCPA	Y	CA-949	24-2	ACTV	DST	38.753146	-122.718258		
09790244	NCPA	Y	CA-949	24A-2	ACTV	INJ	38.753176	-122.718375		
09790245	UNION	N	LFH State 4597	3	ABDN	DST	38.814070	-122.769862	Yes	NA
09790246	FMRP	N	GP	9	ABDN	TG	0.000000	0.000000		
09790247	FMRP	N	GP	10	ABDN	TG	0.000000	0.000000		
09790248	FMRP	N	GP	11	ABDN	TG	0.000000	0.000000		
09790249	FMRP	N	GP	12	ABDN	TG	0.000000	0.000000		
09790250	FMRP	N	GP	13	ABDN	TG	0.000000	0.000000		

Appendix 5 - well data

API number	Operator Company	Confid -ential?	Lease Name	Well Number	Well Status	Well Type	Latitude	Longitude	Got History?	Activity 1989-1994
09790251	*	N	*	*	CANC	*	0.000000	0.000000		
09790252	NCPA	Y	CA-950	81A-3	ACTV	DST	38.760117	-122.723954		
09790253	NCPA	Y	CA-950	81-3	ACTV	DST	38.760081	-122.724106		
09790254	*	N	*	*	CANC	*	0.000000	0.000000		
09790255	UNION	Y	CA-1863	96-18	ACTV	DST	38.803889	-122.782762		
09790256	*	N	*	*	CANC	*	0.000000	0.000000		
09790257	GEP	Y	Aidlin	2	ACTV	EST	38.837456	-122.887115		
09790258	UNION	N	DX State 4596	33	ACTV	DST	38.812612	-122.777508	Yes	PROD
09790259	*	N	*	*	CANC	*	0.000000	0.000000		
09790260	*	N	*	*	CANC	*	0.000000	0.000000		
09790261	*	N	*	*	CANC	*	0.000000	0.000000		
09790262	UNION	N	LF State 4597	25	ACTV	DST	38.805175	-122.776824	Yes	PROD
09790263	UNION	N	LF State 4597	26	ACTV	DST	38.805046	-122.776806	Yes	PROD
09790264	UNION	N	LF State 4597	27	ACTV	DST	38.804917	-122.776792	Yes	PROD
09790265	FMRP	N	Briggs Creek St	1	ABDN	TG	0.000000	0.000000		
09790266	UNION	N	Sulphur Bank	24	ACTV	DST	38.809094	-122.814041	Yes	PROD
09790267	UNION	N	Sulphur Bank	25	ACTV	DST	38.808995	-122.814151	Yes	PROD
09790268	UNION	N	Sulphur Bank	26	ACTV	DST	38.808905	-122.814275	Yes	PROD
09790269	UNION	Y	CA-5634	45-12	ACTV	DST	38.814526	-122.815113		
09790270	GEO	N	GP	1	ABDN	TG	0.000000	0.000000		
09790271	GEO	N	GP	2	ABDN	TG	0.000000	0.000000		
09790272	GEO	N	GP	3	ABDN	TG	0.000000	0.000000		
09790273	GEO	N	GP	4	ABDN	TG	0.000000	0.000000		
09790274	FMRP	N	GP	5	ABDN	TG	0.000000	0.000000		
09790275	FMRP	N	GP	6	ABDN	TG	0.000000	0.000000		
09790276	FMRP	N	GP	7	ABDN	TG	0.000000	0.000000		
09790277	FMRP	N	GP	8	ABDN	TG	0.000000	0.000000		
09790278	FMRP	N	NG	13	ABDN	TG	0.000000	0.000000		
09790279	FMRP	N	NG	14	ABDN	TG	0.000000	0.000000		
09790280	FMRP	N	NG	16	ABDN	TG	0.000000	0.000000		
09790281	*	N	*	*	CANC	*	0.000000	0.000000		
09790282	FMRP	N	NG	18	ABDN	TG	0.000000	0.000000		
09790283	FMRP	N	NG	19	ABDN	TG	0.000000	0.000000		
09790284	FMRP	N	NG	20	ABDN	TG	0.000000	0.000000		
09790285	FMRP	N	NG	21	ABDN	TG	0.000000	0.000000		
09790286	FMRP	N	NG	22	ABDN	TG	0.000000	0.000000		
09790287	FMRP	N	NG	23	ABDN	TG	0.000000	0.000000		
09790288	FMRP	N	NG	24	ABDN	TG	0.000000	0.000000		
09790289	FMRP	N	NG	25	ABDN	TG	0.000000	0.000000		
09790290	FMRP	N	NG	26	ABDN	TG	0.000000	0.000000		
09790291	GEO	N	TG	1	ABDN	TG	0.000000	0.000000		
09790292	GEO	N	TG	2	ABDN	TG	0.000000	0.000000		
09790293	GEO	N	TG	3	ABDN	TG	0.000000	0.000000		
09790294	GEO	N	TG	4	ABDN	TG	0.000000	0.000000		
09790295	GEO	N	TG	5	ABDN	TG	0.000000	0.000000		
09790296	GEO	N	TG	6	ABDN	TG	0.000000	0.000000		
09790297	ANDAR	N	TG	7	ABDN	TG	0.000000	0.000000		
09790298	GEO	N	TG	8	ABDN	TG	0.000000	0.000000		

Appendix 5 - well data

API number	Operator Company	Confid -ential?	Lease Name	Well Number	Well Status	Well Type	Latitude	Longitude	Got History?	Activity 1989-1994
09790299	ANDAR	N	TG	9	ABDN	TG	0.000000	0.000000		
09790300	ANDAR	N	TG	10	ABDN	TG	0.000000	0.000000		
09790301	GEO	N	TG	11	ABDN	TG	0.000000	0.000000		
09790302	ANDAR	N	TG	12	ABDN	TG	0.000000	0.000000		
09790303	GEO	N	TG	13	ABDN	TG	0.000000	0.000000		
09790304	*	N	*	*	CANC	*	0.000000	0.000000		
09790305	THERM	N	TG	15	ABDN	TG	0.000000	0.000000		
09790306	ANDAR	N	TG	16	ABDN	TG	0.000000	0.000000		
09790307	*	N	*	*	CANC	*	0.000000	0.000000		
09790308	ANDAR	N	TG	18	ABDN	TG	0.000000	0.000000		
09790309	ANDAR	N	TG	19	ABDN	TG	0.000000	0.000000		
09790310	GEO	N	TG	20	ABDN	TG	0.000000	0.000000		
09790311	GEO	N	TG	21	ABDN	TG	0.000000	0.000000		
09790312	GEO	N	TG	22	ABDN	TG	0.000000	0.000000		
09790313	GEO	N	TG	23	ACTV	TG	0.000000	0.000000		
09790314	GEO	N	TG	24	ABDN	TG	0.000000	0.000000		
09790315	*	N	*	*	CANC	*	0.000000	0.000000		
09790316	*	N	*	*	CANC	*	0.000000	0.000000		
09790317	*	N	*	*	CANC	*	0.000000	0.000000		
09790318	*	N	*	*	CANC	*	0.000000	0.000000		
09790319	*	N	*	*	CANC	*	0.000000	0.000000		
09790320	*	N	*	*	CANC	*	0.000000	0.000000		
09790321	*	N	*	*	CANC	*	0.000000	0.000000		
09790322	*	N	*	*	CANC	*	0.000000	0.000000		
09790323	*	N	*	*	CANC	*	0.000000	0.000000		
09790324	*	N	*	*	CANC	*	0.000000	0.000000		
09790325	*	N	*	*	CANC	*	0.000000	0.000000		
09790326	*	N	*	*	CANC	*	0.000000	0.000000		
09790327	*	N	*	*	CANC	*	0.000000	0.000000		
09790328	*	N	*	*	CANC	*	0.000000	0.000000		
09790329	*	N	*	*	CANC	*	0.000000	0.000000		
09790330	*	N	*	*	CANC	*	0.000000	0.000000		
09790331	*	N	*	*	CANC	*	0.000000	0.000000		
09790332	*	N	*	*	CANC	*	0.000000	0.000000		
09790333	*	N	*	*	CANC	*	0.000000	0.000000		
09790334	*	N	*	*	CANC	*	0.000000	0.000000		
09790335	*	N	*	*	CANC	*	0.000000	0.000000		
09790336	*	N	*	*	CANC	*	0.000000	0.000000		
09790337	*	N	*	*	CANC	*	0.000000	0.000000		
09790338	*	N	*	*	CANC	*	0.000000	0.000000		
09790339	*	N	*	*	CANC	*	0.000000	0.000000		
09790340	*	N	*	*	CANC	*	0.000000	0.000000		
09790341	*	N	*	*	CANC	*	0.000000	0.000000		
09790342	*	N	*	*	CANC	*	0.000000	0.000000		
09790343	*	N	*	*	CANC	*	0.000000	0.000000		
09790344	*	N	*	*	CANC	*	0.000000	0.000000		
09790345	UNION	N	BG	73-28	ABDN	TG	0.000000	0.000000		
09790346	*	N	*	*	CANC	*	0.000000	0.000000		

Appendix 5 - well data

API number	Operator Company	Confid -ential?	Lease Name	Well Number	Well Status	Well Type	Latitude	Longitude	Got History?	Activity 1989-1994
09790347	*	N	*	*	CANC	*	0.000000	0.000000		
09790348	UNION	N	BG	73-31	ABDN	TG	0.000000	0.000000		
09790349	SHELL	N	Heat Hole	10	ABDN	TG	0.000000	0.000000		
09790350	SHELL	N	Heat Hole	12	ABDN	TG	0.000000	0.000000		
09790351	*	N	*	*	CANC	*	0.000000	0.000000		
09790352	SHELL	N	Heat Hole	21	ABDN	TG	0.000000	0.000000		
09790353	SHELL	N	Heat Hole	22A	ABDN	TG	0.000000	0.000000		
09790354	SHELL	Y	Heat Hole	24	ABDN	TG	0.000000	0.000000		
09790355	SHELL	N	Heat Hole	26	ABDN	TG	0.000000	0.000000		
09790356	SHELL	Y	Heat Hole	36	ABDN	TG	0.000000	0.000000		
09790357	*	N	*	*	CANC	*	0.000000	0.000000		
09790358	*	N	*	*	CANC	*	0.000000	0.000000		
09790359	UNION	N	CMHC	6	ACTV	INJ	38.803995	-122.782733	Yes	INJ
09790360	UNION	N	CMHC	7	ACTV	DST	38.803940	-122.782889	Yes	PROD
09790361	UNION	N	GDC	8	ACTV	DST	38.783825	-122.771744	Yes	PROD
09790362	UNION	N	GDC	9	ACTV	DST	38.783855	-122.771666	Yes	PROD
09790363	UNION	N	GDC	10	ACTV	DST	38.783943	-122.771826	Yes	PROD
09790364	UNION	N	GDC	11	ACTV	DST	38.784058	-122.771900	Yes	PROD
09790365	UNION	N	DX State 4596	38	ACTV	DST	38.833604	-122.797545	Yes	PROD
09790366	UNION	N	DX State 4596	39	ACTV	DST	38.836502	-122.797687	Yes	PROD
09790367	*	N	*	*	CANC	*	0.000000	0.000000		
09790368	NCPA	Y	CA-950	43-3	ACTV	DST	38.755751	-122.732268		
09790369	UNION	N	Ottoboni St 4596	25	ACTV	DST	38.836452	-122.797640	Yes	PROD
09790370	UNION	N	DX State 4596	40	ACTV	DST	38.814396	-122.791710	Yes	PROD
09790371	UNION	N	Sulphur Bank	27	ACTV	DST	38.808806	-122.814392	Yes	PROD
09790372	*	N	*	*	CANC	*	0.000000	0.000000		
09790373	UNION	N	DX State 4596	41	ACTV	DST	38.814465	-122.791565	Yes	PROD
09790374	UNION	N	LF State 4597	29	ACTV	DST	38.809555	-122.779906	Yes	PROD
09790375	UNION	N	LF State 4597	28	ACTV	DST	38.809714	-122.779746	Yes	PROD
09790376	NCPA	Y	CA-950	33-4	ABDN	DST	38.755992	-122.750290		
09790377	UNION	N	GDC	7	ACTV	DST	38.788509	-122.778409	Yes	PROD
09790378	REPUB	Y	M	1	CANC	TG	0.000000	0.000000		
09790379	UNION	N	Angeli	1	ABDN	DST	38.802895	-122.751308	Yes	NA
09790380	UNION	N	DX State 4596	44	ACTV	DST	38.812223	-122.794409	Yes	PROD
09790381	UNION	N	DX State 4596	43	ABDN	DST	38.812292	-122.794265	Yes	NA
09790382	UNION	N	DX State 4596	42	ACTV	DST	38.814536	-122.791423	Yes	PROD
09790383	*	N	*	*	CANC	*	0.000000	0.000000		
09790384	*	N	*	*	CANC	*	0.000000	0.000000		
09790385	*	N	*	*	CANC	*	0.000000	0.000000		
09790386	UNION	N	Curry	1	ACTV	DST	38.797370	-122.806206	Yes	PROD
09790387	GEP	N	Aidlin	3	ACTV	INJ	38.847500	-122.881500	Yes	INJ
09790388	SANFE	N	TG	34-5	ABDN	TG	0.000000	0.000000		
09790389	SANFE	N	TG	56-9	ABDN	TG	0.000000	0.000000		
09790390	SANFE	N	TG	58-8	ABDN	TG	0.000000	0.000000		
09790391	*	N	*	*	CANC	*	0.000000	0.000000		
09790392	NCPA	Y	CA-949	69-2	ABDN	DST	38.745237	-122.710767		
09790393	*	N	*	*	CANC	*	0.000000	0.000000		
09790394	CGC	N	CA-958	37-34	ACTV	DST	38.763800	-122.732500	Yes	PROD

Appendix 5 - well data

API number	Operator Company	Confid -ential?	Lease Name	Well Number	Well Status	Well Type	Latitude	Longitude	Got History?	Activity 1989-1994
09790395	CGC	N	CA-958	37A-34	ACTV	DST	38.763500	-122.732500	Yes	PROD
09790396	CGC	N	CA-958	56A-34	ACTV	DST	38.764100	-122.727500	Yes	PROD
09790397	*	N	*	*	CANC	*	0.000000	0.000000		
09790398	*	N	*	*	CANC	*	0.000000	0.000000		
09790399	FMRP	N	HS	11	ABDN	TG	0.000000	0.000000		
09790400	FMRP	N	HS	12	ABDN	TG	0.000000	0.000000		
09790401	*	N	*	*	CANC	*	0.000000	0.000000		
09790402	*	N	*	*	CANC	*	0.000000	0.000000		
09790403	UNION	N	BG	72-16	ABDN	TG	0.000000	0.000000		
09790404	SRGC	N	CA-1862	37-21	ABDN	DST	38.789105	-122.750596	Yes	PROD; ABDN 7/93
09790405	SHELL	N	Heat Hole	11	ABDN	TG	0.000000	0.000000		
09790406	SHELL	N	Heat Hole	23	ABDN	TG	0.000000	0.000000		
09790407	SHELL	N	Heat Hole	37	ABDN	TG	0.000000	0.000000		
09790408	SHELL	N	Heat Hole	38	ABDN	TG	0.000000	0.000000		
09790409	SHELL	N	Heat Hole	39	ABDN	TG	0.000000	0.000000		
09790410	SHELL	N	Heat Hole	40	ABDN	TG	0.000000	0.000000		
09790411	SHELL	N	Heat Hole	41	ABDN	TG	0.000000	0.000000		
09790412	SHELL	N	Heat Hole	42	ABDN	TG	0.000000	0.000000		
09790413	SHELL	N	Heat Hole	43	ABDN	TG	0.000000	0.000000		
09790414	SHELL	N	Heat Hole	44	ABDN	TG	0.000000	0.000000		
09790415	SHELL	N	Heat Hole	45	ABDN	TG	0.000000	0.000000		
09790416	SHELL	Y	Heat Hole	46	ABDN	TG	0.000000	0.000000		
09790417	SHELL	Y	Heat Hole	27	ABDN	TG	0.000000	0.000000		
09790418	SHELL	Y	Heat Hole	28	ABDN	TG	0.000000	0.000000		
09790419	SHELL	Y	Heat Hole	30	ABDN	TG	0.000000	0.000000		
09790420	SHELL	Y	Heat Hole	32	ABDN	TG	0.000000	0.000000		
09790421	SHELL	Y	Heat Hole	34	ABDN	TG	0.000000	0.000000		
09790422	UNION	N	Geysers	VII	ABDN	DST	38.802530	-122.804224		
09790423	*	N	*	*	CANC	*	0.000000	0.000000		
09790424	DWR	N	Rorabaugh	3	ABDN	DST	38.799339	-122.820129	Yes	SHTN 3/92
09790425	DWR	Y	Rorabaugh	4	CANC	DST	0.000000	0.000000		
09790426	DWR	Y	Rorabaugh	5	CANC	DST	0.000000	0.000000		
09790427	UNION	N	D & V	2	ACTV	DST	38.768681	-122.738056	Yes	PROD
09790428	CGC	N	CA-956A	56-34	ACTV	DST	38.763800	-122.727200	Yes	PROD 1/89-9/93; INJ 11/93-12/94
09790429	UNION	N	GDC	12	ACTV	DST	38.797263	-122.806252	Yes	PROD
09790430	*	N	*	*	CANC	*	0.000000	0.000000		
09790431	*	N	*	*	CANC	*	0.000000	0.000000		
09790432	*	N	*	*	CANC	*	0.000000	0.000000		
09790433	UNION	N	Beigel	1	ACTV	DST	38.778561	-122.763477	Yes	PROD
09790434	UNION	N	LF State 4597	30	ACTV	DST	38.792634	-122.757784	Yes	PROD
09790435	UNION	N	Tocher	1	ACTV	DST	38.780133	-122.736917	Yes	PROD
09790436	GEO	N	Rorabaugh	A-12	ABDN	DST	38.794550	-122.837400	Yes	NA
09790437	UNION	N	DX State 4596	23	ACTV	DST	38.819385	-122.776111	Yes	PROD
09790438	UNION	N	DX State 4596	45	ACTV	DST	38.827926	-122.783612	Yes	PROD
09790439	UNION	N	DX State 4596	46	ACTV	DST	38.827937	-122.783790	Yes	PROD
09790440	UNION	N	DX State 4596	47	ACTV	DST	38.819416	-122.776243	Yes	SHTN
09790441	*	N	*	*	CANC	*	0.000000	0.000000		
09790442	*	N	*	*	CANC	*	0.000000	0.000000		

Appendix 5 - well data

API number	Operator Company	Confid -ential?	Lease Name	Well Number	Well Status	Well Type	Latitude	Longitude	Got History?	Activity 1989-1994
09790443	*	N	*	*	CANC	*	0.000000	0.000000		
09790444	*	N	*	*	CANC	*	0.000000	0.000000		
09790445	GEO	N	Rorabaugh	A-14	ACTV	DST	38.796066	-122.828886	Yes	SHTN 6/91
09790446	NCPA	Y	CA-950	81B-3	ACTV	DST	38.760152	-122.723699		
09790447	UNION	N	DX State 4596	48	ACTV	DST	38.819468	-122.776048	Yes	SHTN
09790448	UNION	N	DX State 4596	49	ABDN	DST	38.819507	-122.776218	Yes	SHTN
09790449	UNION	N	Geysers	III	ABDN	DST	38.781700	-122.801500		
09790450	UNION	N	LF State 4597	34	ACTV	DST	38.804978	-122.776675	Yes	PROD
09790451	NCPA	Y	CA-950	81C-3	ACTV	DST	38.760141	-122.723574		
09790452	UNION	Y	CA-5639	86-30	PROP	DST	38.783863	-122.777222		
09790453	UNION	Y	CA-5634	45A-12	ACTV	DST	38.814564	-122.815000		
09790454	UNION	N	DX State 4596	50	ACTV	DST	38.827956	-122.783875	Yes	PROD
09790455	UNION	N	GD Horner State	2	ACTV	DST	38.827961	-122.783964	Yes	PROD
09790456	UNION	Y	CA-5634	73-12	ACTV	DST	38.816757	-122.807952		
09790457	UNION	N	Angeli	2	ACTV	DST	38.792702	-122.757720	Yes	PROD
09790458	UNION	Y	CA-5639	52-32	ABDN	DST	38.770669	-122.764882		
09790459	ANDAR	N	Exploratory Site	C	ABDN	EST	38.737000	-122.662000		
09790460	*	N	*	*	CANC	*	0.000000	0.000000		
09790461	NCPA	Y	CA-950	43A-3	ACTV	DST	38.755742	-122.732147		
09790462	GEO	N	Rorabaugh	A-13	ACTV	DST	38.801608	-122.832336	Yes	PROD; SHTN 6/91
09790463	NCPA	Y	CA-950	43B-3	ABDN	DST	38.755764	-122.732034		
09790464	REPUB	Y	M	2	CANC	TG	0.000000	0.000000		
09790465	UNION	Y	CA-5634	73A-12	ACTV	DST	38.816856	-122.808076		
09790466	UNION	Y	CA-5634	73B-12	ACTV	DST	38.816957	-122.808197		
09790467	*	N	*	*	CANC	*	0.000000	0.000000		
09790468	DWR	N	Rorabaugh	6	ABDN	DST	38.797370	-122.807952	Yes	SHTN 3/92
09790469	DWR	Y	Rorabaugh	7	CANC	DST	0.000000	0.000000		
09790470	DWR	Y	Rorabaugh	8	CANC	DST	0.000000	0.000000		
09790471	DWR	Y	Rorabaugh	9	CANC	DST	0.000000	0.000000		
09790472	DWR	Y	Rorabaugh	10	CANC	DST	0.000000	0.000000		
09790473	DWR	Y	Rorabaugh	11	CANC	DST	0.000000	0.000000		
09790474	DWR	Y	Rorabaugh	12	CANC	DST	0.000000	0.000000		
09790475	DWR	Y	Rorabaugh	13	CANC	DST	0.000000	0.000000		
09790476	*	N	*	*	CANC	*	0.000000	0.000000		
09790477	GEO	N	Prati	1	ABDN	DST	38.837304	-122.806129	Yes	NA
09790478	CGC	N	CA-958	56B-34	ACTV	DST	38.763500	-122.727000	Yes	PROD
09790479	NCPA	Y	CA-950	43C-3	ACTV	DST	38.755762	-122.731910		
09790480	UNION	N	Modini	1	ACTV	DST	38.773270	-122.736155	Yes	PROD
09790481	UNION	N	Modini	2	ACTV	DST	38.773352	-122.736289	Yes	PROD
09790482	UNION	N	DX State 4596	57	ABDN	DST	38.824770	-122.776285	Yes	NA
09790483	NCPA	Y	CA-949	24B-2	ACTV	DST	38.753190	-122.718478		
09790484	GEO	N	Rorabaugh	A-17	ACTV	DST	38.801564	-122.832277	Yes	SHTN 6/90
09790485	UNION	Y	Sulphur Bank	29	ACTV	INJ	38.809954	-122.829784		
09790486	CCPA	N	Prati State	1	ACTV	DST	38.837440	-122.805954	Yes	PROD
09790487	CGC	N	CA-1862	21-28	ACTV	INJ	38.785300	-122.752500	Yes	PROD 1/89 -8/91; INJ 8/91-12/94
09790488	UNION	N	DX State 4596	55	ACTV	DST	38.822915	-122.792054	Yes	PROD
09790489	NCPA	Y	CA-949	24C-2	ACTV	DST	38.753201	-122.718584		

Appendix 5 - well data

API number	Operator Company	Confid -ential?	Lease Name	Well Number	Well Status	Well Type	Latitude	Longitude	Got History?	Activity 1989-1994
09790490	UNION	N	DX State 4596	58	ACTV	DST	38.824739	-122.776451	Yes	PROD
09790491	GEO	N	Rorabaugh	A-19	ACTV	DST	38.801564	-122.832277	Yes	SHTN 6/91
09790492	NCPA	Y	CA-949	13-2	ACTV	DST	38.756371	-122.720499		
09790493	UNION	N	DX State 4596	56	ACTV	DST	38.822700	-122.791841	Yes	PROD
09790494	UNION	N	DX State 4596	59	ACTV	DST	38.824704	-122.776618	Yes	PROD
09790495	*	N	*	*	CANC	*	0.000000	0.000000		
09790496	*	N	*	*	CANC	*	0.000000	0.000000		
09790497	*	N	*	*	CANC	*	0.000000	0.000000		
09790498	*	N	*	*	CANC	*	0.000000	0.000000		
09790499	*	N	*	*	CANC	*	0.000000	0.000000		
09790500	*	N	*	*	CANC	*	0.000000	0.000000		
09790501	GEO	N	Dunlavy	2	ABDN	TG	0.000000	0.000000		
09790502	*	N	*	*	CANC	*	0.000000	0.000000		
09790503	*	N	*	*	CANC	*	0.000000	0.000000		
09790504	*	N	*	*	CANC	*	0.000000	0.000000		
09790505	GEO	N	WW	1	ABDN	TG	0.000000	0.000000		
09790506	GEO	N	NWW	2	ABDN	TG	0.000000	0.000000		
09790507	UNION	N	Geyser Gun Club	4	ACTV	DST	38.812791	-122.826143	Yes	PROD
09790508	UNION	N	LF State 4597	31	ACTV	DST	38.795982	-122.779097	Yes	PROD
09790509	GEO	N	WS	4-A	ABDN	TG	0.000000	0.000000		
09790510	NCPA	Y	CA-949	13A-2	ACTV	DST	38.756280	-122.720460		
09790511	UNION	N	DX State 4596	60	ACTV	DST	38.824671	-122.776785	Yes	PROD
09790512	GEO	N	Rorabaugh	A-18	ABDN	DST	38.802856	-122.838192	Yes	PROD; SHTN 6/91
09790513	UNION	Y	CA-5639	65-29	ACTV	INJ	38.778622	-122.763626		
09790514	CCPA	N	Prati	2	ACTV	DST	38.837440	-122.806039	Yes	PROD
09790515	UNION	N	Geyser Gun Club	5	ACTV	DST	38.812818	-122.826310	Yes	PROD
09790516	UNION	N	DX State 4596	69	ACTV	DST	38.824663	-122.776898	Yes	PROD
09790517	UNION	Y	CA-5639	14-27	ACTV	DST	38.780263	-122.736982		
09790518	UNION	Y	CA-5635	123-19	ACTV	DST	38.795911	-122.779133		
09790519	CCPA	N	Prati	8	ACTV	INJ	38.836441	-122.825367	Yes	INJ
09790520	CCPA	N	WS	1	ABDN	TG	0.000000	0.000000		
09790521	CGC	N	CA-1862	62-29	ACTV	DST	38.784500	-122.763800	Yes	PROD
09790522	UNION	N	DX State 4596	63	ACTV	DST	38.821542	-122.771276	Yes	PROD
09790523	MSR	N	MSR Abril	5B-1	ABDN	EST	38.804104	-122.855095		
09790524	CCPA	Y	Prati	7	ABDN	DST	38.848097	-122.845074		
09790525	UNION	N	D & V	11	ACTV	INJ	38.763061	-122.739829	Yes	PROD
09790526	CCPA	N	Prati	9	ACTV	INJ	38.836386	-122.825409	Yes	INJ
09790527	UNION	N	D & V	13	ACTV	DST	38.763193	-122.740138	Yes	PROD
09790528	UNION	N	DX State 4596	64	ACTV	DST	38.821669	-122.771592	Yes	PROD
09790529	UNION	N	D & V	12	ACTV	DST	38.763124	-122.739978	Yes	PROD
09790530	GEO	N	Abril	1-1	ABDN	DST	38.798100	-122.845100	Yes	PROD; SHTN 6/91
09790531	UNION	N	Modini	4	ACTV	DST	38.773457	-122.736279	Yes	PROD
09790532	UNION	N	Modini	3	ACTV	DST	38.773377	-122.736151	Yes	PROD
09790533	EEI	N	SS	3	ABDN	CLT	0.000000	0.000000		
09790534	UNION	N	GDC	53A-13	ACTV	INJ	38.802670	-122.810434	Yes	INJ
09790535	UNION	N	D & V	3	ACTV	DST	38.768646	-122.738223	Yes	PROD
09790536	CGC	N	CA-1862	37A-21	ACTV	DST	38.789105	-122.750596	Yes	PROD
09790537	CGC	N	CA-1862	62A-29	ACTV	DST	38.784600	-122.763900	Yes	PROD

Appendix 5 - well data

API number	Operator Company	Confid -ential?	Lease Name	Well Number	Well Status	Well Type	Latitude	Longitude	Got History?	Activity 1989-1994
09790538	*	N	*	*	CANC	*	0.000000	0.000000		
09790539	UNION	N	DX State 4596	72	ACTV	INJ	38.819416	-122.776341	Yes	INJ
09790540	UNION	N	D & V	4	ACTV	DST	38.768695	-122.737882	Yes	PROD
09790541	CGC	N	CA-1862	37B-21	ACTV	DST	38.789105	-122.750596	Yes	PROD
09790542	GEO	N	Abril	1-2	ABDN	DST	38.798100	-122.845100		
09790543	CGC	N	CA-1862	62B-29	ACTV	DST	38.784400	-122.763700	Yes	PROD
09790544	CGC	N	CA-1862	62C-29	ACTV	DST	38.784300	-122.763600	Yes	PROD
09790545	UNION	N	D & V	5	ACTV	DST	38.766867	-122.746526	Yes	PROD
09790546	UNION	Y	CA-5634	32-12	ACTV	DST	38.819512	-122.815819		
09790547	NCPA	Y	CA-950	86A-3	ACTV	DST	38.749804	-122.725554		
09790548	UNION	Y	CA-5639	53-33	ACTV	DST	38.767279	-122.746438		
09790549	UNION	N	GDC	20	ACTV	DST	38.788531	-122.778757	Yes	PROD
09790550	ANDAR	N	TG	26	ABDN	TG	0.000000	0.000000		
09790551	ANDAR	N	TG	27	ABDN	TG	0.000000	0.000000		
09790552	ANDAR	N	TG	28	ABDN	TG	0.000000	0.000000		
09790553	CGC	N	CA-1862	21A-28	ACTV	DST	38.785200	-122.752500	Yes	PROD
09790554	UNION	Y	CA-5634	32A-12	ACTV	DST	38.819627	-122.815915		
09790555	UNION	Y	CA-5635	94-19	ACTV	INJ	38.793463	-122.786415		
09790556	UNION	N	D & V	15	ACTV	DST	38.763034	-122.739492	Yes	PROD
09790557	*	N	*	*	CANC	*	0.000000	0.000000		
09790558	CGC	N	CA-1862	15-21	ACTV	DST	38.792100	-122.755600	Yes	PROD
09790559	UNION	Y	CA-5634	32B-12	ACTV	DST	38.819745	-122.816007		
09790560	UNION	N	D & V	16	ACTV	DST	38.763058	-122.739563	Yes	PROD
09790561	UNION	Y	CA-5635	94A-19	ACTV	DST	38.793537	-122.786277		
09790562	UNION	N	LF State 4597	35	ACTV	DST	38.791133	-122.772198	Yes	PROD
09790563	UNION	N	DX State 4596	61	ACTV	INJ	38.822728	-122.791671	Yes	INJ
09790564	CGC	N	CA-1862	15A-21	ACTV	DST	38.791900	-122.755600	Yes	PROD
09790565	UNION	N	GDC	18	ACTV	INJ	38.786456	-122.775433	Yes	PROD / INJ MIXED
09790566	UNION	N	LF State 4597	36	ACTV	DST	38.791042	-122.772330	Yes	PROD
09790567	UNION	N	71	5	ABDN	TG	0.000000	0.000000		
09790568	UNION	N	71	7	ABDN	TG	0.000000	0.000000		
09790569	UNION	N	71	8	ABDN	TG	0.000000	0.000000		
09790570	UNION	N	71	12	ABDN	TG	0.000000	0.000000		
09790571	UNION	N	71	13	ABDN	TG	0.000000	0.000000		
09790572	UNION	N	71	14	ABDN	TG	0.000000	0.000000		
09790573	UNION	N	71	16	ABDN	TG	0.000000	0.000000		
09790574	UNION	N	71	18	ABDN	TG	0.000000	0.000000		
09790575	UNION	N	71	19	ABDN	TG	0.000000	0.000000		
09790576	UNION	N	71	23	ABDN	TG	0.000000	0.000000		
09790577	UNION	N	71	24A	ABDN	TG	0.000000	0.000000		
09790578	*	N	*	*	CANC	*	0.000000	0.000000		
09790579	UNION	N	Sulphur Bank	30	ACTV	DST	38.805044	-122.816854	Yes	PROD
09790580	UNION	N	Geyser Gun Club	6	ACTV	DST	38.812848	-122.826477	Yes	PROD
09790581	UNION	N	BG	73-1	ABDN	TG	0.000000	0.000000		
09790582	UNION	N	BG	73-4	ABDN	TG	0.000000	0.000000		
09790583	UNION	N	BG	73-5	ABDN	TG	0.000000	0.000000		
09790584	CGC	N	CA-1862	21B-28	ACTV	DST	38.785100	-122.752500	Yes	PROD
09790585	GEO	N	NW	2	ABDN	TG	0.000000	0.000000		

Appendix 5 - well data

API number	Operator Company	Confid -ential?	Lease Name	Well Number	Well Status	Well Type	Latitude	Longitude	Got History?	Activity 1989-1994
09790586	CCPA	N	NW	3	ABDN	TG	0.000000	0.000000		
09790587	CCPA	N	WW	2	ABDN	TG	0.000000	0.000000		
09790588	UNION	Y	CA-5635	94B-19	ACTV	DST	38.793608	-122.786135		
09790589	UNION	Y	CA-5634	21-12	ACTV	DST	38.820056	-122.818260		
09790590	UNION	Y	CA-5639	63-29	ACTV	DST	38.780803	-122.761892		
09790591	UNION	N	DX State 4596	67	ACTV	DST	38.823367	-122.786177	Yes	PROD
09790592	UNION	Y	CA-5639	42-33	ACTV	DST	38.770471	-122.749251		
09790593	UNION	Y	CA-5639	63A-29	ACTV	DST	38.780828	-122.761722		
09790594	UNION	Y	CA-5634	21A-12	ACTV	DST	38.820157	-122.818377		
09790595	UNION	N	Happy Bob State	1	ACTV	DST	38.824530	-122.824750	Yes	PROD
09790596	UNION	Y	CA-5639	42A-33	ABDN	DST	38.770600	-122.749194		
09790597	CCPA	N	Prati State	10	ACTV	DST	38.833700	-122.815700	Yes	PROD
09790598	GEO	N	Rorabaugh	A-22	ACTV	DST	38.794550	-122.837400	Yes	PROD 6/91
09790599	CCPA	Y	Prati State	31	ACTV	DST	38.839856	-122.835678		
09790600	UNION	N	Thermal	15	ACTV	DST	38.802648	-122.805351	Yes	PROD
09790601	UNION	N	DX State 4596	74	ACTV	DST	38.823864	-122.778086	Yes	PROD
09790602	UNION	Y	CA-5633	87A-2	ACTV	DST	38.824537	-122.822750		
09790603	UNION	N	DX State 4596	75	ACTV	DST	38.823812	-122.778154	Yes	PROD
09790604	GEO	N	FG	1	ACTV	TG	0.000000	0.000000		
09790605	CCPA	Y	Prati	30	ACTV	DST	38.848166	-122.845071		
09790606	CCPA	N	WW	3	ABDN	TG	0.000000	0.000000		
09790607	UNION	N	GDC	21	ACTV	INJ	38.775089	-122.752435	Yes	INJ
09790608	UNION	Y	CA-5639	63B-29	ACTV	DST	38.780847	-122.761562		
09790609	GEP	N	Aidlin	5	ACTV	DST	38.832498	-122.874608	Yes	PROD
09790610	UNION	Y	CA-5639	36-28	ACTV	DST	38.774955	-122.752468		
09790611	UNION	Y	CA-5639	42B-33	ACTV	INJ	38.770732	-122.749137		
09790612	UNION	N	GDC	26	ACTV	INJ	38.802014	-122.803947	Yes	INJ
09790613	UNION	N	GDC	23	ACTV	DST	38.774820	-122.752502	Yes	PROD
09790614	UNION	N	DX State 4596	68	ACTV	DST	38.823398	-122.786017	Yes	PROD
09790615	UNION	N	Beigel	2	ACTV	DST	38.778588	-122.763547	Yes	PROD
09790616	GEO	N	NWW	6	ABDN	TG	0.000000	0.000000		
09790617	GEO	Y	Prati State	26	CANC	DST	0.000000	0.000000		
09790618	CCPA	N	Prati	39	ACTV	DST	38.845632	-122.828484	Yes	PROD
09790619	NCPA	Y	CA-950	86B-3	ACTV	INJ	38.749749	-122.725656		
09790620	UNION	N	GDC	19	ACTV	DST	38.786385	-122.775550	Yes	PROD
09790621	UNION	Y	CA-5639	44-28	ACTV	DST	38.779610	-122.749453		
09790622	UNION	Y	CA-5639	44B-28	ACTV	DST	38.779569	-122.749517		
09790623	CCPA	Y	Prati	29	ACTV	DST	38.850106	-122.818153		
09790624	CCPA	N	Prati	27	ACTV	EST	38.849971	-122.818127	Yes	PROD
09790625	GEO	N	Rorabaugh	A-25	ACTV	DST	38.793602	-122.840660	Yes	SHTN 6/91
09790626	GEO	N	BR	10	ABDN	TG	0.000000	0.000000		
09790627	GEO	N	BR	12	ABDN	TG	0.000000	0.000000		
09790628	GEO	N	BR	5	ABDN	TG	0.000000	0.000000		
09790629	UNION	N	Beigel	3	ACTV	DST	38.780863	-122.761469	Yes	PROD
09790630	CCPA	Y	Prati	32	ACTV	DST	38.839919	-122.835714		
09790631	UNION	Y	CA-5639	44A-28	ACTV	DST	38.779648	-122.749385		
09790632	NCPA	Y	CA-949	13C-2	ACTV	DST	38.756357	-122.720985		
09790633	NCPA	Y	CA-949	13D-2	ACTV	DST	38.756299	-122.721063		

Appendix 5 - well data

API number	Operator Company	Confid -ential?	Lease Name	Well Number	Well Status	Well Type	Latitude	Longitude	Got History?	Activity 1989-1994
09790634	UNION	N	GDC	24	ACTV	DST	38.786355	-122.775628	Yes	PROD
09790635	UNION	N	GDC	29	ACTV	DST	38.777625	-122.739985	Yes	PROD
09790636	UNION	Y	CA-5639	85-28	ACTV	DST	38.777626	-122.739983		
09790637	UNION	N	Sulphur Bank	28	ACTV	DST	38.809163	-122.813956	Yes	PROD
09790638	UNION	N	GDC	25	ACTV	DST	38.786415	-122.775681	Yes	PROD
09790639	UNION	N	Angeli	3	ACTV	DST	38.792733	-122.757624	Yes	PROD
09790640	UNION	N	DX State 4596	73	ACTV	DST	38.823400	-122.785950	Yes	PROD
09790641	UNION	Y	CA-5639	85A-28	ACTV	DST	38.777702	-122.739965		
09790642	UNION	Y	CA-5634	32C-12	ACTV	DST	38.819858	-122.816099		
09790643	UNION	N	DX State 4596	62	ACTV	DST	38.822755	-122.791508	Yes	PROD
09790644	UNION	N	Curry	3	ACTV	DST	38.797134	-122.806306	Yes	PROD
09790645	UNION	N	LF State 4597	37	ACTV	DST	38.797779	-122.764250	Yes	PROD
09790646	UNION	Y	CA-5634	21B-12	ACTV	DST	38.820259	-122.818497		
09790647	UNION	Y	CA-5634	32D-12	ACTV	DST	38.819938	-122.816170		
09790648	GEO	N	WS	6	ABDN	TG	0.000000	0.000000		
09790649	*	N	*	*	CANC	*	0.000000	0.000000		
09790650	UNION	Y	CA-5634	21C-12	ACTV	DST	38.820143	-122.818260		
09790651	UNION	Y	CA-5634	21D-12	ACTV	DST	38.820245	-122.818380		
09790652	*	N	*	*	CANC	*	0.000000	0.000000		
09790653	UNION	N	Ottoboni St 4596	27	ACTV	DST	38.826323	-122.803794	Yes	PROD
09790654	UNION	N	Ottoboni St 4596	28	ABDN	DST	38.826376	-122.803848	Yes	NA
09790655	SRGC	N	CA-1862	21C-28	ABDN	INJ	38.785000	-122.752500	Yes	INJ
09790656	GEO	Y	Rorabaugh	A-26	CANC	DST	0.000000	0.000000		
09790657	GEO	N	TG	66	ABDN	TG	0.000000	0.000000		
09790658	GEO	N	TG	67	ABDN	TG	0.000000	0.000000		
09790659	GEO	N	TG	68	ABDN	TG	0.000000	0.000000		
09790660	UNION	Y	CA-5634	45B-12	ACTV	DST	38.814517	-122.814954		
09790661	UNION	N	DX State 4596	71	ABDN	INJ	38.807996	-122.795541	Yes	INJ; ABDN 10/89
09790662	UNION	N	Geyser Gun Club	8	ACTV	DST	38.818686	-122.830134	Yes	PROD
09790663	*	N	*	*	CANC	*	0.000000	0.000000		
09790664	GEO	N	Rorabaugh	A-27	ABDN	DST	38.802195	-122.832684	Yes	PROD; SHTN 6/91
09790665	UNION	N	Ottoboni St 4596	29	ACTV	DST	38.826430	-122.803908	Yes	PROD
09790666	UNION	Y	CA-5634	52-11	ACTV	DST	38.818782	-122.830149		
09790667	UNION	N	DX State 4596	80	ACTV	DST	38.830798	-122.790500	Yes	PROD
09790668	UNION	Y	GD Horner State	6	CANC	DST	0.000000	0.000000		
09790669	UNION	N	DX State 4596	81	ACTV	DST	38.830800	-122.790500	Yes	PROD
09790670	UNION	N	DX State 4596	82	ACTV	DST	38.830796	-122.790525	Yes	PROD
09790671	UNION	N	D & V	6	ACTV	DST	38.766867	-122.746526	Yes	PROD
09790672	UNION	N	LF State 4597	38	ACTV	DST	38.797409	-122.766527	Yes	PROD
09790673	UNION	Y	CA-5635	117-19	ACTV	DST	38.788232	-122.779109		
09790674	UNION	Y	CA-5635	117A19	ACTV	INJ	38.788200	-122.779109		
09790675	*	N	*	*	CANC	*	0.000000	0.000000		
09790676	GEO	N	TG	69	ABDN	TG	0.000000	0.000000		
09790677	UNION	N	LF State 4597	41	ACTV	DST	38.789478	-122.765509	Yes	
09790678	CCPA	N	Prati	4	ACTV	DST	38.839120	-122.821064	Yes	PROD
09790679	UNION	N	LF State 4597	42	ACTV	DST	38.789412	-122.765548	Yes	PROD
09790680	UNION	N	LF State 4597	39	ACTV	DST	38.797453	-122.766608	Yes	PROD
09790681	GEO	Y	Rorabaugh	A-28	CANC	DST	0.000000	0.000000		

Appendix 5 - well data

API number	Operator Company	Confid -ential?	Lease Name	Well Number	Well Status	Well Type	Latitude	Longitude	Got History?	Activity 1989-1994
09790682	CCPA	N	Prati	37	ACTV	DST	38.836038	-122.832184	Yes	PROD
09790683	NCPA	Y	CA-949	13E-2	ACTV	DST	38.756242	-122.721138		
09790684	CCPA	N	Prati	5	ACTV	DST	38.839125	-122.821153	Yes	PROD
09790685	NCPA	Y	CA-950	81E-3	ACTV	DST	38.759793	-122.723124		
09790686	NCPA	Y	CA-950	43F-3	ACTV	DST	38.755698	-122.731608		
09790687	CCPA	N	Prati	38	ACTV	DST	38.836101	-122.832162	Yes	PROD
09790688	NCPA	Y	CA-949	13B-2	ACTV	DST	38.756190	-122.720421		
09790689	NCPA	Y	CA-950	43G-3	ACTV	DST	38.755698	-122.731693		
09790690	NCPA	Y	CA-950	81F-3	ACTV	DST	38.759870	-122.723159		
09790691	UNION	Y	D & V	9	PROP	DST	38.766867	-122.746526		
09790692	UNION	N	DX State 4596	76	ACTV	DST	38.826010	-122.777884	Yes	PROD
09790693	NCPA	Y	CA-950	43H-3	PROP	DST	38.755720	-122.731775		
09790694	UNION	Y	CA-5639	15-28	ACTV	DST	38.774887	-122.755295		
09790695	CCPA	N	Prati	25	ACTV	DST	38.841727	-122.831123	Yes	PROD
09790696	NCPA	Y	CA-949	47-2	ACTV	DST	38.749669	-122.715434		
09790697	NCPA	Y	CA-949	47A-2	ACTV	DST	38.749765	-122.715441		
09790698	UNION	Y	CA-5639	15A-28	ACTV	DST	38.778275	-122.754997		
09790699	UNION	N	DX State 4596	77	ACTV	DST	38.825955	-122.777834	Yes	PROD
09790700	UNION	Y	LF State 4597	51	CANC	DST	0.000000	0.000000		
09790701	UNION	N	DX State 4596	85	ACTV	DST	38.825898	-122.777781	Yes	PROD
09790702	UNION	N	LF State 4597	48	ACTV	DST	38.789500	-122.764500	Yes	PROD
09790703	GEO	Y	D	6	ABDN	TG	0.000000	0.000000		
09790704	UNION	N	GDC	30	ACTV	DST	38.785219	-122.775614	Yes	PROD
09790705	GEO	Y	Rorabaugh	A-32	CANC	DST	0.000000	0.000000		
09790706	NCPA	Y	CA-950	81G-3	ACTV	DST	38.759949	-122.724429		
09790707	NCPA	Y	CA-949	47B-2	ACTV	DST	38.749861	-122.715448		
09790708	GEO	N	Rorabaugh	A-31	ABDN	DST	38.802800	-122.838600	Yes	PROD; SHTN 6/91
09790709	UNION	N	DX State 4596	84	ABDN	DST	38.812777	-122.792838	Yes	SHTN
09790710	NCPA	Y	CA-949	47C-2	ACTV	INJ	38.746768	-122.710777		
09790711	GEO	Y	Prati State	22	CANC	DST	0.000000	0.000000		
09790712	CGC	N	CA-958	37B-34	ACTV	DST	38.763000	-122.732500	Yes	PROD
09790713	UNION	N	Sulphur Bank	31	ACTV	DST	38.809341	-122.814215	Yes	PROD
09790714	CCPA	N	Prati State	24	ACTV	DST	38.833359	-122.805156	Yes	PROD
09790715	UNION	Y	CA-5639	15B-28	ACTV	DST	38.778210	-122.755585		
09790716	CGC	N	CA-1862	62D-29	ACTV	DST	38.784200	-122.763500	Yes	PROD
09790717	NCPA	Y	CA-950	81H-3	ACTV	DST	38.759881	-122.724419		
09790718	NCPA	Y	CA-949	47D-2	ACTV	INJ	38.750053	-122.715463		
09790719	UNION	Y	CA-5639	15C-28	ACTV	DST	38.777874	-122.755142		
09790720	CCPA	N	Prati State	12	ACTV	DST	38.833148	-122.815645	Yes	PROD
09790721	CCPA	N	Prati	50	ACTV	DST	38.840615	-122.812279	Yes	PROD
09790722	NCPA	Y	CA-950	811-3	ACTV	INJ	38.759812	-122.724404		
09790723	UNION	N	LF State 4597	49	ACTV	DST	38.789700	-122.764800	Yes	PROD
09790724	NCPA	Y	CA-950	21-3	ACTV	DST	38.759859	-122.738266		
09790725	CCPA	N	Prati State	54	ACTV	DST	38.833337	-122.805245	Yes	PROD
09790726	NCPA	Y	CA-950	43D-3	ACTV	DST	38.755674	-122.731410		
09790727	NCPA	Y	CA-950	43E-3	ACTV	DST	38.755720	-122.731669		
09790728	NCPA	Y	CA-950	81D-3	ACTV	DST	38.760152	-122.724078		
09790729	UNION	Y	CA-5639	15D-28	ACTV	DST	38.777893	-122.754829		

Appendix 5 - well data

API number	Operator Company	Confid -ential?	Lease Name	Well Number	Well Status	Well Type	Latitude	Longitude	Got History?	Activity 1989-1994
09790730	CGC	N	CA-958	37C-34	ACTV	DST	38.762500	-122.732500	Yes	PROD
09790731	UNION	N	71	1	ABDN	TG	0.000000	0.000000		
09790732	UNION	N	71	2	ABDN	TG	0.000000	0.000000		
09790733	UNION	N	71	3	ABDN	TG	0.000000	0.000000		
09790734	UNION	N	71	4	ABDN	TG	0.000000	0.000000		
09790735	UNION	N	71	6	ABDN	TG	0.000000	0.000000		
09790736	GEO	N	TG	14	ABDN	TG	0.000000	0.000000		
09790737	UNION	N	BG	73-2	ABDN	TG	0.000000	0.000000		
09790738	UNION	N	BG	73-3	ABDN	TG	0.000000	0.000000		
09790739	UNION	N	BG	73-6	ABDN	TG	0.000000	0.000000		
09790740	UNION	N	BG	73-7	ABDN	TG	0.000000	0.000000		
09790741	UNION	N	BG	73-8	ABDN	TG	0.000000	0.000000		
09790742	UNION	N	BG	73-9	ABDN	TG	0.000000	0.000000		
09790743	UNION	N	BG	72-1	ABDN	TG	0.000000	0.000000		
09790744	UNION	N	BG	72-2	ABDN	TG	0.000000	0.000000		
09790745	UNION	N	BG	72-3	ABDN	TG	0.000000	0.000000		
09790746	UNION	N	BG	72-10	ABDN	TG	0.000000	0.000000		
09790747	UNION	N	BG	72-11	ABDN	TG	0.000000	0.000000		
09790748	UNION	N	BG	72-17	ABDN	TG	0.000000	0.000000		
09790749	UNION	N	BG	72-18	ABDN	TG	0.000000	0.000000		
09790750	UNION	N	BG	72-21	ABDN	TG	0.000000	0.000000		
09790751	UNION	N	BG	73-27	ABDN	TG	0.000000	0.000000		
09790752	UNION	Y	CA-5639	14A-27	ACTV	DST	38.780600	-122.736982		
09790753	UNION	N	71	21	ABDN	TG	0.000000	0.000000		
09790754	UNION	N	71	22	ABDN	TG	0.000000	0.000000		
09790755	UNION	N	71	25	ABDN	TG	0.000000	0.000000		
09790756	UNION	N	71	20	ABDN	TG	0.000000	0.000000		
09790757	UNION	N	71	15	ABDN	TG	0.000000	0.000000		
09790758	SHELL	N	Heat Hole	22	ABDN	TG	0.000000	0.000000		
09790759	NCPA	Y	CA-950	21A-3	ACTV	DST	38.759862	-122.738177		
09790760	UNION	N	D & V	23	ACTV	DST	38.767164	-122.736028	Yes	PROD
09790761	CCPA	N	Prati	14	ACTV	DST	38.766800	-122.735500	Yes	PROD
09790762	NCPA	Y	CA-950	21B-3	ACTV	DST	38.838900	-122.809100		
09790763	NCPA	Y	CA-950	21C-3	ACTV	DST	38.759870	-122.738000		
09790764	UNION	Y	ANG	1	CANC	TG	0.000000	0.000000		
09790765	UNION	Y	LFGT	9	ACTV	TG	0.000000	0.000000		
09790766	UNION	Y	G	4	CANC	TG	0.000000	0.000000		
09790767	UNION	Y	G	5	ACTV	TG	0.000000	0.000000		
09790768	UNION	Y	G	8	CANC	TG	0.000000	0.000000		
09790769	UNION	N	G	12	ACTV	TG	0.000000	0.000000		
09790770	UNION	N	G	13	ACTV	TG	0.000000	0.000000		
09790771	UNION	Y	G	14	CANC	TG	0.000000	0.000000		
09790772	CGC	N	CA-1862	62E-29	ACTV	DST	38.784100	-122.763400	Yes	PROD
09790773	UNION	N	D & V	24	ACTV	DST	38.767186	-122.735942	Yes	PROD
09790774	UNION	N	D & V	25	ACTV	DST	38.766800	-122.735400	Yes	PROD
09790775	UNION	Y	G	18	CANC	TG	0.000000	0.000000		
09790776	UNION	Y	G	19	CANC	TG	0.000000	0.000000		
09790777	UNION	N	G	20	ACTV	TG	0.000000	0.000000		

Appendix 5 - well data

API number	Operator Company	Confid -ential?	Lease Name	Well Number	Well Status	Well Type	Latitude	Longitude	Got History?	Activity 1989-1994
09790778	UNION	Y	G	21	CANC	TG	0.000000	0.000000		
09790779	*	N	*	*	CANC	*	0.000000	0.000000		
09790780	UNION	N	G	23	ACTV	TG	0.000000	0.000000		
09790781	UNION	N	G	24	ACTV	TG	0.000000	0.000000		
09790782	UNION	Y	G	25	CANC	TG	0.000000	0.000000		
09790783	UNION	N	G	26	ACTV	TG	0.000000	0.000000		
09790784	UNION	Y	CA-5634	51-11	ACTV	DST	38.819973	-122.829803		
09790785	CGC	N	CA-1862	15B-21	ACTV	DST	38.792100	-122.755100	Yes	PROD
09790786	NCPA	Y	CA-950	21D-3	ACTV	DST	38.759873	-122.737915		
09790787	UNION	N	LF State 4597	40	ACTV	DST	38.791900	-122.766000	Yes	PROD
09790788	UNION	Y	CA-5634	51A-11	ACTV	DST	38.820198	-122.830025		
09790789	UNION	N	G	29	ACTV	TG	0.000000	0.000000		
09790790	UNION	Y	CA-5634	52B-11	ACTV	DST	38.818686	-122.830134		
09790791	UNION	Y	LF State 4597	43	CANC	DST	0.000000	0.000000		
09790792	UNION	Y	CA-5639	88-28	PROP	DST	38.772369	-122.740181		
09790793	UNION	N	Angeli	4	ACTV	DST	38.794412	-122.759234	Yes	PROD
09790794	CGC	N	CA-1862	15C-21	ACTV	DST	38.791900	-122.755100	Yes	PROD
09790795	GEP	N	Aidlin	6	ACTV	DST	38.832600	-122.877100	Yes	PROD
09790796	GEP	N	Aidlin	8	ACTV	DST	38.847500	-122.881700	Yes	INJ
09790797	NCPA	Y	CA-949	24D-2	ACTV	DST	38.753196	-122.718346		
09790798	CCPA	Y	Prati	41	CANC	DST	0.000000	0.000000		
09790799	CCPA	Y	Prati State	11	CANC	DST	0.000000	0.000000		
09790800	NCPA	Y	CA-949	24E-2	ACTV	DST	38.753171	-122.718236		
09790801	UNION	Y	CA-5634	48-2	ACTV	DST	38.822529	-122.834633		
09790802	NCPA	Y	CA-949	24F-2	ACTV	DST	38.753157	-122.718172		
09790803	UNION	Y	CA-5633	48A-2	ACTV	DST	38.822529	-122.834785		
09790804	GEP	Y	Aidlin	4	ACTV	DST	38.837486	-122.886215		
09790805	UNION	Y	CA-5633	27-2	ACTV	DST	38.823914	-122.836583		
09790806	UNION	Y	G	27	CANC	TG	0.000000	0.000000		
09790807	UNION	Y	CA-5633	27A-2	ACTV	DST	38.823914	-122.836583		
09790808	NCPA	Y	CA-949	24G-2	ACTV	DST	38.753143	-122.718105		
09790809	SCPD	Y	SV Geo	1	CANC	NLT	0.000000	0.000000		
09790810	UNION	N	S	1	ACTV	TG	0.000000	0.000000		
09790811	CGC	N	CA-1862	71-28	ACTV	DST	38.785100	-122.744000	Yes	PROD
09790812	CGC	N	CA-956A	56C-34	ACTV	DST	38.762700	-122.736900	Yes	PROD
09790813	NCPA	Y	CA-949	69A-2	ACTV	DST	38.745481	-122.710156		
09790814	NCPA	Y	CA-949	69B-2	ACTV	DST	38.745424	-122.710125		
09790815	CGC	N	CA-1862	71A-28	ACTV	DST	38.784800	-122.743000	Yes	PROD
09790816	NCPA	Y	CA-949	69C-2	ACTV	DST	38.745391	-122.710142		
09790817	GEP	Y	Aidlin	7	ACTV	DST	38.832600	-122.877100		
09790818	NCPA	Y	CA-949	69D-2	ACTV	DST	38.745358	-122.710160		
09790819	NCPA	Y	CA-949	69E-2	ACTV	DST	38.745492	-122.710178		
09790820	SMI	Y	SV	1	ACTV	CLT	0.000000	0.000000		
09790821	CGC	N	CA-1862	37C-21	ACTV	DST	38.789105	-122.750596	Yes	PROD
09790822	NCPA	Y	CA-950	86C-3	ACTV	DST	38.749606	-122.725813		
09790823	NCPA	Y	CA-950	86D-3	ACTV	DST	38.749691	-122.725756		
09790824	NCPA	Y	CA-950	86E-3	ACTV	DST	38.749716	-122.725820		
09790825	GEP	N	Aidlin	9	ACTV	DST	38.832500	-122.876900	Yes	PROD

Appendix 5 - well data

API number	Operator Company	Confid -ential?	Lease Name	Well Number	Well Status	Well Type	Latitude	Longitude	Got History?	Activity 1989-1994
09790826	CGC	N	CA-1862	21D-28	ACTV	DST	38.784900	-122.752500	Yes	PROD
09790827	GEP	Y	Aidlin	10	ACTV	DST	38.832600	-122.877100		

Appendix 6

Listing for program b_D_3d.c

This *C* program was used to calculate the temporal variation in *b* and *D*. See Figure 5.2 for a flow diagram and Section 5.1 for a description of this program.

```
/*   PROGRAM TO FIND B VALUE FOR >100 MAGNITUDES OVER 200 VALUE
     WINDOWS USING FUNCTION DEFINED BY NUMERICAL RECIPE RTBIS
     & PROGRAM TO FIND SPATIAL & TEMPORAL FRACTAL DIMENSION
     OVER 200 VALUE WINDOWS USING FUNCTION FROM HIRATA (1987)
     C Version djb Oct 96
     Use cc -o b_D_3d b_D_3d.c -lm  to compile */

/*   REMEMBER:
     incr is REAL
     ndata is INTEGER
     iwin is REAL */

#include <math.h>
#include <stdio.h>
#define jmax 40
#define iwin 200.0
#define incr 10.0
#define ndata 4000
#define rsmaximum -0.33
#define rsincr 0.05
#define rsstart -1.15
#define rs3dmaximum -0.45
#define rs3dincr 0.05
#define rs3dstart -0.604
#define rtmaximum 1.0
#define rtincr 0.05
#define rtstart -5.0
#define SQR(a) (sqrarg=(a),sqrarg*sqrarg)

double posy[ndata], posx[ndata], posz[ndata], year[ndata], mag[ndata];
double rs[ndata][ndata],rt[ndata][ndata],rs3d[ndata][ndata];
double pow(double, double);
double log10(double);
double log(double);
double fabs(double);
double sqrt(double);
double exp(double);
double max, min, mean, rsmax, rtmax, rs3dmax;
int nltrs = 0;
int nltrs3d = 0;
int nltrt = 0;
static float sqrarg;

main()
        {
        double calcrs(), compares();
        double calcrs3d(), compares3d();
        double calcrt(), comparet();
        void fith(), nrerror();
        double as = 0.0, bs = 0.0, sigas = 0.0, sigbs = 0.0, chi2s = 0.0, qs = 0.0;
        double as3d = 0.0, bs3d = 0.0, sigas3d = 0.0, sigbs3d = 0.0, chi2s3d = 0.0, qs3d = 0.0;
        double at = 0.0, bt = 0.0, sigat = 0.0, sigbt = 0.0, chi2t = 0.0, qt = 0.0;
        double corrs[600], rsx[600], sigs[50];
        double corrs3d[600], rs3dx[600], sigs3d[50];
        double corrt[600], rtx[600], sigt[50];
        double bval1,bval2,akierror,rst=1.0,rtt=1.0,rs3d=1.0;
        double bval3, perror, perrorp, perrorm, sum;
        double page(), pageplus(), pageminus(), rtbis();
```

```
        int i, j, g,k, factor;
        int rscount = 0,rs3dcount = 0,ncount,rtcount = 0;
        sum = 0.0, min = 100.0, max = -100.0;

/*  Read in data */
        scanf("%d\n", &ncount);
        for (g = 0 ; g < ncount ; g++)
    {
        scanf("%lf\t%lf\t%lf\t%lf\t%lf\n", &year[g], &posy[g], &posx[g], &posz[g], &mag[g]);
    }

/*  Examine data in window */
        for ( i = 1; i <= ncount; i+=incr)
    {
        if (i + iwin - 1 <= ncount)
        {
                factor = (int)(i + iwin - 1);
                for (j = i; j <= iwin + i -1 ; j++)
                {
                        if ( mag[j-1] >= max) max = mag[j-1];
                        if ( mag[j-1] <= min) min = mag[j-1];
                        sum += mag[j-1];

/*      calculate values of r (spatial) */
                        for (k = i; k <= (i + iwin - 1); k++)
                {
                        if (j > k) {calcrs(j, k);}
                }
/*      calculate values of r (spatial 3d) */
                        for (k = i; k <= (i + iwin - 1); k++)
                {
                        if (j > k) {calcrs3d(j, k);}
                }
/*      calculate values of r (temporal) */
                                        for (k = i; k <= (i + iwin - 1); k++)
                                        {
                 if (j > k) {calcrt(j, k);}
              }


                }


/*  compare values of r (spatial) */
            for (rst = rsstart; rst<= rsmaximum; rst = rst+rsincr)
                {
                                        rsmax=exp(rst*(log(10)));
                        for (j = i; j <= (i +  iwin - 1); j++)
                        {
                                        for (k = i; k <= (i + iwin - 1); k++)
                        {
                                        if (j > k) {compares(j, k);}
                        }
                        }
                        if  (nltrs > 200)
                {
                        rscount++;
                        rsx[rscount] = log10(rsmax);
                        corrs[rscount] = log10((2.0 / ( iwin * (iwin - 1.0) ) ) * ( (float) nltrs));
/*                                              printf("%lf\t%lf \n", rsx[rscount], corrs[rscount]); */
                  }

      /* reset variables */
                        nltrs = 0;
                }

/*  compare values of r (spatial 3d) */
            for (rs3d = rs3dstart; rs3d<= rs3dmaximum; rs3d = rs3d+rs3dincr)
                {
                                        rs3dmax=exp(rs3d*(log(10)));
                        for (j = i; j <= (i +  iwin - 1); j++)
                        {
                                        for (k = i; k <= (i + iwin - 1); k++)
```

```
                                {
                                        if (j > k) {compares3d(j, k);}
                                }
                                }
                                if (nltrs3d > 200)
                        {
                                rs3dcount++;
                                rs3dx[rs3dcount] = log10(rs3dmax);
                                corrs3d[rs3dcount] = log10((2.0 / ( iwin * (iwin - 1.0) ) ) * ( (float) nltrs3d));
/*                                              printf("%lf\t%lf \n", rs3dx[rs3dcount], corrs3d[rs3dcount]); */
                          }

        /* reset variables */
                                nltrs3d = 0;
                        }

/*  compare values of r (temporal) */
                for (rtt = rtstart; rtt<= rtmaximum; rtt = rtt+rtincr)
                {
                                                rtmax=exp(rtt*(log(10)));
                        for (j = i; j <= (i +  iwin - 1); j++)
                        {
                             for (k = i; k <= (i + iwin - 1); k++)
                             {
                                  if (j > k) {comparet(j, k);}
                             }
                        }
                        if (nltrt > 0)
                        {
                             rtcount++;
                             rtx[rtcount] = log10(rtmax);
                             corrt[rtcount] = log10((2.0 / ( iwin * (iwin - 1.0) ) ) * ( (float) nltrt));
/*                                              printf("t - %lf\t%lf \n", rtx[rtcount], corrt[rtcount]); */
                        }

        /* reset variables */
                        nltrt = 0;
                }

/*                      fith(rtx,corrt,rtcount,sigt,0,&at,&bt,&sigat,&sigbt,&chi2t,&qt); */
                        fith(rsx,corrs,rscount,sigs,0,&as,&bs,&sigas,&sigbs,&chi2s,&qs);
                        fith(rs3dx,corrs3d,rs3dcount,sigs3d,0,&as3d,&bs3d,&sigas3d,&sigbs3d,&chi2s3d,&qs3d);

/*  Calculate bvalues & print results */
/* error on fractal dimensions is 10% - see JRH thesis for theory on this  */
                        mean    = sum / iwin;
                        bval1   = 0.43429 / ( mean - min );
                        bval2   = ( ( iwin - 1 ) * 0.43429 ) / ( iwin * ( mean - min ) );
                        akierror = 1.96 * bval1 / ( pow( iwin, 0.5 ) );
                        bval3   = rtbis(page, -5.0, 10.0, 0.00001);
                        perrorp  = rtbis(pageplus,  -5.0, 10.0, 0.00001);
                        perrorm  = rtbis(pageminus, -5.0, 10.0, 0.00001);
                        perror   = fabs( (perrorp - perrorm) / 2.0);

printf("%lf\t%10.6lf\t%10.6lf\t%10.6lf\t%10.6lf\t%10.6lf\t%10.6lf\t%10.6lf\t%10.6lf\t%10.6lf\t%10.6lf\t%10.6lf\t%10.6lf\n",
year[i+(int)iwin-1]-0.5*(year[i+(int)iwin-1]-year[i]),bval1,bval2,bval3,akierror,perror,bs,bs/10.0,bs3d,bs3d/10.0,bt,bt/10.0);

/*  Reset variables */
                        sum = 0.0, min = 100.0, max = -100.0, rscount = 0, rtcount = 0, rs3dcount=0 ;
                }
                else
                {
                        break;
                }
                }
}

/* BVALUE CALCULATING FUNCTIONS */

/* Bisection function RTBIS from 'Numerical Recipes' */
double rtbis(func, x1, x2, xacc)
    double (*func)(), x1, x2, xacc;
    {
```

```
    int j;
    double dx, f, fmid, xmid, rtb;
    void nrerror();

    f = (*func)(x1);
    fmid = (*func)(x2);
    if (f*fmid >= 0.0) nrerror("Root must be bracketed for bisection in RTBIS.");
    rtb = f < 0.0 ? (dx = x2 - x1, x1) : (dx = x1 - x2, x2);
    for (j = 1; j <= jmax; j++ )
        {
        fmid = (*func)(xmid = rtb + (dx *= 0.5 ));
        if (fmid <= 0.0 ) rtb = xmid;
        if (fabs(dx) < xacc || fmid == 0.0) return rtb;
        }
    nrerror("Too many bisections in RTBIS");
    }

/* page equation function */
double page(x)
    double x;
    {
    double f1,f2,f3;
      f1 = x / 0.434329;
      f2 = exp(-f1*(max-min));
      f3 = (min-(max*f2))/(1-f2);
      return  f1-(1/(mean-f3));
    }

/* page eqn error plus function */
double pageplus(x)
    double x;
    {
    double f1,f11,f12,f13,f2,f3;
      f1=x/0.43429;
      f11=max-min;
      f12=exp(f1*(f11));
      f13=exp(-f1*(f11));
      f2=(pow((1/f1), 2.0)) + (pow(f11, 2.0)/(2.0-f12-f13));
      f3=(1/f1)-mean+((min-(max*f13))/(1.0-f13));
      return ((pow(iwin, 0.5))*(pow(f2, -0.5)) * f3) + 1.96;
    }

/* page eqn error minus function */
double pageminus(x)
    double x;
    {
    double f1,f11,f12,f13,f2,f3;
      f1=x/0.43429;
      f11=max-min;
      f12=exp(f1*(f11));
      f13=exp(-f1*(f11));
      f2=(pow((1/f1), 2.0)) + (pow(f11, 2.0)/(2.0-f12-f13));
      f3=(1/f1)-mean+((min-(max*f13))/(1.0-f13));
      return ((pow(iwin, 0.5))*(pow(f2, -0.5)) * f3) - 1.96;
    }


void nrerror(char *s)
    {
    printf(s);
    exit();
    }

/* FRACTAL DIMENSION CALCULATING FUNCTIONS */

/*    Function to calculate r = sqrt( (x1-x2)^2 + (y1-y2)^2 ) for two sets of co-ords  */
double calcrs(j ,k)

     int j, k;
     {
      rs[j-1][k-1] = pow( pow( (posy[j-1] - posy[k-1]), 2.0) + pow( (posx[j-1] - posx[k-1]), 2.0), 0.5);
      return;
     }
```

```
/*    Function to calculate r = sqrt( (x1-x2)^2 + (y1-y2)^2 + (z1-z2)^2) for two sets of co-ords  */
double calcrs3d(j ,k)

     int j, k;
     {
      rs3d[j-1][k-1] = pow( pow( (posx[j-1] - posx[k-1]), 2.0) + pow( (posy[j-1] - posy[k-1]), 2.0) + pow((posz[j-1] - posz[k-
1]), 2.0), 0.5);
      return;
     }


/*    Function to calculate r = x1 - x2  for two sets of co-ords  */
double calcrt(j ,k)

     int j, k;
     {
      rt[j-1][k-1] = year[j-1] - year[k-1];
      return;
     }



/*    Function to compare calculated value of r with limit in Hirata eqn  (spatial) */

double compares(j, k)
     int j, k;
     {
      if ( (rs[j-1][k-1] <= rsmax) && (rs[j-1][k-1] > 0.0) ) nltrs++;
     }

/*    Function to compare calculated value of r with limit in Hirata eqn  (spatial) */

double compares3d(j, k)
     int j, k;
     {
      if ( (rs3d[j-1][k-1] <= rs3dmax) && (rs3d[j-1][k-1] > 0.0) ) nltrs3d++;
     }

/*    Function to compare calculated value of r with limit in Hirata eqn  (temporal) */

double comparet(j, k)
     int j, k;
     {
      if ( (rt[j-1][k-1] <= rtmax) && (rt[j-1][k-1] > 0.0) ) nltrt++;
     }


/* Routine to fit a straight line to a set of data
  n.b. if standard deviations not needed, mwt = 0
  from Numerical Recipies in C by Press et al. (1988)*/

#include <math.h>
void fith(x,y,ndat,sig,mwt,a,b,siga,sigb,chi2,q)
double x[],y[],sig[],*a,*b,*siga,*sigb,*chi2,*q;
int ndat,mwt;

{
          int i;
          double wt,t,sxoss,sx=0.0,sy=0.0,st2=0.0,ss,sigdat;
          double gammq();
/*
     printf("fith   ndat = %5d \n", ndat);
     for(i=1;i<=ndat;i++)
       {
       printf("%9.6lf   %9.6lf  \n",x[i],y[i]);
       }
*/

          *b=0.0;
          if (mwt) {
                    ss=0.0;
                    for(i=1;i<=ndat;i++){
```

```
                        wt=1.0/SQR(sig[i]);
                        ss+=wt;
                        sx+=x[i]*wt;
                        sy+=y[i]*wt;
                }
        }
        else{
                for (i=1;i<=ndat;i++){
   sx+=x[i];
                        sy+=y[i];
                }
                ss=ndat;
        }
        sxoss=sx/ss;
        if(mwt){
                for(i=1;i<=ndat;i++){
                        t=(x[i]-sxoss)/sig[i];
                        st2 += t*t;
                        *b += t*y[i]/sig[i];
                }
        }
        else{
                for (i=1;i<=ndat;i++){
                        t=x[i]-sxoss;
                        st2 += t*t;
                        *b += t*y[i];
                }
        }
        *b /= st2;
        *a=(sy-sx*(*b))/ss;
        *siga=sqrt((1.0+sx*sx/(ss*st2))/ss);
        *sigb=sqrt(1.0/st2);
        *chi2=0.0;
        if (mwt == 0){
                for(i=1;i<=ndat;i++)
                        *chi2 += SQR(y[i]-(*a)-(*b)*x[i]);
                *q=1.0;
                sigdat=sqrt((*chi2)/(ndat-2));
                *siga += sigdat;
                *sigb += sigdat;
        }
        else
    {
                for(i=1;i<=ndat;i++)
                        *chi2 += SQR((y[i]-(*a)-(*b)*x[i])/sig[i]);
                *q=gammq(0.5*(ndat-2),0.5*(*chi2));
        }
}

/* Other functions referred to in fith */

double gammq(a,x)
double a,x;
{
        double gamser,gammcf,gln;
        void gcf(),gser(),nrerror();

        if (x < 0.0 || a <= 0.0) nrerror("Invalid arguments in routine GAMMQ");
        if (x < (a+1.0)) {
                gser(&gamser,a,x,&gln);
                return 1.0-gamser;
        } else {
                gcf(&gammcf,a,x,&gln);
                return gammcf;
        }
}

#include <math.h>

#define ITMAX 100
#define EPS 3.0e-7

void gcf(gammcf,a,x,gln)
```

```
double a,x,*gammcf,*gln;

{
	int n;
	float gold=0.0,g,fac=1.0,b1=1.0;
	float b0=0.0,anf,ana,an,a1,a0=1.0;
	double gammln();
	void nrerror();

	*gln=gammln(a);
	a1=x;
	for (n=1;n<=ITMAX;n++) {
		an=(float) n;
		ana=an-a;
		a0=(a1+a0*ana)*fac;
		b0=(b1+b0*ana)*fac;
		anf=an*fac;
		a1=x*a0+anf*a1;
		b1=x*b0+anf*b1;
		if (a1) {
			fac=1.0/a1;
			g=b1*fac;
			if (fabs((g-gold)/g) < EPS) {
				*gammcf=exp(-x+a*log(x)-(*gln))*g;
				return;
			}
			gold=g;
		}
	}
	nrerror("a too large, ITMAX too small in routine GCF");
}

#undef ITMAX
#undef EPS
#include <math.h>

#define ITMAX 100
#define EPS 3.0e-7

void gser(gamser,a,x,gln)

double a,x,*gamser,*gln;

{
	int n;
	double sum,del,ap;
	double gammln();
	void nrerror();

	*gln=gammln(a);
	if (x <= 0.0) {
		if (x < 0.0) nrerror("x less than 0 in routine GSER");
		*gamser=0.0;
		return;
	} else {
		ap=a;
		del=sum=1.0/a;
		for (n=1;n<=ITMAX;n++) {
			ap += 1.0;
			del *= x/ap;
			sum += del;
			if (fabs(del) < fabs(sum)*EPS) {
				*gamser=sum*exp(-x+a*log(x)-(*gln));
				return;
			}
		}
		nrerror("a too large, ITMAX too small in routine GSER");
		return;
	}
}

#undef ITMAX
#undef EPS
```

```
#include <math.h>

double gammln(xx)
double xx;
{
        double x,tmp,ser;
        static double cof[6]={76.18009173,-86.50532033,24.01409822,
                -1.231739516,0.120858003e-2,-0.536382e-5};
        int j;

        x=xx-1.0;
        tmp=x+5.5;
        tmp -= (x+0.5)*log(tmp);
        ser=1.0;
        for (j=0;j<=5;j++) {
                x += 1.0;
                ser += cof[j]/x;
        }
        return -tmp+log(2.50662827465*ser);
}
```

Appendix 7

Data table for Geysers results

Well	Latitude	Longitude	# of $M_d \geq$ 0.5 events after 5/1990	Nearby active production wells	Nearby active injection wells	Hypercube length		Range in r for 2D D:		Range in r for 3D D	
						2D D (km)	3D D (km)	r_n/ 3 (km)	r_s (km)	r_n/ 3 (km)	r_s (km)
Whole Geysers	38^0 43' to 38^0 53'	-122^0 55' to -122^0 35'	16142	357	39	16.25	16.25	0.27	2.71	0.74	2.0
09790016	38^0 45.8' to 38^0 46.5'	-122^0 45.4' to -122^0 44.2'	194	25	3	n/a	n/a	n/a	n/a	n./a	n/a
09790020	38^0 48'	-122^0 48.6'	376	12	2	n/a	n/a	n/a	n/a	n/a	n/a
09790026	38^0 48.8'	-122^0 48.2'	324	9	1	n/a	n/a	n/a	n/a	n/a	n/a
09790127	38^0 49.2'	-122^0 48'	888	18	1	1.5	4.2	0.04	0.25	0.065	0.53
09790231	38^0 48'	-122^0 46.5'	1340	33	4	2.75	4.0	0.065	0.45	0.22	0.5
09790487	38^0 47'	-122^0 45.5'	711	26	2	1.4	2.0	0.03	0.25	0.11	0.25
09790519	38^0 50.2'	-122^0 49.5'	774	9	2	1.9	3.2	0.04	0.3	0.18	0.4
09790539	38^0 49.2'	-122^0 46.7'	630	17	2	1.3	2.8	0.03	0.2	0.16	0.35
09790563	38^0 49.3'	-122^0 47.5'	501	11	1	1.3	4.0	0.03	0.2	0.22	0.5
09790565	38^0 47.2'	-122^0 46.5'	803	19	3	2.1	4.0	0.05	0.22	0.35	0.5
09790612	38^0 48.1'	-122^0 48.2'	296	9	1	n/a	n/a	n/a	n/a	n./a	n/a
Lake County	38^{0}45' to 38^{0}47'	-122^0 44' to -122^0 42'	1161	60	10	n/a	n/a	n/a	n/a	n./a	n/a
Prod 1	38^0 49'	-122^0 48.5'	897	4	0	1.7	4.0	0.04	0.3	0.22	0.5
Prod 2	38^0 47.6'	-122^0 44.5'	1020	5	0	2.0	3.0	0.05	0.3	0.17	0.38

Frequency-magnitude statistics and spatial correlation dimensions of earthquakes at Long Valley caldera, California

D. J. Barton, G. R. Foulger and J. R. Henderson[1]
Department of Geological Sciences, University of Durham, Durham, DH1 3LE, England

B. R. Julian
U. S. Geological Survey, Menlo Park, CA 94025, USA

SUMMARY

Intense earthquake swarms at Long Valley caldera in late 1997 and early 1998 occurred on two contrasting structures. The first is defined by the intersection of a north-north-westerly array of faults with the southern margin of the resurgent dome, and is a zone of hydrothermal upwelling. Seismic activity there was characterised by high *b* values and relatively low values of *D*, the spatial fractal dimension of hypocentres. The second structure is the pre-existing South Moat fault which has generated large-magnitude seismic activity in the past. Seismicity on this structure was characterised by low *b* values and relatively high *D*. These observations are consistent with low-magnitude, clustered earthquakes on the first structure, and higher-magnitude, diffuse earthquakes on the second structure. The first structure is probably an immature fault zone, fractured on a small scale and lacking a well-developed fault plane. The second zone represents a mature fault with an extensive, coherent fault plane.

1. INTRODUCTION

The seismic *b* value of a set of earthquakes is the negative slope of the log-cumulative -frequency vs. magnitude plot. It is a measure of the proportion of larger to smaller events within a seismic sequence. A low value of *b* indicates a greater proportion of larger events than in the case where the value of *b* is high. The spatial correlation dimension of hypocentres, *D*, is a measure of the scaling in the spatial distribution of events. Correlations between *b* and *D*, both positive and negative, have been reported in both natural earthquake data (e.g. Hirata, 1989; Henderson *et al.*, 1994) and in laboratory tests (e.g. Meredith *et al.*, 1990). Physical models have been proposed to explain these correlations (e.g. Henderson & Main, 1992) but the causative physical processes are still under debate.

In this study, *b* value and the spatial correlation dimension are calculated for recent volcanic earthquakes from the Long Valley caldera, California, recorded on the permanent Northern California Seismic Network (NCSN). The seismic *b* value, *D* and the correlation between them

[1]Currently at Elf Exploration UK PLC, Aberdeen.

change significantly as the locus of seismicity changes over time. These changes correspond to an abrupt change in the nature of local crustal deformation and the transition from volcanic swarm-type seismicity to seismic activation of the pre-existing South Moat fault near the southern caldera rim.

2. TECTONIC SETTING AND DATA

Long Valley caldera lies on the eastern side of the Sierra Nevada in east-central California (Figure 1). The caldera formed at about 0.76 Ma when a magmatic system erupted cataclysmically and emplaced 600 km^3 of material (Bailey *et al.*, 1976). A ring fault formed on which 2 - 3 km of subsidence occurred, forming a 17 x 32 km oval depression. Subsequent magmatic activity in the centre of the caldera built a resurgent dome.

The current period of unrest in Long Valley commenced in 1978 with an M = 5.7 earthquake 20 km south of the caldera (Rundle & Hill, 1988). In 1980, there was a seismic crisis with four M ~ 6 earthquakes. Since then, seismic activity has been almost continuous with occasional events as large as M = 5.5. The Mammoth Mountain area at the south-western edge of the caldera vents 400-500 tonnes of CO_2 per day (Farrar *et al.*, 1995). Uplift of the resurgent dome also commenced in 1980 and continues to the present day. The deformation pattern is consistent with the inflation of an underlying magma chamber at depths of 6 - 10 km (Rundle & Hill, 1988).

Since June 1997 there has been a great increase in seismic activity to the immediate south of the resurgent dome, culminating in a massive swarm of > 2000 earthquakes 22-25 November 1997. This increase in seismicity coincided with accelerated inflation of the resurgent dome. Ground deformation was monitored by two-colour geodimeter, GPS, tiltmeter and strainmeter measurements.

Earthquakes at Long Valley are continually monitored by the NCSN network which has approximately 50 stations within 50 km of the caldera. The NCSN catalogue contains both earthquake locations and magnitudes based on measurements made by hand (CUSP data) and automatically-picked measurements (Earthworm data). The CUSP and Earthworm results are merged in the catalogue with the CUSP results taking precedence where both exist. Between January 1997 and February 1998, 24,511 earthquakes were catalogued, 4,820 of which were CUSP-processed. The majority occurred in swarms between July and November 1997.

During periods of relatively low activity, CUSP-processed events are complete down to M = 1.2. During intense swarms, however, staff time is only sufficient to hand pick the largest events and many earthquakes larger than M = 1.2 are processed only by the Earthworm system. In addition to having less accurate locations, Earthworm magnitudes are determined from coda lengths and several closely spaced events may be interpreted as a single large event. This causes exaggeration of the numbers of large-magnitude events and underestimation of the numbers of low-magnitude events. The effect of this during intense swarms can be seen from

log-cumulative-frequency vs. magnitude plots (Figure 2). During periods of low activity (Figure 2a), a straight-line distribution following the Gutenberg-Richter equation is exhibited for earthquakes with M ≥1.2. However, during intense swarms (Figure 2b) a distorted log-cumulative-frequency vs. magnitude plot results, which may exhibit two straight segments above M = 1.2, and a correct *b* value cannot be calculated. We therefore restrict our analyses to those time periods where CUSP data are complete down to a threshold value of M = 1.8. By using only the CUSP data we increase our confidence that the observed differences in *b* value are real, and do not arise from systematic errors in automatic magnitude calculation. Furthermore, this also restricts our dataset to those earthquakes most accurately located.

3. METHOD

The threshold magnitude was selected by examining plots of log-cumulative-frequency vs. magnitude. A threshold magnitude of M = 1.8 was the lowest suitable for the set of data used in this study. We used sliding windows of 200 data points to estimate both *b* and *D*, with each window overlapping the next by ten events (Figure 3).

The hypocentral spatial distribution of the CUSP events for 200-event windows was characterised by the correlation dimension *D* (Grassberger and Procaccia, 1983).

$$D = \lim_{r \to 0} \frac{\log C(r)}{\log r}$$

where *r* is the radius of the sphere of investigation and *C(r)*, the correlation integral, is a measure of the fraction of pairs of earthquakes having separations < *r*. In the case of an infinite fractal distribution, a plot of log *C(r)* against log *r* will be a straight line whose gradient is the fractal dimension. A finite data sample typically yields a plot that is only linear for that range of *r* that is above the depopulation limit and below the saturation limit. In this study we estimate the fractal dimension for values of *r* of 0.4 km < *r* < 1 km (Figure 2c).

Although previous work has suggested that large datasets are required to calculate *D* accurately (Smith, 1988), there is evidence that much smaller datasets are adequate, particularly in the situation where it is differences in fractal dimension that are of interest rather than their absolute values (Nerenberg and Essex, 1990). This conclusion is supported by the findings of Havstad and Ehlers (1989) and Eneva (1996).

The value of *D* is an indicator of clustering within the earthquake population. Earthquakes that are diffuse in space are characterised a large value of *D*. As the earthquakes become progressively clustered the value of *D* decreases.

The range of magnitudes is small. For this reason we estimate the *b* value using the maximum likelihood method of Page (1968).

4. RESULTS

Changes in the values of *b* and *D* are shown in Figure 3 and the spatial distributions of the events in different time windows are shown in Figures 4 - 6. Prior to 22 November 1997, most of the earthquakes occurred in clusters which together formed a broad zone trending N 85° E along the southern margin of the resurgent dome and to its immediate south-west (Figure 4). During the period that seismicity occurred in this area, *b* was relatively high and *D* relatively low, consistent with low magnitude, clustered activity (Figure 3a). There is a negative correlation between *b* and *D* (Figure 3b).

Commencing 22 November there is a sharp fall in *b*, accompanied by a sharp rise in *D*. The *b* value mostly recovered 4 December from which date both *b* and *D* decreased overall until 1 January. Between 22 November and 1 January *b* and *D* are uncorrelated (Figure 3c). During this period the seismicity formed a much narrower, linear zone trending N 105° E and located 2 - 3 km south of the pre-22 November activity (Figure 5). This linear feature dips at 80° and contains several events with M > 4.0. The relatively high values of *D* indicate that the activity is diffuse.

After 1 January there was again a negative correlation between *b* and *D* (Figure 3d). There was also a return to a pattern of clusters further north, on the southern edge of the resurgent dome (Figure 6).

5. DISCUSSION

Prior to 22 November, clustered earthquake activity formed an easterly-trending zone beneath the southern margin of the resurgent dome. This zone coincides with the distribution of thermal springs and fumaroles which occur where north-north-westerly-trending faults cross the southern edge of the resurgent dome (Figure 1). The seismic activity was probably caused by accelerated resurgent dome uplift causing extension and allowing the migration of hot fluids up this zone (Foulger *et al.*, 1998).

The linear seismic feature activated on and after 22 November coincides with the South Moat fault, a blind, sub-vertical, strike-slip fault (Denlinger *et al.*, 1985). Motion on this fault may have been facilitated by the same processes that gave rise to the nearby pre-22 November seismicity, or by processes resulting from that activity.

The change in locus of seismicity is associated with a change in locus of deformation as suggested by geodetic measurements. Prior to 22 November, rapid dome inflation occurred with the greatest line lengthening on the two-colour geodimeter lines Casa to Krakatau, Saw, Hot and Knolls (Figure 1). Between 22 - 26 November, accelerated lengthening occurred on the Casa-Krakatau and Saw lines, but lengthening ceased on the Casa-Hot and Casa-Knolls lines. The lines Casa-Tilla and Casa-Miner began to contract. After 26 November the rate of lengthening for the Casa-Krakatau line decreased, and the rates of lengthening of the Casa-Knolls, Saw and Sherwin lines increased abruptly. Also, the Casa-Tilla, Shark and Hot lines

started to shorten. Detailed modelling of the data has yet to be done, but these observations suggest that the locus of greatest deformation moved from beneath the resurgent dome to an area between the geodimeter stations Casa, Miner, Tilla and Saw - the same area as the most intense seismicity on the narrow linear zone that was activated after 22 November.

A number of reasons for variations in *b* value have been suggested. Mogi (1962) pointed to the importance of heterogeneity in contributing to high *b* value. Scholz (1968) demonstrated an inverse correlation between stress level and *b* value in laboratory experiments. Stress level may be affected by pore fluid pressure and thermal stresses, and these have also been proposed as contributing to variations in *b* value (Warren and Latham, 1970; Wyss, 1973). High stress levels at asperities suggest a means of mapping the latter using *b* values (Wiemer and Wyss, 1997). Furthermore, changes in stress levels and degrees of heterogeneity may lead to temporal variations in *b* value (e.g., Wiemer and McNutt, 1997). Wiemer et al. (1998) present a study of seismicity at Long Valley which demonstrates that changes in seismicity can be related to changes in the nature of magmatic activity. Examples of short- to intermediate-term temporal variation in *b* value are also presented by Henderson et al. (1992) and Henderson et al (1994). In addition, Henderson and Main (1992) suggest a mechanism by which *b* values will change over time even in the absence of changes in the external stress, as a consequence of non-linear feedback processes resulting in changes in stress intensity factor associated with the growing population of cracks.

In the examples described here we suggest that variations in *b* and *D* can be explained by considering the different processes operating in the different regimes. In the hydrothermal zone of weakness that was active prior to 22 November, many small faults and small-scale structures, possibly augmented by thermal cracking, provided a highly heterogeneous environment. High permeability and a supply of pore fluids may have resulted in reduced effective stresses and thus the earthquakes were caused by the failure of isolated, small asperities and consequently occurred in clusters. This resulted in high *b* and relatively low *D*. This is consistent with the weak negative correlation shown in Figure 3b.

From 22 November, seismic activity was transferred to the South Moat fault. This fault has failed in the past with M > 6 earthquakes and has a mature, well developed, coherent fault plane. Highly stressed asperities are widely spaced along it. Consequently when it failed large-magnitude earthquakes occurred, causing a low *b* value. The wide distribution of earthquakes along the fault plane caused a relatively high value of *D*.

This study describes an unusual case where adjacent structures with contrasting seismic properties are activated and monitored using a uniform network and data processing techniques, and sufficient earthquakes are available to yield many accurate estimates of *b* and *D*. It also shows that the South Moat fault is a sub-vertical blind fault ~12 km long and ~7 km high, terminating at its western end ~ 1 km east of the town of Mammoth Lakes. Its history of M > 6 earthquakes and behaviour during the 1997 - 1998 period of activation show that, in

contrast to the hydrothermal zone a few kilometres further north, it is capable of generating large magnitude earthquakes. It thus represents a potential hazard to the town of Mammoth Lakes.

ACKNOWLEDGMENTS

The seismic data were obtained from the NCSN catalogue at Berkeley. Valuable advice was given by Mitch Pitt and David Oppenheimer and the geodimeter data were kindly supplied by John Langbein, all at the USGS. DJB was supported by a NERC research studentship. We are grateful for the very thorough reviews of Max Wyss and an anonymous reviewer who pointed out a major error in the original manuscript.

REFERENCES

Bailey, R. A., G. D. Dalrymple and M. A. Lanphere, Volcanism, structure and geochronology of Long Valley Caldera, Mono County, California, *J. Geophys. Res.*, **81**, 725-744, 1976.

Denlinger, R. P., Riley, F. S., Boling, J. K. & Carpenter, M. C., Deformation of Long Valley Caldera between August 1982 and August 1983, *J. Geophys. Res.*, **90**, 11,199 - 11,209, 1985.

Eneva, M., Effect of limited datasets in evaluating the scaling properties of spatially distributed data: an example from mining induced seismic activity, *Geophys. J. Int.*, **124**, 773-786, 1996.

Farrar, C. D., M. L. Sorey, W. C. Evans, J. F. Howle, B. D. Kerr B. M. Kennedy, C.-Y. King, and J. R. Southon, Forest-killing diffuse CO_2 emission at Mammoth Mountain as a sign of magmatic unrest, *Nature*, **336**, 675-678, 1995.

Foulger, G.R., P.E. Malin, E. Shalev, B.R. Julian and D.P. Hill, Seismic monitoring and activity increase in California caldera, *EOS Trans. AGU*, **79**, 357-363, 1998.

Grassberger, P. & Procaccia, I., Measuring the strangeness of strange attractors, *Physica*, **9D**, 189-208, 1983.

Havstad, J. W. & Ehlers, C. L., Attractor dimension of non-stationary dynamical systems from small data sets, *Phys. Rev.*, **39**, 845-853, 1989.

Henderson, J. R. & Main, I. G., A simple fracture-mechanical model for the evolution of seismicity, *Geophys. Res. Lett.*, **19**, 365-368, 1992.

Henderson, J. R., Main, I. G., Pearce, R. G. & Takeya, M., Seismicity in north-eastern Brazil: fractal clustering and the evolution of the b-value, *Geophys J. Int.*, **116**, 217-226, 1994.

Henderson, J. R. & Main, I. G., A simple fracture-mechanical model for the evolution of seismicity, *Geophys. Res. Lett.*, **19**, 365-368, 1992.

Hirata, T., A correlation between the b-value and fractal dimension of earthquakes, *J. Geophys. Res.*, 94, 7507-7514, 1989.

Meredith, P. G., Main, I. G. & Jones, C., Temporal variations in seismicity during quasi-static and dynamic rock failure, *Tectonophysics*, 175, 249-268, 1990.

Mogi, K., Magnitude-frequency relation for elastic shocks accompanying fractures of various materials and some related problems in earthquakes, *Bull. Earthq. Res. Inst., Univ. Tokyo*, 40, 831-853, 1962.

Nerenberg, M. A. H. & Essex, C., Correlation dimension and systematic geometric effects, *Phys. Rev.*, 42, 7065-7074, 1990

Page, R., Aftershocks and micro-aftershocks of the Great Alaska Earthquake of 1964, *Bull. Seism. Soc. Am.*, 58, 1131-1168, 1968.

Rundle, J. B. and Hill, D. P., The geophysics of a restless caldera - Long Valley, California, *Ann. Rev. Earth Planet. Sci.*, 16, 251-271, 1988.

Scholz, C.H., The frequency-magnitude relation of microfracturing in rock and its relation to earthquakes, *Bull. Seis. Soc. Amer.*, 58, 399-415, 1968.

Smith, L. A., Intrinsic limits on dimension calculations, *Phys. Lett.*, 113, 283-288, 1988.

Sorey, M. L., Evolution and present state of the hydrothermal system in Long Valley Caldera, *J. Geophys. Res.*, 90, 11,219-11,228, 1985.

Warren, N.W. & Latham, G.V., An experimental study of thermally induced microfracturing and its relation to volcanic seismicity, *J. Geophys. Res.*, 75, 4455-4464, 1970.

Wiemer, S. & McNutt, S., Variations in frequency-magnitude distribution with depth in two volcanic areas: Mount St. Helens, Washington, and Mt. Spurr, Alaska, *Geophys. Res. Lett.*, 24, 189-192, 1997.

Wiemer, S. & Wyss, M., Mapping the frequency-magnitude distribution in asperities: An improved technique to calculate recurrence times, *J. Geophys. Res.*, 102, 15,115-15,128, 1997.

Wiemer, S., McNutt, S.R. & Wyss, M., Temporal and three-dimensional spatial analyses of the frequency-magnitude distribution near Long Valley caldera, California, *Geophys. J. Int.*, 134, 409-421, 1998.

Wyss, M., Towards a physical understanding of the earthquake frequency distribution, *Geophys. J. Royal astr. Soc.*, 31, 341-359, 1973.

FIGURE CAPTIONS

FIGURE 1

Map of Long Valley caldera showing regional location (inset) and main tectonic features. The caldera rim is indicated by a solid line and the resurgent dome by a dashed line. Thin lines: faults, triangles: hot springs and fumaroles, solid grey line: the South Moat fault. The two-colour Geodimeter stations are shown (hexagons) and grey lines joining them indicate baselines routinely measured. The town of Mammoth Lakes is indicated by a square. Map features from Sorey (1985).

FIGURE 2

Examples of b and D calculated using samples of all the data (CUSP and Earthworm) from the NCSN catalogue. (a) Plot of log-cumulative-frequency vs. magnitude for data from June 1997 when the CUSP (hand-picked) magnitude threshold was M = 1.2. There is a linear relationship above M = 1.2. (b) Same as (a) but for data from late November 1997 during an intense swarm. A highly non-linear plot for earthquakes larger than M = 1.2 results and the threshold indicated on the plot is M = 2.4. (c) A typical plot of log $C(r)$ vs. log r showing the range selected for calculating D (shaded area).

FIGURE 3

(a) Plot of b and D for 200-event windows for the period 1 January 1997 to 28 February 1998. Few CUSP-processed earthquakes were catalogued during the first half of 1997. The error bars for b correspond to the 95% confidence limits. The errors in D are ~ 10% of the calculated value (Henderson *et al.*, 1992; Havstad & Ehlers, 1989). (b) Plot of b vs. D for the period 1 January to 21 November 1997, (c) as (b) except for the period 22 November - 31 December 1997, (d) as (b) except for the period January - 28 February 1998.

FIGURE 4

Seismicity in Long Valley for the period 1 January - 21 November 1997. Events with $M \geq 1.8$ are shown. Events with $M \geq 4$ are shown as open circles. Map features as for Figure 1. (a) Earthquake epicentres, (b) north-south cross section, (c) west-east cross section. On the cross-sections events within ± 10 km of the line of section shown in (a) are plotted.

FIGURE 5

Same as Figure 4 except for the period 22 November - 31 December 1997.

FIGURE 6

Same as Figure 4 except for the period 1 January - 28 February 1998.

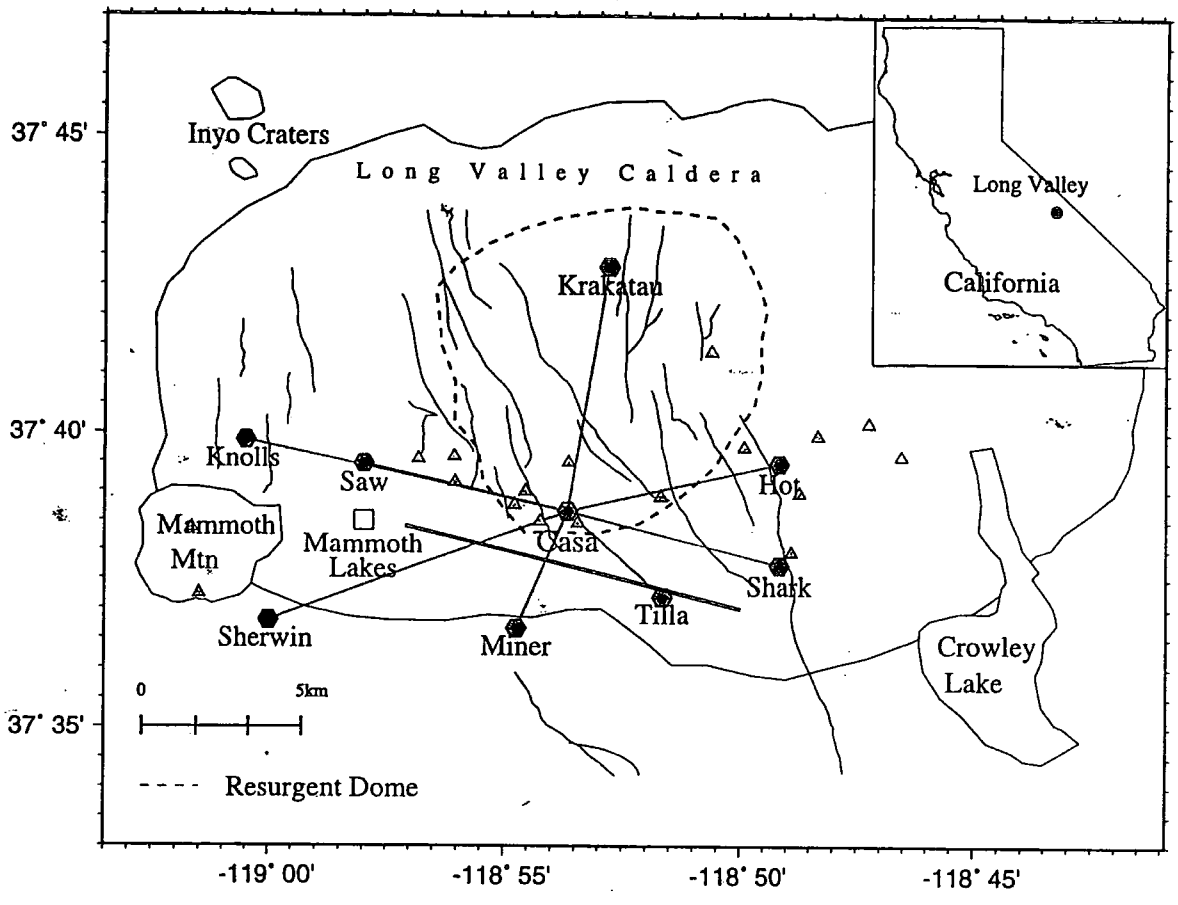
Inyo Craters
Long Valley Caldera
Long Valley
California
Krakatau
Knolls
Saw
Hot
Mammoth Mtn
Mammoth Lakes
Casa
Shark
Tilla
Sherwin
Miner
Crowley Lake
0
5km
Resurgent Dome
37° 45'
37° 40'
37° 35'
-119° 00'
-118° 55'
-118° 50'
-118° 45'

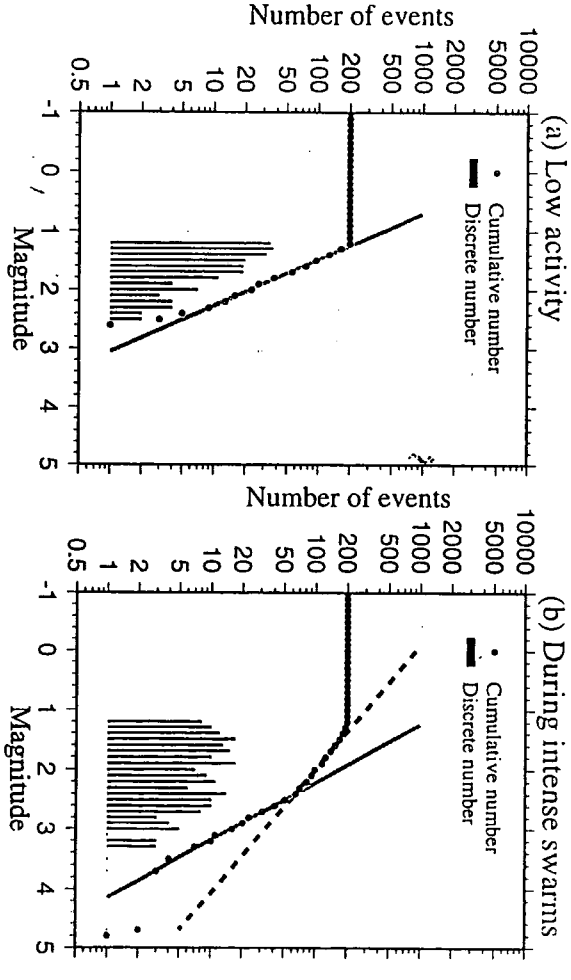
Number of events
Magnitude
Cumulative number
Discrete number
(a) Low activity
(b) During intense swarms

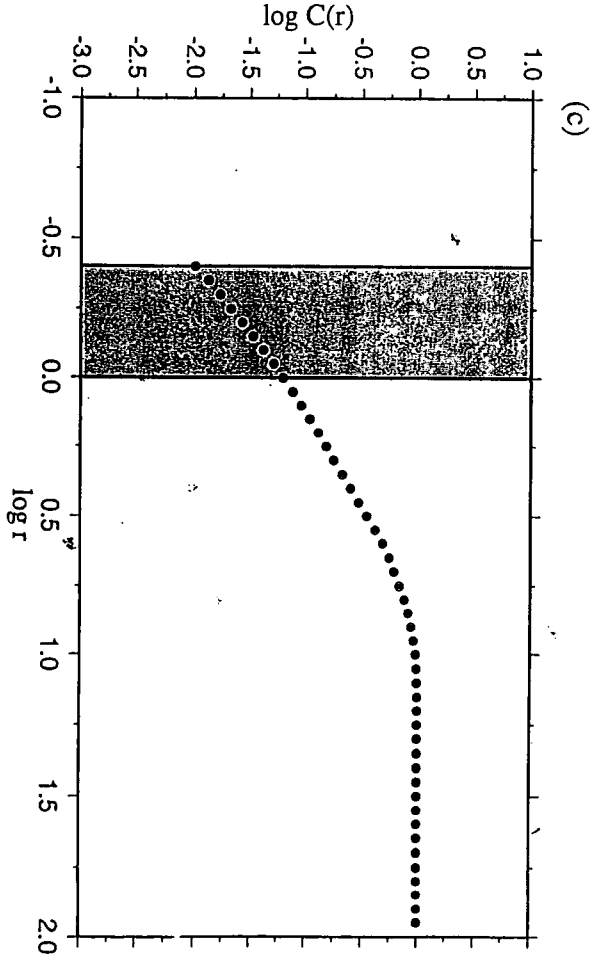
log C(r)
log r
(c)

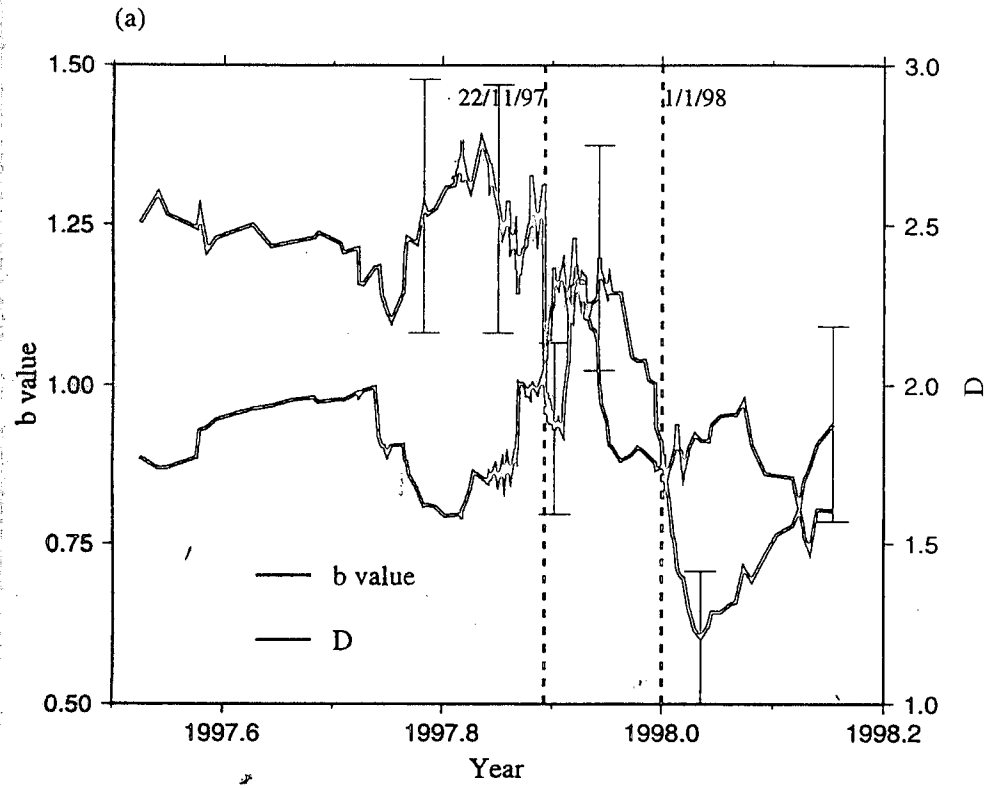
(a)
22/11/97
1/1/98
b value
D
Year

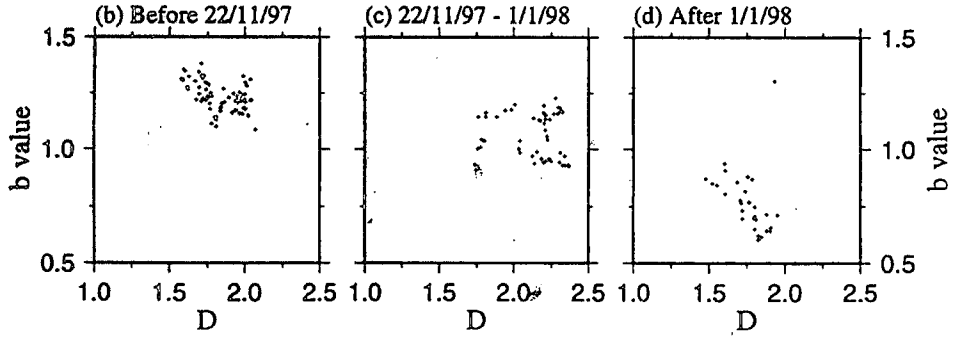
(b) Before 22/11/97
(c) 22/11/97 - 1/1/98
(d) After 1/1/98
b value
D

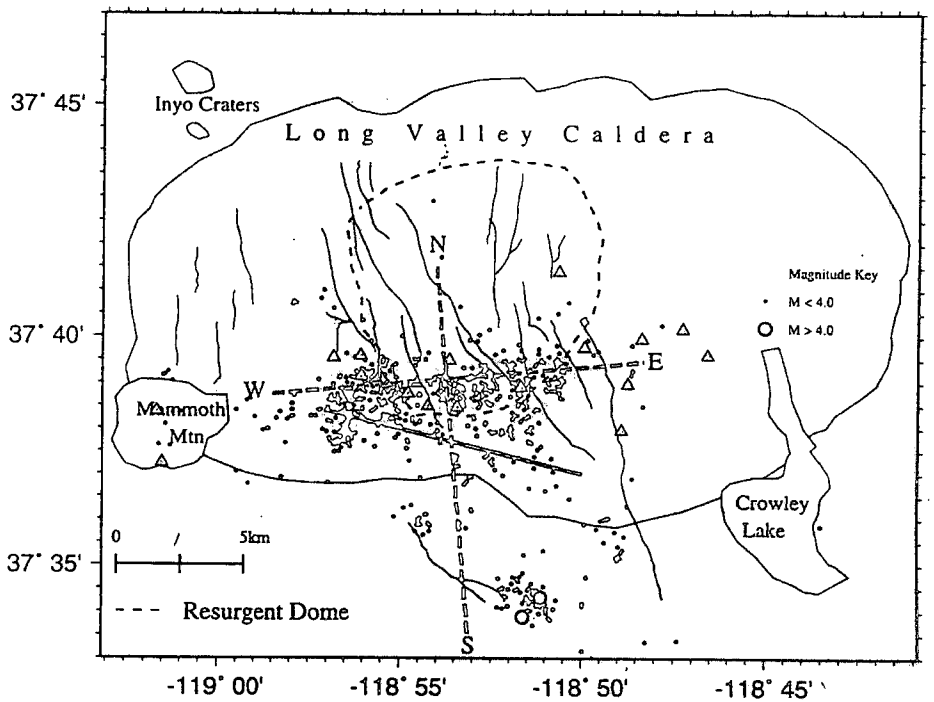
Inyo Craters
Long Valley Caldera
Magnitude Key
M < 4.0
M > 4.0
Mammoth Mtn
Crowley Lake
Resurgent Dome
5km

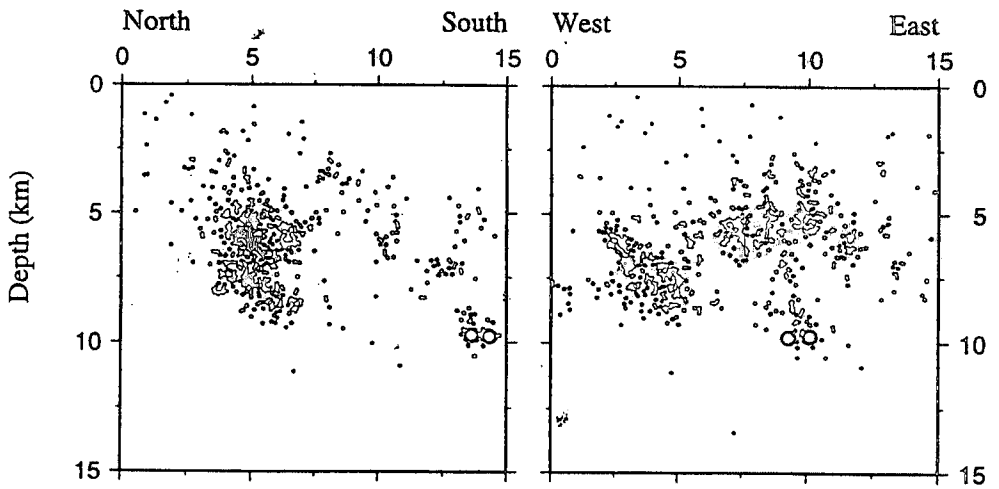
North
South
West
East
Depth (km)

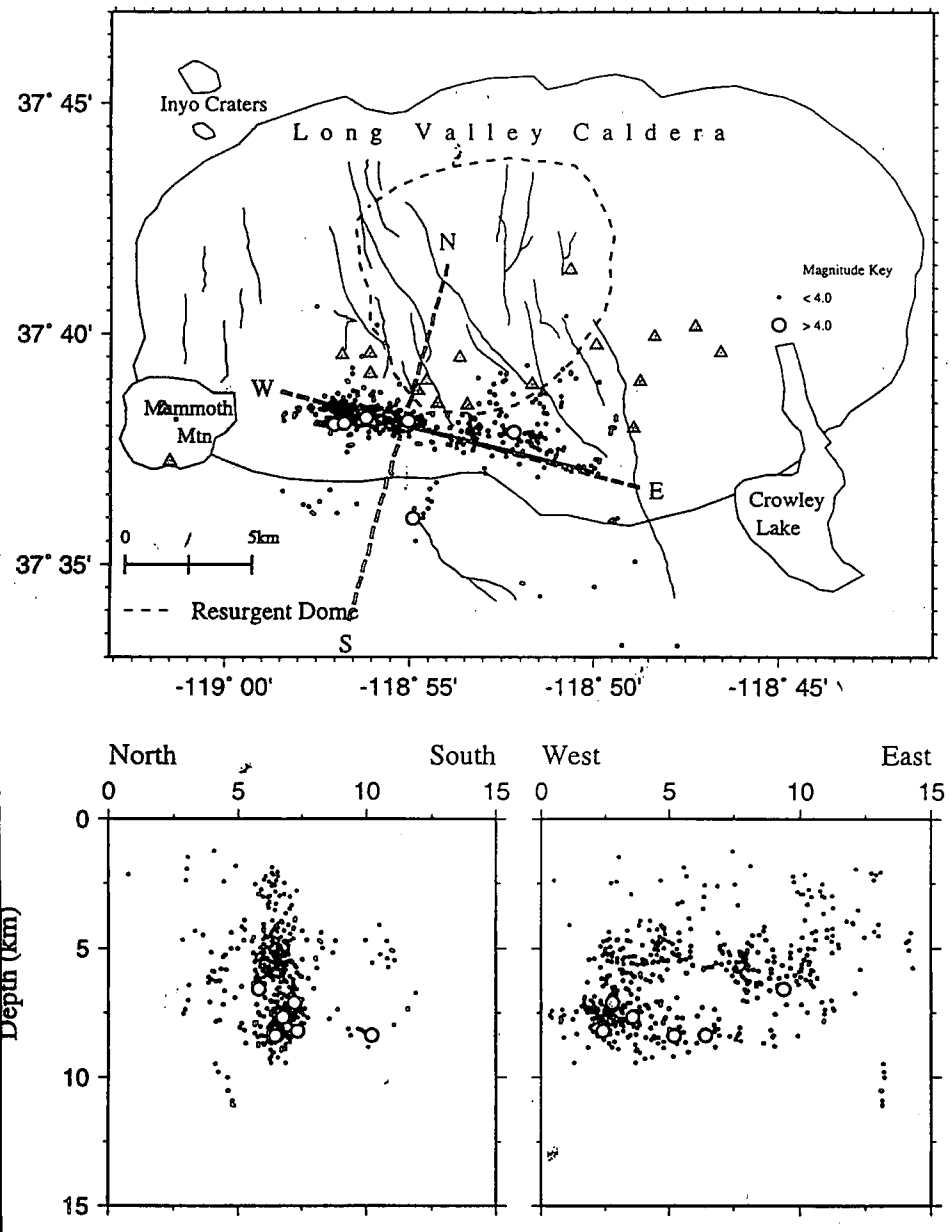
Inyo Craters
Long Valley Caldera
37° 45'
37° 40'
37° 35'
N
W
E
S
Mammoth Mtn
Crowley Lake
Magnitude Key
< 4.0
> 4.0
0 5km
Resurgent Dome
-119° 00'
-118° 55'
-118° 50'
-118° 45'

North
South
West
East
0
5
10
15
Depth (km)

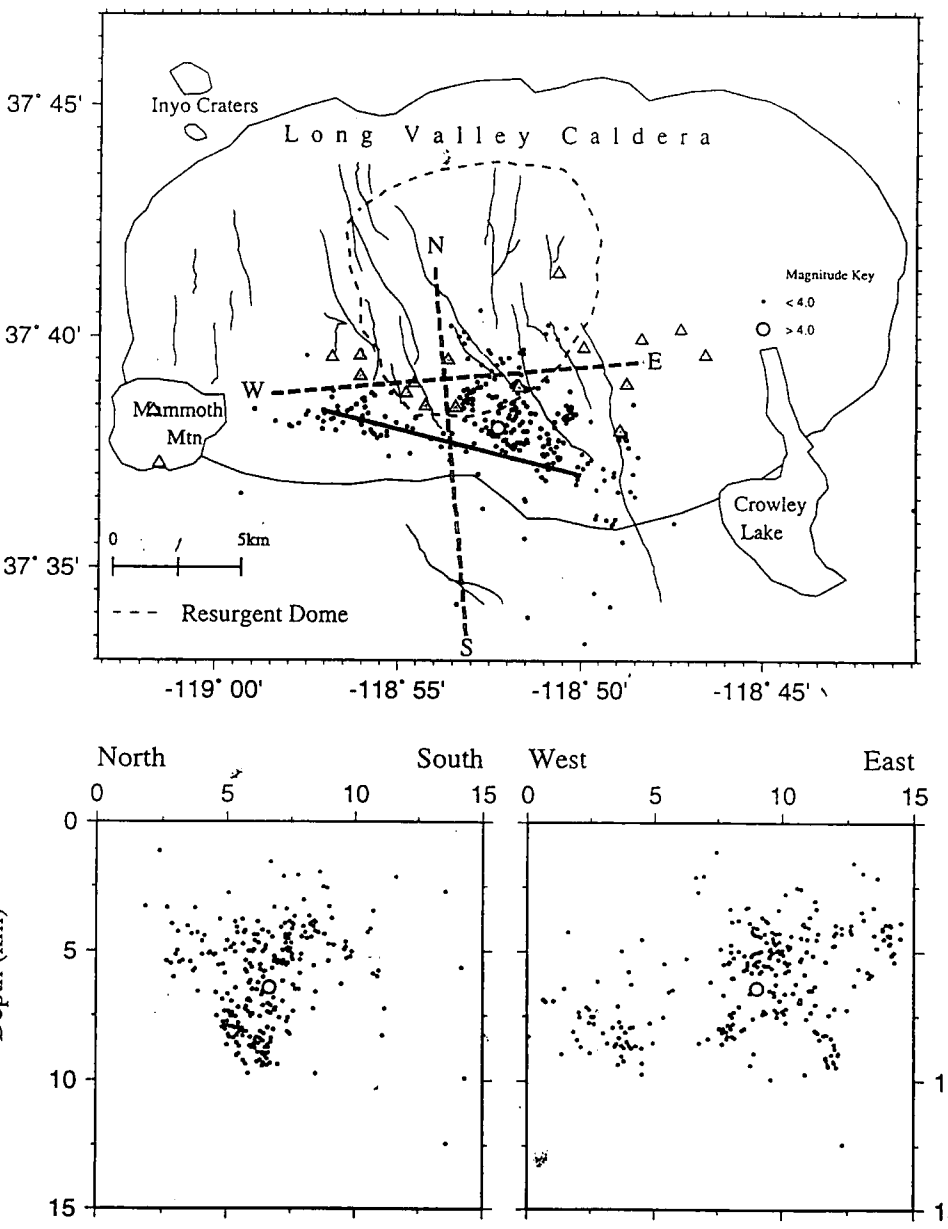
Inyo Craters
Long Valley Caldera
37° 45'
37° 40'
37° 35'
N
W
E
S
Mammoth Mtn
Crowley Lake
Magnitude Key
< 4.0
> 4.0
0 5km
Resurgent Dome
-119° 00'
-118° 55'
-118° 50'
-118° 45'

North
South
West
East
0
5
10
15
Depth (km)

FRACTAL CLUSTERING OF INDUCED SEISMICITY IN THE GEYSERS GEOTHERMAL AREA, CALIFORNIA

J. R. Henderson, D. J. Barton and G. R. Foulger

Department of Geological Sciences, University of Durham, Durham DH1 3LE, England

Abstract

We analyze earthquakes recorded at The Geysers geothermal field in California, an area where industrial activity induces seismicity. The seismicity is characterized by the seismic *b*-value and *D*, the fractal dimension of earthquake hypocentres measured from sliding windows containing 200 events. We study a group of events strongly clustered around an injection well. Over most of the time period examined we find a positive correlation between *b* and *D*. However, during the initiation of injection into a new well we find instead a negative correlation. The differences in correlation are statistically significant at the 1σ level but only marginally so at the 2σ level. These results provide evidence for a transient change in the seismic mechanism operating, and may be explained by a change from conditions of slow stress loading to rapid loading as a result of build up of the rate of water injection into the reservoir.

Introduction

In recent years, fractal concepts have been widely used to characterize various aspects of seismicity. It has been shown that earthquake sizes have a power-law distribution which is often expressed in terms of the Gutenberg-Richter relation. It has been claimed that these fractal measures, particularly the seismic *b*-value and the fractal dimension of hypocentres, *D*, vary in a systematic way related to the earthquake process. For example, it has been observed that the *b*-value may show systematic variation in the period preceding a major earthquake [*Smith*, 1981]. Similar behaviour has been observed for *D* [e.g. *DeRubeis et al.*, 1993; *Legrand et al.*, 1996], and a correlation between *b* and *D* has been reported [e.g. *Hirata*, 1989; *Henderson et al.*, 1992, 1994; *Oncel et al.*, 1995]. Changes in *b* and *D* have also been observed during laboratory studies of rock deformation [*Meredith et al.*, 1990; *Sammonds et al.*, 1992; *Lockner et al.*, 1991], and conceptual models have been produced to explain this [e.g. *Main*, 1992; *Henderson and Main*, 1992]. However, since it is not clear what processes are operating during the seismic cycle, the origins of these changes in *b* and *D*, and hence the validity of the models, are not always obvious.

In this study we use a large and relatively high-quality dataset to examine the temporal changes in fractal clustering of earthquake hypocentres in a geothermal area where seismicity is induced by industrial activity. In such a situation it is possible to relate changes in the correlation between *D* and *b* to specific physical processes.

Data

The Geysers geothermal area lies within the San Andreas shear zone in northern California (Figure 1). The steam-dominated geothermal reservoir has a surface area of about 75 km^2, and extends from about 0.3 km above sea level to at least 3 km below sea level. Commercial development of The Geysers commenced in the mid 1950s. The UNOCAL Corporation commenced large scale development of the area in 1971, reaching a maximum installed capacity of 2043 MW in the mid-1980s.

The area is intensely seismically active, and generates many small earthquakes per day. Despite a dearth of pre-exploitation monitoring, a large majority of the earthquakes are attributed to the commercial extraction of steam [*Hamilton and Muffler*, 1972; *Ludwin and Bufe*, 1980; *Majer and McEvilly*, 1979; *Eberhart-Phillips and Oppenheimer*, 1984] and reinjection of condensate into the reservoir [*Stark*, 1991]. This is in agreement with case histories from other areas around the world where earthquake activity associated with fluid disposal and water impoundment suggests that fluid injection can induce earthquakes. It has been shown that injection activity does not always induce earthquakes [*Stark*, 1991]. *Eberhart-Phillips and Oppenheimer* [1984] state that injection under zero wellhead pressure, as practiced at The Geysers, is unlikely to create the pore pressures required to cause earthquake activity by the *Hubbert-Rubey* [1959] mechanism and that some of the seismic activity may be tectonic. However, later studies suggest that many of the earthquakes studied by *Eberhart-Phillips and Oppenheimer* [1984] were caused by proprietary injection not known to those authors.

Earthquakes at The Geysers are monitored by a permanent seismic network, operated until quite recently by the UNOCAL Corporation, which has comprised between 12 (1989) and 22 stations (1994). Between 1989 and 1994 approximately 130,000 events were recorded. Of these events, we located 30,000 using P arrival times automatically picked from the digital seismograms. Samples of the autopicks were checked by hand and mostly found to be accurate to 0.01 seconds. The earthquakes were located using a three-dimensional velocity model generated from seismic tomography [*Julian et al.*, 1996].

Magnitudes for the events were calculated using the duration of the observed seismic signal, defined as the time from the first arrival to the time at which the signal level fell below some threshold determined with reference to the noise level. The relationship between magnitude and duration is [*Bath*, 1981]:

$$m_r = c_1 \log(L) + c_2\Delta + c_3 \qquad (1)$$

where L is the signal duration in seconds and Δ is the epicentral distance in km. In low attenuation environments such as The Geysers, the coefficient c_2 is typically negligibly small, and the coefficients c_1 and c_3 were determined by calibrating the durations against magnitudes determined for some of the events from the NCSN seismograph network, operated by the U.S. Geological Survey.

Geothermal well activity data were collected from various companies operating in the area. These data consist of production histories for steam and injection histories for water. Figure 1 shows a map of the seismicity and injection well locations.

There is a correlation between injection well locations and distinct clusters of seismic activity, suggesting that the two are related. In order to investigate this phenomenon, a cluster of events was selected for more detailed study (Figures 1 and 2). This cluster was used because interactive examination of hypocentre locations in three dimensions revealed it to be clearly distinct from other areas of seismicity and it contains a large number of events which occurred during a period when the configuration of the UNOCAL seismometer network was stable. Although there are several wells in the vicinity of the cluster, we focus on Well 045 because it is the only well where there was substantial variation in industrial activity, and because it lies adjacent to a large fault cutting across the study area. Well 231, which also lies on the fault, shows less variation in injection.

Although it would be desirable to extend the analysis to the entire dataset, in practice this is problematic because variations in the seismometer network and operating procedures reduce the homogeneity of the catalogue. Such deficiencies have been noted in other studies of seismicity [e.g., *Zuñiga and Wyss*, 1995], and reduce the reliability of conclusions drawn from such studies. Instead we concentrate on a well-understood subset of the data.

Method of analysis

We estimated the *b*-value using the formula of *Page* [1968]:

$$\beta = [\overline{m} - \frac{m_{min} - m_{max}\exp(-\beta(m_{max} - m_{min}))}{1 - \exp(-\beta(m_{max} - m_{min}))}]^{-1} \qquad (2)$$

where $\overline{m}$ is the average magnitude of events exceeding a threshold magnitude, m_{max} and m_{min} are the maximum and minimum magnitudes used, and $b = \beta / \log_{10} e$. The threshold magnitude, m_{min}=0.5, was estimated by observing the deviation from linearity of the frequency-magnitude relationship for the area at low magnitude, and did not vary over the time period of interest. A typical example of a frequency-magnitude plot for a window of 200 events is shown in the upper panel of Figure 3.

The fractal dimension of earthquake hypocentres was estimated using the correlation dimension, D_c [*Grassberger and Procaccia*, 1983]:

$$D_c = \lim_{r \to 0} \frac{\log C(r)}{\log r} \qquad (3)$$

where r is the radius if a sphere of investigation, and $C(r)$ is the correlation integral:

$$C(r) = \lim_{N \to \infty} \frac{1}{N^2} \sum_{i=1}^{N} \sum_{j=1}^{N} H(r - |x_i - x_j|) \qquad (4)$$

where N is the number of points in the analysis window, the x are the co-ordinates of the hypocentres and H is the Heaviside step function $H(x)$=0 for $x \leq 0$, $H(x)$=1 for $x > 0$. In simpler terms, $C(r)$ is a function of the probability that two points will be separated by a distance less than r.

In the case of an infinite fractal distribution, the resulting plot of log $C(r)$ against log r will be a straight line whose gradient is the fractal dimension. In practice, however, for large values of r the gradient is artificially low, whereas for small values of r the gradient is artificially high. These two conditions have been called "saturation" and "depopulation" [*Nerenberg and Essex*, 1990]. Whereas it is common for an estimate of the fractal dimension to be made by fitting a straight line to a subjectively-chosen straight part of the curve, *Nerenberg and Essex* [1990] provide formulae for determining the distances of depopulation and saturation, r_n and r_s:

$$r_n = 2R(\frac{1}{N})^{1/d}, \quad r_s = \frac{R}{d+1} \qquad (5)$$

where d is the dimensionality of the data cluster, and $2R$ is the approximate length of the side of the hypercube containing the data. As discussed by *Eneva* [1996], it is often safe to start the

scaling range at values of r as low as $r_n/3$, but in the case studied here we choose the more conservative approach of measuring a gradient from r_n. In practice, the values used were r_n = 0.08 km and r_s = 0.45 km. An example of a typical plot of log $C(r)$ against log r is shown in the lower panel of Figure 3.

Another area of controversy in the estimation of fractal dimensions concerns the size of the dataset used. It has been suggested that very large datasets are necessary for accurate determination of D [*Smith*, 1988], but there is evidence that much smaller datasets are adequate, particularly in the situation where it is *changes* in fractal dimension that are of interest, rather than their absolute values [*Nerenberg and Essex*, 1990]. This viewpoint is supported by the findings of *Havstad and Ehlers* [1989] and *Eneva* [1996]. In this study we use sliding windows of 200 events, overlapping by 10 events, from which to estimate b and D.

Results

Figure 4 (upper two panels) shows the values of b and D calculated as described above. The error bounds shown for b are the 95% confidence limits (2σ) calculated using the method of *Page* [1968]. These limits are more conservative than those found using the maximum likelihood formula $\delta b = 1.96b/\sqrt{N}$. The error bounds shown for D are 10% of the calculated value, and are approximately appropriate for the 95% confidence limits [*Havstad and Ehlers*, 1989]. The lower panel of Figure 4 shows the injection activity at wells 231 and 045.

There is very little variation in either b or D, relative to their respective error bars (between 1σ and 2σ). There is, however, a decline and subsequent revival of D, marginally significant at the 2σ level, over the period late 1991 to early 1993. This corresponds to an increase in seismic activity (Figure 5), and occurs at the same time as the onset of injection in well 045 (Figure 4, lower panel).

Over the whole period studied there is no obvious correlation between any pair of D, b and the absolute level of injection in the area. However, if the data are divided into temporal subsets, systematic behaviour may be discerned. Figure 6 shows the relationship between b and D for three temporal subsets: before the initiation of activity at well 045; during the period over which injection rapidly increased; and after, when injection continued at a roughly steady rate. These periods are defined with reference to the period over which injection rose from zero to over 5 x 10^7 kg per month, in early 1992. The period labelled "during" refers to all those windows containing a datapoint from this period of rising injection. The change in event rate means that these windows are of various lengths, but they are typically about six months long. Some representative samples are shown in Figure 4.

For the entire dataset, there is no significant correlation between b and D. However, for each temporal subset, a weak correlation exists between b and D, and the nature of this correlation varies (Figure 6). Before the initiation of well activity, there is a weak positive correlation between b and D. During initiation of injection, a negative correlation exists, and after this period the correlation is again positive. Errors were calculated assuming uncertainties in both b and D, and 1σ values are shown in Figure 6. For each subset the slopes calculated are significantly different from zero at the 1σ level but not, or only marginally so at the 2σ level. The evidence presented here must thus be viewed as weak. This illustrates the notorious difficulty of detecting statistically significant variations in the fractal dimensions of earthquake activity, which arises from the very large numbers of high-quality data required to achieve high precisions and the small numbers that are typically available. Nevertheless, these results suggest that the nature of the seismicity, particularly the spatial clustering and the earthquake generation process, changes with the rate of injection of water into the geothermal reservoir.

Discussion

Whereas tectonic seismicity often shows significant changes in b-value associated with changes in event rate and clustering behaviour [e.g., Foulger, 1988], the seismicity observed in the present study shows little change in b-value. D varies no more than b relative to the errors, but a weak negative anomaly and a surge of seismicity is associated with the onset of injection into well 045. A positive correlation between b and D is observed over the periods of time when well activity was fairly constant in the area, but this correlation became negative when the rate of injection was changing rapidly.

Henderson and Main [1992] presented a model for seismicity in which an initial phase where the proportion of small earthquakes is high (high b) occurs in an anti-clustered manner (high D). This is followed by low b-value activity in a strongly clustered geometry (low D). This model, which is based on the notion that small, isolated earthquakes relieve local stresses, predicts a positive correlation between b and D, and is appropriate for a slowly loaded system. This pattern of behaviour is shown by the present dataset during the periods before and after the rapid increase in injection rate. During these periods a preponderance of small earthquakes was associated with a more diffuse spatial distribution.

During the period when the injection rate increased rapidly, the opposite was the case. Then, the negative correlation between b and D shows that a predominance of small earthquakes (high b) was associated with spatial clustering (low D). This behaviour occurred under conditions of rapid loading and, although only weakly statistically significant, has been observed in a

number of other cases at The Geysers [Barton, 1999].

A possible interpretation for these observations is as follows. Preceding and following the initiation of well activity small fluctuations in pore fluid pressure led to seismic activity which had the effect of locally inhibiting further activity. The mechanism for this may have been dilatant hardening [*Scholz et al.*, 1973]. Rapid increase in the rate of injection overcame this and triggered numerous earthquakes by a process involving pore pressure diffusion. Such a style of activity is manifest in spatial clustering of the seismicity (low *D*). *Henderson and Maillot* [1997] proposed that where changes in pore fluid pressure are large compared with fault zone permeabilities, seismicity will be dominated by small events (high *b*-value), and that model seems to be applicable in this case.

These results suggest that there are fundamental differences in the style of seismicity associated with steady-state industrial activity at The Geysers, and periods of rapid changes. They further suggest a relationship between the driving forces of seismicity and the nature of the correlation between *b* and *D*.

Acknowledgments. The seismic data used in this study were supplied by the IRIS-PASSCAL Data Center, Berkeley, and the well data were supplied by the California Division of Oil, Gas and Geothermal Resources and the Northern California Power Agency. DJB was supported by a NERC Research Studentship. This manuscript was considerably improved by the detailed comments of Ian Main, two anonymous reviewers and the Editor.

References

Bath, M., Earthquake magnitude - Recent research and current trends, *Earth Sci. Rev., 17,* 315-398, 1981.

Barton, D.J., Systematics of the frequency-magnitude distribution and spatial fractal dimension at The Geysers geothermal area and Long Valley caldera, California, Ph.D. thesis, Univ. Durham, pp xvi+330, 1999.

DeRubeis, V., Dimitriu, P., Papadimitriou, E. and Tosi, R, Recurrent patterns in the spatial behaviour of Italian seismicity revealed by the fractal approach, *Geophys. Res. Lett., 20,* 1911-1914, 1993.

Eberhart-Phillips, D. and Oppenheimer, D. H., Induced seismicity in The Geysers geothermal area, California, *J. Geophys. Res., 89,* 1191-1207, 1984.

Eneva, M., Effect of limited data sets in evaluating the scaling properties of spatially distributed data: an example from mining-induced seismic activity, *Geophys. J. Int., 124,* 773-786, 1996.

Foulger, G., The Hengill triple junction, SW Iceland: 1. Tectonic structure and the spatial and temporal distribution of local earthquakes. *J. Geophys. Res., 93,* 13,493-13,506, 1988.

Grassberger, P., and Procaccia, I., Measuring the strangeness of strange attractors, *Physica, 9D,* 189-208, 1983.

Hamilton, R. M., and Muffler, L. J. P., Microearthquakes at The Geysers geothermal area, California, *J. Geophys. Res.,* 77, 2081-2086, 1972.

Havstad, J. W., and Ehlers, C. L., Attractor dimension of non-stationary dynamical systems from small datasets, *Phys. Rev. A, 39,* 845-853, 1989.

Henderson, J. R., and Maillot, B, The influence of fluid flow in the fault zone on patterns of seismicity: a numerical investigation, *J. Geophys. Res., 102,* 2915-2924, 1997.

Henderson, J. R., and Main, I. G., A simple fracture-mechanical model for the evolution of seismicity, *Geophys. Res. Lett., 19,* 365-368, 1992.

Henderson, J. R., Main, I. G., Meredith, P. G., and Sammonds, P. R., The evolution of seismicity: observation, experiment and a fracture-mechanical interpretation, *J. Struct. Geol., 14,* 905-914, 1992.

Hirata, T., A correlation between the *b*-value and the fractal dimension of earthquakes, *J. Geophys. Res., 94,* 7507-7514, 1989.

Hubbert, M.K., and Rubey, W.W., Role of fluid pressure in the mechanics of overthrust faulting, *Geol. Soc. Amer. Bull., 70,* 115-166, 1959.

Julian, B. R., Ross, A., Foulger, G. R., and Evans, J. R., Three dimensional imaging of reservoir depletion at The Geysers geothermal area, California, using Vp/Vs ratios, *Geophys. Res. Lett., 23,* 685-688, 1996.

Legrand, D., Cistemas, A., and Dorbath, L., Multifractal analysis of the 1992 Erzincan

aftershock sequence, *Geophys. Res. Lett.*, 23, 933-936, 1996.

Lockner, D. A., Byerlee, J. D., Kuksenko, V., Ponomarev, A., and Sidorin, A., Quasi-static fault growth and shear fracture energy in granite, *Nature, 350,* 39-43, 1991.

Ludwin, R. S., and Bufe, C. G., Continued seismic monitoring of The Geysers, California geothermal area, *Geophysics, 44,* 246-269, 1980.

Main, I. G., Damage mechanics with long-range interactions: correlation between the seismic *b*-value and the two point correlation dimension, *Geophys. J. Int., 111,* 531-541, 1992.

Majer, E.L., and McEvilly, T.V., Seismological investigations at The Geysers geothermal field, *Geophysics, 44,* 246-268, 1979.

Meredith, R G., Main, I. G., and Jones, C., Temporal variations in seismicity during quasi-static and dynamic rock failure, *Tectonophysics, 175,* 249-268, 1990.

Nerenberg, M. A. H., and Essex, C. Correlation dimension and systematic geometric effects, *Phys. Rev.* A, 42, 7065-7074, 1990.

Oncel, A. 0., Alptekin, 0., and Main, I. G., Temporal variations of the fractal properties in the western part of the North Anatolian fault zone: possible artifacts due to improvements in station coverage, *Nonlin. Proc. in Geophys., 2,* 147-157, 1995.

Page, R., Aftershocks and microaftershocks of the great Alaska earthquake of 1964, *Bull. Seis. Soc. Amer., 58,*1131-1168, 1968.

Sammonds, R. R., Meredith, R G., and Main, I. G., Role of pore fluids in the generation of seismic precursors to shear fracture, *Nature, 359,* 228-230, 1992.

Scholz, C. H., Sykes, L. R., and Aggarwal, Y. R, Earthquake prediction: A physical basis, *Science, 181,* 803-810, 1973.

Smith, L. A., Intrinsic limits in dimension calculations, *Phys. Lett. A, 133,* 283-288, 1988.

Smith, W. D., The *b*-value as an earthquake precursor, *Nature, 289,* 136-139, 1981.

Stark, M. A., Microearthquakes - a tool to track injected water in The Geysers reservoir, *Geothermal Resources Council, Monograph on The Geysers Geothermal Field, Special Report No. 17,* 1991.

Zuñiga, F. R., and Wyss, M., Inadvertent changes in magnitude reported in earthquake catalogues: their evaluation through *b*-value estimates, *Bull. Seis. Soc. Amer., 85,* 1858-1866, 1995.

Figure Captions

Figure 1 Map of The Geysers geothermal area, showing the boundary of the area of geothermal production, principal injection wells, hypocentres of 30,000 automatically-located events, and major faults. The box shows the boundaries of the area studied in detail, shown enlarged in Figure 2. Inset shows regional location of The Geysers.

Figure 2 Detailed map showing hypocentre locations of the events used in this study (large grey dots), other nearby events (small black dots), and injection wells in the area (numbered boxes).

Figure 3 Typical examples of frequency-magnitude plot (upper panel) and a plot of log $C(r)$ against log r for a 200-event window (lower panel). The gradient of the frequency-magnitude plot above the threshold magnitude m_{min} gives the *b*-value, and the gradient of the plot of log $C(r)$ against log r at values of log $r < 0.35$ gives the fractal dimension.

Figure 4 Diagram showing the evolution of *b* (upper panel) and *D* (middle panel) for the study area during the periods before, during, and after the onset of injection in Well 045 in early 1992. 2σ error estimates described in the text are indicated by the vertical bars. Horizontal bars show representative window lengths. Lower panel shows the rate of injection for wells 045 and 231.

Figure 5 Rate of seismicity in the study area throughout the period of interest.

Figure 6 Graphs showing the correlation between *b* and *D*, and the associated best-fitting straight lines, for three time periods: before the injection into well 045 (upper panel), during the build-up of injection (middle panel), and following the build-up of injection (lower panel). The sample correlation coefficients, slopes and 1σ uncertainties are shown for each panel.

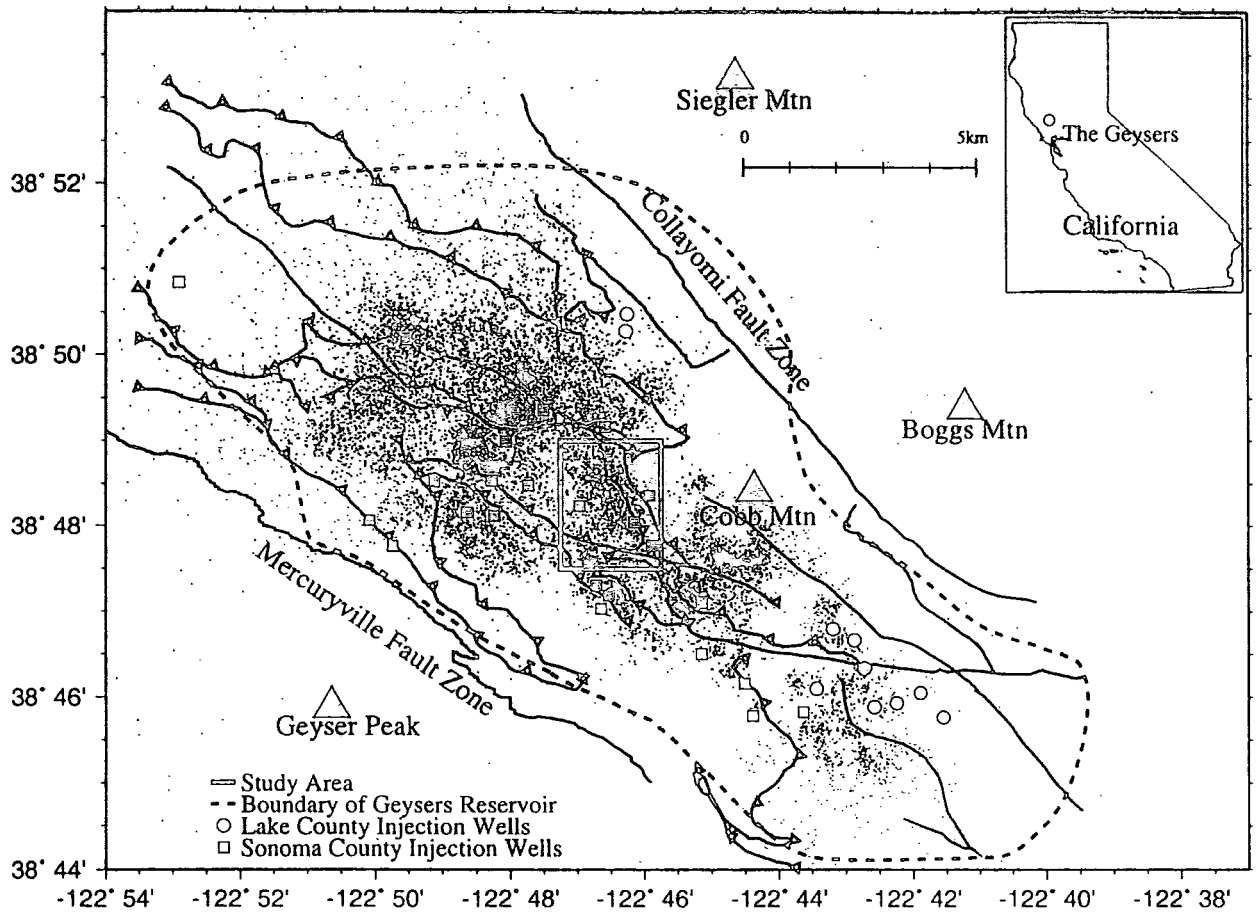
Siegler Mtn
0
5km
The Geysers
California
Collayomi Fault Zone
Boggs Mtn
Cobb Mtn
Mercuryville Fault Zone
Geyser Peak
Study Area
Boundary of Geysers Reservoir
Lake County Injection Wells
Sonoma County Injection Wells
38° 52'
38° 50'
38° 48'
38° 46'
38° 44'
-122° 54'
-122° 52'
-122° 50'
-122° 48'
-122° 46'
-122° 44'
-122° 42'
-122° 40'
-122° 38'

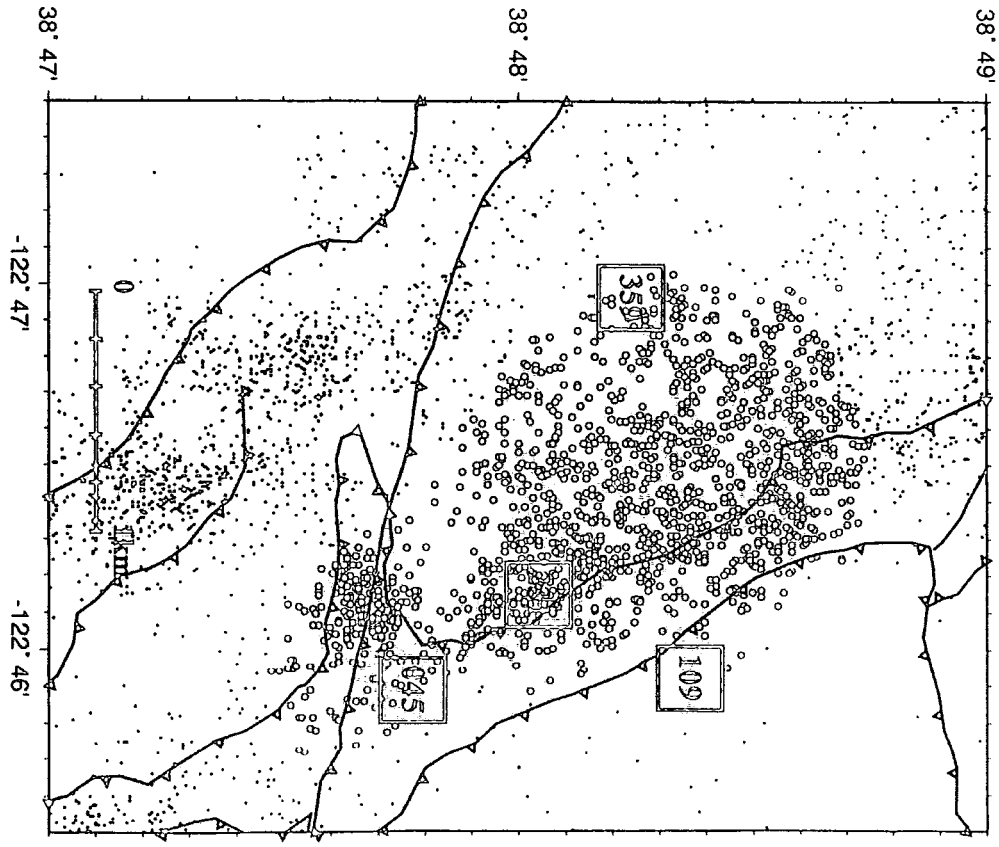
38° 47'
38° 48'
38° 49'
-122° 47'
-122° 46'
0
1km
359
109

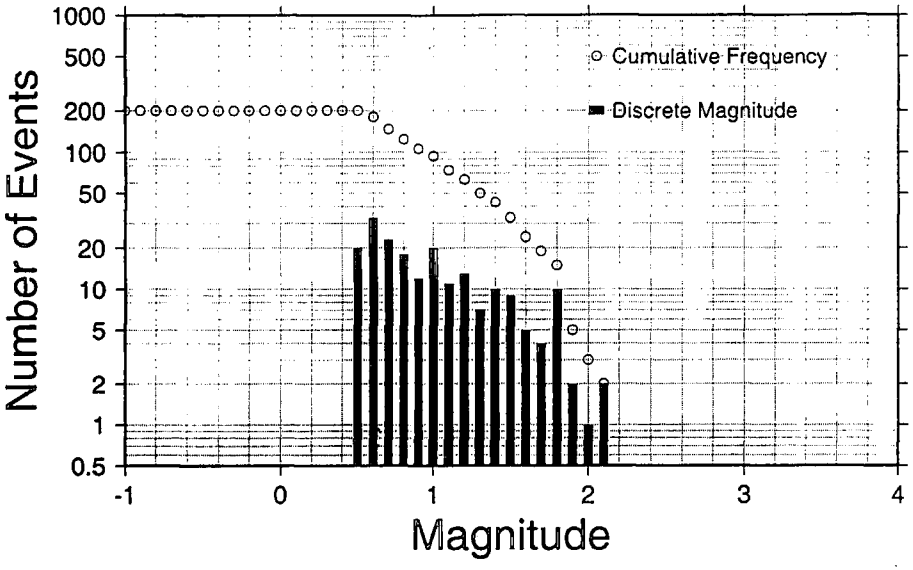
Number of Events
Cumulative Frequency
Discrete Magnitude
Magnitude

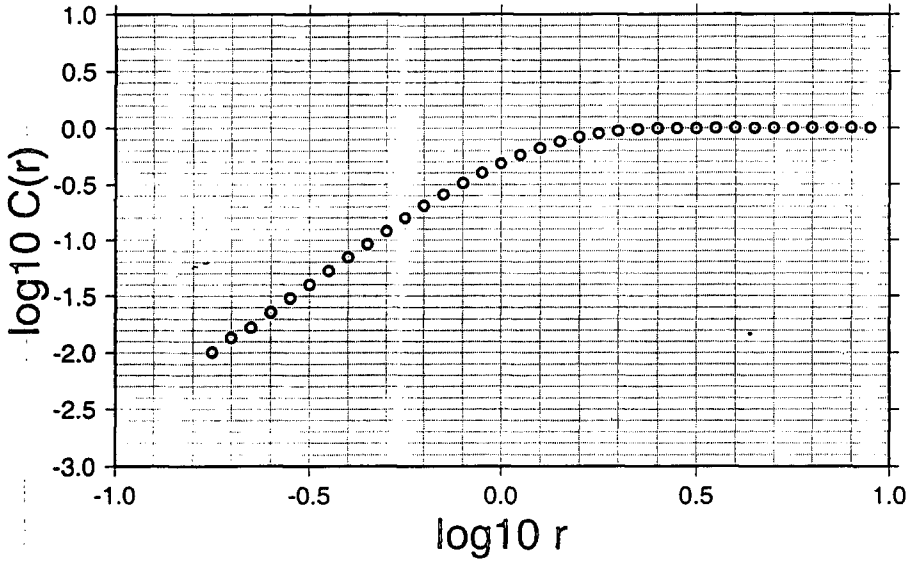
log10 C(r)
log10 r

Fig 3

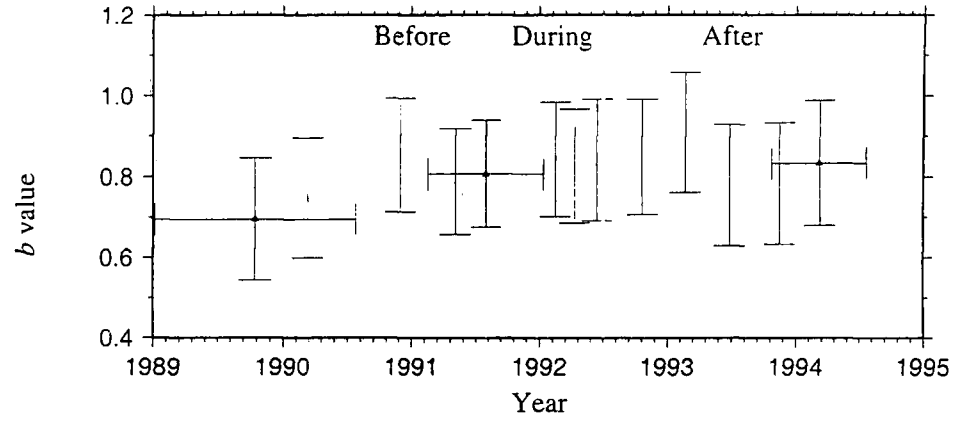
b value
Before
During
After
Year

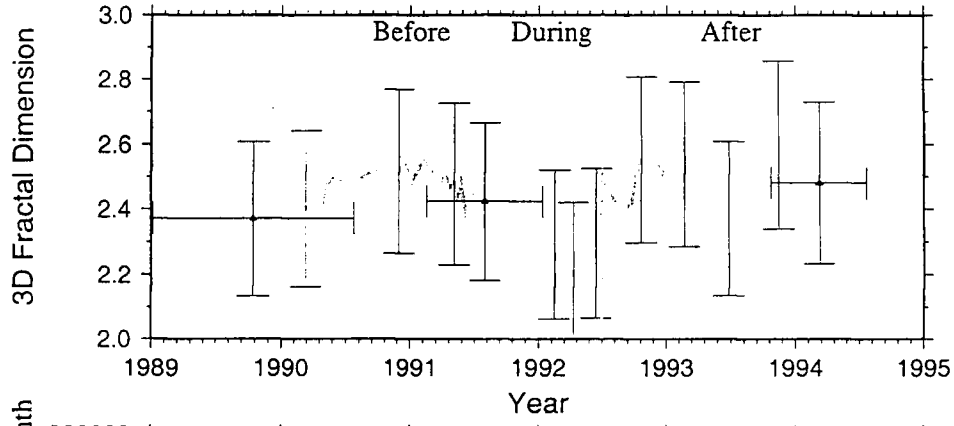
3D Fractal Dimension
Before
During
After
Year

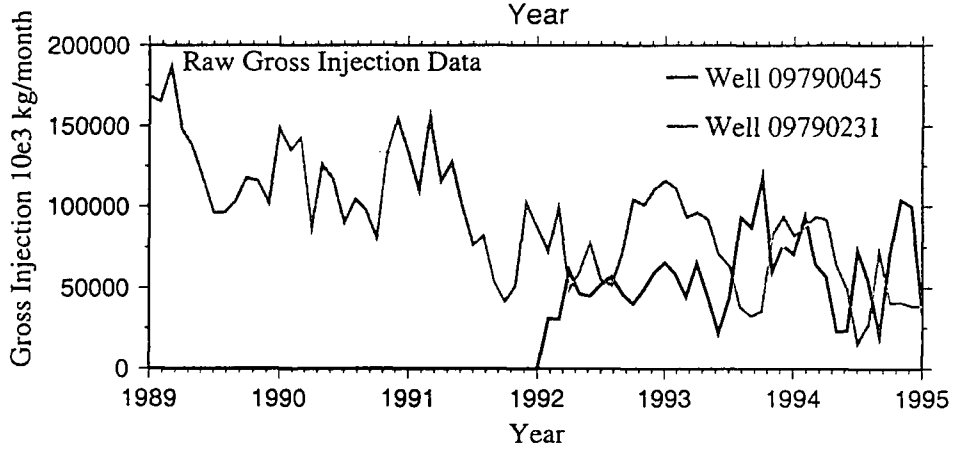
Gross Injection 10e3 kg/month
Raw Gross Injection Data
Well 09790045
Well 09790231
Year

Fig 4

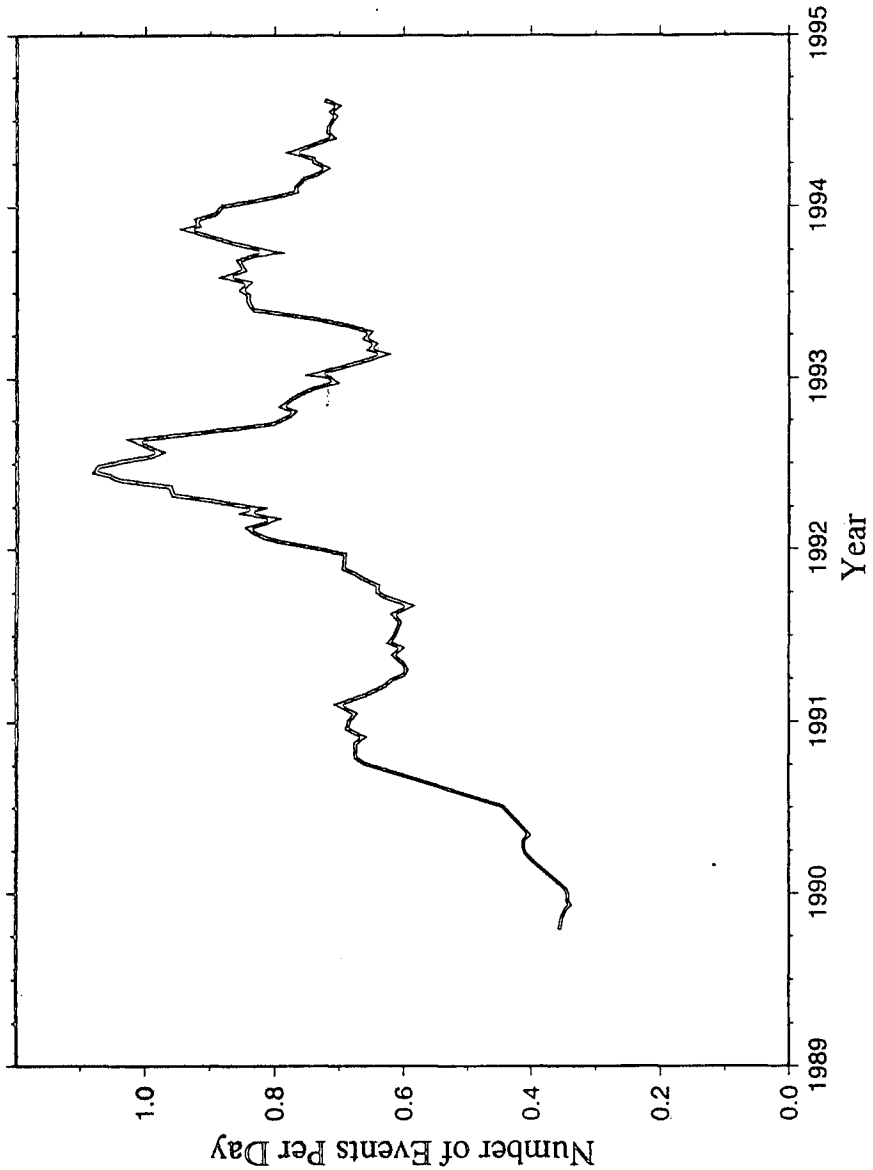
Number of Events Per Day
1.0
0.8
0.6
0.4
0.2
0.0
1989
1990
1991
1992
1993
1994
1995
Year

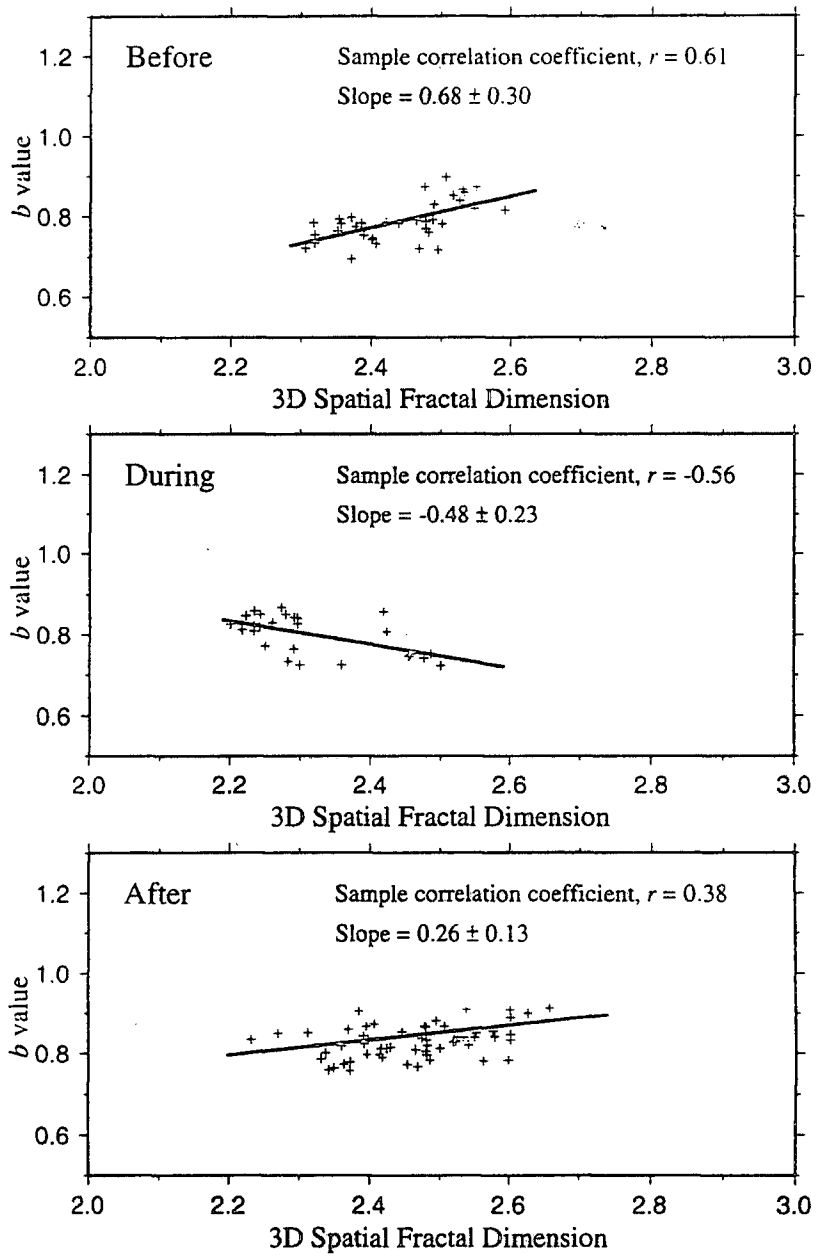
Before
Sample correlation coefficient, r = 0.61
Slope = 0.68 ± 0.30
During
Sample correlation coefficient, r = -0.56
Slope = -0.48 ± 0.23
After
Sample correlation coefficient, r = 0.38
Slope = 0.26 ± 0.13
b value
1.2
1.0
0.8
0.6
2.0
2.2
2.4
2.6
2.8
3.0
3D Spatial Fractal Dimension

Fig 6